

NASA/CP-2016-219016



International VLBI Service for Geodesy and Astrometry 2016 General Meeting Proceedings

“New Horizons with VGOS”

Dirk Behrend (ed.)
NVI, Inc., Greenbelt, Maryland

Karen D. Baver (ed.)
NVI, Inc., Greenbelt, Maryland

Kyla L. Armstrong (ed.)
NVI, Inc., Greenbelt, Maryland

National Aeronautics and
Space Administration

Goddard Space Flight Center
Greenbelt, MD 20771-0001

October 2016

Available from:

NASA Center for Aerospace Information
7115 Standard Drive
Hanover, MD 21076-1320
Price Code: A17

National Technical Information Service
5301 Shawnee Road
Alexandria, VA 22312
Price Code: A10

Preface

This volume is the proceedings of the ninth General Meeting (GM2016) of the International VLBI Service for Geodesy and Astrometry (IVS), held in Johannesburg, South Africa, March 13–17, 2016.



Fig. 1 Logo of the ninth IVS General Meeting.

The keynote of the ninth IVS General Meeting was the opening of new possibilities with the VLBI Global Observing System (VGOS) under the theme “New Horizons with VGOS.” The VGOS network will gradually develop into its full operational state over the next few years, but even during the transition period from the current S/X network to the higher accuracy VGOS systems, new frontiers in science and applications will be opened up by virtue of the increased coverage with VLBI data of unprecedented accuracy.

The ninth General Meeting was held at Ekudeni (Johannesburg), South Africa and was hosted by the Hartebeesthoek Radio Astronomy Observatory (HartRAO), a facility of the National Research Foundation (NRF) of South Africa. The goal of the meeting was to provide an interesting and informative program for a

wide cross-section of IVS members, including station operators, program managers, and analysts.

This volume contains the following:

- **Special report.** The IVS held a retreat in October 2015 which resulted in the preparation of the *Strategic Plan of the IVS for the Period 2016–2025*. IVS Chair Axel Nothnagel introduced the plan in the opening session of the General Meeting. A copy of the strategic plan is reproduced here.
- **The papers presented at the meeting.** There are six major sections of this volume, each corresponding to a meeting session. Poster and oral papers are mixed. The six sessions cover the following topics:
 1. Advances in VGOS Stations and Technology
 2. VGOS Strategies and Expected Results
 3. Stations, Correlators, and Operations Centers
 4. Data Structures and Analysis Strategies in the VGOS Era
 5. Geodetic and Astrometric VLBI Results
 6. VLBI Observations of Space Vehicles

This volume includes 77 papers. The program booklet with abstracts is available online at

[http://events.saip.org.za/
getFile.py/access?resId=
0&materialId=4&confId=56](http://events.saip.org.za/getFile.py/access?resId=0&materialId=4&confId=56)

All papers of this volume were edited by the editors for usage of the English language, form, and minor content-related issues.

- **A list of registered participants.**
- **An author index.**

The contents of this volume also appear on the IVS Web site at



Fig. 2 Participants of the ninth IVS General Meeting at the Lesedi African Lodge and Cultural Village, venue of the meeting banquet.

<http://ivscc.gsfc.nasa.gov/publications/gm2016>

143 registered participants from 22 countries attended the meeting, making this General Meeting as big as the previous one in Shanghai. It was especially nice to see a strong participation from several African countries. In the six sessions of the meeting, the participants gave 112 presentations; 68 of these were talks, and 44 were poster presentations.

The April 2016 issue of the IVS Newsletter has a feature article about the meeting. The Newsletter is available at

<http://ivscc.gsfc.nasa.gov/newsletter/issue44.pdf>

Photographs taken during the meeting week were posted online on the meeting Web site and the IVS Web site:

<http://events.saip.org.za/getFile.py?pageId=11&confId=56>

<http://ivscc.gsfc.nasa.gov/meetings/gm2016/>

The meeting was a huge success, showcasing outstanding research, productive interactions, and diverse social activities, all in a very friendly atmosphere and unique venue. The organization was flawless, and for that, the LOC cannot be thanked enough.



Fig. 3 Mrs. Pandor, Minister of Science and Technology, giving the opening speech.



Fig. 4 Meeting participants during an oral session.



Fig. 5 Axel Nothnagel (IVS Chair, left) and Ludwig Combrinck (Chair of the LOC, right) at the icebreaker reception.



Fig. 6 The 26-m (foreground) and 15-m antennas at HartRAO.



Fig. 7 Groundbreaking for HartRAO's future VGOS telescope.



Fig. 8 Beer and wine tasting at HartRAO.



Fig. 9 More oral presentations are given.

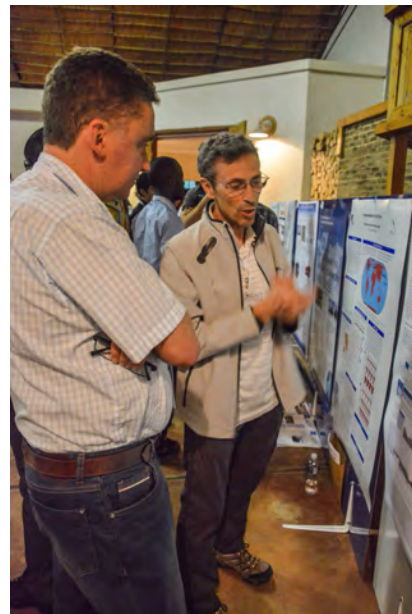


Fig. 10 Jim Lovell (left) and Bill Petrachenko (right) during one of the poster sessions.



Fig. 11 Stunning performance by tribal dancers at Lesedi.

The editors would like to thank the contributing authors to this volume for the timely submission of their papers. Only this made it possible that these proceedings could be produced with such a short turnaround time.

Beyond the General Meeting itself, a number of splinter meetings (large and small) were organized. In the week leading up to the General Meeting, the 2nd IVS Training School on VLBI for Geodesy and Astrometry was held at HartRAO. The school was a big success with 45 participants including 32 students from institutions in different countries in Africa and Asia, Europe, and North America. The participants hailed from Kenya (10), Zambia (9), Germany (7), Austria



Fig. 12 The beautiful landscape of the Swartkop Mountain Range.

(4), U.S.A. (4), China (2), Finland (2), France (2), Sweden (2), Ghana (1), Italy (1), and Spain (1).

During and after the GM, there were side meetings of the VGOS Technical Committee (VTC), the WG on ICRF3, the Monitor and Control Infrastructure (MCI) Group, the Asia-Oceania VLBI Group for Geodesy and Astrometry (AOV), and the WG on Galactic Aberration. Further, an IVS Analysis Workshop was held. All these meetings were held at Ekudeni.

Dirk Behrend, Karen Baver, and Kyla Armstrong
GM2016 Proceedings editors
Greenbelt, MD · September 2016

Table of Contents

Preface	iii	
Special Reports	1	
<i>Axel Nothnagel, Dirk Behrend, Alessandra Bertarini, Patrick Charlot, Ludwig Combrinck, John Gipson, Ed Himwich, Rüdiger Haas, Alexander Ipatov, Ryoji Kawabata, Jim Lovell, Chopo Ma, Arthur Niell, Bill Petrachenko, Torben Schüler, Guangli Wang: Strategic Plan of the IVS for the Period 2016–2025</i> ...	3	
<i>Alexey Melnikov, Pablo de Vicente, Sergei Kurdubov, Andrey Mikhailov: First 2-Gbps Observations between the KVAZAR VGOS Antennas and the Yebes RAEGE Antenna</i>	40	
<i>Arthur Niell, Roger Cappallo, Brian Corey, Chris Eckert, Pedro Elosegui, Russ McWhirter, Ganesh Rajagopalan, Chet Rusczyk, Mike Titus: VGOS Observations with Westford, GGAO, and the New Station at Kokee, Hawaii</i>	44	
<i>Gerhard Kronschnabl, Alexander Neidhardt, Christian Plötz, Torben Schüler, Jan Kodet: The VGOS TWIN Radio Telescope TTW2 at Wettzell</i>	49	
<i>Graham M. Appleby, Giuseppe Bianco, Carey E. Noll, Erricos C. Pavlis, Michael R. Pearlman: Current Trends and Challenges in Satellite Laser Ranging</i>	15	
<i>Evgeny Nosov, Dmitriy Marshalov, Alexey Melnikov: Operating Experience with the Broadband Acquisition System on the RT-13 Radio Telescopes</i>	53	
<i>Mamoru Sekido, Kazuhiro Takefuji, Hideki Ujihara, Tetsuro Kondo, Masanori Tsutsumi, Yuka Miyauchi, Eiji Kawai, Hiroshi Takiguchi, Shingo Hasegawa, Ryuichi Ichikawa, Yasuhiro Koyama, Yuko Hanado, Ken-ichi Watabe, Tomonari Suzuyama, Jun-ichi Komuro, Kenjiro Terada, Kunitaka Namba, Rumi Takahashi, Yoshihiro Okamoto, Tetsuro Aoki, Takatoshi Ikeda : An Overview of the Japanese GALA-V Wideband VLBI System</i>	25	
<i>Gino Tuccari, Walter Alef: BRAND EVN</i>	34	
<i>Leif Morten Tangen: Ny-Ålesund Observatory: What Has Been Done?</i>	37	
<i>Roger Cappallo: Delay and Phase Calibration in VGOS Post-Processing</i>	61	
<i>Hayo Hase, Vincenza Tornatore, Brian Corey: How to Register a VGOS Radio Telescope at ITU and Why It Is Important</i>	65	
<i>Dirk Behrend, Cynthia Thomas, Ed Himwich: Implementation of the VGOS Trials</i>	69	
<i>Daniel MacMillan, Erricos C. Pavlis, Magda Kuzmicz-Cieslak,</i>		
IVS 2016 General Meeting Proceedings		

<i>Daniel Koenig</i> : Generation of Global Geodetic Networks for GGOS	73	<i>A. de Witt, D. Mayer, G. MacLeod, L. Combrinck, L. Petrov, M. Nickola</i> : Optimizing the African VLBI Network for Astronomy and Geodesy	118
<i>Anthony Searle, Bill Petrachenko</i> : Operational VGOS Scheduling	78	<i>Pablo de Vicente</i> : A Technical Overview of the EVN	123
<i>Bill Petrachenko, Patrick Charlot, Arnaud Collioud, Anthony Searle</i> : VGOS Source Selection Criteria	82	<i>Cynthia C. Thomas, Dirk Behrend, Daniel S. MacMillan</i> : From CONT to VGOS: the Evolution of the CONT Campaigns	127
<i>Lucia Plank, Jim Lovell, Jamie McCallum, David Mayer</i> : Observing with Sibling and Twin Telescopes	87	<i>Matteo Stagni, Monia Negusini, Giuseppe Bianco, Pierguido Sarti</i> : The Italian VLBI Network: First Results and Future Perspectives	132
<i>Jim Lovell, Lucia Plank, Jamie McCallum, Stas Shabala, David Mayer</i> : Prototyping Automation and Dynamic Observing with the AuScope Array	92	<i>IGN Yebes Observatory staff</i> : RAEGE Project Update: Yebes Observatory Broadband Receiver Ready for VGOS ..	135
<i>Alexander Neidhardt, Pablo de Vicente, Alessandra Bertarini, Thomas Artz, Sebastian Halsig, Dmitry Ivanov, Alexey Melnikov, Johannes Böhm, Andreas Hellerschmied, David Mayer, Christian Plötz, Gerhard Kronschnabl, Axel Nothnagel, Sergei Kurdubov, Andrey Mikhailov, Dmitry Marshalov, Ilia Bezrukov, Yu. Bondarenko</i> : First Results of the FAST-S/X Sessions with New VGOS Antennas	96	<i>Sang-oh Yi, Yun-mo Sung, Ki-duk Ah, Hong-jong Oh, Doyoung Byon, Hyung-chul Lim, Moon-hee Chung, Do-heung Je, Tae-hyun Jung</i> : Activities at Sejong Station	139
<i>Alexander Neidhardt, Katharina Kirschbauer, Christian Plötz, Matthias Schönberger, Armin Böer, and the Wettzell VLBI Team</i> : Current Status of an Implementation of a System Monitoring for Seamless Auxiliary Data at the Geodetic Observatory Wettzell	101	<i>Nataliya Zubko, Jyri Näränen, Ulla Kallio, Veikko Saaranen, Jenni Virtanen and Markku Poutanen</i> : Metsähovi Geodetic Fundamental Station in Finland — New VGOS Site, Plans, and Current Status	143
<i>Alexander Ipatov, Dmitriy Ivanov, Gennadiy Ilin, Sergei Smolentsev, Iskander Gayazov, Vyacheslav Mardyshev, Leonid Fedotov, Victor Stempkovski, Alexander Vytov, Alexander Salnikov, Igor Surkis, Andrey Mikhailov, Dmitriy Marshalov, Ilya Bezrukov, Alexey Melnikov, Voytsekh Ken, Sergei Kurdubov</i> : New Generation VLBI: Intraday UT1 Estimations	106	<i>Ch. Plötz, A. Neidhardt, T. Klügel, R. Wojdziak, J. Serna Puente, B. Vaquero Jiménez, T. Schüler, VLBI Team Wettzell, DFD Team DLR</i> : The German Antarctic Receiving Station O’Higgins and Its VLBI Capabilities	146
Session 3. Stations, Correlators, and Operations Centers	111	<i>T. Schüler, C. Plötz, S. Mähler, T. Klügel, A. Neidhardt, A. Bertarini, S. Halsig, A. Nothnagel, M. Lösler, C. Eschelbach, J. Anderson</i> : First Local Ties from Data of the Wettzell Triple Radio Telescope Array	149
<i>Sten Bergstrand, Ralf Schmid</i> : Activities of the IERS Working Group on Site Survey and Co-location	113	<i>Ulla Kallio, Michael Lösler, Sten Bergstrand, Rüdiger Haas, Cornelia Eschelbach</i> : Automated Simultaneous Local Ties with GNSS and Robot Tacheometer	154
		<i>Takaaki Jike</i> : VERA Geodetic VLBI with a Newly Developed High-speed Sampler and Recorder	159
		<i>Renjie Zhu, Yajun Wu, Jiyun Li</i> : Progress on the VLBI	

Data Acquisition System of SHAO	163	<i>Zheng</i> : Results from the VLBI Analysis Software Comparison Campaign 2015	203
<i>Federico Perini, Claudio Bortolotti, Mauro Roma, Roberto Ambrosini, Monia Negusini, Giuseppe Maccaferri, Matteo Stagni, Mauro Nanni, Cecilia Clivati, Matteo Frittelli, Alberto Mura, Filippo Levi, Massimo Zucco, Davide Calonico, Alessandra Bertarini, Thomas Artz</i> : The First Geodetic VLBI Field Test of LIFT: A 550-km-long Optical Fiber Link for Remote Antenna Synchronization	166	<i>Tobias Nilsson, Maria Karbon, Benedikt Soja, Susanne Glaser, Robert Heinkelmann, Harald Schuh</i> : Simulations of Near Real-time EOP Estimation from a Future VGOS Network	208
<i>Arno Müskens, Walter Alef, Alessandra Bertarini, Simone Bernhart, Laura La Porta, Helge Rottmann, Gabriele Bruni, Torben Schüler, Walter Briskin</i> : New DiFX Software Correlator Cluster at Bonn and Summary of Recent Activities	171	<i>Linda Messerschmitt, Sabine Bachmann, Daniela Thaller</i> : Options and Functions of the Revised IVS Combination Web Site	213
<i>Wu Jiang, Zhiqiang Shen, Fengchun Shu, Zhong Chen, Tianyu Jiang</i> : Current Status of the Shanghai VLBI Correlator	176	<i>Thomas Artz, Sebastian Halsig, Andreas Iddink, Axel Nothnagel</i> : ivg::ASCOT: Development of a New VLBI Software Package	217
<i>Zhijun Xu, Jiangying Gan, Shaoguang Guo</i> : Hardware Correlator Development at SHAO	180	<i>Sergei Bolotin, Karen Baver, John Gipson, David Gordon, Daniel MacMillan</i> : Transition to the vgosDb Format	222
<i>Jiangying Gan, Zhijun Xu, Shaoguang Guo</i> : High-speed Data Playback of the VLBI Hardware Correlator	183	<i>Gerald Engelhardt, Volkmar Thorandt, Dieter Ullrich</i> : Refinement of the Rapid UT1 Estimation Derived from Tsukuba VLBI Measurements after the 2011 Earthquake	225
<i>David Gordon, Walter Briskin, Walter Max-Moerbeck</i> : Difxcalc – Calc11 for the DiFX Correlator	187	<i>John Gipson, Karen Baver</i> : Improvement of the IVS-INT01 Sessions through Bayesian Estimation	229
Session 4. Data Structures and Analysis Strategies in the VGOS Era	191	<i>Thomas Hobiger, Rüdiger Haas, Eskil Varenius</i> : Hard- and Software Tools for the Education of Geodetic VLBI ..	234
<i>Thomas Artz, Sebastian Halsig, Andreas Iddink, Axel Nothnagel, Corinna Tegtmeier</i> : Constraining Least-Squares VLBI Solutions	193	Session 5. Geodetic and Astrometric VLBI Results	239
<i>Niko Kareinen, Thomas Hobiger, Rüdiger Haas</i> : Robust Ambiguity Estimation for an Automated Analysis of the Intensive Sessions	198	<i>Sabine Bachmann, Daniela Thaller, Ole Roggenbuck, Michael Lösler, Linda Messerschmitt</i> : IVS Contribution to ITRF2014	241
<i>G. Klotek, T. Artz, A. Bellanger, G. Bourda, M. Gerstl, D. Gordon, R. Haas, S. Halsig, G.A. Hjelle, T. Hobiger, U. Hugentobler, A. Iddink, A.S. Kirkvik, S. Lambert, L. Plank, R. Schmid, F. Shu, O. Titov, F. Tong, G. Wang, M. Xu, W.</i>		<i>Sigrid Böhm, Hana Krásná, Sabine Bachmann</i> : Vienna Contribution to ITRF2014	251
		<i>Benedikt Soja, Tobias Nilsson, Susanne Glaser, Kyriakos Balidakis, Maria Karbon, Robert Heinkelmann, Richard Gross, Harald Schuh</i> : Comparison of a VLBI TRF Solution Based on Kalman Filtering and Recent ITRS Realizations	256

<i>Claudia Flohrer, Erik Schönemann, Tim Springer, René Zandbergen, Werner Enderle: VLBI Processing at ESOC</i>	<i>Schuh, Guangli Wang: Source Structure of 0642+449 Derived from CONT14 Observations</i>
261	317
<i>Younghee Kwak, Johannes Böhm, Thomas Hobiger, Lucia Plank, Kamil Teke: Combination of Two Radio Space-Geodetic Techniques with VieVS during CONT14</i>	<i>Bo Zhang: Images of VLBI Calibrators from the BeSSeL Survey</i>
265	321
<i>Chopo Ma, Daniel MacMillan, Karine Le Bail, David Gordon: Aspects of ICRF-3</i>	<i>Sebastian Halsig, Thomas Artz, Andreas Iddink, Axel Nothnagel: An Inequality Constrained Least-Squares Approach as an Alternative Estimation Procedure for Atmospheric Parameters from VLBI Observations</i>
270	326
<i>David Mayer, Hana Krásná, Johannes Böhm: Vienna Contribution to the ICRF3</i>	<i>Kyriakos Balidakis, Florian Zus, Jan Douša, Tobias Nilsson, Susanne Glaser, Benedikt Soja, Maria Karbon, Robert Heinkelmann, Harald Schuh: On the Impact of Different Mapping Functions on Geodetic and Tropospheric Products from VLBI Data Analysis</i>
275	331
<i>David Gordon, Karine Le Bail: Status of the X/S Source Catalog</i>	<i>John Gipson: El Niño and VLBI Measured Length of Day</i>
280	336
<i>Andreas Iddink, Thomas Artz, Sebastian Halsig, Axel Nothnagel: Estimating the Celestial Reference Frame via Intra-Technique Combination</i>	<i>C. Gattano, S. Lambert, C. Bizouard: The Annual Retrograde Nutation Variability</i>
283	341
<i>Karine Le Bail, David Gordon, Chopo Ma: Selecting Sources that Define a Stable Celestial Reference Frame with the Allan Variance</i>	<i>Anastasiia Girdiuk, Michael Schindelegger, Johannes Böhm: Tidal Atmospheric Loading and VLBI</i>
288	346
<i>C. Gattano, S. Lambert: Defining Source Selection and Celestial Reference Frame Stability</i>	<i>Fengchun Shu, Leonid Petrov, Wu Jiang, Jamie McCallum, Sang-oh Yi, Kazuhiro Takefuji, Jinling Li, Jim Lovell: Progress on the VLBI Ecliptic Plane Survey</i>
292	351
<i>Maria Karbon, Robert Heinkelmann, Julian Mora-Diaz, Minghui Xu, Tobias Nilsson, Harald Schuh: About the Modeling of Radio Source Time Series as Linear Splines</i>	<i>Kyriakos Balidakis, Robert Heinkelmann, Apurva Phogat, Benedikt Soja, Susanne Glaser, Tobias Nilsson, Maria Karbon, Harald Schuh: On the Impact of Inhomogeneities in Meteorological Data on VLBI Data Analysis</i>
297	356
<i>A. de Witt, A. Bertarini, C.S. Jacobs, J. Quick, S. Horiuchi, T. Jung, J. Lovell, J. McCallum, G. Bourda, P. Charlot: Completing the K-band Celestial Reference Frame in the North</i>	Session 6. VLBI Observations of Space Vehicles
302	361
<i>C. Gattano, S. Lambert: Source Characterization by the Allan Variance</i>	<i>Geshi Tang, Jing Sun, Xie Li, Shushi Liu, Guangming Chen, Tianpeng Ren, Guangli Wang: APOD Mission Status and Observations by VLBI</i>
307	363
<i>S. Basu, A. de Witt, S. Shabala, J. McCallum, J. Quick, A. Bertarini: How Good is the Deep Southern Sky</i>	<i>Benjamin Männel, Markus Rothacher, Philippe Jetzer,</i>
312	
<i>M. H. Xu, R. Heinkelmann, J. M. Anderson, J. Mora-Diaz, H.</i>	

<i>Steve Lecomte, Pascal Rochat: E-GRIP: A Highly Elliptical Orbit Satellite Mission for Co-location in Space</i>	368
<i>Andreas Hellerschmied, Johannes Böhm, Younghee Kwak, Jamie McCallum, Lucia Plank: VLBI Observations of GNSS Signals on the Baseline Hobart–Ceduna</i>	373
<i>Weimin Zheng, Fengxian Tong, Fengchun Shu: Accurate Spacecraft Positioning by VLBI Imaging</i>	378
<i>Guifré Molera Calvés, Alexander Neidhardt, Christian Plötz, Gerhard Kronschnabl, Giuseppe Cimó, Sergei Pogrebenko: Venus and Mars Express Spacecraft Observations with Wettzell Radio Telescopes</i>	382
About the Meeting	387
Registered Participants	389
Author Index	393

Special Report



March 2016 · Johannesburg · South Africa

Strategic Plan of the IVS for the Period 2016–2025

Axel Nothnagel, Dirk Behrend, Alessandra Bertarini, Patrick Charlot, Ludwig Combrinck, John Gipson, Ed Himwich, Rüdiger Haas, Alexander Ipatov, Ryoji Kawabata, Jim Lovell, Chopo Ma, Arthur Niell, Bill Petrachenko, Torben Schöler, Guangli Wang

Abstract Over the next decade, the IVS is on the cusp of dramatic changes transitioning from using large, slow moving antennas observing at S/X (“legacy” systems) to using small, fast antennas with broad-band receivers, the so-called VGOS systems. Never has there been a time when so many antennas specifically designed for geodetic VLBI are scheduled to come on line in such a short period. VGOS observing will change all aspects of VLBI, from scheduling, to correlation, to observing strategy, to analysis. Compared to current observing, a typical VGOS session will have 1–2 orders of magnitude more data. In this strategic plan we outline some of the operational concepts of VGOS observing, our goals for data accuracy and latency, and some of the challenges and issues we will face during this transition.

Keywords VGOS

1 Prolog

In the period 2016 to 2025 the International VLBI Service for Geodesy and Astrometry (IVS) will enter the era of the VLBI Global Observing System (VGOS), which will be composed of a transition period and subsequent full VGOS operations. To enable overall planning and to give the stakeholders and IVS Associates some guidelines for the investments and activities needed, the IVS Directing Board has developed the *Strategic Plan of the IVS for the Period 2016–2025*.

IVS Directing Board

This strategic plan was developed on the basis of the current composition and framework of the IVS’s operations. The IVS acts as a truly international entity consisting of hardware distributed all over the world, a global organizational structure, and the associated personnel for organizing and administering the IVS. The IVS is not a formal global institution but a collaboration, which operates on a best-effort basis. The full potential of geodetic and astrometric VLBI can only be exploited if baselines beyond a length of about 6,000 km are employed for Earth Orientation Parameter (EOP) and Celestial Reference Frame (CRF) determinations. The same also applies to any Terrestrial Reference Frame (TRF) application. Because of this it would be difficult for the IVS to be replaced by a single country running its own VLBI network, operating its own telescopes, correlating and analyzing the results, and producing the final VLBI products.

In the geodetic and astrometric communities it is well known that the IVS is essential for the monitoring of the Earth orientation parameters and for the maintenance of the celestial and terrestrial reference frames. However, the IVS is little known for its products beyond this limited group. For this reason the organizational relationships of the IVS, external as well as internal, and the administration of the IVS must be developed further. In this context the IVS may benefit from the GGOS and UN-GGIM initiatives (Global Geodetic Observing System, UN-Global Geospatial Information Management), which will help to raise awareness in political circles of the needs for geodetic products. We urge IVS associates to publicize this initiative and the important role of IVS in geodesy.

Another challenge of the future is that many experienced colleagues have reached or are close to retirement age. Hence, we need active recruiting and staff

structure development to replace them. An increased awareness of this issue is needed within the IVS components up to the highest level of their administrations.

On the product side, several separate requirements compete: accuracy, resolution, and timeliness. These need to be balanced for an optimum satisfaction of the product users. There may arise conflicts between what is actually feasible given the current economic and organizational circumstances and the users' desires for higher accuracy, resolution, and timeliness.

Under these premises the *Strategic Plan of the IVS for the Period 2016–2025* was developed to address the following topics and the corresponding goals for operational concepts, including correlation, product lines, and institutional relations.

2 Operational Concepts

2.1 Observing Network

Although not quite correct for a chronological consideration of the IVS's operation, the first group of components to look at is the observatories. Their technical layout was defined in Petrachenko et al. (2009) with comparisons of components documented in Petrachenko (2013a, 2013b). In summary it can be stated that VGOS telescopes should be fast slewing and capable of recording broadband radiation of extra-galactic radio sources from 3–14 GHz continuously. It is conceivable that the upper limit may even be extended to 18 GHz, which offers some advantages for the receiver developments due to the fact that 18 GHz is a multiple of the lower limit of 3 GHz. The development of a suitable feed horn needs to be followed closely, and a recommendation for a certain development line of wide-band feed cannot be made at this stage. The same applies to the final frequency band allocation within the total bandwidth.

Although Ka-band (32 GHz) observations may have their benefit, they are hampered by the degradation of quality by adverse weather conditions and are, thus, not recommended for the routine monitoring purposes, which are needed by the IVS for EOP determinations.

The recently developed Mark 6 recording units were designed to cope with the expected data volume

and should reach an operational stage soon. In parallel to this, commodity based recording systems, such as *Flexbuff*, are suitable for handling today's data volume but still need to prove their suitability for 16 Gbit/s recording. However, these systems are suited for asynchronous or even synchronous eTransfer operations. A firm recommendation for a particular recording system cannot and should not be given at all because the IVS should remain open for development initiatives.

The previous statement has, however, to be seen within the restrictions of technical standards since compatibility must be guaranteed throughout the community. This can be achieved only if standardization in VLBI keeps pace with the technical developments, and the IVS Technology Coordinator has a very special responsibility in this arena. The Technology Coordinator should take care that the necessary standards are developed and adopted in time and that geodesists and astronomers alike abide to these standards.

The VGOS idea as laid out in Petrachenko et al. (2013) foresees an operation of the IVS infrastructure of seven days per week for 24 hours each. This general rule should be interpreted in such a way that the VGOS operation produces EOP, especially UT1–UTC, seven days a week with a certain time resolution. At this stage the main customer, the IERS Bureau for Rapid Service and Prediction at US Naval Observatory, processes its data every six hours. The same time resolution should be attained initially for the IVS products with a goal of higher resolution, i.e., aiming for three-hour intervals. Since the determination of a single UT1–UTC value at a given epoch requires a certain observing time to gain geometrical stability, continuous observations are the necessary consequence. Additionally, since the correct estimates of UT1–UTC are dependent on the other EOP components, it is necessary to employ full-scale VGOS network observations.

The necessity for continuous network observations has led to the advantageous situations that at some observatories twin telescopes are being built. These can be used in cycles allowing sufficient maintenance and repair periods, thus guaranteeing that these observatories can really provide 24/7 operations. They will be the cornerstones of the VGOS observing network.

Such a scheme is not possible at single-telescope observatories, so we cannot expect that each and every station will observe continuously. Instead we anticipate a rotating system of telescopes joining or leaving the

network for full days at a time. This will ensure that observatories where only a single telescope is available have sufficient time for maintenance and repairs.

For the constellation of the networks, it is necessary to take into account how many telescopes are available with VGOS capabilities, so there will be a clear distinction between the transition phase and full operation of the network. The initial observing setup in the transition phase with daily one-hour sessions is laid out in the VGOS Observing Plan (Petrachenko et al. 2013).

Although initial plans called for 30 stations observing simultaneously, reality will determine how many telescopes will be available at any time. However, it is the declared aim of the IVS to exploit the full benefit of at least a 24-station network. For determining the optimal locations of the telescopes, simulations can help to give guidelines. These are being carried out in, for example, the PLATO Working Group of the IAG (Thaller et al. 2015). Without preempting the results of those studies, it can be clearly noted that the IVS network lacks observatories in the Southern Hemisphere. The IVS, the IVS DB, and all IVS Associates should actively encourage and pursue the construction of new telescopes primarily in Africa, South America, and any suitable islands as far south as possible. The operations and continued participation of the rather few existing telescopes in these regions should be safeguarded because they are extremely important for continental motions and Earth orientation variations for reasons of geometric constellation and network sensitivity.

The cost of operating the VGOS telescopes is non-negligible. Automatic, unattended observations may be one way of reducing the financial burden. Remote operations of telescopes are another promising avenue to reduce costs and to allow for quick responses to unforeseen occurrences. The formation of observing control centers which hand over responsibility from time zone to time zone at normal working hours will be considered by the IVS.

Even though the primary operations of the IVS will aim at the regular determinations of EOP with the VGOS network, the so-called legacy antennas continue to be needed in the future. On the one hand, the IVS Observing Program Committee and the IVS Coordinating Center need to take care of suitable mixed-mode observations to locate the new telescopes in the terrestrial reference frame currently defined by the legacy telescopes. On the other hand, the legacy antennas mainly have larger apertures, which make them more

sensitive. They are, therefore, more useful for observations of weaker radio sources and, thus, important for the maintenance of the celestial reference frame. For these purposes, as many as possible legacy antennas that satisfy the sensitivity qualification should be kept in operation for as long as possible. Their use will provide not only dedicated TRF observations but also guarantee a sufficient overlap for maintaining the long position time series of the stations and the transfer of the continental drift information to the new telescopes.

Independent of the legacy telescope CRF work, astrometry with the VGOS antennas should also be taken into account for the future. Here, the observing time available for astrometry heavily depends on the number of telescopes available at a given time. A clear projection of how much dedicated CRF observing will be carried out can, therefore, not be given at this stage.

2.2 Correlators

Correlation of the observed data is a central requirement of VLBI. Due to the fast development in commodity computing, software correlators are almost solely employed for today's VLBI correlations. Correlators are the first instance where the data can be checked, and often the data quality is far from the specifications defined in the session setup. Under the premise that observing efforts are costly, the correlator staff tries to rescue as many observations as possible and inform the stations about possible defects in their systems. Likewise they give feedback on station tests, which are necessary whenever a telescope takes up operations or has undergone major changes in its hardware.

Before correlation results can be used in data analysis, the correlator output needs to be fringe-fitted. This process is considered an integral part of correlation and requires a great deal of expertise, which in most cases has to be separated from the analysis of the group and phase delays. Today, five out of six correlators use the same suit of fringe-fitting software (difax2mark4, fourfit) although other suitable software is available. For broadening the expertise and for benefitting from modern computational capabilities, the IVS strongly encourages further developments in this field.

Several correlators currently share the load of the IVS correlation. Over the long history of VLBI corre-

lations, expertise has been built up in multiple correlation centers such that workloads can be shifted from one correlator to another as needed. This capability will need to be maintained and exploited in the future when the steadily increasing correlator capacity requirement will need to be distributed to multiple correlator centers on an even basis. Unfortunately, the situation with funding and operating the correlators varies greatly among the individual centers. This affects not only the financial background but also technical expertise. On the institutional side, a firm commitment at the level of about ten years is needed to make credible planning feasible and to sustain correlator operations. This does not seem to be possible for some of the institutions involved but is needed to provide guarantees for continuous product delivery. The situation with experienced personnel, is equally critical. VLBI correlation is a very specialized skill, and it takes years to become proficient. While a number of correlator centers gear up their operations and learn, mostly from established groups, how to correlate and how to cope with defective data or unusual setups, the number of experienced personnel that can provide this expertise is diminishing due to aging and retirements. We need to hire and train suitable personnel on a long term basis with sufficient perspectives for the future.

The development of correlator and fringe fitting software is not the domain of geodesists alone but also of astronomers with very similar interests and sometimes more resources. Sharing the operations of a correlation facility with closely aligned disciplines (e.g., with astronomers) is a suitable model for sharing costs and experiences. Synergies should be explored to a greater extent than is done at the moment. This will help to advance the technology much further than geodesists can achieve alone. The same applies to computer scientists, who may have different interests but may be able to provide modern concepts for the ever changing world of computing.

2.3 Data Transport

Closely linked to the correlation proper are data transport issues. Here, the situation is as heterogeneous as the variety of correlators. While some of the observatories may have to ship disk modules, others would send all the data to the correlators by electronic transfer. The

latter poses serious network bandwidth and storage requirements on the respective correlator if this is done by many stations. The situation will only get worse with VGOS, where a typical station will take ~ 40 TB of data during a session.

The other issue in this respect is the data transfer capability of the electronic network. Stations normally subscribe to a provider for a certain bandwidth. The same applies to the correlator with the additional requirement that the data of multiple telescopes must be transferred from the backbone to the final storage area in parallel. This requires multiples of the bandwidth of individual telescopes. In some countries, the costs for that are (still) prohibitive.

In terms of efficient operations, some optimization seems to be possible. For example, the correlator staff could initiate retrieval of the data from the telescope sites at their discretion. This would allow the correlator personnel to efficiently balance the load on the last-mile to the correlator. A second possibility is for correlators to establish high-capacity RAID systems at the backbone node and retrieve the data from there when needed. Both of these measures have their pros and cons, which must be balanced according to the respective situation.

Another option is to set up and operate correlators in a distributed architecture. This will keep the responsibility for session setups and quality control in the hands of the correlator centers but will potentially offer a way to circumvent data transfer problems. The IVS community should also think of and investigate decentralized correlation.

Finally, it should be noted that electronic transfer capacity is likely to limit what will be achievable in the VGOS era. It is hoped that commercial applications and political decisions will work in favor of the IVS's operation.

2.4 Session Planning and Scheduling

Even though a great deal of automation is foreseen for the daily session configuration and for the scheduling of the individual days, good coordination will be necessary to exploit the full benefit of the available resources. The IVS Coordinating Center and the IVS Operations Centers will continue to work closely together in the VGOS era.

Currently, geodetic and astrometric VLBI is organized in sessions, mainly of 24-hour duration. From a planning and organizational point of view this will continue, with the only change being that sessions will run from 0 h UT to 0 h UT. Planned network changes will always take place at day boundaries, i.e., only when the telescopes join or leave the observing networks. Of course, in the pilot phase as described in the VGOS Observing Plan (Petrachenko et al. 2013), some sub-sessions will be of only one-hour duration. For these reasons, the observing plans will be prepared in units of 24 hours also in the future.

Another aspect of session planning is that the IVS should strive for robustness of its products. The first approach to achieving robustness is to schedule a sufficient number of stations in each session. This will mitigate the effects of unforeseen station failures on the accuracy of the IVS products. In order to minimize the impact of a station failure during a session, a flexible response of the network to such a loss should be prepared for. The same also applies when severe degradation of sensitivity occurs. One of the possible solutions to both situations is dynamic scheduling, which can take effect as soon as an unplanned dropout or loss of sensitivity is reported. The exact mechanism of how this would be handled should be developed in the near future.

Another approach might be to operate several networks in parallel in order to provide the opportunity for checking the derived IVS products. However this requires access to a sufficiently large number of VGOS stations that several parallel networks with sufficient geometry can be formed.

3 Data Analysis Considerations and Product Lines

The different VLBI products have varying latency and spatial resolution requirements. The most stringent latency requirement is for EOP, and in particular, UT1–UTC, where accurate near-real-time daily or even sub-daily measurements are desired (As mentioned previously, the IERS produces estimates every six hours.). In contrast, the latency and resolution requirements for the TRF and CRF are much more relaxed. For the CRF we need to measure sources only often enough to monitor their strengths, and much less frequently to mea-

sure their apparent positions. For the most part, these measurements will occur naturally as part of the regular observing, and no special efforts need to be made. Monitoring of the TRF on a daily basis can be achieved more economically with GNSS observations. In addition to the EOP considerations, continuous observations will provide improvement in overall reliability of the geodetic and astrometric VLBI observation setup. Except for the ultra-rapid products (see below) the time resolution of the IVS products will be set to three hours in order to be commensurate with the current six-hour interval of the IERS RS-PC and, additionally, be prepared for the increased resolution.

The whole process of producing geodetic results from VGOS observations is driven by the desire to deliver products which are as accurate as possible at the time the data are taken. However, there may be varying demands with respect to timeliness or precision and accuracy. Since UT1–UTC results used for extrapolations decay rather quickly, VGOS results should be available almost instantly. Since continuity is predominantly determined by the observing capabilities, it is a prerequisite that the processing of the observations cope with this pace by a high level of automation in data analysis. The analysis groups within the IVS always strive for highest quality. Thus it is expected that accuracy and precision will continue to improve based on changes in analysis strategies state-of-the-art modeling and processing. Furthermore it is anticipated that every IVS Analysis Center will be able to perform its analyses from the correlator output onwards so that there will be no dependence on other analysis centers.

Another criterion to be considered is latency, which means how quickly VLBI products are made available to the scientific and user communities. Latency and accuracy are not necessarily in conflict, but in general low latency (quickly available) results are mostly less accurate than those that are delivered after some longer processing and quality control time. One of the reasons is that low latency always requires some compromises with respect to the usage of auxiliary data. These might not be available instantly because they may be provided at the required quality only by another service that does not have the same latency requirement. As mentioned above, depending on the priorities, timeliness may be more important than accuracy for some users. This results in a need for products with different latencies and respective qualities.

Low latency is most important for Earth orientation parameters (EOP), which are used by the scientific and technical community. In particular, the GNSS community needs the UT1–UTC product in near-real-time (Bradley et al., 2015). Low latency is less critical for telescope coordinates, which, to a first approximation, evolve linearly. In this case, measuring telescope coordinates periodically and processing them in less than real-time may be sufficient. An exception to this might be if something abruptly changes the telescope coordinates (e.g., an earthquake) in which case we might want a rapid update and regular measurements thereafter until the station returns to a predictable motion. It should be noted that since the quality of the estimated EOP strongly correlates with that of the station positions, it is important that we have good station positions for those stations involved in EOP measurements of only one hour duration. Analyzing 24-hour sessions for EOP automatically provides good information on station coordinates simultaneously.

The processing steps and their time requirements depend on how the data transport and the correlations are carried out. For this reason two different scenarios need to be considered. The first one relies on a continuous, though retarded, correlation process. Here, the observables may be available on a scan by scan basis. This situation allows for an incremental analysis employing filter solutions with update intervals from a few minutes to virtually any length. In the second scenario, correlations are carried out in batches of three or 24 hours each with some non-negligible delay time.

Finally, in addition to striving always for highest accuracy and precision continuous development of better technical components as well as improvement in analysis strategies and models must be a standing goal of the IVS. In the context of VGOS operations, with technology and analysis always staying state of the art, the accuracy of products achievable clearly depends on the latency time permitted for the results to be available after the observations. For this reason, four different lines of IVS products are foreseen, as specified in Table 1. We emphasize that this lists our goals for the final VGOS network and is not applicable to the transition time.

In this four-level scheme, if immediate correlation is possible on a scan by scan basis and these scans are exported instantly, ULTRA-RAPID PRODUCTS will be produced from the accumulated observations. This will be a task for analysis centers with dedicated processing

facilities that can be devoted to this task. Only one IVS Analysis Center can be the official IVS Real-time AC, but there should be at least one backup and control AC.

The RAPID PRODUCTS will use data of observing periods of predefined lengths. Assuming correlation in batches of three hours, these new data can be added incrementally to the preceding set and analyzed accordingly. If the correlation of these sessions only commences at the end of the 24-hour periods, the observables will not be available until a certain time after these sessions.

In order to minimize latency, the rapid products will be produced by a completely automated process at multiple analysis centers at the time of data availability. These centers may use different software packages and analysis philosophies. At that time, auxiliary files, like log files or those for the Vienna Mapping Function, may often not be available and model values will have to be used. Ideally, the output of the individual analysis centers will be combined at the level of results by the IVS Combination Center in order to ensure quality and to safeguard against mistakes. Outliers will be rejected outright with no further consideration. For this, state-of-the-art statistical techniques for outlier detection will have to be applied.

The processing line for the INTERMEDIATE PRODUCTS will permit the use of some level of intervention and the application of additional information, such as the Vienna Mapping Function and meteorological data from sources other than those provided routinely. The combination may also be carried out in a more sophisticated way, e.g., on the basis of normal equation systems or permitting re-weighting by variance component estimation. It is expected that these products will be more accurate.

The FINAL PRODUCTS for a single week should be available on the Wednesday of the subsequent week. Two days will be allocated for the analysis centers, while the remaining day will be at the discretion of the IVS Combination Center.

In terms of reading the delivery and update times in the table an example for the intermediate products with continuous correlation would be as follows: every day at 1200 UT (update epoch) the IVS will deliver updated results for the epochs 3, 6, 9, 12, 15, 18, 21, and 24 UT of the preceding day with the last data point (24 UT) having a latency of 12 hours.

Independent of latency requirements, the analysis of VGOS data will put severe demands on the capabil-

Table 1 Products, update rates, latencies, and accuracies.

Product	Product epoch	Update epoch	Epochs to be updated	Latency of last data point	Sub-product	Expected accuracy (WRMS)
Ultra-rapid	Every 30'	Every 30'	t–30'...180'	30 min.	UT1–UTC	7 μs
Rapid with continuous near-realtime correlation	Every 3 h at 3, 6, ... 24 h	Every 3 h at 0, 3, 6, ... 21 h UT	t–3...24 h	3 hrs	UT1–UTC	5 μs
					Polar motion	75 μas
					Nutation offsets	75 μas
Rapid with batch correlation of 3 or 24 h blocks	Every 3 h at 3, 6, ... 24 h	Once every correlation data release	t–3...24 h	3–6 days	UT1–UTC	5 μs
					Polar motion	75 μas
					Nutation offsets	75 μas
Intermediate with continuous near-realtime correlation	Every 3 h at 3, 6, ... 24 h	Every 24 h at 12 h UT	t–12...33 h	12 hrs	UT1–UTC	3 μs
					Polar motion	45 μas
					Nutation offsets	45 μas
Intermediate with batch correlation of 3 or 24 h blocks	Every 3 h at 3, 6, ... 24 h	Every 24 h at 12 h UT	t–12...33 h	3–6 days	UT1–UTC	3 μs
					Polar motion	45 μas
					Nutation offsets	45 μas
Final	Every 3 h at 3, 6, ... 24 h	Every 7 d on day 3 at 12 h UT	t–3d...t–10d	7 days	UT1–UTC	1 μs
					Polar motion	15 μas
					Nutation offsets	15 μas
					Telescope coordinates	3 mm
					Source positions	15 μas

ities of the analysis software packages. According to the VGOS Observing Plan (Petrachenko et al., 2013) both the number of stations and the number of observations per baseline will increase considerably compared to the current legacy X/S observing. For a 24-station network and two observations per baseline per minute the total number of delay observations may be close to 800,000. Assuming the current analysis method of least squares adjustments in a Gauss-Markov model with 20-minute atmosphere and clock parameterization, the number of parameters will be close to 4,000. Analyzing this amount of data is not difficult for modern computers, but it will result in some increase in processing time if computing capability or processing algorithms are not improved.

On the other hand, there are other adjustment methods, such as filter techniques, which process the observations sequentially. However, for combination purposes of intermediate results of multiple analysis centers, adjustments with normal equation systems are still the primary choice because these can be produced void of any datum.

In any case, the vast number of observations will preclude manual interaction with the data for editing such as outlier elimination or specification of clock jump location. Currently, analyzing a standard 24-hour session with 10,000 observations takes on the order of 15 minutes if there are no problems. Clearly it would be impractical to analyze a session with 800,000 observations in the same way. This leads to the conclu-

sion that significant effort must be expended to automate this process.

4 Institutional Relations

The existing links of the IVS to institutions and organizations document the strong relationships of the IVS to many activities in various fields. Some of them are very close due to mutual dependencies, others are weak, and some are non-existent even though there seems to be an obvious need for close cooperation. The more formal the links are between the IVS and institutions, associations, and other services, the better it is for its general recognition. The IVS should cooperate with the GGOS project of the IAG and with the UN-GGIM initiative (Global Geospatial Information Management) with its push towards a Global Geodetic Reference Frame (GGRF). These activities will definitely have great benefit for the IVS. Lastly, it should be a declared goal of the IVS and its associates to establish and strengthen further contacts to institutions making direct or indirect use of IVS products to sensitize them to what the IVS has provided. For this reason, active steps to establish contacts and cooperative endeavors with more external institutions using IVS products should be taken by many more IVS associates than is currently the case.

5 Visibility, Public Relations, and Outreach

In the end, it needs to be stressed that public, scientific, and institutional visibility is a fundamental requirement for all components of the IVS. This not only helps to safeguard current funding levels of IVS components but often affects decisions on the pure continuation of operations or investments in new hardware and personnel. These issues begin with observatories running radio telescopes, but also affect coordinating and operations centers, and have a severe effect on correlators. In particular, radio telescopes and correlators are integral parts of VLBI, while coordinating and operations centers provide the organizational structure of the IVS, just to name a few IVS components. All of them need and deserve an appropriate level of visibility. No

institution will maintain or build observing or correlator capabilities and finance personnel and infrastructure for operational aspects if they do not benefit from the success of the observations and the results.

At present, almost all publications of IVS results in the scientific literature are authored by colleagues in the IVS Analysis Centers. We are of course glad that our data are used extensively for scientific achievements, but all parts of the IVS that are doing the basic work, which is not less demanding scientifically, are left unrecognized.

A first step to correct this is the introduction of Digital Object Identifiers (DOI numbers) for the data sets of the IVS, which should be used extensively in all publications using IVS data. However, even more important is recognition in scientific publications. While such references in publications by non-IVS scientists might have the highest value, this practice should begin with those IVS colleagues using IVS data for their publications.

Finally, outreach and public relations should be addressed as well. Although mentioned in previous sections concerning institutional relations, the general public should also be offered paths to information, in particular on the IVS Web sites and in dedicated brochures. Beyond regular IVS schools on VLBI, this may also help to attract young people to the field of geodetic and astrometric VLBI.

References

1. Bradley B, Sibois A, Axelrad P (2015): Influence of ITRS/GCRS Implementation for Astrodynamics: Coordinate Transformations, *Advances in Space Research*, doi: <http://dx.doi.org/10.1016/j.asr.2015.11.006>.
2. Petrachenko B, Niell A, Behrend D, Corey B, Bhm J, Charlot P, Collioud A, Gipson J, Haas R, Hobiger T, Koyama Y, MacMillan D, Nilsson T, Pany A, Tuccari G, Whitney A, Wresnik J (2009): Design Aspects of the VLBI2010 System. Progress Report of the VLBI2010 Committee. NASA Technical Memorandum, NASA/TM-2009-214180, 58 pp.
3. Petrachenko B (2013a): VLBI2010 Feed Comparison. Internal Report, VLBI2010 Project Executive Group (V2PEG), IVS Annual Report 2012, NASA/TP-2013-217511, Greenbelt (MD), pp. 48–51.
4. Petrachenko B (2013b): VLBI2010 Receiver Back End Comparison. Internal Report, VLBI2010 Project Executive Group (V2PEG), IVS Annual Report 2012, NASA/TP-2013-217511, Greenbelt (MD), pp. 39–47.

5. Petrachenko B, Behrend D, Hase H, Ma C, Niell A, Nothnagel A, Zhang X (2013): VGOS Observing Plan. Internal Report, VGOS Project Executive Group (VPEG), IVS Annual Report 2013, NASA/TP-2014-217522, Greenbelt (MD), pp. 70–79.
6. Schuh H, Charlot P, Hase H, Himwich E, Kingham K, Klatt C, Ma C, Malkin Z, Niell A, Nothnagel A, Schlüter W, Takashima K, Vandenberg N (2002): “IVS Working Group 2 for Product Specification and Observing Programs, Final Report”, IVS Document http://ivsc.gsfc.nasa.gov/about/wg/wg2/IVS_WG2_report_130202-letter.pdf.
7. Thaller D and the GGOS Working Group PLATO Team (2015): The GGOS Working Group on Performance Simulations and Architectural Trade-Offs (PLATO); Geophysical Research Abstracts Vol. 17, EGU2015-6281-1, EGU General Assembly 2015.

Session I: Advances in VGOS Stations and Technology



March 2016 · Johannesburg · South Africa

Current Trends and Challenges in Satellite Laser Ranging

Graham M. Appleby¹, Giuseppe Bianco², Carey E. Noll³, Erricos C. Pavlis⁴, Michael R. Pearlman⁵

Abstract Satellite Laser Ranging (SLR) is used to measure accurately the distance from ground stations to retro-reflectors on satellites and on the Moon. SLR is one of the fundamental space-geodetic techniques that define the International Terrestrial Reference Frame (ITRF), which is the basis upon which many aspects of global change over space, time, and evolving technology are measured; with VLBI the two techniques define the scale of the ITRF; alone the SLR technique defines its origin (geocenter). The importance of the reference frame has recently been recognized at the inter-governmental level through the United Nations, which adopted in February 2015 the Resolution Global Geodetic Reference Frame for Sustainable Development. Laser Ranging provides precision orbit determination and instrument calibration and validation for satellite-borne altimeters for the better understanding of sea level change, ocean dynamics, ice mass-balance, and terrestrial topography. It is also a tool to study the dynamics of the Moon and fundamental constants and theories. With the exception of the currently in-orbit GPS constellation, all GNSS satellites now carry retro-reflectors for improved orbit determination, harmonization of reference frames, and in-orbit collocation and system performance validation; the next generation of GPS satellites due for launch from 2019 onwards will also carry retro-reflectors. The ILRS delivers weekly realizations that are accumulated sequen-

tially to extend the ITRF and the Earth Orientation Parameter series with a daily resolution. SLR technology continues to evolve towards the next-generation laser ranging systems and it is expected to successfully meet the challenges of the GGOS2020 program for a future Global Space Geodetic Network. Ranging precision is improving as higher repetition rate, narrower pulse lasers, and faster detectors are implemented within the network. Automation and pass interleaving at some stations is expanding temporal coverage and greatly enhancing efficiency. Discussions are ongoing with some missions that will allow the SLR network stations to provide crucial, but energy-safe, range measurements to optically vulnerable satellites. New retro-reflector designs are improving the signal link and enable daylight ranging that is now the norm for many stations. We discuss many of these laser ranging activities and some of the tough challenges that the SLR network currently faces.

Keywords Satellite Laser Ranging, ILRS, Terrestrial Reference Frame, Earth observation

1 Introduction

In this paper, we review the technique of Satellite Laser Ranging (SLR), which is coordinated by the International Laser Ranging Service (ILRS) (Pearlman et al., 2002). We discuss emerging new technology, the ongoing expanding constellations of satellites that require the high-quality tracking that is afforded by laser ranging, and a number of new or proposed new sites that are under development, often in conjunction with

1. NERC Space Geodesy Facility, Herstmonceux, UK

2. Centro di Geodesia Spaziale G. Colombo, Agenzia Spaziale Italiana, Matera, Italy

3. NASA Goddard Space Flight Center, Greenbelt MD, United States

4. University of Maryland, Baltimore MD, United States

5. Harvard-Smithsonian Center for Astrophysics, Cambridge MA, United States

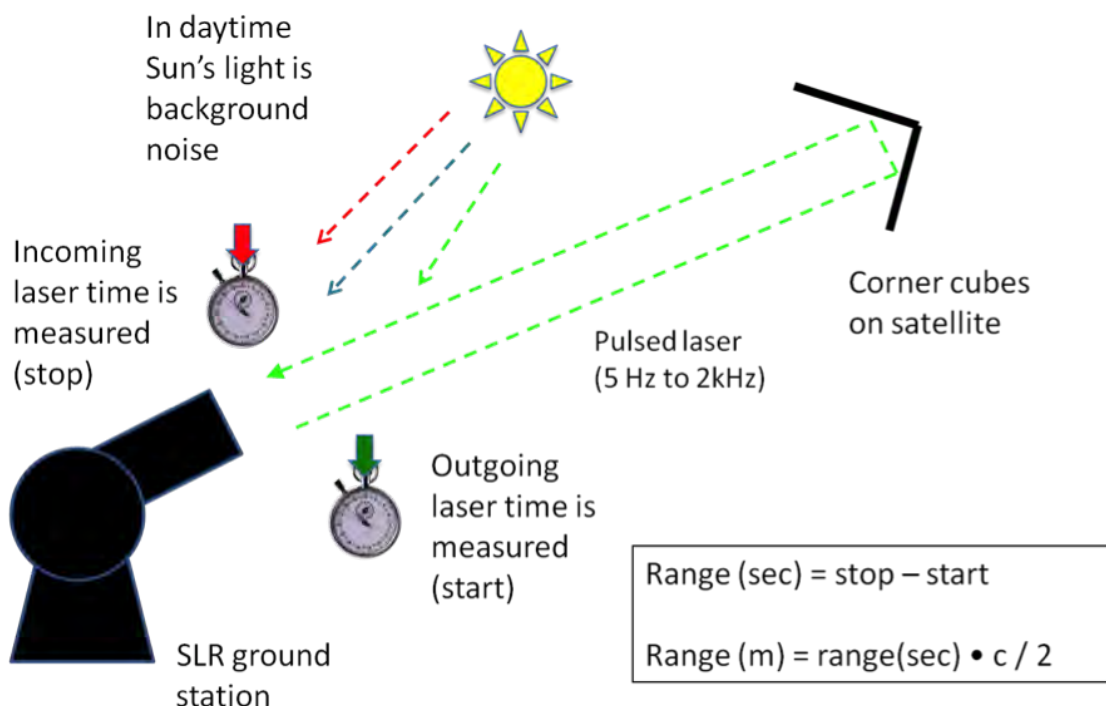


Fig. 1 The technique of satellite laser ranging.

VLBI, GNSS, and DORIS. The ILRS community is also addressing and embracing novel applications for its technique, including satellite attitude determination and debris tracking. The ILRS continues to have a major role within the emerging Global Geodetic Observing System (GGOS) (Plag and Pearlman, 2009), both in support of precise orbit determination for applications satellites and in its crucial role in defining the origin and scale of the terrestrial reference frame. For this work, high-quality, multi-technique sites are essential: the space-observational services—the IDS, IGS, ILRS, and IVS—together supply the data and products to meet the GGOS Mission, which includes as a major challenge the determination of the reference frame with a precision of 1 mm and a stability of 0.1 mm yr^{-1} , which must be realized via inter-technique site ties and combination of analysis products (site position, velocity, Earth orientation). We conclude with a discussion of some recent work carried out at the SGF ILRS Analysis Center on the detection of systematic effects in laser ranging observations and analyses and their impact on ITRF scale.

2 The Technique of Satellite Laser Ranging

Satellite Laser Ranging, shown schematically in Figure 1, directly measures the range between a ground station and a satellite using very short laser pulses, corrected for refraction, satellite center of mass, and the internal delay of the ranging machine.

The state-of-the-art is millimeter precision for averaged measurements (normal points) with centimeter-level accuracies. The most able stations can track satellites at distances from 300 km to more than 22,000 km by day and at night. Each station tracks independently, but overall satellite priorities are set by the ILRS and can be used to encourage the stations to concentrate on new launches, for example. A network of stations can also in principle work together via real-time status exchange to optimize tracking. The key to the technique's success is that it requires only a passive retro-reflector of sufficient optical cross section to be placed on the satellite. The observations, both normal points and full-rate, are made available to the worldwide community in near real-time through the NASA-supported

Crustal Dynamics Data Information System (CDDIS <http://cddis.nasa.gov>) and the European Data Centre (EDC <http://edc.dgfi.tum.de>).

3 SLR Science and Applications

The precise laser range measurements to retro-reflector-carrying satellites lead, in some cases in conjunction with other tracking techniques such as GNSS and DORIS, to precise orbit determination for those satellites and also to a time history of station positions and motions. Arguably the most important product of satellite laser ranging is its critical contribution to the realization of the Terrestrial Reference Frame, upon which a huge number of research projects and societal enterprises depend, from monitoring global sea-level changes, GIA, ice sheet mass-balance, to satellite navigation and surveying for example. The SLR contribution to a series of realizations, including the most recent ITRF2014 (Altamimi et al., 2016), is in the determination of the origin of the frame at the mass center of the Earth system and, together with VLBI, its scale. The primary satellites used for reference frame determination are the two LAGEOS satellites, orbiting at nearly 6,000 km above the Earth; LAGEOS is shown in Figure 2. Future plans to improve the precision and accuracy of the ITRF include the use of range measurements to the ASI LAsER Relativity Satellite (LARES), launched by ESA in 2012 into a circular orbit 1400 km above the Earth.



Fig. 2 The LAGEOS geodetic satellite (courtesy of NASA).

Since the 1970s the laser ranging network has supported more than 150 space missions, including the

earliest altimeter missions Geos-3 and Seasat. Several missions have been ‘rescued’ by laser ranging when other tracking systems have failed; for instance, on the ESA mission ERS-1, the experimental PRARE tracking system failed soon after launch in 1991, and SLR provided the only tracking data for precise orbit determination (POD) and for calibration/validation of the altimeter data. With multi-technique tracking of altimeter missions such as the JASON series, a critical role for laser ranging is independent validation of orbital accuracy and resolution of phase center offsets for on-board GNSS antennae. This role for SLR, which also involves its use in routine POD, will continue into the future; the most recent addition to the ESA Copernicus Programme is the Sentinel-3 two-satellite series, with Sentinel-3A launched in April 2016. These satellites carry radar altimeters, two GPS receivers, a DORIS system, and a laser retro-array, measurements from all of which will be used by such agencies as CNES for POD (Fernández et al., 2015).

4 Recent Tracking Station Initiatives

There has been a recent expansion of the Russian SLR network, for instance, the new system in Brazil and one expected at Hartebeesthoek, primarily to support GLONASS tracking for improved orbital accuracy and for time transfer and to join international efforts to improve the reference frame as per the GGOS initiative. The NASA Space Geodesy Project has ambitious plans to upgrade existing facilities and deploy new instrumentation to create new GGOS core sites, for example at McDonald, Texas and on Hawaii, and other agencies are getting involved in these global efforts to realize the GGOS concepts. These agencies include the Norwegian Mapping Agency with a planned multi-technique site at Ny Ålesund to deploy a NASA SLR system in a few years’ time and the South Korean Astronomy and Space Science Institute that is developing a site at Sejong to include an existing modern kHz-class SLR system. The existing and projected ILRS network of stations is shown in Figure 3.

A growing number of ILRS stations now operate at kHz laser repetition rates. The advantages of operating at these rates compared to the legacy systems that work at rates of 5–10 Hz include much more rapid acquisition of the target, enabling pass-interleaving and thus



Fig. 3 Projected ILRS Network (ILRS CB).

increased coverage, and the ability to reach sub-mm normal-point precision very quickly. The kHz lasers also tend to have very short pulse lengths and low energy per pulse (at 1-mJ level), so an added benefit is high-resolution interrogation of the distribution of corner cubes within the array. An example of this impressive capability is shown in Figure 4, where tracks from individual corner-cubes are clearly visible. The

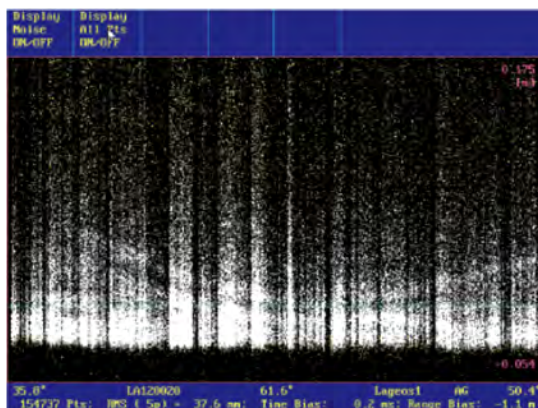


Fig. 4 kHz ranging to LAGEOS from Graz (courtesy G. Kirchner).

availability of this high-resolution, high repetition-rate

range data has led to new work to monitor the time-variation of the spin vectors of many of the geodetic satellites. For instance, recent work by Kucharski and others (Kucharski et al., 2014a) has resulted in a ten-year time series of the direction in inertial space of the spin axes of the two Etalon satellites; the series shows that both axes behave in the same manner, with the direction in declination being very stable and constant throughout. This sort of information has great potential for accurate models of non-gravitational forces on these important classes of geodetic satellites.

5 Space Debris

A growing concern is the lack of accurate orbital information for the huge number of inactive pieces of space junk in orbit around the Earth. Debris includes rocket bodies, heat shields, and other parts of satellites, as well as formerly active satellites. Several, mainly European, stations have carried out some ranging experiments, both to once-active satellites fitted with retroreflectors as well as to non-cooperative, inert satellites. A good example of the results that can be achieved by such monitoring of currently-inactive satellites is that

published by Kucharski et al. (Kucharski et al., 2014b) from laser range observations of the Envisat satellite that suddenly failed on 8 April 2012. On that date, all communication was lost, a few weeks after the satellite had achieved ten productive years in orbit. Laser ranging was resumed in 2013, and Kucharski's analysis showed that Envisat is rotating in a counter-clockwise direction with an inertial period in September 2013 of 135 s. Many stations continue to track Envisat, as well as TOPEX/Poseidon, in order to advance these attitude studies. A recent O-C range plot obtained at the Herstmonceux SLR station from a pass of TOPEX/Poseidon is shown in Figure 5; a clear, steady rotational signature is seen in the track of laser returns.

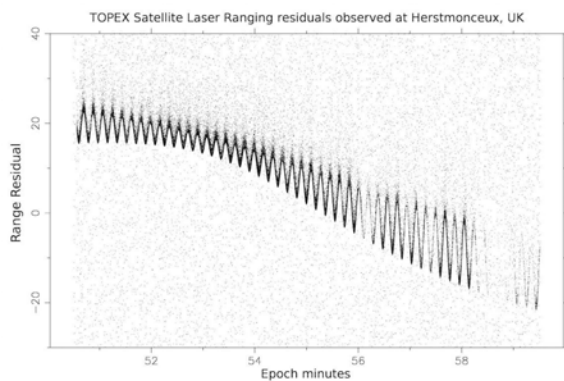


Fig. 5 kHz ranging to defunct satellite TOPEX/Poseidon from Herstmonceux.

6 Increasing Numbers of Satellites

Particularly demanding are the expanding constellations of GNSS satellites, all of which are fitted with laser retro-reflectors: GLONASS (Russia), Galileo (Europe), Beidou (Compass: China), IRNSS (India), and QZSS (Japan). An example of what this demand means for the stations is shown in Figure 6 covering a two-day period, where each point represents a laser range normal point obtained at Herstmonceux from a satellite at the given height above the Earth. Many range measurements are obtained from the GNSS satellites, at heights of approximately 20,000 km, as well as one at geosynchronous distance (IRNSS). The GNSS mission operators request from the ILRS as

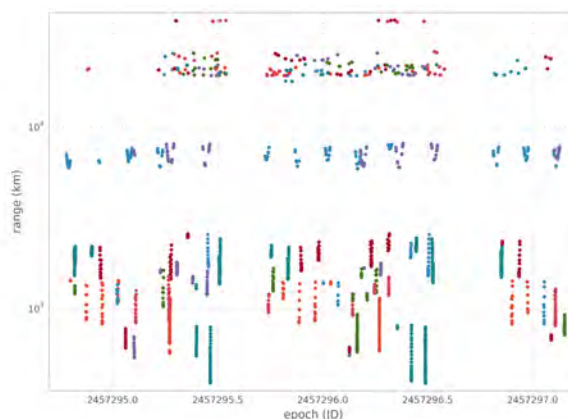


Fig. 6 Example of laser range normal points obtained at Herstmonceux as a function of satellite altitude.

much laser tracking as possible, in order to support investigations into co-location of techniques in space, to strengthen precise clock and orbit determination, and to strengthen links between reference frames. The research community is taking advantage of the greater numbers of laser range measurements to the GNSS satellites to investigate many of these issues; for example, see Soñnica et al. (2015). To test each station's capabilities in tracking GNSS, the ILRS Central Bureau has run a series of three campaigns. Most of the strongest stations took part, as shown in the global map of Figure 7. The stations were asked to track at high priority just six of the possible 24 GLONASS satellites, Compass-M3, and four of the Galileo constellation. The results were that reasonably high data yields can be expected when sky conditions are very good, but that there is a strong need for more data in daylight. Daytime ranging to these high satellites is very challenging for most stations. This point is demonstrated clearly in Figure 8, which gives total numbers of GNSS normal points obtained by the Network during the third campaign (August to October 2015) binned according to local time. It is clear that the numbers of daytime observations are about one third of those during nighttime. Also shown for comparison is an equivalent non-campaign period during 2014, where the total yield is lower by one third and the daytime tracking is disproportionately even lower.

One concern expressed when the ILRS was asked for increasing priority to be given to tracking GNSS was that tracking of the primary geodetic LAGEOS

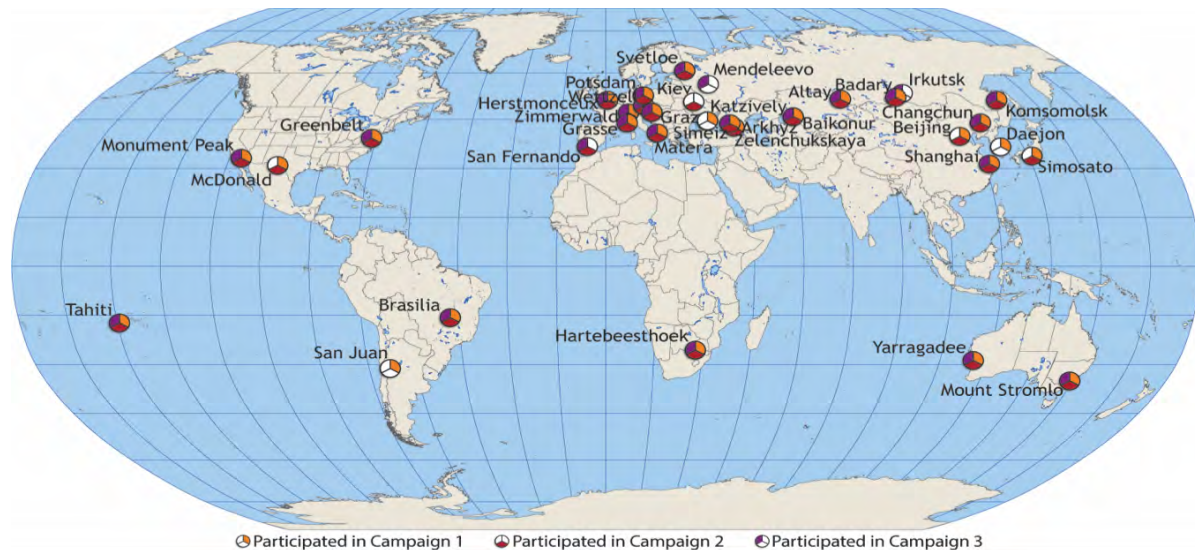


Fig. 7 ILRS stations that contributed to the three GNSS tracking campaigns of 2015.

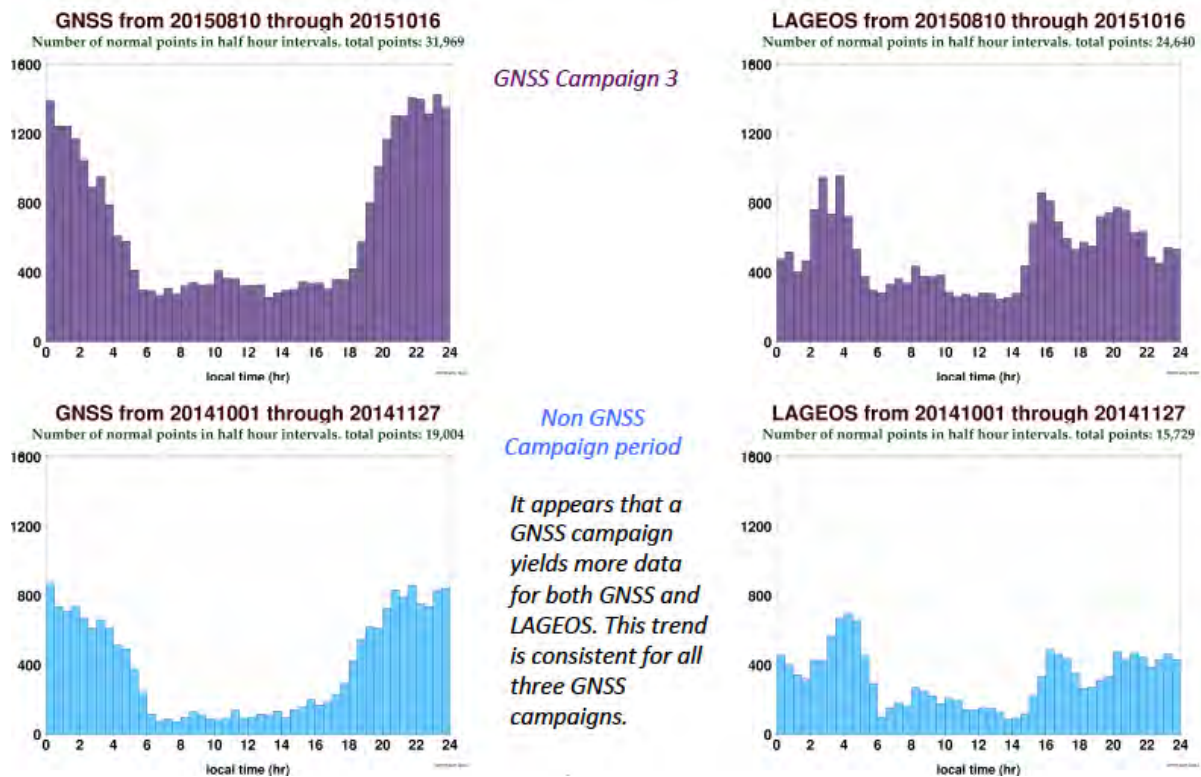


Fig. 8 ILRS Network yield from GNSS tracking: both during and outside Campaign number 3.

satellites would suffer. Interestingly, however, the reverse effect has proven to be true, as also illustrated in Figure 8: during the third GNSS campaign, increased numbers of normal points were obtained on the two

LAGEOS satellites, both by day and night. This very encouraging trend is consistent for all three GNSS campaigns.

7 Terrestrial Reference Frame

Of course, the primary application of SLR is in the realization of the International Terrestrial Reference Frame (ITRF), e.g., ITRF2014 (Altamimi et al., 2016). The need for a consistent global reference frame to support a huge number of societal needs from global sea-level monitoring and disaster management to bridge-building was recognized at the UN level in 2015: the Resolution A Global Geodetic Reference Frame for Sustainable Development, (GGRF) (United Nations General Assembly, 2015) was passed by 52 Member States. The geodetic Services' contributions to the realization of the ITRF are:

- **SLR:** Uniquely provides Earth center of mass, the origin of the ITRF;
- **VLBI:** Provides EOP parameters and the connection with the Celestial Reference Frame;
- **SLR and VLBI:** Independently provide Scale;
- **GNSS:** Global coverage and density;
- **DORIS:** Global coverage.

Figure 9 shows the numbers of passes of the two LAGEOS satellites tracked by the ILRS stations during the past year. The high-performing stations include Zimmerwald, Changchun, Monument Peak, Har-tebeesthoek, and, of course, the most prolific station in the Network, Yarragadee, Western Australia.

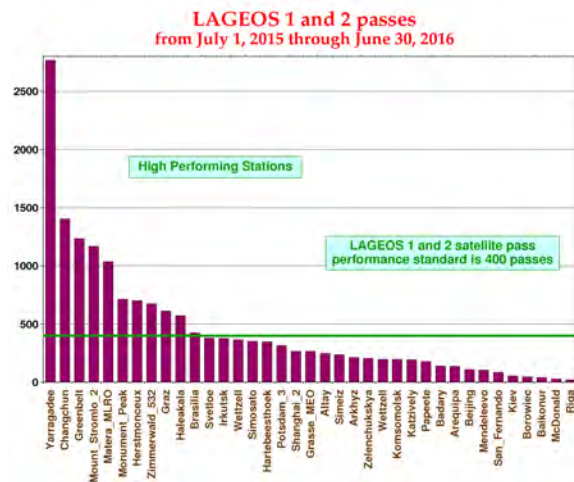


Fig. 9 Tracking of the LAGEOS satellites during the past year (ILRS CB).

7.1 ITRF Scale

Of particular interest in recent realizations of the terrestrial reference frame, ITRF2008 (Altamimi et al., 2011) and ITRF2014 (Altamimi et al., 2016), is the persistent systematic difference in scale as determined from the two techniques of SLR and VLBI, which alone are capable of high-precision scale determination. The difference in scale for ITRF2014 is 1.37 ± 0.01 ppb (Altamimi et al., 2016), more than 8 mm at the equator, and in the sense that the scale determined by the SLR technique is smaller than that from VLBI. This persistent difference in scales is intriguing and points to systematic problems in either or both techniques as well as to potential site-tie problems. To ascertain the extent to which possible systematic effects in laser ranging to the LAGEOS satellites may be responsible for at least some of the scale discrepancy with the VLBI result, the UK ILRS Analysis Center at the Space Geodesy Facility, Herstmonceux (SGF AC) carried out an investigation using fifteen years of LAGEOS and LAGEOS-2 observations. The standard ILRS reference-frame determination procedure, as agreed by the ILRS Analysis Standing Committee (Pavlis and Luceri, 2013), is to treat a number of ranging stations as error-free in the weekly orbital solutions, along with other stations for which a systematic range error (range bias, RB) may be solved for simultaneously with station geocentric coordinates and Earth orientation parameters. This was the procedure used in the production of the ILRS contribution to the realization of ITRF2008 and ITRF2014. The thesis of the SGF AC work is that, if indeed some systematic range error is present in any of the stations that are assumed error-free, then that systematic error will have been absorbed during the least-squares estimation process primarily in station height and thus enter in corrupted form the ITRF. On-going daily and weekly quality checks regularly carried out at several ILRS Analysis Centers (<http://ilrs.gsfc.nasa.gov/science/analysisCenters/>) that use coordinates taken from, for example, ITRF2008, will thus not detect the hidden range error. Causes of small systematic range errors may be non-linearity in the time-of-flight counters (Appleby et al., 2008), error in the survey distance of the calibration board, and inappropriate center-of-mass corrections applied to the range measurements to refer them to the centers of

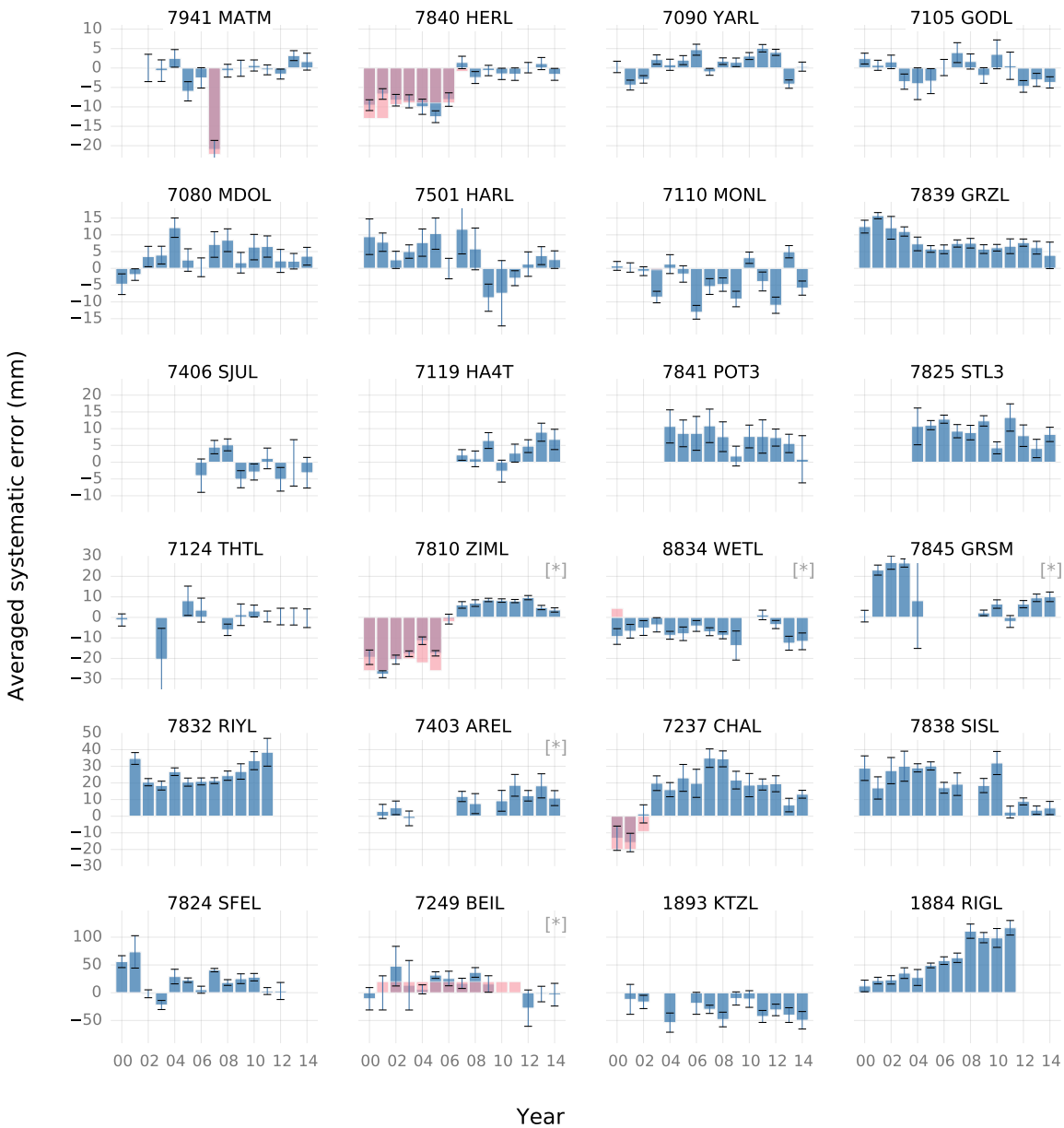


Fig. 10 Yearly-averaged station range bias determined simultaneously with reference frame in weekly solutions: shaded values correspond to previously-known systematics.

the LAGEOS satellites (Otsubo and Appleby, 2003). The SGF AC approach was, for the period 2000 to 2014, to compute weekly solutions for LAGEOS and LAGEOS-2 state vectors, station coordinates, daily Earth orientation parameters, and a single range bias value for each of the contributing stations, using SGF's in-house SATAN analysis package. No *a priori* range bias values were applied to any of the observations.

The solutions for stations' range bias, averaged yearly from the weekly solutions, are shown in Figure 10. It is clear that most stations have some level of systematic bias, with some being consistent throughout the time period. There is evidence at some stations of dramatic improvement, such as the change from large (12 mm) negative bias at Herstmonceux to very small values from 2007 onwards. This problem was caused by

the difficulty in application of known non-linearity in time-of-flight counters in use at the station until replacement by a high-accuracy event timer in February 2007 (Appleby et al., 2008). A similar dramatic improvement is evident at Hartebeesthoek from 2011 onwards. An example of a consistent range bias is that at Graz, where a positive bias of at least 5 mm is present throughout despite an upgrade to kHz ranging in 2002. The final step in this analysis is to carry out 7-parameter Helmert solutions (three translations, three rotations, and one scale difference) between the all-station weekly RB solutions and standard ILRS solutions where RB is solved only for a subset of the stations; to re-iterate, this latter scheme was used by all ACs for the ILRS contribution to ITRF2014. From the time series of scale differences, the final solution for mean scale is found to be $+0.7 \pm 0.1$ ppb, approximately half the difference in scale between the SLR and VLBI solutions in ITRF2014 (Altamimi et al., 2016). A full account of this work is given in a recent publication (Appleby et al., 2016).

8 Conclusions

The ILRS Satellite Laser Ranging technique is in a situation of continuing growth and improvement. New applications are emerging, and the list of new missions that require laser support for precise orbit determination is ever increasing. New stations are being built, and it is particularly encouraging to see new and planned sites at geographically important locations, such as at high latitudes. Care must continue to be taken that the primary geodetic application of SLR, that of realization of the origin and scale of the ITRF, be addressed at the highest level of accuracy and by prolific observations of the LAGEOS satellites by the core ILRS SLR stations, including the long-running excellent system nearby at Hartebeesthoek.

Acknowledgements

The lead author is very grateful to the Program Committee for the invitation and support to attend and take part in the 9th IVS General Meeting.

References

- Altamimi, Z., X. Collilieux, and L. Métivier. 2011. ITRF2008: an improved solution of the International Terrestrial Reference Frame. *Journal of Geodesy* 85 (8): 457–473.
- Altamimi, Z., P. Rebischung, L. Métivier, and X. Collilieux. 2016. ITRF2014: A new release of the International Terrestrial Reference Frame modeling non-linear station motions. *Journal of Geophysical Research*. doi:10.1002/2016JB013098.
- Appleby, G., M. Wilkinson, V. Luceri, P. Gibbs, and V. Smith. 2008. Attempts to separate apparent observational range bias from true geodetic signals. In *Proceedings of the 16th International Workshop on Laser Ranging*. Poznan, Poland.
- Appleby, G. M., J. Rodríguez, and Z. Altamimi. 2016. Assessment of the accuracy of global geodetic satellite laser ranging observations and estimated impact on ITRF scale: estimation of systematic errors in large observations 1993–2014. *Journal of Geodesy*. doi:DOI 10.1007/s00190-016-0929-2.
- Fernández, J., F. Ayuga, P. Féménias, and H. Peter. 2015. The COPERNICUS SENTINEL-3 mission. In *Proceedings of the 2015 ILRS Technical Workshop*. Matera, Italy.
- Kucharski, D., et al. 2014a. Attitude and spin period of space debris envisat measured by satellite laser ranging. *IEEE Transactions on Geoscience and Remote Sensing* 54(11). doi:10.1109/TGRS.2014.2316138.
- Kucharski, D., G. Kirchner, L. Hyung-Chul, and F. Koidl. 2014b. Spin parameters of high earth orbiting satellites etalon-1 and etalon-2 determined from khz satellite laser ranging data. *Advances in Space Research* 54(11): 2309–2317.
- Otsubo, T., and G. M. Appleby. 2003. System-dependent center-of-mass correction for spherical geodetic satellites. *Journal of Geophysical Research: Solid Earth* 108 (B4).
- Pavlis, E. C., and V. Luceri. 2013. Analysis report. In *International Laser Ranging Service 2009–2010 Report*, eds. C. Noll and M. Pearlman, 6–164. NASA/TP 2013-217507.
- Pearlman, M. R., J. J. Degnan, and J. M. Bosworth. 2002. The International Laser Ranging Service. *Advances in Space Research* 30 (2): 135–143.
- Plag, H-P., and M. Pearlman, eds. 2009. *Global Geodetic Observing System: Meeting the Requirements of*

- a Global Society on a Changing Planet in 2020*. Springer.
- Sośnica, K., D. Thaller, R. Dach, P. Steigenberger, G. Beutler, D. Arnold, and A. Jäggi. 2015. Satellite laser ranging to GPS and GLONASS. *Journal of Geodesy* 89: 725–743.
- United Nations General Assembly. 2015. UN Resolution on Global Geodetic Reference Frame for Sustainable Development. <http://un-ggim-europe.org>.

An Overview of the Japanese GALA-V Wideband VLBI System

Mamoru Sekido¹, Kazuhiro Takefuji¹, Hideki Ujihara¹, Tetsuro Kondo¹, Masanori Tsutsumi¹, Yuka Miyauchi¹, Eiji Kawai¹, Hiroshi Takiguchi¹, Shingo Hasegawa¹, Ryuichi Ichikawa¹, Yasuhiro Koyama¹, Yuko Hanado¹, Ken-ichi Watabe², Tomonari Suzuyama², Jun-ichi Komuro¹, Kenjiro Terada¹, Kunitaka Namba¹, Rumi Takahashi¹, Yoshihiro Okamoto¹, Tetsuro Aoki¹, Takatoshi Ikeda¹

Abstract NICT is developing a new broadband VLBI system, named GALA-V, with the aim of performing frequency comparisons between atomic time standards over intercontinental baselines. The development of the broadband GALA-V system is coordinated to be as compatible as possible with the VGOS system. Two types of original broadband feed systems were developed for the Kashima 34-m antenna of modified Cassegrain optics. The first prototype feed, called IGUANA-H, works in the 6.5–16 GHz frequency range, while the second feed, NINJA, works in the 3.2–14 GHz range. The GALA-V observation system is designed to capture four bands of 1024 MHz width in the 3–14 GHz range. Two types of data acquisition modes are available. One is a narrow channel mode, which acquires multiple channels with 32-MHz bandwidth. This mode is compatible with the NASA Proof-of-Concept (PoC) system developed by MIT Haystack Observatory. The other is a broad channel acquisition mode, in which a signal of 1024 MHz width is digitized as a single channel. A radio frequency (RF) direct sampling technique was used in this mode as a new approach for broadband observation taking advantage of the high-speed sampler K6/GALAS and its digital filtering function. This technique has several advantages in the precise delay measurement of the broadband bandwidth synthesis. VLBI experiments were conducted between the Kashima 34-m antenna and the Ishioka 13-m VGOS station of GSI, Japan. The first broadband observation over 8-GHz bandwidth was successful on this baseline in early 2015. The

results of the broadband bandwidth synthesis over 8-GHz bandwidth proved sub-pico-second resolution group delay measurement with one second of integration time. Time series of the group delay data showed several picoseconds of fluctuation over a few hundred seconds of time. The Allan standard deviation is consistent with the frozen flow model of Kolmogorov tropospheric turbulence.

Keywords GALA-V, broadband VLBI

1 Introduction

The time interval of the SI second as time scale is defined by counting the microwave emission from Cs atom at 9,192,631,770 Hz. Recent technological progress in quantum physics and optics allows to realize more accurate frequency standards by using optical emission of atoms [1]. A re-definition of the time scale has been discussed as a subject in metrology [2]. NICT is charged as a national institute with keeping Japan Standard Time and is engaged in research and development of optical frequency standards. A confirmation of the identity of the frequency generated by independent optical atomic standards is an important subject for a re-definition of the SI second.

Currently two-way satellite time and frequency transfer (TWSTFT) and observation of GNSS satellites are operationally used for distant frequency transfer. Advanced TWSTFT technology with carrier-phase [3] might provide enough precision over inter-continental distances, but it depends on the availability of satellite transponders. VLBI has the potential to enable distant

1. National Institute of Information and Communications Technology

2. National Institute of Advanced Industrial Science and Technology, National Metrology Institute of Japan

frequency transfer, which has been investigated in several studies [4]–[9]. One of the advantages of VLBI is that it is independent of the availability of satellites. The development of a more precise VLBI observation technology is in progress, and it is expected to advance the VLBI application in geodesy and metrology.

The IVS is promoting the deployment of VGOS as the new generation geodetic VLBI system. The VGOS system is characterized by a high temporal resolution of the observations by using fast slewing antennas and a broad radio frequency bandwidth. The fast source switching is necessary for VGOS to improve on the correct atmospheric delay modeling and its temporal resolution. The VLBI group at NICT is developing a broadband VLBI system named GALA-V in order to apply the VLBI technique to distant frequency transfer. The GALA-V system is basically designed to use a compatible radio observation frequency range as well as data acquisition system with the VGOS. The concept of the GALA-V system and the development of an original feed and data acquisition system are described in Section 2. Domestic broadband VLBI experiments between Kashima 34-m and the Ishioka 13-m VGOS station were conducted in 2015. The observation conditions and the derived broadband delay are discussed in Section 3. Finally, in Section 4 we summarize the overall progress.

2 Broadband VLBI System: GALA-V

2.1 Distant Clock Comparison with Small Antennas

A frequency comparison with VLBI is made by clock parameter estimation just as with geodesy. The standard signal from the atomic frequency standard is used as reference for the VLBI observations at each station; thus, the VLBI delay observable on that baseline contains the difference between those atomic clocks. To utilize VLBI for atomic frequency transfer, the VLBI stations need to be located near the atomic frequency standard, except for the case that the reference signal comes from a remote atomic clock via a stable fiber link (e.g., [10]). Thus our GALA-V system uses transportable small VLBI stations as the terminal of the comparison. Figure 1 shows the concept of the

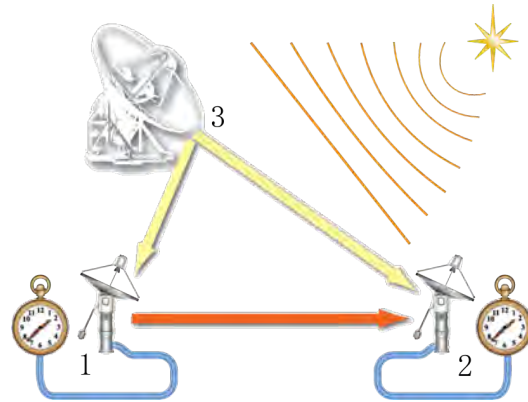


Fig. 1 Concept of the GALA-V broadband VLBI system.

GALA-V broadband VLBI system. The GALA-V observation system can be characterized by the following:

1. High-speed sampling: 1 GHz \times 4 bands, 8 Gbps per polarization.
2. Combination use of small antennas with a large diameter antenna.
3. Non-redundancy array of observation frequency allocation to get a fine delay resolution function.
4. Broadband observation: 3–14 GHz.
5. RF direct sampling without frequency conversion.

The disadvantage of the lower sensitivity due to the small collecting area is mitigated by using (1) broadband observations and (2) the combination observation with a large-diameter antenna. The data acquisition rate of the GALA-V system is 8192 Mbps corresponding to 4 \times 1-GHz bands, whereas the conventional geodetic VLBI observation uses about 256 Mbps. GALA-V brings about a 5.6 ($=\sqrt{8192/256}$) times improvement in SNR when compared to conventional VLBI. The signal-to-noise ratio of the VLBI observation is expressed by the product of the system equivalent flux densities (SEFD) of two stations as

$$SNR = \frac{S}{SEFD_1 \cdot SEFD_2} \sqrt{2Bt}, \quad (1)$$

where S is the flux of the radio source, B is the observation bandwidth, and t is the integration time. Thus, even if the SNR of the VLBI observation with a pair of small antennas ‘1’+‘2’ is not sufficient for reaching a target SNR, the joint observation with the large-diameter (boost) antenna ‘3’ enables the interferometer to work. The delay observable of the baseline $\tau_{21}(t_1)$ is computed by combining the two observables τ_{13} and

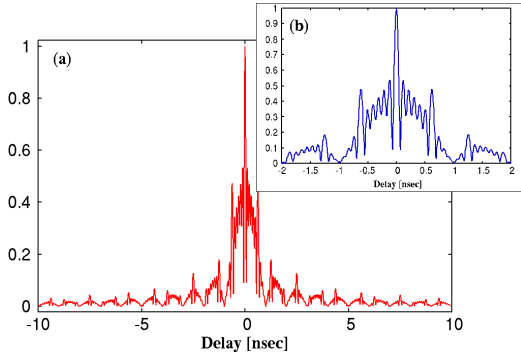


Fig. 2 (a) Delay resolution function as expected from the frequency array at 4.0 GHz, 5.6 GHz, 10.4 GHz, and 13.6 GHz with 1-GHz bandwidth and (b) a magnified plot around the center.

τ_{23} and using the closure delay relation as follows:

$$\tau_{21}(t_1) = \tau_{23}(t_3) - \tau_{13}(t_3) - \tau_{13} \times \dot{\tau}_{21} + \frac{1}{2} \tau_{13}^2 \times \ddot{\tau}_{21} + o_3, \quad (2)$$

assuming that radio source structure effect is negligible. Although the error of the observable τ_{12} increases by the root-square sum of the errors τ_{23} and τ_{13} , the advantage of this method is that systematic errors caused by the boost station cancel out. The radio source structure effect in the broadband observation is a subject of investigation.

After a local survey of the radio interference environment, we selected the nominal frequency array of the GALA-V system at 4.0 GHz, 5.6 GHz, 10.4 GHz, and 13.6 GHz for the center frequencies of the observation bands. By allocating the array in a non-redundancy interval, the delay resolution function has a fine peak and low side-lobes as indicated in Figure 2.

‘RF Direct Sampling’ is our original approach to enable easily do the broadband phase calibration by observation of a radio source. A stable phase relation between the observing bands is a prominent feature of this method. More details of this technique are described in Section 2.3.

It is well known that the atmospheric delay is the dominating error source with space-geodetic techniques including VLBI. For that a fast source switching is essential to improve the precision of both the geodetic results and the distant clock comparison. Therefore, the GALA-V project expects to make joint VLBI observations with a VGOS station as boost station in order to improve both the SNR and the temporal resolution.

2.2 Broadband Feed Development

The GALA-V system is designed to have a common radio observation frequency range with VGOS for joint observations. Most of the VGOS stations use the Eleven Feed [11] or the Quad-ridged Flared Horn (QRFH) [12] to receive the broadband radio signal. These feeds have a broader beam size at around 90–120°. Therefore, all new VGOS antennas are of the special optics design called “ring focus” in order to adapt to the broad beam size.

Using a different approach, we developed an original broadband feed with narrow beam size (34°) for the Cassegrain optics of the Kashima 34-m antenna. The first prototype feed “IGUANA-H” was produced in 2014. The design was based on a multi-mode wave composition, and it works at the frequency range 6.5–16 GHz. The second prototype feed “NINJA” was mounted on the 34-m antenna in 2015. It is sensitive in the frequency range 3.2–14 GHz.

Figure 3a shows the broadband receiver system of the Kashima 34-m antenna. The left hand side of the picture is the NINJA feed, the right hand side shows the IGUANA-H feed. The frequency dependence of the SEFDs of each feed is indicated in Figures 3b and 3c.

2.3 RF Direct Sampling with K6/GALAS(OCTAD-G)

The current standard VGOS observation system is based on the Proof-of-Concept (PoC) VLBI system developed at MIT Haystack Observatory [13, 14]. This system uses UpDown converters (UDC) for selecting four bands of 1-GHz bandwidth in the 2–14 GHz range. The signals are converted to intermediate frequencies (IF) in 32 channels of 32-MHz bandwidth using digital baseband conversion (DBBC, e.g., [15]–[17]) for each band. The phase relation among the 32 video channels must be stable, because each video frequency channel is separated in the digital signal processing after the IF signal is converted to digital data. The phase relations between the selected four bands using the UDC are not always constant; they may change and could even be sensitive to temperature mainly because of the analog mixing components and the local oscillators for each band. The concept

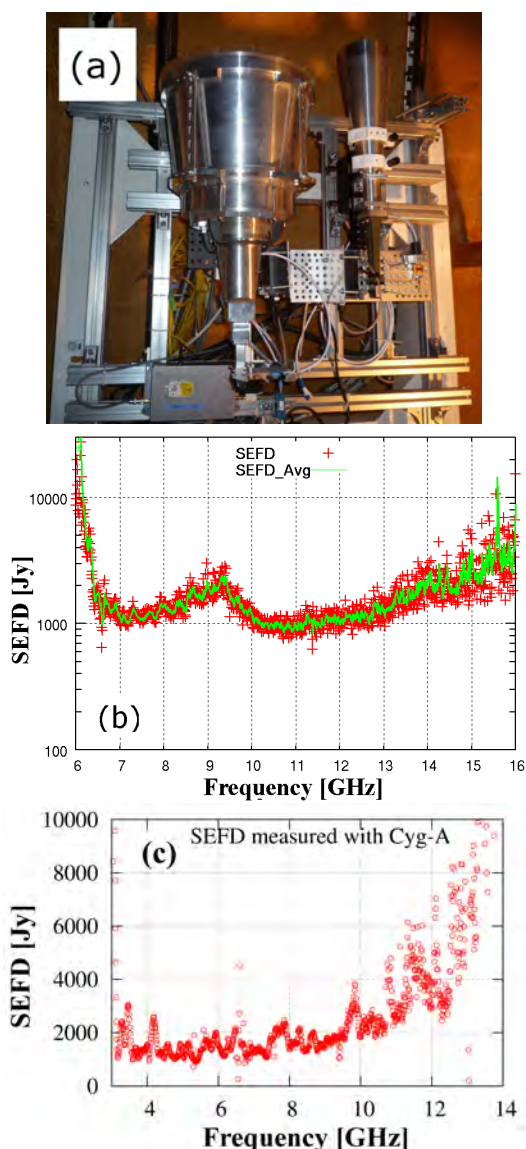


Fig. 3 Picture (a) of the NINJA (left) and IGUANA-H (right) feeds and SEFDs of the IGUANA-H (b) and NINJA (c) feeds.

of VGOS aims at deriving the so-called ‘broadband delay’ [18] from the coherent synthesis of the fringe phase over the four bands. The phase calibration signal, which is injected into the signal path at the front end and later digitally recorded, is essential for calibrating the phase variation.

Our GALA-V system takes a different approach: sampling the radio frequency (RF) signal without analog frequency conversion, an ‘RF Direct Sampling’ technique [19]. This technique was enabled by the 16-

Table 1 K6/GALAS Sampler specification parameters.

Input	
Number of inputs	2
Input freq. range	0.1–16.4 GHz
Sampling rate	16,384 MHz or 12,800 MHz
Quantization bit	3 bit
Output	
Sampling mode	Broadband mode 3200 Msps: 1, 2 bit 6400 Msps: 1, 2 bit 12800 Msps: 1 bit
	DBBC mode LO resolution of frequency is 1 MHz. Nch: 1, 2, 3, 4 Sample rate: 2048 Msps Quantization bit: 1 or 2 bit
Max data rate/sampler	16,384 Mbps
Output interface port	10GBASE-SR (SFP+), 4 ports
Data format	VDIF/VTP over UDP/IP
Control	Telnet /1000BaseT

GHz, high-speed sampler K6/GALAS (OCTAD-G). An image of this sampler is displayed in Figure 4a. The National Astronomical Observatory of Japan (NAOJ) and Elecs Co Ltd have been developing a series of a VLBI observation system called OCTAVE [20]. The high-speed sampler OCTAD is a member of the OCTAVE family with a 3-bit quantization at a 8,192 MHz sampling rate. The K6/GALAS is an upgraded version of OCTAD; this sampler realizes the analog-digital (A/D) conversion at a 16,384 MHz sampling rate with a 3-bit quantization. Then digital filtering via internal FPGA is applied to extract the 1024-MHz bandwidth signal at the requested frequency. The nominal observing mode is 2048 Msps-1bit-4band; the observed data come out at a data rate of 8,192 Mbps via the 10 GBASE-SR port with VDIF/VTP protocol as UDP/IP data stream.

A block diagram of the signal input to the sampler is shown in Figure 4b. The power divider and anti-aliasing filters have to be used to eliminate folding of the signal at 8,192 MHz. Then the signal is fed to two RF input ports to obtain four 1024-MHz bands distributed over the 3–14 GHz frequency range. Since the dynamic range of the A/D conversion at the input is limited, the input power level needs to be equalized over the broad frequency range. The data acquisition parameters and interface specifications of the K6/GALAS sampler are summarized in Table 1.

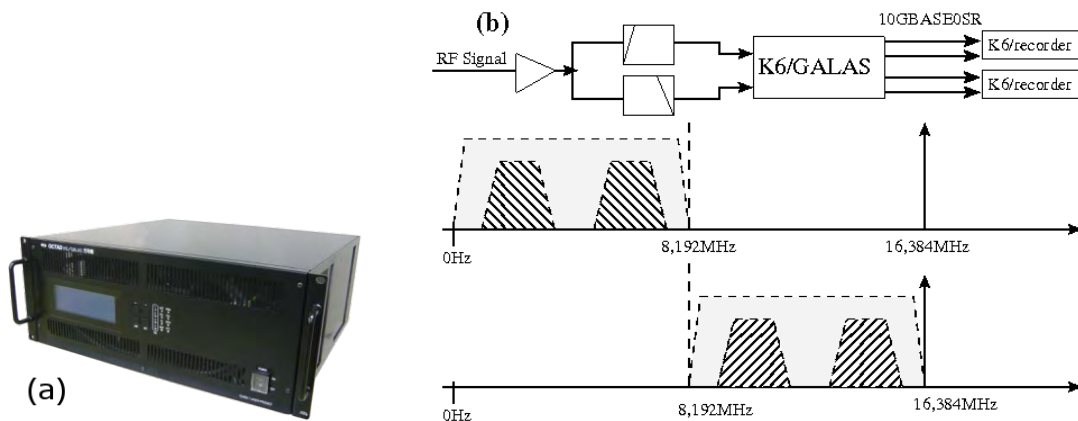


Fig. 4 (a) Picture of the K6/Galas sampler. (b) Block diagram from sampler input to data recording. Two anti-alias filters are used to eliminate folding of the signal at a sampling rate of 16,384 MHz.

2.4 Wideband Bandwidth Synthesis without Pcal Signal

A prominent feature of the ‘RF Direct Sampling’ is its stable phase relation that enables broadband bandwidth synthesis without a phase calibration (Pcal) signal. The phase calibration technique with Pcal signal has been used since the 1980’s [21] to utilize the invention of bandwidth synthesis [22]. The most significant phase change in the signal chain of the observation system happens during frequency conversion. It is unavoidable that the local oscillator’s initial phase is included in the converted signal. Consequently, large phase differences between signals happen naturally. The Pcal signal has effectively corrected phase differences in the signal chain of multi-channel VLBI systems (e.g., [21, 23]). The frequency range to be synthesized has been up to 1-GHz width in the conventional VLBI system, whereas with VGOS and GALA-V the bandwidth to be synthesized is about ten times wider than the conventional VLBI. The broadband phase calibration is an essential technology to achieve such high delay resolution; hence, the broadband Pcal signal has to be quite stable.

The ‘RF Direct Sampling’ technique enables broadband phase calibration without a Pcal signal. The observed signal is converted to digital data in the radio frequency region without frequency conversion; the phase relation of the signal is conserved at this point. The required frequency bands are extracted via digital signal processing in the following step. Since frequency conversion is a major cause for inserting

phase differences between bands, we can expect that the phase relation over the captured broad frequency range will be stable enough to eliminate the need for calibration with Pcal signal.

A wideband bandwidth synthesis algorithm (WBWS) [24] is being developed, in which the band-pass cross spectrum phase for a strong radio source is used to perform the broadband phase calibration. The WBWS estimates the ionospheric dispersive delay and the broadband group delay simultaneously. Instead of using a Pcal signal, the WBWS method requires a ‘calibration scan’ (CalScan) within a VLBI session. The CalScan is an observation of a compact strong radio source with relatively long duration to get a sufficiently small phase error in the cross correlation spectrum. Since the CalScan cross correlation phase data contains not only the instrumental delay, but also the geometrical, ionospheric, and atmospheric propagation delays of the scan, the user has to be aware that the group delay obtained by the WBWS is a differential delay with respect to the CalScan.

3 Broadband VLBI Experiment and Delay Variation

3.1 Kashima–Ishioka Experiment

The Geospatial Information Authority of Japan (GSI) has constructed a new 13.2-m diameter VLBI station [25] at Ishioka city in Japan. The Ishioka station

Table 2 Observation parameters of the broadband VLBI experiment in August 2015 on the Kashima 34-m – Ishioka 13-m baseline.

Date and Duration	2015y226d06h40m – 227d14h59m (32h20m),
Scan	2 scans of 1200 seconds and 1188 scans of 30 seconds
Frequency Array [MHz]	3200–4224, 4600–5624, 8800–9824, 11600–12624
Effective bandwidth	3.3 GHz
Data Acquisition	K6/GALAS & K6/recorder
Data Acquisition Mode	2048Mpsps-1bit-4band
Polarization	Vertical – Vertical

is fully compliant with the VGOS specifications. Thus Kashima 34-m of NICT and Ishioka 13-m of GSI are the only two stations in Japan with a broadband receiver system with an SEFD better than 2000 Jy. In collaboration with GSI, we have installed K6/GALAS DAS at Ishioka in August 2015. A test VLBI experiment in the observation frequency range of 3.2–12.6 GHz was conducted on this baseline. The observation parameters of this experiment are listed in Table 2.

Only one linear polarization was available with the NINJA feed of the Kashima 34-m station at the time. As the baseline between Ishioka 13-m and Kashima 34-m is very short (48.6 km), the parallactic angle of the polarization is negligible. The observation was done with one vertical linear polarization at both stations. The experiment included two long scans (1,200 s) and many short scans (30 s) in the more than 24 hours. The reasons for the long scans were twofold: examining the broadband delay behavior in the experiment and obtaining CalScan data for the WBWS processing. The cross correlation processing was done by the software correlator GICO3 [26] for each band. Finally, the post-correlation data were processed with the upgraded bandwidth synthesis software ‘komb’ (Ver. 2015-4-27) [24].

The process of WBWS includes the estimation of the dispersive delay and the broadband group delay. The cross spectrum phase is modeled by

$$\phi_{\text{meas}}(f) = \alpha \frac{\delta \text{TEC}}{f^2} + \delta \tau_a + \phi_o, \quad (3)$$

where the first term on the right hand side is the dispersive delay corresponding to the difference of the total electron content (δTEC) in the lines-of-sight from each observation station, and the second term is the non-dispersive delay including the geometrical delay and the tropospheric delay. Figure 5a shows the cross spectrum phase and 5b shows the time series of estimated

δTEC . Let me remind the reader that these data are differential quantities with respect to the CalScan used in the process. It is notable that up to several TECU^1 of dispersive delay contribution exist even on the short 48.6-km baseline.

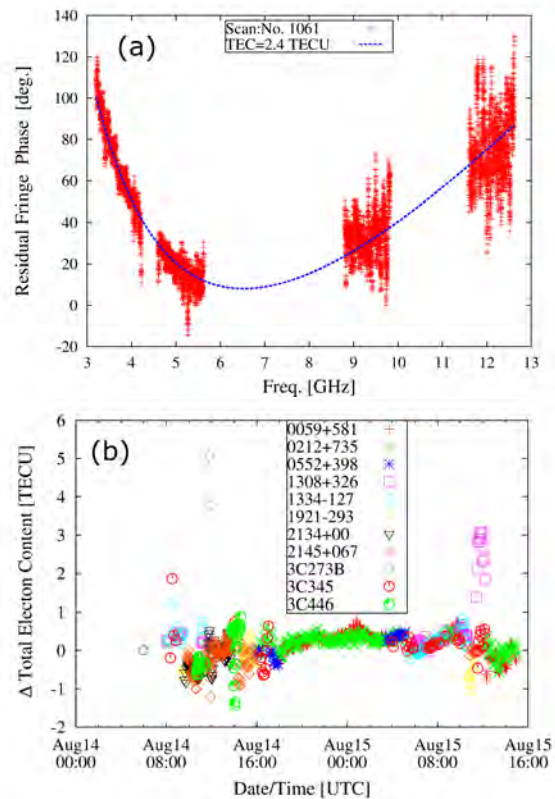


Fig. 5 (a) An example of the cross correlation phase spectrum. The dashed line is a plot of Equation (4) with parameters fitted to the data. (b) Time series of the estimated δTEC obtained in the experiment. Each symbol corresponds to one radio source.

¹ 1 TECU = 10^{16} electrons/m²

3.2 Broadband Delay

Figure 6a shows a time series of the group delay data of one-second integration after removal of a second-order polynomial for the slow delay change, and its Allan standard deviation (ASD) is displayed in Figure 6b. That scan was about 1,000 seconds long observing source 3C273B. The plot of the ASD indicates that the broadband delay of this case (effective bandwidth 3.3 GHz) reaches sub-pico-second precision at one-second observation when strong radio sources are observed.

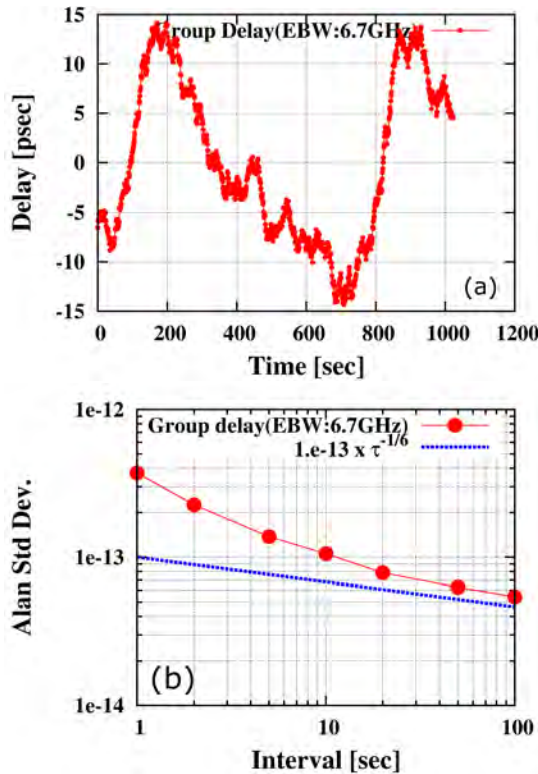


Fig. 6 (a) Time series of group delay data derived by WBWS after removal of a second order polynomial for the slow delay change. (b) Allan standard deviation of the delay data. The dashed line is a plot of $\sigma_y = 10^{-13} \tau^{-1/6}$.

It is notable that the group delay change on the order of ten picoseconds over hundreds of seconds of time was observed with a very high precision. There are several candidate causes which can affect the group delay variation: troposphere propagation excess delay, instrumental delay, radio source structure effect, ionospheric delay, and model error of the geometrical de-

lay. A model error of the geometrical delay will cause a slow variation related to Earth rotation. Also, the radio source structure effect will change the group delay with the rotation of the projected baseline with respect to the source. Thus, these two are unlikely to be the reason for the short time variation. A rapid change of the ionospheric delay may be caused by traveling ionospheric disturbances (TID, e.g., [27]), which is 100 km scale with order of 1 TECU amplitude traveling with velocity around 400 km/hour. Its time scale is about 1,000 seconds, then it seems to be too long to explain this variation. The tropospheric delay is known to be the dominating error source in space-geodetic observations. The Allan variance of the tropospheric delay in interferometric observations is modeled by the frozen flow of the Kolmogorov turbulence [28].

$$\sigma_y^2(\tau) = 1.3 \times 10^{-17} C_n^2 L v_s^{5/3} \tau^{-1/3}, \quad (4)$$

where $C_n^2 L$ is the constant of the turbulence, v_s is the wind velocity on the ground surface in m/s, and τ is the time interval. Armstrong and Sramek [29] have measured $C_n^2 L$ as $2 \times 10^{-13} \sim 2 \times 10^{-9}$ for a 35 km spatial scale. By using wind speed (4 m/s) measured on the ground at the time of observation, the ASD can be computed as $4.8 \times 10^{-13} \sim 2 \times 10^{-15}$ at $\tau = 1$ second interval. Figure 6b shows the ASD derived from the time series of the group delay and plot of $\sigma_y(\tau) = 10^{-13} \tau^{-1/6}$. This good agreement between measurement and model in both slope and magnitude of ASD suggests that the delay fluctuation may be attributed to tropospheric turbulence.

The baseline analysis was made with CALC/SOLVE [30] for this broadband VLBI experiment. Although the delay precision is better than one picosecond for each data point, the root mean square (RMS) of the post-fit delay residual after standard parameter estimation was 34 picoseconds with a large Chi-square value. That means that the scattering of the residuals cannot be explained by the magnitude of the delay error computed from the SNR and bandwidth. Re-weighting of the data with additive noise of 55 picoseconds reduced Chi-square to unity. This result suggests that an unmodeled error dominates the errors of the VLBI analysis, and that this is likely the tropospheric delay as suggested by the delay fluctuation data. The formal errors of the station coordinates in the final solution were 3–4 mm in the horizontal and 1.3 mm in the vertical direction.

4 Summary

NICT is developing a wideband VLBI system (GALAV) for frequency transfer over long distances. The observed radio frequency range is compatible with the VGOS specifications. To enable broadband observations with the Kashima 34-m radio telescope of Cassegrain optics, two types of original broadband feeds named IGUANA-H (6.5–16 GHz) and NINJA (3.2–14 GHz) were developed. A new high-speed sampler K6/GALAS was introduced for using the ‘RF Direct Sampling’ technique. An outstanding feature of ‘RF Direct Sampling’ is the stable phase relation between the bands selected by digital filtering. Since the signal path is simple and the data is digitized in an early stage, a high stability in phase and path length of the signal can be anticipated. The broadband delay is derived by the WBWS processing via phase calibration with a radio source signal (CalScan).

We have conducted a broadband VLBI experiment between the Kashima 34-m antenna and the Ishioka 13-m station, which is the only fully VGOS compliant station in Japan built by GSI in 2014. The experiment was composed of a geodetic session with 1,188 scans of 30 seconds in duration and two scans of long 1,200 seconds in duration. The cross correlation processing was done with the software correlator GICO3. The phase characteristic of the post-correlation data of whole bandwidth was calibrated with the phase data of a reference radio source (CalScan). Then the broadband group delay and the dispersive δTEC were simultaneously estimated in the WBWS process. The experiment has proven that the broadband delay enables sub-pico-second precision group delay measurements with one-second integration time. The behavior of the delay observable shows a fluctuation, which is consistent with the frozen flow model of the Kolmogorov tropospheric turbulence.

Acknowledgements

We express our gratitude to Yoshihiro Fukuzaki, Ryoji Kawabata, and Takahiro Wakasugi of GSI Japan for the collaboration in the joint observation with Ishioka 13-m station. We thank the “New Generation Network Testbed JGN-X” for supporting our project by providing a 10-Gbps network environment.

References

1. B. J. Bloom et al., “An optical lattice clock with accuracy and stability at the 10^{-18} level”, *Nature*, 506, DOI 10.1038/nature12941, 71–77, 2014.
2. J. Guèna et al., “Contributing to TAI with a secondary representation of the SI second”, *Metrologia*, 51(1), DOI 10.1088/0026-1394/51/1/108, pages 108–120, 2014.
3. M. Fujieda et al., “Carrier-Phase-Based Two-Way Satellite Time and Frequency Transfer”, *IEEE Ultrason. Ferroelectr. Freq. Control*, 59(12), DOI 10.1109/TUFFC.2012.2503, pages 2625–2630, 2012.
4. R. J. Coates and Clark, T. A., “Worldwide time and frequency synchronization by planned VLBI networks”, *In Its Proc. of the Sixth Ann. Precise Time and Time Interval (PTTI) Planning Meeting*, pages 361–371, 1974.
5. S. Hama et al., “First international Time and Frequency Comparison Experiment by using Very Long Baseline Interferometry”, *J. Radio Res. Lab.*, 34(142), 85–93, 1987.
6. H. Takiguchi et al., “VLBI Measurements for Frequency Transfer”, *Highlights of Astronomy*, Vol.15, Proc. of XXVIIIth IAU General Assembly in August 2009, DOI 10.1017/S1743921310008926, pages 225, 2010.
7. C. Rieck et al., “VLBI time-transfer using CONT08 data” *EFTF-2010 24th European Frequency and Time Forum*, DOI 10.1109/EFTF.2010.6533654, pages 1–8, 2010.
8. R. Haas et al., “VLBI and GNSS Frequency Link Instabilities during CONT Campaigns”, *IVS 2012 General Meeting Proceedings* Edited by Dirk Behrend and Karen D. Baver NASA/CP-2012-217504, pages 425–430, 2012.
9. C. Rieck et al., “VLBI Frequency Transfer using CONT11”, *Proc. of European Frequency and Time Forum (EFTF) 2012*, DOI 10.1109/EFTF.2012.6502358, pages 163–165, 2012.
10. K. Przemyslaw et al., “Remote Atomic Clock Delivery to the VLBI Station in Torun”, *Proc. of European Frequency and Time Forum 2016*, pages 183, 2016.
11. J. Yang et al., “Development of the Cryogenic 2-14 GHz Eleven Feed System for VLBI2010”, *6th European Conference on Antennas and Propagation*, DOI 10.1109/EuCAP.2012.6206604, pages 621–625, 2011.
12. A. Akgiray et al., “Circular Quadruple-Ridged Flared Horn Achieving Near-Constant Beamwidth Over Multi-octave Bandwidth: Design and Measurements”, *IEEE Trans. Antennas Prop.*, 61(3), DOI 10.1109/TAP.2012.2229953, pages 1099–1108, 2013.
13. C. Beaudoin and A. Niell, “Post-correlation Processing for the VLBI2010 Proof-of-concept”, *IVS 2010 General Meeting Proceedings* Edited by Dirk Behrend and Karen D. Baver NASA/CP-2010-215864, pages 35–39, 2010.
14. A. Niell, and Broadband Development Team, “The NASA VLBI2010 Proof-of-concept Demonstration and Future Plans”, *IVS 2010 General Meeting Proceedings* Edited by Dirk Behrend and Karen D. Baver NASA/CP-2010-215864, pages 23–27, 2010.
15. G. Tuccari, “Development of a Digital Base Band Converter (DBBC): Basic Elements and Preliminary Results”, *New Technologies in VLBI*, Asto. Soc. Pacific Conf. Ser. ISSN 1050-3390, Vol. 306, pages 177–252, 2004.

16. H. Takeuchi et al., "Development of a 4 Gbps Multifunctional Very Long Baseline Interferometry Data Acquisition System", *Publ. Astr. Soc. Pacific*, 118, pages 1739–1748, 2006.
17. A. Niell et al., "RDBE Development and Progress", *IVS 2010 General Meeting Proceedings*, Edited by Dirk Behrend and Karen D. Baver NASA/CP-2010-215864, pages 396–399, 2010.
18. B. Petrachenko et al., "Design Aspects of the VLBI2010 System", *Progress Report of the VLBI2010 Committee. NASA Technical Memorandum*, NASA/TM-2009-214180, June 2009.
19. K. Takefuji et al., "High-order Sampling Techniques of Aliased Signals for Very Long Baseline Interferometry", *Publ. Astr. Soc. Pacific*, 124, pages 1105–1112, 2012.
20. T. Oyama et al., "New VLBI Observing System 'OCTAVE-Family' to Support VDIF Specifications with 10 GigE for VERA, JVN, and Japanese e-VLBI (OCTAVE)", *IVS 2012 General Meeting Proceedings* Edited by Dirk Behrend and Karen D. Baver NASA/CP-2012-217504, pages 91–95,
21. T. A. Clark et al., "Precision Geodesy Using the Mark-III Very-Long-Baseline Interferometer System", *IEEE Trans. Geosci. Remote Sensing*, GE-23(4), IOD 10.1109/TGRS.1985.289433, pages 483–449, 1985.
22. A. E. E. Rogers, "Very long baseline interferometry with large effective bandwidth for phase-delay measurements", *Radio Science*, 5(10), DOI 10.1029/RS005i010p01239, pages 1239–1247, 1970.
23. H. Kiuchi et al., "K-3 AND K-4 VLBI VLBI DATA ACQUISITION TERMINALS", *J. Comm. Res. Lab.*, 38(3), pages 435–457, 1991.
24. T. Kondo and K. Takefuji, "An algorithm of wideband bandwidth synthesis for geodetic VLBI", submitted to *Radio Science*, 2016.
25. Y. Fukuzaki et al., "Construction of a VGOS Station in Japan", *IVS 2014 IVS General Meeting*, Edited by Dirk Behrend, Karen D. Baver, and Kyla L. Armstrong Science Press (Beijing) ISBN 978-7-03-042974-2, pages 32–35, 2014.
26. M. Kimura, "Development of the software correlator for the VERA system II", *IVS NICT-TDC News*, 28, pages 22–25, 2007.
27. A. Saito, S. Fukao, and S. Miyazaki, "High resolution mapping of TEC perturbations with the GSI GPS network over Japan", *Geophys. Res. Lett.*, 25(6), DOI 10.1029/98GL52361, pages 3079–3082, 1998.
28. A. R. Thompson, J. M. Moran, and G. W. Swenson, JR., "Interferometry and Synthesis in Radio Astronomy", KIEGER Pub., Malabar, Florida, ISBN 0-89464-859-4, pages 428–436, 1986.
29. J. W. Armstrong, and R. A. Sramek, "Observations of Tropospheric phase scintillations at 5GHz on vertical path", *Radio Science*, 17(6), DOI:10.1029/RS017i006p01579, pages 1579–1586, 1982.
30. D. Gordon et al., "GSFC VLBI Analysis Center Report", *IVS 2014 Annual Report*, edited by K. D. Baver, D. Behrend, and K. L. Armstrong, NASA/TP-2015-217532, pages 221–224, 2015.

BRAND EVN

Gino Tuccari^{1,2}, Walter Alef²

Abstract A multi-band concurrent observation capability for the frequency bands commonly used in the EVN could greatly improve the VLBI scientific opportunities, even enabling an important simplification of the radio telescope operations. The project for a 1.5–15.5 GHz fully digital receiver is presented with possible solutions for a smooth introduction in the EVN radio telescopes, which differ widely from each other.

Keywords VGOS, EVN, DBBC, VLBI, backends

1 Introduction to the BRAND Project

Today EVN observing sessions are covered by separate receivers, and a sequence of about three or four bands per session are used in succession. Considering frequencies lower than 22 GHz the following bands are involved: 18 cm (L-band), 13 cm (S-band), 6 cm (C-band), 5 cm (C-band Methanol-OH), 4 cm (X-band), and at some stations even 2 cm (Ku-band) is available.

Having to use different physical receivers implies a number of restrictions including taking seconds to hours (depending on the radio telescope) to switch between bands, different mechanical positions at the antenna focus, more cryogenic cooling systems and receivers to be maintained, and different pointing models. So multi-band observations are not possible, while frequency agility in the EVN has been a high priority

goal for more than 15 years. Compared to the VLBA, which has been offering fast frequency switching on the order of seconds since the beginning, this has obviously created a high user demand motivated by the possibility of saving valuable observing time, by the chance to obtain spectral index maps, and even more by the potential for precise registration of source positions via phase-referencing, which allows the measurement of frequency dependent core-shifts, and so on.

The new emerging geodetic network VGOS is implementing simultaneous multi-frequency observations. The goal for this network is to achieve an improved positioning accuracy down to 1 mm. To achieve this, fringe-fitting over a very-wide frequency range is applied, which includes an accurate determination of the ionosphere contribution.

The EVN can develop multi-wavelength VLBI now, starting a development that makes use of recent achievements in the relevant fields: existing implementations of broadband feeds and LNAs, backends with very high data rates (DBBC3 backend), and analog-to-digital converters which can sample the proposed frequency range. The latter will allow the introduction of new solutions where no frequency conversions are necessary to handle a huge sky frequency range. This will open a full set of new scientific opportunities such as real multi-wavelength VLBI mapping, multi-wavelength spectroscopy, multi-wavelength polarimetry, and multi-wavelength single-dish, geodetic VGOS compatibility. All of that would result in observing capabilities which are even superior to the fast frequency switching.

1. INAF Istituto di Radioastronomia

2. Max-Planck-Institut für Radioastronomie

2 Scientific Drivers

The implementation of a concurrent multi-band observing capability greatly enhances the potential for new scientific projects. This also offers an important simplification for the operation of the radio telescopes. It has an economic impact in the daily use and maintenance of the receiver systems.

In particular the scientific motivation for simultaneous multi-wavelength observations underlines the high priority of our project:

- VLBI mapping: using fringe-fitting over the whole band (including an ionospheric solution) will naturally allow precise registration of maps at different frequencies.
- VLBI spectroscopy: the simultaneous study of several different maser types in different frequency bands, and the alignment of different maser species allows, for instance, the determination of conditions in complex flow patterns.
- VLBI polarimetry: variations of polarized emissions as a function of frequency over a very wide frequency range can be measured, and precise rotation measures can be determined without ambiguities, which will improve studies of physical conditions of various astronomical objects.
- single dish: flux variation studies in several bands simultaneously (especially interesting for intraday variability) are possible, and rotation measures over large bandwidths can be made.
- compatibility with VGOS antennas: joint observations with geodetic VGOS antennas would be possible, for precise positions of astronomical antennas and celestial reference frame observations. Huge arrays for astronomical observations could be formed when needed.

In short, advantages could be envisaged for the EVN users: new improved science and additional available observing time due to the reduced/removed observation down-time. Advantages for the EVN telescopes are: having fewer receivers that require maintenance, more efficient use of the increased observing time, in addition to a reduction of daily cost for maintaining cooled receiver systems, and a simplification of their medium and long-term maintenance. EVN, like VGOS, could take the lead in VLBI observing because of the new multi-band simultaneous capability.

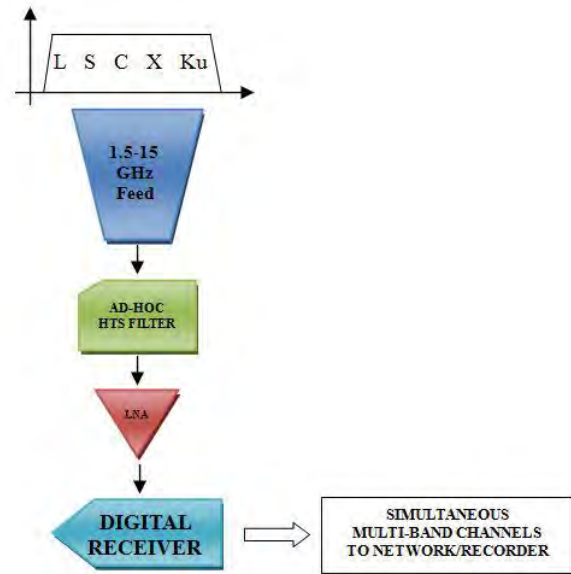


Fig. 1 Schematic view of the complete receiver.

3 Implementation

The BRAND project is a Joint Research Activity in the RadioNet4 proposal, which was submitted to the EU Horizon2020 call for proposals. In the BRAND project it is planned to develop a single cryogenic cooled receiver covering the broadband for astronomy with linear polarization feeds covering the frequency range 1.5–15 GHz. Figure 1 shows a schematic description of the proposed complete receiver system, including the analog front-end part (without any frequency conversion) and the broadband digital receiver.

The development work will take advantage of and start from state-of-the-art existing know-how, which will be adapted and extended for the EVN network. Here in summary, possible contributions of the various participants in the project are given with their expertise in the different parts of the project:

- Broadband antenna feed from ten years of technology developed for VGOS (OSO (QRFH), IGN (DYQSA))
- Low noise amplifiers developed for VGOS (MPI, IGN, IAF)
- Analog signal processing without any frequency conversion (INAF, MPI)

- Analog signal processing — only LNA and amplification chain with HTS filtering of strong RFI (INAF, MPI)
- Fully digital broadband sampling and data processing (DBBC3H INAF and MPI)
- Broadband digital receiver (INAF, MPI)
- Fully digital down-conversion and/or band selection with DSC/PFB/DDC modes (INAF, MPI)
- FPGA-based digital polarization conversion (ASTRON)
- Output channel selection and network routing/recording for multi-band simultaneous observations (INAF, MPI, OSO).
- Broadband DDC/PFB/DSC observing modes firmware implementation
- Multi-band total power detector firmware implementation
- Multi-band polarimeter firmware implementation
- Multi-band spectrometer firmware implementation
- Development of a complete prototype receiver for a selected antenna
- Integration and testing in the selected antenna
- Development of station control software
- Development of correlation and astronomical data processing software.

Different work packages are required to accomplish the project:

- Studies of the boundary conditions for antenna status of the EVN stations
- Determination of local RFI “fingerprints” at the EVN stations with homogeneous tools
- Ad-hoc development of the antenna feed
- Ad-hoc filtering implementation
- Broadband LNA development
- Broadband analog multi-bit to digital conversion
- Antenna system — digital receiver link connection
- Digital unit hardware implementation
- Method and implementation of digital polarization conversion from linear to circular
- Additional digital RFI mitigation firmware implementation

4 Conclusions

If the RadioNet4 proposal is successful, it might already start in December 2016, with a duration of four years. In RadioNet4, BRAND will develop a state-of-the-art digital receiver for radio astronomy, which, if deployed in the EVN, will change the way in which we do VLBI in Europe dramatically, opening new scientific opportunities. A great boost will be also given to the extreme wide-band technologies whose applications can be envisaged to bring possible benefits to the fields of telecommunication and diagnostic medical instrumentation.

Ny-Ålesund Observatory: What Has Been Done?

Leif Morten Tangen¹

Abstract The existing 20-m radio telescope in Ny-Ålesund was put into operation in 1994. The telescope is more than 20 years old now and is ready for retirement. We decided to build a VGOS core site with twin telescopes. The existing telescope is just 70 meters away from the airport runway and the CAA did not allow us to build anything new as close. The new site is about 1,500 meters northwest of the old telescope and we had to build a road with a bridge. This was finished in summer 2014 and the construction work at the new site started in October 2014. It is challenging to do construction work during the winter time at 79°N with permafrost. During the winter, the VLBI foundation was built. The station, SLR, and gravity buildings were built as well. This presentation will show what has been done until now and different solutions for the telescopes. The telescopes are scheduled to arrive in April 2016.

Keywords Radio telescope, VGOS

1 Introduction

We started in 2013 and built the first part of the road and a bridge. The rest was completed in 2014 and Veidekke started the construction work at the new site in October 2014. One year later all of the buildings have finished construction.

Norwegian Mapping Authority

2 Construction Work

First we had to dig the holes for the VLBI foundation. We found bed rock in a depth of four meters. This was just as test drillings had indicated. After cleaning the bedrock with steam everything was ready for the concrete. We built the VLBI, SLR, and gravity foundations. During winter time you have to use tents and heat where you will do concrete work. This created some extra work and during winter storms it was rather difficult. All houses are made of wood and stand on steel pipes (120 of them) drilled down one meter into bedrock.

3 Control Points and GNSS

At the site we established several control points and three GNSS points. The latter are made like a tripod with steel pipes drilled one meter down into bedrock and welded together at the top. A steel tower will be put on the tripod.

4 Telescopes

The first FAT was done in October 2015 and the second in January 2016. The telescopes are ready for shipment and will arrive in Ny-Ålesund at the beginning of April 2016. The telescopes have everything inside. This will keep all instruments and cables at controlled temperatures. We have also made a temperature controlled box for the VLBI signal cables in the walk ways. The front end will use a trolley and a railway will be made in the



Fig. 1 Site overview in February 2015.



Fig. 2 The station in late summer 2015.

feed cone. When the front end must be taken down for maintenance, the railway can be extended and a hoist on the azimuth cabin can lift the trolley down. The telescopes have an invar wire system and tiltmeters.

5 Other Things

The Maser will arrive in July 2016. We have not decided yet what feed to use but will do so in spring



Fig. 3 First telescope at FAT.

2016. GNSS was up and running in November 2015. The SLR system will come in 2019. For more information, please visit Veidekke's Web page: <http://veidekkearctic.no>.

First 2-Gbps Observations between the KVAZAR VGOS Antennas and the Yebes RAEGE Antenna

Alexey Melnikov¹, Pablo de Vicente², Sergei Kurdubov¹, Andrey Mikhailov¹

Abstract A series of joint test observations using three 13-m VGOS antennas was carried out between September and November 2015. These included experiments at two different recording rates: 256 Mbps and, for the first time, 2 Gbps. Two different DBBC2 working setups, Digital Down Conversion and Polyphase Filter Bank, were used at Yebes; the data recorded was e-transferred to the IAA Correlator Center. Combined correlation of mixed bandwidth data from the KVAZAR antennas and Yebes were performed with DiFX 2.4, and some results were obtained.

Keywords VLBI, VGOS, KVAZAR, RAEGE

1 Introduction

A series of eight experiments were carried out with the 13.2-m antenna network of Zelenchukskaya (Zv) and Badary (Bv) in Russia and the 13.2-m antenna at Yebes (Yj) in Spain. All antennas are of ring-focus design and are equipped with an S/X/Ka-receiver. There are differences between the antennas' data acquisition and recording systems: Yebes uses a DBBC2 and a Mark 5B+; Badary and Zelenchukskaya have a BRoadband Acquisition System (BRAS) [5, 6, 7] and a Data Transmitting and Recording System (DTRS) [1]. Observation scheduling, data correlation, and analysis were performed at the IAA in Russia. A short summary of all experiments is presented in Table 1.

1. Institute of Applied Astronomy RAS

2. Observatorio de Yebes, Instituto Geográfico Nacional

2 Scheduling

Geodetic scheduling was performed with a modified version of the SKED software (version 2007Feb13) [4]. On-source times ranged from 22 to 100 s (RU0179, RU0180, RU0181), 30–100 s (RU0191, RU0192), 90–150 s (RU0222, RU0224), 50–180 s (RU0263), and a target signal-to-noise (SNR) of 20 dB in both X- and S-band. The scan sequence was automatically optimized for UT1-UTC estimation. NRAO SCHED key-files were prepared with the frequency setup, and the scan sequence from the skd-file was added later. Final vex-files were transferred to the stations.

The setup for Badary and Zelenchukskaya included three 512-MHz-wide frequency channels in X-band covering the range between 7568 and 9104 MHz and a single 512-MHz-wide channel in S-band covering the 2164–2676 MHz bandwidth.

For the first experiments, we tested the PFB mode of the DBBC2 at the RAEGYEB station. Frequencies were selected in the second Nyquist zone to cover 512 MHz in X-band and S-band with gaps; in S-band the KVAZAR receivers have filters between 2400–2500 MHz to avoid local RFI (see Table 2). Several scans in DDC mode were added in subsequent experiments to ease diagnostics and the fringe search.

3 Data Correlation

The recorded data were e-transferred to the IAA Correlator Center in St. Petersburg via optical fiber. Correlation was done with DiFX 2.4 [2] on the new blade-server hybrid cluster in the IAA using the “*zoom band*” capability of the software correlator because the

Table 1 Brief summary of the experiments. In RU0191, RU0222, RU0224 several scans at the beginning were recorded in the DDC mode and the rest in the PFB mode. DBBC mode, the number of intermediate frequency bands, their polarizations and bandwidths are specified in the *Frequency setup* column for each station.

Session name	Start date and time, UT	Duration, h	Number of scans	Frequency setup
RU0179	2015-09-09 19:00	1	40	ZvBv: 3X LCP and 1S RCP, 512 MHz
RU0180	2015-09-10 19:00	1	39	Yj:PFB, 8X RCP and 8S LCP, 32 MHz
RU0181	2015-09-11 19:00	1	39	
RU0191	2015-10-14 07:00	1	44	ZvBv: 3X and 1S RCP, 512 MHz Yj:DDC, 8X, RCP, 16 MHz Yj:PFB, 8X and 8S, RCP, 32 MHz
RU0192	2015-10-15 07:00	1	44	ZvBv: 3X and 1S RCP, 512 MHz Yj:DDC, 4X and 4S, RCP, 16 MHz
RU0222	2015-11-09 09:00	3	75	ZvBv: 1X and 1S, RCP, 512 MHz
RU0224	2015-11-10 09:00	3	77	Yj:DDC, 8X, RCP, 16 MHz
RU0263	2015-11-20 09:00	4	109	Yj:PFB, 8X and 8S, RCP, 32 MHz

Table 2 Sky frequency values (MHz) for scheduled experiments.

RU0179	X	9072	9008	8944	8880	8816	8752	8688	8624
RU0180	S	2612	2580	2548	2388	2356	2324	2292	2260
RU0181									
RU0191	X	9076	9044	8980	8916	8852	8788	8724	8660
	S	2612	2580	2548	2388	2356	2324	2292	2260
RU0192	X	8964	8948	8932	8916				
	S	2324	2308	2292	2276				
RU0222	X	9076	9044	9012	8980	8948	8916	8884	8852
RU0224	S	2612	2580	2548	2388	2356	2324	2292	2260
RU0263									

KVAZAR stations are equipped with BRAS and able to record only 512 MHz-wide frequency channels and Yebes with DBBC2 in DDC mode has 16 MHz-wide channels and in PFB mode 32 MHz per channel. Detailed frequency setups for every experiment are presented in Table 2.

During the experiments, we experienced different kinds of problems: in RU0179, Zelenchukskaya was misconfigured with the wrong VDIF frame size. Additionally, the DBBC2 at Yebes was not properly configured. Thus only RU0180 and RU0181, which yielded fringes for the Bv-Zv baseline, were analyzed for EOPs. RU0191 required corrections to the setup, but only fringes between Badary, Zelenchukskaya, and Yebes in DDC mode were found, whereas the scans in PFB mode at Yebes yielded no fringes. RU0192 was also unsuccessful because data from the KVAZAR stations were lost during transfer. RU0222 and RU0224 were correlated with successful results both in the DDC mode and the PFB mode at Yebes. RU0263 is currently in the correlator queue.

4 Analysis

The *PIMA* software [8] was used for data post-processing and to produce NGS-card files. This includes the resolution of the delay ambiguities and the calculation of the ionospheric contribution. The analysis was done with the “*Quasar*” software suite [3]. All sessions were analyzed, but due to different problems that arose during the sessions, only a few sessions can be considered successful. Pre-fit residuals of the session RU0224 are shown in Figure 1. Yebes shows a linear clock offset. Zelenchukskaya’s position was fixed, and the following parameters were estimated: station positions, a linear zenith wet delay, and linear clocks. The corresponding post-fit residuals of the session RU0224 are shown in Figure 2. Root mean square residuals (RMS) are presented in Table 3. The final weighted root mean square residuals (WRMS) are about 49 ps, and the corresponding mean ionospheric free group delay error is about 114 ps. In comparison, the typical WRMS for the 512 MHz-wide bands of the Bv-Zv baseline is below 10 ps.

Table 3 Root-mean-square residuals for the RU0224 experiment.

Baseline	RMS, ps
Badary-Yebes	239
Badary-Zelenchukskaya	67
Yebes-Zelenchukskaya	205
average	138

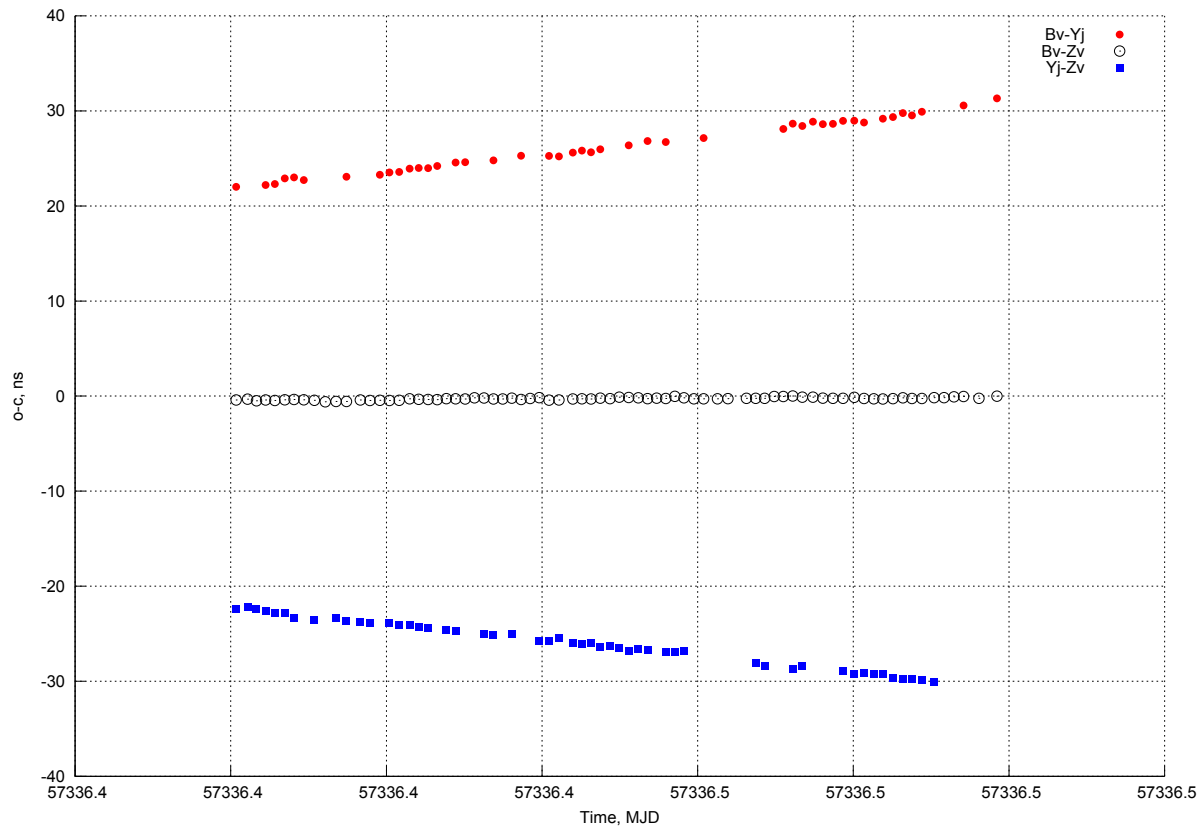


Fig. 1 Pre-fit residuals of the session RU0224 on November 10, 2015.

5 Conclusions

A first analysis of an international Intensive experiment using a VGOS network has been done. The Yebes DBBC2 setup in PFB mode is compatible with KVAZAR's Badary and Zelenchukskaya equipment. The successful combined correlation of KVAZAR stations and RAEGYEB in the PFB mode of the DBBC2 was performed.

Acknowledgements

The activities for the construction of the 13.2-m RAEGYEB radio telescope are being co-financed by ERDF/FEDER 2007-2013 under the project: "VGOSYEBES: Radiotelescopio de VLBI Geodesico y Astrometrico para su integracion en la red VGOS".

The RAEGYEB telescope received partial funding from MINECO grant FIS2012-38160 for the activities described here.

References

1. I. Bezrukov, A. Salnikov, A. Vylegzhanin (2014). Russian Data Recording System of New Generation. In: *International VLBI Service for Geodesy and Astrometry 2014 General Meeting Proceedings*. Science Press, Beijing, China, 130–133, 2014.
2. A. T. Deller, S. J. Tingay, M. Bailes, C. West (2007). DiFX: a software correlator for very long baseline interferometry using multiprocessor computing environments, *Publications of the Astronomical Society of the Pacific* 119, 318, 2007.
3. S. L. Kurdubov, V. S. Gubanov (2011). Main results of the global adjustment of VLBI observations. *Astronomy Letters*, Volume 37, Issue 4, DOI 10.1134/S1063773711010063, 267–275, 2011.
4. A. Melnikov, J. Gipson (2005). Running SKED under Linux. In: *Proceedings of the 17th Working Meeting on Eu-*

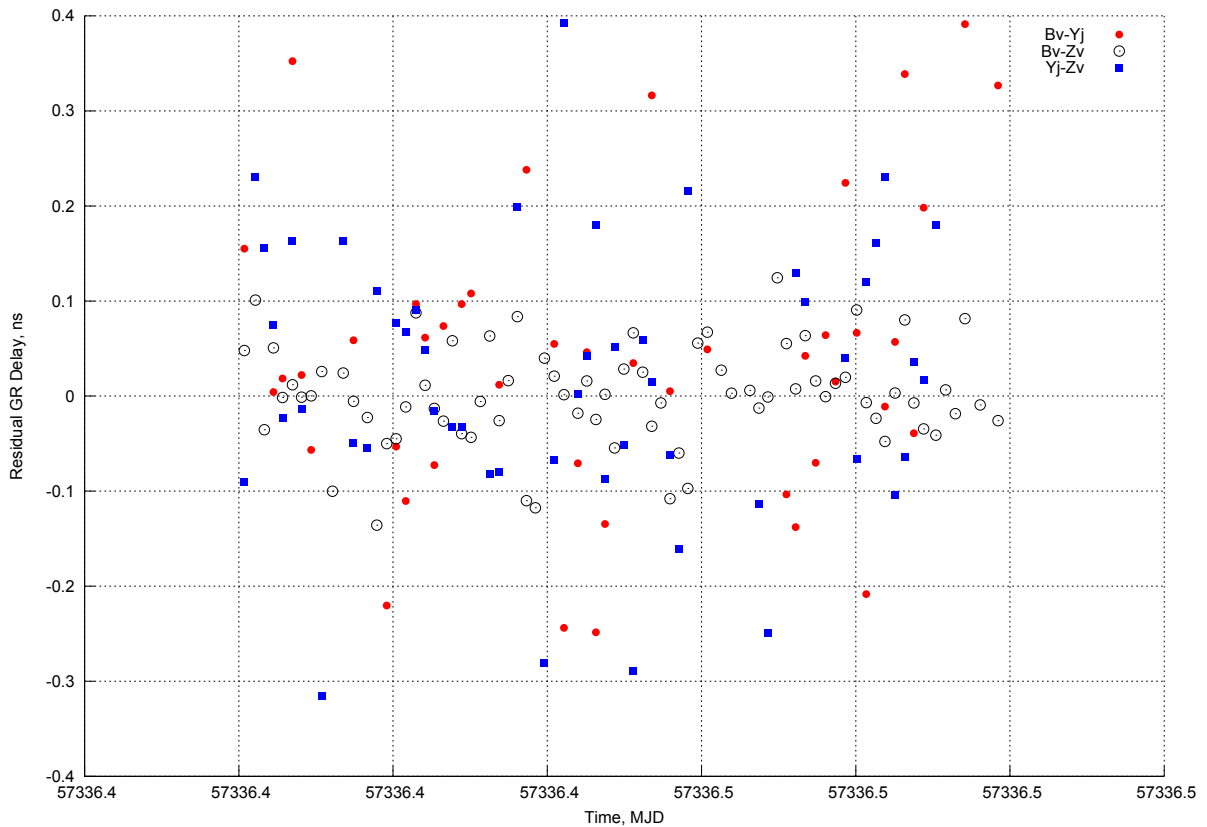


Fig. 2 Post-fit residuals of the session RU0224 on November 10, 2015.

- ropean VLBI for Geodesy and Astrometry*, M. Vennebusch, A. Nothnagel (eds.), INAF, Italy, 131–132, 2005.
5. N. E. Koltsov, D. A. Marshalov, E. V. Nosov, L. V. Fedotov (2013). A data acquisition system of the S/X-wave range of the radio interferometer for the universal time on-line monitoring. *Instruments and Experimental Techniques*, Vol. 56, No. 3, 339–346, 2013.
 6. E. Nosov, A. Berdnikov, S. Grenkov, D. Marshalov, A. Melnikov, L. Fedotov (2014). Current Development State of the Russian VLBI Broadband Acquisition System. In: *International VLBI Service for Geodesy and Astrometry 2014 General Meeting Proceedings*. Science Press, Beijing, China, 82–85, 2014.
 7. D. A. Marshalov, A. S. Berdnikov, S. A. Grenkov, A. V. Krohalev, E. V. Nosov, L. V. Fedotov, A. V. Shemanaev (2015). The results of Preliminary Tests of Broadband Digital Conversion System for Radiotelescopes. *IAA Transactions*. Issue 32. St.-Petersburg, 27–33, 2015.
 8. L. Petrov, Y.Y. Kovalev, E.B. Fomalont, D. Gordon (2011). The VLBA Galactic Plane Survey — VGaPS. *Astron. J.*, 142, 35, 2011.

VGOS Observations with Westford, GGAO, and the New Station at Kokee, Hawaii

Arthur Niell, Roger Cappallo, Brian Corey, Chris Eckert, Pedro Elosegui, Russ McWhirter, Ganesh Rajagopalan, Chet Rusczyk, Mike Titus

Abstract The GGAO 12-m and Westford 18-m antennas are instrumented with the four-band broadband signal chain to provide VGOS capability. These antennas have been making VGOS geodetic observations for more than a year. Preliminary analysis of the thirteen sessions, which range in duration from one to 15 hours, gives a weighted RMS deviation of 2 mm from the mean baseline length (601 km). The 12-m VGOS antenna at Kokee Park Geophysical Observatory on Kauai, HI, was completed in early 2016, and the broadband signal chain, built by MIT Haystack Observatory, was installed. Observations with the GGAO12M and Westford antennas began in February. These will increase in duration from one to 24 hours with completion of the Commissioning Phase for KOKEE12M expected in May 2016.

Keywords VGOS, broadband VLBI, geodesy

1 Introduction

The goal of the next-generation geodetic VLBI system is to achieve station position uncertainty of approximately 1 mm and velocity uncertainty of better than 0.1 mm/year. Studies by the IVS Working Group 3 [4] determined that the primary error source is expected to be unmodeled atmosphere delay variation and that this error is reduced by increasing the number of observations per hour. This implies faster antennas, but for economic reasons the resulting antenna collecting

area for the same cost is significantly smaller, thus implying lower sensitivity for the same receiver systems. To recover the sensitivity a higher recording data rate was proposed, to be achieved by utilizing more RF bandwidth and by implementing dual polarization on the antennas. The delay uncertainty would be reduced, for the same antenna efficiency, by covering a wider frequency range than the 2 to 9 GHz of the existing geodetic VLBI network. The result of the WG3 studies was to propose the use of four 1-GHz bands spanning the radio frequency band from S-band (2.2 GHz) to 14 GHz.

This broadband design, originally called VLBI2010 but now referred to as VGOS (VLBI Global Observing System), was implemented on two prototype systems: a 12-m antenna at the Goddard Geophysical and Astronomical Observatory (GGAO) of the Goddard Space Flight Center near Washington, D.C., and the Westford 18-m antenna at Haystack Observatory near Boston, Massachusetts, USA, to prepare for the development and implementation of the first operational VGOS antenna at Kokee Park Geophysical Observatory (KPGO). The KPGO VGOS antenna, which began observations in February 2016, has been a cooperative project of the U.S. Naval Observatory, NASA, and MIT Haystack Observatory.

The GGAO and Westford antennas began geodetic VLBI observations in December 2014 with the VGOS Demonstration Series (VDS). Results from that set of sessions spanning 14 months are reported here, along with some preliminary results for the KPGO VGOS antenna. Additional information about the KPGO system is provided in the reports in this volume by Rajagopalan (2016) [5] and by Rusczyk (2016) [6].

MIT Haystack Observatory

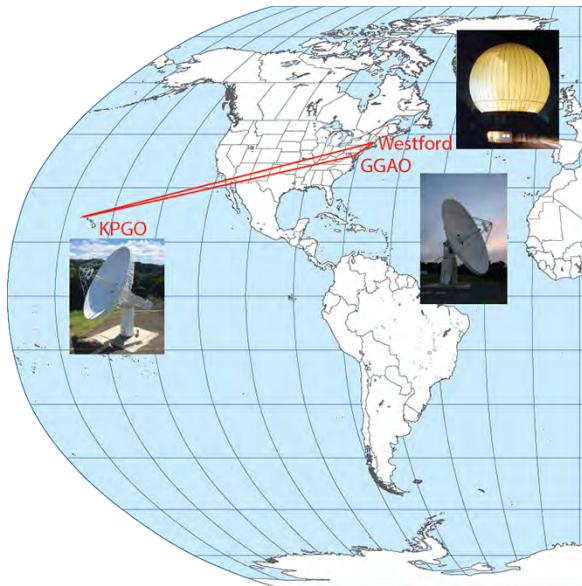


Fig. 1 The first operational VGOS antenna systems.

2 VGOS Broadband System Features

The features of the VGOS system as implemented on the GGAO12M and Westford antennas are repeated here for reference:

- four bands of 512 MHz each, rather than the two (S and X) for the legacy Mark IV systems,
- dual-linear polarization in all bands,
- multitone phasecal delay for every channel in both polarizations,
- group delay estimation from the full spanned bandwidth (3.0 GHz to 10.5 GHz),
- simultaneous estimation of the group delay and the total electron content difference (dTEC) between sites using the phases across all four bands.

A major difference between the broadband systems and the legacy S/X systems is the use of both linear polarizations rather than just one circular polarization.

The current configuration of the broadband signal chain for GGAO12M, Westford, and KOKEE12M is shown in Figure 2.

Two significant differences between the analysis of broadband data and that of standard S/X geodetic VLBI data are the required use of multitone phase cal delay to align the four bands and the simultaneous estimation of the group delay and the dispersive effect of the differential along-path charged particle content

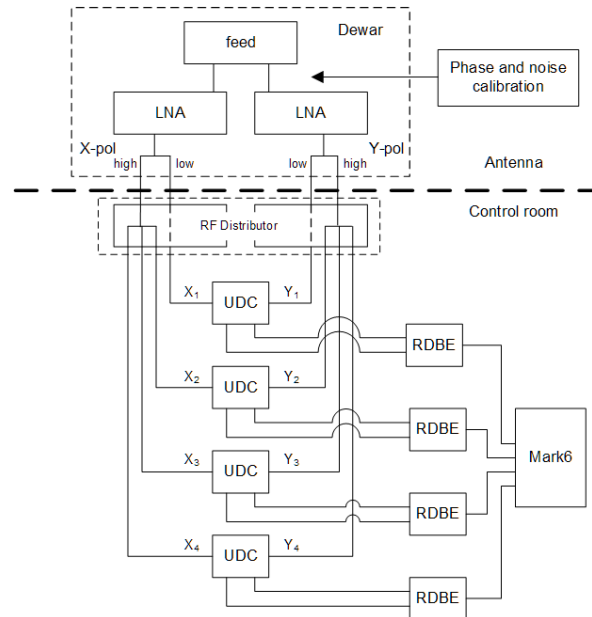


Fig. 2 Broadband signal chain configuration for GGAO 12-m, Westford, and Kokee 12-m antennas (Haystack implementation).

(the ‘ionosphere’). An additional instrumental effect that required investigation and implementation is the difference, between polarizations, of the uncalibrated delays and phases that arise primarily in the feed and cables that precede injection of the phase calibration signal in the front end.

3 Observations, Correlation, and Analysis

In late 2014 a series of bi-weekly one-hour sessions, called the VGOS Demonstration Series (VDS), was initiated in order to bring the new observation technique to operational capability. The emphasis has been on completion of Field System control of all equipment, evaluation of the equipment for sustained operation, implementation of the additional correlation and post-correlation analysis tools needed for the broadband hardware capability, and development of the procedures for all of these steps to provide minimum personnel interaction at all stages. Each of these leads toward the goal of unattended operation.

An objective of the VGOS design is the ability to observe with the legacy systems at S and X bands. However, radio frequency interference (RFI) at S-band

can severely degrade the sensitivity of the systems. For the results reported here, and perhaps for future VGOS-only sessions, the lower frequency bound was chosen to be 3 GHz. Also, while the goal for the upper frequency of the VGOS observations is 14 GHz, the GGAO and Westford systems, which are prototypes, are limited by the down-conversion hardware (UDC in Figure 2) to an upper bound of about 11 GHz. Taking into account the need to estimate the line-of-sight charged particle dispersion, the optimum band frequencies were calculated by Bill Petrachenko to be centered on approximately 3.3 GHz, 5.5 GHz, 6.6 GHz, and 10.5 GHz.

From December 2014 through February 2016 thirteen sessions were successful. Hardware problems plagued both antennas through the second half of 2015, but observations resumed in November.

The following list summarizes the various processes involved in the data collection and processing of the recent VGOS observing sessions:

- make a schedule,
- perform the observations,
- transfer the data to the correlator, either by shipping the disk modules or by network transfer,
- correlate simultaneously all four polarization products for all four bands directly from the Mark 6,
- estimate the group delay using *fourfit*
 - applying multitone phasecal delays and phases to align the phases of the four bands,
 - correcting for uncalibrated delay and phase offsets between polarizations,
 - combining the four polarization products (HH/VV/HV/VH) to produce a pseudo-Stokes I visibility [2] providing a single amplitude, group delay, and phase,
- create a database,
- estimate the geodetic and ancillary parameters with *nuSolve* [1].

More details on the observation, correlation, observable extraction (fringe fitting), and geodetic analysis are provided in [3]. Since that report a significant advance has been made towards the realization of the VGOS goal of improved analysis capability by incorporating the use of the new *vgosDB* and associated utilities [1] for all sessions in 2016.

4 Preliminary Results from VDS

The geodetic analysis was done for each session separately using the new program *nuSolve* from GSFC [1]. *nuSolve* provides all of the needed operations and modeling that is useful for inspection, evaluation, and parameterization of the VDS sessions.

For the *nuSolve* analysis, since these were mostly only one-hour sessions, the model parameterization was relatively simple. Only the clock behavior at GGAO, the position of GGAO, and the atmosphere zenith delays and gradients at both stations were estimated. The clocks and atmospheres were modeled as one-hour piecewise-linear (PWL) functions using the default constraints from *nuSolve*. While the median formal uncertainty for the group delay for the VDS sessions is less than three picoseconds (including accounting for the correlation of the group delay and charged particle dispersion (e.g., ionosphere)), the actual scatter is much larger, probably due primarily to unmodeled atmosphere fluctuations. To achieve a chi-square per degree of freedom of ~ 1 , an additional delay of 5–10 picoseconds was added quadratically to the formal uncertainty of each scan. The post-fit delay residuals for the longest VDS session are shown in Figure 3. Outliers greater than 3-sigma after re-weighting were excluded. The weighted RMS value is 6.8 ps.

The length of the baseline between the two antennas is approximately 601 km, oriented northeast-southwest. The residuals of the length estimates about the mean for the thirteen sessions are shown in Figure 4. The durations of the sessions are 1–1.5 hours

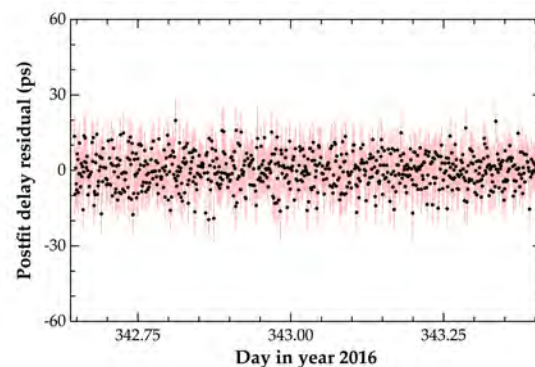


Fig. 3 Group delay post-fit residuals for V15342 after re-weighting.

for all but DOY 328 (five hours) and DOY 342 (15 hours). Possible reasons for the apparent inconsistency in length estimate are discussed in the next section.

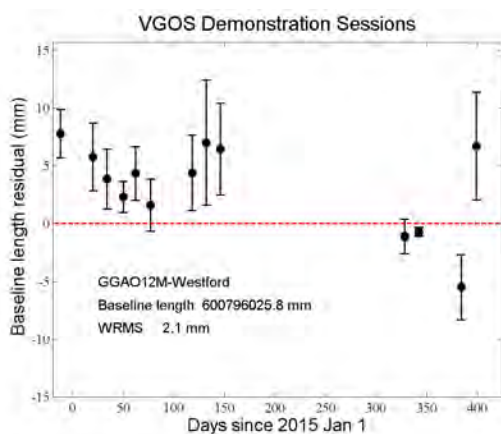


Fig. 4 Length residuals of the 13 VDS sessions.

5 Cable Delay Calibration

A shortcoming in the instrumentation at both sites is the lack of the new cable delay measurement system (CDMS, developed for KOKEE12M) for the cable carrying the 5-MHz reference signal from the maser to the phase calibration generator in the front end. Any variation of delay in this cable would produce an uncorrected variation in the observed delay. If this variation is correlated with antenna position, it may result in an error in the estimated position. The most common problem is for the delay to vary due to cable stretching with motion in elevation or in azimuth (or both). In order to assess the possible magnitude of this effect, the multitone phase delay was measured while moving each antenna in azimuth and elevation (not as part of a VLBI session), with the results given in the following section.

5.1 Westford

A Mark IV cable calibrator was installed at Westford in December 2015 but was not used consistently. However, measurements of the azimuth and elevation de-

pendence of the multitone phase cal delay in a special observing session and measurements of the cable delay for the sessions, where present, indicate that any uncalibrated horizontal position error, and thus baseline length change, is probably less than two millimeters.

5.2 GGAO

In June 2015 (DOY 180) the peak-to-peak variation in multitone phase cal delay was less than 10 ps as the antenna was moved systematically in azimuth and elevation. By November (DOY 322) it was up to 60 ps and reached over 100 ps by the last session reported. The variation in multitone phase cal delay in all bands at GGAO, when corrected for, could possibly change the apparent position of GGAO by up to 10 mm. This degradation in cable stability is inferred to be due to changes in the coaxial cable carrying the 5-MHz reference signal to the phase cal generator, since the large variation decreased to almost zero when that cable was replaced.

A potential method of correcting for this effect is to use the multitone phase cal delay dependence on azimuth and elevation as a proxy for the cable delay measurement, but this has not been evaluated yet.

6 KOKEE12M

The KOKEE12m antenna, funded by the U.S. Naval Observatory, built by InterTronics Solutions, and implemented with the four-band broadband delay signal chain, is the first operational system meeting most VGOS specifications. While the optics are identical to the GGAO 12-m antenna, the Kokee antenna has improved az-el motion and achieves the slew rates of 12°/second in azimuth and 5°/second in elevation that is specified for VGOS-compatible systems. The signal chain, funded by NASA and implemented by MIT Haystack Observatory, evolved from the version that was constructed for the GGAO 12-m antenna but has some improvements, most notably the inclusion of the CDMS and a somewhat wider frequency coverage. Access to frequencies up to 14 GHz is attained through changes in the UpDown Converter and the use of later

versions of the low-noise amplifiers and QRFH feed from Caltech.

KOKEE12M has made broadband observations in several sessions with GGAO12M and Westford. The post-fit delay residuals (without re-weighting) are shown in Figure 5 for one session. See the papers in this volume by Rajagopalan (2016) [5] and by Ruzczyk (2016) [6] for additional information about KOKEE12M.

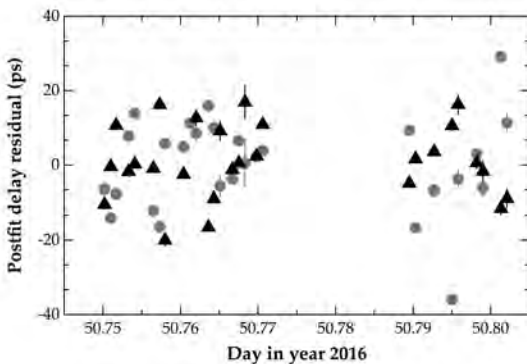


Fig. 5 Post-fit delay residuals for the KOKEE12M-GGAO12M (circles) and KOKEE12M-Westford (triangles) baselines with no re-weighting. The 1-sigma formal delay uncertainties, based solely on signal-to-noise ratio, are indicated by the error bars, most of which are smaller than the symbols. The median uncertainty is less than two picoseconds for each of the thirty-second scans.

7 Plans

Following completion of the KOKEE12M VGOS system, observing will switch to commissioning sessions to develop and demonstrate the capabilities and operations of the new antenna in conjunction with GGAO12M and Westford. A sequence of one-hour sessions, similar to the VDS, will initiate the series, and the duration will increase until several successful 24-hour sessions have been completed.

Acknowledgements

The success of the GGAO12M–Westford VGOS system observations and data analysis is due to the dedication of the entire Broadband Development Group, whom we thank for their efforts in constructing, implementing, and operating the systems at GGAO and at Westford, for participating in the testing and observations, and for development and modification of analysis software: Alex Burns, Mark Derome, Mike Poirier, Jason Soohoo, Sergei Bolotin, John Gipson, David Gordon, Ed Himwich, Katie Pazamikas, and Jay Redmond.

Special thanks go to Bill Petrachenko for his creative ideas, contributions, and continued encouragement.

References

1. Bolotin, S. (2016), Transition to the vgosDb format, *9th IVS General Meeting*.
2. Corey, B.E. (personal communication), (2012): Notes on antenna polarization and VLBI observables (Prepared for 2006 September 15 VLBI2010 workshop; revised 2012 Jan 11).
3. Niell, A. (2015) Status report on observations with the GGAO–Westford VGOS systems, *Proceedings of the 22nd European VLBI Group for Geodesy and Astrometry Working Meeting*. ISBN 978-989-20-6191-7, pages 80–85.
4. Petrachenko, B., Niell, A., Behrend, D., Corey, B., Bohm, J., Charlot, P., Collioud, A., Gipson, J., Haas, R., Hobiger, Th., Koyama, Y., MacMillan, D., Malkin, Z., Nilsson, T., Pany, A., Tuccari, G., Whitney, A.R., Wresnik, J. (2009) Design Aspects of the VLBI2010 System, *Progress Report of the IVS VLBI2010 Committee, NASA/TM-2009-214180*.
5. Rajagopalan, G. (2016) Unveiling the VGOS Signal Chain at the Kokee Park Geophysical Observatory, *9th IVS General Meeting*.
6. Ruzczyk, C. (2016) KPGO 12-m Signal Chain Update, First Light and Beyond, *9th IVS General Meeting*.

The VGOS TWIN Radio Telescope TTW2 at Wettzell

Gerhard Kronschnabl¹, Alexander Neidhardt², Christian Plötz¹, Torben Schüler¹, Jan Kodet²

Abstract The southern Wettzell antenna Ws of the TWIN Radio Telescope Wettzell (TTW), which is compliant with the VLBI Global Observing System (VGOS), is equipped with the Elevenfeed, which offers a continuous frequency range from 2 GHz — 14 GHz. We will present the status of the broadband receiving system and the data acquisition systems installed at the Ws antenna (TTW2) of the Wettzell Observatory. Additionally, the future plans for both antennas of the TWIN radio telescopes Wettzell will be presented.

Keywords TWIN Radio Telescopes Wettzell, Elevenfeed, ring focus antenna, first results

1 Introduction

The Wettzell TWIN radio telescopes, with a diameter of 13.2 meters, are based on the ring focus reflector principle. The antenna design was developed in close cooperation with Vertex Antennentechnik GmbH in Duisburg, Germany, the MIRAD Microwave AG in Switzerland, and the Geodetic Observatory Wettzell (GOW).

The initial idea to use such a type of antenna design is the general specification of the International VLBI Service for Geodesy and Astrometry (IVS) for the new generation of VGOS antennas, which is described in the reports about VLBI2010 [1]. The goal was to find a very agile antenna system which had a relatively small

1. BKG Wettzell, Germany
2. FESG Wettzell, Germany



Fig. 1 TWIN radio telescopes TTW1 and TTW2.

main reflector of about 12 meters with a high system performance over a frequency range from 2 to 14 GHz or even more. In the year 2011, BKG decided to buy a newly developed feed horn from Professor Kildal, the “Elevenfeed”, as the specifications showed it to be the best candidate for the antenna type at Wettzell.

2 The VGOS Ring Focus Antenna TTW2 at Wettzell

The ring focus design was not quite familiar for use as a receiving system in radio astronomy, but it was selected for the TWIN radio telescopes Wettzell because of its performance parameters (see Figure 1). It has advantages for broadband feed horns, such as the Elevenfeed, which usually have a wider flare angle of 65° compared to traditional feeds in geodetic VLBI, such as the existing Radio Telescope Wettzell (RTW), which

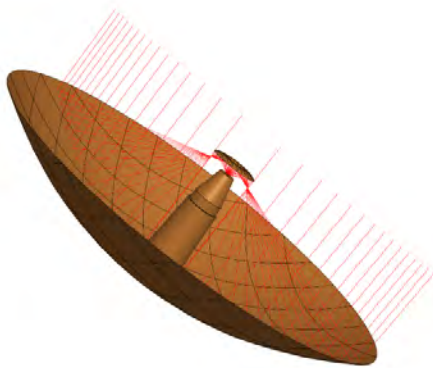


Fig. 2 Ring focus principle (courtesy of Vertex Antennentechnik GmbH).

has a Cassegrain design (22°). The shape of the main reflector of this design is geometrically generated by the offset section of a parabola at the focus line which is rotated at the antenna's axis of symmetry. The result is a main reflector that creates a ring-shaped first focus line in front of the subreflector. Figure 2 illustrates the optical path of rays for such a ring focus design, as it was originally designed. The advantage of this configuration is that all microwaves from the sensitive parts of the main reflector area are focused to the most sensitive region of the feed system. This will enhance the antenna efficiency and minimize backward reflections at the subreflector. But because of this high efficiency, the antenna system has also to deal with higher spill-over effects.

3 The Elevenfeed of the TTW2

The development of the Elevenfeed began at the Chalmers University in Gothenburg in Sweden in the early years of the 21st century. It is a broadband feed with a fixed phase center at the ground plate (see Figure 3). The Geodetic Observatory Wettzell (GOW) ordered a newly built version of this feed that is able to operate at a cryogenic temperature from Omnisys Instruments in Sweden at the end of 2011. The new design offered a better performance at higher frequencies. Unfortunately, the improved version had a worse system temperature, which reduced the benefits of the higher efficiencies. Therefore, some adaptation had to be made, and after several iteration steps, it was

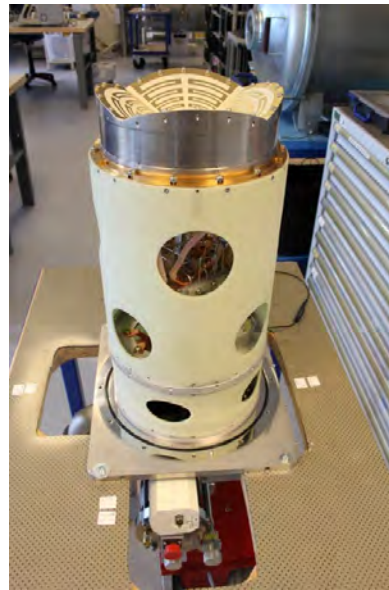


Fig. 3 Elevenfeed front-end (courtesy of Omnisys Instruments).

possible to solve the issues within the last three years [2].

After a successful factory acceptance test at Omnisys Instruments in Gothenburg [3], the front-end of the Elevenfeed was delivered to the GOW in October 2014. Additional tests were performed at the GOW. The front-end system operates smoothly and reliably. In January 2015, a measurement of the complete set of patterns was done in an anechoic chamber at MIRAD AG to get the receiving parameters for an antenna simulation. The test results of the simulation were encouraging, showing efficiencies up to 70% over the whole bandwidth for the used antenna system [4].

Additionally, the measured cross polarization discrimination was roughly 20 dB with some spikes up to 15 dB in horizontal and vertical polarization, which is also a very good result. The measurement of the receiver temperature, which was done at Wettzell using an absorber and the cold sky, showed a T_{rec} of 20 to 25 K almost over the whole frequency range of 2 to 14 GHz.

A new feed cone to mount the Elevenfeed into the antenna was developed by MIRAD AG to enable an easier installation of the feed. An internal rail system supports the mounting of the feed into the feed cone to simplify the feed handling for the personnel doing maintenance. This is advantageous for maintaining the cold head. Furthermore, special attention was laid on

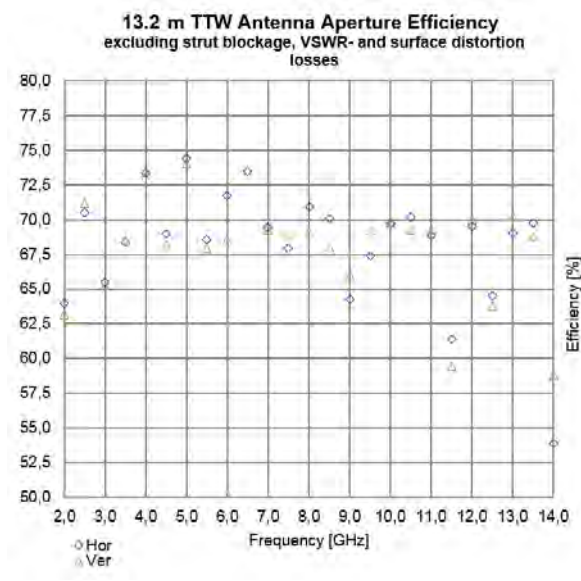


Fig. 4 Calculated aperture efficiency of TTW2.

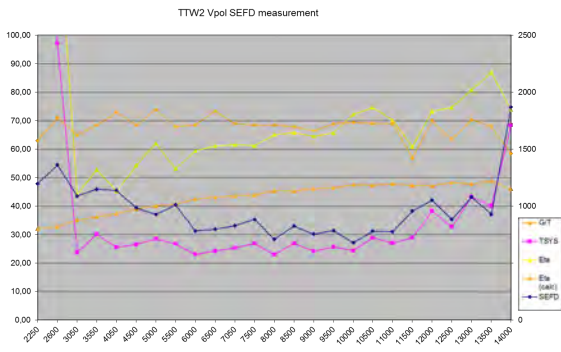


Fig. 5 SEFD, T_{sys} , and Eta measurements.

avoiding icing at the foil window to prevent a ring of ice on the window at low environmental temperatures. For this purpose, a feed blower was installed to blow warm air to the front of the feed window when low outside temperatures and high humidity are detected.

4 Final Test and Measurement Results at the Antenna TTW2

In February 2016, some measurements with radio stars (Cassiopeia A and Taurus A) showed a really good performance for the System Equivalent Flux Density (SEFD), which results in a good system temperature

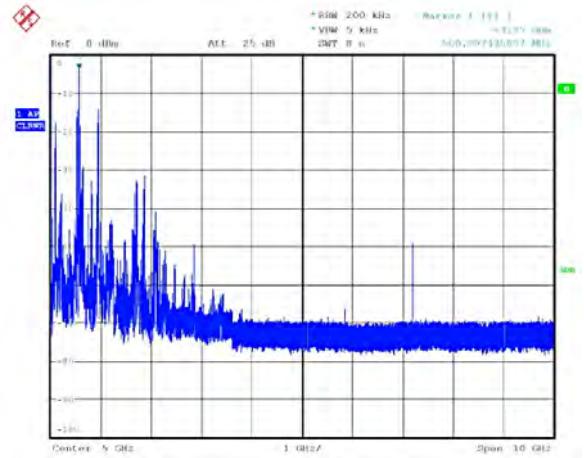


Fig. 6 Spectrum of the horizontal output signal.

and efficiency (see Figure 5). The measurement values at lower and higher frequencies are distorted by Radio Frequency Interference (RFI) from local and extraterrestrial radio transmitters. Therefore, further investigations must be made to get the final performance parameters.

The broadband capability of the feed is as good as modeled. Even at frequencies above 12 GHz a reasonable system performance at all measurements is given. Unfortunately, the lower end of the frequency range is at about 500 MHz, which leads to a high RFI level due to terrestrial TV stations (see Figure 6 at 560 MHz). To avoid a saturation of the post amplifiers, an additional high pass filter was mounted at the LNA outputs.

5 The New Wettzell Phase Calibration Unit

For the use in both TWIN radio telescopes, a new phase calibration (pcal) unit was designed (see Figure 7). The phase calibration box contains all necessary post amplifiers for all bands and polarizations. The noise calibration sources and power dividers for the T_{sys} measurement are included there as well. The pcal tones are adjustable to different intervals and can be locked to different reference frequencies (5 MHz, 10 MHz, and 100 MHz). The box is designed very compactly and is temperature-stabilized.



Fig. 7 Wetzell Phase Calibration Unit.

6 Conclusion and Outlook

The TWIN radio telescope TTW2 at the Wetzell observatory is equipped with the broadband Elevenfeed. The telescope and equipment required is operational for VGOS tests. Initial delays were caused by different issues during the development of the feed and feed mounting. Nevertheless, the performance measurements by the GOW and by MIRAD AG are in good compliance with simulations for all system parameters.

The overall system performance was obtained using reference radio sources at the beginning of this year. The first results presented are promising. After the installation of the new broadband down converter, some first VGOS tests with other stations were planned and already executed while this paper is being published.

References

1. NIELL, A., A. WHITNEY, W. PETRACHENKO, W. SCHLÜTER, N. VANDENBERG, H. HASE, Y. KOYAMA, C. MA, H. SCHUH, G. TUCCARI (2005). VLBI2010: Current and Future Requirements for Geodetic VLBI Systems, IVS WG3 Report, <http://ivscc.gsfc.nasa.gov/about/wg/wg3>, Download 2016-05-13.
2. OLSSON, R., KILDAL, P.-S., WEINREB, S. (2006). The Eleven antenna: a compact low-profile decade bandwidth dual polarized feed for reflector antennas, *IEEE Transactions on Antennas and Propagation*, vol. 54, no. 2, pt. 1, pp. 368-375, Feb. 2006.
3. EKEBRAND, T. (2014). VLBI2010 11 Feed Front-end, Omnisys Instruments, ADUTRP002, Date: 2014-09-05.
4. WIEDLER, R. (2015). Testreport Elevenfeed Strahlungscharakteristik, TER0011_90239500, MIRAD microwave AG, Date: 12.01.2015.

Operating Experience with the Broadband Acquisition System on the RT-13 Radio Telescopes

Evgeny Nosov, Dmitriy Marshalov, Alexey Melnikov

Abstract The Broadband Acquisition System (BRAS) was designed to digitize wideband signals from receivers of radio telescopes, pack the digital samples into VDIF frames, and transmit them through 10G Ethernet interface. The system has been installed at the Badary and Zelenchukskaya observatories on the recently constructed 13-meter radio telescopes (RT-13) in February–March 2015 [1]. Since November 2015, IAA RAS performs regular observations with the RT-13 equipped with BRAS. In addition, BRAS has been used in several international experiments. The paper describes the design of BRAS and its performance and results.

Keywords Digital backend, BRAS, DAS, RT-13, radio telescope, VLBI, Quasar network, Kvizar

1 Introduction

In 2015, the Institute of Applied Astronomy finished constructing a new radio interferometer based on fast-slewing 13-meter antennas built at the Zelenchukskaya and Badary observatories. To compensate for the sensitivity loss caused by the small antenna diameter the recorded signal bandwidth had to be significantly increased. The then-existing narrow-band data acquisition systems like R1002M DAS [2] could not satisfy the new requirements. To equip these new radio telescopes with a wide bandwidth digital backend, IAA RAS has designed the Broadband Acquisition System (BRAS). The system is in operation since the begin-

ning of 2015 and it works on a regular basis in everyday VLBI observations.

2 Structure of the Broadband Acquisition System

BRAS contains eight identical units (wideband channels) that allow to digitize the input signals of 512 MHz bandwidth (Figure 1). Each unit is based on high-speed ADC and low-cost FPGA performing the necessary signal processing. The required Nyquist zone is selected by an input antialiasing filter, with the third Nyquist zone from 1024 to 1536 MHz being the default. Each wideband channel of BRAS outputs data packed into VDIF frames through a 10 Gigabit Ethernet fiber link. BRAS is relatively small in size (one 19" rack with 6U units) and is located in the focal cabin of the antenna close to the receivers. It allows eliminating the transmission of analog signals over a long distance and all related instabilities and performance degradation.

A matrix switch in the receiving system (Figure 2) provides two possible switching modes: S/X and X/Ka. In S/X mode, BRAS digitizes one signal in S-band and three signals in X-band for both right (RCP) and left (LCP) circular polarizations (Figure 3). In X/Ka mode, BRAS digitizes one signal in X-band and three signals in Ka-band, also in both polarizations. The local oscillators of the receiving system allow the frequencies of the wideband channels in all ranges marked in Figure 3. More information about the BRAS structure and performance can be found in [3, 4].

Institute of Applied Astronomy of RAS (IAA RAS)

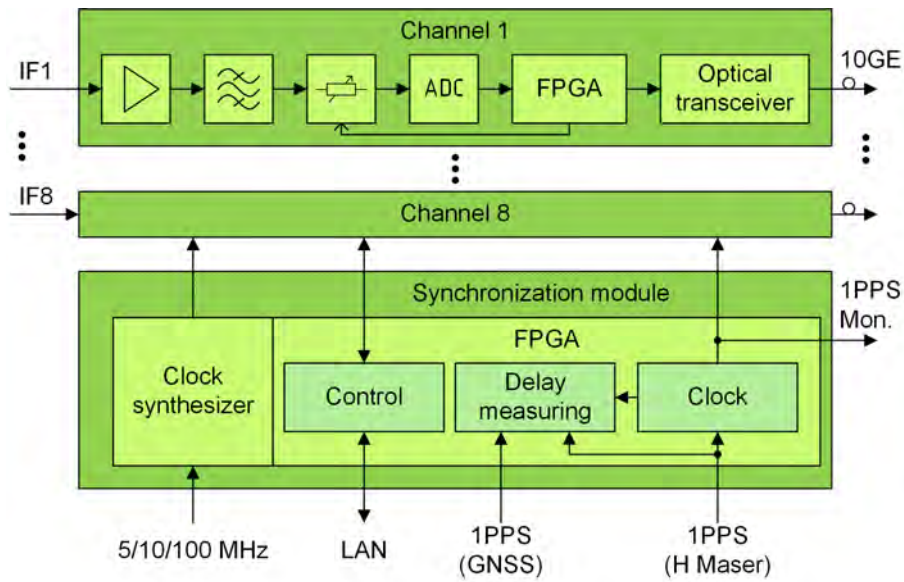


Fig. 1 Structure of the Broadband Acquisition System (BRAS).

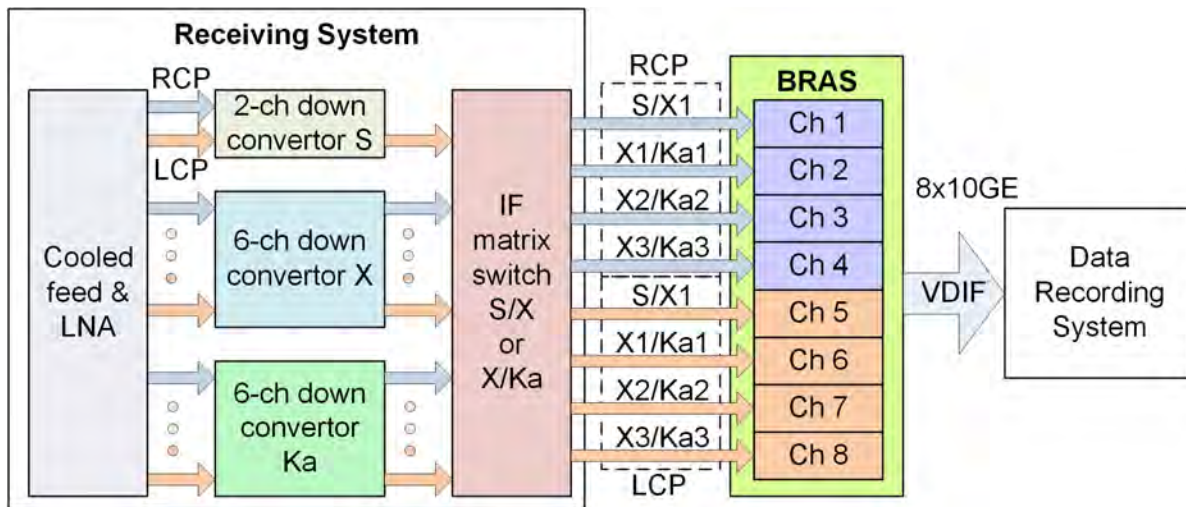


Fig. 2 Signal chain of the RT-13 radio telescopes.

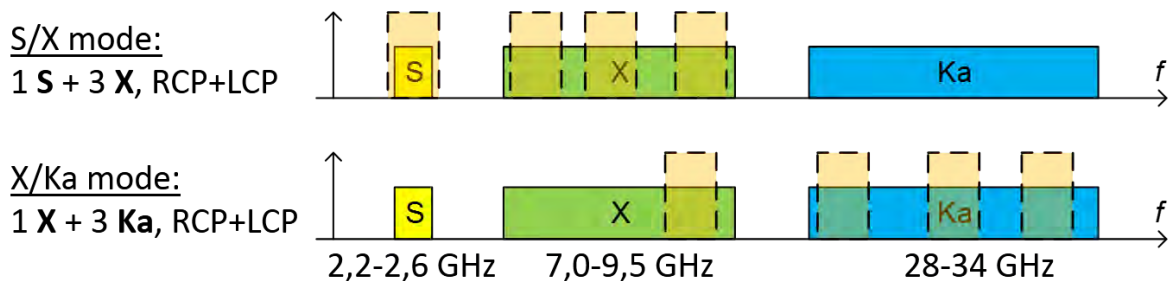


Fig. 3 Switching modes of the RT-13 radio telescopes.

3 System Diagnostics and Signal Analysis Features

Since BRAS is located in the focal cabin and most of the signal processing is digital, it is impossible to use traditional methods of system diagnostics based on indicators and electronic measuring instruments. Instead, BRAS implements a rich set of embedded functions for remote control of the system status and input signal behavior. Along with monitoring the conventional parameters like currents in power circuits, temperatures inside the system, and lock detect signals of the clock synthesizers, BRAS provides the following features:

- Signal power measurement,
- 2-bit sample distribution estimation,
- 1PPS internal-external delay monitoring,
- Input/output (8/2-bits) signal capture, and
- Phase calibration (PCAL) signal extraction.

The signal power measurement is performed in each wideband channel four times per second. The measurements are used to control the signal chain condition and evaluate the system temperature. The estimation of 2-bit sample distribution is convenient for automatic detection of input signal distortions and strong RFI. As an example, Figure 4 represents a 2-bit distribution in S-band measured at Badary observatory with enabled (top) and disabled (bottom) DORIS transmitter. When the DORIS transmitter is disabled, the distribution corresponds to a Gaussian white noise (0.16, 0.34, 0.34, 0.16 with 1σ quantization threshold), while when the DORIS transmitter is enabled the distribution is like sinusoidal (0.25 for each bin).

Another useful feature is the 1PPS delay monitoring implemented in BRAS for the delay measurement between the internal clock of BRAS and the 1PPS signals from the H-maser and the GNSS receiver. Comparing these delays one can detect and isolate failures in the time synchronization system. The accuracy of the time delay measurement is 4 ns. The other two features are input and output (8- and 2-bits) signal capture and PCAL extraction. On request BRAS can capture 1 μ s of input and output signals and send it to the control software so that they can be viewed in the digital oscilloscope and analyzed in the time and frequency domain. Figure 5 gives an example of the power spectral density (PSD) estimated using Fast Fourier Transform and averaging among several realizations of the captured input signal in X-band. This feature is a handy

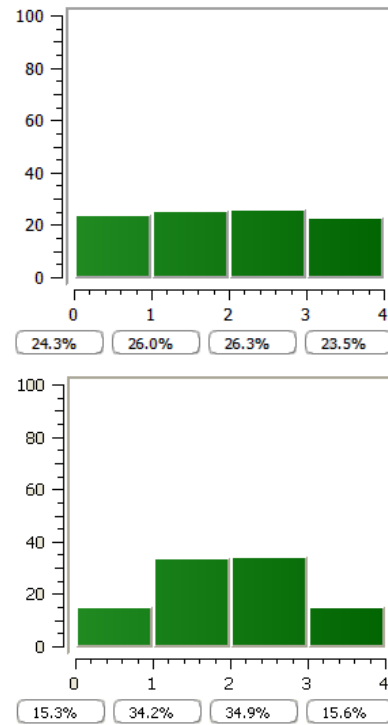


Fig. 4 Measured 2-bit distribution with enabled (top) and disabled (bottom) DORIS transmitter at S-band at Badary.

tool for on-the-fly control of the signal chain condition and their maintenance and repair.

The injection of the PCAL signal into the signal chain not only helps with wide bandwidth synthesis, but it also simplifies hardware debugging. BRAS extracts the PCAL signal by averaging it in one-second intervals. By extracting the PCAL signal from the noise, it is possible to estimate the phases and amplitudes of the PCAL tones and its variation in time as well as the group delay of the PCAL signals for each channel.

4 Observation Results and Conclusions

In the end of 2014, BRAS was tested for the first time with real observations on the RT-32 radio telescopes and fringes were obtained [5]. In the beginning of 2015, it was installed on the new RT-13 radio telescopes and used for their adjustment. On 16 April 2015, BRAS was used in the first VLBI observation with the RT-13 radio telescopes and first

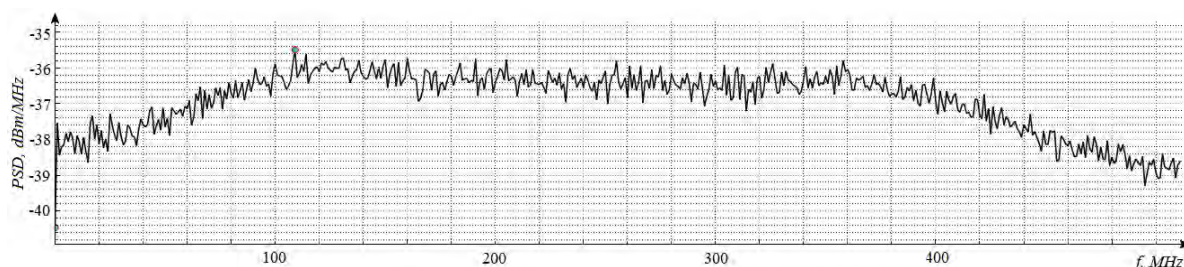


Fig. 5 PSD estimated by using captured input signal in X-band at the Zelenchukskaya observatory.

Mk4/DiFX fourfit 3.11 rev 1142

3C279.ytrcop, No0001, bz
BADAR13M - ZELEN13M, fgroup X, pol RR

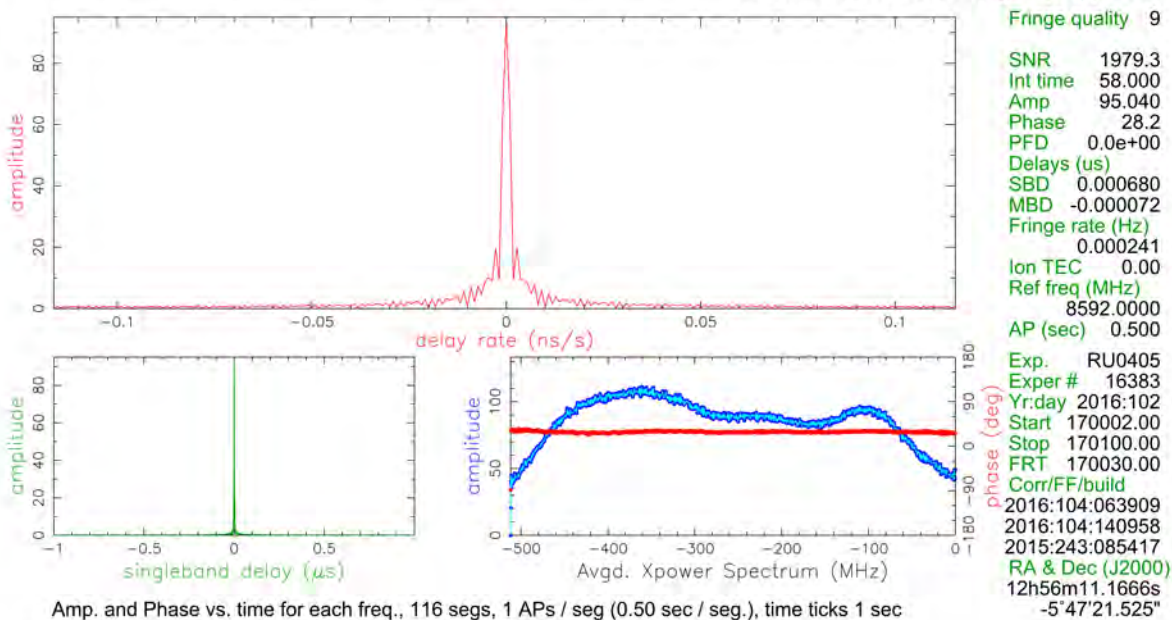


Fig. 6 Fringes found with BRAS on the Badary–Zelenchukskaya baseline in the RU0405 experiment.

fringes were successfully obtained. On 29 April 2015, the first international observations were performed with the Yebes and Wettzell observatories. On 19 May 2015, the official inauguration of the new radio interferometer equipped with BRAS took place during the EVGA 2015 meeting [6]. The recorded data was processed by three correlators: the GPU-based and DiFX correlators of IAA RAS in St. Petersburg and the DiFX correlator of MPIfR in Bonn. During a year of BRAS service, several minor hardware and software bugs were detected and fixed. Figure 6 shows an example of fringes found with BRAS. It is important to point out that compatibility between the BRAS and DBBC systems was confirmed with real observations [7, 8]. Currently BRAS is used on a regular basis in the

day-to-day work. Altogether BRAS was used in about two-hundred international and domestic observations in 2015 and in about 300 observations in the first quarter of 2016.

References

1. A. Ipatov, D. Ivanov, G. Ilin, V. Olifirov, V. Mardyshev, I. Surkis, L. Fedotov, I. Gayazov, V. Stempkovsky, Yu. Bondarenko. “Russian Radio Interferometer of New Generation.”, In: R. Haas, F. Colomer (eds.), Proceedings of 22nd EVGA Working Meeting, 2015, pages 75–79.
2. S.A. Grenkov, E.V. Nosov, L.V. Fedotov, N.E. Koltsov. “A Digital Radio Interferometric Signal Conversion System.”,

- Instruments and Experimental Techniques, Vol.53. No.5, 2010, pages 675–681.
3. N.E. Koltsov, D.A. Marshalov, E.V. Nosov, L.V. Fedotov. “A data acquisition system of the S/X-wave range of the radio interferometer for the universal time on-line monitoring.” *Instruments and Experimental Techniques*, Vol.56, No.3, 2013, pages 339–346.
 4. E. Nosov, A. Berdnikov, S. Grenkov, D. Marshalov, A. Melnikov, L. Fedotov. “Current Development State of the Russian VLBI Broadband Acquisition System.” *IVS 2014 General Meeting Proceedings*. Science Press, Beijing, China, pages 82–85.
 5. D.A. Marshalov, A.S. Berdnikov, S.A. Grenkov S.A., A.V. Krohalev, E.V. Nosov E.V., L.V. Fedotov, A.V. Shemanaev. “The results of Preliminary Tests of Broadband Digital Conversion System for Radiotelescopes” . *IAA Transactions*. Issue 32. St.Petersburg, 2015. Pages 27–33.
 6. V. Ken, I. Surkis, Y. Kurdubova, A. Melnikov, N. Mishina, V. Mishin, V. Shantyr. “IAA VGOS GPU-based Software Correlator: current status and broadband processing.” In: R. Haas, F. Colomer (eds.), *Proceedings of 22nd EVGA Working Meeting*, 2015, pages 40–42.
 7. A. Neidhardt, P. De Vicente, A. Hellerschmied, D. Mayer, A. Melnikov, C. Plötz, G. Kronschnabl, “First results of the FAST-S/X-sessions with new VGOS antennas.” In this proceedings.
 8. A. Melnikov, P. De Vicente. “First 2 Gbps observations between KVAZAR VGOS antennas and Yebes RAEGE antenna.” In this volume.

Session 2: VGOS Strategies and Expected Results



March 2016 · Johannesburg · South Africa

Delay and Phase Calibration in VGOS Post-Processing

Roger Cappallo

Abstract In recent years, large amounts of data have begun to flow through the VGOS pipeline, and significant real-world issues are now being encountered in the fringe-fitting process. In order to create a high-quality geodetic observable it is important to minimize the sensitivity of the group delay to instrumental parameters that may change over time, while at the same time maximizing the amount of information that is extracted. This paper addresses a number of topics relevant to those goals, such as matching of delays in polarization products and receiving bands, and coherent phasing of the four polarization products. We describe the software that automates the somewhat tedious determination of the calibration parameters. The ionosphere is highly correlated with the group-delay observable, so its accurate characterization and removal are central to the determination of the calibration parameters.

Keywords VLBI, calibration, ionosphere

1 Introduction

The VLBI Global Observing System has been many years in development, but only relatively recently has it started to generate appreciable quantities of data. Its wide spanned bandwidths, dual-linear polarization, and the desire to push the envelope on short, and thus weak, observations lead to added complexity during the post-processing stage. It is necessary to exercise extra diligence during the post-correlation processing, with additional calibration steps inserted, in order to ensure

MIT Haystack Observatory

that a minimum of information is lost from the raw observations.

2 Characteristics of the Observations

The RF spectrum of the VGOS system spans about 10 GHz, and it is split into four bands, each of 512-MHz width. In turn, each of those bands is further broken into sixteen 32-MHz channels, with eight in each linear polarization. Thus there are a total of $4 \times 8 = 32$ channels in each of the four polarization products (XX, YY, XY, and YX) that are produced by the correlator. The VGOS system uses a series of phase-calibration tones, which are separated by 5-MHz intervals. The principal use of these tones is to remove instrumental differences in channel phase incurred in the signal path between the receiver and the samplers. A secondary purpose, though, is to adjust for inter-channel variability in delay. This is done in the fourfit program by (in essence) seeing how the phase within each channel varies as a function of tone frequency.

3 Pseudo Stokes-I Mode

In order to extract the most accurate group delay estimate from the four polarization products coming from the correlator, it is desirable to coherently combine them in a single fit, yielding a single estimate of the group delay. In principle, it would be possible to have no fringes detected in any one of the four products, but to still have detectable fringes in their coherent sum. A formulation for combining the products was given

by Corey (2011), producing a quantity similar to the Stokes intensity, or I, product:

$$I = (\overline{X_a \star X_b} + \overline{Y_a \star Y_b}) \cos(\Delta p) + (\overline{X_a \star Y_b} - \overline{Y_a \star X_b}) \sin(\Delta p) \quad (1)$$

where Δp is the differential parallactic angle between sites a and b , and $\overline{X_a \star Y_b}$ is (for example) the time-averaged correlation product of site a 's X polarization with site b 's Y polarization. The trigonometric functions of the parallactic angle difference account for the projection of the linear polarizations into one other.

4 Optimal Determination of Polarization-dependent Phase and Delay Offsets

The combination of the four polarization products into a single Stokes-I observable without too much loss of signal-to-noise ratio (snr) due to insufficient coherence (see Figure 1) requires matching of both residual phase and delay. Two products will suffer at most a 1% decoherence if either of two conditions are true:

- the phases differ by 8° , and
- the multiband (group) delays differ by 10.2 ps. This corresponds to a slope in the phase vs. frequency relation, and causes a peak-to-peak phase change

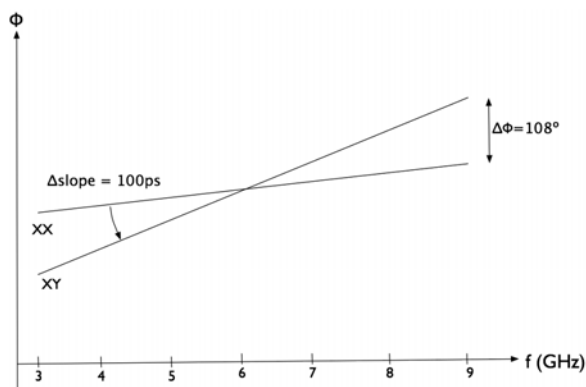


Fig. 1 Example of mismatching residual group delays between two polarization products, which leads to reduced coherence across the VGOS observing range. In this extreme example, the data near the ends of the range are actually anti-correlated with the bulk of the data, and would reduce the fringe amplitude.

of 28° across the current VGOS RF bandwidth of 7.65 GHz.

These values, 8° and 10 ps, should be considered as upper bounds in the allowable discrepancy between polarization products prior to coherent combination.

4.1 Fourphase

In order to accommodate the phase and delay offsets, the *fourfit* program has been modified to allow both a phase and a delay offset between the two polarizations at each station. These offsets must be set for an observing session to values that ensure the coherence of all four polarization products going into the fringe fits. A new program, *fourphase*, has been written to automate the process of finding the offset phase and delay values. It does so by going through the following steps:

1. On each baseline, such as baseline ab in Figure 2, a single value of the differential TEC, or ΔTEC , of the ionosphere is found by performing fringe-fitting ionosphere searches on each polarization product, and then applying snr-based weights to find the optimal value of ΔTEC for that baseline.
2. The baseline ΔTEC values are then used in a weighted least-squares fit to find an optimal set of (relative) station-based TEC values.
3. Each baseline then has four fringe-fits (one per polarization product) performed using the TEC estimates from Step 2. This produces output data consisting of a multiband delay, a phase, and an snr for each of the four products. For n stations, this step produces $2n(n-1)$ phases and delays.
4. Using the data from Step 3, a global weighted least-squares solution for the Y offsets relative to X (e.g., $Y_a - X_a$) in both delay and phase is produced for each of the n stations.
5. For convenience, a *fourfit* control file is written out, with the delay and phase parameters that were found in the least-squares fit of Step 4.
6. Based upon the new values for the parameters, new fringe fits are performed and various statistical quantities are calculated to verify that the fitting process was successful.

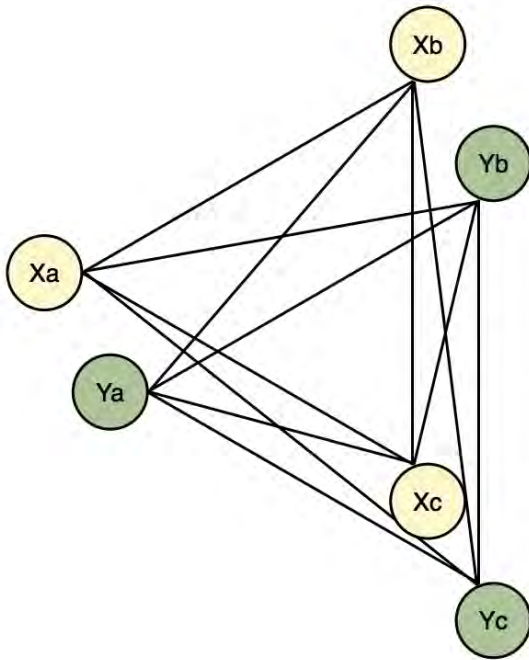


Fig. 2 An example of the geometry of the phase and delay offset fitting process in the three-station case. Stations a, b, and c, each have two polarizations (e.g., X_a and Y_a), and each baseline has four polarization products (e.g., $X_a Y_a$, $Y_a Y_b$, $X_a Y_b$, $Y_a X_b$) that are measured.

5 The Effect of the Ionosphere

In the VGOS system, due to the multiple bands, wide RF spanned bandwidth, and the desire to allow observations with low snr, the ionosphere is estimated and removed at fringe-fit time, rather than later during database creation (for details on the algorithm employed, see Cappallo, 2014). Briefly, the fringe fit in *fourfit* is performed by finding that group delay which maximizes the coherent sum over time and frequency of the fringe phasors residual to the correlator model. When the ionosphere is fit, *fourfit* simply and robustly searches over a grid of potential differential ionosphere TEC values, in order to find the maximum coherent phasor sum. This trial value is then improved by iteration on finer grids, followed by a parabolic interpolation of the gridded values. This method of finding the maximum coherent sum with respect to the group delay has been shown to be equivalent to using least-squares estimation in the region of the maximum.

5.1 Correlation of the Ionosphere with the Multiband Delay

Despite the wide distribution of the observing bands, the differential TEC parameter is still highly correlated with the group-delay estimate. For that reason we determine the errors in the delay and TEC estimates by performing a covariance analysis using linear least squares. Let us model the observed phase as a function of frequency as follows

$$\phi(f) = \tau_g * (f - f_0) + \phi_0 - 1.3445/f * \Delta TEC \quad (2)$$

where:

- ϕ phase (rot)
- f frequency (GHz)
- f_0 *fourfit* reference frequency (GHz)
- τ_g group delay (ns)
- ΔTEC differential TEC (TECU $\equiv 10^{16}/m^2$)
- ϕ_0 phase at f_0 (rot)

The constant phase parameter, ϕ_0 , might be usefully estimated at a variety of reference frequencies. In the future, it is possible that the broadband system will use phase delays referenced to a constant phase at DC. For now, though, *fourfit* currently performs a group-delay fit to the slope of phase vs. frequency just over the RF region of the frequency channels that were employed, and it produces a group delay along with a phase at a centered reference frequency. *fourfit's* algorithm, which maximizes the coherent sum of the counter-rotated phasors, has the effect of solving for the mean phase over the sampled frequency channels. The reported standard deviation for the phase is simply $1/snr$ radians. This standard deviation needs to be adjusted if the reference frequency is not equal to the mean frequency, as there is then a term taking into account the uncertainty in the group delay, multiplied by the difference between the reference frequency (at which the phase is reported) and the mean frequency of the sequence.

By performing a covariance analysis using the phase model in Equation 2, we find that the current VGOS observing frequency sequence leads to a correlation coefficient of 0.93 between τ_g and ΔTEC . This somewhat ill-conditioned state of affairs can be seen graphically in Figure 3, which shows an idealized noise-free case of fringe amplitude as a function of ΔTEC and τ_g . The irregular frequency spacing of

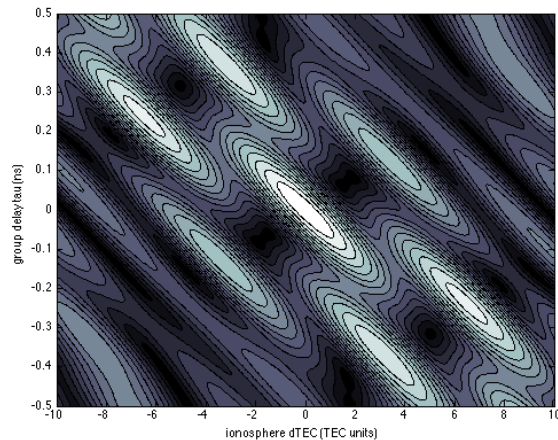


Fig. 3 Fringe amplitude as a function of differential TEC (ΔTEC) and group delay (τ). Synthetic data based upon the current VGOS frequency sequence with a flat spectrum and no added noise were used.

channels results in islands of coherence, of which the central peak is the highest. The diagonal elongation demonstrates how a modest amount of added noise might cause a large shift in τ and an offsetting shift in ΔTEC along the preferred symmetry axis.

$$\sigma_{mbd} = 1 / (2\pi \cdot f_{rms} \cdot snr) \quad (3)$$

The previous *fourfit* group delay error calculation (see Equation 3), did not take the ionosphere into account, and was based solely upon rms spanned bandwidth and snr. As such, it was an underestimate of the true error, as it did not take into consideration the extra degree of freedom introduced by the ionospheric TEC. We find that the estimate of the VGOS group-delay standard deviation increases by about a factor of about 2.6 when the ionosphere is simultaneously estimated.

6 Conclusions

The process of determining appropriate phase and delay offsets for each VGOS station certainly makes the job of post-processing more complex, but it is unavoidable. Software has been written to ease the burden. On the other hand, solving for the ionosphere does not add to the serial complexity of the post-processing operations, but it is fairly demanding in terms of computing resources. When the ionosphere is solved for, it is essential that the group delay error properly reflects the added uncertainty due to the ionosphere fit.

Acknowledgements

Arthur Niell, Bill Petrachenko, and Brian Corey took part in discussions that produced significant ideas related to this work.

References

1. Brian Corey, private communication, 2011.
2. Roger Cappallo. Correlating and Fringe-fitting Broadband VGOS Data, in International VLBI Service for Geodesy and Astrometry 2014 General Meeting Proceedings, edited by D. Behrend, K. D. Baver, and K. L. Armstrong, 91–96, 2014.

How to Register a VGOS Radio Telescope at ITU and Why It Is Important

Hayo Hase¹, Vincenza Tornatore², Brian Corey³

Abstract VGOS radio telescopes enable observations in the range of 2–14 GHz and are much more receptive for unwanted radio frequency interference. Some spaceborne transmitters may cause detrimental radiation to VGOS receivers. The registration of new VGOS sites at ITU is important for obtaining administrative protection. This may help to avoid direct illumination by strong radars. This paper introduces the risk of damage and explains the registration procedure.

Keywords VGOS, spectrum management, RFI, SAR radar, ITU registration

1 The Problem: Satellite Signals are Strong

VGOS radio telescopes with wideband feeds are receptive to radiation at least in the spectral range between 2 and 14 GHz. In this range we find some very small spectral bands which are protected for radio astronomy use, but the majority is used by other (commercial and military) applications.

Radio frequency interference (RFI) is a threat to VLBI observations, because affected observations will not produce fringes in the correlation or will result in lower SNR and hence less accuracy.

If a detected RFI source is local, that means it is located at the observatory site, and it should be possible to identify and eliminate its origin (e.g., a WLAN

device). If the RFI source is external, it can be either ground based (e.g., telecommunication transceiver) or space based (e.g., satellite transmitter). RFI can be picked up by the antenna sidelobes or by accidentally pointing directly at the RFI source.

Problematic RFI signals have much higher power levels than the expected quasar radiation for which the very sensitive wideband receivers are built. In general strong radio signals have to be avoided in the reception in order not to damage the receiver amplification chain, in particular, the low-noise amplifier (LNA), which is the first and most sensitive amplifier following the antenna feed. Wideband VGOS radio telescope systems are much more exposed to unwanted RFI radiation than the narrow band legacy S/X systems.

During recent years satellite based radars became popular in Earth Exploration Satellite Systems (EESS). Table 1 lists some satellite missions with strong transmitters. Synthetic Aperture Radars (SAR), which have some of the highest power transmitters, use microwaves to map the Earth, independent of cloud coverage. Applying interferometry to radar images of different epochs, areal deformations can be made visible.

In order to coordinate the use of the microwave spectrum among space agencies, the Space Frequency Coordination Group (SFCG) was founded. Its mission statement reads: “SFCG is the pre-eminent radio-frequency collegiate of Space Agencies and related national and international organizations through which global space systems spectrum resources are judiciously husbanded for the benefit of humanity.” (Read more at <https://www.sfcgonline.org/About/default.aspx>).

At the conference SFCG-31 document SF31-9DR1 on the “Potential Damage to RAS Sites by EESS (Ac-

1. Bundesamt für Kartographie und Geodäsie

2. Politecnico di Milano

3. MIT Haystack Observatory

Table 1 Overview of satellite missions with active sensors in the VGOS wideband frequency range of 2–14 GHz (excerpt from Table 4 in [2]).

Frequency Band [GHz]	Bandwidth [MHz]	Missions carrying spaceborne active transmitters			
		SAR	Alti-meter	Scattero-meter	Precipi-tation radar
3.100–3.300	200	ALMAZ	•	•	•
5.250–5.570	320	Radarsat, ERS, Envisat, RISAT, Sentinel-1	Topex, Jason	ERS-2, MetOp	•
9.500–9.800	300	Cosmo-SkyMed, TerraSAR-X	•	•	•
13.250–13.750	500	•	Topex, Jason, ERS, Envisat	QuikSCAT, Envisat	TRMM

tive)” [2] was presented by NASA, providing calculations of the power levels received from EESS transmitters vis-à-vis damaging power levels given in Report ITU-R RA.2188 [4]. The SFCG-31 report [2] compares the power flux density (PFD) levels of EESS with the damage levels for radio astronomy receiving systems (Table 2). The Radio Astronomy Services (RAS) damage level is determined by the most sensitive telescopes, typically 100 m in diameter.

Satellite radiation has the potential to damage the receiver LNAs at large radio telescopes, as seen by the negative RAS margins in three of the four cases in Table 2.

The VGOS radio telescope reflectors are typically 13.2 m in diameter and therefore less sensitive than a 100-m RAS telescope. With a VGOS antenna efficiency of about 80%—versus 50% of legacy systems—the PFD threshold for VGOS radio telescopes can be calculated to be -40 dB(W/m²) instead of -60 dB(W/m²) for 100-m radio telescopes, where an LNA damage threshold of 10 mW is assumed in both cases. The calculation of PFD VGOS damage level PFD_{VGOS}^{dl} for a 13.2-m radio telescope is:

Table 2 Comparison of typical EESS power flux densities at the Earth’s surface with RAS and VGOS damage thresholds (excerpt from Table 8 in [2] with information added for VGOS).

Parameter	Sensor type			
	SAR	Altimeter	Scattero-meter	Precipita-tion radar
Radiated power [W]	4400	20	4000	1013
Antenna gain [dB]	36.4	43.3	34	47.7
Orbital altitude [km]	225	1396	785	400
Incidence angle [deg]	21	0	32	0
PFD [dB/(W/m ²)]	-45.8	-77.2	-50.4	-45.3
RAS PFD damage level [dB/(W/m ²)]	-60	-60	-60	-60
Margin RAS	-14.2	+17.2	-9.6	-14.7
VGOS PFD damage level [dB/(W/m ²)]	-40	-40	-40	-40
Margin VGOS	+5.8	+37.2	+10.2	+5.3

$$\begin{aligned}
 PFD_{VGOS}^{dl} &= \frac{P_{LNA}^{dl}}{A_e} = \frac{P_{LNA}^{dl}}{\eta_A \cdot \pi \cdot R^2} \\
 &= \frac{0.01 \text{ W}}{109 \text{ m}^2} = 0.000091 = -40 \text{ dB(W/m}^2\text{)}
 \end{aligned}$$

where

P_{LNA}^{dl} is the LNA input power that causes damage

A_e is the effective area of the radio telescope

η_A is the antenna efficiency ~ 0.8

R is the radio telescope radius.

The VGOS threshold level of -40 dB(W/m²) is fortunately above the EESS radiation level, i.e., the VGOS margins in the last line of Table 2 are all positive. But some of the margins are small. There will be a potential danger if future radar systems are equipped with stronger transmitters or flown at lower altitude.

These margins are estimated assuming the satellite and VGOS antennas point directly at each other. While such an occurrence is unlikely, the consequences of even a momentary mutual alignment of their beams would be serious if the satellite PFD exceeded the LNA damage threshold. It is not necessary for a VGOS antenna to track a satellite to cause a problem. Even momentary exposure when a satellite passes through a stationary VGOS beam or when a VGOS antenna points at a satellite as it slews from one source to another

could damage the LNA. For example, a satellite at 500 km altitude will pass through the main beam of a stationary VGOS antenna in 0.1 to 1 second, depending on frequency. That time scale is long compared with typical LNA thermal time constants. As a result the LNA will suffer as much damage as if the exposure lasted much longer.

EESS have typical repetition periods of two days to two weeks. That means that the VGOS observatories are being observed again and again from space and hence exposed to radiation from satellites. In order to minimize the risk of losing VLBI observations or eventually receiving equipment, it is advised to register the VGOS radio telescope at the International Telecommunication Union (ITU).

The ITU-Regulation RA.2188 report [4] lists two options for avoiding LNA damage: (a) blanking satellite transmitters so they do not transmit toward RAS sites and (b) not allowing a VGOS radio telescope to be pointed at a satellite transmitter. The latter option is neither implemented yet at stations, where most often the survival position is the zenith position, nor in the VGOS scheduling process, which could check for satellites crossing the line of sight of the radio telescope. A third option is adding diode limiters at the LNA input to limit the voltage seen by the active components. Whether this is feasible for a specific LNA will depend on its characteristics.

Space agencies are using the ITU list of radio telescope sites for planning of their observation schedule and may respect or even get in contact with a radio telescope site, if a space maneuver will illuminate a radio telescope site. If a VGOS radio telescope site is not listed as sensitive receiving infrastructure at ITU, it might be difficult to claim losses due to RFI or to complain to the responsible space agency.

2 A Partial Solution: Get Registered at ITU

The ITU is the United Nations specialized agency for information and communication technologies. It is allocating global radio spectra and satellite orbits and developing the technical standards that ensure that networks and technologies seamlessly interconnect. The administrations operating radio astronomy stations may register them with the Radiocommunication Bureau (RB) of ITU.



Fig. 1 Artist's view of a damaged frontend of a radio telescope being hit by too strong transmission power of a SAR transmitter.

It is important to point out that at the ITU the (passive) radio astronomy service is recognized with an official status. There is no geodetic VLBI service known at ITU. Although the IVS programs observe quasars primarily for geodetic applications with geodetic observatories, from the perspective of the ITU it is a radio astronomy service.

ITU is used to dealing with dedicated portions of spectral ranges over the entire electromagnetic spectrum [1]. The VGOS frequency range from 2 to 14 GHz is full of such portions of spectral bands. Each band has allocated primary and secondary uses. Radio astronomy services have some allocated spectral bands as primary in which astronomers are observing spectral lines of atoms and molecules in the universe. Those allocated bands for RAS are protected and should not be interfered by other users, not even by out-of-band emissions of transmitters from adjacent bands. The RAS bands are usually different from those of the EESS.

Unfortunately, VGOS came up too late to claim the entire 2–14 GHz range for the exclusive use of VLBI. It is only possible to register a new site for the existing portions of bands allocated for RAS, which fall into the 2–14 GHz range.

As the VGOS range covers many RAS bands, VGOS radio telescopes may be registered as RAS sites. A registered RAS site should then be protected from strong signals according to RAS bands and other bands where footnotes in the regulations apply in favor of RAS.¹

¹ Although protected, the trend of using the limited number of available bands is band-sharing. In regions where there is no suitable RAS observatory, the protected bands might be made avail-

Registration of radio astronomy stations (VGOS observatories) must take place through the telecommunications authority of the national administrations. The required characteristics of the radio astronomy station (kinematic and receiving parameters) are described in Annex 2 of Appendix 4 of the Radio Regulations (RR) [3]. Before starting the registration process the most recent version of the RR should be consulted, because parts of them are continuously updated according to the outcome of the World Radio Conferences (WRC).

The advantages of being registered are:

1. Several footnotes in the Radio Regulations provide protection to radio astronomy stations from unwanted emissions by satellites.
2. Examining a satellite system for compliance with footnotes, the Radiocommunication Bureau will consider only registered radio astronomy observatories.
3. Establishing a chronological priority for the registered station. It may claim protection from unwanted emissions of satellite systems filed for operation in adjacent or nearby bands at a later date.
4. Producing awareness of the national authorities about your protection-worthy RAS.

However, registering with ITU is far from a full solution, because it protects stations only in the RAS bands, but EESS generally transmit outside the RAS bands. Therefore the previously mentioned option (b) of not allowing a VGOS radio telescope to be pointed at a satellite transmitter should also be considered for VGOS network stations. This requires information on the geographical locations of the satellite beam ground tracks (or on satellite positions if the emission is at a constant nadir direction). This information is available at the space agencies which operate the satellites. If the satellite transmission cannot be stopped over a VGOS site, we propose that satellite operators study the feasi-

able to other users. Band-sharing is not only restricted to regions, but also in time. If an observatory does not observe, the protected bands might be used otherwise.

bility of providing a 24h/7d dedicated beam alert system service which may interact directly with the antenna control unit of the VGOS radio telescope to avoid detrimental illuminations.

3 Summary

The ITU registration gives administrative protection. The following steps are necessary:

- Contact your national telecommunication administration.
- Supply to the national authority the information required for the ITU registration of the VGOS radio telescope according to the recent Radiocommunication Regulations.
- Check via the national telecommunication administration about the successful registration at ITU.

For protection against detrimental illuminations of VGOS radio telescopes by satellite radar systems, we propose to study the feasibility of a satellite beam monitoring system service that could be provided by the satellite operating space agencies.

References

1. Handbook on Radio Astronomy, 3rd edition, Radiocommunication Bureau, ITU, 2013.
2. NASA: Potential Damage to RAS sites by EESS (Active), (SFCG Action Item 30/8), SFCG-31, San Francisco, CA, USA, 7-15 June 2011 <https://www.sfcgonline.org/Public%20Documents/SF31-09DR1.pdf>.
3. Radio Regulations Appendices, ITU, 2012.
4. Power flux-density and e.i.r.p. levels potentially damaging to radio astronomy receivers, Report ITU-R RA.2188, (10/2010) RA Series, Radio astronomy <https://www.itu.int/pub/R-REP-RA.2188-2010>.

Implementation of the VGOS Trials

Dirk Behrend, Cynthia Thomas, Ed Himwich

Abstract In February 2014, the VGOS Project Executive Group (VPEG) presented the VGOS Observing Plan, which outlined possible steps on how to go from initial VGOS broadband tests to intermediate observing scenarios to the fully operational VGOS system. The document introduced VGOS trial campaigns as the initial means to accustom the VGOS stations as well as the subsequent component types to the VGOS processing load: scheduling, data taking, data transport, correlation, and analysis. Three different trial campaigns of six to eight weeks each were envisioned. The Coordinating Center—in conjunction with the Observing Program Committee (OPC)—was tasked with their implementation. This paper describes the progress made on implementing the trial campaigns.

Keywords VGOS, trial campaigns, pilot project

1 Introduction

The technical development of the VLBI Global Observing System (VGOS) has made good progress in the past several years. While the progress was not as fast as anticipated, the development has now reached a point where VGOS can gradually be phased into operations. That is, in addition to the activities of the technology development groups, under the supervision of the VGOS Technical Committee (VTC), now other parts of the IVS are getting involved. The VGOS Project Executive Group (VPEG) prepared the VGOS Observing Plan [1] in February 2014 outlining the various

NVI, Inc.

phases of the VGOS implementation for operational work. The various stages go from broadband tests, to VGOS trial campaigns, to a pilot project, and eventually to full VGOS operations. In this paper we focus on the implementation of the VGOS trials, but we will also cover the other stages to some degree. The implementation task was given to the Coordinating Center and the Observing Program Committee (OPC). The following summarizes the state of affairs as of early 2016.

2 VGOS Broadband Test Sessions

Starting in calendar year 2015, test sessions were organized on the baseline Westford to Goddard using the installed broadband signal chains at both sites. These sessions were initially one-hour long and were observed every two weeks. After gaining some experience with and steadily improving the system, the observing time was increased to two hours, then to six hours, and, eventually, to a full 24-hour session. The two-week rhythm was only interrupted to perform necessary repairs at the antennas (e.g., azimuth motor repair at the GGAO12M telescope at GSFC). These test sessions are being continued in 2016; the network will be expanded to include new telescopes as they become available: Kokee Park, Wettzell, Yebes, and Ishioka.

3 VGOS Trial Campaigns

The main purpose of the trial campaigns is to evaluate and improve aspects of VGOS operations [1]. In order to properly assess the sustainability of all as-

pects of operations, each trial will have six observing weeks ensuring the completion of a full operational cycle for ‘*schedule – acquire – ship/transmit – correlate/process/analyze – ship/transmit*’ without backlog. There will be a break of two months between successive trials, which will allow time to compensate for an eventual backlog, to assess performance, to recommend improvements, and to prepare for the subsequent trial [1].

3.1 Observing Scenarios

In the VGOS Observing Plan [1], three trial VGOS campaigns are foreseen to be observed:

- **Trial 1:** *Sustained weekly 24-hour sessions.*
 - all available VGOS stations,
 - optimized for very fast slewing,
 - observe on Sunday (to foster unattended observing),
 - observe UT days (0–24 UT),
 - ship modules.
- **Trial 2:** *Sustained daily VGOS EOP sessions.*
 - all available VGOS stations,
 - optimized for very fast slewing,
 - daily sessions with reduced duty cycle (four one-hour bursts per UT day),

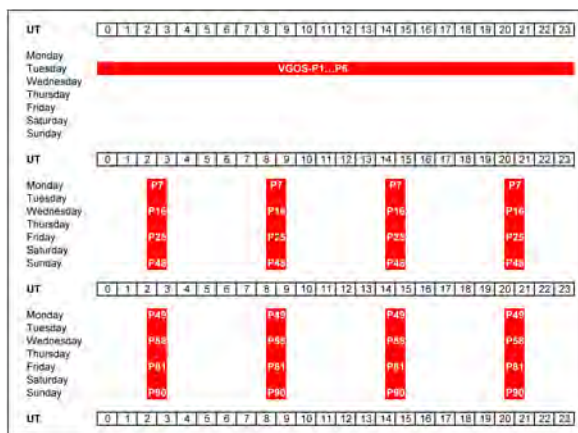


Fig. 1 Observing scenarios of the VGOS trial campaigns: Trial 1 (upper panel), Trial 2 (middle panel), and Trial 3 (lower panel). The naming of the one-hour bursts indicates the grouping of the individual sessions. For instance, session VGOS-P25 consists of four one-hour bursts to be observed on a Friday. It is anticipated that altogether 90 sessions will be observed in the three VGOS trials.

- observe UT days (0–24 UT),
- ship modules.
- **Trial 3:** *Sustained daily VGOS EOP sessions with timely transmission of data.*
 - same as Trial 2 but...
 - e-transfer of data as much as possible.

The observing scenarios for all three trials are depicted in Figure 1. Unlike initially planned, Trial 1 will be observed as a UT-day on a weekday (not Sunday) and every two weeks (as opposed to every week) until six 24-hour sessions have been observed.

The move to a weekday is due to the fact that the automation of the observing procedures is not advanced enough to allow for unattended observing. Further, the now planned Tuesday may be changed to Wednesday enabling Westford (and possibly other stations) to participate in the R1 sessions. This allows the VGOS stations to be tied to the existing legacy network.

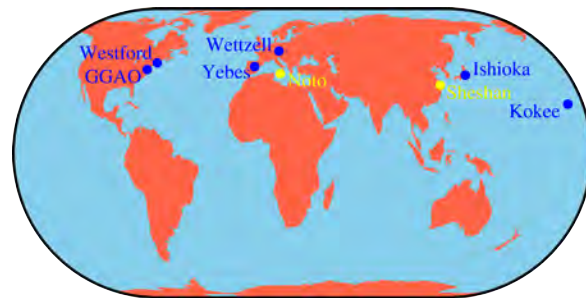


Fig. 2 Network of the VGOS trials. The three trial campaigns will be observed on the network Westford, GGAC, Wettzell, Yebes, Ishioka, and Kokee. The VGOS stations at Noto and Sheshan are not available yet. Other stations may be added if they become available on time (e.g., Santa María or the AuScope stations).

Because of observing only every other week for a total of six sessions, Trial 1 will take twelve weeks (three months) to complete. For the subsequent trial campaigns the decision has not been made on whether weekly or bi-weekly observing will be used. At this point in time, weekly observing is favored, as it is closer to the final VGOS operations.

Trial 2 and Trial 3 observe four hours per day every day of the week. Their only difference lies in the way the data are transmitted from the stations to the correlator: physical shipment of recording modules is replaced as much as possible by electronic data transfer.

3.2 Network

The network for the VGOS trial campaigns was anticipated to consist of eight stations (Figure 2). Two stations (Noto and Sheshan) will not be ready for the first trial campaign and will likely not be ready for the two subsequent ones either.

The VGOS stations currently planned to observe in the trial campaigns are GGAO, Westford, Kokee Park, Wettzell, Yebes, and Ishioka (blue/dark stations in Figure 2). If other stations become available before the end of the trials, they will also be included as much as possible. The trials so far only have stations in the northern hemisphere. However, some southern hemisphere stations (e.g., HartRAO and the AuScope stations) will become available as VGOS sites in subsequent years.

3.3 Timing

All three trials were foreseen to be observed in the calendar year 2015. Figure 3 depicts the spread of the trials over the year with two months of break between the trial campaigns.

2015		
Jan	Feb	
	May	Jun
		Sep
Oct		

Fig. 3 The original time plan for the three VGOS trial campaigns: Trial 1 in January/February, Trial 2 in May/June, and Trial 3 in September/October.

The planning of the trials was based on information available by February 13, 2014. Since then, several local VGOS projects have slipped in time (e.g., due to delays in getting broadband feeds). For this and other constraints, the trials are currently foreseen to be observed as shown in Figure 4.

2016			2017		
			Jan	Feb	
				May	Jun
Jul	Aug	Sep			

Fig. 4 Current time plan for the three VGOS trial campaigns. The Master Schedule for 2016 has Trial 1 included; that is, the first trial campaign was scheduled. The observing periods for Trial 2 (January/February 2017) and Trial 3 (May/June 2017) are tentative at the point of writing. The two-months observing period for these inherently assumes that the observing will take place on a weekly basis as opposed to a bi-weekly basis.

Hence, the first trial campaign will start 1.5 years later than initially anticipated. The test sessions have shown that a two-week turnaround time is still needed to complete the cycle from observing to correlation to analysis. Thus at least Trial 1 will be kept observation-free every other week.

The observing slots for Trial 2 and Trial 3 are not finalized yet. There will be four one-hour bursts on a daily basis. However, the start and duration (including whether to observe every other week only) still need to be determined.

4 Resource Management

In addition to the station time, the resources necessary for the success of the trials include recording media, data transport, correlation and fringe fitting, and analysis. In order to address these needs, the Coordinating Center has commenced holding monthly teleconferences with the various groups involved in the effort. The teleconferences are also helpful in addressing technical issues that may need to be resolved.

The following provides a brief summary of the resources being discussed:

- **Data transport:** The amount of recorded data is so high that an e-transfer (even for a single station) of the data will easily become too unwieldy. Hence,

the data transport will mostly be physical shipment of recording modules (Mark 6).

- **Mark 6 modules:** A media pool with Mark 6 modules has been started. Each station needs to contribute at least as many modules as required for the trials. The module size is preferably 48 TB in order to fit a single session onto one module (test schedules indicate a need of 37 TB per 24-hour session per station).
- **Correlation and fringe-fitting:** MIT Haystack Observatory is developing the correlation and fringe-fitting capability based on the DiFX software correlator. Haystack will do the correlation/fringe-fitting work.
- **Analysis:** The analysis is based on *vgosDB* as the storage format. The analysis work will be done at Haystack and Goddard using *nuSolve*.

5 Pilot Project

After the successful completion of three trial campaigns, a pilot project can commence. The main purpose of the pilot is to gain experience with the operational mode but without making a full commitment to product delivery [1]. The pilot will be a combination of the observing scenarios of the trials with steadily increasing observing load over time. In order to get to 24/7 observing one of two avenues will be followed: either increasing the burst lengths (Figure 5) or increasing the number of bursts (Figure 6).

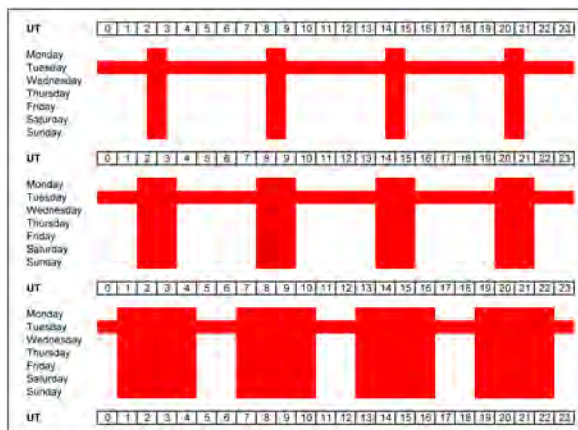


Fig. 5 Pilot project with increasing the burst lengths.

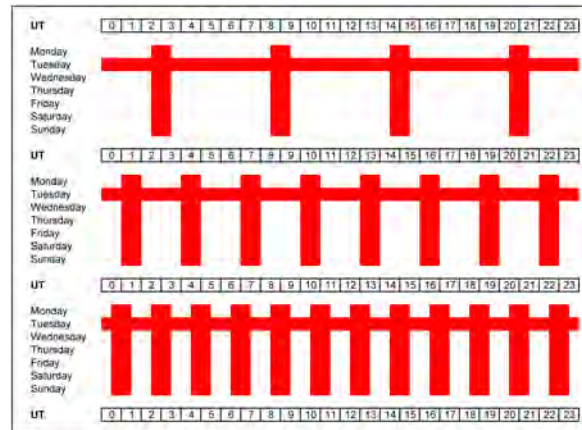


Fig. 6 Pilot project with increasing the number of bursts.

An argument in favor of increasing the number of bursts is that it allows the determination of dUT1 in an Intensive-type approach. However, it has not been decided yet which avenue will be taken. In terms of timing, the pilot project can be scheduled as early as the fourth quarter of 2017 or at the beginning of 2018. This is somewhat dependent on the success of the trial campaigns.

6 Outlook

In the next several years a substantial number of new VGOS antennas will come online. By the year 2018 we expect some 18 VGOS sites altogether. The new stations will be integrated into the trials (if possible) as well as the pilot project. The pilot project will eventually culminate into full VGOS operations by 2020.

References

1. B. Petrachenko, D. Behrend, J. Gipson, H. Hase, C. Ma, D. MacMillan, A. Niell, A. Nothnagel, and X. Zhang. VGOS Observing Plan. *IVS 2014 General Meeting Proceedings 'VGOS: The New VLBI Network'*, edited by D. Behrend, K. D. Baver, and K. L. Armstrong, Science Press (Beijing), ISBN 978-7-03-042974-2, pp. 16–19, 2014.

Generation of Global Geodetic Networks for GGOS

Daniel MacMillan¹, Erricos C. Pavlis², Magda Kuzmicz-Cieslak², Daniel Koenig²

Abstract We simulated future networks of VLBI+SLR sites to assess their performance. The objective is to build a global network of geographically well distributed, co-located next-generation sites from each of the space geodetic techniques. The network is being designed to meet the GGOS terrestrial reference frame goals of 1 mm in accuracy and 0.1 mm/yr in stability. We simulated the next generation networks that should be available in five years and in ten years to assess the likelihood that these networks will meet the reference frame goals. Simulations were based on the expectation that 17 broadband VLBI stations will be available in five years and 27 stations in ten years. We also consider the improvement resulting from expanding the network by six additional VLBI sites to improve the global distribution of the network. In the simulations, the networks will operate continuously, but we account for station downtime for maintenance or because of bad weather. We ran SLR+VLBI combination TRF solutions, where site ties were used to connect the two networks in the same way as in combination solutions with observed data. The strengths of VLBI and SLR allows them to provide the necessary reference frame accuracy in scale, geocenter, and orientation. With the +10-year extended network operating for ten years, simulations indicate that scale, origin, and orientation accuracies will be at the level of 0.02 ppb, 0.2 mm, and 6 μ s. Combining the +5-year and +10-year network realizations will provide better estimates of accuracy and estimates of stability.

Keywords VLBI, SLR, TRF, GGOS, VGOS

1. NVI Inc./NASA GSFC

2. Joint Center for Earth Systems Technology/UMBC

1 Introduction

Progress is already being made on building next generation stations for the geodetic networks for future observing by all of the geodetic techniques. The GGOS terrestrial reference frame goals of 1 mm in accuracy and 0.1 mm/yr in stability impose strong requirements on the geodetic networks. Future networks will contain sites with legacy, next-generation, and mixed equipment. We have performed simulations for the +5-year and the +10-year time frames. The two network designs are based on the existing stations' plans for the future and an extensive database of information for future system deployments collected from proposals submitted to the GGOS Bureau of Networks and Observations (GBNO). Although we have no guarantee that all these proposed plans will materialize exactly as planned, these are the best available information that we can rely upon. As a first step, we have made simulations for the VLBI+SLR combinations. The rationale for this combination is that SLR uniquely provides the origin of the TRF since it is directly sensitive to the geocenter. VLBI provides the reference frame orientation since it can measure orientation relative to the distant quasar reference frame, which provides essentially fixed reference points. Both techniques provide the TRF scale. A next step will be to incorporate GNSS into the combination. GNSS will be available at all sites, including those that have less than the complete ensemble of techniques that would provide a direct tie. With the presence of GNSS these non-core sites are tied to the rest of the network via this third technique.

For our simulations, we assumed that in the +5-year time frame, there would be both legacy and next-generation systems. In the +10-year time frame, VLBI will be assumed to be observing only with next gener-

ation broadband networks; the SLR network would be composed of about 50% next-generation systems and 50% legacy systems because the high cost of replacement of many legacy sites is prohibitive.

2 Simulations for Future VLBI + SLR Networks

For the VLBI simulation, next-generation stations will all have broadband (2–14 GHz) receivers. Most of these antennas will be “very fast” being capable of slewing at $12^\circ/\text{s}$ in azimuth and $6^\circ/\text{s}$ in elevation. At present there are five antennas in the “fast” category (GGAO12M at GSFC, three Australian, and one in New Zealand) slewing at $5\text{--}6^\circ/\text{s}$ in azimuth and $1\text{--}2^\circ/\text{s}$ in elevation. We included the legacy antenna at Westford, which has an azimuth slew rate of $3^\circ/\text{s}$.

Figure 1 shows the locations of broadband VLBI sites used in our simulations. In five years we expect that there will be 17 sites. It is clear from the map that there are large areas without stations, most notably South America, South Pacific, Africa, and Central Asia. The additional sites we foresee in ten years fill in these holes. NASA Headquarters requested that we extend the +10-year network to include six sites that help to further fill in geographical holes. Figure 2 shows the corresponding map for SLR for the +10-year and +10-year-extended cases. For the purpose of the simulations we did not include a few sites (which we know will have future stations) that are close to our chosen sites because the Calc/Solve analysis software limits the number of sites in a session to a maximum of 32 sites.

Table 1 VLBI observing day comparison.

Session Type	Number of Stations	Site average scans/hr	Range scans/hr	Number of Observations
Weekly R1	8–10	15	12–21	5,100
CONT11	14	16	12–20	10,900
CONT14	17	19	14–24	20,300
+5-year	17	79	58–97	141,800
+10-year	27	76	61–86	274,200

The new VLBI broadband antennas will make far more observations than current operational networks. The large antenna slew rates enable many more observations to be made and the high data rate (16 Gbps)



Fig. 1 Global distribution of future VLBI broadband stations. Stations (at 17 sites) expected in five years (solid black circles), added stations (at ten sites) in ten years (solid red stars), and additional stations (at six sites) in an extended network in ten years (blue diamonds).

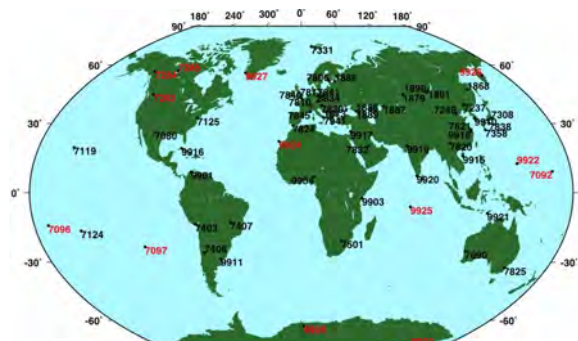


Fig. 2 Global distribution of future SLR stations. Stations expected in ten years (black number codes) and additional stations in an extended network in ten years (red number codes).

allows observation scan times to be short (20–30 s depending on the source flux). Table 1 compares network performance statistics of the weekly R1 operational networks, CONT campaign networks, and the future broadband networks that we have simulated. The big increase (factor of 3 to 4) in the network size and the increase (factor of 5 to 8) in station scans/hour lead to about a factor of more than 50 in the number of observations made by the network in a 24-hour session.

To generate the VLBI input to the combination, we first made an observing schedule for a network of stations with the desired properties (antenna slew rates, data rates, antenna SEFDs). This was done using the scheduling software SKED. The schedule is converted into a simulation database, which can be run with the VLBI analysis software package Calc/Solve. Calc/Solve is set up to generate three VLBI Geodyn

input files: 1) observations, 2) solution setup information, and 3) a simulated delay for each observation. For each observation, the observation file gives the epoch, the stations, and the radio source that was observed. The solution setup file contains the a priori station positions and velocities, the parametrization of the estimation of clock and troposphere parameters, and constraint information. Simulated delays consist of three contributions: clock delays, wet tropospheric delays, and observation uncertainty. Clock delays for each station are modeled as the sum of random walk and integrated random processes with the expected (required) clock Allan standard deviation 1×10^{-14} @ 50 minutes. The wet delay contribution is based on a Kolmogorov turbulence delay model, where the model parameters are the effective troposphere height, wind velocity, and site dependent refractive index structure constants C_n . A white noise contribution corresponding to the observation uncertainty is included. The simulation delay model was validated by applying it in the analysis of CONT11 data. Baseline length repeatabilities using simulated delays were compared to repeatabilities from analysis of observed data. Simulated repeatabilities are within about 30% of observed repeatabilities. The average ratio of repeatabilities was close to one (0.97 ± 0.32).

The SLR simulation procedure starts by using GEODYN with a suite of models for gravity, tides, and so on that represent the “true” Earth System, to predict all available passes of LAGEOS and LAGEOS-2 over the network of SLR stations for a year of continuous system operations. Data are then deleted in several steps, to eliminate tracking of two targets simultaneously, to account for other effects including local weather and system downtime. In the next step, the data set is split into daylight and nighttime passes and sampled according to the system capabilities and performance for each site. For legacy sites, the sampling is done to match multi-year performance statistics. For next-generation SGSLR-class sites, 25% and 50% of data is kept for day and night passes, respectively (see Figure 3). In the final step we corrupt the data by adding simulated errors to the observed ranges, using the systematic and random error levels corresponding to each category of sites. For legacy sites, this is based on current performance statistics, while for SGSLR-class systems on the system specifications, using for each pass a random walk error model with a standard deviation of 1 mm plus white noise of 1 mm.

3 VLBI + SLR TRF Combination Solution

Figure 4 provides an overview of the calculation of the combination TRF with the Geodyn software. The first step involves ingesting the simulated observations from VLBI and from SLR. For SLR, GEODYN generates weekly normal equations (Sunday to Saturday). In the case of SLR data, GEODYN uses a slightly inferior set of models for gravity, tides, and so on compared to what was used in generating the “real” data. In this way we include a systematic error component in the reduction process to represent the real situation where the models used in data reductions are only approximations of the “true” Earth models. The difference of the parameters describing each model (true vs. approximate) being commensurate with our best estimate of the uncertainty in the used model. In the case of VLBI the data are processed by GEODYN in sessions (daily) and normal equations are formed. In a second step, we use the companion program to GEODYN, “SOLVE” (not the one associated with Calc), to form a weekly set of normal equations by stacking the appropriate session files. Uncertainties from each weekly solution are scaled to make the chi-square (per degree of freedom) equal to 1. In the next step, SOLVE combines the VLBI and SLR normal equations. In our solution, there were 12 co-located SLR and VLBI sites in the +5-year sim-

Table 2 Projection of combined TRF quality results.

Case	σ_{Tx} mm	σ_{Ty} mm	σ_{Tz} mm	σ_{Ds} ppb	σ_{Rx} μ as	σ_{Ry} μ as	σ_{Rz} μ as	σ_{3D} mm
+5 years	0.77	0.79	0.81	0.12	32.2	31.7	30.7	1.37
+10 years	0.66	0.65	0.88	0.10	34.4	37.1	23.5	1.28
+10 years (extended)	0.42	0.41	0.50	0.06	21.4	22.0	15.7	0.77

ulation. For the +10-year and +10-year-extended cases there were 15 and 21 sites, respectively. To account for (model) the ties between the sites, the covariance matrix included the 3-dimensional site-tie covariance. For the current simulation, we assumed a 3D covariance of 3 mm, consistent with an estimate of the quality of ground survey measurements of site ties from Z. Altamimi. Better local site tie vector determination could reduce this below the 1-mm level. We plan further tests using other values for the tie covariance including more pessimistic values.

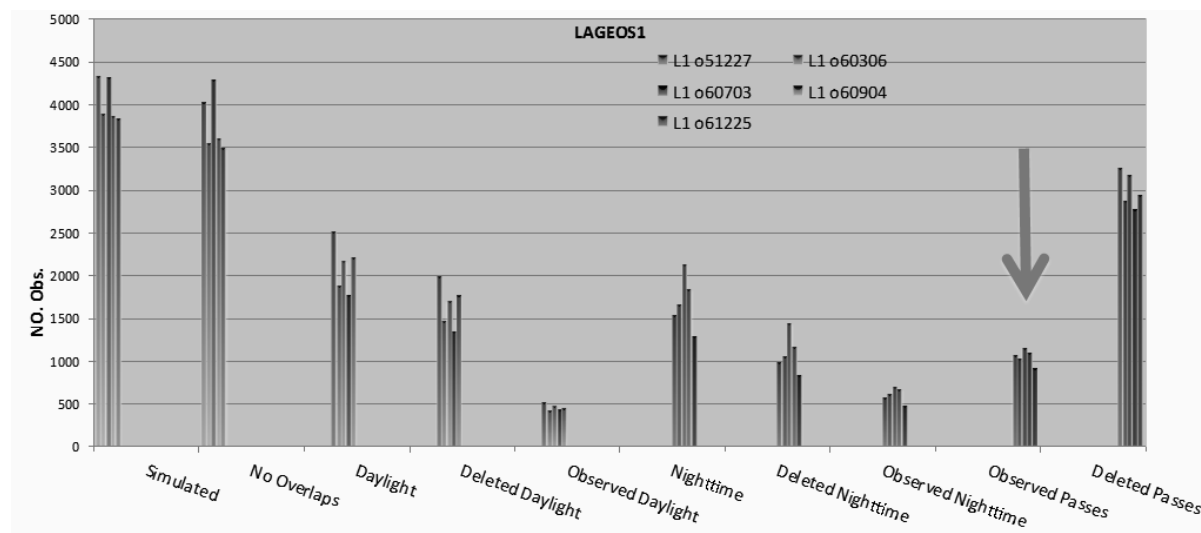


Fig. 3 Five weekly LAGEOS arcs, examples of SLR data going through the preprocessing steps for the generation of a realistic set of observed data: (a) generating all possible data, (b) eliminating the data overlapping with tracking other targets, (c) splitting the data in daytime and nighttime tracking, (d) sub-sampling the data according to the individual system’s expected performance. The last two columns indicate the final number of accepted and rejected passes.

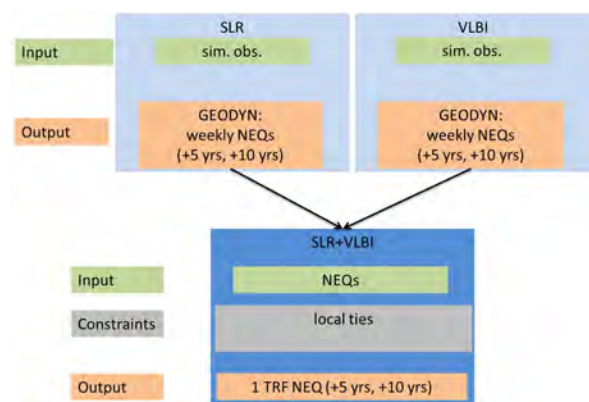


Fig. 4 Overview of the process of combining VLBI and SLR input to produce an SLR+VLBI combined TRF solution.

The quality of the combination TRF is summarized in Table 2. For each network case, the uncertainties of the seven-parameter Helmert transformation parameters are shown. The increase in network size from the +5-year network to the extended network in ten years improved the 3D uncertainties by a factor of 1.78 to 0.77 mm. Scale improved by a factor of 2 to 0.06 ppb (0.38 mm), and orientation by a factor of 1.45 to 22 μ s. Even with just one year of continuous observations, the GGOS TRF accuracy goal of 1 mm is met. Of course, at this point we have not considered reference frame

stability. To estimate this, we will combine the +5-year and +10-year TRF realizations.

4 Conclusions

We simulated the SLR and VLBI network operations for one year at two different epochs of its future evolution: five years and ten years from present. The predictions for how the networks will “look” like at these two instances are based on the information collected and tabulated by the GGOS Bureau of Networks and Observations. The major differences from previous simulations is that here special care was taken to generate realistic tracking data for the mixed (legacy + next generation) SLR networks and, additionally, the processing of a vast amount of VLBI data generated by an all next-generation broadband system network, compared to the legacy systems that were used in the past. Based on our combined VLBI and SLR TRF realizations, these networks seem to be sufficiently robust in delivering the required accuracy of 1 mm for the origin, scale, and orientation of the TRF, which are the goals of GGOS. If we further assume that the network realization of ten years operates for ten continuous years, we find that a combination of these ten years will lead

to a TRF model with an origin (3D) accurate to 0.4 mm, a scale at 0.2 mm, and an orientation at 0.5 mm. At the request of NASA/HQ we also examined an extended network for the period of ten years. This network considers the addition of about a dozen more sites to the standard network, half of which are core sites with collocated SLR and VLBI systems, and these are placed in areas void of sites in the standard network, that is they fill-in gaps. The improved coverage demonstrates the critical importance of establishing uniform networks, as it improves the TRF accuracy delivered by the standard network by about 40%. If such an extended network were to operate for ten years, it would deliver a TRF accurate to 0.2 mm in origin, 0.13 mm in scale and 0.33 mm in orientation. Our immediate plans are the combination of the two networks five years apart (the one after five with the one after ten years from present), which will provide us with a first estimate of the stability that we can expect these two networks to deliver for the TRF models of the very next years.

Acknowledgements

D. MacMillan acknowledges support from NASA contract NNG12HP00C. E. C. Pavlis, M. Kuzmicz-Cieslak, and D. Koenig acknowledge the support of NASA Grant NNX14AN50G. Resources supporting this work were provided by the NASA High-End Computing (HEC) Program through the NASA Advanced Supercomputing (NAS) Division at Ames Research Center through SMD-15-5810.

Operational VGOS Scheduling

Anthony Searle¹, Bill Petrachenko^{1,2}

Abstract The VLBI Global Observing System (VGOS) has been designed to take advantage of advances in data recording speeds and storage capacity, allowing for smaller and faster antennas, wider bandwidths, and shorter observation durations. Here, schedules for a “realistic” VGOS network, frequency sequences, and expanded source lists are presented using a new source-based scheduling algorithm. The VGOS aim for continuous observations presents new operational challenges. As the source-based strategy is independent of the observing network, there are operational advantages which allow for more flexible scheduling of continuous VLBI observations. Using VieVS, simulations of several schedules are presented and compared with previous VGOS studies.

Keywords VGOS, operations, scheduling

1 Introduction

Since the publishing of the VLBI2010 specification [1], many countries have invested in new VLBI antennas that adopt the new standard. In the coming years, a global network of these smaller, fast antennas will become available for VGOS operations. This new mode of operation will require re-evaluating how stations are scheduled and how to make optimal use of their new capabilities. Further, the new frequency regime will affect source selection and observation lengths. There remains a question of how many sources exist that

can be observed over the new wide bandwidths. Here we present a simulation using four different prospective frequency sequences and a simulation using source lists of various sizes. Both simulations use a scheduling algorithm that is designed to maximize observations while minimizing station bias.

2 Source-Based Scheduling

Because VGOS will operate using expanded frequency bandwidths and smaller, fast antennas, scan durations will be shorter and observations more frequent. The “opposite sky” source-based scheduling algorithm used in this study aims to maximize observations at each site, independent of the ground network.

The scheduling algorithm randomly selects a source that has not been observed recently and then selects a second source roughly opposite on the sky. A majority of stations should be able to observe one of the two sources and each station joins the observation if it is able to slew there in time. A new set of sources is selected every 30 seconds. Sources are chosen so that sources have an equal number of observations.

Scan duration was calculated using the correlated flux for the source, the antenna/receiver sensitivity, and the frequency sequence. Because it was shown that geodetic/astrometric performance does not degrade significantly until delay measurement error exceeds 16–32 ps [2], there was no attempt to improve delay precision beyond 8 ps. As a result the calculation of integration time, Δt , was divided into three regimes, i.e.,

$$\text{If } SC_{src} < 58ps \text{ then } \Delta t = 10s$$

1. Natural Resources Canada, Canadian Geodetic Survey

2. Dominion Radio Astrophysical Observatory

If $SCsrc > S8ps$ then $\Delta t = 10s(S8ps/SCsrc)^2$

If $\Delta t < 1s$ then $\Delta t = 1s$

where $SCsrc$ is the correlated flux of the source and $S8ps$ is the correlated flux at which a particular frequency sequence achieves 8 ps delay precision. In addition to the scan duration, a three second buffer was added to each scan to allow each antenna time to “settle” and acquire the source.

There are operational advantages in using a simple scheduling algorithm:

- An algorithm that is unaffected by the ground network is easier to operate; stations can drop out with minimum influence on the schedule and rejoin as soon as they are available.
- The fastest sites are used more effectively. More complicated schemes have to decide whether to wait for slower dishes, which tends to prioritize the slower dishes.
- More sparsely populated hemispheres are observed at the same rate as densely occupied regions. Algorithms that maximize observations prefer dense parts of the network.

Prerequisites for a source based solution to work effectively include a globally distributed ground network and a well-distributed source list.

3 VGOS Simulation Network



Fig. 1 VGOS simulation network.

The VGOS simulation network which includes 19 sites that are either built, under construction, or planned, plus a Yellowknife station, can be seen in Figure 1. Up-to-date antenna specifications are used

for known antennas; VGOS specifications are used for anticipated sites (see Table 1). The antenna distribution is quite good, but there are notable gaps in South America, Russia, and the Middle East. Europe and the eastern United States have some short baselines, but these may be valuable if regular imaging of radio sources becomes part of VGOS operations.

Table 1 Station characteristics of VGOS network.

Station Name	Az. Rate (deg/min)	El. Rate (deg/min)	$C_n \times 10^{-7} m^{-1/3}$
KOKEE12M	720	360	1.78
WETTZ13S	720	360	1.8
WESTFORD	720	360	3.67
NYALES12	720	360	0.95
ISHIOKA	720	360	2.3
HART12M	720	360	1.47
ONSALA12	720	360	2.09
GGAO12M	300	66	2.3
HOBART12	300	75	1.6
KATH12M	300	75	1.68
METSA12M	720	360	2.09
MCD_12M	720	360	1.45
RAEGCANA	720	360	1.5
RAEGFLOR	720	360	1.5
RAEGYEB	720	360	1.5
SESHA12M	720	360	1.79
TAHIT12M	720	360	2.19
WARK12M	300	60	1.6
YARRA12M	300	75	1.76
YELLOW12	720	360	1.24

4 Frequency Sequence Simulation

The VGOS system will use four bands of frequencies in the 3–14 GHz range. The exact placement of the frequencies has not yet been determined. It is known that the frequency sequence will affect the scheduling by varying the scan durations for a target delay precision and limiting the ability to connect the phase across the observing band for weaker sources.

To investigate the effect of the frequency sequence on scheduling, four prospective VGOS frequency sequences were used to create day-long schedules using the sky-based algorithm and the 128-source list from the source number simulation (see Section 5). In order to determine scan lengths for each sequence, minimum source fluxes for which the delay observable

Table 2 Characteristics of frequency sequences.

Sequence number	Min Flux (mJy)	Avg $\Delta\tau$ (ps)	SNR @min	Flux for 8ps (mJy)	BW (MHz)	Data Rate(Gbps)	Number of Scans	# Obs.	F1 (MHz)	F2 (MHz)	F3 (MHz)	F4 (MHz)
1	80	9.36	10	208	1024	31.7	5710	165644	3008	4896	8288	9696
2	110	11.129	10	255	1024	16.4	5701	159610	3008	5062	6688	9696
3	130	11.194	12	148	1024	16.4	5706	161398	3008	5792	8032	12704
4	190	11.426	17	290	512	15.4	5683	156841	3008	4960	7872	9280

uncertainty would equal 8 ps in 10 seconds (see Table 2), were determined (see Section 2). Observations were simulated with a turbulent troposphere with Treuhaft-Lanyi parameters and site-dependent structure constants taken from Sun [3] (see Table 1); clocks were modeled with Allan Standard Deviations of 1×10^{14} at 50 minutes, and the delay measurement precision was determined by the flux method described in Section 2.

Least-squares parameter estimations of EOPs, site positions, tropospheric parameters, and site clocks were completed using VieVS [4]. Zenith troposphere delay offsets were determined at 15-minute intervals with a piece-wise linear constraint of 15 mm between adjacent offsets; gradients were estimated at 30-minute intervals with 1 mm absolute constraints; clocks were determined as second order polynomials with linear offsets determined every hour relatively constrained to 13 mm, and station positions were determined once per 24 hours constrained with no-net-rotation and no-net-translation conditions. EOPs were determined once per day.

5 Source Number Simulation

To study the impact of the number of sources available in the source list, five prospective source lists of varying length were used to produce day-long schedules using the “opposite sky” source-based algorithm and frequency sequence number 2 from Table 2. Source catalogs of 32, 64, 128, 256, and 512 sources were subsets of the Bordeaux VLBI Image Database [5] with sources with declinations below -45 degrees added from the Goddard Space Flight Center SKED source list [6]. The catalogs were determined by adjusting a cut-off minimum flux and maximum median delay error until the desired number of sources was included.

Observations were simulated using the same troposphere, clock, and noise models as in Section 4. EOPs,

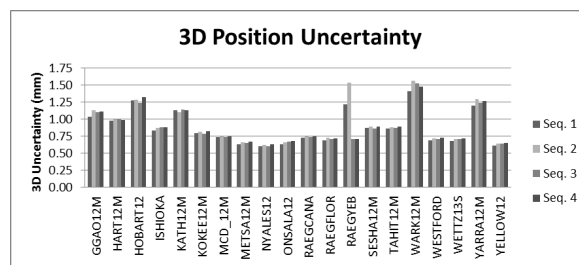
site positions, tropospheric parameters, and site clocks were determined using least-squares parameter reduction with the same strategy as in Section 4.

Table 3 Characteristics for source schedules.

	32	64	128	256	512
#Scans	5723	5696	5701	5679	5695
#Obs.	180119	163948	159610	151764	140882
Avg $\Delta\tau$ (ps)	8.248	10.06	11.129	12.586	13.737

6 Results

Station positions were determined for each schedule. For the frequency sequence simulation, the mean 3D rms station position scatter was 0.88, 0.93, 0.88, and 0.89 mm for sequences 1, 2, 3, and 4, respectively. In the source list size simulation the mean 3D rms station position scatter was 1.08, 0.91, 0.93, 0.90, and 0.96 mm for the 32, 64, 128, 256, and 512 source lists, respectively. In both simulations, larger values of station position uncertainty corresponded to stations with slower slewing speeds and fewer observations.

**Fig. 2** 3D rms of stations in frequency sequence study.

The EOP estimate formal uncertainty is shown in Table 4 for the different frequency sequence schedules and in Table 5 for different source lists. EOP determi-

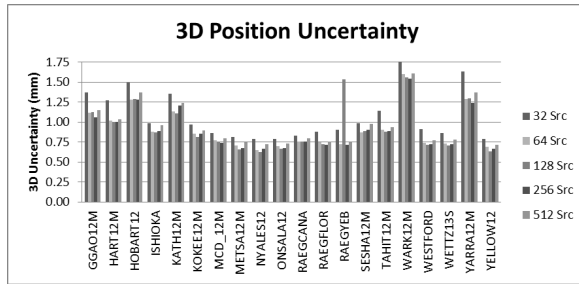


Fig. 3 3D rms of stations in source number study.

Table 4 EOP uncertainty for sequence simulations.

	Seq. 1	Seq. 2	Seq. 3	Seq. 4
Xp(μ as)	3.68	3.84	3.71	3.77
Yp(μ as)	3.74	3.87	3.84	3.83
dUT(μ s)	0.178	0.183	0.184	0.184
dX(μ as)	2.57	2.64	2.63	2.67
dY(μ as)	2.56	2.63	2.61	2.65

Table 5 EOP uncertainty for source simulations.

	Source Number				
	32	64	128	256	512
Xp(μ as)	4.25	3.68	3.84	3.89	4.10
Yp(μ as)	4.39	3.79	3.87	3.97	4.19
dUT(μ s)	0.210	0.184	0.183	0.187	0.195
dX(μ as)	2.94	2.76	2.64	2.78	2.97
dY(μ as)	2.93	2.60	2.63	2.77	2.95

nation appears to be insensitive to sequence, though there was a small degradation in EOP results for the 32 and 512 source lists.

7 Conclusions

- Neither the frequency sequence nor the source list had significant impact on the geodetic parameters of interest. Geometry and observation density are more important factors.
- Sites with greater than ~ 13000 observations per day have position uncertainties of less than 1mm, which is a goal of VGOS.
- While the 32 source list schedule has the most observations, the limited geometry degraded the results. As the number of sources increased beyond 256, solutions become marginally worse due to the addition of a number of weaker sources resulting in fewer observations.

- After approximately 100 sources, the geometry is sufficient for station positions and EOPs, though there may be other reasons to expand the source list.
- Position determination was worse for the southern stations because many of the antennas in the south are slower and miss scans due to slewing.
- Operationally, having observations at regular intervals reduces complications in scheduling while increasing the number of observations and eliminating station and hemisphere bias.
- As the VGOS network matures, proper estimates of observation interval and scan duration could further improve the technique.

Acknowledgements

This research has made use of material from the Bordeaux VLBI Image Database (BVID).
<http://www.obs.u-bordeaux1.fr/BVID>

References

1. B. Petrachenko, A. Niell, D. Behrend, B. Corey, J. Böhm, P. Charlot, A. Collioud, J. Gipson, R. Haas, T. Hobiger, Y. Koyama, D. MacMillan, T. Nilsson, A. Pany, G. Tuccari, A. Whitney, J. Wresnik, “Design Aspects of the VLBI2010 System. Progress Report of the VLBI2010 Committee”. NASA Technical Memorandum, NASA/TM-2009-214180, 58 pp., June 2009.
2. D. MacMillan, J. Böhm, J. Gipson, R. Haas, A. Niell, T. Nilsson, A. Pany, B. Petrachenko, and J. Wresnik, “Simulation Analysis of the Geodetic Performance of the Future IVS VLBI2010 System”, 2008 Fall AGU poster, 2008. http://lupus.gsfc.nasa.gov/files_presentations/2008_fall_agu_v2c.ppt
3. J. Sun, J. Böhm, T. Nilsson, H. Krásná, S. Böhm, and H. Schuh, “New VLBI2010 scheduling strategies and implications on the terrestrial reference frames”, *J. Geodesy* 88:449-461. doi 10.1007/s00190-014-0697-9, 2014.
4. J. Böhm, S. Böhm, T. Nilsson, A. Pany, L. Plank, H. Spicakova, K. Teke, and H. Schuh, “The New Vienna VLBI Software VieVS”, In S. Kenyon, C. M. Pacino, and U. Marti, editors, “Geodesy for Planet Earth: Proceedings of the 2009 IAG Symposium, Buenos Aires, Argentina, 31 August — 4 September 2009”, Springer Berlin Heidelberg, Berlin, Heidelberg, pages 1007–1011, doi 10.1007/978-3-642-20338-1_126, 2012.
5. A. Collioud, P. Charlot, “The Bordeaux VLBI Image Data base”, 19th EVGA working meeting proceedings, G. Bourda, P. Charlot, and A. Collioud editors, 2009.
6. <ftp://gemini.gsfc.nasa.gov/pub/sked/catalogs/source.cat>, accessed January 18, 2016.

VGOS Source Selection Criteria

Bill Petrachenko¹, Patrick Charlot², Arnaud Collioud², Anthony Searle¹

Abstract Source structure has long been recognized as a significant risk factor for the broadband method. The issue of greatest concern is that structure related phases and delays will lead to cycle slips during broadband phase connection. These errors are subtle to detect and difficult or impossible to correct after the fact. As the advent of VGOS operations draws near, criteria will be needed to generate lists of candidate VGOS sources that are at the same time strong enough to be detected and simple enough not to cause broadband phase connection errors. The purpose of this study is to propose useful VGOS source selection criteria and to understand their relation to broadband frequency sequences, source lists, and geodetic/astrometric performance. In order to increase the number of available sources, an attempt will be made to find frequency sequences that operate reliably below the typical VGOS flux cut-off of 250 mJy. Candidate source lists will be generated using the Bordeaux VLBI Image Data Base (BVID) as input.

Keywords VGOS, source, selection, criteria

1 Introduction

Source structure is a significant cause of systematic error in geodetic VLBI. It varies with both time and frequency, manifesting in some cases as apparent motion of the source but always as a systematic variation of delay, phase, and amplitude as the length and orientation of the interferometer baseline changes. For VGOS,

variation of structure with frequency introduces an additional challenge: it has the potential to compromise phase connection between bands.

Traditionally two approaches have been considered for mitigating the negative impact of source structure. The more active of the two is the application of structure corrections. This involves the use of a high quality source image to calculate delay, phase, and amplitude corrections in the uv-plane (a plane perpendicular to the direction to the source that contains instantaneous projected baseline vectors expressed in units of wavelengths). If corrections have been applied successfully, the source appears as a point source situated at the reference location of the image. Unfortunately, the use of phase closure in VLBI removes all absolute position information from the image, making it difficult to overlay images from one epoch to another and from one frequency band to another, which is a significant challenge for the structure corrections approach. Up to the present time, structure corrections have not produced significant enough performance improvements to be considered for operational use.

The second approach is to generate lists of sources that have acceptably small amounts of structure and to use only those sources. This is the approach taken traditionally and is the approach taken in this paper. Operationally this requires meaningful criteria for selecting sources along with frequent observations of candidate sources to evaluate their changing structure and flux. To be useful, the criteria need to incorporate: correlated flux and structure delay over the uv-plane; the fact that, in broadband delay, dispersive and non-dispersive delays are calculated simultaneously, and the impact of broadband frequency sequences.

If this approach is taken, it is pertinent to ask whether the selection criteria will provide a large

1. Natural Resources Canada

2. Laboratoire d'Astrophysique de Bordeaux

enough sample of sources for VGOS observing. There is some evidence from Monte Carlo simulations [1] that weak improvement in geodetic/astrometric performance results if the number of scheduled sources increases from 32 to 64 with diminishing benefit above 64. However, there are other benefits of increasing the size of the source list, e.g., reduced impact of source structure related systematics, better connection to the ICRF, and improved maintenance of the ICRF. It is difficult to be quantitative about the number of sources required, but it is reasonable that the target should be a list of at least a couple hundred sources. Furthermore, it will be difficult to estimate the number of broadband sources available given that, although plentiful structure data is available at S- and X-bands, little is available at the frequencies planned for the broadband method. For this reason, a criterion for selecting broadband sources based on S/X observations will be useful.

Questions to be answered in this paper include:

- Are there good criteria for evaluating the suitability of broadband sources?
- Will there be at least about two hundred suitable sources for VGOS observing?
- Is it useful to optimize broadband frequency sequences to increase the number of suitable sources?

2 Background

2.1 Bordeaux VLBI Image Database (BVID)

The BVID [2] is used extensively in this study both as a source of S/X-band structural information and as a model for the type of quality metrics that might be used as VGOS broadband source selection criteria. The BVID includes in excess of 1,200 sources, each of which has been observed in both S- and X-band. Although a large number of the BVID sources were observed only once, many were observed in excess of 20 or 30 times. Each time a BVID source is observed, S- and X-band images are produced, and these are then used to calculate a uv-plane distribution of structure delay and visibility. The S- and X-band structure delays are further scaled to reflect the impact of that band on the ionosphere corrected delay. The median structure delay over the uv-plane (scaled according to its impact

on the ionosphere corrected delay) forms the basis for the S- and X-band structure indices [see Table 1], and the median visibility is used as a measure of the source compactness. Finally, the total flux is provided, which, when combined with the source visibility, produces the correlated flux over the uv-plane.

Table 1 Structure Index definition [5].

Structure Index (SI)	Median structure delay (ps)
1	0-3
2	3-10
3	10-30
4	>30

2.2 Frequency Sequences

The VGOS broadband system uses four bands in the 3–14 GHz range. Each band has nominally 1 GHz bandwidth with a cumulative data rate for all four bands of 16 Gbps. The exact frequency placement of the bands influences the ability to connect phase between bands. For example, phase connection is improved if: the frequency range from lowest to highest band is decreased; the bands are spread in some optimal fashion instead of, for example, being arranged in groups, or the bandwidth of each band is increased. [Note that although the ability to connect phase improves for narrower sequences, the ability to resolve delay degrades in proportion.] Four sample optimized sequences have been generated, and the fluxes below which the delay resolution peak starts to be mis-identified (assuming integrations of 10 s, SEFDs of 2500 Jy, and the use of 200,000 tries at peak identification) have been determined. The sequences are summarized in Table 2. Note that in all cases, the minimum fluxes are significantly below the typical VGOS flux cut-off of 250 mJ.

Table 2 Frequency Sequence summary.

Seq	BW (MHz)	Data rate (Gbps)	Start (GHz)	Stop (GHz)	Min Flux (mJy)
1	512	15	3.0	9.8	145
2	1024	16	3.0	13.7	120
3	1024	16	3.0	10.8	100
4	1024	32	3.0	10.8	75

2.3 Broadband Delay Calculation

The output of a VLBI correlator is a set of complex correlation coefficients, one for each frequency channel, i.e.,

$$\Gamma_i = A_i e^{-j\phi_i} \quad (1)$$

where A_i is the amplitude of the i^{th} channel and ϕ_i is the phase of the i^{th} channel. The phase can further be expanded as,

$$\phi_i = 2\pi f_i \left(\tau + \frac{K}{f_i^2} \right) \quad (2)$$

where f_i is the frequency of the i^{th} channel, τ is the non-dispersive delay of the signal (due to, for example, the interferometer geometry, the neutral atmosphere, the instrumentation, and the offset of the reference oscillators), $\frac{K}{f_i^2}$ is the dispersive (phase) delay due to the ionosphere, and K is a factor proportional to the total electron content (TEC) along the line of sight to the source.

Because the ionosphere delay varies with frequency, it can be eliminated if data are taken at more than one band. For legacy S/X systems, a linear delay is calculated separately for both S- and X-band, and then the delays from each of the two bands are combined to produce an ionosphere corrected delay. For VGOS broadband systems, the non-dispersive and dispersive delays are calculated in a single step. A grid of trial values, $\hat{\tau}_m$ and \hat{K}_n , are subtracted from τ and K in Equation (2) to give,

$$\Delta\phi_{imn} = 2\pi f_i \left((\tau - \hat{\tau}_m) + \frac{(K - \hat{K}_n)}{f_i^2} \right) \quad (3)$$

Then, for each value of m and n , the trial correlation coefficients (i.e. the correlation coefficients with $\hat{\tau}_m$ and \hat{K}_n subtracted, see Equation (3)) are summed over all frequencies to produce the delay resolution function (DRF), i.e.,

$$DRF_{mn} = \sum_i A_i e^{-j\Delta\phi_{imn}} \quad (4)$$

The values of $\hat{\tau}_m$ and \hat{K}_n that maximize DRF_{mn} are the maximum likelihood estimates of τ and K . The DRF for a typical broadband sequence is depicted in Figure 1. The elongated diagonal peak is an indication that

the non-dispersive delay and TEC are significantly correlated.

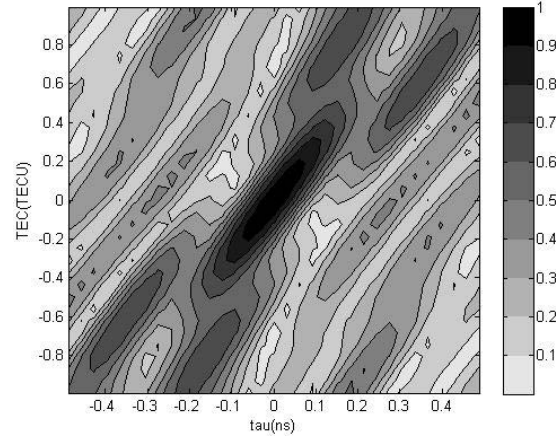


Fig. 1 The delay resolutions function (DRF) for a typical broadband frequency sequence.

3 Broadband Source Selection Criteria

A similar approach to that based on the BVID structure index and source compactness for legacy S/X sources (see Section 2.1) could be extended to broadband delay except that four bands would need to be handled instead of two. Although this provides valuable information about the individual bands, the cumulative effect on the final broadband result is more difficult to assess. Hence it may be efficient and meaningful to find quality factors that consider the whole broadband frequency sequence at the same time. This will be particularly useful when several hundred sources need to be evaluated automatically on a frequent basis.

The broadband DRF suggests a method for doing this. The following steps could be applied to generate uv plots of broadband correlated flux and broadband structure delay bias:

1. Generate high quality source images for each band and align the images relative to each other. [Note: the loss of absolute position information resulting from the use of phase closure makes it impossible to rigorously align the images; hence assumptions are required.]

2. Transform the images to the uv-plane to give correlated fluxes and structure phases at all points in the uv-plane and for the observing frequencies of all broadband channels.
3. For each point in the uv-plane, use the correlated fluxes and structure phases (for each channel) to simulate complex correlation coefficients and input these into the DRF calculation (see Section 2.3).
4. Determine the broadband correlated flux as the height of the DRF peak.
5. Determine the broadband delay bias as the location of the DRF peak.
6. Repeat Steps 3 to 5 for each point in the uv-plane to produce uv plots of broadband correlated flux and broadband structure delay (see Figure 2).

[Note: These plots no longer apply to individual bands (as was the case for the BVID S/X plots) but to the full broadband sequence.]

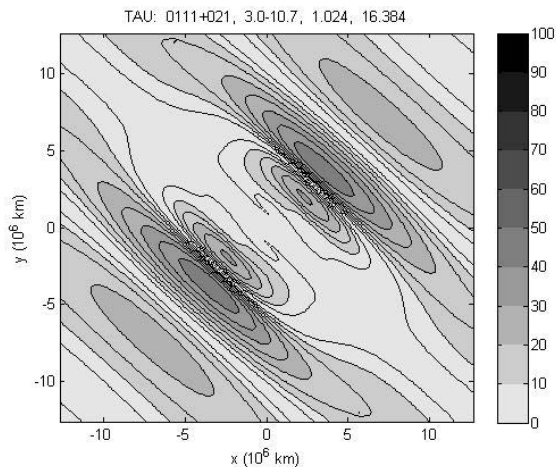


Fig. 2 uv-plot of broadband structure delay for source 0111+021. Source 0111+021 was observed 12 times between 1997 and 2010 and consistently had a structure index of 3 at X-band and a structure index of either 1 or 2 at S-band. Grey scale in the plot is in ps.

This can be taken one step further to consider the impact of correlated flux and source structure on broadband delay precision. The process for doing this involves the addition of gaussian pseudo random noise (prn) values to the source-based correlation coefficients that are input to the DRF calculation. In order to generate realistic noise signals, it is necessary to assume values for integration time, data rate, and antenna SEFD. If the process is repeated a number of times (e.g.,

25–50 times) using different prn sequences then the scatter of delay estimates will reflect the expected delay precision. This can be repeated for all points of the uv-plane to produce a uv-plot of expected delay precision (see Figure 3). [Note: These uv-plots depend on assumed values of integration time, data rate, and antenna SEFD and hence are not unique. They need to be scaled if different values of these parameters are appropriate.]

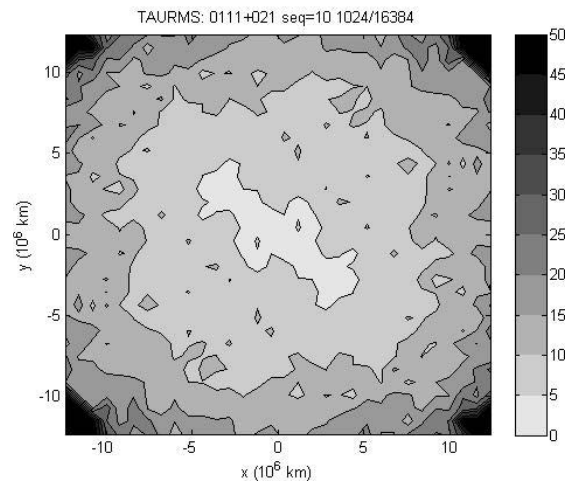


Fig. 3 uv-plot of broadband rms delay error for source 0111+021. Grey scale in the plot is in ps.

4 Number of Broadband Sources

The final goal of the paper is to predict the number of sources that will be available for use with the broadband system. Unfortunately, the current lack of source related data at all frequencies expected for broadband observing makes this difficult. So the challenge is to find a way to use legacy S/X-band data, which is plentiful, to predict which sources will work with the VGOS broadband systems. Because actual broadband data is not yet available, this cannot be done with a high degree of reliability; however, the conclusions arrived at through the use of S/X-band data should be at least reliable enough to get a rough idea of the number of sources that will be available for use with broadband observing.

A method for doing this was suggested by Arthur Niell in 2006 [3]. It relies on a paper by Fey and Charlot [5] in which S- and X-band elliptical component models were reported for 225 sources. In order to interpolate to arbitrary frequencies, hand picked assumptions were made regarding the spectral indices of the component fluxes. Because each source required individual attention, the approach was applied to only five of the 225 sources [4], making it difficult to draw general conclusions.

In this paper, a single set of spectral rules was applied to each source, making it possible to automate the interpolation process. The rules were: a) hold the S-band component fluxes fixed below 2.3 GHz, falling linearly above 2.3 GHz to zero at 8.5 GHz and b) hold the X-band component fluxes fixed above 8.5 GHz, falling linearly below 8.5 GHz to zero at 2.3 GHz. The only exception was for the main component flux, in which case an exponential was fitted to the S- and X-band values. Based on these rules, component models could be derived at arbitrary frequencies hence simulating actual broadband data.

Through cut and try methods an equation was then developed that combined ratios between S- and X-band median correlated flux, visibility, and structure delay and respective threshold values of the same parameters. The threshold values were then adjusted until the equation had the highest success rate (based on the 225 sources with broadband data simulated from component models) for predicting the truth of specified broadband conditions. The conditions tested are listed in the first column of Table 3 where here the focus was on rms delay error but could be expanded to also include delay bias. The process was repeated for each of the four test frequency sequences proposed in Section 2.2. When tested against the 225 sources with component models, the process was 85% to 90% successful in predicting broadband conditions based on S/X-band data. This was then applied to the full set of sources in the BVID, and the results are summarized in Table 3.

Table 3 Prediction of the number of BVID sources available for broadband observing based on S/X-band correlated flux and structure delay data.

Criterion	Seq#1	Seq#2	Seq#3	Seq#4
90% of uv-plane below 8 ps rms	191	212	213	269
90% of uv-plane below 16 ps rms	269	261	310	388
60% of uv-plane below 8 ps rms	350	408	412	566
60% of uv-plane below 16 ps rms	566	530	644	729

5 Summary and Conclusions

- Frequency sequences were proposed that work significantly below the typical VGOS flux cut-off of 250 mJ.
- A method was proposed for calculating broadband structure delay.
- A method was proposed for predicting expected rms delay error based on both correlated flux and structure phase.
- A method was proposed for using S/X median structure delay, visibility and flux to predict the number of sources available for broadband observing. Based on this method, it is expected that there will be at least 200 sources available for broadband observing.
- It was found that optimized frequency sequences can increase the number of available sources by roughly 50%.

Acknowledgements

This research has made use of material from the Bordeaux VLBI Image Database (BVID): <http://www.obs.u-bordeaux1.fr/BVID>.

References

1. Searle, A. and Petrachenko, B., "Operational VGOS Scheduling", 2016, Proceedings of the 9th IVS General Meeting (this volume).
2. Collioud, A. and Charlot, P., "The Bordeaux VLBI Image Data base", 19th EVGA Working Meeting Proceedings, eds. G. Bourda, P. Charlot, and A. Collioud, 2009.
3. Niell, A., "Source Structure Simulation", 2006, IVS memo 2006-017v01, <ftp://ivscc.gsfc.nasa.gov/pub/memos/ivs-2006-017v01.pdf>
4. Niell, A., "Source Structure Examples", 2006, IVS memo 2006-018v01, <ftp://ivscc.gsfc.nasa.gov/pub/memos/ivs-2006-018v01.pdf>
5. Fey, A. and Charlot, P., "VLBA Observations of Radio Reference Frame Sources. II. Astrometric Suitability Based on Observed Structure", 1997, ApJS, 111, 95.

Observing with Sibling and Twin Telescopes

Lucia Plank¹, Jim Lovell¹, Jamie McCallum¹, David Mayer²

Abstract With the transition to VGOS, co-located radio telescopes will be common at many sites. This can be as a sibling telescope when a VGOS antenna is built next to a legacy one, or as the concept of a twin telescope with two identical VGOS antennas. The co-location of two antennas offers new possibilities in both operation and analysis. The immediate question for observing with sibling/twin telescopes is the applied observing strategy and its realization in the scheduling software. In this contribution we report about our efforts implementing new scheduling modes for sibling and twin telescopes in the Vienna VLBI Software. For the example of the sibling telescope in Hobart, several types of sessions will be discussed: an improved tag-along mode for the 26-m antenna (Ho), a proper implementation of the twin-mode using the antenna with the shorter slewing time, and an astrometric support mode enabling the observation of weak sources with the AuScope array.

Keywords Scheduling, twin telescopes, sibling telescopes

1 Introduction

The idea of the VLBI Global Observing System (VGOS, e.g., Petrachenko et al., 2009) initiated a global infrastructure upgrade effort, with many new telescopes completed or being built worldwide. In general, the new telescopes are smaller ($\sim 12\text{--}15\text{ m}$)

and slew faster (up to $12^\circ/\text{s}$ in azimuth) than traditional antennas used for geodesy. Often these new antennas are co-located with existing, legacy antennas. Until the VGOS broadband system is widely adopted, there will be a period of common compatibility in terms of frequency and mode of operation.

Currently, there are co-located antennas in Hobart (Hb-12m, Ho-26m), HartRAO (Ht-15m, Hh-26m), Yebes (Yj-13m, Ys-40m), and Wettzell (Wn-13m, Wz-20m) which have participated in common observations in legacy S/X-mode. Others are on their way (e.g., Ny-Ålesund, Kokee) and often plan an overlapping period. This is important for establishing a local tie realized by VLBI measurements, complimentary to local surveys. In the following, we call such co-located telescopes of different capabilities *sibling telescopes* (Figure 1, left).

Alternatively, the VGOS concept also includes so-called *twin telescopes* (Figure 1, right). These are two co-located antennas of identical capabilities, as realized in the future in Wettzell, Ny-Ålesund, and Onsala.



Fig. 1 Terminology of a sibling telescope with different attributes in sensitivity and slew speeds and a twin telescope with identical capabilities.

1. University of Tasmania

2. Technische Universität Wien

Common operation of co-located telescopes requires new ideas in observing as well as in analysis. In this contribution we concentrate on the immediate question of the scheduling, meaning the planning of common experiments. Using the scheduling module of the Vienna VLBI software (Böhm et al., 2012; Sun, 2013; Sun et al., 2014), we report on new implementations for scheduling the sibling telescopes in Hobart.

2 Scheduling within the AUSTRAL Network

Our testbed is the AUSTRAL network shown in Figure 2. This comprises the AuScope VLBI array (Lovell et al., 2013) with the 12-m telescopes in Hobart (Hb), Katherine (Ke), and Yarragadee (Yg); the antenna in Warkworth (Ww) having the same design as the AuScope dishes; and the 15-m telescope in Hartebeesthoek (Ht). In addition, there are two 26-m legacy antennas in Hobart (Ho) and Hartebeesthoek (Hh).

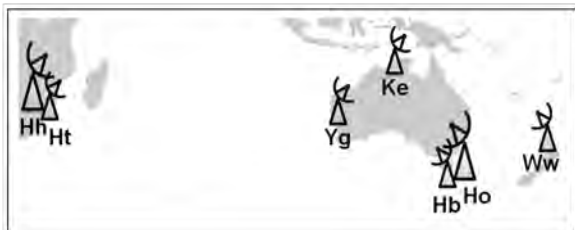


Fig. 2 Antennas in the AUSTRAL network.

Before discussing several new scheduling modes, it is important to understand the basic theory of scheduling. For a deeper understanding the interested reader is referred to scheduling-specific literature such as Gipson (2016) or Sun (2013).

In the schedule, one has to decide which antennas will observe which source and when. As a basic scheduling strategy one can say that the more scans (two or more antennas observing the same source) the better, a second optimization criteria would be *sky coverage*, based on the assumption that scans at different elevation and azimuth help to better resolve the tropospheric errors. Based on a given target SNR (signal-to-noise ratio) of usually 15 or 20, the scan length

t_{scan} is determined based on the strength of the source (source flux), the sensitivities of the contributing antennas (measured in antenna specific *system equivalent flux density* (SEFD)), and the data rate as a measure how much data is recorded per time unit:

$$t_{scan} \approx \left(\frac{\text{SNR}}{\text{flux}} \right)^2 \cdot \frac{\text{SEFD}_1 \cdot \text{SEFD}_2}{\text{data rate}} \quad (1)$$

The scan length has to be determined for each baseline, meaning each antenna pair in the network of antennas observing the same source. It is the weakest partner antenna that determines how long a telescope has to stay on source.

In between scans, the slewing time an antenna needs to move from one source to the next has to be calculated. In general one can say that the old, typically larger, legacy antennas are more sensitive but slower, while the new small dishes are less sensitive but can slew much faster. Also, weaker sources have to be observed longer than strong ones. To overcome the longer on-source times, the VGOS concept includes the transition to a much higher data rate of up to 32 Gbps, compared to 256 Mbps that is commonly used today. In the AUSTRAL network we usually perform AUSTRAL experiments (Plank et al., 2015) with a 1-Gbps data rate.

While scheduling telescopes of a similar type is rather simple, it becomes more complicated when different types of antennas are used. It then has to be decided, for example, whether one should wait for a slow antenna and accept idle time for the fast telescopes or skip the slow antenna in a scan and allow more observations for the fast antennas. Additional complications arise when multiple sub-nets are observing at the same time. In this work we concentrate on the AUSTRAL network without the African antennas where there is almost no sub-netting necessary.

2.1 New Tag-along Mode

In the first example we have the four 12-m telescopes in Australia/New Zealand and intend to add the 26-m Ho antenna. In order to distinguish between different scheduling options, we give the number of scans per hour for each station in Table 1. For improved schedules, we aim for a high number there.

When only scheduling the four fast 12-m antennas (HbKeYgWw), we find 37 scans per hour per station. When we add the 26 m to the network, this number reduces to 24 scans for the 12-m stations and to 23 scans for Ho, respectively. Without special measures, Vie_sched favors larger networks causing the fast antennas to wait for Ho. This leads to about 45% idle time for the 12-m dishes.

Table 1 Number of scans per hour for each antenna of the Australian/New Zealand network plus the 26-m Ho antenna. The new mode is the improved tag-along mode.

# of scans/h	fast 12-m	Ho
HbKeWwYg	37	–
+ Ho	24 (45% idle)	23
+ Ho new mode	37	16

The classical way to include a telescope in a schedule without *disturbing* it is the so-called tag-along mode. For this, the schedule is first created without this additional antenna. In the end the software goes through the schedule and looks for scans that the new antenna can reach in time and which are long enough to get sufficient SNR on all baselines. For our schedule we chose a slightly different approach: we simply decided not to wait for Ho when determining the start time of a scan and Ho can take part whenever it can reach the source in time. The advantage over the classical tag-along mode is the fact that our strategy includes Ho in all other optimization criteria such as the sky-coverage or higher weight for scans with more antennas. Applying this new *improved tag-along mode* we find that Ho does not weaken our schedule. We keep the 37 scans/h for the small dishes and get a decent 16 scans/h for Ho.

This new mode allows us to schedule the Ho antenna in the AUSTRAL network without influencing the number of scans for the small antennas. Hence we expect to keep the high precision in geodetic results (e.g., baseline lengths) and additionally get local baseline observations for the determination of the local tie. However, a thorough comparison with the standard tag-along mode or in terms of sky coverage has not been done so far.

2.2 Twin Mode

The second newly implemented scheduling mode is the proper scheduling of twin telescopes. Before going into detail on this, let us recall the main reasons for the twin concept:

- the main idea is to get more observations at one site. While one antenna is observing, the other can already slew to the next source;
- a second motivation is to overcome maintenance without disturbing continuous observations;
- a third interesting mode is simultaneous observations of different sources. This would allow for a better scanning of the troposphere, the largest error source in VLBI today.

For the implementation of the twin mode we chose that only one dish of the twin is observing while the other has time for slewing. For a scan, the software picks whichever antenna has the shorter slewing to come on source. In our example schedule, we chose the Hobart *twin* in the AuScope network. To simulate a twin telescope, both antennas were given the sensitivity and *fast* slew speeds of the Hb antenna ($5^\circ/\text{s}$ in azimuth and $1.25^\circ/\text{s}$ in elevation).

We find that in the AuScope network with three identical antennas, a twin is not much use. Whether Hb is scheduled as a twin or as single dish, we find 49 scans/h (Table 2).

Table 2 Number of scans per hour for different schedules, illustrating that a *fast* twin telescope can overcome its shortcomings in a network of *very fast* antennas.

# of scans/h	AuScope
3 slow	49
3 fast	58
2 fast + Hb	51
2 fast + Hb + Ho	58

We then simulated three *very fast* antennas ($12^\circ/\text{s}$ in azimuth and $6^\circ/\text{s}$ in elevation) in 1-Gbps AUSTRAL mode, which would give us 58 scans/h.

When we further assume that only Ke and Yg are *very fast* while Hb keeps its real speed, the number of scans per hour drops to 51. If finally Hobart is replaced with a *fast* twin telescope, this can compensate for the reduced slew speed and we find again 58 scans per station (counting Hb and Ho as one station).

This means, that in a network of *very fast* VGOS telescopes a twin telescope with reduced slew speeds can keep up with the high cadence source switching.

2.3 Star Mode

The final new mode is the so-called star mode. The motivation for it was enabling the AUSTRAL network with its small and low-sensitivity antennas to carry out experiments with astrometric demands. The idea is to add the Ho antenna to the network and increase the network's sensitivity allowing for observations of weaker sources.

However, while adding the Ho antenna would give higher sensitivity on baselines with this large antenna, it would not change anything on the other baselines, e.g., between Yg and Ke. As a consequence, the total length of the scan in the whole network will not change, neither would it become possible to observe weaker sources. With the AuScope array, sources down to 0.4 Jy flux can be observed with scan lengths of up to 500 seconds.

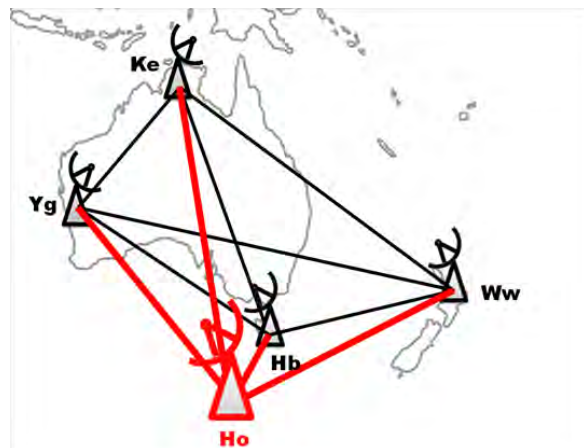


Fig. 3 Illustration of the star mode. The scan length is determined only using the baselines including Ho (thick red lines).

In order to fully exploit the contribution of an additional, more sensitive antenna, we developed the star mode as illustrated in Figure 3. In cases of weak sources, the scan length is determined only using the baselines to Ho. It is then most likely that on the other baselines between two small antennas only an insuffi-

cient SNR will be achieved leading to non-detections on these observations. On the other hand, it allows the observation of much weaker sources. In the case of the AuScope array plus Ho, keeping the scan lengths under ten minutes allows sources down to about 0.15 in X-band and 0.2 in S-band to be observed.

It is then the task of the scheduling software to properly mix *normal* scans for the whole network and those to *special sources* in the star mode.

We have realized this new mode for the session AUA009 observed on February 23, 2016. Participating antennas were the 12-m antennas Hb, Ke, Yg, and Ww plus the 26-m antenna Ho. In addition we selected a list of seven weak sources (Table 3).

Table 3 List of target *special* sources for AUA009 including their flux in X- and S-band.

source	X-flux	S-flux
0244–470	0.40	0.25
0212–620	0.40	0.30
0758–737	0.15	0.20
0918–534	0.16	0.50
1334–649	0.20	0.20
1941–554	0.20	0.20
2333–528	0.40	1.00

Without modification in the scheduling, these target sources would be observed with scan lengths of up to 60 minutes or more, which is not very practicable. When applying the new mode, these lengths were reduced to reasonable one–ten minute scans.

Practically we realized a combination of classical geodetic scans with the 12-m antennas to strong sources with Ho in tag-along. Every thirteenth scan was scheduled to one of the target sources applying the star mode. This gives about ten scans for each of these target sources over the 24-hour session. While the parameter for balancing between standard and target scans (13:1) was determined iteratively, all other scheduling is fully automated.

For AUA009, we find 34 scans/h for the 12-m antennas and 12 scans/h for Ho (Table 4).

Table 4 Overview of scan numbers in AUA009 for the 12-m antennas, the large Ho antenna, and for the special target sources.

# of scans/h	12-m	Ho	special sources
AUA009	34/h	12/h	~10/24h

Small shortcomings of this mode at the moment are that for Ho the *old* tag-along mode (see Section 2.1) is used without considering Ho for the sky coverage. Also, as already mentioned above, it is only semi-automated so far.

3 Summary and Outlook

For the example of the sibling telescope in Hobart and its application in AUSTRAL sessions we have developed three new scheduling modes, all implemented in a preliminary version of *Vie_sched*.

The new tag-along mode allows for local baseline measurements between the new and the legacy telescopes, without degrading the schedule for the small and fast dishes. The star mode is an innovative schedule with the new concept of determining the scan lengths for only a sub-set of baselines within a network. This new strategy is very promising and was already applied in AUA009 (with correlation under way at the moment). This new mode allows the AuScope array to undertake much more responsibilities in monitoring sources in the southern sky, as by addition of one or more large telescopes the sensitivity can be significantly increased.

Future developments of these new modes will include refinements in the software implementation, application to real sessions, as well as investigations concerning the extension to larger networks comprising several sibling and twin telescopes.

Acknowledgements

This work was supported by the Austrian Science Fund (FWF, projects J 3699-N29 and I 2204) and the AuScope Initiative, funded under the National Collaborative Research Infrastructure Strategy (NCRIS), an Australian Commonwealth Government Programme.

References

- Böhm J, Böhm S, Nilsson T, Pany A, Plank L, Spicakova H, Teke K, Schuh H (2012) The new Vienna VLBI Software *VieVS*. In: Proceedings of the 2009 IAG Symposium, Buenos Aires, Argentina, International Association of Geodesy Symposia, vol 136, doi: doi:10.1007/978-3-642-20338-1_126.
- Gipson J (2016) SKED VLBI Scheduling Software. Goddard Space Flight Center ftp://gemini.gsfc.nasa.gov/pub/sked/SkedManual_v2_016Jan31.pdf.
- Lovell J, McCallum J, Reid P, McCulloch P, Baynes B, Dickey J, Shabala S, Watson C, Titov O, Ruddick R, Twilley R, Reynolds C, Tingay S, Shield P, Adada R, Ellingsen S, Morgan J, Bignall H (2013) The AuScope geodetic VLBI array. *J Geod* 87:527–538
- Petrachenko B et al. (2009) Progress Report of the IVS VLBI2010 Committee: Design Aspects of the VLBI2010 System. NASA/TM-2009-214180 <ftp://ivscg.gsfc.nasa.gov/pub/misc/V2C/TM-2009-214180.pdf>.
- Plank L, Lovell JE, McCallum J, Rastorgueva-Foi E, Shabala SS, Böhm J, Mayer D, Sun J, Titov O, Weston S, Gulyaev S, Natusch T, Quick J (2015) Results from the regional austral VLBI sessions for southern hemisphere reference frames. International Association of Geodesy Symposia, Springer Berlin Heidelberg, pp 1–6, doi: doi:10.1007/1345_2015_132.
- Sun J (2013) VLBI scheduling strategies with respect to VLBI2010. *Geowissenschaftliche Mitteilungen* 92, Schriftenreihe der Studienrichtung Vermessung und Geoinformation, Technische Universität Wien, ISSN 1811-8380.
- Sun J, Böhm J, Nilsson T, Krásná H, Böhm S, Schuh H (2014) New VLBI2010 scheduling strategies and implications on the terrestrial reference frames. *J Geod* 88:449–461.

Prototyping Automation and Dynamic Observing with the AuScope Array

Jim Lovell¹, Lucia Plank¹, Jamie McCallum¹, Stas Shabala¹, David Mayer²

Abstract The continuous observing mode envisioned for the new array of VGOS stations would benefit greatly from a high level of automation, from scheduling through to analysis. The centrally-operated AuScope VLBI array of three 12-m antennas in Australia is serving as a testbed for these automation techniques. Here we describe the challenges we are addressing and how we are using simulations to understand where the most beneficial improvements can be obtained (in dynamic scheduling for example), and we present the progress we have already made.

Keywords VLBI, VGOS, observations, techniques

1 Introduction

The AuScope Very Long Baseline Interferometry (VLBI) array, consisting of three 12-m diameter radio telescopes at Yarragadee (WA), Katherine (NT), and Hobart (TAS), is an important southern component of the global IVS network [1]. The array was constructed as part of the Australian Federal Government's National Cooperative Research Infrastructure Strategy (NCRIS), funded in 2006, and is a component of AuScope, an infrastructure framework to support geological, geochemical, geophysical, and geospatial research. The VLBI array is currently participating in ~ 140 IVS 24-hour sessions per year but has demonstrated sustained operations at a level of 210 days per year over a 12-month period in 2014/15. The increased

number of stations and observations in the southern hemisphere that AuScope provides has significantly addressed the north-south imbalance in global geodetic solutions [2]. Being a self-contained VLBI array with centralized operations and a scheduling, correlation, and analysis capability, it also serves as a useful facility for testing new technologies and techniques.

The main focus in geodetic VLBI at the moment is the transition to VGOS, the VLBI Global Observing System [3]. The VGOS vision includes a global array of small, fast slewing antennas with broadband receiving systems and high data recording rates. The array would operate continuously, and initial data products are required within 24 hours of observing. It has been suggested that VGOS would benefit greatly from a centralized operations model where a handful of Operations Centers (OCs) manage the scheduling, observing, correlation, and analysis for the entire array (e.g., [4]).

Centralized operations of the VGOS array would provide the opportunity to make the best use of the available resources of antennas and correlators. Remote control and monitoring of these facilities would allow observing programs to be optimized to best meet their aims, and these decisions could be made in real time if necessary rather than months in advance as is typical in the current paradigm. This concept has been termed Dynamic Observing [4]. For example, rapid dUT1 observations could be configured with two antennas with the best long east-west baseline and an idle small correlator with good network connectivity. Meanwhile an experiment to determine Earth Orientation Parameters could be configured with an array with a well-balanced geometry. Before a 24-hour session is started, a short observation could be made to check for fringes and measure telescope sensitivity (SEFD). This

1. University of Tasmania

2. Technische Universität Wien

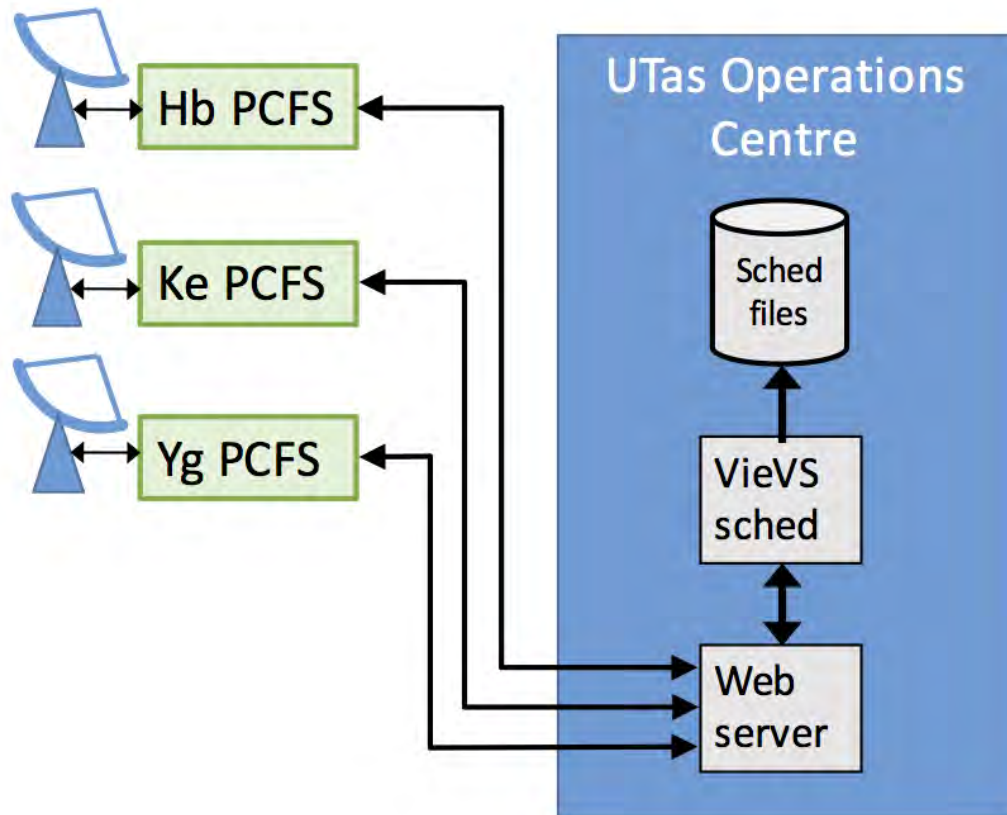


Fig. 1 A schematic showing the main components of the Dynamic Observing test made with the AuScope array in March 2016. Scheduling was handled from UTas with a 15-minute refresh cycle, and observatories were able to communicate with the operations center to report their availability and retrieve schedules.

information could be used to generate a schedule that is optimized for current telescope performance.

A significant problem with the Dynamic Observing concept is that, for reasons such as security, many facilities will not permit remote access or control. In this paper we describe a possible solution to this problem and present a demonstration of its implementation using the AuScope array.

2 A Demonstration of Secure Dynamic Observing

A facility could still take part in Dynamic Observing if it maintained full control over participation in operations and could join or leave the pool of resources at any time. However, under this scenario it would be nec-

essary for the Operations Center to respond quickly to these changes and adapt the observing program accordingly. In turn, the remote facility (telescope or correlator) would be required to send the Operations Center the necessary status information and, in the case of an observatory, regularly obtain and execute schedule information.

In March 2016 we began work to test the feasibility of this solution using the AuScope VLBI array where scheduling of the observations was coordinated from the operations room at the University of Tasmania. At this stage, no attempt at correlator operation was made. All three 12-m telescopes were used with monitoring and automated scheduling carried out from the operations room. The telescopes were configured with a 1-Gbps observing mode (S/X-band, 16-MHz bands, and 2-bit sampling).

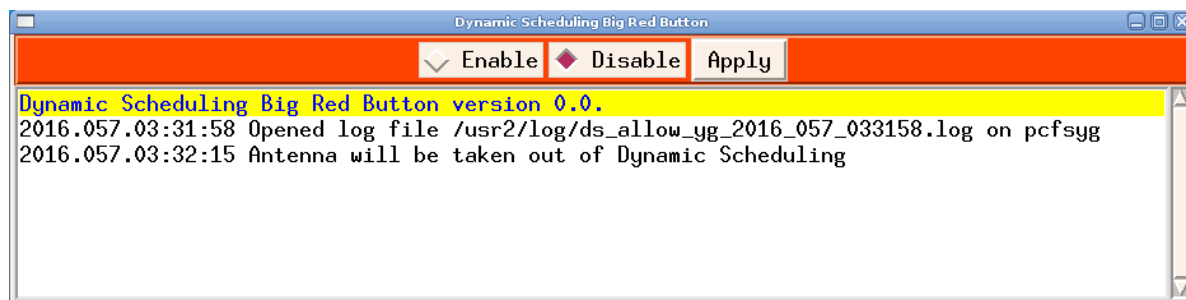


Fig. 2 The user interface running at Katherine that permits the observatory to opt in or out of Dynamic Observing sessions at any time.

At the operations center a version of the VieVS scheduler `vie_sched` (running under Octave) was used [5]. This software was configured to generate a new piece of schedule every 15 minutes based on information on telescope availability: a schedule was only generated for an observatory if it reported that it could participate. A 15-minute cycle time was chosen as this is the minimum amount of time that a tropospheric solution could be obtained under the observing mode in use. Once a new schedule file was generated, the information on the scheduled telescopes, the schedule file name, and the start time were all published on a Web server. At 0 UT every day, the scheduling software produced a VEX file of the past 24 hours of observations ready for correlation (Figure 1).

At the observatories, the standard PC Field System (PCFS) software was used but with three additions. The first was a simple application with a graphical interface that allows a local user to join or leave the observations at any time. The user can simply choose to participate or not, and this status information is sent immediately to the operations center (Figure 2). The second piece of software is called `dysched.pl`, a script that runs on a continuous one minute cycle. It uses an additional PCFS program called `mondump` to send status information to the schedule server, retrieve a new schedule if one is available, and append it to the dynamic observing schedule that is currently running. If the observatory has chosen not to participate in an observation, `dysched.pl` will not update the schedule but will continue to run and reactivate the observations when the local user chooses to do so. The monitoring information, including the antenna availability status, is received at the Operations Center and displayed on a Web page.

The demonstration session lasted for approximately eight hours. During this time, antennas were locally added and removed, and it was confirmed that the scheduling software adapted accordingly. Following the observations, the data from Katherine and Yarragadee were shipped to Hobart for correlation on a local PC cluster using DiFX. Good fringe detections were obtained on all baselines.

The scheduling software keeps a record of the last source observed in the previous 15-minute segment, the antenna position, and cable wrap information. This is used as a starting point for the following 15 minutes. This (currently) has the disadvantage that an optimization of source and sky coverage over a longer period (24 hours in the case of current IVS observations) is not done. It will be necessary to compare the quality of results from these two observing modes and assess if a 15-minute cycle is suitable or not. If not, then longer cycle times may be needed, or changes to how the scheduling software uses previous observations to optimize for future ones may be required.

3 Conclusions and Outlook

The AuScope VLBI array has been used to make some preliminary demonstrations of the Dynamic Observing concept while allowing local stations to maintain control and, thereby, hopefully alleviating restrictions that might prevent centralized coordination of operations in a VGOS scenario.

We plan to continue developing and demonstrating the Dynamic Observing concept, firstly by increasing the duration of experiments to 24 hours and making comparisons of data products with those from the

traditional 24-hour block concept. We will investigate whether the 15-minute cycle time is optimal and if there is a benefit in making this a dynamic quantity that changes depending on telescope parameters and data rates. Other developments will include adding a correlator feedback loop for fringe checking and antenna sensitivity measurements which can be used by `vie_sched` for optimization. Further, we will include telescopes from other institutes to further test and demonstrate the capabilities of Dynamic Observing. Routine application of Dynamic Observing could lead to a significant increase in observing time. Whenever an IVS network station finds itself idle for a few hours (e.g., an astronomy session was cancelled due to bad weather) and is willing to observe, it can be easily included in global observations.

A further aim is to move from development to implementation, making Dynamic Observing the routine procedure for the AuScope VLBI array.

Acknowledgements

This study made use of data collected through the AuScope initiative. AuScope Ltd is funded under the

National Collaborative Research Infrastructure Strategy (NCRIS), an Australian Commonwealth Government Programme. The authors thank the Austrian Science Fund (FWF) for supporting this study (projects J 3699-N29 and I 2204). This work was supported by the Australian Research Council (FS1000100037, FS110200045, and DE130101399).

References

1. J. Lovell et al. 2013, *J. Geod* 87, 527.
2. L. Plank, J. Lovell, S. Shabala, J. Böhm, O. Titov 2015. *Adv Sp Res* 56:304–313.
3. B. Petrachenko et al., 2009, NASA/TM-2009-214180, June 2009.
4. J. Lovell et al. 2014, in *IVS 2014 General Meeting Proceedings*, Edited by Dirk Behrend, Karen D. Baver, and Kyla L. Armstrong Science Press (Beijing), ISBN 978-7-03-042974-2.
5. J. Sun, J. Böhm, T. Nilsson, H. Krásná, S. Böhm, H. Schuh (2014) New VLBI2010 scheduling strategies and implications on the terrestrial reference frames. *J Geod* 88:449–461.

First Results of the FAST-S/X Sessions with New VGOS Antennas

Alexander Neidhardt¹, Pablo de Vicente², Alessandra Bertarini^{3,7}, Thomas Artz³, Sebastian Halsig³, Dmitry Ivanov⁴, Alexey Melnikov⁴, Johannes Böhm⁵, Andreas Hellerschmied⁵, David Mayer⁵, Christian Plötz⁶, Gerhard Kronschnabl⁶, Axel Nothnagel³, Sergei Kurdubov⁴, Andrey Mikhailov⁴, Dmitry Marshalov⁴, Iliia Bezrukov⁴, Yu. Bondarenko⁴

Abstract During the VTC meeting in Ponta Delgada, Portugal, it was decided to form a group with the goal of testing the fast slewing mode of the VGOS antennas on intercontinental baselines. The goal is to observe S/X-schedules regularly using fast slewing modes of the antennas. Two sessions, FAST02 and FAST03, were scheduled with VieVS at the Vienna University of Technology, employing the new VGOS antennas at Yebes in Spain, Wettzell in Germany, and Zelenchukskaya and Badary in Russia. FAST02 was a 24-hour session observed in DDC mode. FAST03 was a six-hour session to test the PFB mode. The correlation was done both in Bonn, where also the main geodetic analysis was made, and at the IAA in Russia. Unfortunately, FAST03 was not successful due to incompatible frequency setups. In this paper, we report on the first results of the FAST02 session.

Keywords FAST, S/X observations, VGOS antennas

1 Introduction

The first international 24-hour long session, FAST02, was observed on December 16/17, 2015 using the fast slewing modes of the new VGOS antennas with a standard S/X-frequency setup. The goal was to demon-

strate and test the capabilities of scheduling, running, correlating, and analyzing sessions in the new modes. While the VGOS tests directly focus on broadband experiments, the FAST sessions should demonstrate which improvements for standard setups can be made by increasing the number of observations within 24 hours. While FAST02 used a standard frequency setup, FAST03 tested the polyphase filterbank mode with 16x32 MHz continuous channels in combination with the direct sampling mode at the Russian sites. While FAST02 provided usable results, except for some existing issues, FAST03 could not be correlated due to the missing overlap of frequencies observed.

2 Scheduling of FAST Sessions

The FAST sessions were scheduled with VIE.SCHED [9], the scheduling module of the Vienna VLBI Software (VieVS) [1]. VIE.SCHED automatically generates geodetic VLBI schedules with an optimized sky coverage at each station. On-source times are determined to meet the defined target SNR (15 dB and 20 dB for S- and X-band respectively), considering source fluxes, antenna sensitivities, and the recorded data rates. Slew times are calculated according to the antenna specifications.

We chose to stay close to the standard setting of S/X observations. Basically, the GEO-SX mode was used with increased data rates of 1 Gbps and 2 Gbps for FAST02 (DDC mode) and FAST03 (PFB mode), respectively. Badary and Zelenchukskaya used data rates of 6 Gbps and 4 Gbps for FAST02 and FAST03, respectively. Due to constraints and a very high sampling rate at the Russian stations, a special relaxed

1. FESG Wettzell, Germany
2. Observatorio de Yebes-IGN, Spain
3. IGG Bonn, Germany
4. Institute of Applied Astronomy RAS, Russia
5. Technische Universität Wien, Austria
6. BKG Wettzell, Germany
7. MPIfR Bonn, Germany

mode (only every 4th scan was observed) was implemented for ZELEN13M (Zv) and BADAR13M (Bv). The minimum scan length was set to 20 seconds, and sub-netting was enabled in order to get a reasonable sky coverage at all sites.

A summary of the schedule can be found in Table 1. With this setup, WETTZ13N (Wn) and RAE-GYEB (Yj) get about 70 scans/hour which is an increase of about a factor of 3 compared to normal IVS-R1 and IVS-R4 sessions. Another apparent fact is that about 30% of the time is used for calibration. In order to get the most scans/hour this limiting factor has to be decreased by revising the calibration procedures. However, this was not done for this schedule and is subject to future investigations.

Table 1 Schedule summary for FAST02 and FAST03. With the fast VGOS antennas a remarkably large number of observations was reached, with an average of 70 and 73 scans/hour at Wn and Yj respectively (Russian antennas only participated in every fourth scan).

	FAST02				FAST03			
Session start	2015-12-16 13:00 UT				2015-12-21 9:00 UT			
Duration [h]	24				6			
Site statistics	Wn	Yj	Bv	Zv	Wn	Yj	Bv	Zv
Obs. time [%]	42	43	12	11	42	42	11	10
Cal. time [%]	31	31	8	8	32	32	8	8
Slew time [%]	19	25	13	14	19	26	13	14
Idle time [%]	8	1	67	67	7	0	67	67
Scans total	1658	1658	413	415	510	510	126	128
Scans/hour	70	70	18	18	73	73	19	19
Avg. scan [sec]	22	23	25	24	21	21	21	21

3 Observation Network

A network of the antennas at Badary (Bv), Wettzell (Wn), Yebes (Yj), and Zelenchukskaya (Zv) was used. All antennas are VGOS-compliant and use 13.2-m dishes with ring-focus design. For the FAST-sessions they were at least temporarily equipped with S/X/Ka-band feeds and receivers. While Yj uses six down-converted intermediate frequency bands (IF) with two polarizations, the other antennas support eight bands from an up-down-converter, for example, to offer four bands in both polarizations. The European antennas used a DBBC2 and a Mark 5B+ for digitization and recording backend for digital down

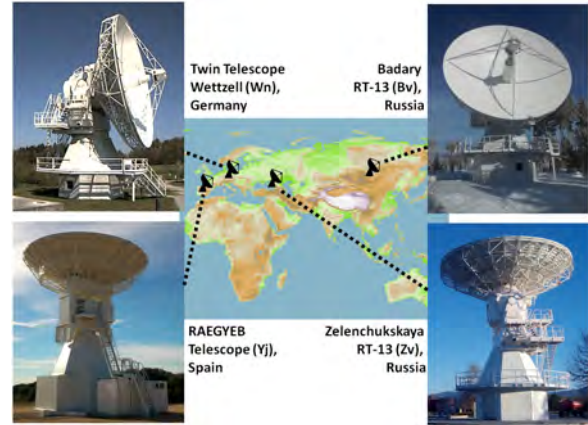


Fig. 1 The observation network used for FAST02 and FAST03.

conversion (FAST02) or polyphase filter bank mode (FAST03). The Russian antennas used the proprietary Broadband Acquisition System (BRAS) [5, 6, 7] which implements direct sampling conversion and the Data Recording System (DRS) for high speed recording. Both systems are developed in Russia.

Badary and Zelenchukskaya radio telescopes observed every fourth scan of the 24-hour FAST02 experiment due to limited disk capacity. The reason is that the current version of the DRS software cannot automatically switch to a free disk pool during a running session. Therefore, this could have been changed manually by the operator, using a patched software but to avoid potential operator mistakes, we decided to observe without manual switching.

4 Correlation

The correlation was successfully done at Bonn, Germany and at the IAA in Russia to do extended investigations into different aspects.

4.1 Correlation at the Bonn Correlator, Germany

FAST02 was correlated in Bonn using the DiFX ([3]) software correlator. To correlate this experiment, “zoom band mode” was used to deal with the different backend setups: the Russian antennas recorded the data

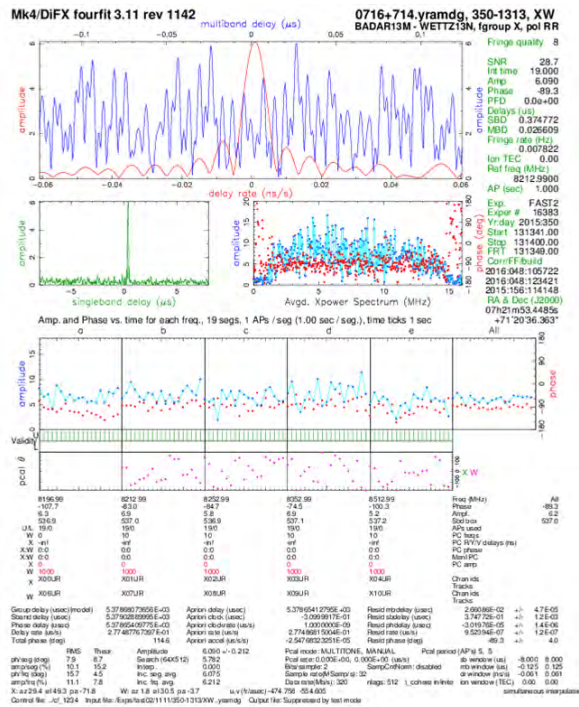


Fig. 2 Baseline Bv-Wn (zoom band). In this case only five X-band channels are seen because of the splitting of Bv data into three files, of which only one was used for the correlation.

using direct sampling (3 x 512 MHz channels), whilst Yebe and Wettzell used 16 x 16 MHz-wide channels. DiFX was instructed to extract and cross-correlate only the part of the bands which were common to all four stations. Because the Russian antennas wrote the data into three different files (one per IF output), three processes of correlation would have been required. We only performed one pass, hence we correlated only five X-band channels (see Figure 2).

4.2 Correlation by the IAA, Russia

Correlation was also performed at the IAA RAS with DiFX 2.4.0 on the new blade-server hybrid cluster together with a new GPU-based correlator [4]. Because of the mixed bandwidth setup (Wn and Yj with 16 MHz-wide channels; Bv and Zv with 512 MHz), and also shifted sky frequencies by 10 kHz at Wn and Yj, it was necessary to use the *zoom band* mode of DiFX. It allows extraction of exact frequency ranges from spectra for the correlation. One method is to set

10.24 MHz bandwidths of every zoom band channel to get power of two spectral points in correlated data used with HOPS (first time suggested by the Chinese RU0197 fringe test). Another method is to shift the LO by 10 kHz and put proper values into the VEX file for the Bv and Zv antennas (suggested by W. Brisken). Both methods were applied, and fringes were obtained. Additionally, analysis data were used for a second correlation method. The data of the Russian antennas from three individual 512 MHz-wide channels were merged into a single VDIF file, and all 16 frequency channels were correlated in one pass. We also performed correlation of the Bv-Zv baseline only with 512 MHz-wide channels and an independent correlation of three groups of 16 MHz-wide channels: two in X-band and one in S-band. Post-processing was done with the PIMA software [8] without adaption of phase calibration (pcal).

5 Analysis

5.1 Analysis by the IGG Bonn, Germany

The data processing has been done with vSolve [2]. This includes the resolution of ambiguities and the calculation of the ionospheric contribution. In the least-square adjustment, clocks (reference clock: Wettzell) and zenith wet delays were estimated in the form of 60-minute continuous piece-wise linear functions (CPWLF) and gradients as daily CPWLF. The corresponding residuals are depicted in Figure 3. Significant offsets can be seen between Wettzell/Yebes and Badary/Zelenchukskaya, which are currently unexplained. Further investigations are in progress to find the reasons for these inconsistencies. Most probably this is due to inconsistencies of the station setups.

To overcome this issue, we estimated baseline clock offsets for the baselines Yebe-Badary and Yebe-Zelenchukskaya and ended up with weighted root mean squared residuals at the level of legacy VLBI sessions, i.e., 57 ps. As can be seen in Figure 4, there is a saw-like structure in the residuals for all baselines with Yebe. This slightly degrades the solution. However, this feature can be explained by the behavior of the air conditioning system.

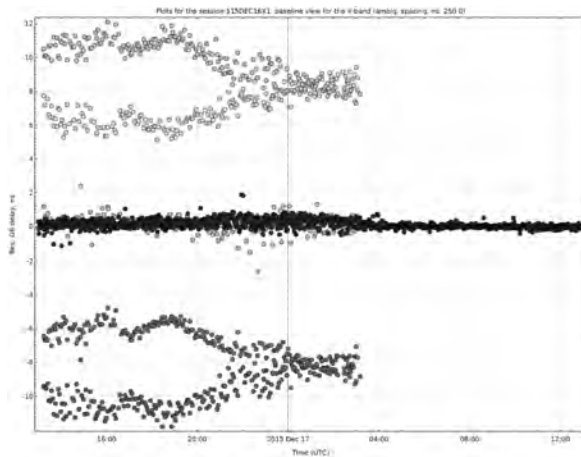


Fig. 3 Post-fit residuals for all baselines. Residuals around zero belong to Wetzell-Yebes (black) and Badary-Zelenchukskaya (gray).

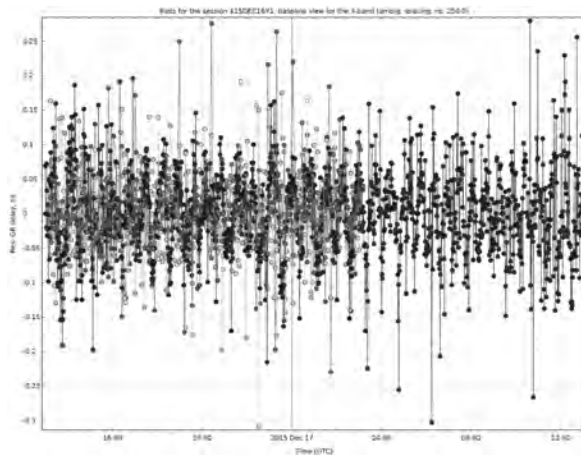


Fig. 4 Post-fit residuals when estimating baseline clock offsets for all baselines, especially the residuals for the Wetzell-Yebes baseline (black), which represent the spurious saw-like variations at Yebes due to the air conditioning system.

5.2 Analysis by the IAA, Russia

The analysis was also done with the “Quasar” software suite (see Figure 5). The top panel a) of Figure 5 looks rather noisy, but there are no significant triangle closures. The baselines with Badary (panel b) of Figure 5: WnBv and YjBv) allow the assumption of several clock breaks. However, ZvBv (panel c) of Figure 5) does not show such peculiarities, but on the contrary there are strong saw-like patterns of clock irregularities. The data from WnZv and YjZv do not show anything unusual.

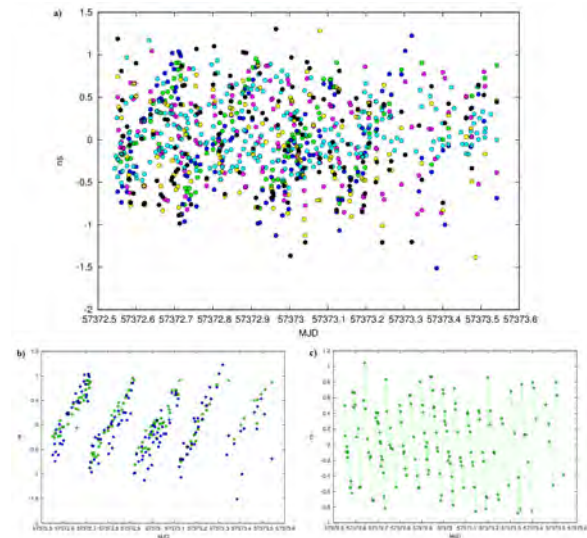


Fig. 5 Intermediary solution: a) residual plot for baselines WnBv (blue), YjBv (green), BvZv (violet), YjWn (gray), YjZv (yellow), WnZv (black), b) focus on baselines WnBv (blue) and YjBv (green), and c) focus on baseline ZvBv.

As a result, the triangle disclosures are about 0.5 ns in magnitude revealing a saw-like pattern, which have different periodicities for different baseline combinations.

6 Conclusion and Outlook

The scheduling and observation of the first FAST sessions were a first step using VGOS antennas for fast-slewing experiments. FAST02 delivered results using existing formats and recording systems. The correlation ran smoothly within ten hours. We had high SNRs and a detection rate of 99% because in only one percent of the scans telescopes were late on source. This demonstrates that the network is able to observe fast-slewing experiments. The analysis used the S/X-legacy mode which is comparable to all other IVS experiments. There was a higher temporal resolution, but there is also the need to investigate 17 ns triangle misclosures, which might be caused by different station setups and by a problem with the cycling of the air conditioning system at Yebes, which influenced the analysis results and needs to be eliminated.

The data analysis was successful with WRMS residuals at the level of legacy VLBI sessions. Unfor-

tunately, there is a spurious signal in the residuals due to the behavior of the air conditioning system at Yebe, which degrades the solution. Thus, estimating zenith wet delays with a higher temporal resolution than one hour has no physical meaning. However, due to the huge amount of observations, it would be possible to go down below ten minutes, which represents the success and opportunities of our observing mode.

After having gained experience from the two FAST campaigns, where we demonstrated the possibility of scheduling, observing, correlating, and analyzing the fast slewing mode, we can now follow-up with better designed observations. Furthermore, we would like to enlarge our array to more VGOS antennas that are equipped with S/X-receiving systems. We plan to improve and smooth the processing, by using a common setup and a standardized way of observation. An important result obtained from these campaigns is that shorter scan lengths are possible: ten seconds might be achieved while keeping the good performance.

Acknowledgements

This research is based on observations processed at the Bonn Correlator, jointly operated by the Max Planck Institute for Radio Astronomy (MPIfR) and the Federal Agency for Cartography and Geodesy (BKG).

The RAEGYEB telescope received partial funding from MINECO grant FIS2012-38160 for the activities described here. The activities for the construction of the 13.2-meter RAEGYEB radio telescope were co-financed by ERDF/FEDER 2007–2013 under the project: “VGOSYEBES: Radiotelescopio de VLBI Geodesico y Astrometrico para su integracion en la red VGOS.”

References

1. Böhm, J., Böhm, S., Nilsson, T., Pany, A., Plank, L., Spicakova, H., Teke, K., and Schuh, H. (2012). The new Vienna VLBI Software VieVS. In *Proceedings of the 2009 IAG Symposium, Buenos Aires, Argentina*, Vol. 136, 1007–1011, International Association of Geodesy Symposia, 31 August - 4 September 2009.
2. S. Bolotin, K. Bayer, J. Gipson, D. Gordon, D. MacMillan (2012). The First Release of *nuSolve*. In: *IVS 2012 General Meeting Proceedings*, D. Behrend and K. Bayer (eds.), NASA/CP-2012-217504, 222–226, 2012.
3. Deller, A. T., Tingay, S. J., Bailes M., West, C. (2007). DiFX: a software correlator for very long baseline interferometry using multiprocessor computing environments, *Publications of the Astronomical Society of the Pacific* 119, 318, 2007.
4. V. Ken, I. Surkis, Y. Kurdubova, A. Melnikov, N. Mishina, V. Mishin, V. Shantyr (2015). IAA VGOS GPU-based Software Correlator: current status and broadband processing. In: R. Haas, F. Colomer (eds.), *Proceedings of 22nd EVGA Working Meeting*, 40–42, 2015.
5. N. E. Koltsov, D. A. Marshalov, E. V. Nosov, L. V. Fedotov (2013). A data acquisition system of the S/X-wave range of the radio interferometer for the universal time on-line monitoring. *Instruments and Experimental Techniques*, Vol.56, No.3, 339–346, 2013.
6. E. Nosov, A. Berdnikov, S. Grenkov, D. Marshalov, A. Melnikov, L. Fedotov (2014). Current Development State of the Russian VLBI Broadband Acquisition System. In: *International VLBI Service for Geodesy and Astrometry 2014 General Meeting Proceedings*. Science Press, Beijing, China, ISBN 978-7-03-042974-2, 82–85, 2014.
7. D. A. Marshalov, A. S. Berdnikov, S. A. Grenkov, A. V. Krohalev, E. V. Nosov, L. V. Fedotov, A. V. Shemanaev (2015). The results of Preliminary Tests of Broadband Digital Conversion System for Radio telescopes. *IAA Transactions*. Issue 32. St.-Petersburg, 27–33, 2015.
8. L. Petrov, Y. Y. Kovalev, E. B. Fomalont, D. Gordon (2011). The VLBA Galactic Plane Survey - VGaPS. *Astron. J.*, 142, 35, 2011.
9. Sun, J., Böhm, J., Nilsson, T., Krásná, H., Böhm, S., and Schuh, H. (2014). New VLBI2010 scheduling strategies and implications on the terrestrial reference frames. *Journal of Geodesy*, 88, 449–461, 2014.

Current Status of an Implementation of a System Monitoring for Seamless Auxiliary Data at the Geodetic Observatory Wettzell

Alexander Neidhardt¹, Katharina Kirschbauer², Christian Plötz³, Matthias Schönberger³, Armin Böer³, and the Wettzell VLBI Team³

Abstract The first test implementation of an auxiliary data archive is tested at the Geodetic Observatory Wettzell. It is software which follows on the Wettzell SysMon, extending the database and data sensors with the functionalities of a professional monitoring environment, named Zabbix. Some extensions to the remote control server on the NASA Field System PC enable the inclusion of data from external antennas. The presentation demonstrates the implementation and discusses the current possibilities to encourage other antennas to join the auxiliary archive.

Keywords Seamless auxiliary data, system monitoring, Zabbix

1 Introduction

The Global Geodetic Observing System (GGOS) requires permanent monitoring systems (e.g., for the determination of the local ties at sub-millimeter accuracy) to achieve the positioning precision goals ([5]). Besides the main products, several additional parameters might be worth being monitored to improve the final geodetic solution. Therefore, the IVS Task Force for Seamless Auxiliary Data was founded during the Analysis Workshop in Shanghai 2014 to discuss and find solutions to improve the current situation (for the following see [4]). Possible implementations should be

demonstrated. Further on, suggestions could be made about the type of data which are useful and how observatories can contribute to the real-time data stream. It would also have some positive effects on the accuracy of IVS data products if data were to be continuously available. Real-time auxiliary data can also contribute in a dynamic observing scenario where scheduling decisions are automatically made.

Therefore the main goals are:

- Continuous, auxiliary data (are of high interest),
- Additional data (might be interesting for research),
- Centralized data repository,
- Real-time overview of the observation network, and
- Preparations for dynamic observations.

The implementation of a seamless auxiliary database follows two phases (see Figure 1). The first is a proof-of-concept section lasting one year. The NASA Field System and the e-RemoteCtrl software ([3]) should be extended with a sending functionality during this development section so that currently available auxiliary data can be sent. Tests are ongoing at Wettzell including other data propagation mechanisms, such as the one from the mm-VLBI group [6]. To enable a centralized data repository, a server hardware with suitable RAID-sets of hard drives is under preparation at the Geodetic Observatory Wettzell, where the operating system and the software will be installed in the coming months. It is a set of hierarchical servers for the data acquisition and Web presentation.

Currently, the implementation is delayed because of the focus on tasks which are related to developments for the VLBI Global Observing System (VGOS). Some of the server hardware is prepared. Local extensions to the system monitoring at Wettzell are made. Expe-

1. FESG Wettzell, Germany

2. Student, THD — Technische Hochschule Deggendorf, Germany

3. BKG Wettzell, Germany

4. University of Tasmania, Tasmania/Australia

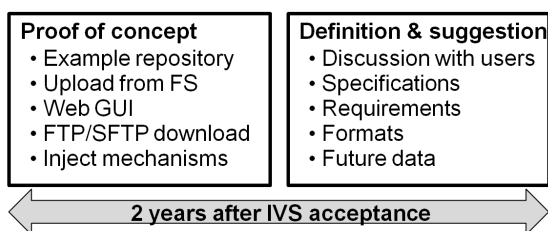


Fig. 1 The planned phases of the IVS Task Force on Seamless Auxiliary Data.

periments with different solutions to propagate data between the servers are already tested.

2 Local System Monitoring

The foundation of each global monitoring system is the local data nodes, which collect data and make them available. They collect data for science and analysis, data for system operations, and data for diagnostics. Because the data are essential for the operation of the antennas, the different observatories developed and use individual solutions. In a global context, the MoniCA system in Australia ([1]), the MIT Monitoring and Control Infrastructure for the new VGOS antennas in Haystack, Washington and Kokee Park, the mm-VLBI Radio Lab VLBI Monitor [6], and the Wettzell SysMon [2] are relevant. The following focuses on the Wettzell SysMon suite.

The main part of a sensor node in SysMon software is a data storage system using the Data Base Management Systems (DBMS) PostgreSQL. The database contains the short-term and current data sets. Monitoring data are kept in the PostgreSQL database for a few months to make a presentation of current data with suitable plots. It is extended with a file system server, to build up hybrid storage possibilities. The file system contains the historic and long-term data. The presentation layer on such a node is ZABBIX and a Web server [7]. ZABBIX is an open-source monitoring system which offers all capabilities of presenting and interacting with monitoring data.

Each monitoring count is configured with a configuration file. Using the program “sysmon_sender -R test.conf” (where “test.conf” contains the sensor details, see Figure 2), a count can be registered at the system. The configuration file contains all relevant infor-

mation about a sensor, for example a sensor identification number, a sensor name, the used unit, information about type and the manufacturer of the sensor, and data about the limits to set warnings and alerts. The registration prepares the database tables and the file system directories and even produces a template file for Zabbix, which simplifies the implementation of a ZABBIX Web page having graphs, triggers, and data injectors.

```

<MCI sensorControlPoint>
  ControlPointID          = Test
  ControlPointType        = test
  ControlPointPort        = 52666
  <MCI sensorProprietarySettings>
  ...
</MCI sensorProprietarySettings>
<MCI ZabbixConnection>
  ...
</MCI ZabbixConnection>
<MCI DBConnection>
  ...
</MCI DBConnection>
<MCI BackupSettings>
  ...
</MCI BackupSettings>
<MCI sensor>
  SensorID                = Test1
  SensorName               = Test1Sensor
  SensorUnit               = Deg C
  SensorManufacturer       = HEM
  SensorModel              = AED9001A
  SensorPosition           = Midway in azimuth axis
  SensorUpdateInterval     = 180s
  SensorResolution         = 0.05
  SensorDataAvailabilityTime = 1d
  SensorMinLimit           = -20
  SensorMaxLimit           = 50
  SensorMinWarningLimit    = 5
  SensorMaxWarningLimit    = 35
  SensorMinAlertLimit      = 0
  SensorMaxAlertLimit      = 40
  SensorFlagProvider        = yes
  SensorFlagConsumer        = no
  SensorFlagCommandable     = no
  SensorFlagManageable      = no
  SensorDataArchiveDirectory = /archive/MCI
  SensorPropArchiveDirectory =
</MCI sensor>
<MCI sensor>
  ...
</MCI sensor>
  ...
</MCI sensorControlPoint>

```

Fig. 2 A configuration skeleton for SysMon.

“sysmon_sender” is also used to transparently inject single sensor values and counts to the database, the file system, and the presentation layer. There are two ways: data which should be injected can be defined as arguments to the program (“sysmon_senderc -s test.conf TestID1 200.0 1”, where “TestID1” is the sensor identification, “200.0” is the value, and “1” is an additional trigger for alert levels) or can be written as a table in a file (“sysmon_senderc -f test.conf datafile.txt”, where “datafile.txt” contains a table of sensor inputs structured in the same way as used as program arguments), which is then completely imported. The version using a file makes a complete update of several sensor values possible.

After the import of the template file to ZABBIX, it can directly be used to present data via a Web server on a Web browser (see Figure 3). ZABBIX provides several interactions, so that one can zoom into the data series to check specific events. Several types of charts can be adapted to an individual style of data presentation.



Fig. 3 A possible Web page showing the monitoring data which are collected from the cryo-system of the dewar.

The development of the local SysMon was one of the highly prioritized tasks at the Wettzell observatory, as it makes automated and autonomous observations possible while keeping the overview of the different telescope systems. Therefore, some projects extended the capabilities of SysMon. Even if SysMon is specifically used at Wettzell, it is interoperable to all the other systems, as data injectors can simply take data from other systems, such as MoniCA or MCI, to send them to SysMon with a simple call of the “sysmon_sender” software.

3 Combination with FS Control

The main part of the control of VLBI telescopes is the NASA Field System, which processes schedules, controls hardware, and collects all necessary system data to log them to a session log file. This system is extended with a local station code to implement the ac-

cess to the station-specific data from different sensors of the SysMon nodes, so that all data are accessible for the operator in the Field System. Additionally, an e-RemoteCtrl server offers remote access to all functionalities using a role-based authentication system. Related e-RemoteCtrl clients can be used all over the observatory network and also over the world-wide networks to access control remotely.

New observation strategies, such as the use of unattended night shifts, require a higher-level of safety. This additional requirement is provided by the SysMon nodes. Each node operates in parallel to the Field System and has all necessary data about the system to make decisions about the safety and the current system status. Because some of the standard monitoring data only arrive at the Field System, for example the meteorological data or the antenna parameters, the Field System must propagate these data to the SysMon node. Therefore, the SysMon nodes of a telescope and the controlling Field System interact closely. Critical situations are then directly visible for the operator in the Field System and in the ZABBIX Web pages (see Figure 4).

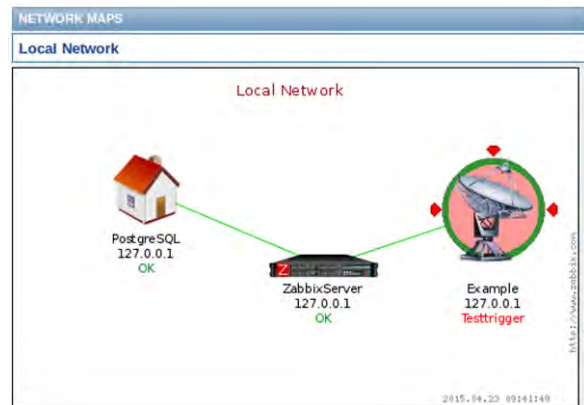


Fig. 4 The notification of a critical situation in the telescope control forced by a trigger signal to test the propagation.

Additionally, the status and auxiliary data are then propagated to a central monitoring node from where they are sent to the IVS repository for auxiliary seamless data.

4 Propagation to a Central IVS Repository

A proof-of-concept implementation of a centralized IVS repository for auxiliary seamless data is currently under development at the Wettzell observatory (see Figure 5). It will collect data from a limited number of observatories using a centralized SysMon node with a suitable RAID-set of hard drives and different data access points. The simplest way to receive data is an upload with Secure Copy (SCP) or Secure File Transfer Protocol (SFTP) to an incoming directory. The update times are defined by the participating stations. The uploaded file just contains meteorological data in a first step.

But in the near future, the server should enable the receiving of incoming data sets in different formats on different access points (such as the JSON-based format of the Radio Lab VLBI Monitor [6] or the currently used format for dynamic observations of the AuScope network in Australia, see presentations of J. Lovell). It will have a suitable ZABBIX frontend to access current values. Historic data files are archived in separate download areas.

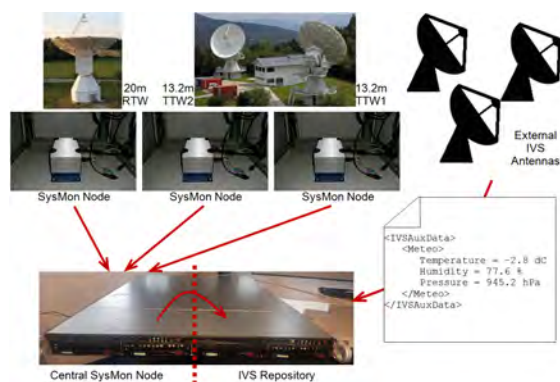


Fig. 5 The data from participating antennas are propagated to a centralized IVS repository for auxiliary seamless data.

5 Special Features

Having such centralized archives and reporting systems, a central failure and error management for the complete network of antennas is possible. Some first example developments at the Wettzell observatory im-

plement notification services with text messages to mobile phones and output of dynamic audio messages to regular phones.

A mini-PC with Voyage-Linux is used to run the open-source software “Asterisk”, which can be used to automatically make phone calls (see Figure 6). If a trigger is activated by a critical limit of a value, the SysMon system sends text messages with the error codes to the mini-PC which converts it to audio files and makes phone calls to the responsible operator. He can then use e-RemoteCtrl and Virtual Network Computing (VNC) to access the system remotely. In most cases, this remote access can fix the problem to continue the regular operation. This technique can be used to run night shifts unattended.

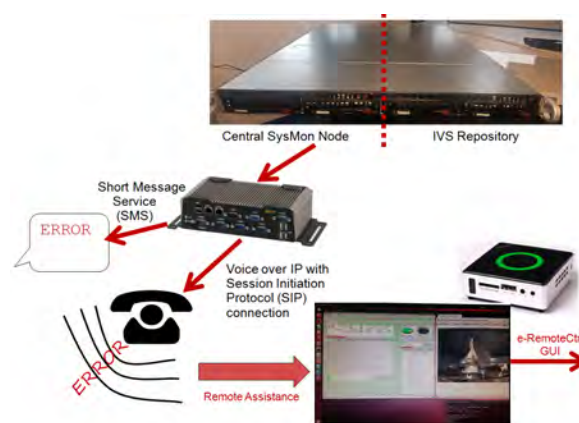


Fig. 6 Failure management and notification service tested at Wettzell to make unattended observations and remote assistance possible.

6 Conclusion and Outlook

The implementation of a centralized IVS repository for auxiliary seamless data is an ongoing task. Even if the project is delayed, several sub-tasks were developed with the focus on tools and equipment which are essential for future observation modes at the Wettzell observatory. The complete design is interoperable with other systems, so that parallel existing system monitoring software can inject data as well. After final tests, it will be accessible also for external partners and for the IVS components.

References

1. BRODRICK, D. (2015). “MoniCA” Monitoring Software. Web document <https://www.narrabri.atnf.csiro.au/monitor/monica/>, Download 2015.
2. Ettl, M., Neidhardt, A., Plötz, C., Mühlbauer, M., Dassing, R., Hase, H., Beaudoin, C., Himwich, E. (2010) SysMon - a robust and flexible remote monitoring system for VLBI and more. Proceedings of Science (PoS) - 10th European VLBI Network Symposium and EVN Users Meeting: VLBI and the new generation of radio arrays, EID PoS (10th EVN Symposium) 025, Scuola Internazionale Superiore di Studi Avanzati (SISSA), 2010.
3. Ettl, M., Neidhardt, A., Schönberger, M., Alef, W., Himwich, E., Beaudoin, C., Plötz, C., Lovell, J., Hase, H. (2012). e-RemoteCtrl: Concepts for VLBI Station Control as Part of NEXPreS. In: Behrend, D., Baver, K.D. (eds.) *Launching the Next-Generation IVS Network*. IVS 2012 General Meeting Proceedings, NASA/CP-2012-217504, pp 128–132, National Aeronautics and Space Administration, 2012.
4. Neidhardt, A., Lovell, J., Kirschbauer, K., Schönberger, M., Himwich, E., McCallum, J., Plötz, C., Quick, J. (2015). Results from a test realization of a system monitoring for seamless auxiliary data. In: Haas, R., Colomer, F. (eds.) *Proceedings of the 22nd European VLBI Group for Geodesy and Astrometry Working Meeting*. pp 30-34, Ponta Delgada, Azores, May 2015.
5. Rothacher, M., Beutler, G., Bosch, W., Donnellan, A., Gross, R., Hinderer, J., Ma, C., Pearlman, M., Plag, H.-P., Richter, B., Ries, J., Schuh, H., Seitz, F., Shum, C.K., Smith, D., Thomas, M., Velacogna, E., Wahr, J., Willis, P., Woodworth, P. (2009). The future Global Geodetic Observing System (GGOS). In: Plag, H.-P., Pearlman, M. (eds.) *The Global Geodetic Observing System. Meeting the Requirements of a Global Society on a Changing Planet in 2020*, Springer-Verlag, 2009.
6. Schellart, P., et al. (2016). Radboud Radio Lab VLBI Monitor. Online monitoring for Very Long Baseline Interferometry campaigns. https://gitlab.science.ru.nl/radiolab/vlbi_monitor, Download 2015/05/15.
7. ZABBIX (2015). The Ultimate Enterprise-class Monitoring Platform. Web document <http://www.zabbix.com/>, Download 2015.

New Generation VLBI: Intraday UT1 Estimations

Alexander Ipatov, Dmitriy Ivanov, Gennadiy Ilin, Sergei Smolentsev, Iskander Gayazov, Vyacheslav Mardyshekin, Leonid Fedotov, Victor Stempkovski, Alexander Vytov, Alexander Salnikov, Igor Surkis, Andrey Mikhailov, Dmitriy Marshalov, Ilya Bezrukov, Alexey Melnikov, Voytsekh Ken, Sergei Kurdubov

Abstract IAA finished work on the creation of the new generation radio interferometer with two VGOS antennas co-located at Badary and Zelenchukskaya. 48 single baseline one-hour VLBI sessions (up to four sessions per day) were performed from 04 Nov to 18 Nov 2015. Observations were carried out using wideband S/X receivers, three X-band and one S-band 512 MHz channels at one or two circular polarizations. Sessions consisted of about 60 scans with a 22-second minimum scan duration. The stations' broadband acquisition systems generated 1.5–3 TB data per session, which were transferred via Internet to the IAA FX correlator. The accuracy of the group delay in a single channel was 10–20 ps, which allows the use of every single channel's observations for geodetic analysis without synthesis. 156 single channel NGS-cards were obtained in total. The RMS of the differences between UT1–UTC estimates and IERS final values is 19 μ s.

Keywords VLBI, VGOS, UT1

1 Introduction

The construction of the new generation VGOS interferometer proposed at the previous General Meeting [1] was finished in 2015. In order to test the capabilities and the performance of the newly built facility, we started a special UT1–UTC estimation program. This paper reports the state-of-the-art conditions of the interferometer components and the first results of the UT1 campaign.

Institute of Applied Astronomy RAS

2 Antenna System and Feed

The 13.2-m antenna system produced by Vertex Antennentechnik GmbH was chosen for the purpose of fulfilling VLBI2010 (VGOS) requirements. The main antenna characteristics are shown in Table 1.

Table 1 13-m antenna specifications.

Main mirror diameter	13.2 m
Mount	alt-azimuth
Sub-reflector scheme	Ringfocus
Sub-reflector Mount	Hexapod
Azimuth speed	12°/sec
Elevation speed	6°/sec
Limits by Az, El	$\pm 270^\circ$, 0° – 110°
Operation	24h/7d
Tracking accuracy	± 15 arcsec
Surface accuracy (RMS)	Bv 0.053 mm / Zv 0.057 mm
Frequency range	2–40 GHz
Surface efficiency	> 0.7
Polarization	LCP and RCP
Ambient temperature	-35°C to $+50^\circ\text{C}$
Humidity	up to 100%
Snow load	100 kg/m ²
Wind velocity	50 m/sec

The new tri-band S-X-Ka receiving systems were developed and mounted for VGOS observations [2]. General receiver system parameters are presented in Table 2. In order to improve the signal-to-noise ratio, the tri-band feed and the frontend LNAs were mounted in a single unit and cooled by a closed cycle refrigerator to the temperature of liquid helium (20 K).

Synchronization of the frequency converters is provided by the frequency-time synchronization system of the radio telescope. The radio telescope receiver units are placed in the focal cabin.

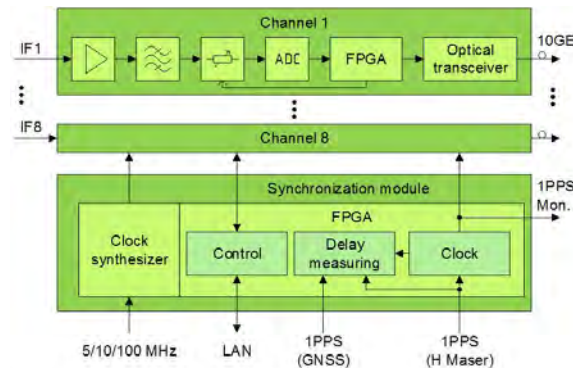
Table 2 Tri-band receiving system parameters, results of on-site measurements, 14.04.2014, Badary, 60°.

Band	S (13 cm)	X (3.5 cm)	Ka (1 cm)
Freq. (GHz)	2.2–2.6	7.0–9.5	28.0–34.0
Polarization	RCP and LCP		
$T_{sys}(K)$	35	25	70
SEFD (Ja)	1000	670	2100
Surface efficiency	0.7	0.8	0.7

3 Broadband Data Acquisition System

The Broadband Acquisition System (BRAS) contains eight identical units (wideband channels) that allow the digitization of the input signals of 512 MHz bandwidth (Figure 1) into the intermediate frequency range from 1024 to 1536 MHz [1].

Each unit is based on a high-speed 8-bit analog-to-digital converter (ADC) and low-cost field-programmable gate array (FPGA) performing the necessary signal processing. The main purpose of the FPGA is to receive data from the high-speed ADC, pack the input samples into frames in VLBI Data Interchange Format (VDIF) with timestamps, and to send the derived frames to the recording systems through a 10 Gigabit Ethernet fiber link. The BRAS is designed based on standard plug-in 6U Europack units, which provide ease of operation. Vibration resistance and good electromagnetic shielding of the housing made it possible to place the system in the focal cabin of the antenna close to the receivers. This eliminates the transmission of analog signals over a long distance and all related instabilities and performance degradation. More information on the BRAS structure, performance, and applications can be found in [3].

**Fig. 1** BRAS structure.

4 Buffering and Data Transmission System

In 2015 IAA RAS created the Data Transmission and Registration System (DTRS) for the new two-station radiointerferometer based on the 13.2-m diameter antennas (RT-13). DTRS may be used in the international VGOS program. The main objectives of the new system are:

- Recording eight data streams (with scalability up to 16) in the VDIF format at a 2 Gbps data rate for each channel;
- Transferring data to the Correlation and Processing Center (CPC) at a 10 Gbps rate simultaneously with recording and buffering;
- Storing up to 20 TB of observation data with a set of disk pools.

DTRS is based on a Dell PowerEdge R720 rack server with two Dell PowerVault MD1220 disk enclosures. Up to four dual-port 10 G Ethernet Intel network cards (Intel X520) are used. DTRS runs FreeBSD 10.1 with ZFS. For data registration and recording, DTRS uses special software developed by IAA RAS. This software exploits the netmap framework for high-speed packet processing.

To solve the problem of efficient transfer of large amounts of data it is necessary to use modern high-speed protocols. It is important to avoid losses and errors during simultaneous data transfer and registration at 16 Gbps. Maximum utilization of the channel bandwidth is essential for broadband communications over the Internet. That can be provided by transmitting data with multiple streams. The implementation of the UDP protocol provides such an opportunity. A software package (server) includes an algorithm which adapts to channel capacity, which is essential in case of data transmission during simultaneous recording. Observation data from stations were transferred to the CPC via broadband channel over the Internet. During research we used 2 Gbps links to each station and a 4 Gbps link to the CPC at St. Petersburg. One-hour VLBI data transmission was carried out by four or eight UDT streams: four streams were used for simultaneous transfer and registration, and when the observations ended we switched to eight streams. Analysis of the experiment results shows that multi-threaded data transmission in a broadband communication channel provides the desired efficiency of data delivery to the CPC from stations.

5 Software Correlator

The six-station software correlator was developed and assembled by the end of 2014. The correlator is able to process VDIF data from up to six stations simultaneously at a maximum rate of 16 Gb/s from each station in a near-real time mode. Table 3 presents the main correlator specifications.

Table 3 Correlator specifications in near-real time mode.

Input data format	VDIF
Sampling	1/2 bit
VGOS station	up to six
Spectra channels	up to 4096
Input data stream	up to 16 Gb/s
Frequency bands	four
Polarization	1/2
Pcal tones	up to 32
Delay (RMS)	< 10 ps

The main design feature is the use of graphical processing units (GPUs) for the main computations such as fringe stopping, bit repacking, Fourier transformation, spectra multiplication, and phase calibration signal extraction.

The correlator hardware is based on a hybrid blade server cluster. The present hardware contains 32 hybrid blade servers, which are inserted into seven chassis, and eight 19-inch cache servers. Each blade server contains two Intel CPUs, two Nvidia Tesla K20 GPUs, and 64 GB RAM. These servers are used for FX data processing algorithms (fringe stopping, FFT, and spectra multiplication) computing. The 19-inch servers also contain two CPUs, two GPUs, and 2x10 Gb fiber optic input, but the RAM is increased up to 256 GB. Each of them provides data reception, pcal extraction, delay tracking, and bit repacking. The 256 GB memory allows the VGOS data to be cached in response to any delays during data transmission. Data storage is based on the PANASAS system with a total capacity of 196 TB. The interblock data communication is provided by the infiniband network. Cluster components are mounted in a four rack unit. The air conditioning system is mounted in a three rack unit.

6 Observation Schedule for UT1 Estimations

Regular UT1–UTC sessions on the BADAR13M–ZELEN13M baseline were launched 4 Nov 2015. The 93 one-hour sessions were conducted in X/S band up to four times per day in November. A data stream of 4,096 Mbps was recorded for four-channel sessions, and 8,192 Mbps were recorded for eight-channel sessions (two polarizations). The bandwidth of each channel was 512 MHz. There are about 60 scans per hour in the November sessions. In late November we performed several experiments with scheduling parameter optimizations in order to increase the average number of scans per hour by two or more times. Test sessions with a six second minimum scan duration and disabled calibration were carried out and yielded 137 scans per hour. In subsequent sessions we set a ten-second minimum scan duration requirement and 15 dB minimum SNR. This mode yielded about 120 scans/hour, which allowed the generation of half-hour sessions while retaining the same number of scans per session. During the period from December 2015 to March 2016 the 145 half-hour sessions were carried out in two frequency channels (S and X) with 2,048 Mbps rate. Regular test observations in X/Ka bands started in Feb 2016. From February to March, 20 one-hour sessions were observed at the 2,048 Mbps rate in two frequency channels (X/Ka). Several tests were carried out with two X-channels with maximum spacing at 1.5 GHz.

7 Frequency Channel Setup

As one can see from above, VLBI observations with RT-13 were conducted using two, four, or eight BRAS frequency channels, corresponding to data streams of 2,048, 4,096, or 8,192 Mbps, respectively. Figure 2 shows a schematic arrangement of frequency channels in the S, X, and Ka bands. The rectangles with a gray (light) background show the boundaries of the operating ranges of the S, X, and Ka RT-13 receivers. The red (dark) rectangles show the actual frequency channel setup in different sessions. The scheme of the frequency channel setup for the RT-13 UT1–UTC sessions was:

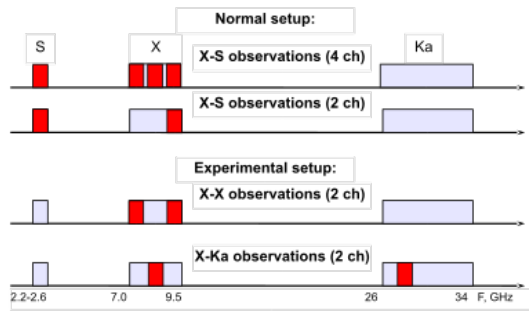


Fig. 2 Bands and channels.

- observation in November 2015 with one S channel (2,164–2,676 MHz) and three X channels (7,568–8,080 MHz, 8,080–8,592 MHz, and 8,592–9,104 MHz), with the three X channels forming a continuous channel strip and two polarizations doubling the channel set;
- observations from December 2015 to March 2016 with one S channel (2,164–2,676 MHz) and one X channel (8,592–9,104 MHz);
- experimental observations in X/Ka-band, in which the X channel was set to the frequency of 8,080–8,592 MHz and the Ka channel to 27,952–28,464 MHz;
- experimental observations in X-band with a maximum spacing of two frequency channels: 7,464–7,976 MHz and 8,964–9,476 MHz.

8 Session Features

When the single channel registration bandwidth is 512 MHz, the group delay accuracy from the correlator ranges from a few to tens of picoseconds in the single channel (depending on the scan length and brightness of the source). Thus at the picosecond level, the delay formal errors are apparently predominated by instrumental effects, and further enhancement of the formal precision at this stage is meaningless. Based on this, now we process observations in independent channels separately without wideband synthesis and consider different channels of observations as independent VLBI sessions. As a result, a one hour session with four channels gives us three independent determinations of universal time. Observations in the S channel were used to calibrate the ionospheric delay. In this case observations in two polarizations doubled

the number of independent observations. In November 2015, in the presence of a 2 Gbps data channel to the observatories, one-hour sessions were conducted daily for four or eight channels. After processing each of those sessions, we obtained three to six independent estimations of UT1. From December to March the communication channel was decreased to average 0.2 Gbps, and we could only observe two half-hour sessions per day, with two frequency channels (one S + one X or one X + one Ka) and obtained only one UT1 estimation per session.

The data analysis was accomplished with the QUASAR software [5], and a set of seven parameters was estimated: the linear clock offset, a linear wet tropospheric zenith delay for each station, and the UT1–UTC correction.

9 Comparisons with IERS and IVS

In order to show the quality of the results, we calculated the differences of our UT1–UTC estimates and the IERS finals values. The results of the comparison are presented in Figure 3. Dark/blue points present the IVS-Intensive results on the WETTZEEL–KOEKE baseline. Light/green points present the ZELLEN13M–BADAR13M results during the same period. The one-hour S/X sessions held in November 2015 give us a WRMS of 21 μ s when differenced with the IERS finals values. The WRMS of the differences to the half-hour sessions from December 2015 to March 2016 is 27 μ s; the entire set’s WRMS is 24 μ s. The IVS-Intensive series from Nov 2015 to Mar 2016 has a 16 μ s WRMS with respect to the IERS finals.

Comparison of the results for S-X and X-Ka observations are presented in Figure 4. Despite the fact that the X-Ka band pair looks more promising, at this moment the X-Ka estimations of UT1–UTC have a bit more scatter and worse formal errors. Apparently this is due to the usage of radio source S-X positions and the current lack of a catalog of good X-Ka positions.

10 For Further Investigations

Currently, with the brand new wideband VLBI, we encountered several problems, such as:

- When making a synthesis of a wide-wide band from several 512 MHz channels it was found that the

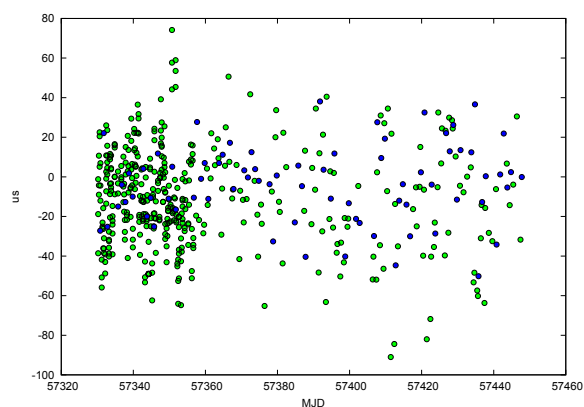


Fig. 3 Differences vs. IERS finals (light/green points are ZELN13M-BADAR13M (S/X); dark/blue points are WETTZELL-KOKEE).

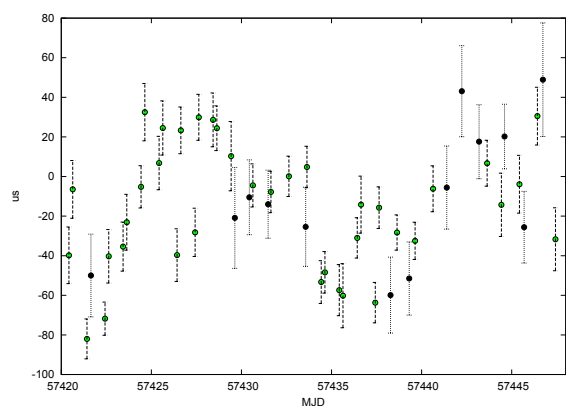


Fig. 4 Differences vs. IERS finals (light/green points are ZELN13M-BADAR13M (S/X); dark/black points are ZELN13M-BADAR13M (X/Ka)).

synthesized result is worse than the results for individual channels.

- In processing the observations in different frequency channels, the UT1 estimates obtained from different X band channels lies within units of microseconds, whereas the use of different S channel causes a shift in the results of several tens of microseconds.
- Some observations produce formal errors significantly less than 10 ps; often such observations significantly affect UT1 estimation due to their excessive weight.
- To obtain more accurate results in the prospective pair of X-Ka bands, we need to build an X-Ka version of ICRF.

- Joint processing of the new broadband with the old narrow-band observations is needed.

11 Conclusions

Since 2012, we have improved the accuracy of the national UT1 estimates from 60 to 20 microseconds. The accuracy obtained on small 13-m antennas is comparable to the accuracy of the IVS-Intensives, which is reached at 2.5 times less base. Our UT1 estimates are much more rapid than the standard IVS-Intensives; the delay between the beginning of the observations and the UT1-UTC result is about two to three hours. Currently, the IAA holds three sessions per day for the estimation of Universal Time (two half-hour sessions with the 13-m antennas and one one-hour session with the 32-m antennas). We encourage the IVS Analysis Centers to begin to use our observations in routine processing—it would significantly improve the quality of the IVS products, as IVS begins to provide UT1 four times per day and makes a step forward towards VGOS standards.

References

1. Alexander Ipatov et al., “Russian VLBI System of New Generation”. In: *IVS 2014 General Meeting Proceedings*, pp. 25–29, Edited by Dirk Behrend, Karen D. Bayer, and Kyla L. Armstrong, Science Press (Beijing), ISBN 978-7-03-042974-2, 2014.
2. Alexander Ipatov et al. “Tri-band System for the Russian Interferometer”. In: *IVS 2014 General Meeting Proceedings*, pp. 118–121. Edited by Dirk Behrend, Karen D. Bayer, and Kyla L. Armstrong, Science Press (Beijing), ISBN 978-7-03-042974-2, 2014.
3. Evgeny Nosov et al. Current Development State of Russian VLBI Broadband Acquisition System. In: *IVS 2014 General Meeting Proceedings*, pp. 82–85. Edited by Dirk Behrend, Karen D. Bayer, and Kyla L. Armstrong, Science Press (Beijing), ISBN 978-7-03-042974-2, 2014.
4. I. Bezrukov et al. “Russian Data Recording System of New Generation”. In: *IVS 2014 General Meeting Proceedings*, pp. 130–133. Edited by Dirk Behrend, Karen D. Bayer, and Kyla L. Armstrong, Science Press (Beijing), ISBN 978-7-03-042974-2, 2014.
5. S. L. Kurdubov, V. S. Gubanov, “Main results of the global adjustment of VLBI observations”, *Astronomy Letters*, Volume 37, Issue 4, pp. 267–275, DOI 10.1134/S1063773711010063, 2011.

Session 3: Stations, Correlators, and Operations Centers



March 2016 · Johannesburg · South Africa

Activities of the IERS Working Group on Site Survey and Co-location

Sten Bergstrand¹, Ralf Schmid²

Abstract The objective of the International Earth Rotation and Reference Systems Service (IERS) Working Group on Site Survey and Co-location is to improve local measurements at space geodesy sites. We appointed dedicated Points of Contact (POC) with the four different services of IERS as well as the NASA Space Geodesy Project in order to improve the efficiency of internal communication within the working group. Following the REFAG2014 conference, the POCs agreed on a common and general terminology on local ties that clarifies the communication regarding site surveying and co-location issues between and within the IERS services. We give brief introductions to the different observation techniques and mention some contemporary issues related to site surveying and co-location.

Keywords Site survey, local tie, IERS, co-location

1 Introduction

The combination of space-geodetic solutions is critically reliant on the availability of local tie vectors, which are the relative positions of the reference points of co-located space-geodetic instruments determined by some survey technique. In order to combine the four space-geodetic techniques DORIS, GNSS, SLR, and VLBI, tie vectors enter the combination of space-geodetic solutions effectively as a fifth technique. The tie vectors are not only necessary for rigorous terrestrial reference frame realization but also serve to high-

light the presence of technique-specific and/or site-specific biases. With the ultimate objective of improving the accuracy and consistency of space-geodetic solutions through adequate utilization of local measurements, the International Earth Rotation and Reference Systems Service (IERS) Working Group on Site Survey and Co-location (WG Sisuco) provides an authoritative source of surveying methodology advice, promotes technical discussion, provides a forum for the evaluation of existing and new procedures and analysis strategies, and supports the exchange of relevant information across the Global Geodetic Observing System (GGOS) and between the International Association of Geodesy (IAG) technique services. The working group also acts as an entity of the GGOS Bureau of Networks and Observations under the IERS name, as well as of the IAG Subcommittee 1.2 as WG 1.2.1.

GGOS is the Observing System of the International Association of Geodesy (IAG). GGOS works with the IAG components to provide the geodetic infrastructure necessary for monitoring the Earth system and for global change research. It provides observations of the three fundamental geodetic observables and their variations, that is, the Earth's shape, the Earth's gravity field, and the Earth's rotational motion. In order to meet the most demanding requirements on GGOS as a whole, the system needs to provide data in a frame that is accurate to 1 mm and stable to 0.1 mm/yr over decadal time scales, which is approximately an order of magnitude better than currently provided. Current tie and space geodesy discrepancies of the ITRF2014 [9] are of the order of 3 mm, which indicates that there is still room for improvement in the treatment of local ties. Here we give examples of recent and current work on:

- the working group's organization,
- adequate terminology when discussing local ties,

1. SP Technical Research Institute of Sweden, SP

2. German Geodetic Research Institute, DGFI-TUM

- insights into DORIS, GNSS, and SLR local tie work,
- ongoing IVS activities within the WG scope, e.g., telescope deformation, VLBI–GNSS baseline comparison through automatic reference point determination, and GNSS-based telescope ties.
- Each site should assign a single point or marker to represent the site as a whole. These markers should ideally consist of a brass bolt or something similar and, wherever possible, be attached to the lithosphere.
- Movements of the site should be monitored or modeled in standardized ways.

The WG has existed in various forms for some twenty years and has 36 listed members. In order to advance the speed of constructive communication, a group of dedicated points of contact (POC) has been established among the involved entities: the four IERS services, the IERS surveying entity, and the NASA Space Geodesy Project. These POCs are:

- IDS: Jerome Saunier,
- IGS: Ralf Schmid,
- ILRS: Erricos C. Pavlis,
- IVS: Rüdiger Haas,
- NASA SGP: James L. Long,
- IERS surveying entity: Xavier Collilieux.

The IERS surveying entity, through IGN France, is undertaking an effort to collect and issue its comprehensive experiences from different surveying campaigns for the benefit of improved surveying practices for all.

2 Terminology

As a consequence of the increasing awareness of the geodetic contribution to various scientific fields, e.g., different aspects of climate change, the importance of a coherent combination of space-geodetic techniques is becoming more imminent. In order to improve the information exchange between the different players in the field, the need for a common terminology was accentuated at an open WG workshop in Paris in 2013. The discussion ended up in a combined effort to implement a common terminology, which has been submitted as a resolution to the proceedings of the REFAG2014 conference and published in its submitted form at the WG homepage [1]. The resolution is conformant to the DOMES [10]:

- Each instrument (defined by a DOMES number) has a unique geometric reference point, and it is the task of the services to define these reference points. The term “reference” is reserved for these points.

3 International DORIS Service, IDS

This text is largely taken from [4]. Since 1994, thanks to its network of more than fifty permanent beacons (including three on the African mainland), DORIS has contributed to the IERS activities for the realization and maintenance of the ITRS (International Terrestrial Reference System). On July 1, 2003, the International DORIS Service officially started as an IAG Service. Positions and velocities of the reference sites at the cm and mm/yr accuracy level contribute to scientific studies in the fields of global and regional tectonics.

Locating a satellite in space is complicated by the fact that it is in motion on a trajectory dictated by launch parameters and forces acting on the satellite. Chief among these forces are the pull of Earth’s gravity, which keeps the satellite in orbit, and surface acceleration forces such as solar radiation pressure and atmospheric drag. A good understanding of the Earth’s gravity field and the satellite’s environment is used to calculate the real trajectory with respect to the elliptical orbit described by Kepler’s laws of motion. The DORIS antenna onboard satellites receives signals emitted by the network of terrestrial stations. When the receiver and the source are moving with respect to each other, the receiving wavelength differs from the emitting wavelength through the Doppler effect. The frequency of the signal received by DORIS instruments onboard the satellite is higher than the emitted signal when the satellite moves closer to the emitting beacons and lower when it moves away. On a plot of the frequency received by the satellite as a function of time, the slope of the curve at the point of near maximum (TCA point: Time of Closest Approach) allows calculation of the distance between the beacon on the ground and the transmitting satellite.

The DORIS ground network is now being upgraded, and new definitions have been adapted in line with a WG resolution [14, 13, 1]. The geometric refer-

ence point of the Doris ground antennas, the so-called “antenna reference point” (ARP), is the center of a painted ring on the lower part of the antenna radome.

4 International GNSS Service, IGS

The IGS was established in 1994 as the “International GPS Service for Geodynamics” [5]. In view of other global navigation satellite systems (GNSS) evolving, it has been called “International GNSS Service” since 2005. The IGS operates as a voluntary federation of over 200 agencies, universities, and research institutions in more than 90 countries. The basis of all activities is a global network of about 500 stations continuously tracking a variety of GNSS signals. On the African continent, the network is still sparse. Of the approximately 40 available African IGS stations, nearly half are located in South Africa.

Traditionally, carrier frequencies in the L-band ranging from 1176.45 MHz (e.g., GPS L5) to about 1602 MHz (GLONASS G1) have been used for GNSS purposes [8]. The Indian Regional Navigation Satellite System (IRNSS) is the first to transmit signals in the S-band (2492.028 MHz). The primary products of the IGS are orbit and clock information for the GNSS satellites. Whereas the accuracy of the final GPS orbits has reached a level of 2–3 cm, the orbit quality for the new GNSS is substantially lower (due to, e.g., uncertainties in the observation modeling, sparse tracking networks, incomplete constellations affecting the ambiguity success rate, or constellations with geostationary or geosynchronous orbits). Key aspects of the current IGS activities are the transition from a GPS/GLONASS to a multi-GNSS processing and the provision of products in real-time.

The geometric reference point of the receiving GNSS antennas is the so-called “antenna reference point” (ARP). For all antenna types installed within the IGS network, the ARP is defined in the file *antenna.gra* [6] together with the “north reference point” (NRP), which defines the proper orientation of the antenna with respect to the true north direction. Preferably, the ARP is an easily accessible point on the lowest non-removable horizontal surface of the antenna. Typically, it coincides with the axis of attachment of the antenna to the monument.

Several IGS antenna calibration facilities determine elevation- and azimuth-dependent phase center corrections with respect to the ARP. Thus, it is possible to model the position of the phase center where GNSS signals are actually received. However, IGS station coordinates do not refer to the ARP, but to a permanent marker. The IGS Site Guidelines [7] demand that eccentricities from the station permanent position marker to the ARP be surveyed and reported in site logs and RINEX headers to ≤ 1 mm accuracy. Apart from that, the three eccentricity components should not exceed 5 m.

Local ties with respect to a GNSS antenna have to be measured from a co-located instrument to the GNSS station’s permanent marker. The biggest systematic error sources affecting the estimated GNSS station position are probably near- and far-field multipath. However, also the phase center corrections are not free of errors. Calibrations from different institutions do not agree on the 1-mm level, and the resulting error in the phase center position is even amplified by forming the ionosphere-free linear combination. For 6.5% of the IGS stations (status as of January 2016), purely elevation-dependent converted field calibrations are still applied, and about 10.5% of the antennas in the IGS network are covered by uncalibrated radomes. The IGS aims at a network with full coverage of state-of-the-art absolute robotic calibrations.

5 International Laser Ranging Service, ILRS

LAGEOS (short for Laser Geodynamic Satellite) was launched in 1976 and was the first NASA orbiter dedicated to the measurement technique called laser ranging. Laser ranging activities are organized under the International Laser Ranging Service (ILRS), which provides global satellite and lunar laser ranging data and their derived data products to support research in geodesy, geophysics, Lunar science, and fundamental constants. The ILRS was established in September 1998 to support programs in geodetic, geophysical, and lunar research activities and to provide the IERS with products important to the maintenance of an accurate International Terrestrial Reference Frame (ITRF). Satellite Laser Ranging (SLR) and Lunar Laser Ranging (LLR) use short-pulse lasers and

state-of-the-art optical receivers and timing electronics to measure the two-way time of flight (and hence distance) from ground stations to retroreflector arrays on Earth orbiting satellites and the Moon. Scientific products derived using SLR and LLR data include precise geocentric positions and motions of ground stations, satellite orbits, components of Earth's gravity field and their temporal variations, Earth Orientation Parameters (EOP), precise lunar ephemerides, and information about the internal structure of the Moon. Laser ranging systems are already measuring the one-way distance to remote optical receivers in space and can perform very accurate time transfer between sites far apart. As with VLBI, the geometric reference point of an SLR telescope is the projection of the secondary axis onto the primary axis.

6 IVS Site Surveying Issues

The IVS was inaugurated in 1999, and the VLBI technique should be familiar to the reader of this publication. As with SLR, the reference point of the telescope is the projection of the secondary axis onto the primary axis. However, there are some issues with VLBI that are more articulated and have attracted some recent attention.

6.1 Telescope Deformation

Large structures such as radio telescopes are subject to external forces and deform, particularly under the influence of temperature and gravitation. Modern surveying systems such as terrestrial laser scanners have been used to determine the shape variation of the reflector and supporting elements [2]. Here, we also take the opportunity to introduce a continuously operating lidar monitoring system that measures selected internal length variations of the Onsala 20-m telescope and provide data in real-time [3].

6.2 VLBI–GNSS Baseline Comparison

One of the main objectives of the WG Sisuco is to resolve technique specific biases. In a recent project [15] in the European Metrology Research Program (EMRP), comparisons of the VLBI and GNSS baselines between the Metsähovi and Onsala sites, together with independent GNSS and terrestrial based local tie monitoring schemes, are made on both sites. The project is presented in some detail in [11].

A customized, VLBI-schedule-adapted terrestrial system called the “High-End Interface for Monitoring and spatial Data Analysis using L2-Norm” (Heimdall) has been developed. It consists of a robotic total station monitoring system adapted to the local observation schedule, and it determines the reference point of the telescope by observing retro-reflecting prisms attached to the structure. Heimdall was operational during the CONT14 experiment. The system is presented in further detail in [16].

With the end objective of observing all techniques in a truly common reference frame, some transfer functions still need to be applied in order to exchange data between different observation frames of the separate techniques. As GNSS coordinates are available everywhere, they have been designated to carry the information between the techniques. A pure GNSS tie has been developed that determines the reference point of the telescope indirectly, through hinge-mounted GNSS antennas on the sides of the telescope.

7 Limiting Factors

As it turns out for most repeated local surveys, the weakest link in the chain is the orientation of the local system with respect to the global terrestrial reference frame. The length of the vector between two reference points surveyed at different occasions is quite often reproducible within 1 mm, which can be justified by control measurements, instrument calibrations, and so on. However, as the vector between the reference points needs to be oriented in the ITRF, and the GNSS point observations that constitute the foundation of these orientations are often perturbed by a series of unknown parameters, the orientation of the local network often varies between surveys.

Furthermore, the evolution and improvement of the space-geodetic techniques have been dramatic, and observations are now being performed on a regular basis at extremely high repeatability within the separate techniques. However, with the objective of improving current performance by an order of magnitude, every opportunity to improve the system has to be evaluated.

Acknowledgements

The EMRP is jointly funded by the EMRP participating countries within EURAMET and the European Union.

References

1. S. Bergstrand, X. Collilieux, J. Dawson, R. Haas, J. L. Long, E. C. Pavlis, J. Saunier, and A. Nothnagel. Resolution on the nomenclature of space geodetic reference points and local tie measurements. REFAG 2014 Proceedings (submitted). (available at http://www.iers.org/SharedDocs/Publikationen/EN/IERS/WorkingGroups/SiteSurvey/Bergstrand_etal_REFAG2014_TieResolution.pdf)
2. T. Artz, A. Springer, and A. Nothnagel. A complete VLBI delay model for deforming radio telescopes: the Effelsberg case. *Journal of Geodesy*, Vol. 88(12), 2014.
3. S. Bergstrand, C. Rieck, and J. Spetz. (available at <http://193.11.166.19/ilr/>)
4. CNES. (available at <http://www.aviso.altimetry.fr/en/techniques/doris.html>)
5. J. M. Dow, R. E. Neilan, and C. Rizos. The International GNSS Service in a changing landscape of Global Navigation Satellite Systems. *J Geod* 83(3): 191–198, doi:10.1007/s00190-008-0300-3, 2009.
6. IGS Central Bureau. antenna.gra, 2016 (available at <ftp://ftp.igs.org/pub/station/general/antenna.gra>)
7. IGS Infrastructure Committee. IGS Site Guidelines, 2015 (available at <http://kb.igs.org/hc/en-us/articles/202011433>)
8. IGS RINEX Working Group. RINEX – The receiver independent exchange format, Version 3.03, 2015 (available at <ftp://igs.org/pub/data/format/rinex303.pdf>)
9. ITRF2014 URL (available at: http://itrf.ign.fr/ITRF_solutions/2014/doc/ITRF2014-Tie-Residuals.dat)
10. ITRF DOMES URL (available at http://itrf.ign.fr/domes_desc.php)
11. U. Kallio, Michael Lösler, S. Bergstrand, R. Haas, and C. Eschelbach. Automated Simultaneous Local Ties with GNSS and Robot Tachymeter. This volume.
12. P. Sarti, L. Vittuari, and C. Abbondanza. Laser Scanner and Terrestrial Surveying Applied to Gravitational Deformation Monitoring of Large VLBI Telescopes' Primary Reflector. *J. Surv. Eng.*, 10.1061/(ASCE)SU.1943-5428.0000008, 136–148, 2009.
13. J. Saunier. Assessment of the DORIS network monumentation. *Advances in Space Research*, <http://dx.doi.org/10.1016/j.asr.2016.02.026>.
14. C. Tourain, G. Moreaux, A. Auriol, and J. Saunier. DORIS starec ground antenna characterization and impact on positioning. *Advances in Space Research*, <http://dx.doi.org/10.1016/j.asr.2016.05.013>.
15. SIB60 team (available at <https://www.ptb.de/emrp/sib60-home.html>)
16. T. Schüller, C. Plötz, S. Mähler, T. Klügel, A. Neidhardt, A. Bertarini, S. Halsig, A. Nothnagel, M. Lösler, C. Eschelbach, and J. Anderson. First Local Ties from Data of the Wettzell Triple Radio Telescope Array. This volume.

Optimizing the African VLBI Network for Astronomy and Geodesy

A. de Witt¹, D. Mayer², G. MacLeod¹, L. Combrinck¹, L. Petrov³, M. Nickola¹

Abstract

The African VLBI Network will be a pan-African network of radio telescopes comprised of converted redundant satellite Earth-station antennas and new purpose-built radio telescopes. The first of these antennas, in Ghana, is currently being converted to a radio telescope and current funding is estimated to permit the conversion of two more antennas in Africa. These antennas will initially be equipped with a 5-GHz and 6.7-GHz receiver and the next receiver likely to be fitted is a 1.4–1.7-GHz receiver. While it would be advantageous for the AVN antennas to be able to participate also in geodetic and astrometric VLBI observations, there is no funding currently for this. In this paper we re-visit the scientific justifications for the AVN in an attempt to optimize the AVN for each science case, both astronomical and geodetic.

Keywords VLBI, geodesy, astrophysics, instrumentation and methods for astrophysics

1 Introduction

The African Very Long Baseline Interferometry Network (henceforth referred to as the AVN), when initially conceived, was to be a modest network of new-built 12-m class radio telescopes in the African Square Kilometre Array (SKA) partner countries. However, it was discovered that, as a result of new optical fiber connectivity into Africa, many large 30-m class telecom-

munications antennas were redundant and could be converted for astronomy purposes [3].

Currently the SKA, South Africa (SA), and the Hartebeesthoek Radio Astronomy Observatory (HartRAO) are converting the redundant 34-m telecommunications antenna in Ghana to a radio telescope [1]. The Ghanaian radio telescope will be the second element, HartRAO being the first, of what will become the AVN. There are 29 documented 30-m class telecommunications antennas in 19 African countries (though some antennas were destroyed). It is proposed that more of these can be converted and added to the AVN [3]. Each addition will improve the present global VLBI networks; some will have greater impact than others. Currently there are plans, and limited funding, to convert antennas in Kenya, Madagascar, and Zambia. It is presently proposed that each of these new AVN stations will be equipped with the same receivers as Ghana: a 5-GHz and 6.7-GHz receiver and later a 1.4–1.7-GHz receiver [3, 4]. New radio telescopes may also be built. However, no significant evaluation of the optimization of the AVN has been completed. Such an analysis will inform which to convert first, where to build new stations, and what next-generation instruments and receivers they should have.

We discuss our results from analysis of weather data and assessment of the radio frequency interference (RFI) environment for potential AVN sites. Plots of the u - v coverage for existing VLBI networks together with potential AVN locations are also presented and we show the impact of AVN antennas on geodetic products through simulated VLBI observations. We discuss the potential contributions the AVN can make to current global VLBI experiments, as well as what a stand-alone AVN can do and where co-location of other geodetic instruments can be implemented.

1. Hartebeesthoek Radio Astronomy Observatory, South Africa

2. Vienna University of Technology, Austria

3. Astrogeog Center, USA

2 Site Selection and Evaluation

Currently, the only VLBI-capable radio telescopes in Africa are the 26-m and 15-m radio telescopes at HartRAO, SA. An antenna in Ghana is in the process of being converted for radio astronomy. Telecommunications antennas in African SKA partner countries likely to be converted next are in Kenya, Madagascar, and Zambia. There are also plans for a new radio telescope in Mauritius. The above mentioned sites, referred to as Group 1 (see Table 1), were included in all of our analyses as they are most likely to be converted first. All of our analyses and simulations also include the HartRAO site.

The above mentioned sites were assessed to determine viability for both radio astronomy and geodesy purposes. An excellent site is one where there is low precipitable water vapor (PWV), minimal RFI, provide excellent north-south and east-west baselines, and offer exceptional southern skies viewing. The first two criteria speak to the frequency range in which the facility will operate optimally. The latter three provide a measure of how to best improve present science experiments, e.g., VLBI experiments and southern skies accessibility.

Table 1: Potential sites in Africa selected for our analysis. The diameter of the telecommunications antenna at each site as well as the altitude of the site is listed.

Country	Site	Diam (m)	Alt (m)
Group 1			
Ghana	Kuntunse	32	70
Kenya	Longonot	34	1720
Madagascar	Arivonimamo	32	1450
Mauritius	Cassis	new-build	20
Zambia	Mwembeshi	34	1125
Group 2			
Egypt	Cairo	32	40
Ethiopia	Sululta	30	2725
Morocco	Souk el Arba des Sehoul	30	90
Nigeria	Lanlate	32	670
Senegal	Gandoul	30	50

For the purpose of the u - v coverage plots and the geodetic VLBI simulations we also included some additional telecommunications antennas that can be converted in Morocco, Egypt, Senegal, Nigeria, and Ethiopia. These sites were chosen strategically in terms of their location in order to optimize the network

distribution for a stand-alone AVN. These sites will be referred to as Group 2 (see Table 1) throughout this paper.

3 Weather Data

In order to assess atmospheric effects we used the NASA global numerical weather model GEOS-FPIT [5] that assimilates basically all available satellite, radiosonde, and ground meteorological data. The output of this model, at $0.625^\circ \times 0.5^\circ \times 72$ vertical layers $\times 3^h$ resolution, was used to derive the state of the atmosphere at a regular grid. Using the state of the atmosphere, we computed atmosphere air temperature and atmosphere specific opacity at a set of frequencies using the ITU-R (2013) [6] expressions.

In Figure 1 we present, as examples, the atmospheric opacity time series for the Ghanaian and Kenyan sites. We show results for three frequencies (22, 43, and 100 GHz) for the interval from 01 January 2013 to 08 November 2015, using a step size of three hours.

From the weather data, the Ghanaian site is best suited for low- to mid-frequency operations. HartRAO is an excellent site in comparison to the other proposed sites. For experiments requiring high-frequency observations, e.g., 22-GHz observations, the site in Kenya is favored. Though the HartRAO, Malagasy, and Zambian sites have comparable weather patterns the latter two sites have more extreme variations and would only be useful for higher frequency observations during the winter months.

4 Radio Frequency Interference

A number of precautions can be taken to minimize the effect of human generated RFI, e.g., to choose remote locations away from urban centers and industrial zones and implement radio quiet zones. However, most of the AVN stations are existing facilities close to cities and will operate in an already established environment.

A reliable proxy for RFI measurements can be determined from visual inspection of each site using Google Earth maps, where little infrastructure suggests little RFI. Satellite imagery, taken at an altitude of 4.2

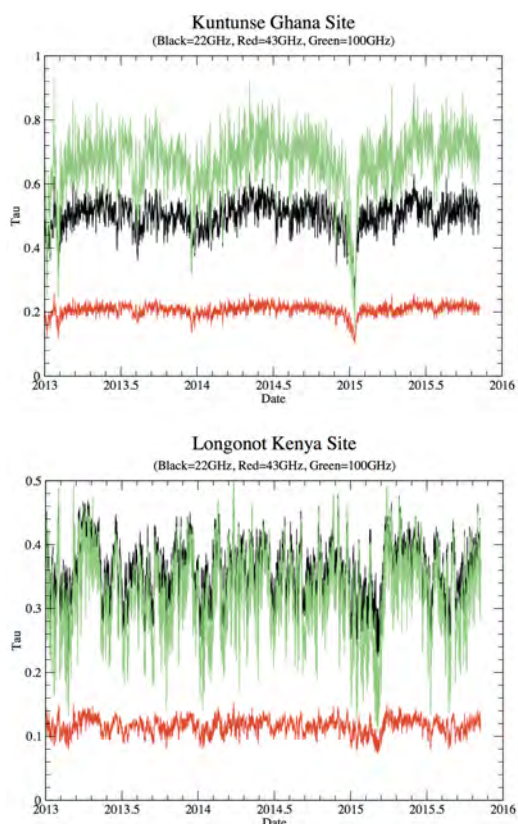


Fig. 1: Time series of atmospheric opacity for the Ghana and Kenya sites at 22, 43, and 100 GHz.

km, of the Ghanaian and Kenyan sites are presented in Figure 2 as examples. At 4.2 km the types of dwellings can be identified generally as residential, agricultural, or industrial.

The Kenyan and Zambian sites are in rural settings but each are located in flat areas with no protection, such as the hills surrounding HartRAO. The Ghanaian, Mauritian, and Malagasy sites are in urban areas with significant RFI. All these AVN sites should be characterized for sources of RFI. Since RFI is primarily a problem within the low frequency bands (< 5 GHz), it might be more advantageous for some AVN sites to concentrate on frequency bands at or above 5 GHz.

5 u - v Coverage Plots

The HartRAO 26-m radio telescope is valuable in providing long baselines to radio telescope arrays

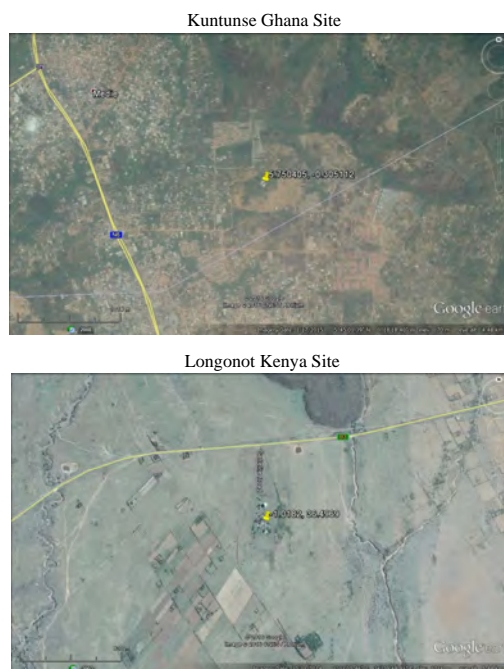


Fig. 2: Satellite imagery for the Ghana and Kenya sites.

on other continents, e.g., Europe (European VLBI Network, EVN) and Australia (Australia Long Baseline Array, LBA), and thus high angular resolution imaging. However, telescopes that can fill the gap between SA and Europe as well as SA and Australia would substantially increase the image quality.

We generated sample u - v coverage plots for existing VLBI networks (EVN and LBA) together with some potential AVN locations, to investigate the possible improvement in the density and the distribution of the u - v tracks. The results (see Figure 3 a, b) show that the antennas located roughly half-way between SA and Europe (i.e., Ghana, Kenya, Ethiopia, and Nigeria) provide the biggest improvement, as they fill the gap in u - v coverage between the northern EVN antennas and HartRAO. A telescope in Mauritius would be most valuable in filling some of the gaps in the u - v coverage between HartRAO and antennas in Australia.

The AVN would greatly facilitate VLBI observations of southern objects. As a stand-alone facility, AVN stations that would make the greatest contributions are in Ghana, Madagascar, Mauritius, Senegal, and Zambia. However, the AVN would still benefit from the long baselines to Australia (e.g., Figure 3 c). An AVN-LBA VLBI network would benefit greatly

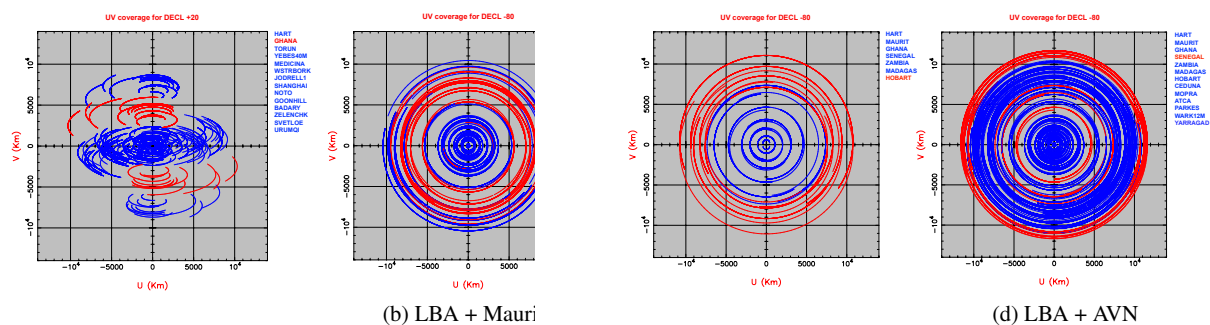


Fig. 3: Plots of the u - v coverage for a source at $+20^\circ$ (a) and -80° (b, c and d) declination, observed over a period of 24 hours. The red tracks show how a telescope in Ghana (a) and a telescope in Mauritius (b) will significantly improve the u - v coverage in the north and south, respectively. For a stand-alone AVN, an antenna in Australia (e.g., Hobart, c) is still needed for the long-baseline components. A telescope in Senegal (d) will contribute to both the long baselines and filling some of the gap between Australia and Africa.

from another antenna on the West coast of Australia (see Figure 3 d).

6 Simulated Geodetic Observations

In order to assess the influence of the AVN on geodetic products, we scheduled and simulated sessions with different station lists and compared them among themselves and with a state-of-the-art geodetic session (this session was not rescheduled but observations were simulated with the same parametrization). The Vienna VLBI Software (VieVS) [2] was used for scheduling, simulating, and analyzing these sessions.

Figure 4 depicts all the stations which were included in the present analysis. The AVN stations are grouped according to Table 1, the station HartRAO 15 m (Ht) was added and the stations from the session R1675 were used in different setups.

The scheduling parametrization resembles the IVS-R1 sessions as closely as possible. For the simulation of observations the default VieVS parameters (e.g., $C_n = 2.5 \cdot 10^{-7} m^{-1/3}$, $H = 2000$ m, $v_e = 8$ m/s) were used for every station. This does not resemble the true troposphere variability at every site but at the moment there is not enough information about troposphere turbulence at these stations. In order to get statistical information about the estimated parameters, the sessions were simulated 50 times and then analyzed. A standard

geodetic analysis was performed with the same models and parameters for every session.

In Table 2 the average formal error and its standard deviation are listed. One can see that adding additional African stations to a typical IVS-R1 session will increase the accuracy of the Earth Orientation Parameters (EOP) by roughly a factor of 2.

Coordinate stability was also examined, but we found no significant differences between the baseline length repeatability of the networks.

Another interesting aspect is the accuracy of source estimates. In the present analysis sources were fixed to their a priori positions but could be estimated session-wise and compared. However, this was not done so far and is subject to future work.

7 Co-location of Geodetic Instruments

There is a scarcity of non-VLBI geodetic instruments in Africa resulting in insufficient data for the International Terrestrial Reference Frame (ITRF). There are only two Satellite Laser Ranging (SLR) systems in Africa: HartRAO and Helwan, Egypt (no longer functional). Global Navigation Satellite Systems (GNSS) stations are the most suitable geodetic technique to densify the ITRF; GNSS stations are low cost, low maintenance, and can operate on solar-powered batteries. It is suggested that each AVN telescope be co-located with at least a geodetic-quality GNSS receiver

Table 2: Average formal EOP errors and their standard deviations.

Network	x_pol (μas)	y_pol (μas)	dut1 (ms)	nutdx (μas)	nutdy (μas)
R1675	41.43 ± 0.95	65.45 ± 1.49	5.12 ± 0.12	26.29 ± 0.60	25.36 ± 0.58
Group 1 + Ht	287.55 ± 6.73	170.87 ± 4.00	16.80 ± 0.39	56.66 ± 1.33	58.53 ± 1.37
Group 1 + 2 + Ht	113.61 ± 1.86	43.80 ± 0.72	7.84 ± 0.13	22.99 ± 0.38	23.64 ± 0.39
Group 1 + R1675	22.54 ± 0.37	30.65 ± 0.51	2.57 ± 0.04	14.69 ± 0.24	15.18 ± 0.25
Group 1 + 2 + R1675	21.78 ± 0.30	22.19 ± 0.31	2.13 ± 0.03	12.50 ± 0.17	12.32 ± 0.17

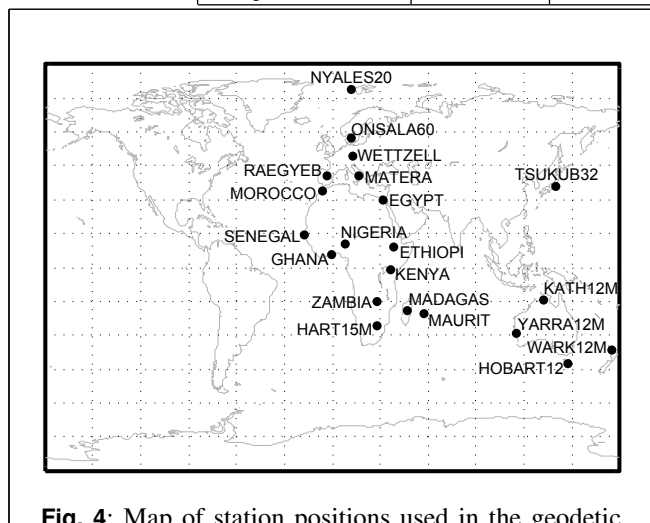


Fig. 4: Map of station positions used in the geodetic simulations. The stations shown in the map are stations from the IVS-R1675 session as well as the AVN antennas from Group 1 and Group 2 listed in Table 1.

and a meteorological station. Suitable stations can also be equipped with a seismometer, accelerometer, and gravimeter.

If funding could be obtained, astronomical VLBI antennas, and specifically new-built VLBI antennas should be considered for geodetic/astrometric work. This would greatly increase the benefit to the hosting nation for several reasons:

- The hosting nation would have a fundamental link to the ICRF, and via the EOP, to the ITRF.
- Such a station would be extremely valuable to the global geodetic community.
- Smaller co-located instruments would be sponsored from global sources at a rapid rate.
- There would be the possibility to eventually become a core (fundamental) site.
- The station would become its country's modern datum defining point, and would allow its realization and contributions to not only the ITRF, but also to the Global Geodetic Reference Frame (GGRF).

Co-location and geodetic/astrometric VLBI equipped antennas would allow the country to start transforming its (often very dated) geodetic Datum. This would allow for the creation of modern maps, land management, cadastral surveying, and civil engineering, which are all crucial to modern economies.

8 Conclusions

We have investigated the impact on global VLBI networks and found that the AVN will significantly improve each. Antennas in Mauritius and Kenya will greatly improve the EVN and LBA networks, respectively. Co-location of geodetic techniques will best serve the development of the ITRF and African Reference Frame.

References

1. D. Asabere et al., Radio astronomy in Africa: the case of Ghana, *astro-ph*, 1503.08850, 2015.
2. J. Böhm et al., The new Vienna VLBI Software VieVS. In *Proceedings of the 2009 IAG Symposium, Buenos Aires, Argentina*, Vol. 136, 1007–1011, International Association of Geodesy Symposia, 31 August – 4 September 2009.
3. M. J. Gaylard et al., An African VLBI Network of radio telescopes, In *Proceedings of SAIP2011, the 56th Annual Conference of the South African Institute of Physics*, pages 473–478, 2012.
4. A. Loots, The African VLBI network project, *American Astronomical Society Meeting Abstracts*, 225, pages 126.02, 2015.
5. A. Molod, et al., The GEOS-5 Atmospheric General Circulation Model: Mean Climate and Development from MERRA to Fortuna, *NASA/TM–2012*, 104606, vol. 28, 2012, <http://gmao.gsfc.nasa.gov/pubs/docs/tm28.pdf>
6. Recommendation ITU-R P.676-10, Attenuation by atmospheric gases, 2013, <https://www.itu.int/rec/R-REC-P.676/en>

A Technical Overview of the EVN

Pablo de Vicente

Abstract In this paper we present an overview of the European VLBI Network (EVN) from the technical side. We describe the frequency bands used, the equipment at the stations, the different types of observations, and how they are organized. There is also a description of the latest technical developments, whose main goal is to achieve two polarizations 512-MHz wide with a recording rate of 4 Gbps. All these tasks lie within the role of the Technical and Operations Group (TOG) of the EVN that is also in charge of maintaining the quality of the results of the network.

Keywords VLBI, EVN

1 Introduction

The European VLBI Network (EVN) is a collaboration of the 14 major radioastronomical institutes in Europe (including the Joint Institute for VLBI ERIC), Africa, and Asia, whose main goal is to perform astronomical high angular observations of cosmic sources. This is achieved using Very Long Baseline Interferometry (VLBI) among telescopes at the different observatories of the institute members. The EVN operates 21 telescopes and two correlators.

The EVN has a governing body formed by the Consortium Board of Directors (CBD), a Technical and Operations Group (TOG), and a Programme Committee (PC). The chairs of the two latter groups report to the CBD every six months.

Observatorio de Yebes, Instituto Geográfico Nacional

2 The TOG

The Technical and Operations Group dates back to 1982 (by that time it started being called the TWG), although minutes from past meetings are public available only since 1992. The TOG is in charge of the operations and technical developments of the network. It is composed of VLBI friends at the stations and personnel at the correlators. The TOG meets periodically approximately every nine months, rotating the location through the different observatories. The meetings are open and are also regularly attended by non-EVN members, like the FS main developer or staff from Haystack and NRAO. The meetings are organized so that they do not coincide with EVN sessions. Once every three meetings the TOG chair tries to match it with the EVN symposium and EVN users' meeting, looking for a direct interaction between the technical personnel and the users. Beginning in 2016, the TOG will meet together with the Global Millimeter Array (GMVA) Technical Group every other meeting. The goal is to exploit synergies, look for common developments, and benefit from the exchange of information between both communities.

The TOG resources are distributed among different EVN partners who host different servers. The main TOG Web page is currently hosted at <http://www.oan.es/evn/tog.html> and it acts as starting point to access all the resources. This page is also reachable from the main EVN Web page: <http://www.evlbi.org>. The sources of information are the TOG wiki, hosted by MPIfR in Bonn: https://deki.mpifr-bonn.mpg.de/Working_Groups/EVN_TOG.html and the Radionet3 wiki Web page: <http://www.radionet-eu.org/radionet3wiki/doku.php?id=na:eratec:tog>. The

first wiki contains information about disk status, disk purchases, spares, last and permanent action items, and technical information, including scripts, procedures, and descriptions to perform tasks at the stations. The second wiki is basically devoted to TOG meetings. It archives the agenda, minutes, reports, and talks from past meetings. The JIVE Web page and servers maintain all information regarding feed back from observations, observed and correlated experiments, and about real time correlation. The schedules and logs are stored in the EVN FTP hosted by the Istituto Nazionale di Astrofisica (INAF) in Italy. The main communication channel is the mailing list hosted by Jodrell Bank and is known as the EVNtech email list.

3 EVN Observations

The EVN observes between 21 cm and 7 mm. There are seven main bands whose frequencies were chosen to make them match with interesting spectral molecular or atomic lines. Table 1 lists the frequencies, bandwidths, and lines on which they are centered. The 21-cm band is centered on the atomic H line, and the 18-cm band is centered on the OH maser line. 13 cm and 3.6 cm are also bands chosen because they are compatible with geodetic S/X observations. Other bands are 6 cm and 5 cm, the latter centered around the CH₃OH maser line. Finally the upper bands are 1.3 cm around the H₂O maser line and 0.7 cm around the SiO maser line. Available instantaneous bandwidths depend on the frequency ranges and vary between stations, the largest being 500 MHz. Many telescopes can tune their local oscillators and the observable bands are larger than 500 MHz, for example several GHz for 22 and 43 GHz at some telescopes. This information is kept in one of the catalogs at JIVE. The most used bands during EVN observation are 5 cm, 6 cm, and 18–21 cm.

Most of the EVN telescopes are equipped with DBBC2 backends built by HAT-Lab in collaboration with MPIfR. The DBBC2s contain four IFs and four COREs and a Fila10G board which can generate VDIF data rates up to 8 Gbps. However, not all telescopes have fully equipped DBBC2s. The Russian KVAZAR telescopes use their own DAS R1002 backend, and the Korean stations also use a Korean Data Acquisition System. Robledo uses a data acquisition unit (DVP) built by JPL. The recorders used are Mark 5A,

Table 1 Frequency bands covered by the EVN. Band widths depend on the individual stations.

Band	Bandwidth	Main interest
21 cm	60–500 MHz	H maser
18 cm	60–500 MHz	OH maser
13 cm	300 MHz	S/X geodetic S band
6 cm	500 MHz	Continuum emission
5 cm	425, 500 MHz	6.6 GHz CH ₃ OH maser
3.6 cm	500 MHz	S/X geodetic X band
1.3 cm	100, 400, >500 MHz	22 GHz H ₂ O maser
0.7 cm	>500 MHz	43 GHz SiO maser

Mark 5B, Mark 5B+, Mark 5C, Flexbuf, and Mark 6. Updated information on the recorders and the firmware that they use is compiled on the following Web page: <http://mark5-info.jive.nl/>. Most of the stations record in Mark 5B format, although during 2015 two stations, Ef and On, began recording data in VDIF format.

Standard observations at the EVN consist in observing two bands 128-MHz wide each at right and left circular polarization, which corresponds to a recording rate of 1024 Mbps. This rate is limited by a DBBC2 equipped with two COREs and a Mark 5B recorder if Mark 5B format is used. Higher rates require four COREs in DDC mode and at least a Mark 5B+ recorder. Since EVN 2015-3 the EVN offers two bands 256-MHz wide with a recording rate of 2 Gbps at all stations except two.

The EVN groups observations along the year in three blocks called sessions. Several weeks prior to each session there is a call for proposals which are evaluated by the Program Committee (PC). Proposals rated best are scheduled and observed. Each session is divided into blocks according to the observing frequency. The sessions usually take place in February/March, May/June, and October/November. The scheduler keeps contact with the Global Millimeter Array (GMVA) scheduler and the IVS scheduler to avoid observational conflicts, because some EVN telescopes also belong to the GMVA and IVS networks. The number of observations programmed depends on the available disk space at the stations and correlator. Currently, with a recording rate of 1 Gbps, the typical usage per station and session is 60 TB. The schedules are made by JIVE where a customized catalog and a patched version of SCHED is kept.

Apart from the standard science observations during sessions, the EVN performs other types of observations. Network Monitoring Experiments (NME)

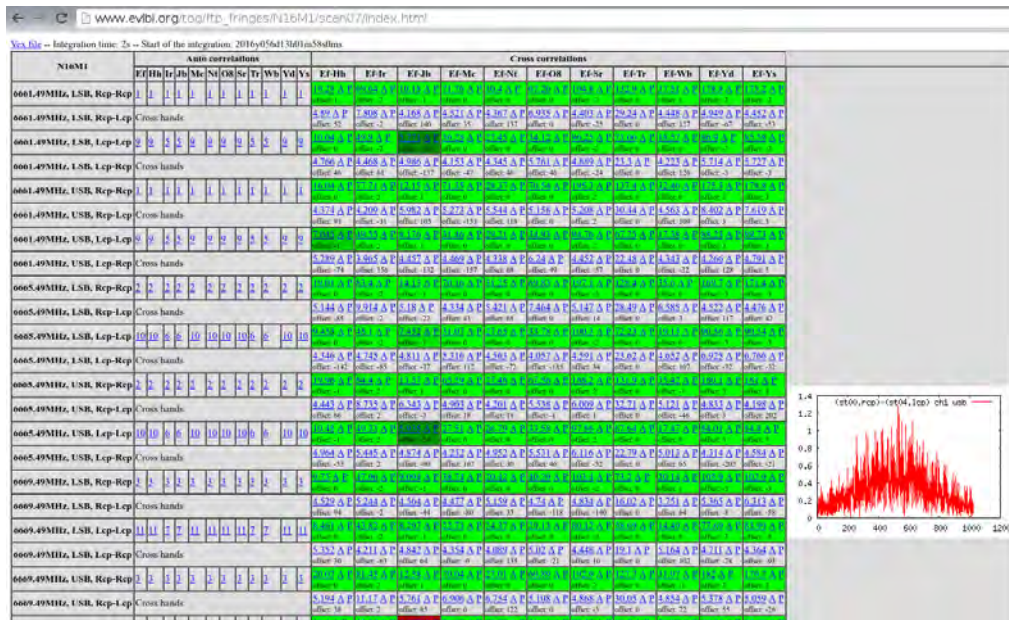


Fig. 1 The Web page evlbi.org showing results from the correlation after transferring a part of a scan to JIVE correlator. Results from all baselines to a single reference station are shown. Amplitude and phase together with autocorrelation are displayed for both polarizations and for cross polarizations.

are observations that precede a frequency block during an EVN session. The stations transfer slots of selected scans to the correlator where the data is correlated. The goal of these observations is to debug problems some hours before the science observations to be able to tackle them. Fringe tests are another kind of EVN observation and their purpose is to test a development not restricted to the EVN sessions. They can be scheduled at any time and usually are restricted to a subset of telescopes, namely those that are available and willing to implement the new features to test. Both types of observations are correlated in near-real time, and the results displayed on a Web page at JIVE: http://www.evlbi.org/tog/ftp_fringes/. Figure 1 shows an example. There are some cases in which some fringe tests are diskless and the data is transferred in real time to the correlator.

Out-of-session Observations (OoS) happen six days per year. They require a long-term cadence and time specific requirements and they are usually associated with the Radioastron project. e-VLBI observations are diskless transfers of data to the correlator where they are correlated in real time. Each observation usually takes 30 hours and they are distributed along the year, in several periods. Usually the first hours of the observation are reserved

for tests. Target of Opportunity (ToO) observations is another category of observations. Their goal is to react to a transient event. They require a fast review and scheduling and if their rating is high enough they can override a running schedule. For the time being, ToO observations can only happen during an e-VLBI period.

All observations automatically send the LOG to the EVN FTP server hosted in Bologna, Italy, and observers fill a feedback form after the observation has completed. Previous to the EVN sessions, telescopes should reserve time for an amplitude calibration observation that allows to determine the gain of the antenna and noise temperature of the diodes along a frequency band. This is achieved with ONOFF observations. The EVN is trying to extend the usage of continuous calibration driven by a 80-Hz signal to all telescopes. This method reduces the time devoted to calibration and monitors the gain changes through the receiving chain.

4 Technical Developments

One of the short-term technical goals of the EVN is a recording rate of 2 Gbps for e-VLBI and recorded ex-

periments, and 4 Gbps for recorded experiments in the near future. 2 Gbps, which corresponds to two bands of 256 MHz, should be implemented at all stations by 2017 and 4 Gbps (2 bands 512-MHz wide) one year later. To achieve this goal the EVN signed a contract with NVI in 2015 to provide new features in the FS which had to be completed in one year approximately. This agreement was composed of three steps which had to be covered by a FS release each time.

The first goal was to provide support for 32 MHz per channel in DDC mode. FS version 9.11.7 released in April 2015 and the DBBC firmware V105E_1 released by HAT-Lab in January 2015 covered this goal. This mode is available within the EVN since then and it is offered in the call for proposals since fall 2015. This is currently implemented and working.

The second step consisted in providing support for VDIF data and therefore for Fila10G, Mark 5C, Flexbuff, and Mark 6 recorders. This was accomplished by Fila10G firmware version 3.3, FS version 9.11.8, and jive5ab versions above 2.6.0. This has been supported and available since October 2015. Currently, three EVN stations benefit from this development and within the next months others will follow. This step is closely related to the jive5ab software. jive5ab is a crucial software in the EVN; the TOG agreed in 2014 to replace Dimino by jive5ab at all EVN stations. jive5ab is a development mainly by Harro Verkouter (JIVE) and it manages the recording of data. It works on Mark 5A, Mark 5B, Mark 5B+, Mark 5C, Mark 6, and Flexbuff. It is supported in 32 and 64 bit OS Linux versions and works for several Debian versions: Etch, Lenny, and Wheezy. jive5ab supports VDIF and Mark 5B format. Together with jive5ab there are some useful tools like m5copy to copy data between the different recorders. This can be used to transfer data between the stations and the correlator at high speeds, up to 800 Mbps. In the Flexbuff and the Mark 6 there is also a virtual file system, based on a fuse that allows to gather the data from an experiment distributed in different disks. For further information see Verkouter in this same volume.

The third step consisted in providing support for the PFB mode. This is the mode that will be required for 4-Gbps operations. Currently, there are several FS beta versions, 9.11.9 to 9.11.13, that address the issues that have arisen. The successive versions have been tested successfully in January, April, and May 2016 (experiments FR028, FR030, FR031, FRO033, and FR034).

Support for radiometry is already in place and, at the time of this paper, some tests still need to be performed to check the validity of the last version.

One of the latest technical developments accomplished by the TOG was the adoption of 2-Gbps e-VLBI. This mode has been implemented after extensive tests performed during the last months. The usage of Mark 5Bs imposed a limitation of 1 Gbps in the transfer of data in real time. The correlator connected to the station's Mark 5B or Mark 5C and managed the data flow using jive5b. However, increasing the data rate to 2 Gbps required that the DBBC2 sent the data directly to the correlator. The DBBC2 generates data in VDIF format that can be sent in a single thread with different frames, one per frequency band, or in different threads, one per frequency; both cases were tested. The single thread multi-frame works with a payload of 8,000 bytes per frame and the multi-thread single-frame one with 2,000 bytes. The former matches the requirements of the correlator. The second one, although it also matches the capability of the correlator, imposes a load on the CPU: smaller frames require more processing. The data flow control from the correlator was achieved by a proxy, a server program that listens to the FS and to a second client (from the correlator), and which forwards commands to the DBBC2 and receives answers which are sent back to the caller. This is the way to control the data flow and start and stop it when required at the correlator. The proxy is installed on a host in the public local area network to prevent malicious access to the FS which controls the radio telescope.

After this development, the EVN has announced in the last call for proposals, in May 2016, the possibility to perform e-VLBI observations at a rate of 2 Gbps with at least six stations. Once the 4-Gbps recording rate mode is fully tested, this mode will be announced at the EVN and it should also be available for e-VLBI observations, provided the stations have 10 Gbps connection lines to the Internet.

References

1. Harro Verkouter (JIVE — ERIC). "Of Flexing your buffers and Marking your 6's". 4th International VLBI Technology Workshop, 2015.

From CONT to VGOS: the Evolution of the CONT Campaigns

Cynthia C. Thomas, Dirk Behrend, Daniel S. MacMillan

Abstract Continuous VLBI campaigns (CONT) started in 1994 with the goal of demonstrating state-of-the-art VLBI over a continuous period of time. The first CONT was followed by campaigns in 1995 and 1996. After a six year hiatus, CONT campaigns were organized approximately every three years from 2002 through 2014. In this paper we primarily focus on the cornerstones of each CONT campaign. Specifically, we review the developments in networks, scheduling techniques, recording media, correlation, and other resources used. A timeline of the history of the CONTs and the goals for future campaigns will be presented. The CONTs used a significant amount of IVS resources to produce a large volume of high quality data and demonstrated the advantages of continuous observing which will soon be realized with VGOS.

Keywords Continuous VLBI, CONT, VGOS

1 Introduction

Over more than two decades continuous VLBI campaigns (CONTs) have been organized to demonstrate and exploit the capabilities of the geodetic/astrometric VLBI technique at its maximum potential at the time. The state-of-the-art of VLBI was first demonstrated over an extended continuous period of time in 1994 (CONT94). This was followed by campaigns in the

two subsequent years (CONT95 and CONT96) and then, after a gap of six years, every three years starting in 2002 (CONT02, CONT05, CONT08, CONT11, and CONT14). Thus, a total of eight CONT campaigns have been observed so far.

All past eight CONT campaigns provide a snapshot of the capabilities of the legacy S/X systems in various stages of its development. As the technology advanced, analog systems were gradually replaced by digital systems. So while the early CONTs made use of thin tapes and video converters, later ones employed recording disks (Mark 5) and digital backends. Likewise the correlation went from early hardware correlators (Mark IIIA) to advanced hardware correlators (Mark IV) and eventually to software correlators (DiFX).

With the gradual implementation of the broadband VGOS system, VLBI is heading towards continuous operations by the year 2020 or shortly thereafter. Hence, once VGOS is fully established, the main characteristic of a CONT campaign—namely continuous observing—will have become the regular modus operandi of VLBI. In other words, CONT campaigns will lose their purpose by then. However, in the transitional period, CONTs may continue to be an important assessment tool of the progress of VLBI. As such, the CONT campaigns in 2017 and 2020 may be quite useful.

In the following we provide a brief history of the CONT campaigns. We address the resources used such as station and correlator time as well as recording media. We conclude with an outlook for the future CONT campaigns. The continuous VLBI campaigns can clearly be viewed as a precursor of the VGOS.

NVI, Inc.

Table 1 Overview of the history and possible future of the CONT campaigns.

Campaign	Observing period	Description
CONT94A	12–25 January 1994	13 continuous days with two independent networks running simultaneously: seven non-VLBA stations (A) and seven VLBA stations (B)
CONT94B		
CONT95	23–29 August 1995	Six continuous days
CONT96A	2 Sep. – 16 Nov. 1996	11-week campaign with non-continuous observing with ARSAC sequence the first seven weeks—observed biweekly, two weeks not observing, and two parallel networks the last two weeks: (A) five non-VLBA stations, (B) 10 VLBA plus up to two non-VLBA stations
CONT96B		
CONT02	16–31 October 2002	15 continuous days
CONT05	12–27 September 2005	15 continuous days
CONT08	12–27 August 2008	15 continuous days
CONT11	15–30 September 2011	15 continuous days
CONT14	6–21 May 2014	15 continuous days
CONT17	<i>tbd, in planning phase</i>	<i>15 continuous days on two networks (e.g., 19 legacy S/X stations and seven VGOS stations)</i>
CONT20	<i>tbd, under consideration</i>	<i>15 continuous days with VGOS stations</i>

2 History and Goals of the CONT Campaigns

Table 1 summarizes the timeline and provides a brief description of the various CONT campaigns. In the following we elaborate in more detail on the goals of the CONTs.

CONT94, CONT95, and CONT96 are three campaigns that were a prelude to the Continuous Observation of the Rotation of the Earth (CORE) VLBI project. CONT94 was a resource-intense campaign that observed two seven-station networks simultaneously: network A with non-VLBA stations and network B with VLBA stations for 13 days. CONT94A produced the lowest formal errors ever obtained using VLBI until CONT05. CONT95 was the shortest campaign. It ran for six days (August 23–29) with six participating stations. According to Clark et al., CONT95 was conducted in order to better understand the effects of higher tropospheric water vapor content and larger tropospheric delays during the Northern Hemisphere summer, which contrasts with the CONT94 winter campaign [1]. CONT96 was not observed continuously over a period of time, but it ran for 11 weeks from September 2 to November 16. CONT96 adopted an innovative observation scheme to maximize the usefulness of the data on timescales from subdaily to monthly under the correlator constraint [1]. Twenty-four observation days were selected during a period of 77 days starting September 2, 1996, according to the “ARSAC zero-redundancy sequence” 1100101, which gave the pattern of observing days within a week as well as the pattern of observing

weeks [1]. After the six-year hiatus, the CONT campaigns were observed every three years starting with CONT02. All of the campaigns were observed for 15 days with various number of stations.

CONT02 (October 16–31) had eight participating stations with the goals of obtaining scientific analysis of daily and sub-daily tidal models, VLBI technique improvement for atmosphere studies, reference frame repeatability, and comparisons with other geodetic techniques. Water Vapor Radiometer (WVR) data was collected at Kokee, Onsala, and Wettzell.

CONT05 was observed for 15 days beginning September 12 with 11 participating stations. There were several goals for CONT05. Two weeks of continuous high frequency (sub-daily) EOP addressed the discrepancies seen between the tidal and atmospheric models, specifically the observations at the M2 and S1 frequencies and the long-term and short-term values of tidal amplitudes. Continuous data allowed a comparison of the estimates of the troposphere zenith delay and gradients across experiment boundaries as a measure of the accuracy of the observations and analysis. Analysis of reference frame repeatability day to day was made and compared with previous continuous VLBI series. CONT05 was strongly endorsed by the IERS because it was an important source of data for the IERS Combination Pilot Project.

The CONT08 campaign was observed on August 12–27 with two improved characteristics. One significant change for CONT08 from previous CONTs was increasing the recording rate from 256 Mb/s to 512 Mb/s. With 512 Mb/s recording and a network with larger geographical coverage, the sub-daily precision

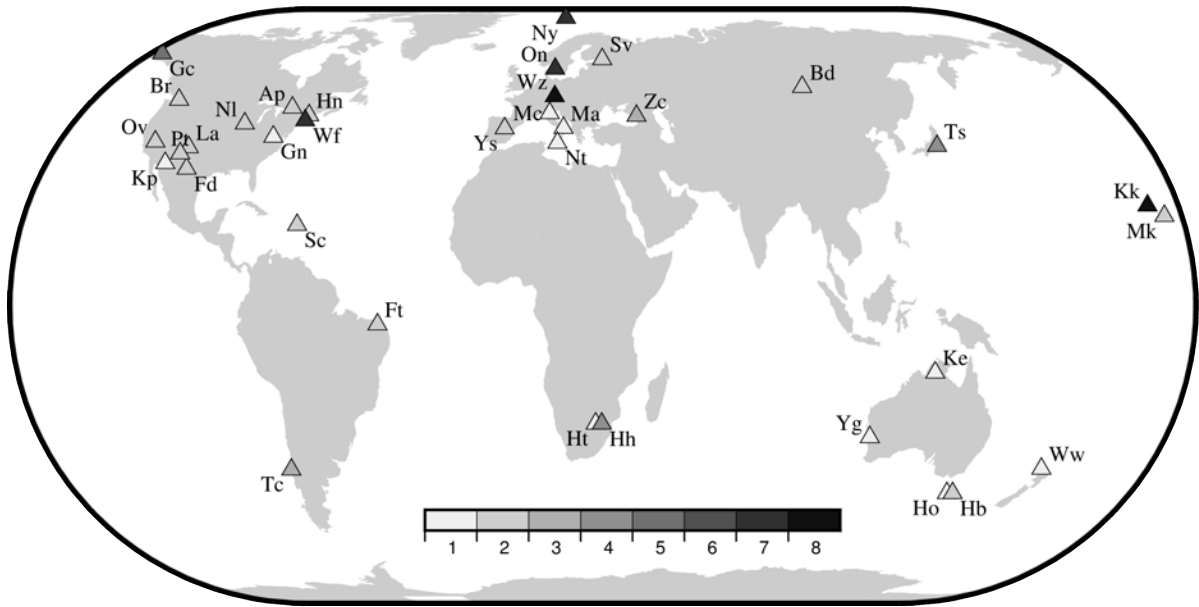


Fig. 1 Thirty-five stations have contributed to CONT campaigns during the last 20 years. The light grey triangles show the stations participating in one to four CONTs, whereas the dark grey triangles display the stations participating in five to eight CONTs.

was expected to be better than earlier CONT campaigns, thus allowing for further testing of theoretical tidal models. First detection of ter-diurnal signals related to M3 and S3 tidal phenomena in the oceans and the atmosphere was achieved with the CONT94, CONT02, and CONT05 data. The anticipated precision of the CONT08 allowed further investigation of these phenomena. The CONT08 network had a larger geographical coverage than previous CONT campaigns and thus promised to be more sensitive to smaller scale features in the ionospheric activity. A combination of VLBI and GPS for the derivation of total electron content (TEC) maps was possible. The CONT08 troposphere delay estimates were also compared with WVR results, GPS estimates, and Numerical Weather Models (NWM).

The large 13-station network of CONT11 (September 15–30) had a reasonably balanced geographical distribution between the northern and southern hemispheres. CONT14, observed during May 6–21, had the largest network of all the previous CONTs—17 stations with reasonably balanced geographical distribution between the northern and southern hemispheres. Both campaigns allowed further studies of high frequency EOP variations, analysis of ocean tide models, tests of theoretical models, and derivation of TEC maps.

3 Resources and Quality

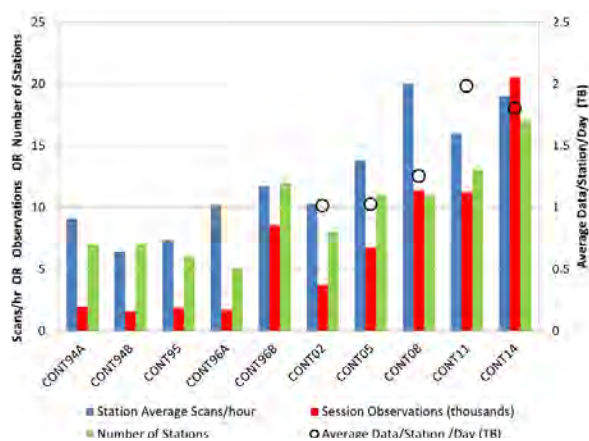
Figure 1 shows how many times a station participated in a CONT campaign. There have been eight CONT campaigns thus far. Two stations, Wettzell and Kokee have participated in all eight campaigns. The global coverage of the CONT campaigns improved with more coverage in the south. HartRAO-26m was added to the CONT campaigns in 2002, but there was a significant improvement in polar motion when both HartRAO-26m and Tigo were included in the CONT05 campaign (see Figure 3).

The CONT campaigns used, and will continue to use, a large amount of resources including station time, recording media, and correlator time. Table 2 displays how much correlator time was used to support the CONT campaigns. This required that all other sessions, except the IVS-R1 and IVS-R4, not be processed until the CONT campaigns were completed. The CONT14 campaign was processed with the DiFX Correlator at Bonn in 38 days. This was a significant improvement from previous CONT campaigns. It shows that we are moving in the right direction with the DiFX correlator so that we will be able to process the massive amount of VGOS data that we plan to obtain.

Figure 2 shows the general increase in several measures of the size of the CONT campaigns. The sta-

Table 2 Resources used for the eight CONT campaigns. The IVS was established in 1999 between CONT96 and CONT02.

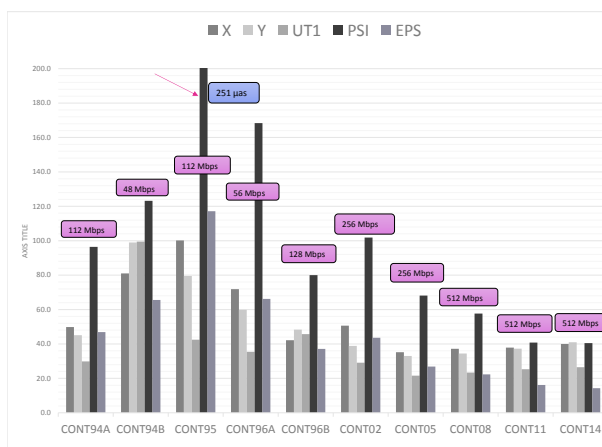
Campaign	#stations	#sources	Media	Recording rate	Correlator center	Correlation time	Correlator type
CONT94A	7	41	thin tape	112 Mbps	Haystack	n/a	Mark IIIA
CONT94B	7	41	thin tape	48 Mbps	Haystack	n/a	Mark IIIA
CONT95	6	34	thin tape	112 Mbps	Washington	n/a	Mark IIIA
CONT96A	5	40	thin tape	56 Mbps	Haystack/Washington	n/a	Mark IIIA
CONT96B	12	44	thin tape	128 Mbps	VLBA	n/a	Mark IIIA
CONT02	8	50	thin tape	256 Mbps	Bonn/Haystack/Washington	58/89/45 days	Mark IV
CONT05	11	74	Mark 5	256 Mbps	Bonn/Haystack/Washington	50/81/68 days	Mark IV
CONT08	11	80	Mark 5	512 Mbps	Washington	163 days	Mark IV
CONT11	13	117	Mark 5	512 Mbps	Washington	146 days	Mark IV
CONT14	17	73	Mark 5	512 Mbps	Bonn	38 days	DiFX

**Fig. 2** Size of CONT campaigns: sources, scans, and observations.

tion average scans per hour were better in CONT08 than in CONT14, but CONT14 had five more stations than CONT08. That is why the number of session observations in CONT14 was much higher than previous CONTs. The average data per station per day was largest in CONT11. The average data per station went down slightly in CONT14, which may be due to the larger network, which allows more subnetting during the scheduling of the stations. The formal errors did not improve significantly for X, Y, or UT1 when the recording rate was increased from 256 Mb/s to 512 Mb/s in CONT08, but it did improve for PSI and EPS.

4 Future CONTs

We are in the planning stage of CONT17. The Coordinating Center and the Observing Program Committee (OPC) began discussions about CONT17 in early

**Fig. 3** The EOP formal uncertainties steadily improved after CONT02. This was due to larger networks and increased recording rates.

2016. There were discussions regarding simultaneous networks, media, and correlator(s). CONT20 has not been discussed yet (see Table 1).

The plan is to have the next CONT campaigns in late 2017. We want to have as many VGOS stations as possible observing simultaneously with the legacy stations. As mentioned earlier, a vast amount of resources will be needed to support this campaign. Currently only the Haystack correlator can process the VGOS data; so, we need at least two correlators to process the data: one to correlate the VGOS data and the other to process the legacy data. Due to limited correlator resources, the huge amount of data from a dual network cannot be processed by one correlator. Mark 6 modules need to be purchased to support the VGOS observing. Depending on the recording rate, additional Mark 5 modules may need to be purchased as well. There have been additional discussions about including the VLBA in the

The Italian VLBI Network: First Results and Future Perspectives

Matteo Stagni¹, Monia Negusini¹, Giuseppe Bianco², Pierguido Sarti^{1,3}

Abstract A first 24-hour Italian VLBI geodetic experiment, involving the Medicina, Noto, and Matera antennas, shaped as an IVS standard EUROPE, was successfully performed. In 2014, starting from the correlator output, a geodetic database was created and a typical solution of a small network was achieved, here presented. From this promising result we have planned new observations in 2016, involving the three Italian geodetic antennas. This could be the beginning of a possible routine activity, creating a data set that can be combined with GNSS observations to contribute to the National Geodetic Reference Datum. Particular care should be taken in the scheduling of the new experiments in order to optimize the number of usable observations. These observations can be used to study and plan future experiments in which the time and frequency standards can be given by an optical fiber link, thus having a common clock at different VLBI stations.

Keywords VLBI, correlation, time and frequency, local ties, national datum

1 Italian VLBI Network Status

The Italian VLBI network is composed of four antennas. Three of them are part of the IVS [1] network: Medicina, Noto, and Matera. The fourth antenna is the Sardinia Radio Telescope (SRT), recently becoming operational. When not involved in VLBI observations they also work as single dishes and perform a number

1. IRA - INAF
2. ASI
3. Italian Embassy - Pretoria - South Africa

of VLBI observations including the ones organized internally.

Since 2012, VLBI observations have gained momentum due to the installation of the DiFX [2] software correlator in Bologna. Progressive updates shown in Table 1 have transitioned the antennas from previous Mark IV and VLBA backends to present DBBC ones.

Table 1 Hardware setup of the Italian antennas.

Antenna	Backend	Formatter	Recorder
Medicina - 32 m	DBBC2	Fila10G	Mark 5C
Noto - 32 m	DBBC2	Fila10G + Mark 5B	Mark 5B
SRT - 64 m	DBBC2	Fila10G + Mark 5B	Mark 5B+5C
Matera - 20 m	VLBA	Mark 5B	Mark 5B

Significant advancements have also been made in network connectivity, providing 10-Gbit connections to Noto and Medicina, and the installation of a POP (Point of Presence) by the Italian research provider (GARR) in Bologna. The POP router provides up to 1-Tbit backplane connectivity to the research network, which is currently under major upgrades.

Table 2 Network connectivity.

Facility	Network connection
Medicina	10 Gbit
Noto	10 Gbit
Sardinia	10 Gbit ¹
Matera	500 Mbit
Bologna	10 Gbit

¹Expected in 2017

All stations are at least co-located with GNSS systems, while at the Matera fundamental geodetic station there is also an SLR system. The relevant local tie vec-

\$14MAR18XI <4> Post-fit residuals

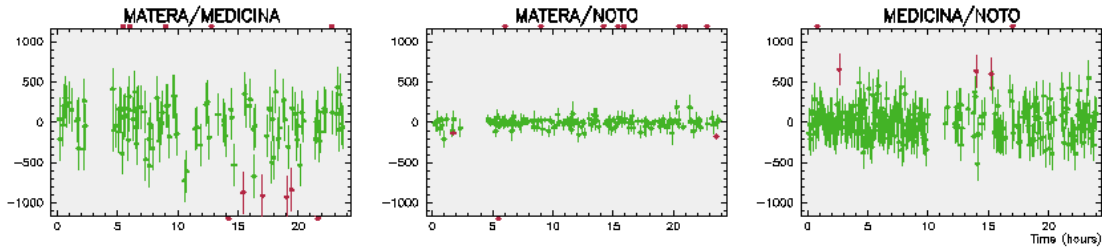


Fig. 1 SOLVE residuals from the first Italian geodetic VLBI experiment.

tors are available. In Italy there are several GNSS networks managed by various institutions, but all of them may benefit from the geodetic VLBI observations. A series of geodetic VLBI experiments has been planned to contribute to realizing an improved national datum.

Table 3 Co-located techniques and their local ties with VLBI.

Antenna	GNSS	DORIS	SLR
Medicina	YES	NO	NO
Noto	YES	NO	NO
Sardinia	YES	NO	NO
Matera	YES	NO	YES

2 Geodetic Experiments

Planning of geodetic experiments followed first fringes obtained with astronomical observations in 2013. The establishment of the experiments pipeline was not straightforward due to the backend transitioning time and working out the processing chain to obtain a dataset which could be analyzed with CALC/SOLVE. The most critical aspects were updating catalogs in SKED that could match the new setups at the antennas, Noto being first in adopting the new DBBC backend and with Medicina following in 2015 (though going directly to VDIF data format). The residuals shown in Figure 1 were obtained after working out the correct definition of Noto station which was scheduled by SKED as having a VLBA backend, but the station at the time was already using a DBBC backend.

3 Time and Frequency

Optical fiber links are beneficial not only for frequency metrology but also for other fields of physical research, such as radio astronomy and geodesy. Within the LIFT Project, the first optical fiber link from the National Institute of Metrology (INRIM) to the Medicina radio telescope was realized [3]. Comparing the hydrogen maser used as a frequency reference at Medicina with the Italian Cs fountain primary frequency standard, it was demonstrated that optical links can provide radio astronomical facilities with very accurate and stable frequency references, potentially better than the currently used hydrogen masers. The investigation experiment EUR137 has seen the participation of Medicina in a double manner [5], utilizing both the local maser clock and the remotely distributed frequency clock. The principal aim of the experiment was to test the accuracy of the remote clock over long periods of time, typically the timescale of a geodetic experiment (24 hours). The experiment was carried out alternating the observation scans between the local clock and the remote clock. This observation strategy was dictated by the fact that it was not possible to observe simultaneously with two different clocks (as this would have required two backends) and by the necessity to observe the same source at least three times for obtaining a single closure within the time of the experiment.

The secondary aim of the experiment was technical: it was the first time Medicina observed using the VDIF data format. The VDIF data format is in fact a more convenient and network-friendly format for VLBI data that can speed up and more reliably enable data transfers over networks rather than disk shipments. The

Fila10G complimentary formatter to the DBBC is able to easily produce this format as network packets output; however, a difficulty for the scheduling and correlation softwares is to interpret this. Table 4 shows the rearranged channels and BBC order for the DiFX software to correctly process the VDIF data.

Table 4 Geodetic VDIF channel and BBC assignment.

GEO VDIF			
CH	Sideband	BBC	Pol
1	U	BBC1	R
2	U	BBC2	R
3	U	BBC3	R
4	U	BBC4	R
5	U	BBC5	R
6	U	BBC6	R
7	U	BBC7	R
8	U	BBC8	R
9	L	BBC1	R
10	L	BBC8	R
11	U	BBC9	R
12	U	BBC10	R
13	U	BBC11	R
14	U	BBC12	R
15	U	BBC13	R
16	U	BBC14	R

4 Conclusions

Recent technical and technological advancements in networks, backends, data formats, and time and frequency distribution contribute to better plan VLBI experiments. The encouraging results shown in this paper could be the first of a series of Italian experiments to be integrated with GNSS solutions through local ties to contribute to a national reference system. The time and frequency distribution opens new perspectives in

the ultimate limits of VLBI and a more precise space geodesy. In the framework of this unique opportunity more Italian geodetic experiments have been planned for 2016 and 2017 to reliably test the new VDIF setups at Medicina and Noto and also involving Matera where the next remote time and frequency distribution link will be set up. During these newly planned tests, real-time recording at the correlation facility in Bologna has also been scheduled to significantly reduce the correlation processing time.

References

1. Nothnagel, A., et al, "The IVS data input to ITRF2014". International VLBI Service for Geodesy and Astrometry, <http://doi.org/10.5880/GFZ.1.1.2015.002>, 2015.
2. A. T. Deller, S. J. Tingay, M. Bailes and C. West, "DiFX: A Software Correlator for Very Long Baseline Interferometry Using Multiprocessor Computing Environments", In Publications of the Astronomical Society of the Pacific, <http://www.jstor.org/stable/10.1086/513572>, pages 318–336, 2007.
3. C. Clivati, R. Ambrosini, C. Bortolotti, G. A. Costanzo, M. Frittelli, F. Levi, A. Mura, F. Perini, M. Roma, M. E. Zucco, D. Calonico, "The optical fiber link LIFT for Radioastronomy", In Frequency Control Symposium and the European Frequency and Time Forum (FCS), 2015 Joint Conference of the IEEE International, doi: 10.1109/FCS.2015.7138955, pages 769–772, 2015.
4. D. Calonico, C. Clivati, M. Frittelli, A. Mura, M. Zucco, F. Levi, F. Perini, C. Bortolotti, M. Roma, R. Ambrosini, G. A. Costanzo, "Time and frequency optical fiber link for Space Metrology", In 2nd IEEE International Workshop on Metrology for AeroSpace, June 4-5, 2015, Benevento, Italy, 2015 IEEE, doi: 10.1109/MetroAeroSpace.2015.7180654, pages 204–208, 2015.
5. F. Perini, C. Bortolotti, M. Roma, R. Ambrosini, M. Negusini, G. Maccaferri, M. Stagni, M. Nanni, C. Clivati, M. Frittelli, A. Mura, F. Levi, M. Zucco, D. Calonico, A. Bertarini, T. Artz, "The first geodetic VLBI field test of LIFT: a 550-km-long optical fiber link for remote antenna synchronization", this volume.

RAEGE Project Update: Yebes Observatory Broadband Receiver Ready for VGOS

IGN Yebes Observatory staff

Abstract An update of the deployment and activities at the Spanish/Portuguese RAEGE project (“Atlantic Network of Geodynamical and Space Stations”) is presented. While regular observations with the Yebes radio telescope are on-going, technological developments about receivers for VGOS are progressing at the Yebes laboratories.

Keywords VGOS, broadband

1 Introduction

The Yebes Observatory of the Spanish *Centro de Desarrollos Tecnológicos* in the National Geographical Institute (IGN CDT) has developed an ultra-low noise and broadband (2–14 GHz) cryogenic receiver for the VLBI Global Observing System (VGOS) project which has been installed in the new 13.2-m radio telescope (see Figure 1).

The 13.2-m radio telescope is an elevation-over-azimuth turning-head antenna with a ring-focus optical design and fast moving capabilities. It has been recently upgraded with a cladding in the back-up structure to reduce thermal gradients and extend its operating frequency.

Instituto Geográfico Nacional (IGN, Spain)

2 The Broadband Receiver

The block diagram is shown in Figure 2. The front-end (Figure 3a) consists of a dewar with a dual linear polarization quadruple-ridged flared horn (QRFH) feed, directional couplers for noise calibration and phase calibration and two ultra-low noise hybrid amplifiers developed at the Yebes laboratories. The cryostat is built over a Sumitomo SRDK-408S2 cold head in a cylindrical dewar made of stainless steel. The top and bottom covers are made of aluminum. In the top cover a vacuum window lets the broadband radiation go through. In the bottom cover are all the RF connectors (signal outputs and calibration inputs), vacuum flanges, the pressure monitor, DC cabling, and housekeeping connectors. Inside the cryostat there is a cylindrical radiation shield made of aluminum and with multilayer isolation (MLI). The temperature of this stage is less than 40 K. Removing the radiation shield, the entire receiver can be easily reached. It is the coldest part of the receiver at a temperature < 10 K. The cold stage is made of copper. The RF output signals from the dewar are sent to RF-over-fiber transmitters, allowing signal transportation through single-mode fiber up to the 40-m radio telescope back-end room (450 meters). In this place, the optical receivers are installed, together with an RF distribution module and four up/down converters (Figure 3b).

These converters are fed by the outputs of the distribution module. They allow the selection of four dual polarization sub-bands in the range 2–14 GHz and its conversion to base-band to feed the VLBI back-ends. NoiseCal and PhaseCal modules were developed too.



Fig. 1 RAEGE “Jorge Juan” radio telescope in Yebes Observatory (Spain).

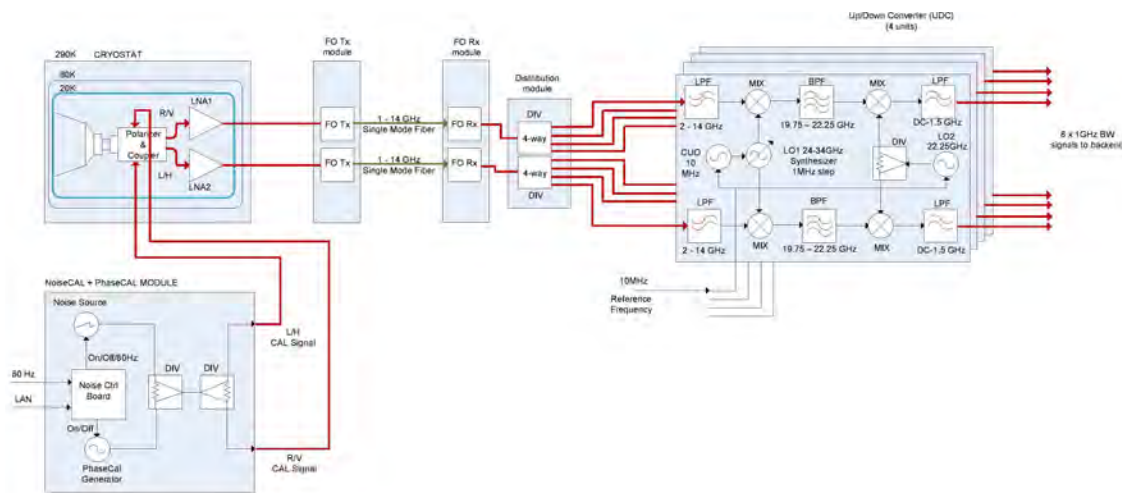


Fig. 2 Block diagram of the VGOS broadband receiver developed at IGN Yebes CDT.

3 Receiver Performance

The measured receiver noise temperature is shown in Figure 4. It can be seen that noise temperature values are distorted by large RFI at low frequencies. Due to these RFI signals, the fiber optic transmitter pre-amplifier had to be removed, to avoid saturation and intermodulation products. The actual T_{sys} value is estimated to be 43 K at 45° elevation.

4 On-site Tests

After the installation in the radio telescope, the spectrum of the RF signal at the output of the distribution module was measured at four elevation angles (see Figure 5). It can be seen that, even at high elevation angles, there are large RFI signals in the low frequency part of the spectrum. Actions to mitigate these signals have to be evaluated.

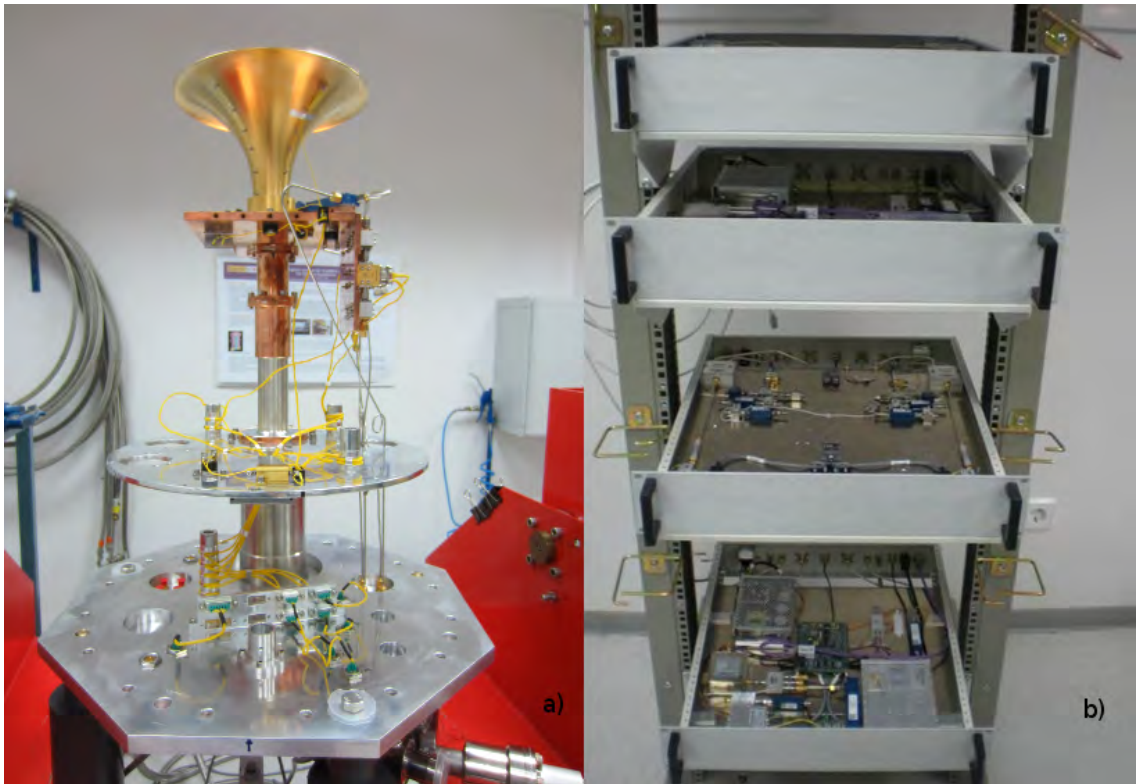


Fig. 3 IGN Yebes CDT broadband receiver: a) dewar, b) modules for RF distribution and up/down converters.

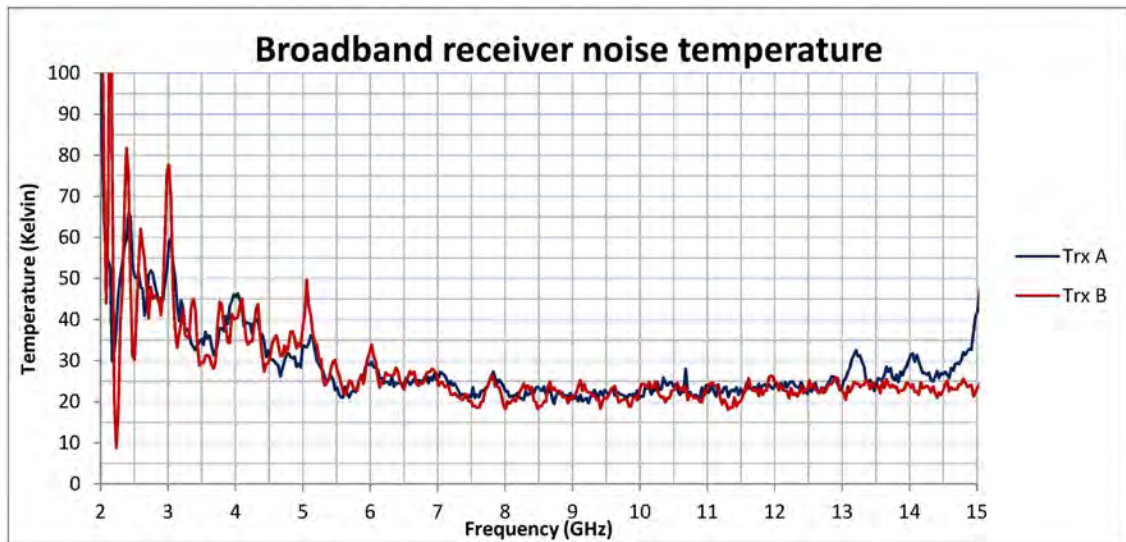


Fig. 4 IGN Yebes CDT broadband receiver performance.

We carried out the first single dish observations with the 13.2-m RAEGE VGOS “Jorge Juan” antenna (see Figure 6). The observations consisted of pointing drifts along the azimuth and elevation axes towards

Cas-A, a supernova remnant. This source is intense, and its size is smaller than the beam of the telescope at frequencies below 14 GHz. The first series of observations was uncalibrated because the calibration sys-

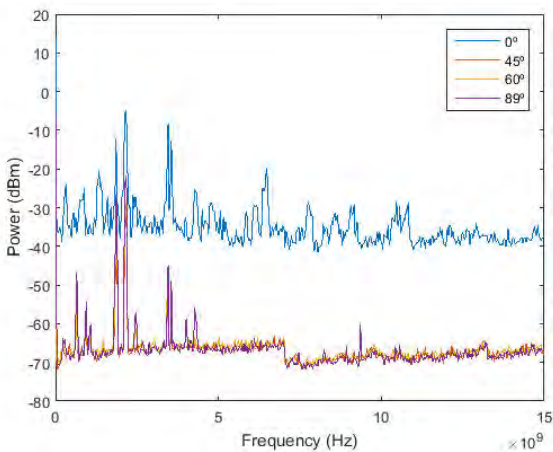


Fig. 5 IGN Yebes CDT broadband receiver RF spectrum.

tem was still undergoing tests. No focus optimization was performed, but the focus position determined with the three-band receiver (S/X/Ka) was used. In order to test the four UDCs, observations at different frequencies and with different units were done. Observations show, in some cases, some lack of repeatability in the pointings for each frequency and different UDCs. We believe this may be caused by RFI. Further observations should be performed to confirm this behavior.

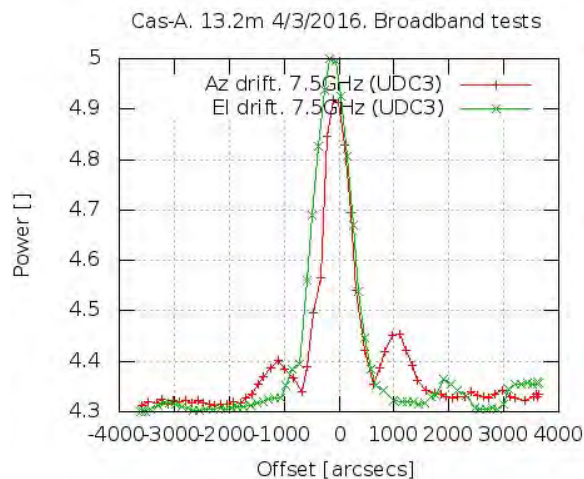


Fig. 6 First observations with the new IGN Yebes CDT broadband receiver.

5 Conclusions

A VGOS compliant broadband receiver has been developed at IGN Yebes CDT and installed on the RAEGE “Jorge Juan” 13.2-meter radio telescope. First light is reported, and work towards the first broadband VLBI fringes is progressing well.

Acknowledgements

This project has been co-funded by European ERDF/FEDER funds under the IGN-MINECO VGOS YEBES agreement.

References

1. P. García-Carreño, M. Patino-Esteban, J.A. López-Pérez. “Medidas del receptor de banda ancha durante su instalación en el radiotelescopio de 13 metros del Observatorio de Yebes”. IGN Yebes CDT Technical Report CDT 2016-4 (in Spanish).
2. P. de Vicente, J. González, L. Barbas, B. Córdoba. “Preliminary results from the 13.2m Yebes antenna after the VGOS update”. IGN Yebes CDT Technical Report CDT 2016-5. <http://bit.ly/1R3AQY9>
3. C. Albo, J. Fernández. “Instalación del compresor SUMITOMO en el radiotelescopio RAEGE de Yebes”. IGN Yebes CDT Technical Report CDT 2016-7 (in Spanish).

Activities at Sejong Station

Sang-oh Yi¹, Yun-mo Sung¹, Ki-duk Ah¹, Hong-jong Oh¹, Do-young Byon², Hyung-chul Lim², Moon-hee Chung², Do-heung Je², Tae-hyun Jung²

Abstract The Sejong station is a part of the SGOC (Space Geodetic Observation Center) which belongs to the NGII (National Geographic Information Institute). This report will briefly describe the Sejong S/X system issues that we need to improve, establishment of a server cluster for S/W correlation, and installation of the ARGO-M (mobile SLR system, 40 cm in diameter) which is developed by KASI (Korea Astronomy and Space Science Institute) at the Sejong station. Construction of the Korea VLBI Network KVNG (Korea VLBI Network for Geodesy) is currently underway.

Keywords Sejong station, NGII, KASI, ARGO-M

1 General Information

Sejong is located about 120 km south of Seoul at longitude $127^{\circ}18'12''$, latitude $36^{\circ}31'12''$ and 153 meters high in the middle of Sejong city, which serves as a new administrative capital. Sejong station has a VLBI antenna, is an IGS station (SEJN), has four pillars for co-location, is a mobile SLR system (40 cm in diameter), has an MWR (Microwave Water vapor Radiometer), and does astrometric surveying by optics (theodolite).

A considerable change is the installation of the SLR system at Sejong station. KASI (Korea Astronomy Space and Science Institute) developed the 40-cm SLR system and installed it near Sejong station. VLBI, GNSS, and the SLR system are directly measured by

electronic distance measuring instruments. There are about 195 meters in distance between the VLBI and SLR systems and about 130 meters in distance between the GNSS and SLR systems.

2 VLBI Observation Activities in 2015

Sejong station started to join IVS regular sessions in September 2014. The Sejong antenna participated in only five sessions in 2014. In 2015, 50 sessions (40 R1, two T2, two APSG, and two AOV) were observed. As for local sessions, Sejong and the KVN (Korea VLBI network, KASI) carried out ten sessions for a performance test.

There are known issues to improve in the Sejong system. One issue is that the DC component sometimes appears in X-band. The NGII and KASI tried to correct this issue by measuring at the Sejong site. However, we could not find and correct this issue. The other issue is quite high SEFDs due to the cooling ability in the cooling box. As you can see in Figure 2, the SEFDs of both X and S are 15,000 Jy and 4,500 Jy respectively. Figure 3 shows S/X feeds in the antenna. It is not the dual one but the individual S and X feeds. Figure 4 shows that eleven cables are connected on the side of the cooling chamber. These cables cause higher physical temperatures inside.

1. National Geographic Information Institute

2. Korea Astronomy Space and Science Institute



Fig. 1 Site layout and equipment at the Sejong station (KASI's newly installed SLR station in October 2015).

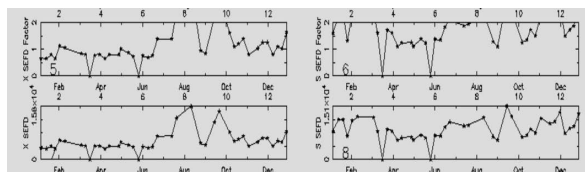


Fig. 2 A captured image of station performance on the IVS Web site for the Sejong antenna.



Fig. 3 Sejong S/X feed system.

3 Status of Korea VLBI Network for Geodesy

The Sejong station is preparing for the local Korean VLBI network with high frequencies (22 GHz and



Fig. 4 LNA cooling chamber. Inside the chamber, LNAs for S/X, a cabling system for calibration, and mode switch cables (Hot/Cold/Sky) are installed.

43 GHz). The purpose is for the co-utilization of geodesy and astrometry. There are four VLBI sites (Sejong, Ulsan, Tamna, and Yonsei) in Korea. KVN (Korea VLBI Network: Ulsan, Tamna, and Yousei) began VLBI observations in 2007. They have K (22 GHz), Q (43 GHz), W (86 GHz), and D (129 GHz) receiver systems with a 21-meter main dish. Among

the receivers, K- and Q-band are the same as in the Sejong VLBI system. In 2015, Sejong and KVN carried out a fringe test. We received fringes for both K- and Q-bands.

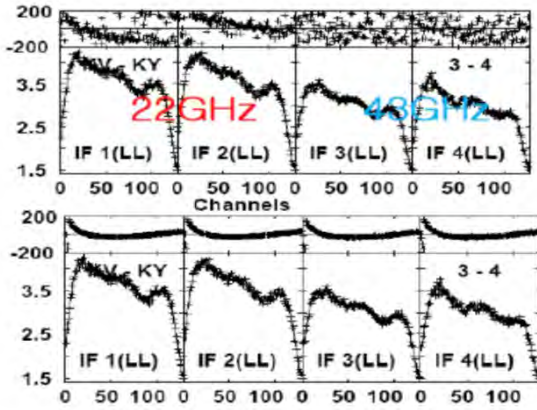


Fig. 5 Phase arranging results in both K- and Q-band.

4 Preparations to Build Sejong Correlator

In order to operate a correlator in Sejong, we constructed a server cluster system with 100 TB of data storage. DiFX and K5 correlation software was installed. Sejong took charge of the AOV004 and AOV005 sessions; however, imperfect fringes were detected during the correlation process, and progress in solving the problem was slow. Thankfully, Shanghai observatory and GSI took over the AOV data for Sejong. We will keep looking into solving the problems. The results will be reported to the AOV board and the IVS when they are finished.

5 Development of Broadband Feed for VGOS by KASI

Normally, feedhorn specification depends on the antenna optic system. It is assumed that the optic system is the same as the VGOS antenna. Here are the feedhorn specifications that we made: a. Operation frequency bandwidth: 2–14 GHz; b. 10 dB bandwidth: 60–90 degrees; c. Input return loss: less than -10 dB;

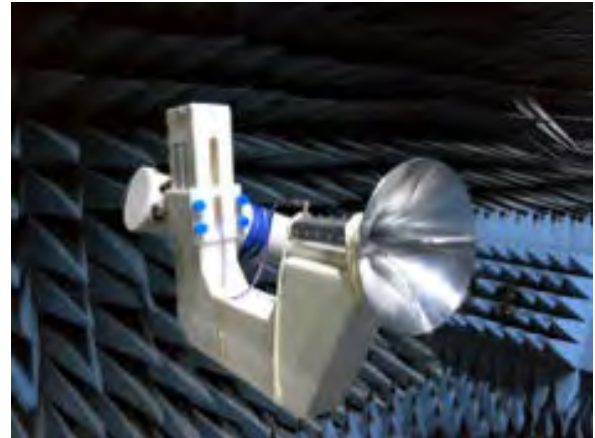


Fig. 6 Far-field pattern measurement setup.

d. Isolation: less than -30 dB; e. Possibility of receiving linear dual polarization; and f. Input impedance: 50 Ohm. As for the results, almost all frequencies' (all except 2 GHz) 10 dB bandwidth levels are satisfied. The specified input return loss and isolation levels are satisfied. KASI will compensate for the failure to satisfy the 10 dB bandwidth level at 2 GHz that appeared during the test.

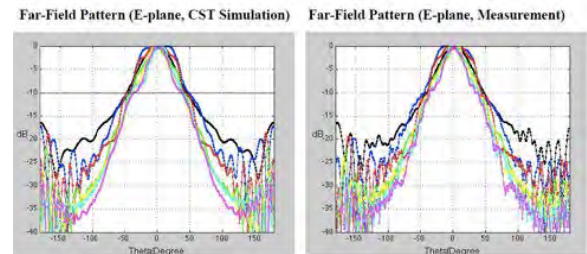


Fig. 7 Comparison for far-field pattern between the simulation and the measured results (Left: Simulation results; Right: Measured results).

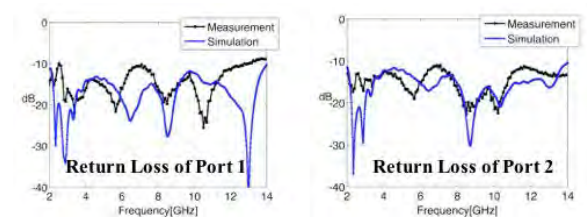


Fig. 8 Comparison for return losses between the simulation and the measured results (Left: Port 1; Right: Port 2).

6 Future Plans

The sessions and the amount of IVS participation of the Sejong station in 2016 will be similar to the 2015 Sejong annual observation schedule. As for the Korea local VLBI network project in 2016, the upgrade for relevant equipment and software development will progress. To operate the correlator properly, the Sejong station will keep solving whatever problems the Sejong correlator may have. Over the next few years, the Sejong station hopes to become an IVS Correlator.

Metsähovi Geodetic Fundamental Station in Finland — New VGOS Site, Plans, and Current Status

Nataliya Zubko, Jyri Näränen, Ulla Kallio, Veikko Saaränen, Jenni Virtanen and Markku Poutanen

Abstract A new VGOS telescope will be built at the Metsähovi Geodetic Fundamental Station. We present here our plans concerning the VGOS project. Also we give an overview of the instruments located at the Metsähovi Geodetic Fundamental Station.

Keywords VGOS, fundamental station

1 Introduction

The Metsähovi Geodetic Fundamental Station in Southern Finland (60.2N, 24.4E) is a key infrastructure of the Finnish Geospatial Research Institute (FGI)[1]. It is a Global Geodetic Observing System (GGOS) core site, i.e., a member of the global network of geodetic stations which is used for maintaining global terrestrial and celestial reference frames, for computing precise orbits of satellites, and for geophysical studies. Metsähovi is one of the few geodetic stations that has all major geodetic observing instruments co-located. These include satellite laser ranging (SLR), very long baseline interferometry (VLBI), global navigation satellite systems (GNSS), superconducting and absolute gravimeters, and a DORIS beacon. The station has been operational since 1978. It contributes to several global services of the International Association of Geodesy (IAG) and, due to its long existence, helps to retain sustainability in the maintenance of global reference frames.

Finnish Geospatial Research Institute

2 VGOS Project

In the autumn of 2015, FGI obtained funding to build a new VGOS-compatible radio telescope system. This project is funded by the Finnish Ministry of Agriculture and Forestry and the National Land Survey. The site chosen for a new telescope is within 100 m of other facilities of the Metsähovi Geodetic Fundamental Station. We aim for a 12–13 m telescope and expect to complete the procurement process of the telescope during summer 2016. The telescope will be founded on bedrock (Figure 1).



Fig. 1 Future VGOS telescope site.

The site preparation will begin with forest removal around the place selected for the new telescope. Also other infrastructure work will be started in summer 2016. The instrumentation and operation rooms will be placed in Metsähovi's main building. The selection and procurement of signal chain components will start

	2016	2017	2018
Telescope procurement	██████████		
Telescope manufacture		██	
Telescope installation			██████
Signal chain procurement	██████████		
Signal chain manufacture		██	
Signal chain installation			██████████
Infrastructure work	██		

Fig. 2 Preliminary schedule for the Metsähovi VGOS project.

after the telescope tendering has finished. The plan is to be operational by the end of 2018. The preliminary schedule for the Metsähovi VGOS project is presented in Figure 2.

3 Metsähovi Geodetic Fundamental Station



Fig. 3 Superconducting gravimeter.

The Ministry of Agriculture and Forestry has allocated a special funding for the renewal of Metsähovi instruments and infrastructure during 2012–2018.

- Finnish Permanent GNSS Network FinnRef (~20 receivers)
- Superconducting gravimeter; new instrument in 2014 (Figure 3)
- Upgrade of the absolute gravimeter
- Satellite laser ranging; new 2-kHz system. Work ongoing, expected to be operational in 2016 (Figure 4)
- VGOS telescope system



Fig. 4 The new Metsähovi SLR observatory.

The following major instruments or facilities exist at Metsähovi (Figure 5):

- Satellite laser ranging (SLR) facility. First observations were started in 1978, but during recent years



Fig. 5 Metsähovi Geodetic Fundamental Station.

the SLR system has been under renovation. A new SLR will be completed in 2016, with a brand new 0.5 m telescope and a 2-kHz laser [2].

- GNSS receivers. Metsähovi has been a part of the IGS network since the early 1990s. Recently GNSS receivers have been modernized, and they are capable of tracking all GNSS satellite systems [3].
- VLBI radio telescope. Geodetic VLBI observations have been made since 2004 using the radio telescope of Aalto University Metsähovi station. A few IVS campaigns per year have been carried out.
- Gravimeters. A new superconducting gravimeter and the upgrade of the FG5X-221 absolute gravimeter have been done in 2013.
- The CNES/IGN Doris beacon, located a few kilometers from Metsähovi.
- TerraSAR-X retroreflector (DLR and Technical University of Munich).

Additionally there are necessary infrastructure, weather stations, a local geodetic network for local ties, a leveling test line, and a calibration and test field for GNSS antennas.

References

1. Poutanen, M., Kallio, U., Koivula, H., Näränen, J., Raja-Halli, A., and Zubko, N. (2013, August). Renewal of Metsähovi Observatory. In 21st Meeting of the European VLBI Group for Geodesy and Astronomy, held in Espoo, Finland, March 5-8, 2013, Eds: N. Zubko and M. Poutanen, Reports of the Finnish Geodetic Institute, Vol. 2013:1, ISBN 978-951-711-296-3, pp. 67–72.
2. Raja-Halli, A. and Näränen, J., Progress Report on the New SLR System of GGOS's Core Site Metsähovi, Finland, Proceedings of the 19th International Workshop on Laser Ranging, Annapolis MD, Oct. 27–31, 2014.
3. Koivula, H. et al. "Finnish permanent GNSS network: From dual-frequency GPS to multi-satellite GNSS." Ubiquitous Positioning, Indoor Navigation, and Location Based Service (UPINLBS), 2012. IEEE, 2012.

The German Antarctic Receiving Station O’Higgins and Its VLBI Capabilities

Ch. Plötz¹, A. Neidhardt², T. Klügel¹, R. Wojdziak³, J. Serna Puente⁴, B. Vaquero Jiménez⁴, T. Schüler¹, VLBI Team Wettzell, DFD Team DLR

Abstract The German Antarctic Receiving Station (GARS) O’Higgins started in the early 1990s with regular VLBI operations. Because of its remote position on the Antarctic Peninsula, the VLBI observing was mostly restricted to the Antarctic summer months. New equipment, a continuous operation by the German Aerospace Center (DLR), and new realizations of observation schedules may open the door for regular observations over the whole year. This paper reports the upgrades carried out in hard- and software and the latest results.

Keywords Antarctica VLBI, O’Higgins, GARS

1 Introduction: GARS O’Higgins at a Glance

The German Antarctic Receiving Station (GARS) is jointly operated by the German Aerospace Center (DLR) and the Federal Agency for Cartography and Geodesy (BKG, Geodetic Observatory Wettzell). The Institute for Antarctic Research Chile (INACH) coordinates the activities and logistics. The 9-m radio telescope at O’Higgins is mainly used for downloading of remote sensing data from radar satellites and for the commanding and monitoring of spacecraft telemetry.

1. Federal Agency for Cartography and Geodesy, Geodetic Observatory Wettzell
2. Technische Universität München, Forschungseinrichtung Satellitengeodäsie, Geodetic Observatory Wettzell
3. Federal Agency for Cartography and Geodesy Leipzig
4. Instituto Geográfico Nacional, Observatorio de Yebes



Fig. 1 9-m radio telescope O’Higgins.

During dedicated campaigns it is also used for geodetic VLBI in the Antarctic summer.

In recent years, special flights using “C-130 Hercules” aircraft and small “DHC-6 Twin Otter” aircraft, as well as transportation by ship, were organized by INACH in order to transport staff, technical material, and food for the entire stay from Punta Arenas via Base Frei on King George Island to O’Higgins. The conditions for transport and landing are strongly weather dependent and involve an increasing, challenging task.

The site is also equipped with other geodetic instruments:

- different time receivers in combination with an H-maser and Cs-standard,
- several GNSS receivers,
- a meteorological station,
- a radar tide gauge and an underwater sea level gauge.

2 Installed Equipment

2.1 Receiver Frontend

The VLBI receiver was renewed because of failures of the cryogenic system and some HF-components. This new receiver for both receiving frequency ranges in S- and X-band for standard dual-band and right-hand circular polarization was designed and built in the labs of the Observatory Yebes, Spain. New high performance cryogenic low noise amplifiers are used for first stage amplification of the incoming noise signal from the quasars. This improves the SEFD of the entire receiving chain. The down-converters were also renewed to simplify the maintenance.



Fig. 2 New S-/X-band VLBI receiver at O'Higgins.

The monitoring of the VLBI receiver is Ethernet-based. This gives more flexibility for remote control and supervision from Wettzell.

2.2 Data Acquisition Backend

To complete the receiving chain with new, stable equipment, a new data acquisition rack was populated with state-of-the-art components in parallel to the existing VLBA4 rack.

The focus was on digital sampling components. Therefore a very stable and flexibly configurable ADS3000+ baseband converter was installed in combination with a Mark 5B+ data recording system.

A new Field System PC is available with one of the latest NASA Field System versions to control all the equipment.

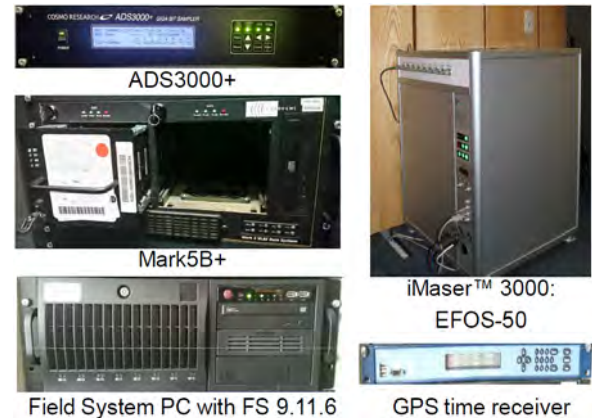


Fig. 3 Newly installed data acquisition systems for VLBI.

An EFOS-50 maser now builds the basis for stable frequency and timing. The UTC connection is managed with a new GPS time receiver with NTP.

2.3 Control Room



Fig. 4 New combined satellite tracking and VLBI control room.

To enable flexible control of satellite missions as well as of VLBI sessions, a new combined control room was built together with the DLR. The tasks can be controlled there from two operator desks.

First plans were discussed to integrate VLBI schedules into the scheduling system Remote Planning System (RPS) and the control software Satellite Mission Control System (SMCS) of the DLR to enable flexible scheduling of observations of satellite passages and intermediate VLBI sessions.

The VLBI sessions can also be controlled remotely at the new control room of the TWIN radio telescopes in Wettzell, using the software e-RemoteCtrl. This should extend the possibilities for VLBI observations.

3 Integration Tests in January and February 2015

The integration of the new receiver frontend and the data acquisition backend was done during the VLBI campaign from January to February 2015. The new VLBI receiver was successfully installed into the antenna's elevation cabin. The VLBI sampler ADS3000+ and the Mark 5B+ were mounted into an existing and available rack in the DLR control room in parallel to the old and still working VLBA4 rack with the Mark 5A VLBI data recorder.

The new system was tested in parallel to the existing equipment during four VLBI sessions:

- OHIG94
- OHIG95
- OHIG96
- T2102

Since then the T2 sessions T2106 and T2108 and the OHIG sessions OHG100, OHG101, and OHG102 were successfully recorded, proving the technical capability of the entire receiving and recording chain as well as the remote accessibility.

The OHIG sessions are dedicated to measure the southern reference frame. The T2 sessions are used to determine the terrestrial reference frame. Sample data scans were copied and sent to the Bonn correlator already during the ongoing sessions to evaluate the data quality of the new VLBI instrumentation. The first feedback from the correlator showed good data quality and performance.

4 Conclusion and outlook

Goals for the upgrades are an increase of the amount of time in which maintenance is not needed and higher automation. The idea behind these goals is to enable the observation of one geodetic VLBI session per month in a more frequently used southern VLBI network (see Figure 5). The VLBI sessions should be scheduled as intermediate observations within the satellite tracking and control sessions of the DLR. Parts of the VLBI sites may be operated remotely in such a scenario.

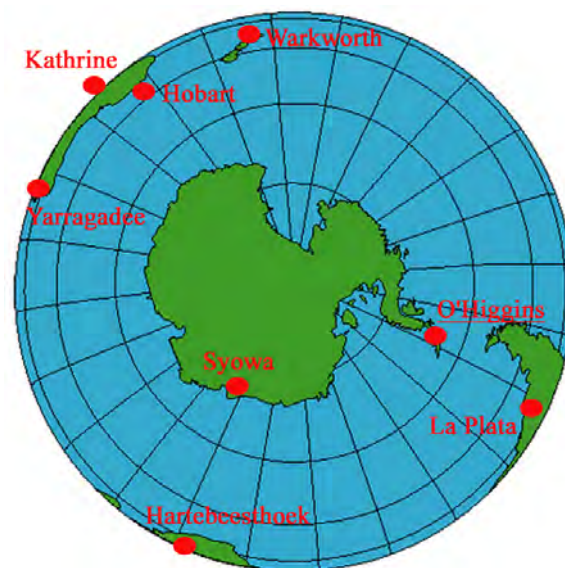


Fig. 5 A possible southern VLBI network for geodesy. The map is courtesy of Bruce Jones Design Inc. and FreeUSandWorldMaps.com.

References

- [BKG(2015)] Bundesamt für Kartographie und Geodäsie. Geodätisches Observatorium O'Higgins/Antarktis. Web document <http://ivs.bkg.bund.de/vlbi/ohiggins/>, Download 2015.

First Local Ties from Data of the Wettzell Triple Radio Telescope Array

T. Schüller^{1,6}, C. Plötz¹, S. Mähler¹, T. Klügel¹, A. Neidhardt², A. Bertarini³, S. Halsig³, A. Nothnagel³, M. Lösler⁴, C. Eschelbach⁴, J. Anderson⁵

Abstract The Geodetic Observatory Wettzell features three radio telescopes. Local ties between the reference points are available from terrestrial precision surveying with an expected accuracy below 0.7 mm. In addition, local VLBI data analysis is currently investigated to provide independent vectors and to provide quality feedback to the engineers. The preliminary results presented in this paper show a deviation from the local survey at the level of one millimeter with a clear systematic component. Sub-millimeter precision is reached after removal of this bias. This systematic effect is likely caused by omission of thermal expansion and gravity deformation, which is not yet implemented in our local VLBI analysis software.

Keywords Local baseline processing, local ties, local correlation, Wettzell radio telescope triple

1 Introduction

The Geodetic Observatory Wettzell features a 20-m radio telescope (RTW) as well as two new 13.2-m TWIN telescopes. While RTW has performed routine oper-

ations since 1984, the first of the TWIN telescopes, TTW1, entered its productive phase in mid-2014, and TTW2 has just been equipped with an Eleven feed broadband receiving system.

The triple telescope array at Wettzell establishes a geodetic short baseline interferometry network. Local correlation yields group delay observations for baseline estimation from VLBI data alone without any immediate augmentation by terrestrial measurements. Apart from relative positioning of the telescopes, these are versatile capabilities for an end-to-end quality control of the VLBI data.

Most components of such a local VLBI-based monitoring system are already available, with the exception of the local VLBI-data correlator (up to now, this part has been carried out at the Bonn Correlator). Moreover, the scheduling mechanisms will have to be optimized for short baseline observations in the future.

Results from local VLBI data analysis will be portrayed in this contribution and compared to the local ties from precision terrestrial surveying.

2 Regional and Local Monitoring

The region around the Geodetic Observatory Wettzell is regularly monitored by geodetic means:

1. *Footprint network*: The footprint network consists of geodetic GNSS reference stations located at distances ranging from 4–14 km (inner ring of stations) up to 90 km (outer ring). Six of these stations are directly operated and maintained by the Observatory's staff, six sites are operated by the regional surveying authority, and one EUREF station completes the network.

1. Geodetic Observatory Wettzell, Federal Agency for Cartography and Geodesy (BKG)
2. Geodetic Observatory Wettzell, Technische Universität München
3. Rheinische Friedrich-Wilhelms Universität Bonn, IGG
4. Faculty 1: Architecture, Civil Engineering, Geomatic, University of Applied Sciences Frankfurt
5. Deutsches GeoForschungsZentrum (GFZ), Department 1: Geodesy, Section 1.1: Space Geodetic Techniques
6. University of the Federal Armed Forces Munich, Faculty of Aerospace Engineering



Fig. 1 The three Wetzell radio telescopes and the 3D distances between them as derived from local terrestrial precision surveying (survey data from the year 2012).

2. *Local GNSS network*: Similarly to the footprint network, an array of more than seven local GNSS receivers is operated on site. The term “on site” (at the Observatory) means that these receivers are located at distances not exceeding 250 m.
3. *Local survey network*: The local surveying network covers the area of the Geodetic Observatory Wettzell and some surrounding places. This network is measured with precision terrestrial total stations yielding a point precision of usually 0.2–0.4 mm. Digital leveling is performed to enhance the accuracy of the vertical coordinate component. Several GNSS points can be co-located with terrestrial equipment and serve as ground control points to transform the local coordinates into Earth-centered, Earth-fixed (ECEF) coordinates.
4. *Reference points*: The monitoring of the reference points is theoretically a part of the local network surveying. However, the reference points of the SLR and VLBI telescopes are usually not accessible directly. Consequently, special surveying procedures must be applied to indirectly determine the reference points.

The motivation behind all these efforts can be characterized as follows. The footprint network is primarily operated in order to verify that the local measurements at the Wettzell Observatory are representative for the entire region (i.e., neither local nor regional deformation is occurring). Surveying the local network also helps to sense small variations in position (e.g., during dry summer periods), but the primary purpose is to provide the vectors between the various co-located instruments (commonly referred to as “local ties”).

Recently, we have started to compute independent, weekly system-specific ties for the local GNSS array that partially coincides with the terrestrial network, and more care is exercised to provide physical connections between the two networks (combined targets with reflectors and GNSS antennas). As an extension, this contribution deals with the determination of system-specific ties between the radio telescopes from VLBI data.

3 Methodology

The methodology is explained in more detail in [Schüler et al. (2015a)]. Group delay observations are used to determine the vector between the two telescopes. The local surveying results are taken as a reference here. The 3D distances between all three telescopes are graphically illustrated in Figure 1.

The work-flow is illustrated in Figure 2. A suitable *schedule* is generated depending on the specific purpose. A schedule to quickly deliver quality information to the VLBI engineers regarding the overall system performance may require an experiment of just one hour duration. In contrast, a local baseline determination may preferably be based on an experiment covering a full day.

Subsequently, the quasar signals are *measured* by the radio telescope receiving systems. Currently, only the 20-m RTW (Radio Telescope Wettzell) and the TTW1 (TWIN Telescope Wettzell 1) are available for this purpose. TTW2’s availability is scheduled for mid-2016. Also note that only TTW1 and TTW2 are currently connected to a common maser frequency refer-

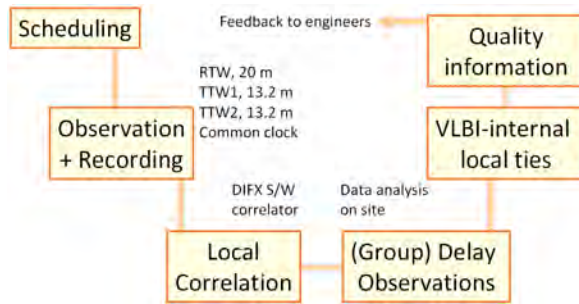


Fig. 2 Basic flowchart for the local end-to-end VLBI observation and analysis sessions.

ence, whereas RTW is connected to a different one. A clock common to all three telescope is foreseen during 2016 too.

Data correlation between the telescopes is carried out right after completion of the measurements. This is a central part of the processing chain, and it will be very beneficial to perform this correlation step locally at the Geodetic Observatory Wettzell, preferably using the same software and methods employed at the Bonn correlator. Up to now, the data have been transferred to Bonn and correlated there using the DiFX correlator [Deller et al. (2011)].

The *group delay observations* are adjusted using in-house software particularly tailored to the needs of the Observatory. Each band can be analyzed independently in such a way that separate S- and X-band results can be computed. Clock drifts are currently compensated via a polynomial compensation approach from order 1 (one hour sessions) up to order 4 (full day sessions). In the future, using a common clock should reduce the number of parameters required for that purpose. Note that the set of radio source positions in the analysis is currently directly taken from the header section of the NGS Card File supplied. Identification and usage of radio sources particularly suited for short baseline interferometry is the subject of future work.

Finally, the *estimated baseline vectors* from VLBI data are reviewed and collected for a further network adjustment. Since we currently only have two telescopes available for real use, the network adjustment module has not been fully implemented yet. Equally important, *quality information* can be extracted from the various results, providing feedback to the VLBI engineers in order to improve the systems.

4 Realization

Apart from organizational aspects regarding the realization of this end-to-end planning-measurement-analysis-feedback chain, the technical aspects with special focus on the receiving systems of the three individual telescopes can be guessed from Figure 3.

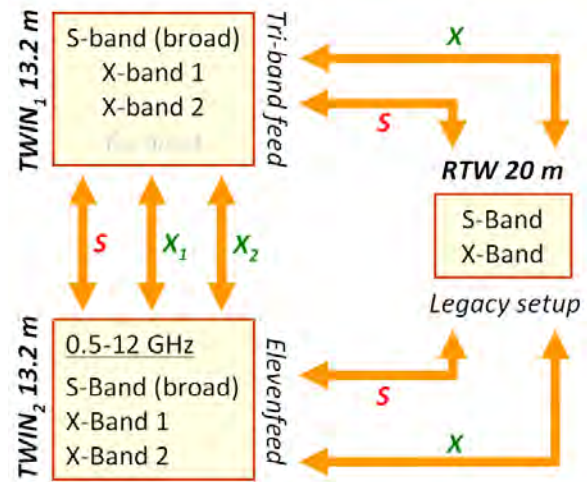


Fig. 3 Current receiving systems in the Wettzell radio telescopes and common observation modes.

1. *RTW (20 m)*: This telescope entered routine operation in 1984 and is equipped with a legacy S/X receiving system. Although there are plans to upgrade the telescope regarding improved capabilities for astrometry, there is no plan to upgrade it with a focus on VGOS capabilities. This means that all baselines processed in conjunction with RTW are naturally limited to this legacy observing mode. This applies to all results presented in this paper.
2. *TTW1 (13.2-m)*: This VGOS-ready telescope is currently equipped with a tri-band receiving system featuring a 700 MHz S-band window, a 4 GHz X-band window, and a Ka-band section. Ka-band can only be measured, but not analyzed locally, because there is no partner telescope available at Wettzell. A specific plan to upgrade TTW1 to broadband capabilities does exist but will not turn into action until late 2017.
3. *TTW2 (13.2-m)*: This second TWIN telescope features a broadband receiving system sensitive from 0.5 to 12 GHz. Consequently, baselines between

TTW1 and TTW2 could be observed using one S-band window and up to two X-band windows (frequencies between 6 and 10 GHz). Theoretically, even a fourth band could be extracted, but the down-converter in TTW1 does not support that, because its fourth receiving chain is dedicated to the Ka-band support.

Note that the TTW1 results obtained from S-band group delays are heavily contaminated by radio-frequency interference (RFI). In legacy mode, these delay observations are already less precise compared to X-band due to their smaller bandwidth. Hence, we only present results derived from X-band observations (the ionosphere correction is disabled, because it is not of concern over a 123 m baseline).

5 Results

Figure 4 portrays an excerpt of baseline estimation results from X-band data deduced from experiments (24-hour duration) during the summer period of 2015 (June to September). The baseline names have the following meaning:

1. *WETTZELL*: RTW (20-m) telescope, analog backend (video converters).
2. *WETTDBBC*: RTW (20-m) telescope with DBBC digital backend [Tuccari et al. (2010)].
3. *WETTZI3N*: TWIN 1 (13.2-m) telescope with DBBC digital backend.

Consequently, the baseline “*WETTZELL-WETTDBBC*” refers to one and the same telescope—that is, it features a zero baseline. Although, these measurements were purposefully collected, we do not discuss that part in this paper.

Moreover, the following columns are part of the table of results:

1. *FREQ*: frequency in gigahertz (here: X-band only).
2. *OBS*: number of observations actually used in the adjustment procedure.
3. *DEL*: percentage of observations (group delays) automatically deleted by the two-stage outlier cleaning procedure upon adjustment.
4. *DX*, *DY*, *DZ*: deviation of the (X, Y, Z)-coordinate component (ECEF) from the local precision survey in millimeters.

5. *DS*: deviation of 3D spatial distance from the local precision survey in millimeters.

Regarding the data processing, it is worth mentioning that the estimated parameters may comprise:

1. The three baseline vector coordinate components.
2. Up to four clock error compensation coefficients.
3. One tropospheric adjustment factor.

Note that the tropospheric adjustment factor is usually not statistically significant for this short baseline. However, a tropospheric delay model is applied in order to account for the difference in height between the two telescopes.

When looking at the results, it is obvious that most results deviate by about 1 mm from the local survey. A clear systematic difference between these two sets of results can be identified. We intentionally did not remove it here. Please refer to the following section for an explanation and interpretation.

Subtraction of the systematic part yields sub-millimeter precision as is usually required for local ties. Note that one important goal of this work is to quickly transfer reference coordinates to a new telescope. From this point of view, these results are promising for future work in this field. This method is attractive, because the very high degree of correlation of all atmospheric propagation delays yields a higher accuracy of the new telescope’s coordinates compared to long baseline adjustment procedures that have to deal with the annoying effects of tropospheric delays.

6 Conclusions

Following some initial values presented in [Schüler et al. (2015b)], the results given in this paper for the telescope vector between the 20-m radio telescope RTW and the new 13.2-m TWIN 1 telescope show a very satisfactory level of agreement with the results from the local precision survey.

A bias of about 1 mm between the two techniques can be identified. The possible sources of these discrepancies are likely related to the fact that the following corrections/reductions have not been implemented in our local analysis software yet:

YYYYMMDD	HH	FROM	TO	FREQ	OBS	DEL	DX	DY	DZ	DS
20150622	17	WETTDBBC	WETTZ13N	8.213	441	15%	1.4	0.7	1.5	2.0
20150622	17	WETTDBBC	WETTZELL	8.213	477	3%	0.9	0.4	1.0	1.3
20150622	17	WETTZ13N	WETTZELL	8.213	439	5%	0.9	0.6	1.0	1.3
20150629	17	WETTZ13N	WETTZELL	8.213	386	4%	1.2	0.7	1.4	1.8
20150713	17	WETTDBBC	WETTZ13N	8.213	320	5%	1.2	0.7	1.3	1.7
20150713	17	WETTDBBC	WETTZELL	8.213	361	4%	0.5	0.2	0.5	0.8
20150713	17	WETTZ13N	WETTZELL	8.213	369	6%	1.0	0.6	1.2	1.5
20150723	18	WETTZ13N	WETTZELL	8.213	271	4%	0.9	0.6	1.2	1.5
20150730	18	WETTZ13N	WETTZELL	8.213	234	6%	1.1	0.8	1.2	1.6
20150804	17	WETTZ13N	WETTZELL	8.213	508	5%	0.9	0.6	1.0	1.2
20150811	17	WETTZ13N	WETTZELL	8.213	391	1%	1.1	0.7	1.4	1.7
20150817	17	WETTZ13N	WETTZELL	8.213	344	7%	1.0	0.7	1.1	1.5
20150831	17	WETTZ13N	WETTZELL	8.213	414	3%	1.0	0.6	1.1	1.3
20150914	17	WETTZ13N	WETTZELL	8.213	386	2%	1.3	0.7	1.6	2.0
20150928	17	WETTZ13N	WETTZELL	8.213	437	1%	1.0	0.6	1.0	1.3

zero baselines!

Fig. 4 Results from local VLBI experiments conducted in common observation mode between RTW (20 m) and TTW1 (13.2 m); excerpt from a longer list of results. The FREQ values have units of gigahertz, and the DX, DY, DZ, and DS values have units of millimeters.

1. *Telescope expansion:* The effect of thermal expansion of the telescope structures has not been taken into account.
2. *Gravitational correction:* Similarly, no model to account for the deformation of the antenna dish due to the weight of the structure was used.

We assume that inclusion of these two main corrections should further improve the results.

Acknowledgements

This research is based on observations processed at the Bonn Correlator, jointly operated by the Max Planck Institute for Radio Astronomy (MPIfR) and the Federal Agency for Cartography and Geodesy (BKG). We made use of the Swinburne University of Technology software correlator, developed as part of the Australian Major National Research Facilities Programme and operated under license.

References

- [Schüler et al. (2015a)] T. Schüler, G. Kronschnabl, C. Plötz, A. Neidhardt, A. Bertarini, S. Bernhart, L. La Porta, S. Halsig, and A. Nothnagel. Initial Results Obtained with the First TWIN VLBI Radio Telescope at the Geodetic Observatory Wettzell. *Sensors* 2015, 15(8), 18767-18800. DOI10.3390/s150818767. Available online: <http://www.mdpi.com/1424-8220/15/8/18767> (accessed on 19 August 2015).
- [Deller et al. (2011)] A. T. Deller, W. F. Brisken, C. J. Phillips, J. Morgan, W. Alef, R. Cappallo, E. Middelberg, J. D. Romney, H. Rottmann, S. J. Tingay & R. Wayth. DiFX-2: A More Flexible, Efficient, Robust, and Powerful Software Correlator, *PASP*, 2011, 123, 275–287.
- [Tuccari et al. (2010)] G. Tuccari, W. Alef, A. Bertarini, S. Buttaccio, G. Comoretto, D. Graham, A. Neidhardt, P.R. Platania, A. Russo, A. Roy, M. Wunderlich, R. Zeitlhöfler, Y. Xiang. DBBC VLBI2010. In *Proceedings of the IVS 2010 General Meeting*, Hobart, Tasmania, Australia, 7–14 February 2010; pp. 28-30.
- [Schüler et al. (2015b)] T. Schüler, G. Kronschnabl, A. Neidhardt, C. Plötz, A. Bertarini, L. La Porta, S. Bernhart, A. Müskens, S. Halsig, and A. Nothnagel. Results from the TWIN Commissioning Phase *Proceedings of the 22nd European VLBI Group for Geodesy and Astrometry Meeting*, 18–21 May 2015, Ponta Delgada, Azores, pp. 15–19. ISBN 978-989-20-6188-7.

Automated Simultaneous Local Ties with GNSS and Robot Tacheometer

Ulla Kallio¹, Michael Lösler², Sten Bergstrand³, Rüdiger Haas⁴, Cornelia Eschelbach²

Abstract We have used GPS-based local-tie measurements simultaneously with geo-VLBI observations since 2008 during every geodetic VLBI session at Metsähovi. This system uses gimbal-mounted GNSS antennas that are mounted on the reflector of the Metsähovi 14-m radio telescope. A similar system was installed in 2013 at the Onsala 20-m radio telescope and has been used for a large number of VLBI sessions, including, e.g., the 15-day-long CONT14 campaign. In order to verify the results of the two systems, we performed a dedicated measurement campaign in the framework of the SIB60 project, involving both Metsähovi and Onsala. During this campaign the local ties at the two stations were measured simultaneously during two VLBI sessions in August and September 2015 where both stations participated. The robot tacheometer monitoring system HEIMDALL was used for the automated classical monitoring of the telescopes at both stations. Moreover, additional local terrestrial measurements were performed several times to derive the full IVS–IGS local ties at both sites. The kinematic GPS measurements at the two stations were analyzed with two independently developed analysis programs. We present here the preparations of the campaign, the measurement process, and preliminary results.

Keywords Local ties, robot tacheometer, GNSS, IVS, IGS, reference frame

1. Finnish Geospatial Research Institute

2. Frankfurt University of Applied Sciences, Laboratory for Industrial Metrology

3. SP Technical Research Institute of Sweden

4. Chalmers University of Technology, Onsala Space Observatory

1 GNSS Local Tie

For a GNSS local tie, two GPS antennas are attached permanently at both sides of the radio telescope dish. They are on a gimbal which keeps them pointed upwards independent of the position of the radio telescope. The reference point of the radio telescope, antenna structure elements, axis orientation, and offset are estimated using the post-processed coordinates of the GNSS antennas and the telescope antenna position angle readings. Synchronizing the telescope position angles and trajectory coordinates is performed using time stamps of trajectory coordinates and telescope angles.

Like with terrestrial local ties, calibrated instruments are needed. The GNSS antennas should be absolute calibrated individually with a robot or in an anechoic chamber. Because the GNSS antennas rotate with the telescope, the orientation of the GNSS antenna should be taken into account when applying the PCC of the antenna. The orientation of the local tie vector comes from the satellite orbits. It is necessary to use precise orbits in ITRF in kinematic post-processing.

Despite massive multipath and blockage of the visibility by the radio telescope antenna, we are able to retrieve enough data for a reliable solution. The multi-stage outlier detection, together with a robust mathematical model, enables the use of kinematic GNSS solution to determine the coordinates of the VLBI antenna reference point. GNSS-based local tie systems have been successfully used at Metsähovi since 2008 and at Onsala since 2013 (e.g., [Kallio and Poutanen (2012)], [Ning et al. (2015)]).

The software development at FGI (Metsähovi) concentrated mainly on the antenna model parts and recently also on the uncertainty in the modeling and com-

mercial or open source software packages used in kinematic post-processing. At Onsala the GNSS local tie system development includes also the kinematic post-processing software [Ning et al. (2015)].

GNSS local ties are well suited for real-time continuous local tie measurements. Once the system is installed, it can be used at any time during the normal use of the radio telescope. A local area network is not needed. The measurements are fully automated and the local tie is achieved directly in the ITRF.

2 Terrestrial Local Tie with Automated Monitoring

Local ties are mainly derived by terrestrial measurements using total stations and levelling instruments, because they cover the high accuracy requirements. The GGOS specifies an accuracy level below 1 mm for the local tie vector and 0.1 mm/yr for its variation. Because the local tie should be provided in a global reference frame, additional GNSS observations are needed. To fulfill these requirements, some preconditions must be met, for instance:

- Usage of calibrated or even certified equipment and instruments,
- Configuration of the local site network, e.g., the construction of the pillars,
- Consideration of new scientific evidence, e.g., applying [Ciddor (2002)] first velocity correction, or
- Thermal expansion corrections for the radio telescope structure.

At Metsähovi as well as at Onsala the radio telescope is enclosed by a protection radome. Thus, the combination of the observations inside and outside the radome is an additional challenge and requires special equipment and an adapted observation concept. E.g., at the Onsala Space Observatory, a special reflector support was mounted at the radome wall to combine both network parts at the local site. While the IVS reference point can be observed in an automated way, the other part of the network as well as the IGS reference point must be measured in a classical way. To avoid the influence of refraction and to minimize local temperature differences during the observation process, the measurement campaigns are preformed in the evening or at night. For this purpose, a second total station (TS30

Leica) was involved. Thus, both network parts as well as both reference points could be observed in parallel.

The big advantages of an automated reference point determination are saving time and manpower. Conventional reference point determinations need maintenance of the radio telescope, whereas an automated monitoring can be done at any time especially during normal operations. Through the automated reference point determination, the portability of conventional measurement methods and their related uncertainties propagations must be validated, reviewed, and adjusted, because additional parameters influence the dynamic measurement process, e.g., synchronization errors or effects caused by misaligned reflectors. On the other hand, an automated monitoring provides long time series and proofs the stability of the geodetic space techniques.

3 HEIMDALL – Milestones of Development

The first version of the monitoring system HEIMDALL had been developed at Karlsruhe Institute of Technology (KIT) in 2010. The developed system was able to monitor quasi-fixed positions at an object, e.g., the non-rotatable tower of a radio telescope was deployed at the Geodetic Observatory Wettzell (GOW) (cf. [Lösler et al. (2010)]). The VGOS agenda as well as the Global Geodetic Observing System (GGOS) call for an automated and continuous monitoring of the reference points of space geodetic techniques. To meet this goal an advanced version of the HEIMDALL system was developed at the Laboratory for Industrial Metrology of the Frankfurt University of Applied Sciences (FRA-UAS). Whereas the first version was able to observe only quasi-fixed positions, the new version allows for a monitoring of movable reflectors that are mounted at the turnable part of a radio telescope (e.g., [Lossin et al. (2014)]).

In general, manually operated terrestrial measurement campaigns depend on, e.g., the available time and personnel resources for maintenance of the radio telescope or weather conditions (cf. [Kallio and Poutanen (2013)]). As shown by [Kallio and Poutanen (2013)] an optimal observation strategy becomes unworkable because of the small timeframe. For example, [Kallio and Poutanen (2013)] attached six reflective tape targets at the turnable part

of the Metsähovi radio telescope and planned to observe the targets in 108 different telescope orientations (12 azimuth and nine elevation positions). Due to the small timeframe, only 18 telescope positions and 68 out of theoretical 648 points were observed. This is a 75% mismatch between the planned and the realized observation strategy. At Metsähovi, the kinematic GPS instead proved to be the best strategy for the local tie measurements ([Kallio and Poutanen (2013)]), and since 2008 this approach has been successfully applied during every geo-VLBI campaign in which Metsähovi has participated. The time frame problem was overcome in 2015 when the HEIMDALL system was installed and used at Metsähovi during two geo-VLBI sessions.

Thus, we can specify the GGOS intended automated and continuous monitoring requirement in more detail by the additional specification during normal operations of the radio telescope. The first fully automated terrestrial monitoring campaign during normal VLBI operations was carried out successfully at the Onsala Space Observatory (OSO) using the HEIMDALL system in 2013 ([Lösler et al. (2013)]). The influence of systematic errors caused by the angle of incidence on the measured reflector positions was studied and corrected analytically for the first time in the framework of reference point determination. In contrast to static stop and go campaigns, when the telescope stops at pre-defined azimuth and elevation positions, an in-process monitoring requires an extended parameterization of limiting factors. Following the *Guide to the Expression of Uncertainty in Measurement* (GUM) a comprehensive uncertainty budgeting was suggested by [Lösler et al. (2016)] and applied during CONT14 at OSO. The success rate between the planned and the realized observation strategy was about 95%.

Based on a VLBI schedule, HEIMDALL predicts the positions of the mounted reflectors and checks the measurability by the angle of incidence. For sensor communication several interfaces are provided, e.g., serial communication or socket connection. The data management is completely realized by an embedded SQL database. The results of external sensors, which are not connected to the system, can be imported to the database and synchronized by the recorded timestamp. In general, the post-processed data analysis starts with a network adjustment to connect the recorded data of several stations and

to provide the estimated Cartesian coordinates and the related uncertainties. The whole network can be defined as a local topocentric coordinate system (cf. [Lösler et al. (2013)]) or as a global geocentric coordinate system (cf. [Lösler et al. (2016)]). The network definition should be aligned to the project goals. For continually proving the stability of the network and the reference point a local topocentric coordinate system is sufficient and descriptive. For deriving local tie vectors a global geocentric coordinate system is preferred, because a final global transformation becomes dispensable.

Beside the network adjustment module, HEIMDALL contains an analysis component for the IVS reference point determination. The implemented mathematical model is based on a rotating model of a radio telescope considering the irregularities in the construction of the radio telescope. This model, presented in 2008, is the first one that allows for continued IVS reference point determination during normal operations and is a major step forward in the research of automated monitoring of local ties (e.g., [Lösler (2009)]). The prototype software HEIMDALL allows an independent, economical, time-effective, and continued monitoring of the IVS reference point.

4 Preliminary Results

In August and September 2015, automated local tie measurements were carried out at the co-location sites Metsähovi and Onsala. The geo-VLBI sessions T2105 (2015-08-25) and EUR137 (2015-09-07) were selected because both stations were participating. The local tie vectors at each site were observed and derived by classical terrestrial measurements involving the monitoring system HEIMDALL and by GNSS observations. Thus, two independent observation methods are used and can be compared to each other. Moreover, at the Onsala site, another representation of the mathematical model of the IVS reference point determination is available and allows for an independent validation.

4.1 Preliminary Results at Onsala

At Onsala, four local measurement campaigns were performed close to the dates of the VLBI sessions to derive the IGS reference point as well as control points that were partially equipped by GNSS antennas and to connect both network parts using a Leica total station TS30. The IVS reference point as well as the radome network were observed automatically by an additional total station MS50 (Leica). To get a homogeneous point distribution, 14 reflectors were mounted at the turnable part of the Onsala 20-m radio telescope. Currently, the GNSS observations are still under investigation and only the local terrestrial observations have been analyzed. Thus, a local topocentric coordinate system was used instead of a global geocentric one. Table 1 summarizes the results of the local tie determination at the Onsala Space Observatory. During the 15-day-long CONT14 campaign, the local tie vector was derived to respond to the IERS call for the ITRF2014. The length of the local tie vector given in SINEX is 79.5709 m and the estimated axis offset is -5.9 mm. The new estimated values confirm the results of the CONT14 measurement campaign very well.

Table 1 Preliminary results of the local tie estimation at the Onsala Space Observatory based on terrestrial observations. The total number of observations is NOO and the number of observed telescope points is denoted by OTP. LEN and AO are the length of the local tie vector and the axis offset with related uncertainties, respectively.

Session	T2105	EUR137
NOO	4761	4686
OTP	1022	1016
LEN	79.5708 m ± 0.5 mm	79.5707 m ± 0.5 mm
AO	-5.9 mm ± 0.2 mm	-6.0 mm ± 0.2 mm

4.2 Preliminary Results at Metsähovi

The local area pillar network was measured in 2014 and in 2015 first with a 40-day GPS campaign and then terrestrially using T2003 tacheometer and TS50 robot tacheometer. A special campaign for the height differences from the pillars to the GPS masts was per-

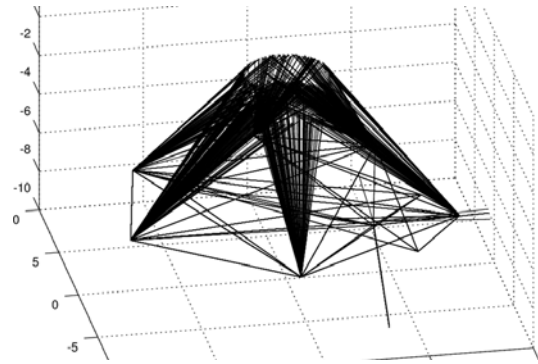


Fig. 1 Geometry of the measurements in automated monitoring at Metsähovi.

formed. The connection of the radome network and the local area network was measured soon after the SIB60 VLBI campaign. The height differences of the pillar points and some points under the radome were levelled. The monitoring observations and the measurements in radome network and the local area network were computed in one combined free network adjustment in ITRF. The orientation and positions of the network are based on the coordinates of 16 GPS points of combined solution of the 40-day campaign. Eight Leica GPR121 prisms were mounted at the rotating part of the 14-m radio telescope and used as targets in automated monitoring (Figure 1). GPS local tie measurements were performed simultaneously (Figure 2). The results reveal small systematic differences in coordinates which is best seen in the time series (Table 2).

Table 2 Preliminary results of the local tie estimation at Metsähovi. The total number of observations is NOO and the number of observed telescope points is denoted by OTP. LEN and AO are the length of the local tie vector and the axis offset with related uncertainties, respectively.

Session Technique	T2105 GPS	EUR137 GPS	T2105 & EUR137 Terrestrial
NOO			4023
OTP	1574	1898	834
LEN	128.8833 m ± 0.8 mm	128.8836 m ± 0.8 mm	128.8818 m ± 0.4 mm
AO	-4.4 mm ± 1.2 mm	-3.3 mm ± 1.2 mm	-1.8 mm ± 0.3 mm

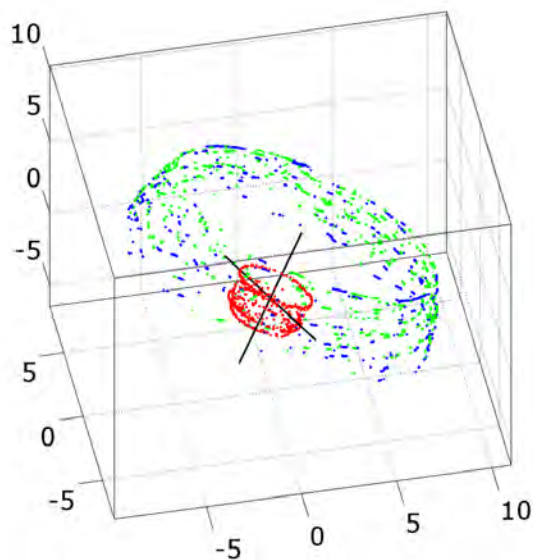


Fig. 2 Geometry of the measured points in GPS local tie (green and blue) and in terrestrial monitoring (red) at Metsähovi.

Acknowledgements

We gratefully acknowledge Sebastian Bieker and Andreas Rüter for supporting this work during their Bachelor theses. The project work of NLS and SP is funded by the European Metrology Research Program (EMRP). The EMRP is jointly funded by the EMRP participating countries within EURAMET and the European Union.

References

[Ciddor (2002)] Refractive Index of Air: 3. The Roles of CO₂, H₂O, and Refractivity Virials *Applied Optics*, Vol. 41(12), 2292–2298, 2002.

- [Kallio and Poutanen (2012)] Can we really promise a mm-accuracy for the local ties on a Geo-VLBI antenna. In: S. Kenyon, M. Pacino, U. Marti, editors, *Geodesy for Planet Earth*, International Association of Geodesy Symposia, Vol. 136, pages 35–42, 2012.
- [Kallio and Poutanen (2013)] U. Kallio and M. Poutanen, Local Ties at Fundamental Stations. In Z. Altamimi, X. Collilieux, editors, *Reference Frames for Applications in Geosciences*, International Association of Geodesy Symposia 138, NASA/TP-2013-217511, pages 147–152, 2013.
- [Lösler (2009)] M. Lösler, New Mathematical Model for Reference Point Determination of an Azimuth-Elevation Type Radio Telescope. *Journal of Surveying Engineering*, Vol. 135(4), pages 131–135, 2009.
- [Lösler et al. (2010)] M. Lösler, C. Eschelbach, A. Schenk, A. Neidhardt, Permanentüberwachung des 20m VLBI-Radioteleskops an der Fundamentalstation in Wettzell. *Zeitschrift für Geodäsie, Geoinformatik und Landmanagement*, Vol. 2010(1), 135, pages 40–48, 2010.
- [Lösler et al. (2013)] M. Lösler, R. Haas, C. Eschelbach, Automated and continual determination of radio telescope reference points with sub-mm accuracy: results from a campaign at the Onsala Space Observatory. *Journal of Geodesy*, Vol. 87(8), pages 791–804, 2013.
- [Lösler et al. (2016)] M. Lösler, R. Haas, C. Eschelbach, Terrestrial monitoring of a radio telescope reference point using comprehensive uncertainty budgeting – Investigations during CONT14 at the Onsala Space Observatory. *Journal of Geodesy*, Vol. 90(5), pages 467–486, 2016.
- [Lossin et al. (2014)] T. Lossin, M. Lösler, A. Neidhardt, R. Lehmann, S. Mähler, The usage of recursive parameter estimation in automated reference point determination. In D. Behrend and K.D. Baver, K.L. Armstrong, editors, *Proceedings of the 8th IVS General Meeting - VGOS: The New VLBI Network*, Science Press (Beijing), Shanghai, China, pages 344–348, 2014.
- [Ning et al. (2015)] T. Ning, R. Haas, G. Elgered, Determination of the local tie vector between the VLBI and GNSS reference points at Onsala using GPS measurements. *Journal of Geodesy* Vol. 89(7), pages 711–723, 2015.

VERA Geodetic VLBI with a Newly Developed High-speed Sampler and Recorder

Takaaki Jike

Abstract By using 1-Gbps recording and increasing the number of scans, VERA has improved the accuracy of the parameter estimation in geodetic VLBI, guaranteeing accurate VERA astrometry. However, further increasing the number of scans will be difficult given the slow speeds of the VERA antennas. OCTAD and OCTADISK2 are candidates for the next-generation data processing system of VERA. The sampling/recording rate of the new system is 8 Gbps. The broadening of the recording bandwidth leads to an improved delay estimation accuracy and is expected to improve the accuracy of the geodetic results. We performed several geodetic VLBI experiments using the new high-speed sampler and recorder.

Keywords VERA, 8-Gbps sampler

1 Introduction

VERA is a Japanese VLBI array aimed for obtaining a three-dimensional map of our Galaxy. Four antennas (Mizusawa, Iriki, Ogasawara, and Ishigakijima) form the VERA network. Employing a phase-referencing VLBI technique, VERA will measure distances and motions of radio sources in our Galaxy with an accuracy of 10^{-9} , unveiling the true structure of our Galaxy. In order to guarantee the accuracy of VERA astrometry, VERA is carrying out two kinds of geodetic VLBI observations. One is the participation of VERA-Mizusawa in IVS sessions (T2, AOV) tying the VERA network into the TRF. The other is VERA-

National Astronomical Observatory of Japan

internal geodetic VLBI in K-band for monitoring the VERA network at the mm-level (H: 1 mm, V: 3–4 mm). The current observation specifications of the VERA-internal geodetic VLBI are shown in Table 1.

Table 1 Specifications of the current VERA-internal geodetic VLBI in K-band.

Number of scans	500–800
Sampling mode	1024Mbps-2bit-1ch
Digital filter mode	16MHz-2bit-16ch, 32-MHz interval
Received radio frequency	22,800–23,328 MHz
Data storage system	OCTADISK
Recording rate	1024 Mbps
Correlator	Mizusawa GICO3

From the site positions derived from the VERA-internal geodetic VLBI observations, the following features are discernible. The largest feature for all stations except Mizusawa is a linear change in position caused by plate motion. For Mizusawa, a co-seismic step and post-seismic creeping are predominant. With the other stations, velocity changes from slow-slip-events (SSE) can be seen. They exert fluctuations from several millimeters to several centimeters on the site positions, and it is difficult to predict the time of the SSE event and the size of the fluctuations. Typical errors for the position results are 1 mm in horizontal and 4 mm in the vertical, but the variation between the results is about twice the size of the errors.

Is it possible to improve the reliability of the estimated site coordinates to 2–3 mm? One of the approaches for improving the accuracy of the estimated geodetic parameters is the acquisition of more precisely and more accurately observed delays. The desired accuracy for the estimated delays is a few millimeters in length (less than 10 ps, 5–6 ps on average).

Broadening the recording bandwidth is effective to improve the fringe detection sensitivity and the accuracy of the estimated delay. OCTAD and OCTADISK2 of the OCTAVE series [1] are a newly developed high-speed sampler and recorder, respectively, developed by NAOJ. The specifications of OCTAD are given in Table 2. Experimental geodetic VLBI observations were carried out using the high-speed sampler and recorder in order to confirm the improvement in the accuracy of the geodetic estimation parameters by the broadening of the recording bandwidth.

Table 2 Specifications of OCTAD.

Maximum sampling rate	10,384 Mbps
Quantifying bit number	2 or 3 bit
Output	10GbE
10GbE ch. number	4 in maximum
10GbE application layer protocol	VDIF

2 Selection of Radio Sources

It is required that the effect of the radio source structure on the uncertainty of the delay amounts to less than 10 ps. Hence, radio sources with a median value for the delay correction due to source structure of less than 10 ps become candidates for observation. In practical terms, radio sources with a structure index of less than two are chosen from the list of K/Q band sources [2]. Each source in this list may or may not have a successful fringe detection. A judgment is performed under the following conditions: delays are estimated with an error of 10 ps or less, each radio source is observed simultaneously at all VERA sites, and fringes are detected with an integration time of 120 seconds or less. Table 3 summarizes the prediction results us-

Table 3 Predicted performance of the fringe detection.

Sampling mode (MHz-bit)	512-2	1024-2	4096-2
Minimum SNR	280	65	45
Minimum flux density (Jy)	4.54	0.80	0.28
Number of sources with fringes	0	8	170

ing three sampling/recording modes: VERA's currently used 1-Gbps mode, 2-Gbps as the maximum performance of the currently used sampler at VERA, and

8-Gbps as the highest possible bit rate. Accordingly, in order to realize geodetic VLBI observations with a delay accuracy of 10 ps or better, the sampling/recording rate of 8-Gbps is indispensable.

3 Observation

Details of the geodetic VLBI experiment are shown in Table 4. Three recording modes were used during the experiment: 1-Gbps, 2-Gbps, and 8-Gbps; their respective parameters to achieve the needed accuracy change in the geodetic parameter estimation with a broadened recording bandwidth are listed in Table 5. Although the observation period was originally planned to be 24 hours, the actual observing time length became 13 hours because of a data transfer problem in the middle of the observation period.

Table 4 Details of the geodetic VLBI experiment.

Date	06:00 Jan. 27 – 06:06 Jan. 28, 2016
Baseline and length	Mizusawa–Ishigakijima, 2280 km
Sky condition	fine@Mizusawa, rain@Ishigakijima
Predicted minimum SNR	38
Number of usable scans	255

Table 5 Comparison of the three data acquisition systems.

Mode name	1-Gbps	2-Gbps	8-Gbps
Sampler	ADS1000	ADS3000+	OCTAD
Filter (MHzBW-bit-ch)	16-2-16	512-2-1	512-2-4
Recorder	OCTADISK	VSREC	OCTADISK2
Min. freq. (MHz)	22,700	21,971	21,459
Rec. rate (Mbps)	1024	2048	8196
Effective BW (MHz)	147.51	147.80	591.21

4 Results of Delay Estimation

Table 6 shows the estimation results of the delays acquired with the three sampling modes. These delays were estimated using the same scan observing radio source 0016+731 for 40 seconds. The estimated delay error is a few ps for 8-Gbps. Table 7 lists the average SNR ratios for 8-Gbps/1-Gbps and 2-Gbps/1-

Table 6 Results of the delay estimation.

Rec. Rate	Delay Error (ps)	SNR
1-Gbps	18.8	57.1
2-Gbps	10.7	100.2
8-Gbps	1.2	219.3

Table 7 Theoretical and actual SNR ratios.

	2-Gbps/1-Gbps	8-Gbps/1-Gbps
Theoretical SNR ratio	1.45	2.88
Average SNR ratio	1.77	3.72

Gbps as determined from the delay estimation. Hence, the actual measured ratio is larger than the theoretical one. This result suggests that the coherence loss occurring in the 1-Gbps signal transfer system is larger than the ideal value. The standard deviation (S.D.) of the delay differences were 30.44 ps between 8-Gbps and 2-Gbps and 74.40 ps between 2-Gbps and 1-Gbps, respectively. The scatter of the delay decreased when the recording bandwidth was broadened and/or the SNR was increased.

5 Results of Rapid Geodetic Estimation

The antenna coordinates, clock polynomials, and zenith atmospheric delay correction parameters (dZAD) were estimated simultaneously. Table 8 shows the offsets and errors of the antenna coordinates as estimated from observations in each sampling mode. The distribution of the error ellipsoids is shown in Figure 1. The offsets from the initial coordinates are settled in less than several millimeters. The ratio of the magnitude of the error for 1-Gbps:2-Gbps:8-Gbps is 2.0:1.4:1.0.

Table 8 Estimated offsets and errors of the Ishigakijima antenna coordinates (in mm).

	1-Gbps		2-Gbps		8-Gbps	
	offset	error	offset	error	offset	error
U-D	2.1	7.0	-5.3	5.2	2.6	3.4
E-W	1.5	2.0	1.4	1.7	-2.3	1.1
N-S	1.0	2.3	-0.4	1.6	-0.8	1.1

The estimated errors are shown in Table 9. For the 1-Gbps and 2-Gbps modes, the RMS of the post-fit delay residuals and the RMS of the observed delay er-

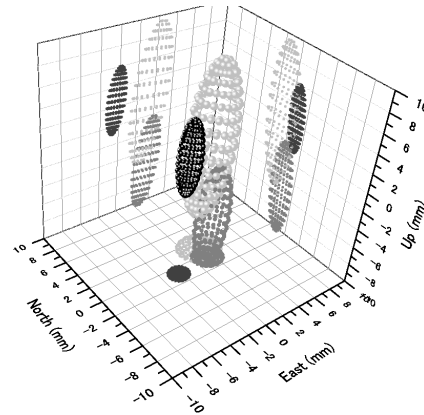


Fig. 1 Distribution of the error ellipsoids from the initial coordinates. The smallest ellipsoids show the error distribution for 8-Gbps, the medium-sized for 2-Gbps, and the largest for 1-Gbps.

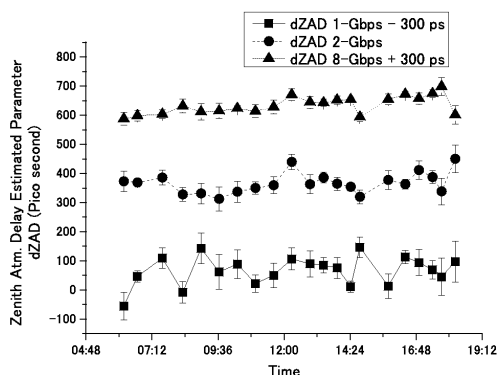
rors are close in value. This suggests that the magnitude of the errors of the estimation parameters is dependent on the magnitude of the thermal noise error of the observed delay. However, with 8-Gbps, the RMS of the post-fit delay residuals is 4.2 times larger than the RMS of the observed delay error. Thus, the ability of the delay estimation is not used effectively in the analysis. Possible reasons for this could be: the instability of the observation system, a time variation of the inter-band phase characteristics, unsuitableness of the fitting function of the fringe peak search processing, skewness of the delay resolution function, and insufficient precision of the physical model and observation equation.

A misestimation of dZAD and its time variation exerts large uncertainties on the estimated coordinates. It is confirmed that the estimation ability of dZAD can be improved by reducing the delay estimate errors. Figure 2 depicts the time series of the estimated dZAD obtained from 1-Gbps, 2-Gbps, and 8-Gbps, respectively. Table 10 lists the average value of the estimated dZAD and its standard deviation. It can be seen that the error scale and time variation of dZAD decreases with decreasing observed delay errors. The error of the estimated dZAD is about six times larger than the RMS of the observed delay error in 8-Gbps. If the atmospheric propagation delay model can trace delays with higher accuracy, it is likely that the estimation of the dZADs will become more exact. Also, it will be effective to go to a higher scanning frequency to estimate dZAD. It is necessary to confirm that a stabilization of the dZAD

Table 9 Estimation errors.

Mode Name	1-Gbps	2-Gbps	8-Gbps	2-Gbps/1-Gbps	8-Gbps/1-Gbps
RMS of post-fit residuals [ps]	32.2	23.0	14.0	0.71	0.43
Sample standard deviation [ps]	2.4	1.7	1.0	0.70	0.42
Degrees of freedom	177	185	186		
Error of baseline length [mm]	8.6	6.0	4.1	0.69	0.48
RMS of observed delay error [ps]	34.7	21.0	3.3	0.61	0.10
Delay rejection criterion [ps]	159.6	115.3	71.5		

results contributes to the stability of the antenna coordinates results.

**Fig. 2** Time series of the estimated zenith atmospheric delay correction. The mapping function used in the estimation was NMF.**Table 10** Average and standard deviation of the estimated dZAD parameters (in ps).

Mode	Average	Std. Dev.
1-Gbps	367.17	38.25
2-Gbps	366.89	26.86
8-Gbps	334.20	18.73

6 Conclusions

A geodetic VLBI experiment was carried out with three data processing systems in order to confirm an improvement in the accuracy of the geodetic

estimation parameters by broadening the recording bandwidth. The employed sampling/recording modes were 1-Gbps, 2-Gbps, and 8-Gbps. When compared to 1-Gbps recording, the SNR of the fringes increased 1.5-fold for 2-Gbps and 3.5-fold for 8-Gbps. The RMS of the observed delay error reached 3 ps for 8-Gbps, thanks to a widening of the recording bandwidth. The delay scatter was also reduced. The magnitude ratio of the geodetic solution error is 2.0, 1.4, and 1.0 for 1-Gbps, 2-Gbps, and 8-Gbps, respectively. The time series stability of the zenith atmospheric delay correction also improved.

Future goals are to perform test observations with 800 or more scans per 24 hours, repeating test observations in order to confirm the stability of the estimated antenna coordinates, establishment of regular operation with 8-Gbps recording, and the use of OCTAD for international VLBI observations at VERA-Mizusawa.

References

1. Y. Kono, T. Oyama, N. Kawaguchi, S. Suzuki, K. Fujisawa, H. Takaba, K. Sorai, M. Sekido, S. Kurihara, Y. Murata, H. Uose, "Real-time VLBI Network with 10GbE Connection, OCTAVE", In D. Behrend and K. Baver, editors, *International VLBI Service for Geodesy and Astronomy 2012 General Meeting Proceedings*, NASA/CP-2012-217504, pages 96–98, 2012.
2. P. Charlot, D. A. Boboltz, A. L. Fey, E. B. Fomalont, B. J. Geldzahler, D. Gordon, C. B. Jacobs, G. E. L. Lanyi, C. Ma, C. J. Naudet, J. D. Romney, O. J. Sovers, and L. D. Zhang, "The Celestial Reference Frame at 24 and 43 GHz. II. Imaging", *The Astronomical Journal*, 139, pages 1713–1770, doi:10.1088/0004-6256/139/5/1713, 2010.

Progress on the VLBI Data Acquisition System of SHAO

Renjie Zhu^{1,2}, Yajun Wu^{1,2}, Jiyun Li¹

Abstract The Shanghai Astronomical Observatory (SHAO) started to develop a VLBI digital backend in 2004. In 2010, the first generation of digital backends named CDAS (Chinese VLBI Data Acquisition System) was installed at the CVN VLBI stations and applied in several projects. This paper introduces the history, the current status, and the future of the VLBI digital backends developed at SHAO.

Keywords VLBI, CDAS

1 Introduction

In 2004, the Shanghai Astronomical Observatory started to develop VLBI digital backends. In 2010, the first generation of digital backends named CDAS (Chinese VLBI Data Acquisition System) [1] was installed at the CVN VLBI stations. During the past ten years, CDAS has supported not only the Chinese Lunar Projects but also astrometric, geodetic, and astrophysical observing.

In 2016, a new VGOS station will be established near the Tianma station. The new generation backend CDAS2 [2] will be installed to meet the requirements of the VGOS. And CDAS3 [2] is still under development.

1. Shanghai Astronomical Observatory, CAS

2. Key Laboratory of Radio Astronomy, SHAO, CAS

2 The Application of CDAS

The CDAS has served the Chinese Lunar Project for several years. In the project, a narrow-band mode such as 2 MHz or 4 MHz x 8 channels was applied due to the speed limitation of the data link from the stations to the data center. The total data rate was no more than 64 Mbps, and the data was sent to the data center in real time by Mark 5B.

Furthermore, the full bandwidth mode such as 32 MHz x 16 channels was applied in a VLBI ecliptic plane survey. The total data rate is 2048 Mbps. In June 2013, the first trial of VEPS observations was made using a 1024(Mbps)-16(Channel)-1(bit) mode. Last year, eight sessions were observed, and a 2048(Mbps)-16(Channel)-2(bit) mode was applied by CDAS at the CVN stations [3].

3 CDAS2

The hardware of CDAS2 was finished in 2014. The full IF bandwidth that can be accepted is 1024 MHz, which can be split into 2 x 512 MHz. The most significant improvement is that a 10Gig Ethernet interface is available. So it can connect with Mark 6 or the commercial disk array through Ethernet.

Now the firmware for PFB mode is almost finished. It can split the IF into several basebands in the same bandwidth. The maximum data rate is 4096 Mbps. The data that is sent by the UDP protocol by 10Gig Ethernet can be monitored by the DATA CAPTURE function in near-real time as Figure 1 shows. In 2 x 512 MHz mode, a thread id can be assigned to each IF.

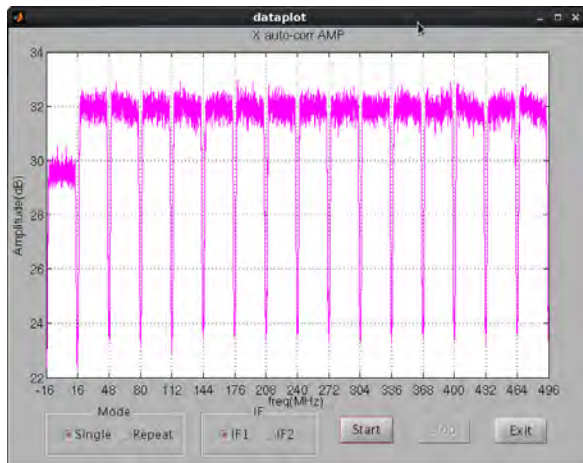


Fig. 1 Control Panel for DDC.



Fig. 2 Control Panel for PFB.

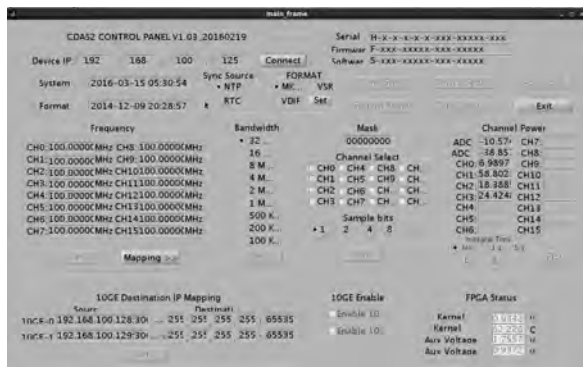


Fig. 3 Control Panel for PFB.

The DDC mode, in which the frequency and bandwidth are changeable, is in development. It is more suitable for astrophysics and deep space applications. The narrow bandwidth (below 1 MHz) and multi-sample-bits (4/8/16-bit) design is aimed at spacecraft tracking.

Figure 2 and Figure 3 show the different parameters needed by the firmware.

4 CDAS3

CDAS3 has improved the full IF bandwidth from 1024 MHz to 2048 MHz. Also it can be split into 2 x 1024 MHz or 4 x 512 MHz. The maximum data rate can be up to 8192 Mbps.

The performance of the ADC module has been tested. An 8 MHz sine wave has been sent to the ADC, and the digitalized data can be captured by FPGA. Then the data can be exported, and the ENOB and SFDR can be calculated using Matlab. Figure 4 shows the results for one channel.

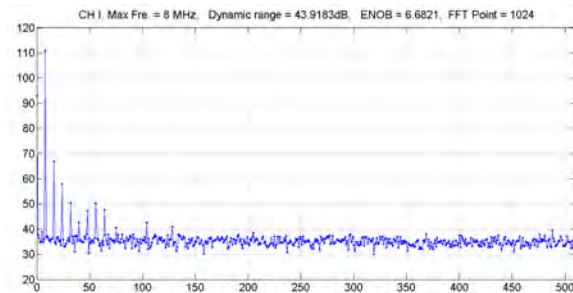


Fig. 4 The ADC performance of CDAS3.

5 Solution for VGOS Station

For the new VGOS station that will be built in Shanghai, a 512-MHz bandwidth observation mode will be achieved first. The maximum data rate is 1024 Msps x two bits x two polarizations x four bands = 16 Gbps. In this case, four sets of CDAS2 can meet the requirement because each set can deal with two polarizations for the 512 MHz bandwidth. And four data streams that come out from CDAS2 can be connected to four SPF+ ports in Mark 6 directly.

In the future, a 1024-MHz bandwidth observation mode will be achieved, and the data rate will be doubled. There are two solutions to meet the new requirement. One solution is simply to double the number of CDAS2 sets of equipment, from four to eight. Due

to the number of SFP+ ports in Mark 6, a 10Gigabit switch would be needed. The other solution is upgrading the four sets of CDAS2 to CDAS3 because each CDAS3 can deal with two polarizations for the 1024 MHz bandwidth.

2. Renjie Zhu, Xiuzhong Zhang, Yajun Wu, et al. "A New Generation of Platforms for CDAS", in *IVS 2014 General Meeting Proceedings*, edited by Dirk Behrend, Karen D. Baver, and Kyla L. Armstrong, Science Press (Beijing), ISBN 978-7-03-042974-2, pp. 215–218, 2014.
3. Fengchun Shu, Leonid Petrov, Wu Jiang, et al. "Progress on VLBI Ecliptic Plane Survey", this volume.

References

1. Renjie Zhu, Ying Xiang, Jintao Luo, and Xiuzhong Zhang, "The Design and Application of High Speed Data Acquisition and Processing Platform for Radio Astronomy", *Progress in Astronomy*, Vol 30, 2012, pp. 236–245.

The First Geodetic VLBI Field Test of LIFT: A 550-km-long Optical Fiber Link for Remote Antenna Synchronization

Federico Perini¹, Claudio Bortolotti¹, Mauro Roma¹, Roberto Ambrosini¹, Monia Negusini¹, Giuseppe Maccaferri¹, Matteo Stagni¹, Mauro Nanni¹, Cecilia Clivati², Matteo Frittelli², Alberto Mura², Filippo Levi², Massimo Zucco², Davide Calonico², Alessandra Bertarini^{3,4}, Thomas Artz⁴

Abstract We present the first field test of the implementation of a coherent optical fiber link for remote antenna synchronization realized in Italy between the Italian Metrological Institute (INRIM) and the Medicina radio observatory of the National Institute for Astrophysics (INAF). The Medicina VLBI antenna participated in the EUR137 experiment carried out in September 2015 using, as reference systems, both the local H-maser and a remote H-maser hosted at the INRIM labs in Turin, separated by about 550 km. In order to assess the quality of the remote clock, the observed radio sources were split into two sets, using either the local or the remote H-maser. A system to switch automatically between the two references was integrated into the antenna field system. The observations were correlated in Bonn and preliminary results are encouraging since fringes were detected with both time references along the full 24 hours of the session. The experimental set-up, the results, and the perspectives for future radio astronomical and geodetic experiments are presented.

Keywords Optical fiber, clock synchronization, metrology

1. Istituto Nazionale di Astrofisica, Istituto di Radioastronomia, Bologna, Italy
2. Istituto Nazionale di Ricerca Metrologica, Divisione di Metrologia Fisica, Torino, Italy
3. Max-Planck-Institute for Radio Astronomy, Bonn, Germany
4. Rheinische Friedrich-Wilhelms-Universität Bonn, Institut für Geodäsie und Geoinformation, Bonn, Germany

1 Introduction

A coherent fiber link for application in very long baseline interferometry (VLBI) for radio astronomy and geodesy has been realized thanks to the LIFT (the Italian Link for Time and Frequency) project [1]. The map of the present LIFT backbone is shown in Figure 1. A dedicated fiber (dark fiber) is used from INRIM to Bologna, where the signal is split: one of the arms reaches the European Laboratory for Non Linear Spectroscopy in Florence (LENS) and the other arm extends the link to the Medicina Observatory. The last 30 km of the link, from Bologna to the radio telescope, are shared with the data channel with a DWDM (Dense Wavelength Division Multiplex) architecture. The system already demonstrated to be capable of operating for several hours without interruptions and without loss of coherence [2]. For the VLBI application it is mandatory to guarantee long-term operation so one of the aims of the experiment was to test in the field some technical improvements, such as automatic polarization adjustment.



Fig. 1 The present LIFT backbone.

Conceivably, a fiber-based network of multiple antennas connected to a single clock can be envisaged, with improved spectral purity and long-term stability.

This will be useful for high-resolution VLBI and could open the possibility of direct fringe comparisons in addition to the well-established protocols where the data are processed at a correlator. This experiment opened the possibility of replacing the local hydrogen masers at the VLBI sites with optically-synthesized Radio Frequency (RF) signals. This could improve the VLBI resolution by providing more accurate and stable frequency references and, in perspective, by enabling common-clock VLBI based on a network of telescopes connected by fiber links. We planned an experiment at Medicina during a measurement campaign that took place in September 2015. In Section 2 we present the experiment set-up, in Section 3 the EUR137 Experiment, and in Section 4 the conclusion and the perspectives for further developments.

2 Experiment Set-up

The optical link to Medicina is based on the distribution of an ultra-narrow linewidth laser at $1.5 \mu\text{m}$ along a phase-stabilized telecom fiber, which does not affect the uncertainty of the delivered frequency at the 10^{-19} level of accuracy (in terms of relative frequency) [1]. To inject the signal of the H-maser at INRIM into the optical link, an optical frequency comb is used. At Medicina, the received light is regenerated by phase-locking a local diode laser. The obtained signal is then used to phase-lock a second optical frequency comb that generates a 100-MHz RF signal. A detailed description of the setup and its characterization can be found in [2]. The signal synthesized from the comb is then processed and sent to a low-noise digital frequency divider which generates both the 5 and 10 MHz RF signals and a Pulse Per Second (PPS) signal needed for the instrumentation of the radio telescope (i.e., as references for the local oscillator of the RF receivers and for the synchronization of the acquisition systems). Particular attention has been devoted to the detection and processing electronics, to ensure that its instability does not affect the overall system performances. To efficiently compare the performances of the local and the fiber-delivered clocks during a VLBI campaign, we added an electronic system to the radio telescope instrumentation which is capable of switching between the two references (Figure 2).

The set-up used for the experiment was composed by the standard VLBI backend, local and remote H-maser Time and Frequency (T&F) references with the switching unit, and the Field System control software. The VLBI backend is composed by a sampling equipment DBBC (Digital Base Band Converter), a data formatting unit (FILA10G) [3], and a recording unit (Mark 5C, <http://www.haystack.edu/tech/vlbi/mark5/>). The switch between the two references is controlled through the IF3 switch-box driven by the observation schedule, when an ad-hoc procedure is called, inserted in the original schedule. The long-term correction of the local H-maser is obtained through a dedicated Global Positioning System (GPS) receiver (on the left in Figure 2) which also provides the initial synchronization of the reference PPS signal generated by the local H-maser. The latter signal is also used for the initial synchronization of the remote PPS only after every possible unlocking of the optical link, i.e., the unlocking of the servo loops on the laser sources, or the optical combs, or link noise compensation. Since the reference switching breaks the DBBC synchrony, a resynchronization is necessary after each switch and a consequently automatic FILA10G time counter adjustment, provided by means of a dedicated GPS antenna (on the right in Figure 2), just for this purpose.

3 EUR137 Experiment

In order to test the remote clock, we used the International VLBI Service for Geodesy and Astrometry (IVS, [4], [5]) Europe experiment (EUR137), already scheduled for September 7, 2015. Since for this experiment Medicina station was not scheduled, we decided to add it to the official schedule in the so-called “tag-along” mode. We established to use both time standards (optical link and local H-maser) throughout the experiment. We split the session into two different sub-sessions, based not on time but rather on two sets of sources that were observed alternately as shown in Table 1. This gives us the possibility to have two 24-hour long observations with both reference clocks.

The data recorded at six European stations (namely DSS65, MEDICINA, METSAHOVI, NYALES20, ONSALA60, and WETTZELL) were sent to the Bonn correlator. The EUR137 experiment was correlated using the Bonn DiFX correlator [6]. In the correlation,

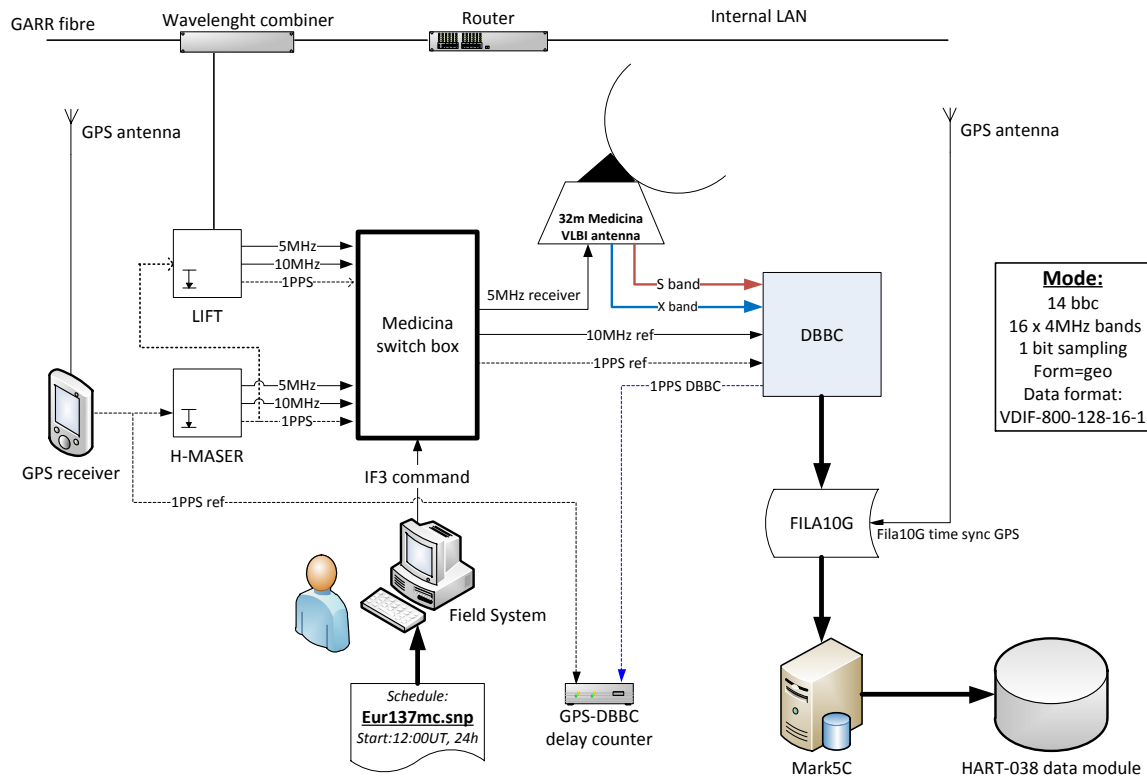


Fig. 2 Schematic experimental set-up.

Table 1 Observed sources.

Clock 1 (H-Maser)	Clock 2 (LIFT)
0059+581	OJ287
0552+398	1803+784
0229+131	1751+288
0119+115	1749+096
1849+670	3C274
0823+033	1128+385
3C418	0716+714
CTA26	0202+319
0017+200	0642+449
1418+546	1726+455
1741-038	0016+731
0454-234	1334-127
0727-115	1519-273
1156+295	

the observations performed at Medicina with the two different clocks were treated as two different VLBI stations: MEDICINA and MEDILIFT. This gave us the opportunity to compare the two geodetic outputs. Fol-

lowing all the standard correlation and post-correlation steps, we created a Mark IV database and analyzed it with vSolve [7]. The MEDILIFT observations had more problems (as opposed to MEDICINA) that were mainly due to the clock behavior: some jumps together with some planned resets at INRIM caused clock breaks. In Figure 3 the MEDILIFT group delay residuals with unresolved clock breaks (on the left) and the residuals (on the right) after setting up eight breaks are presented, respectively. Actually there were more than eight breaks, but between some intervals there were only a few observations leading to singularities. Thus, these observations were removed.

In Figure 4 the final residuals for MEDILIFT (on the left) and MEDICINA (on the right) baselines with full parametrization are displayed: 2nd degree polynomial + one-hour CPWLF (Continuous Piece Wise Linear Functions) clocks, one-hour ZWD (Zenith Wet Delay), 24-hour horizontal tropospheric gradients, station positions for MEDICINA and MEDILIFT, PM (Polar Motion), UT1 (Universal Time), and nutation offsets.

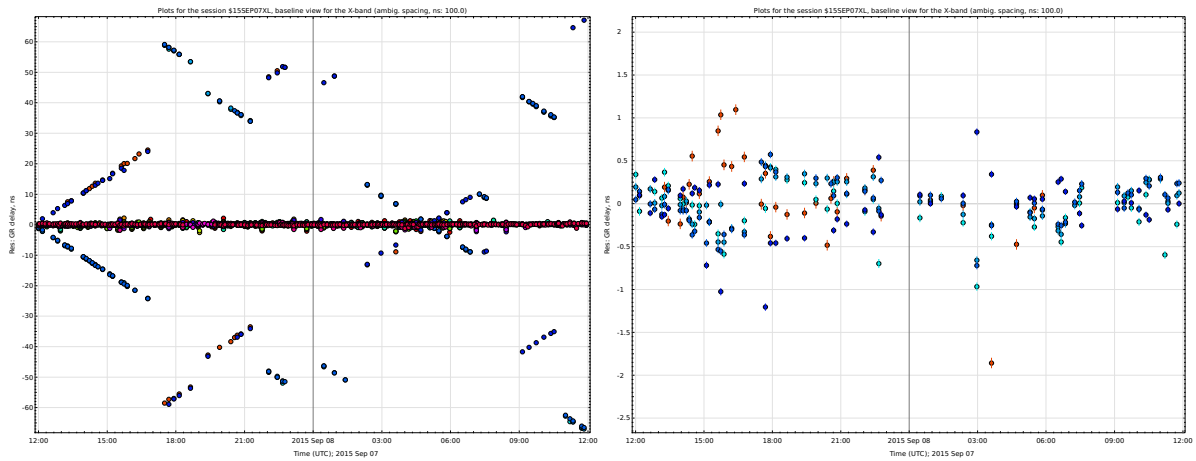


Fig. 3 Group delay residuals for MEDILIFT baselines with unresolved (on the left) and resolved (on the right) clock breaks (in ns).

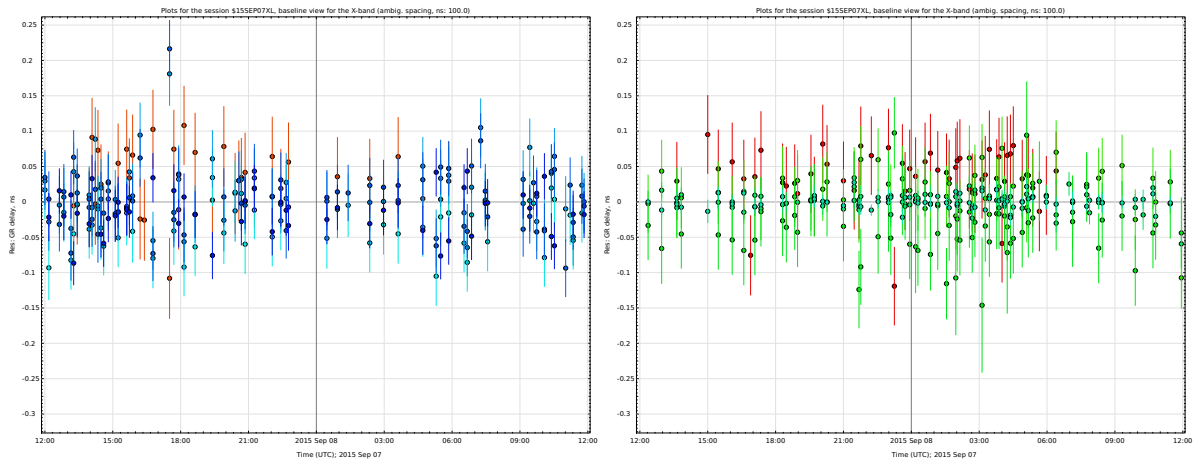


Fig. 4 Final vSolve solution for MEDILIFT (on the left) and MEDICINA (on the right) baselines (in ns).

For MEDILIFT the visible gaps are due to outlier handling.

The problems related to the clock behavior lead to difficulties in the data analysis of the baselines containing MEDILIFT. Resolving the clock breaks gives reasonable results, but the solutions for MEDICINA and MEDILIFT are different, in spite of dealing with the same station. The residuals of the MEDILIFT observations are somewhat larger than those of the MEDICINA observations. This, however, might be due to the imperfect estimation of the clock breaks in vSolve and needs further investigations. Furthermore, the coordinates obtained from the two different data series differ by a few centimeters, mainly in the height component, which reflects obviously on the tropospheric delay. The data are still under analysis

for a full assessment of this difference and the related uncertainty.

4 Conclusions

The IVS EUR137 24-hour experiment demonstrated the feasibility of using the LIFT optical fiber link to distribute the time from INRIM in Turin to the Medicina Observatory. Some technical issues were encountered when making it possible to observe with both clock standards (local and remote clocks). Problems with the observations done with the remote clocks have been found during the data analysis. A key point is to improve the robustness of the remote clock for ex-

tended times. We have planned new experiments for 2016, involving the other INAF antenna in Noto and possibly in coordination with the ASI radio telescope in Matera (ASI), to further test the stability of the system. A newly funded project will possibly extend the fiber link to the Matera geodetic observatory and allow for possible common clock experiments as early as the beginning of 2017. In the future, a fiber-based network of multiple antennas connected to a single clock can be expected. This experiment opens the possibility of replacing the local hydrogen masers at the VLBI sites with optically-synthesized RF signals.

Acknowledgements

This research is based on observations processed at the Bonn Correlator, jointly operated by the Max Planck Institute for Radio Astronomy (MPIfR) and the Federal Agency for Cartography and Geodesy (BKG).

References

1. D. Calonico et al, “High-accuracy coherent optical frequency transfer over a doubled 642-km fiber link”, *Appl. Phys.*, vol. 117, no. 3, pp. 979–986, 2014.
2. C. Clivati et al, “A Coherent Fiber Link for Very Long Baseline Interferometry”, *IEEE Trans on UFFC*, vol. 62, pp. 1907–1912, 2015.
3. G. Tuccari, W. Alef, A. Bertarini, S. Buttaccio, G. Comoretto, D. Graham, A. Neidhardt, P.R. Platania, A. Russo, A. Roy, M. Wunderlich, R. Zeitlhofer, Y. Xiang. “DBBC2 Backend: Status and Development Plan”. In: *International VLBI Service for Geodesy and Astrometry 2010 General Meeting Proceedings*, edited by D. Behrend and K. Baver, NASA/CP-2010-215864, pp. 392–395, 2010.
4. H. Schuh and D. Behrend, “VLBI: A fascinating technique for geodesy and astrometry”, *Journal of Geodynamics*, 2012, 61, 68–80, doi:10.1016/j.jog.2012.07.007.
5. A. Nothnagel. “International VLBI Service for Geodesy and Astrometry (IVS); 2015: The IVS data input to ITRF2014. International VLBI Service for Geodesy and Astrometry, GFZ Data Services. <http://doi.org/10.5880/GFZ.1.1.2015.002>”
6. A. T. Deller, W. F. Brisken, C. J. Phillips, J. Morgan, W. Alef, R. Cappallo, E. Middelberg, J. Romney, H. Rottmann, S. J. Tingay, R. Wayth, “DiFX-2: A More Flexible, Efficient, Robust, and Powerful Software Correlator”, *The Astronomical Society of the Pacific*, vol. 123, no. 901, pp. 275–287, 2011.
7. S. Bolotin, K. Baver, J. Gipson, D. Gordon, D. MacMillan: “The First Release of vSolve”. In: *International VLBI Service for Geodesy and Astrometry 2012 General Meeting Proceedings “Launching the Next-Generation IVS Network”*, edited by D. Behrend and K. Baver, NASA/CP-2012-217504, pp. 222–226, 2012.

New DiFX Software Correlator Cluster at Bonn and Summary of Recent Activities

Arno Müskens¹, Walter Alef², Alessandra Bertarini^{1,2}, Simone Bernhart¹, Laura La Porta¹, Helge Rottmann², Gabriele Bruni², Torben Schüler³, Walter Briskén⁴

Abstract We report on the status of the Bonn Correlator Center for the period 2015/2016. The correlator center has been operated jointly by the Max Planck Institute for Radio Astronomy (MPIfR) in Bonn and the Federal Agency for Cartography and Geodesy in Frankfurt with support from the Institute of Geodesy and Geoinformation in Bonn for more than 25 years. Since 2010 we have been using the DiFX software correlator [Deller et al. (2011)] for astronomical and geodetic correlation on a High Performance computing Cluster (HPC). We summarize our first experience with correlating on our new upgraded cluster, which was designed to be compatible with the VGOS requirements. The new cluster was purchased in December 2015. We also report on newly implemented features, like playback of Mark 6 recordings, and on other software improvements.

Keywords VLBI correlation, DiFX correlator, geodetic VLBI, VGOS

1 Introduction

Since 1978, the MPIfR has been hosting five generations of VLBI correlators: Mark II, Mark III, Mark IIIA, Mark IV [Whitney et al.(2004)], and the Distributed FX software correlator (DiFX). The

1. Rheinische Friedrich-Wilhelms Universität Bonn, IGG
2. Max-Planck-Institut für Radioastronomie (MPIfR)
3. Bundesamt für Kartographie und Geodäsie (BKG)
4. National Radio Astronomy Observatory (NRAO)

correlator center has been operated jointly by the three partners MPIfR, BKG, and IGG.

In 2009 the correlation was switched to DiFX, after 30 years of operating hardware VLBI correlators. The reasons were the significantly lower investment costs and the far greater flexibility of a software-based solution. The DiFX correlator is Open Source and is maintained by a community of developers mostly located at National Radio Astronomy Observatory (NRAO), Netherlands Institute for Radio Astronomy (ASTRON), MPIfR, Commonwealth Scientific and Industrial Research Organisation (CSIRO), and Massachusetts Institute of Technology (MIT) Haystack Observatory. Since 2010, the geodetic correlation has been done exclusively with the DiFX.

2 Background and Present Correlator Status

The DiFX software correlator was developed at Swinburne University in Melbourne, Australia by Adam Deller and collaborators [Deller et al. (2011)]. It has been adapted to the VLBA operational environment by Walter Briskén and NRAO staff, and has been further developed for years by the worldwide DiFX developers group.

DiFX is executed on an HPC, which was upgraded in December 2015 after about seven years of operation. The upgrade was financed by the Max Planck Society with a significant contribution from the German mapping authority BKG. The upgrade went smoothly with a correlator downtime according to plan of less than two weeks. The new cluster is roughly ten times faster than the old one, and will be able to handle wide-band

VLBI observations in the mm-domain and geodesy for at least the next five years.

Some of the features of the new VLBI cluster are:

- 68 compute nodes;
- each node with two processors with 20 compute cores, which adds to 1,360 compute cores in total;
- ~960 TB disk storage (14 RAIDS; 740 TB for VLBI);
- 56 Gbps Infiniband fabric as interconnect (plus 1 GE Ethernet for service tasks);
- 48 TB disk space for correlated data;
- 40 TB backup for correlated data;
- two head nodes for correlation (several correlations can be run in parallel);
- one head node for other tasks;
- one appliance computer for cluster installation and monitoring;
- 17 Mark 5 units for playback of data into the correlator (all Mark 5 formats);
- six Mark 6 units plus two expansion chassis for 1 mm VLBI data and VGOS data;
- 1 Gbps connection to the Internet reserved for VLBI data transfers (soon 2 Gbps).

In addition to the standard DiFX versions (e.g., latest stable = 2.4, development), which are used for “normal” correlation, a DiFX branch for the correlation of RadioAstron data was developed at MPIfR: DiFX-RA. The most significant part of this effort involved modifying the delay model server (Calc, from the Calc/Solve package) to be able to calculate delay information for telescopes with arbitrary coordinates and velocities (that is, not fixed on the ground), and changes to the DiFX metadata system to deal with the changing position and velocity of the spacecraft as a function of time. The delay model was also modified to correct for (general) relativistic effects as the highly elliptical orbit of the spacecraft results in large changes in velocity and gravitational potential compared to the terrestrial frame. DiFX-RA was used extensively to correlate a number of RadioAstron projects in Bonn, but also to help debug the Astro Space Center (ASC) correlator in Moscow.

To perform the fringe search for RadioAstron data, we installed the PIMA¹ software with the help of L. Petrov and the ASC in Moscow.

¹ <http://astrogeo.org/pima>

Other enhancements are the implementation of a database for experiment status and disks, and archiving of the raw correlated data together with their FITS-IDI² or HOPS³ exports on the new MPIfR archive server.

We have implemented native Mark 6 playback into the correlator, the handling of the Mark 6 modules by the correlator, and in addition special VDIF modes for the DBBC3 VLBI backend, all of which are available in the latest development release.

At present we are running Mark 6 recorders in native playback mode for data from VGOS and the Event Horizon Telescope (EHT). The usage of multiple data streams per station was implemented by W. Brisken financed by MPIfR. For instance, an EHT observation at 64 Gbps would deliver the data spread over four Mark 6 recorders with extension chassis, resulting in 16 disk modules to be played into the correlator. We expect that DiFX 2.5 with full Mark 6 playback support will become available in a couple of months. Table 1 lists some important capabilities of the Bonn DiFX correlator.

Table 1 Capabilities of the Bonn DiFX correlator.

Feature	Description
Geometric model	Calc 9 (Calc 11 as plugin)
Phase Cal	Phase-cal extraction of all tones in all sub-bands simultaneously
Pre-averaging time	From milliseconds to seconds
Spectral resolution	Up to 256,000 channels have been used
Signal	Single- and dual-frequency, all four Stokes parameters
Export	Fits export, Interface to MK IV data format for HOPS
Pulsars	Pulsar correlation with incoherent de-dispersion

In general the Bonn Correlator will be powerful enough for the requirements of VGOS for the next five years, in particular as the present estimates of the readiness of VGOS antennas seem to be a bit optimistic. We expect that the EHT will deliver 64 Gbps in the next two years, which should not be an issue either.

² <ftp://ftp.aoc.nrao.edu/pub/software/aips/TEXT/PUBL/AIPSMEMO102.PS>

³ <http://www.haystack.mit.edu/tech/vlbi/hops.html>



Fig. 1 The correlator room at MPIfR—cluster side. The four racks of the cluster are visible behind the glass wall.



Fig. 2 The correlator room at MPIfR—playback side. The three racks on the left house Mark 5 units. The two racks on the right contain Mark 6 units. A glass wall with door shields the operators from the noise.

3 Correlator Usage 2015

The Bonn correlator is the only VLBI correlator worldwide which is shared by astronomers and geodesists with a usage fraction of about 50% for geodesy and 50% for astronomy.

The geodetic throughput of the Bonn correlator in 2015 was roughly identical to the previous years:

- 52 R1 sessions,
- six EURO sessions,
- seven T2 (with up to 20 antennas) sessions,
- six OHIG sessions,
- four R&D sessions,
- 48 INT3 (in e-VLBI mode) Intensives,

- 30 INT2b (30 days, baseline Ts–Wn; e-VLBI mode) Intensives, and
- several additional correlations for DBBC testing (Onsala, Yebes, Wettzell).

Most of the tests for the DBBC development and performance evaluation are correlated in Bonn. Testing of the DBBCs usually consists of parallel observations (whenever possible) of a geodetic session with both analog and digital backends. If requested, we support every station when new software or hardware for recording or transferring data are introduced like Flexbuff, VDIF format, or jive5ab.

It should be noted that most geodetic observatories do not send disk modules anymore, but transfer the data via Internet.

One part of the astronomy load of the correlator is data from the Global mm VLBI Array (GMVA), which observes two sessions per year of up to five days duration at 3-mm wavelength. Up to 15 antennas participate in GMVA observations. For the last two years the data-rate has been increased to 2 Gbps which results in about 500 TB of total disk space recorded in each session.

Correlation of RadioAstron observations has been a big load in the last few years. It requires a very time consuming additional correlation pass, because the RadioAstron clock has to be searched for every scan. As the orbit of RadioAstron is only known to about 500 m, the changes in delay and delay-rate can be quite large, so that an additional acceleration term has to be taken into account. So far, nine observations with up to 30 antennas at 256 Mbps, full track on the source, have been correlated. At times a third correlation pass with an improved satellite orbit was necessary.

Currently the details of correlating high-bandwidth data recorded at 32 Gbps by EHT at 1-mm wavelength are being investigated.

4 Staff Management

The Bonn geodesists have operated their correlation independently of the astronomers from the very beginning. Experiment preparation and post-processing are handled separately for geodetic and astronomical observations.

- **Geodesy:** A. Bertarini, L. La Porta, S. Bernhart, and A. Müskens. Their tasks are:
 - Schedule preparation of nearly all experiments correlated in Bonn.
 - Preparation of correlator control files.
 - Fringe search.
 - Supervision of correlation.
 - Verification of the correlation results and setting up of possible re-correlation.
 - Management of recording media logistics and electronic data transfer.
- **Astronomy:** W. Alef, A. Bertarini, H. Rottmann, G. Bruni, H. Sturm, and R. Märtens.
 - Management of the correlator center.
 - Set-up and verification of astronomical correlation.
 - Cluster management, including operating system and IT security.
 - Maintenance of Mark 5 and Mark 6 playback units as well as of disk modules and cluster hardware.

General computing services and the archive server are provided by the MPIfR computer division.

As a great benefit it turned out that three of the four main geodetic VLBI tasks (*Schedule preparation, Recording, Correlation and Analysis*) are done by our group—the Bonn Geodesists. This allows a tight feedback loop and has resulted in a highly motivated group of people, complemented by the excellent work done by the personnel at the participating geodetic stations.

5 Experiment Distribution among IVS Correlators

Table 2 gives a short overview of the experiment distribution among the IVS correlators worldwide. Unfortunately CRTN (Curtain University software correlator, Australia) is not operational anymore since 2015. Due to the fact that Bonn and WACO have reached their full workload, other IVS correlators need to takeover those experiments. Nevertheless, in the next years several other correlators could become available for IVS correlation. IAA in St. Petersburg/Russia and SHAO (Shanghai VLBI Correlator) plan to upgrade their ex-

isting correlator for VGOS correlation. In addition Vienna/Austria plans to acquire a cluster for correlation.

Table 2 Typical workload of the IVS correlators. Note that the Curtin correlator (CRTN) was shutdown in 2015.

Correlator	Percentage	Session type
BONN	32	R1, T2, Eur, OHG, R&D, INT3
WACO	30	R4, CRD, INT1
CRTN	22	AUS-GEO, AUST, AUS-AST
GSI	10	JADE, AOV, JAXA, INT2
SHAO	3	AOV, APSG, CRF
HAYS	2	R&D, T2
NGII	1	AOV

A different common strategy will be needed and a better distribution of the increasing VGOS correlations is required to ensure that the future correlation demand for VGOS can be satisfied. New ideas and discussions about load balancing are essential for the future of the IVS community and the success of the VGOS program. Discussions are in progress whether it is better to have several effective and very well networked correlators spread over the world or only one big correlator center. Both options need a great and well-connected data center (cloud) where all recorded IVS data can be stored and prepared for further processing. It goes without saying that an experienced staff is required to guarantee an excellent scientific correlation and post-correlation analysis for all IVS sessions.

6 e-transfer

Nowadays 90% of the stations e-transfer their data to Bonn. The average amount of e-transferred data per week for the regular R1 and INT3 observations alone is more than 10 TB.

Most transfers utilize the UDP-based Tsunami protocol and the `jive5ab` (`m5copy`) script. The achieved data rates range from 100 to 800 Mbps. The present Internet connection to the MPIfR is a 1-Gbps dedicated line to the GÉANT node in Frankfurt. The upgrade to 10 Gbps Internet connection to meet the requirements of VGOS has not yet been realized due to cost issues.

For future VGOS observations we should expect a typical data volume of around 40 TB/day/antenna recorded with 8 Gbps data rate. Therefore the increase of the Internet connection for correlators and stations is

essential. In addition, large data buffers have to be provisioned at the stations and at the correlators for each station. In a transition phase Mark 6 modules can be shipped to ease the financial burden of the above two requirements of fast data lines and local large disk storage. But this will lead to a large investment in Mark 6 disk modules and a significant increase in shipping costs. It should be noted that Mark 6 modules can also be used as local storage as implemented, for instance, at Effelsberg.

7 Brain Drain and Outlook

A problem, which is easily overlooked, is that several important VLBI experts will retire in the near future. This is a general problem: VLBI needs new well educated practitioners. The IVS training school is an excellent facility for all young and new members, but experts need many years to become skilled and to gain experience—the special VLBI know-how—which is required.

Some new antennas will become available for use in the next few years. For example, at Wettzell in Germany the new Twin Telescope Wettzell (TTW) for VGOS is close to completion; South Korea has a new antenna for Geodesy at Sejong (NGII, National Geographic Information Institute); in Spain and Portugal, the RAEGE (Atlantic Network of Geodynamical and

Space Stations) project aims to establish a network of four fundamental geodetic stations that will fulfill the VGOS specifications. In Spitsbergen/Norway (NMA, Norwegian Mapping Authority) and in Sweden, Onsala Space Observatory, twin telescopes are in the construction phase. Therefore, broadband geodetic sessions at more regular intervals will be scheduled and processed in the near future. The Bonn Correlator will be powerful enough for the requirements of VGOS for the next five years.

References

- [Whitney et al.(2004)] A.R. Whitney, R. Cappallo, W. Aldrich, B. Anderson, A. Bos, J. Casse, J. Goodman, S. Parsley, S. Pogrebenko, R. Schilizzi & D. Smythe. Mark 4 VLBI correlator: Architecture and algorithms *Radio Science*, 2004, 39, 1007.
- [Deller et al. (2011)] A. T. Deller, W. F. Brisken, C. J. Phillips, J. Morgan, W. Alef, R. Cappallo, E. Middelberg, J. D. Romney, H. Rottmann, S. J. Tingay & R. Wayth. DiFX-2: A More Flexible, Efficient, Robust, and Powerful Software Correlator, *PASP*, 2011, 123, 275–287.
- [Kardashev et al. (2012)] N. S. Kardashev, Y. Y. Kovalev, & K. I. Kellermann. *The Radio Science Bulletin*, 2012, 343, 22–29.
- [Bruni et al. (2014)] G. Bruni, J. Anderson, W. Alef, A. Lobanov, & A. J. Zensus. Space-VLBI with RadioAstron: new correlator capabilities at MPIfR, in *Proceedings of the 12th European VLBI Network Symposium and Users Meeting*, Cagliari, Italy, 2014, ID: 119.

Current Status of the Shanghai VLBI Correlator

Wu Jiang^{1,2}, Zhiqiang Shen¹, Fengchun Shu¹, Zhong Chen¹, Tianyu Jiang¹

Abstract Shanghai Astronomical Observatory has upgraded its DiFX cluster to 420 CPU cores and a 432-TB storage system at the end of 2014. An international network connection for the raw data transfer has also been established. The routine operations for IVS sessions including CRF, AOV, and APSG series began in early 2015. In addition to the IVS observations, the correlator is dedicated to astrophysical and astrometric programs with the Chinese VLBI Network and international joint VLBI observations. It also worked with the new-built Tianma 65-m radio telescope and successfully found fringes as high as at X/Ka and Q bands in late 2015. A more powerful platform is planned for the high data rate and massive data correlation tasks in the future.

Keywords VLBI correlator, IVS, astrometry, radio telescope

1 Introduction

The VLBI group at the Shanghai Astronomical Observatory (SHAO) has a long history in the development of VLBI correlators. The domestic software correlator and hardware correlator are mainly developed and applied for the VLBI tracking system in the Chinese deep space missions. The worldwide open source software correlator called DiFX was adopted at SHAO in 2012 and works as a dedicated correlator for astrophysics and geodesy. The computer cluster and the data storage

1. Shanghai Astronomical Observatory, Chinese Academy of Sciences

2. University of Chinese Academy of Sciences

system of the DiFX correlator has been upgraded in the end of 2014. It has 420 CPU cores and a 432-TB storage capacity (Figure 1). An international high-speed network connection for raw data transfer among the main correlators and geodetic stations is established. As of the beginning of 2015, the DiFX correlator also serves as an IVS correlator. So far, more than ten IVS sessions such as CRF, AOV, APSG, and CRDS sessions as well as a few Australian geodetic VLBI sessions have been processed by the platform.



Fig. 1 Hardware deployment of the Shanghai VLBI correlator.

Besides the IVS correlations, the platform also serves the astrophysical and astrometric programs conducted with the Chinese VLBI Network (CVN) and international joint VLBI observations. Meanwhile, the newly-built Tianma 65-m telescope will cover the frequency range from the L to the Q band together with two dual-frequency receivers in S/X and X/Ka. The DiFX correlator successfully worked with the Tianma 65-m and found fringes as high as at X/Ka and Q bands in late 2015.

2 Performances and Operations

2.1 Platform Performances

The computer cluster shown in Figure 1 is divided into two groups for routine operations. Each head node manages ten computing nodes and 200 CPU cores in total. The main features including the hardware, the software, and the network conditions are as follows. The maximum correlation speed is around 1 Gbps per station when processing ten stations simultaneously (Figure 2). There are more than six staff members

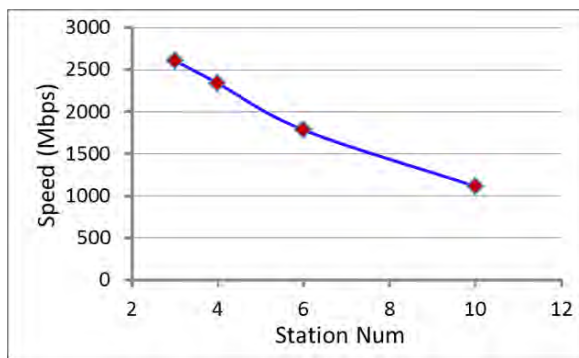


Fig. 2 Correlation speed of the Shanghai VLBI correlator.

(about 50% working time) for different parts of the operations from data delivery to giving out the final outputs.

- Correlator: DiFX-2.2/2.3/2.4/trunk
Post-processing software: HOPS 3.9/3.10/3.11/3.12
- Head nodes: DELL R820 (E5-4610 CPU, 2.4 GHz, 2*6 cores), 64 GB Memory; DELL R730 (E5-2623 CPU, 3.0 GHz, 2*4 cores), 64 GB Memory
- Computing nodes: 20 DELL R630 nodes, 400 cores in total, two socket Intel E5-2660 CPU (2.6 GHz, ten cores), 64 GB Memory
- I/O nodes: RAID6, 432 TB raw storage capacity
- Mark 5 units: three Mark 5A and three Mark 5B.
- 56 Gb Infiniband for internal computing network connection
- 1/10 Gb Ethernet for internal & external network connection

2.2 e-transfer

In order to process global IVS sessions, the network links to Fortaleza, HartRAO, Hobart, Kashima, Noto, and Sejong stations as well as the Bonn correlator have been established (Figure 3). However, the links are not connected in a real time mode and some time slots of connections are negotiated before the data transfer. The two Shanghai VLBI stations are in a 10 Gb link to the VLBI center while other CVN stations are in a much lower rate connection. Most of the high data rate and long duration recording experiments are still through shipment of the diskpicks in CVN.

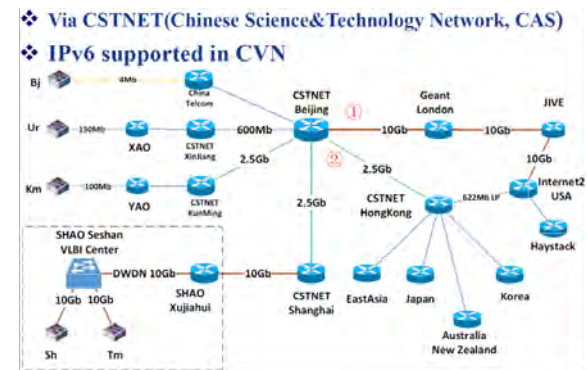


Fig. 3 Network conditions at Shanghai VLBI center.

2.3 Statistics of Correlation Operations

Some comparisons of the outputs after correlation and post-processing were made between the Shanghai DiFX correlator and the Bonn DiFX correlator in late 2014. The RMS of the group delay differences in the X band extracted from an S/X session were within a few picoseconds. In early 2016, a similar comparison was made between the two correlators. The results listed in Table 1 implied the group delay of the two correlator outputs coincided at the picosecond level.

Besides serving the global IVS sessions, the DiFX correlator is open to make correlations for the astrophysical and astrometric programs with CVN, east Asian, and Australian joint VLBI observations. Table 2 gives a summary of the correlations.

Table 1 Comparison results of the Shanghai DiFX and Bonn DiFX correlators. Group delay and rate as WRMS of the differences.

Baseline	S band			X band		
	SNR ratio	Group delay (ps)	Rate (ps/s)	SNR ratio	Group delay (ps)	Rate (ps/s)
Ny-Ts	1	2.4	0.0127	0.992	1.1	0.0085
Ny-Wn	1	5.6	0.0208	1.002	1.6	0.0095
Ny-Wz	1	3.8	0.0156	0.994	0.9	0.0041
Ts-Wn	1	4.6	0.0198	1	1.7	0.0091
Ts-Wz	1	2.8	0.0113	0.994	0.9	0.0063

Table 2 Summary of correlations processed. [In CVN-(CN): Js (Jiamusi), Ks (Kashi), and two deep space stations of China.]

Session Code	Observation Type	Times in a year	Stations participated	Recording rate
AUS-(AST,GEO)	Geodesy	12 (2016)	Australian, more than 4 st.	1024 Mbps
CVN-(CN)	Geodesy	4	CVN, Js and Ks, more than 3 st.	512 Mbps
CVN-(PSR)	Pulsar Astrometry	not fixed	CVN, 3 or 4 st.	1024 Mbps
CVN/EAVN	Astrophysics	not fixed	CVN or EAVN, more than 4 st.	1024 Mbps
IVS-(AOV, APSG, CRDS, CRF, RD)	Geodesy	>10	Global, up to more than 10 st.	256/1024 Mbps
VEPS	Astrometry	6	east Asian and Australian, 3 or 4 st.	2048 Mbps

3 Some Results

3.1 IVS and Astrometric Programs

Thus far, there were 15 IVS sessions (including eight CRF, three AOV, two APSG, one AUG, and one CRDS sessions) processed and databases given out to the Analysis Center by the Shanghai correlator. The main time consumption was in the raw data delivery. Three CVN stations including Kunming 40-m, Shanghai 25-m, and Urumqi 26-m participate in regular IVS sessions. The accuracy of their station positions achieves a few centimeters due to these long-term global geodetic sessions. It helps to carry out some astrometric programs based on the three stations. As also presented in these proceedings, an ecliptic plane survey program was based on the above three stations together with one more session with Hobart, Kashima, and Sejong. The capability of the DiFX correlator made it possible to have different quantifications and baseband bandwidth among different stations. In the first phase of observations, there were 435 target sources detected in three or more observations among more than 2000 candidates in the source pool. The detection rate was near 20%. A pulsar astrometry program has conducted with the S-band receivers at the three stations. Five epoch phase-referenced VLBI positionings of the millisecond pulsar B1937+21 were carried out from 2012 to 2015. The signal-to-noise ratio of the pulsar signal was improved by pulsar gating during the correlations. After EOP, station positions, and ionospheric delay correc-

tions, the best fitted proper motion in RA and DEC were 0.1237 ± 0.18 mas/yr and -0.2585 ± 0.52 mas/yr with a problematic parallax $\Pi = -0.678$ mas. Regardless of the parallax, the proper motion parameters were consistent with the 15.5 year timing solutions of $0.087(16)$ mas/yr in RA and $-0.41(3)$ mas/yr in DEC. A deeper analysis is needed for the error mitigation.

3.2 Tianma 65-m Related

The new-built Tianma 65-m radio telescope is about 6.1 km away from the Shanghai 25-m telescope. The receivers that were installed provide a continuous frequency coverage from L-band to Q-band. Two dual-frequency receivers in S/X and X/Ka bands play an important role in the geodetic activities. Besides of single dish observations, Tianma 65-m is also an important site for the VLBI community. Some joint observations with the KaVA, the EVN, and the VLBA have already been carried out in the low frequency bands. Fringes at high frequency bands including X/Ka and Q were found in late 2015 (Figure 4-a, 4-b). The X/Ka experiment was carried out with Tianma-Wettz13n-Zelen13m in RU0197 session. While the Q-band experiment was a Tianma-KaVA joint observation, an ad-hoc room temperature receiver was used in the experiment and the cooled dual-beam receiver is under installation in 2016.

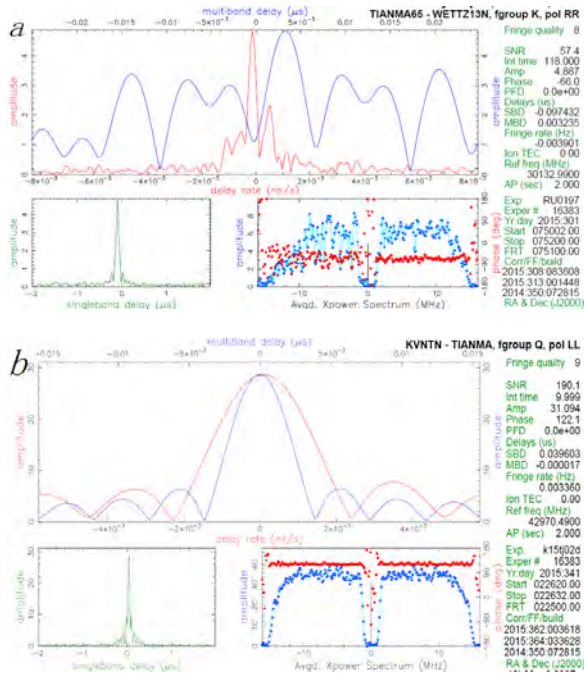


Fig. 4 a. Ka (X/Ka) band fringes to Tianma 65-m. b. Q-band fringes to Tianma 65-m.

4 Conclusions

The DiFX platform at SHAO is dedicated to the astrophysical and the geodetic VLBI observations. It has served as an IVS correlator since 2015. The platform is also open to the CVN and the joint international VLBI observations. Concerning the next generation

broadband and dual polarization VLBI observations, the Shanghai correlator will continue to make its contributions to the data correlation and processing. For the future high data rate and massive data correlations, current network conditions will be one of the bottlenecks and must be improved. A more powerful platform with a high performance computing cluster and a competent storage system is also needed.

Acknowledgements

The work is supported by the National Natural Science Foundation of China (No. Y247021001) and the Joint Funds of the National Natural Science Foundation of China (No. U1331205).

References

1. Deller A T, et al. *PASP*, 2011, 123(901): 275.
2. <http://www.haystack.mit.edu/tech/vlbi/hops.html>.
3. Reardon, D J, et al. *MNRAS*, 2016, 455(2):1751.
4. Shu, F C, et al. *IVS 2014 Annual Report*, 2014.

Hardware Correlator Development at SHAO

Zhijun Xu, Jiangying Gan, Shaoguang Guo

Abstract Hardware correlators have been used in the Chinese Chang'E missions. Recently, a hardware correlator based on uniboard has been developed. This article presents the development of the hardware correlator at SHAO and some results.

Keywords Hardware correlator, FPGA, Uniboard

1 Introduction

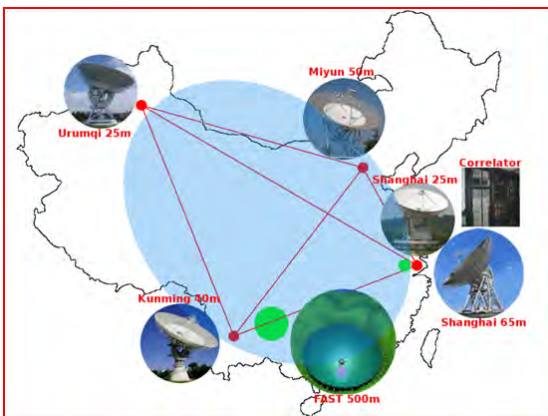


Fig. 1 Chinese VLBI Network.

The Chinese VLBI Network (CVN) has five stations located in Shanghai, Beijing, Kunming, and Urumqi and a VLBI center in Shanghai processing four stations' data in real time. In the Chang'E-1

Shanghai Astronomical Observatory, Chinese Academy of Sciences

project, a Mark IV hardware correlator and, in the Chang'E-2 project, a Mark 5B hardware correlator were used to process the four stations' data in real time, as shown in Figure 2.



Fig. 2 Chang'E-1 and Chang'E-2 hardware correlators.

In the Chang'E-3 and Chang'E-5T1 missions, the Chang'E-3 hardware correlator has been used and performed well. The hardware correlator includes five FPGA boards. Each FPGA board has the same hardware, which consists of one Xilinx Virtex-4 FX60 and four LX160 FPGAs.



Fig. 3 Chang'E-3 hardware correlator.

The FX60 FPGA includes a 1 Gigabit Ethernet port and two embedded PowerPC405 processors for sending and receiving processing data and control information to and from the outside network.

The FX60 also connects to four LX160 FPGAs via a 64-bit bus to send and receive processing data and control information to each LX160 FPGA. Each LX160 FPGA has a 32-bit cPCI bus connection to the mother board, which connects all five FPGA boards. The FPGA board and the correlator pictures are shown in Figure 3.

2 Hardware Correlator in Uniboard

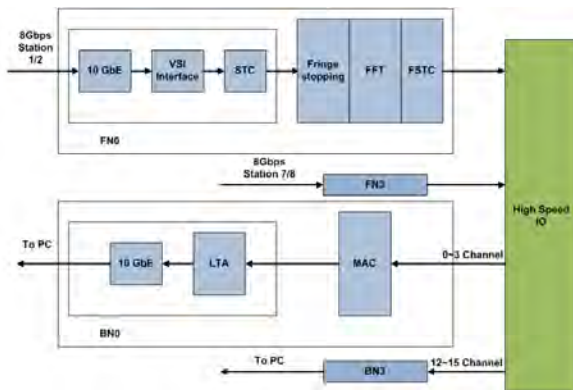


Fig. 4 Previous hardware correlator diagram.

Right now, we are designing the hardware correlator in Uniboard for the next generation correlator. At first we wanted to use the previous design, as shown in Figure 4.

Module	Function	Volume	Max Vol.
10GbE Interface	128MHz*1bits*1station*32channel	8Gbps/chip	30Gbps/chip
Quantification	128MHz*16bits*1station*32channel	128Gbps/chip	/
Fringe Stopping	128MHz*16bits*1station*32channel*2complex	256Gbps/chip	/
FFT	128MHz*16bits*1station*32channel*2complex /2symmetry	128Gbps/chip	/
FSTC	128MHz*16bits*1station*32channel*2complex /2symmetry	128Gbps/chip	/
IO Interface	128MHz*16bits*4station*8channel*2complex /2symmetry	128Gbps/chip	75Gbps/chip
MAC	128MHz*32bits*10baseline*8channel*2complex /2symmetry	640Gbps/chip	/
LTA	(32bits*32channel*2complex*10baseline*1024fft -size/2symmetry)/1s integration	10Mbps/chip	1Gbps/chip

Fig. 5 Data speed table for previous design.

But soon we found that this design will have a speed bottleneck. As shown in Figure 5, in the previous design the IO interface is after FSTC (fractional sample time correction). So when the input data speed is 8 Gbps, a speed of 128 Gbps will be needed after FSTC to accommodate the system, but the IO interface is limited to 75 Gbps, so to address the speed bottleneck, the input speed has to be reduced.

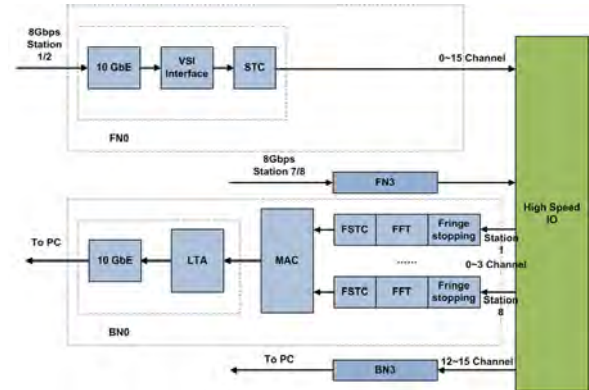


Fig. 6 Uniboard hardware correlator diagram.

As shown in Figure 6, in the recent Uniboard hardware correlator design, we are now moving the IO interface after the data playback.

Module	Function	Volume	Max Vol.
10GbE Interface	256MHz*1bits*1station*32channel	8Gbps/chip	30Gbps/chip
IO Interface	256MHz*1bits*4station*8channel	8Gbps/chip	75Gbps/chip
Quantification	256MHz*16bits*4station*8channel	128Gbps/chip	/
Fringe Stopping	256MHz*16bits*4station*8channel*2complex	256Gbps/chip	/
FFT	256MHz*16bits*4station*8channel*2complex /2symmetry	128Gbps/chip	/
FSTC	256MHz*16bits*4station*8channel*2complex /2symmetry	128Gbps/chip	/
MAC	256MHz*32bits*10baseline*8channel*2complex /2symmetry	640Gbps/chip	/
LTA	(32bits*32channel*2complex*10baseline*1024fft -size/2symmetry)/1s integration	10Mbps/chip	1Gbps/chip

Fig. 7 Data speed table for Uniboard design.

As shown in Figure 7, after the 10GbE interface and data playback, the data speed is still 8 Gbps, so the IO interface does not have a speed bottleneck in this case. The following processing that generates a data explosion will be done inside the FPGA chip, so the system will not have a speed bottleneck.

3 Some Results

Implementation of the previous Uniboard hardware correlator functions has been completed, and we have performed some testing on one source sampled by two CDAS2s, as shown in Figure 8. We also tested the previous Chang'E data and compared the results with the Chang'E-3 hardware correlator. Right now, we are designing the new functions for the next mission.

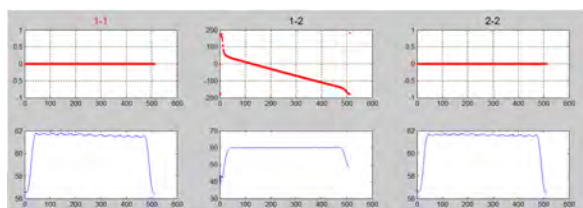


Fig. 8 Test of the same source, sampled by two CDAS2 (16 channel 2 bit 512 MHz BW).

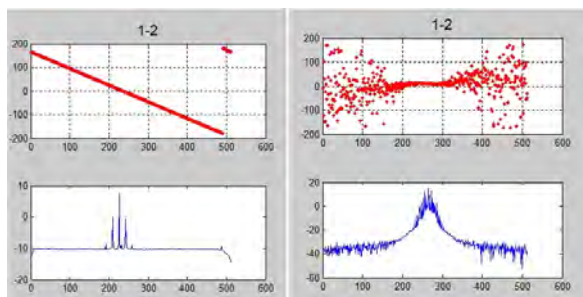


Fig. 9 Test of previous Chang'E data.

4 Future Plans

- Deep Space Correlator will:
 - Be expanded to an eight station, 32 channel system;
 - Support the VDIF VSR format;
 - Support multi-target parallel processing;
 - Support 4, 8 and 16 bit sampled data.
- VGOS Correlator will:
 - Be expanded to a 16 station, 32 channel system;
 - Support a real time mode;
 - Support an output SWIN format;
 - Be updated to Xilinx board or Uniboard2;
 - Support VGOS mode with a maximum of 16 Gbps per station.

References

1. Xu, Z. J., et al. Real Time Correlator in FPGA, in International VLBI Service for Geodesy and Astrometry 2006 General Meeting Proceedings, edited by Dirk Behrend and Karen Baver, NASA/CP-2006-214140, p. 89-92, 2006.
2. Zhang, X. Z., et al. CVN Correlator and its Future, New Technologies in VLBI. Astronomical Society of the Pacific, Conference Series Volumes, v. 306, 287-300, 2003.
3. Zhang, X. Z., et al. Progress of Wideband VLBI Digital System Development at SHAO. IVS 2008 General Meeting Proceedings, "Measuring the Future", edited by Andrey Finkelstein and Dirk Behrend, pp. 381-385, 2008.

High-speed Data Playback of the VLBI Hardware Correlator

Jiangying Gan, Zhijun Xu, Shaoguang Guo

Abstract VLBI (Very Long Baseline Interferometry) is an important radio astronomy technique and is widely used in deep-space probes and high-precision measurements. The performance of the correlator, as the core data pre-processing equipment of VLBI, is very important. At present, the Chinese VLBI data acquisition system (CDAS) can collect 2 Gbps of data, and a multi-band combination can reach 16/32 Gbps. To ensure that the requirements of high speed and high precision are met, Uniboard was used as the hardware platform, 10 G Ethernet was used as the data playback interface, and 1 G Ethernet was used as the control interface. Also research was done into the VLBI data playback, which reaches speeds up to 4 Gbps for a single CDAS, and a pre-processing method that provides data correction and data decoding specific to the VLBI data characteristics has been designed. Now we have finished the preliminary system, and here we will show the design and some results.

Keywords VLBI, Hardware Correlator, data playback, high-speed

1 Introduction

VLBI (Very Long Baseline Interferometry) is an important radio astronomy technique and is widely used in deep-space probes and in high-precision measurements. We have successfully used it to perform VLBI observations for several Chang'E missions [1]. Figure 1 is the Chinese VLBI Center architecture. The

Shanghai Astronomical Observatory

VLBI center is comprised of VLBI stations, data pre-processing, a correlator, a POST correlator, SKD, orbit determination, position determination, and so on. The hardware correlator is the VLBI core data pre-processing equipment, and it can calculate important parameters such as the delay, delay rate, correlation amplitude, interferometric phase, and so on.

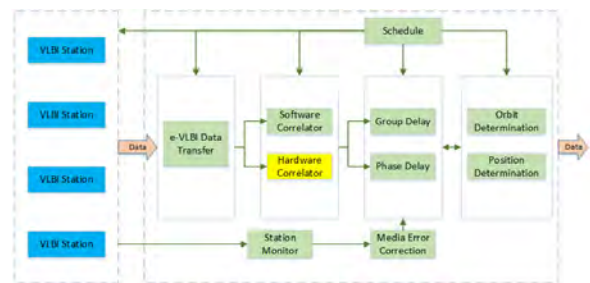


Fig. 1 Chinese VLBI Center.

Already in use, the hardware correlator has five FPGAs, which are configured in two columns. The front column contains four FPGAs to process data from four stations, and the back column contains one FPGA, which processes all channels of data from four stations at the same time. So the speed of the system is restricted. Now, our team has used a Uniboard as the hardware platform. The Uniboard, as the name suggests, is a universal processing platform which will be used in multiple processing applications such as the future EVN correlator. The board consists of eight processing FPGAs configured in two columns. The front column contains the front nodes. These FPGAs are each connected to four 10 GbE SFP+ inputs making copper and optical interfacing possible. Via mesh on the board, a front node is connected to each back node

with a 10 Gbps link. The back side or back node FPGA is connected to a backplane. The control of the board is done via an onboard 1 GbE switch with four copper interfaces on the front panel and eight 1 GbE connections, one for each processing FPGA [2].

2 VLBI Data Playback System

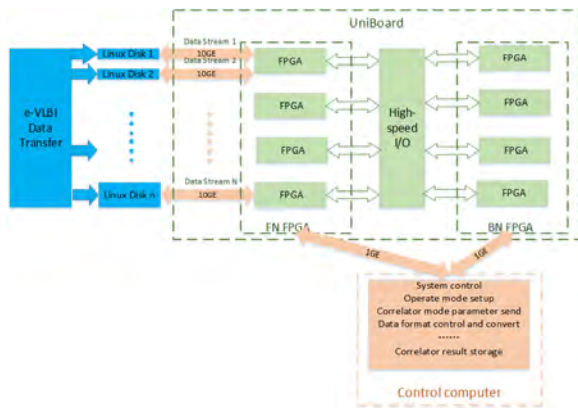


Fig. 2 UniBoard hardware correlator system.

In Figure 2 a block diagram of the UniBoard showing the connections can be seen [3]. The system has characteristics such as:

- Eight processing FPGAs are divided into four front FPGAs and four back FPGAs.
- One station can correspond to one 10 GbE interface, so each front FPGA can accommodate four stations at most.
- Four back FPGAs synchronously process all channels of data, so that data processing can occur more quickly.
- The 1 GbE connection can be used not only to control every board, but also to send the data results to a control computer.

VLBI Data Playback includes a 10 GbE interface, a data playback control module, a data receiver and memory, a strip-head module, a cross switch, a fan-in, a SOPC system, and a 1GbE interface [4]. In Figure 3, the 1 marks the 10 Gb Ethernet interface initialization and control parameters, the 2 marks the playback parameters — including reset, start time, stop time, fan-in code, data bit, FFT size and so on, and the 3 indicates

that frame header information is sent to a control computer in real-time to ensure time synchronization.

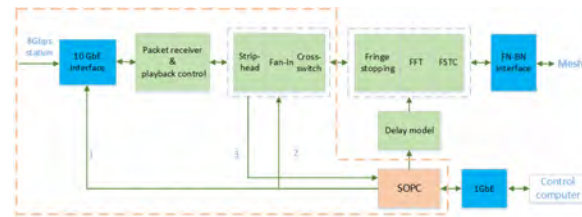


Fig. 3 One station front FPGA.

2.1 10GbE Module

The 10 GbE Network module includes a 10 GbE interface and a data playback control module, which is used to receive data, cache data, and control data playback. Figure 4 is the 10GbE communication and control block diagram. It uses an ACK to control the data playback start or stop. The processing is:

- A Linux disk sends N packets to the FPGA via 10 GbE and waits for a replay packet.
- The FPGA receives N packets and if the post-processing is not full, then sends a replay packet to the Linux disk.
- The Linux disk waits until it receives the ACK packet and then continues to send data packets.

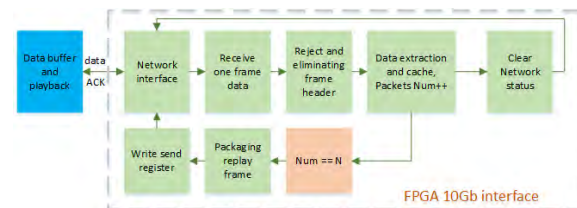


Fig. 4 FPGA 10 G interface.

In theory, the speed of data transmission is 10 G per second for the no load condition and could reach 8 Gbps for pre-processing, but it only reaches 4 Gbps in fact.

2.2 SOPC

The SOPC system is the bridge between the embedded software core system and the hardware IP module, intended to maintain data communication on both sides. The embedded software system NiosII's main functions are to:

- Receive and analyze the network packets and write data to the corresponding hardware IP module.
- Receive data from the hardware IP module and process and send information to the control computer.

The 1 GbE is used to receive data from the control computer and send the data to the target computer. The 1 GbE receives parameter packages for each processing FPGA and sends confirmation information. It also sends results to a PC when the TX data mode is triggered. The 1 GbE Ethernet transmission has two operating modes:

1. RX-TX mode. Receives the 1 GbE packets at first and sends replay packets afterwards.
2. TX only. Packages and sends data to the control computer under control.

Figure 5 shows the RX-TX mode working state.

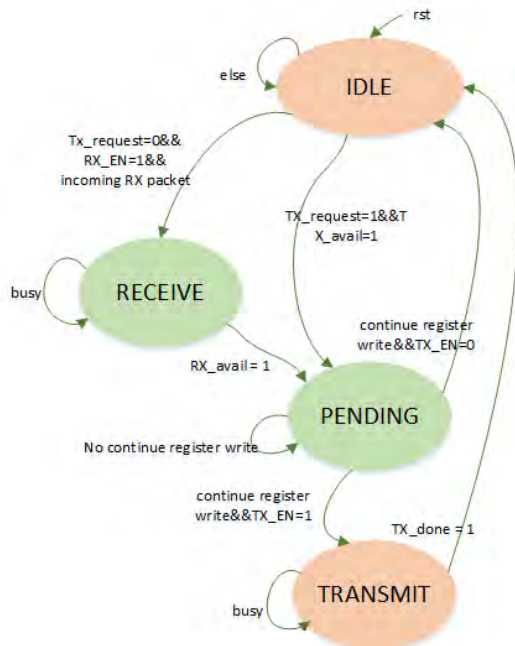


Fig. 5 1 GbE RX-TX mode.

3 Analysis

Figure 6 shows the results of real-time correlation of the data from the CE5-T1 (Chinese Lunar Mission). There are four stations, but the pictures only show two stations. Real-time correlation of the mission data gives the same results as are obtained from correlation using the current correlator.

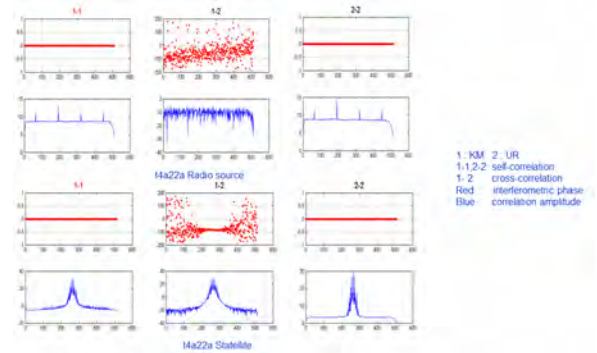


Fig. 6 Results of correlation.

4 Conclusions

The Uniboard correlator has already been finished, and some of its characteristics are shown in Table 1.

Table 1 Characteristics of the Uniboard correlator.

Mode	Near Real-time	Real-time
10 GbE Interface	4 Gbps	8 Gbps
IO Interface	6.25 Gbps	6.25 Gbps
Delay Tolerance	20 s	1 s
Buffering	Disk	Memory
Design Difficulty	10 GbE, high speed IO	DDR3, System
Applications	Deep space exploration	VGOS, SKA

But some capabilities need to be improved, and more astronomical applications will be added.

5 Future Plan

As a near-real-time-style correlator, the data latency needs to be fewer than 25 seconds during the CE-3 mis-

sion [5], and the number of stations must be fewer than five. So some work must still be done to meet more requirements for the new mission, such as: like:

- Support of 4, 8, and 16 bit sampled data,
- VDIF, VSR format data playback,
- Support of more stations (six/eight or more),
- Multi-target processing,
- Multi-bandwidth processing, and
- Adding DDR3 to cache data.

References

1. X. Z. Zhang, "CVN Correlator and Its Future", New Technologies in VLBI Astronomical Society of the Pacific Conference Series, pages 287–300, 2012.
2. Jonathan Hargreaves, Harro Verkouter, "EVN Correlator Design, Version 2.0", http://www.radionet-eu.org/fp7/wiki/lib/exe/fetch.php?media=jra:uniboard:evn_correlator_design_mar2011.pdf.
3. Zhijun Xu, Jiangying Gan, Shaoguang Guo, Xiuzhong Zhang, Renjie Zhu, Yajun Wu, Ying Xiang, "Hardware Correlator Development at SHAO", In IVS 2014 General Meeting Proceedings, edited by Dirk Behrend, Karen D. Baver, and Kyla L. Armstrong, Science Press (Beijing), ISBN 978-7-03-042974-2, pages 228-230, 2014.
4. Jiangying Gan, Zhijun Xu, Xiuzhong Zhang, Shaoguang Guo, Renjie Zhu, Ying Xiang, "VLBI Data Playback in FPGA", In IVS 2014 General Meeting Proceedings, edited by Dirk Behrend, Karen D. Baver, and Kyla L. Armstrong, Science Press (Beijing), ISBN 978-7-03-042974-2, pages 219-223, 2014.
5. Weimin Zheng, Juan Zhang, Yun Yu, Wenbin Wang, Tong Li, "Software Correlator in the Chang'E-3 Mission", In IVS 2014 General Meeting Proceedings, edited by Dirk Behrend, Karen D. Baver, and Kyla L. Armstrong, Science Press (Beijing), ISBN 978-7-03-042974-2, pages 188-190, 2014.

Difxcalc – Calc11 for the DiFX Correlator

David Gordon¹, Walter Brisken², Walter Max-Moerbeck³

Abstract A new program, difxcalc, has been created from calc11 to produce the interferometer model files for the DiFX software correlator. Difxcalc is a stand-alone program intended as a replacement for the calc9.12 calcserver program currently used by DiFX. It handles both infinite distance sources and finite distance sources.

Keywords DiFX correlator, calc11, near-field models

1 Introduction

The Calc program dates back to the late 1970s with the first version developed by Chopo Ma at GSFC. Calc computes a theoretical VLBI delay between two radio telescopes using models of nutation, precession, polar motion, Earth rotation, and various geophysical models to account for phenomena such as solid Earth tides, pole tides, ocean loading, and other effects. Calc has been updated numerous times since its inception to include improved models, and it is now at version 11. Calc was originally written in Fortran 77 and is now in Fortran 90. Calc has been tied to the Mark III database handler since its inception, which also dates to the late 1970s. This system has been the standard for geodetic VLBI since its inception, but it has made using calc difficult for other purposes. Still, various versions have been incorporated into most of the world's VLBI correlators beginning with the Mark III correlators in the early 1980s. The DiFX [1] software corre-

lator currently uses calc version 9.12 in the form of an RPC server. This version is somewhat out-of-date, especially with respect to the nutation/precession model.

2 What Is Difxcalc?

Because of the complications involved in using calc for correlation, it was desired to create a version specifically for DiFX correlator usage. During the update from version 10 to 11, calc was restructured to consolidate all Mark III database calls (ADDs, GETs, and PUTs) into a single module. For the correlator version, this module was then replaced with new input, initialization, and output routines designed to work with DiFX. The flow of the program was also modified to eliminate many computations not needed for correlation. Also, the ability to compute delays for near-field targets (Earth satellites, planetary spacecraft, or other solar system objects) was added. D. Gordon at GSFC worked with W. Brisken at NRAO/Socorro to smooth out initial problems and get difxcalc working properly.

Difxcalc uses many of the same modules as calc11 but has different inputs and outputs and does not use any Mark III database calls. It gets most of its input from the '.calc' files that are created during the DiFX processing stream. It also reads the JPL DE421 ephemeris, an ocean loading coefficients file, an ocean pole tide coefficients file, and an antenna fixed axis tilt file (for Pietown). To work in the near-field mode, it also requires a 'SPACECRAFT' section in the .calc file giving the near field object's coordinates, velocities and epochs. The output of difxcalc is a standard '.im' correlator model file, where the delays and other quantities are represented by fifth degree polynomials for

1. NVI, Inc.

2. NRAO

3. Max-Planck-Institute for Radioastronomy

two-minute intervals. Difxcalc works in the geocenter mode (reference station at the geocenter) but could be easily modified to work in a baseline mode.

Difxcalc contains three separate near-field models. Because of initial difficulties with the Sekido-Fukushima near-field model [2] (which are still being investigated), the Duev near-field model [3] and the satellite ranging model of the IERS Conventions (2010) [4] were both added. Near-field correlation is still an open subject with several different models available that all produce slightly different delays.

Difxcalc is also designed to handle correlator jobs with multiple phase centers. Because of the way difxcalc is structured, it should run much faster than the calc9.12 calcservice when many phase centers are used.

3 Difxcalc vs. Calc9.12

Difxcalc and calc11 use the IAU2006/2000 precession/nutation model, whereas calc9.12 uses the IERS 1996 precession/nutation model, which was an earlier fit to VLBI and lunar laser ranging data. This can result in differences of typically 1–2 milli-arc-seconds (mas) in the precession/nutation angles, which can produce typically 3–6 cm differences in the J2000 site positions. This can in turn, give delay differences of ~50–100 psec or so on long baselines. Also, small changes in the solid Earth tides, ocean loading, the pole tide, and the Earth rotation angle can result in effective site position changes of around a centimeter or more. Difxcalc also models the ~3 arc-minute tilt of the Pietown antenna, which can result in differences of up to around ± 7 psec on Pietown baselines. Difxcalc also has the new ocean pole tide correction and high frequency corrections to UT1 and polar motion, which can produce mm level changes from calc9.12.

4 Difxcalc Validation

Difxcalc has been tested at the VLBA¹ by W. Brisken and W. Max-Moerbeck. Some tests of the regular (far-

¹ The VLBA is operated by the National Radio Astronomy Observatory, which is a facility of the National Science Foundation and is operated under cooperative agreement by Associated Universities, Inc.

field) model are reported in ‘VLBA Sensitivity Upgrade Memo 45’². Delay differences from calc9.12 approaching 100 psec were found. Mostly these were smooth differences for a given source and indicative of small (cm level) differences in the J2000 site positions due to the model differences described in the previous section. Maps made from the same observations correlated with the two versions showed only small differences, with perhaps slightly better results from difxcalc. Near-field tests have also been conducted by W. Brisken using some GPS satellite observations. Fairly good results were obtained using the Duev near-field model.

5 Reasons to Switch to Difxcalc

There are numerous reasons for DiFX correlator users to switch to difxcalc. Difxcalc is a stand-alone program that is well-integrated with DiFX. Unlike the standard calc9.12 implementation currently used in the DiFX suite, difxcalc does not require running an RPC server process. Running of this process is a common stumbling block for new users and during migration to new operating systems, due to the operating system quirks associated with RPC. Difxcalc also uses the latest geophysical models [4], as well as modelling the tilt of the Pietown antenna. It contains three near-field models and has the geometry in place for other possible near-field models. Its structure should also enable much faster generation of .im files for jobs using many phase centers.

Another reason to switch from the calc9.12 calcservice to difxcalc is for consistency between the model and the aprioris. Most DiFX astronomy users get site positions from the SCHED sites catalog, and these positions come from a calc11 solution at GSFC. Most users also get their Earth orientation parameters (EOPs) from GSFC’s version of the ‘usno_finals.erp’ file, which comes from USNO but is rotated to match the GSFC calc11 solution. Therefore, greater consistency between the model and the aprioris will be obtained with difxcalc. This should produce better imaging, particularly when phase-referencing is not used.

² http://library.nrao.edu/public/memos/vlba/up/VLBASU_45.pdf

6 Additional Work

Some additional work still needs to be done on difxcalc before it can completely replace the calc9.12 calcserver. The computation of U, V, W coordinates needs to be modified to match the way it is currently done by the calc9.12 calcserver. Also, support for RadioAstron observations is planned but not yet implemented. And some miscellaneous operational changes will be made. Future upgrades could include improvements in the atmosphere delay computations, or options to use GPS ionosphere maps for ionosphere corrections. Suggestions for future enhancements are welcome. Difxcalc should also be usable with other correlators, perhaps with some modifications required. Contact D. Gordon if you are interested in that possibility.

References

1. Deller, A.T., Brisken, W.F., Phillips, C.J., Morgan, J., Alef, W., Cappallo, R., Middelberg, E., Romney, J., Rottmann, H., Tingay, S.J., and Wayth, R., 'DiFX-2: A More Flexible, Efficient, Robust, and Powerful Software Correlator', 2011, Publications of the Astronomical Society of the Pacific (PASP), 123, 275. doi:10.1086/658907.
2. Sekido, M. and Fukushima, T., 'A VLBI delay model for radio sources at a finite distance', 2006, J. Geodesy, 80, 137. doi:10.1007/s00190-006-0035-y.
3. Duev, D.A., Molera Calvés, G., Pogrebenko, S.V., Gurvits, L.I., Cimó, G., and Bocanegra Bahamon, T., 'Spacecraft VLBI and Doppler tracking: algorithms and implementation', 2012, Astronomy and Astrophysics, 541, A43. doi:10.1051/0004-6361/201218885.
4. Petit, G. & Luzum, B. (editors), 2010, IERS Conventions (2010), IERS Technical Note No. 36, (Frankfurt am Main: Verlag des Bundesamts für Kartographie und Geodäsie). (<http://www.iers.org/TN36>).

Session 4: Data Structures and Analysis Strategies in the VGOS Era



March 2016 · Johannesburg · South Africa

Constraining Least-Squares VLBI Solutions

Thomas Artz, Sebastian Halsig, Andreas Iddink, Axel Nothnagel, Corinna Tegtmeier

Abstract In a traditional least-squares adjustment of parameters to the Very Long Baseline Interferometry (VLBI) observations, typically tropospheric as well as clock parameters are determined in the form of continuous piece-wise linear functions with a given temporal resolution. As the VLBI observations are not equidistant, but on the contrary exhibit gaps of sometimes several hours, singularities arise due to unresolvable parameters inside these gaps. For this reason, it is common practice to constrain the respective parameters in the solution. In this paper we analyze the singularities that arise within the geodetic VLBI data analysis by means of a Singular Value Decomposition of the Jacobian matrix. Furthermore, we show the ramifications of traditional constraining. Finally, we present an alternative approach for optimizing the least-squares solution by omitting the constraints within the VLBI solution and performing a Tikhonov regularization. In this way, we obtain a minimally regularized solution, which leads to reliable target parameters without being influenced by constraints on auxiliary parameters such as clocks or troposphere.

Keywords VLBI, least-squares adjustment, constraints, Tikhonov regularization

1 Introduction

Geodetic Very Long Baseline Interferometry (VLBI) observations are used for the determination of fundamental geophysical parameters, such as, e.g., Earth ori-

Institute of Geodesy and Geoinformation, University of Bonn

entation parameters (EOPs), as well as the celestial and terrestrial reference frames (CRF and TRF). This parameter estimation is typically done in a classical least-squares adjustment. Together with the mentioned target parameters, auxiliary parameters have to be estimated with high temporal resolutions even below one hour. In most cases, these are parameters for clock synchronization as well as tropospheric parameters.

In a routine parameter estimation process, a single solution set-up is chosen to process a lot of VLBI sessions. Unfortunately, not all sessions permit estimation of the entire set of parameters, leading to instabilities of the least-squares solution, which are typically cured by adding constraint equations, whether needed or not. Basically, there are two reasons for these singularities. On the one hand, radio telescopes might miss observations due to various reasons, e.g., too strong winds; data gaps of up to several hours can appear. On the other hand, some observing network geometries are not sensitive for all of the parameters.

Even in the next generation VLBI Global Observing System (VGOS, [4]) era, where large global networks will operate with high data rates, the constraining still might be an issue. Especially, when automatic processing is considered due to the huge number of observations, this will become a crucial point which has to be handled with care.

2 Least-Squares Adjustment and Diagnosis by Singular Value Decomposition

In most of the VLBI analysis packages, an ordinary least-squares approach [3] is chosen to estimate the

necessary parameters \mathbf{x} from the observations \mathbf{b} . The basic idea of the least-squares adjustment is to minimize the sum of the squared residuals \mathbf{r} to deal with the overdetermined linear or linearized equation system

$$\mathbf{b} + \mathbf{r} = \mathbf{A}\mathbf{x} \quad (1)$$

where the matrix \mathbf{A} represents the linear(ized) relationship between observations and parameters, i.e., the Jacobian matrix $\mathbf{A} = \partial\mathbf{b}/\partial\mathbf{x}$. In other words, a solution has to be found, where the gradient of the residuals vanishes. This directly leads to the solution via the normal equations

$$\mathbf{x} = (\mathbf{A}^T \boldsymbol{\Sigma}_{bb}^{-1} \mathbf{A})^{-1} \mathbf{A}^T \boldsymbol{\Sigma}_{bb}^{-1} \mathbf{b}, \quad (2)$$

where a weighting is included based on the inverted covariance matrix of the observations $\boldsymbol{\Sigma}_{bb}$.

Applying a Cholesky decomposition [1] on the weight matrix

$$\boldsymbol{\Sigma}_{bb}^{-1} = \mathbf{R}^T \mathbf{R}, \quad (3)$$

leads to a full de-correlation and, thus, to a modified Jacobian matrix and observation vector

$$\mathbf{X} = \mathbf{R}\mathbf{A}, \quad \boldsymbol{\xi} = \mathbf{R}\mathbf{b} \quad (4)$$

$$\Rightarrow \mathbf{x} = (\mathbf{A}^T \mathbf{R}^T \mathbf{R} \mathbf{A})^{-1} \mathbf{A}^T \mathbf{R}^T \mathbf{R} \mathbf{b} \quad (5)$$

$$= (\mathbf{X}^T \mathbf{X})^{-1} \mathbf{X} \boldsymbol{\xi}. \quad (6)$$

Finally, a Singular Value Decomposition (SVD, [1]) of the transformed Jacobian matrix can be performed

$$\mathbf{X} = \mathbf{U}\mathbf{S}\mathbf{V}^T \quad (7)$$

leading to a new representation of the solution [1]

$$\mathbf{x} = \sum_i \frac{\mathbf{u}_i^T \boldsymbol{\xi}}{s_i} \mathbf{v}_i. \quad (8)$$

Obviously, problems arise if (numerically) zero singular values s_i exist, because in this case the null space of the Jacobian matrix does not disappear, i.e., some parameters are not indeterminable. Thus, the SVD can be used as a tool to diagnose the numerical stability of the solution. If a singular value s_i is numerically zero, the largest entries of the corresponding right singular vector \mathbf{v}_i indicate weakly or undefined parameters. Furthermore, this singular vector is a base vector of the null space.

3 Effects of Standard Constraints

Typically, a stabilization of the least-squares adjustment can be achieved by constraining the solution, i.e., by adding some pseudo-observations which have sufficient information in the null space. Thus, a constraint matrix \mathbf{C} with corresponding standard deviations can be constructed and added to the normal equations (Eq. 2)

$$\mathbf{x} = (\mathbf{A}^T \boldsymbol{\Sigma}_{bb}^{-1} \mathbf{A} + \mathbf{C}^T \boldsymbol{\Sigma}_{cc}^{-1} \mathbf{C})^{-1} \mathbf{A}^T \boldsymbol{\Sigma}_{bb}^{-1} \mathbf{b} \quad (9)$$

as the constraints and the original observations are uncorrelated and the actual pseudo-observations are zero. If the solution should be solved and analyzed by means of SVD, the constraining can be equally achieved by extending the corresponding matrices and vectors

$$\mathbf{A} = \begin{pmatrix} \mathbf{A} \\ \mathbf{C} \end{pmatrix}, \quad \mathbf{b} = \begin{pmatrix} \mathbf{b} \\ \mathbf{0} \end{pmatrix}, \quad \boldsymbol{\Sigma}_{bb} = \begin{pmatrix} \boldsymbol{\Sigma}_{bb} & \mathbf{0} \\ \mathbf{0} & \boldsymbol{\Sigma}_{cc} \end{pmatrix}. \quad (10)$$

It is important to note that the constraints do not have to be the basis of the null space. They only need to have components in the null space.

In routine VLBI data analysis, three types of constraints are relevant. These are offset constraints, rate constraints, and no net translation/no net rotation conditions to define the geodetic datum. In this paper, we focus on offset constraints which force a parameter to be zero where a column of the constraint matrix has the form

$$\mathbf{C}_i = (0 \dots 0 \ 1 \ 0 \dots).$$

Furthermore, rate constraints

$$\mathbf{C}_i = (0 \dots 1 \ -1 \ 0 \dots)$$

are investigated, which force the difference between two parameters to be zero. To overcome the datum deficiency, station and quasar positions are simply not estimated. Thus, only the EOPs are estimated as well as clock parameters (quadratic polynomial and continuous piece-wise linear functions (CPWLF) with a resolution of 1 h), zenith wet delays (ZWDs, 1 h CPWLF), and tropospheric gradients (1 d CPWLF). All auxiliary parameters are set up per station; however, the clock parameters for one station need to be fixed to realize a reference.

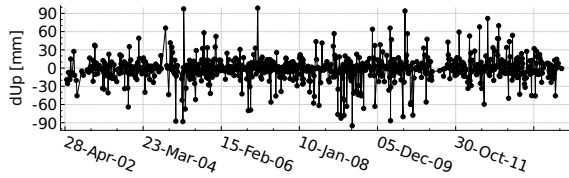


Fig. 1 Height differences for the station TIGOCONC with two different weights for the troposphere constraints. Note that larger differences (> 100 mm) are excluded.

In mass processing of VLBI sessions (batch solutions), a set of offset and rate constraints are always applied regardless of whether the null space of the Jacobian matrix exists or not. Thus, often constraining information is added although it is not necessary. To evaluate this procedure, we performed two different solutions:

1. with standard constraints
 - $\sigma_{ZWD_{rate}} = 40$ ps/h
 - $\sigma_{grad_{offset}} = 1$ mm, $\sigma_{grad_{rate}} = 2$ mm/d
 - $\sigma_{clock_{rate}} = 10^{-14}$
2. with modified weights for the constraint equations
 - $\sigma_{ZWD_{rate}} = 10$ ns/h
 - $\sigma_{grad_{offset}} = 0$ mm, $\sigma_{grad_{rate}} = 0$ mm/d
 - $\sigma_{clock_{rate}} = 10^{-14}$

for VLBI sessions between 2000.0 and 2016.0. With the modified set-up, about 15% of the solutions failed, indicating that the constraints have been necessary. However, for the other sessions differences appear up to the decimeter level (see Figure 1). Even for the currently best VLBI dataset from the continuous VLBI campaign 2014, height differences of up to 7 mm appear (not shown here) indicating that the effects are also relevant in the VGOS era. However, it has to be noted that the differences are typically not significant when compared to the standard deviations of the parameters.

4 Development of an Alternative Approach

When investigating the least-squares solution without any constraint, always a rank deficiency is present. As can be seen in Figure 2, the null space of the Jacobian

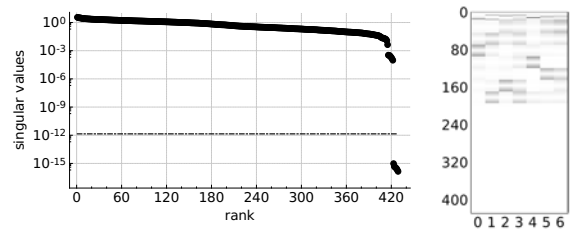


Fig. 2 Singular values (left) and null space of the Jacobian matrix (right). The rank deficiency of seven is related to eight sessions in this experiment, and the basis vectors of the null space are dominated by clock polynomial parameters (one station is the reference station).

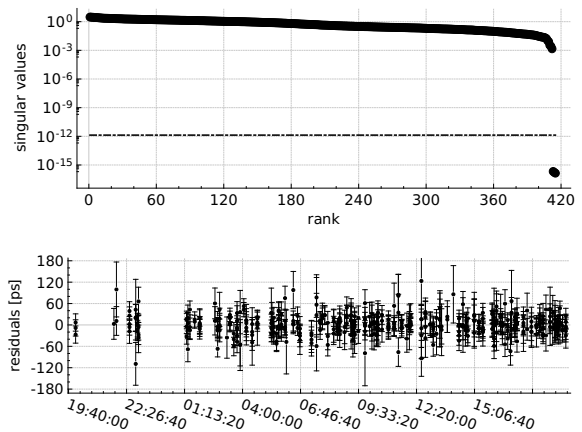


Fig. 3 Singular values (top) for the session 02OCT16XA and the residuals for ALGOPARK from the standard solution (bottom) representing the temporal distribution of the observations.

matrix is dominated by the linear and quadratic clock polynomial parameters. Thus, eliminating the clock polynomials from the functional model of the least-squares solution leads to a regular solution for a well-observed session. In this case, a solution without any constraints leads to a reasonable result with a weighted root mean squared (WRMS) post-fit residual of 27.2 ps, which is 0.3 ps below the WRMS of the standard constrained solution with full clock set-up. However, for another session the approach fails (see Figure 3) due to observation gaps for the station ALGOPARK. These gaps lead to an over-parameterization and, thus, to a singularity. However, none of the parameters are entirely undefined. As a consequence, simply dropping individual parameters is not a feasible approach.

Unfortunately, for this session there are a few observations in every parameterization interval causing a

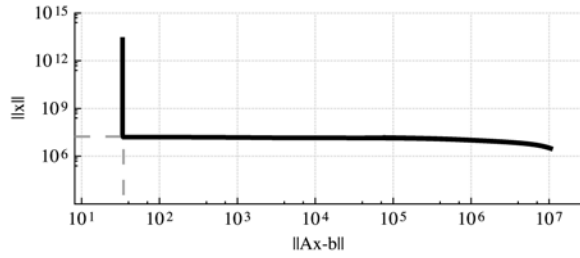


Fig. 4 L-curve, i.e., plot of the solution norm w.r.t. residual norm, which is used to determine the regularization parameter depending on the solution representing the corner.

bad condition of the least-squares problem. To overcome this without the need for constraining, a regularization can be performed. Here, the Tikhonov regularization [5] has been chosen, where the squared parameter norm is minimized in addition to the squared residual norm

$$\min_x \{ \|\mathbf{Ax} - \mathbf{b}\|_2^2 + \lambda^2 \|\mathbf{x}\|_2^2 \}. \quad (11)$$

The Tikhonov parameter λ is considered to balance between smoothing the estimates and minimizing the residuals. In the actual solution, the regularization parameter is used to filter out the impact of the small singular values

$$f_i = \frac{s_i^2}{\lambda_i^2 + s_i^2}, \quad (12)$$

$$\mathbf{x}_{filtered} = \sum_{i=1}^n f_i \frac{\mathbf{u}_i^T \boldsymbol{\xi}}{s_i} \mathbf{v}_i. \quad (13)$$

Thus, the singularity of the initial approach is eliminated. However, the choice of λ is crucial for the success of this approach.

There are various possibilities for choosing the Tikhonov parameter. We make use of the so-called L-curve [2] (see Figure 4), which is a plot of the size of the regularized solution versus the size of the corresponding residual norm for all valid regularization parameters. To obtain this curve, 200 solutions are performed where the minimal and the maximal λ are chosen according to the singular values

$$\begin{aligned} \lambda_{min} &= \max[s_{min}, \varepsilon \cdot s_{max}] \\ \lambda_{max} &= s_{max} \end{aligned} \quad (14)$$

with a tiny value ε , which is sixteen times the next positive representable value after zero. The optimal regularization is the one in the lower left corner of the L-shape as this represents minimal smoothing of the parameters and minimal residual norm.

This procedure, i.e., a totally unconstrained solution with hourly clocks and ZWDs as well as daily tropospheric gradients and the full set of EOPs, has been applied to the continuous VLBI campaign 2002. For sessions where rank deficiencies appear, parameters without any observations have been eliminated. If further ill-conditioning has been present, the Tikhonov regularization parameter has been determined from the L-curve and used for the regularized solution. The resulting UT1–TAI time series is depicted in Figure 5. Slight differences can be seen between our new solution and the standard approach. However, these are only indirect changes of one of the target parameters due to modified handling of the auxiliary parameters.

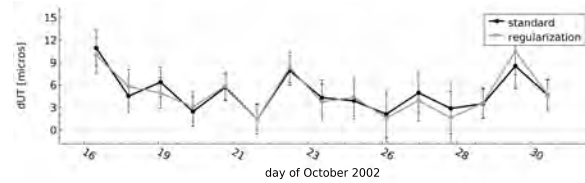


Fig. 5 UT1–TAI for the standard (black) and the new regularized approach without constraints (gray).

In Figure 6 the effects on ZWDs are shown. On the one hand it can be noted that fixing the clock polynomials has only a minor effect on the ZWDs.

This step is one of the necessary changes of our new approach, as it eliminates extremely high correlations between the clock parameters and, thus, allows for neglecting the constraint equations. On the other hand it can be seen from Figure 6 that the parameters which are affected by the regularization have no physical meaning as they are far too large. However, they can easily be declared as outliers if ZWDs should be investigated. Thus, the new approach can be considered successful as no constraints are necessary for the regularized solutions. The resulting time series of target parameters are, therefore, not influenced by model assumptions.

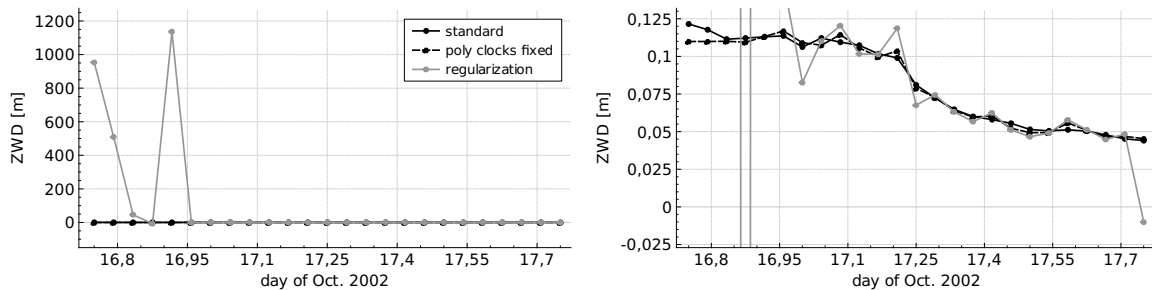


Fig. 6 ZWDs for the standard solution (black circles), a solution without clock polynomials but with constraints (black triangles w/ dashed lines) and the new regularized approach without constraints (gray diamonds). The entire times series (left), clearly shows the outliers for regularized parameters. The zoom to a reasonable range of the parameters (right), however, shows that the other parameter estimates are reasonable.

5 Conclusions

We analyzed the effect of routinely applied constraint equations in VLBI data analysis. The reason for these constraints, which are usually applied in the form of pseudo-observations weighted by standard deviations, are implied to overcome deficiencies in the solution set-up. For instance, the observing geometry might not allow for estimating tropospheric gradients if the local hemispheres above any telescope are not regularly sampled. Furthermore, gaps in the observations can lead to some over-parameterization.

We have shown that changing the standard deviations of the tropospheric parameters can lead to station position changes at the cm-level. Even for the currently most precise set of observations from the continuous VLBI campaign 2014, changes of the station positions of up to 7 mm have been detected.

Furthermore, we demonstrated that it is not possible to simply remove the constraints even for sessions where almost perfect data distribution is given. The reason is the set-up for the clock synchronization where second degree polynomials are estimated simultaneously with CPWLF leading to high mathematical correlations. By removing the clock polynomials, still a reasonable solution can be derived. Subsequently, it is possible to eliminate all constraint equations if the data distribution is homogeneous over a session. If this is not the case, still rank deficiencies appear. With our modified solution approach implementing the Tikhonov regularization we, however, are able to deal with such situations without applying constraints. In this way, we derive time series of target pa-

rameters that are not influenced by model assumptions. Parameters which are strongly affected by the filtering process as they represent the null space of the Jacobian matrix are derived with unrealistic estimates. However, these could be handled as outliers in, e.g., an analysis of ZWDs.

Thus, we presented a new approach for geodetic VLBI data analysis. This approach is not based on any constraint equations and, therefore, permits a set-up for the VGOS era where the equation system is stabilized only in situations where it is necessary.

References

1. J. W. Demmel (1997) Applied numerical linear algebra. Siam, Philadelphia.
2. P.C. Hansen (1999) The L-curve and its use in the numerical treatment of inverse problems. IMM, Department of Mathematical Modelling, Technical University of Denmark.
3. K.R. Koch (1999) Parameter Estimation and Hypothesis Testing in Linear Models, vol 2., upd. and enl. ed. Springer, Berlin; Heidelberg; New York; Barcelona; Hong Kong; London; Milan; Paris; Singapore; Tokyo.
4. A. Niell., C. Beaudoin, R. Cappallo, B. Corey, M. Titus (2013) First results with the GGAO12M VGOS System, *In: Proceedings of the 21nd European VLBI Group for Geodesy and Astrometry Working Meeting*, Helsinki, Finland, Reports of the Finnish Geodetic Institute, ISBN: 978-951-711-206-3, 217–221.
5. A. Tikhonov, V.Y. Arsenin (1977) Solutions of ill-posed problems. 1977. Wiley, New York.

Robust Ambiguity Estimation for an Automated Analysis of the Intensive Sessions

Niko Kareinen, Thomas Hobiger, Rüdiger Haas

Abstract Very Long Baseline Interferometry (VLBI) is a unique space-geodetic technique that can directly determine the Earth's phase of rotation, namely UT1. The daily estimates of the difference between UT1 and Coordinated Universal Time (UTC) are computed from one-hour long VLBI Intensive sessions. These sessions are essential for providing timely UT1 estimates for satellite navigation systems. To produce timely UT1 estimates, efforts have been made to completely automate the analysis of VLBI Intensive sessions. This requires automated processing of X- and S-band group delays. These data often contain an unknown number of integer ambiguities in the observed group delays. In an automated analysis with the `c5++` software the standard approach in resolving the ambiguities is to perform a simplified parameter estimation using a least-squares adjustment (L2-norm minimization). We implement the robust L1-norm with an alternative estimation method in `c5++`. The implemented method is used to automatically estimate the ambiguities in VLBI Intensive sessions for the Kokee–Wettzell baseline. The results are compared to an analysis setup where the ambiguity estimation is computed using the L2-norm. Additionally, we investigate three alternative weighting strategies for the ambiguity estimation. The results show that in automated analysis the L1-norm resolves ambiguities better than the L2-norm. The use of the L1-norm leads to a significantly higher number of good quality UT1-UTC estimates with each of the three weighting strategies.

Keywords VLBI, UT1, robust estimation, ambiguities, Intensives

Chalmers University of Technology

1 Introduction

VLBI is a unique space-geodetic technique capable of simultaneously determining all Earth Orientation Parameters (EOPs). These parameters include Universal Time (UT1), the Earth's phase of rotation. Space-geodetic techniques such as Global Satellite Navigation Systems (GNSS) depend on regular UT1 estimates from VLBI. For this purpose the International VLBI Service for Geodesy and Astrometry (IVS) [1] organizes daily one-hour Intensive (INT) VLBI sessions to provide timely UT1-UTC estimates. The currently observed INT sessions include the INT1 (Kokee–Wettzell, Monday to Friday), INT2 (Tsukuba–Wettzell, Saturday and Sunday), and INT3 (Wettzell, Tsukuba, and Ny-Ålesund, Monday) series.

The relatively low number of observations and the baseline geometry of the INT sessions pose challenges for the data analysis and limit the UT1-UTC accuracy that can be achieved. To produce timely UT1 estimates the turnaround time of the INT sessions needs to be minimized. This requires a streamlined VLBI processing chain. A way to achieve this is to automatically process and analyze the data. Aspects and results related to automated near-real time analysis of INT sessions have been demonstrated in, e.g., Hobiger et. al. (2010) [2] and Kareinen et. al. (2015) [3]. The operational INT sessions are observed on the legacy S/X frequency band. The two bands are formed by individual channels, which are in the post-correlation process combined on the respective bands using the bandwidth synthesis technique [4]. This leads to an unknown number of integer ambiguities in the observed group delays. These ambiguities need to be resolved before ionospheric calibration and parameter estima-

tion. If unresolved, the group delay ambiguities will propagate into the UT1-UTC estimates.

C5++ [2], Vienna VLBI Software (VieVS) [5], CALC/SOLVE [6], GEOSAT [7], and OCCAM [8] are some of the currently used VLBI software packages. Of these software packages only c5++ and CALC/SOLVE are able to resolve the group delay ambiguities and to produce ambiguity-free and ionosphere-free X-band databases.

The standard parameter estimation method in these VLBI software packages is the least-squares adjustment [9] (i.e., L2-norm minimization). In this work we implement the robust L1-norm for the parameter estimation and apply it to automatically resolve the ambiguities in the INT sessions. Starting from Version 1 databases, we use a modified version of c5++ which includes the implemented L1-norm estimation to analyze and estimate UT1-UTC from 1,885 INT1 sessions observed between 2001 and 2015.

2 L1-norm Minimization

Both the L1- and L2-norm minimizations can be derived from the general expression for a p-norm, which is given by

$$\|x\|_p = \left(\sum_{i=1}^p |x_i|^p \right)^{\frac{1}{p}}. \quad (1)$$

The objective functions to be minimized for the L1- and L2-norms are given respectively by

$$\text{L1} : \mathbf{p}^T |\mathbf{v}| \rightarrow \min, \quad (2)$$

$$\text{L2} : \mathbf{v}^T \mathbf{P} \mathbf{v} \rightarrow \min. \quad (3)$$

With the L2-norm the absolute value in the summand disappears. Thus it can be solved analytically, making it computationally straightforward. For the L1-norm, however, the absolute value of the residual vector \mathbf{v} remains. Thus, the objective function is not differentiable at zero, and we are unable to directly derive the value for the vector of unknowns \mathbf{x} that will minimize the sum of the weighted absolute values of the residuals.

The formulation for an L1-norm minimization was described in, e.g., Amiri-Simkooei (2003) [10]. Following this general formulation, in order to deal with the absolute value function in Equation 2, we re-write

the vectors \mathbf{v} and \mathbf{x} with the help of slack variables. This will reduce the problem to that of linear programming. These vectors are now given by

$$\mathbf{v} = \mathbf{u} - \mathbf{w}, \quad \mathbf{u}, \mathbf{w} \geq 0, \quad (4)$$

$$\mathbf{x} = \boldsymbol{\alpha} - \boldsymbol{\beta}, \quad \boldsymbol{\alpha}, \boldsymbol{\beta} \geq 0, \quad (5)$$

where a condition u_i or $w_i = 0$ holds for the residual vector components. Now, given the conditions in Equation 4, Equation 2 can be written as

$$\mathbf{p}^T |\mathbf{v}| = \mathbf{p}^T |\mathbf{u} - \mathbf{v}| = \mathbf{p}^T (\mathbf{u} + \mathbf{w}), \quad (6)$$

subject to the conditions in Equation 5,

$$\mathbf{u} - \mathbf{w} = \mathbf{A}(\boldsymbol{\alpha} - \boldsymbol{\beta}) - \mathbf{y}. \quad (7)$$

The objective function can thus be written as

$$\min \left(\begin{bmatrix} \mathbf{0}^T & \mathbf{0}^T & \mathbf{p}^T & \mathbf{p}^T \\ \boldsymbol{\alpha} \\ \boldsymbol{\beta} \\ \mathbf{w} \\ \mathbf{u} \end{bmatrix} \right), \quad (8)$$

subject to

$$\begin{bmatrix} \mathbf{A} & -\mathbf{A} & \mathbf{I} & -\mathbf{I} \end{bmatrix} \begin{bmatrix} \boldsymbol{\alpha} \\ \boldsymbol{\beta} \\ \mathbf{w} \\ \mathbf{u} \end{bmatrix} = \mathbf{y}, \quad (9)$$

given the same conditions as earlier. Denoting the objective function with z this form is equivalent to

$$z = \mathbf{c}^T \mathbf{x}, \quad (10)$$

subject to

$$\mathbf{A} \mathbf{x} = \mathbf{b}, \quad \mathbf{x} \geq 0. \quad (11)$$

The L1-norm minimization was implemented in c5++ with an external python script. The corresponding linear programming problem was solved using a Simplex-method [11] implemented in the *linprog* function of the optimization module in SciPy [12].

The main advantage of the L1-norm over the L2-norm is its robustness against outliers. The L1-norm sums absolute deviations instead of squared values. This means that large residuals are not emphasized as they are with the L2-norm. Thus, the L1-norm is better at detecting the magnitude of large outliers, while the L2-norm overcompensates the influence of large deviations. These errors will propagate to the unknown parameters in the adjustment.

Table 3 Statistics for the post-fit residuals from the UT1-UTC estimation with the L1- and L2-norm approaches and weighting strategies W1, W2, and W3. Included are RMS, mean of absolute values, and median of absolute values.

	L1			L2		
	$\overline{\text{RMS}}$ [ns]	$\overline{ \text{res} }$ [ns]	$M(\text{res})$ [ps]	$\overline{\text{RMS}}$ [ns]	$\overline{ \text{res} }$ [ns]	$M(\text{res})$ [ps]
W1	0.39	0.26	29.68	1.07	0.75	32.24
W2	1.51	1.10	35.69	1.98	1.47	38.69
W3	1.38	1.00	34.69	1.81	1.34	37.69



Fig. 2 Venn-diagrams for the weighting strategies W1, W2, and W3 illustrating the overlap between the sets of sessions obtained with the L1- and L2-norm ambiguity estimation, that pass the $|\text{UT1-UTC}| < 1,000 \mu\text{s}$ and $\sigma_{\text{UT1-UTC}} < 50 \mu\text{s}$ criteria.

The Venn-diagrams in Figure 2 illustrate the overlap between the good sessions from the L1- and L2-norm approaches. These diagrams show the number of good sessions which are found in the results for both L1 and L2, only L1, or only L2. To investigate the differences in the sessions, where either the L1- or L2-norm approaches fail or succeed, we consider subsets of the diagrams illustrated in Figure 2. The following subsets are considered for all weighting strategies:

- Subset-1: select all sessions that are good with the L1-norm approach and select the same sessions from the L2-norm solutions.
- Subset-2: select all sessions that are exclusively good with the L1-norm approach and select the same sessions from the L2-norm solutions.
- Subset-3: select all sessions that are exclusively good in the L2-norm approach and select the same sessions from the L1-norm solutions.

The number of sessions in each of the subsets and all three weighting strategies are given in Table 4.

The L1-norm leads to approximately 5% more sessions compared to the L2-norm. In general, the big advantage of using the L1-norm for the ambiguity estimation is the increased number of successfully processed sessions. The overall accuracy in the WRMS remains at the level of approximately 18 μs .

Table 4 The number of sessions in Subset-1, Subset-2, and Subset-3 for all weighting strategies W1, W2, and W3.

	Number of sessions		
	Subset-1	Subset-2	Subset-3
W1	1564 + 85 = 1649	85	1
W2	1403 + 66 = 1469	66	4
W3	1426 + 67 = 1493	56	2

In Subset-1 (see Table 5) the inclusion of sessions which fail with the L2-norm shows up as high RMS values compared to that of the L1-norm. This is not seen in the WRMS values, which are on a normal level for both norms, with only slightly (sub-microsecond) higher values for the L2-norm.

Table 5 Number of sessions and corresponding RMS/WRMS of UT1-UTC values for the sessions included in Subset-1.

Units: [μs]	#Sessions	L1		L2	
		RMS	WRMS	RMS	WRMS
W1	1649	22.58	18.39	938.09	18.70
W2	1469	22.32	18.43	805.21	18.82
W3	1493	22.25	18.43	1096.07	18.74

In Subset-1 (see Table 5) the inclusion of the sessions that are filtered in the L2-norm solution is seen as high L2-norm WRMS values compared to the respective L1-norm WRMS values. This indicates that the large values for the UT1-UTC corrections, causing the large RMS in the L2-norm, have correspondingly large formal errors. Thus, these sessions get downweighted in the WRMS computation.

Table 6 Number of sessions and corresponding RMS/WRMS of UT1-UTC values for the sessions included in Subset-2.

Units: [μs]	#Sessions	L1		L2	
		RMS	WRMS	RMS	WRMS
W1	85	18.83	22.54	3934.66	4130.73
W2	66	17.11	19.38	3280.11	3797.42
W3	67	19.48	19.55	2646.68	5173.04

In Subset-2 (see Table 6) we see a clear difference both in RMS and WRMS values between the two norms. The large WRMS values for the L2-norm indicate that the formal errors for the filtered UT1-UTC estimates have similar magnitudes compared to one another.

5 Conclusions

The use of the L1-norm shows a clear improvement for the automated ambiguity estimation for the INT sessions in terms of the increased number of sessions that produce a good quality UT1-UTC estimate. Smaller RMS and WRMS values of the post-fit residuals from the ambiguity estimation also indicate that the ambiguity estimation benefits from the L1-norm. The sessions where the L1-norm performs better in ambiguity estimation are almost identical in terms of average number of observations compared to the whole data set of the analyzed INT1 sessions. Thus, the benefit gained with the L1-norm is not correlated with a particularly high or low number of observations in these sessions. The number of sessions that are improved by the L1-norm approach greatly outnumber the ones where the issues of stability result in a failed ambiguity estimation. The computational complexity of solving the linear programming problem compared to inverting the normal equations does not generally cause significant overhead in the processing time of an individual session. The L1-norm using the W1 weighting (i.e., equally weighted) produced the biggest increase in good quality UT1-UTC estimates. Further information can be found in [14].

Acknowledgements

We acknowledge the IVS [1] for providing the VLBI databases used in this work.

References

- Behrend, D., 2013. Data Handling within the International VLBI Service. *Data Science Journal* 12, WDS81–WDS84.
- Hobiger, T., Otsubo, T., Sekido, M., Gotoh, T., Kubooka, T., Takiguchi, H., 2010. Fully automated VLBI analysis with c5++ for ultra-rapid determination of UT1. *Earth, Planets and Space* 62 (12), 933–937.
- Kareinen, N., Hobiger, T., Haas, R., 2015. Automated analysis of Kokee–Wettzell Intensive VLBI sessions—algorithms, results, and recommendations. *Earth, Planets and Space* 67, 181.
- Rogers, A. E., 1970. Very long baseline interferometry with large effective bandwidth for phase-delay measurements. *Radio Science* 5 (10), 1239–1247.
- Böhm, J., Böhm, S., Nilsson, T., Pany, A., Plank, L., Spicakova, H., Teke, K., Schuh, H., 2012. ‘The new Vienna VLBI software VieVS’. In: *Geodesy for Planet Earth*. Springer, pp. 1007–1011.
- Ma, C., Sauber J. M., Bell L. J., Clark, T., Gordon, D., Himwich W. E., Ryan J. W., 1990. Measurement of horizontal motions in Alaska using very long baseline interferometry. *Journal of Geophysical Research: Solid Earth* 95 (B13), 21991–22011.
- Andersen, P., 2000. Multi-level arc combination with stochastic parameters. *Journal of Geodesy* 74 (7–8), 531–551.
- Titov, O., Tesmer, V., Böhm, J., 2004. ‘OCCAM v. 6.0 software for VLBI data analysis’. In: Vandenberg, N. R., Baver, K. D. (Eds.), *IVS 2004 General Meeting Proceedings*. NASA/CP-2004-212255, pp. 267–271.
- Koch, K. R., 1977. Least squares adjustment and collocation. *Bulletin géodésique* 51 (2), 127–135.
- Amiri-Simkooei, A. R., 2003. Formulation of L_1 norm minimization in Gauss-Markov models. *Journal of Surveying Engineering* 129 (1).
- Murty, K. G., 1983. *Linear programming*. John Wiley & Sons.
- Walt, S., Colbert, S. C., Varoquaux, G., 2011. The NumPy Array: A Structure for Efficient Numerical Computation. *Computing in Science & Engineering* 13 (2), 22–30.
- Bizouard, C., Gambis, D., 2011. IERS C04 08. <https://hpiers.obspm.fr/iers/eop/eopc04/C04.guide.pdf>, the combined solution C04 for Earth Orientation Parameters consistent with International Terrestrial Reference Frame 2008. Accessed: 2016-04-29.
- Kareinen, N., Hobiger, T., Haas, R., 2016. Automated ambiguity estimation for VLBI Intensive sessions using L1-norm. Under review in *Journal of Geodynamics*.

Results from the VLBI Analysis Software Comparison Campaign 2015

G. Klopotek¹, T. Artz², A. Bellanger³, G. Bourda³, M. Gerstl⁴, D. Gordon⁵, R. Haas¹, S. Halsig², G.A. Hjelle⁶, T. Hobiger¹, U. Hugentobler⁷, A. Iddink², A.S. Kirkvik⁶, S. Lambert⁸, L. Plank⁹, R. Schmid⁴, F. Shu¹⁰, O. Titov¹¹, F. Tong¹⁰, G. Wang¹⁰, M. Xu¹⁰, W. Zheng¹⁰

Abstract The aim of the VLBI Analysis Software Comparison Campaign 2015 (VASCC2015) was to compare different VLBI analysis software packages on the basis of computed theoretical delays. Eleven research groups and institutes participated in this project, which allowed us to compare software packages that are used in operational VLBI analyses or that are still under development. We present the first results, and we show how well the individual software packages agree at this stage.

Keywords VLBI theoretical delay, IERS Conventions, VLBI analysis software packages

1 Introduction

The IERS Conventions (2010) [11] contain recommendations, definitions, and models for space geodetic

1. Department of Earth and Space Sciences, Chalmers University of Technology, Sweden

2. Institute of Geodesy and Geoinformation, University of Bonn, Germany

3. Laboratoire d'Astrophysique de Bordeaux, France

4. Deutsches Geodätisches Forschungsinstitut der Technischen Universität München, Germany

5. Goddard Space Flight Center, National Aeronautics and Space Administration, USA

6. Norwegian Mapping Authority, Norway

7. Institut für Astronomische und Physikalische Geodäsie, Technische Universität München, Germany

8. Paris Observatory, France

9. University of Tasmania, Australia

10. Shanghai Astronomical Observatory, Chinese Academy of Sciences, China

11. Geoscience Australia, Australia

techniques including geodetic VLBI. In practice, different analysis software packages follow diverse estimation methods, use a variety of different correction models, and sometimes adhere to conventions that might not be the latest. This may lead to discrepancies in the results that should not appear between analysis software packages dealing with the same observational data sets. Consistency of geodetic VLBI analyses is of great importance for reaching one of the VLBI Global Observing System (VGOS) envisaged goals [9], i.e., 1 mm measurement accuracy on global baselines.

In the VLBI Analysis Software Comparison Campaign 2015 (VASCC2015), existing VLBI analysis software packages were compared on the basis of computed theoretical delays and in accordance with the models described in the IERS Conventions (2010). Eleven research groups and institutes expressed their interest in participating in this project (Table 1). The comparison campaign started in September 2015, and theoretical delays computed with various analysis software packages were investigated thereafter. Preliminary results and conclusions are presented here.

2 Data

Fifteen fictitious consecutive 24-hour sessions (22 June 2015 – 6 July 2015) with one minute resolution formed the basis of this comparison campaign. Two networks, one in the northern and one in the southern hemisphere, were designed in a way that a single source could be tracked at all stations continuously (Figure 1). With that geometry it was possible to compare 16 baseline delays per observation epoch. From all sites of both networks, the source was visible

Table 1 Participants of the VASCC2015 at the present stage of the project.

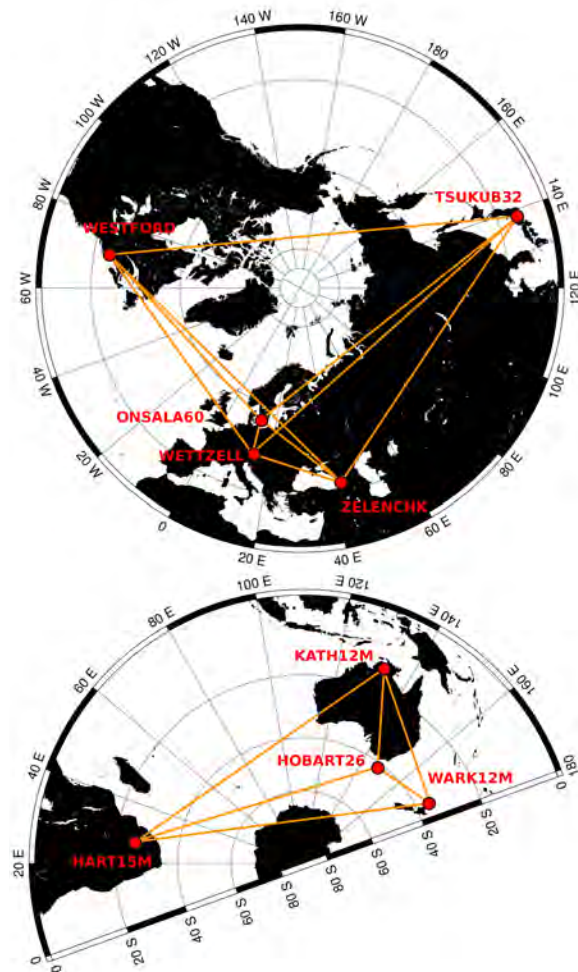
	Software	Participant (provision of results)
1.	Bernese [12]	Technische Universität München (TUM)
2.	c5++ [6]	Chalmers University of Technology
3.	Calc11 [5]	Goddard Space Flight Center (GSFC), NASA
4.	Calc11 [5] SCORR [14]	Shanghai Astronomical Observatory (SHAO), Chinese Academy of Sciences
5.	DOGS-RI [13] OCCAM [17]	Technische Universität München, Deutsches Geodätisches Forschungsinstitut (DGFI-TUM)
6.	GEOSAT [7]	Norwegian Mapping Authority (NMA)
7.	GINS [2]	Laboratoire d' Astrophysique de Bordeaux (LAB)
8.	GLORIA [8] Calc11 [5]	Paris Observatory (OPAR)
9.	ivg::ASCOT [1]	University of Bonn
10.	OCCAM [17]	Geoscience Australia
11.	VieVS [3]	University of Tasmania

with varying local elevation angles, allowing us to draw conclusions concerning elevation-dependent effects.

A priori values and displacement models (Table 2) were defined, and all participants were asked to follow the proposed computation routine as closely as possible. Tidal S1 and S2, as well as non-tidal atmosphere loading, zenith wet delay, and station eccentricities, were not considered. Information about the network geometry, a priori values, and meteorological and auxiliary data was provided to all participants using NGS, VGOSDB, MK3DB, and text files created for the purpose of this comparison campaign.

Table 2 Delay computation settings of the VASCC2015.

1.	EOP	High frequency EOP variations Leap second: 30 June, 24:00:00 UTC Constant values for: X_{pol} , Y_{pol} , UT1, dX, dY
2.	Displacement models	Solid Earth tides, pole tide, ocean and ocean pole tide loading
3.	Technique-specific models	Thermal expansion Axis offset
4.	Mapping function	GMF [4]
5.	Meteorological data (all sites)	Pressure: 1000 hPa Rel. hum.: 50 % Temp.: 20 °C
6.	Cable delays (all sites)	0 s

**Fig. 1** Networks located on the northern (top) and southern hemisphere (bottom). Eight of the nine sites have alt-azimuth type antennas. In case of HOBART26, the mount type is X/Y with the primary axis set to the east-west direction.

3 Results

The consistency of the theoretical delays from different VLBI analysis software packages was evaluated in terms of RMS. At present, sub-mm RMS agreement of the full VLBI delay model could be achieved for six VLBI analysis software packages (Table 3). The complete theoretical delay model consists of a geometrical part and contributions from effects and models described in the IERS Conventions (2010). As an ex-

ample, differences between results from two software packages are depicted in Figure 2.

Table 3 RMS of differences between theoretical delays (full delay model) for both networks over a period of 15 days. The acronym in parenthesis refers to the participant providing the solution. No results for the Calc11 - DOGS-RI pair are shown, as no DOGS-RI solution without antenna thermal expansion and zero value celestial pole offsets was available.

RMS [mm]	Calc11(GSFC)	c5++	DOGS-RI	ivg::ASCOT	SCORR	VieVS
Calc11(GSFC)	x	0.43	-	0.38	0.57	0.44
c5++	-	x	0.61	0.17	0.44	0.22
DOGS-RI	-	-	x	0.59	0.71	0.59
ivg::ASCOT	-	-	-	x	0.41	0.17
SCORR	-	-	-	-	x	0.44
VieVS	-	-	-	-	-	x

0.0 - 1.0 mm RMS

In the case of comparisons with respect to Calc11 (GSFC), celestial pole offsets were not considered, and antenna thermal expansion models [10] were excluded as this is not implemented in Calc11. In addition, one needs to be aware that theoretical delays from Calc11 (GSFC) rely on static TRF station coordinates valid at the middle session which, in this case, is June 29th. An increase of the RMS by about 0.1 mm can thus be explained.

Maximum absolute differences between the results are summarized in Table 4. Software packages not listed in Table 3 require further investigation to draw conclusions concerning the agreement on the basis of theoretical delays. We expect to obtain smaller maximum absolute residuals after all participants have validated their software packages and updated them to the latest agreed-on standards.

During the comparison campaign, some discrepancies were detected and studied in more detail. Most differences were caused by unidentified bugs or numerical issues. But it was also noticed that the definition of the source elevation angle is not well-documented in the IERS Conventions (2010). In particular, a recommendation about whether troposphere bending effects [16], for the computation of axis offset and thermal expansion delays, have to be considered or not is missing. Related papers (e.g., [10, 15]) also lack a clear

Table 4 Maximum residual values between theoretical delays (full delay model) from both networks over a period of 15 days.

Max. abs. value [mm]	Calc11(GSFC)	c5++	DOGS-RI	ivg::ASCOT	SCORR	VieVS
Calc11(GSFC)	x	1.76	-	1.82	2.68	2.06
c5++	-	x	1.87	1.04	1.48	1.14
DOGS-RI	-	-	x	1.52	2.05	1.71
ivg::ASCOT	-	-	-	x	1.24	0.83
SCORR	-	-	-	-	x	1.37
VieVS	-	-	-	-	-	x

0.0 - 1.0 mm RMS
1.0 - 2.0 mm RMS
>2.0 mm RMS

recommendation on this issue. Depending on whether bending effects for the calculation of the source elevation angle are considered or not, differences of up to 0.5 mm can be detected for antennas with axis offsets larger than 1 m (Figure 3). This effect should not have any significant impact on the VGOS-type telescopes, which are expected to have zero or mm order axis offsets. But a conventional mathematical formulation for bending effects on elevation angles could definitely be beneficial for software developers and analysts.

Another finding that is worth mentioning is related to the fact that differences between different software packages started to grow significantly as soon as high-frequency EOP variations [11] were introduced. In terms of RMS over a 24-hour period, this effect is represented by an increase of disparities between solutions by about 0.1 mm. Other geophysical models did not reveal such large discrepancies after being turned on in the software packages. Certainly, further investigation is needed in order to understand the causes of these differences.

4 Conclusions and Outlook

VASCC2015 made it possible to find out how well different software packages agree on the basis of theoretical delay models. We were also able to identify numerical issues and to correct several bugs in some of the analysis packages. Initial results show that a sub-mm agreement of theoretical delays, computed by

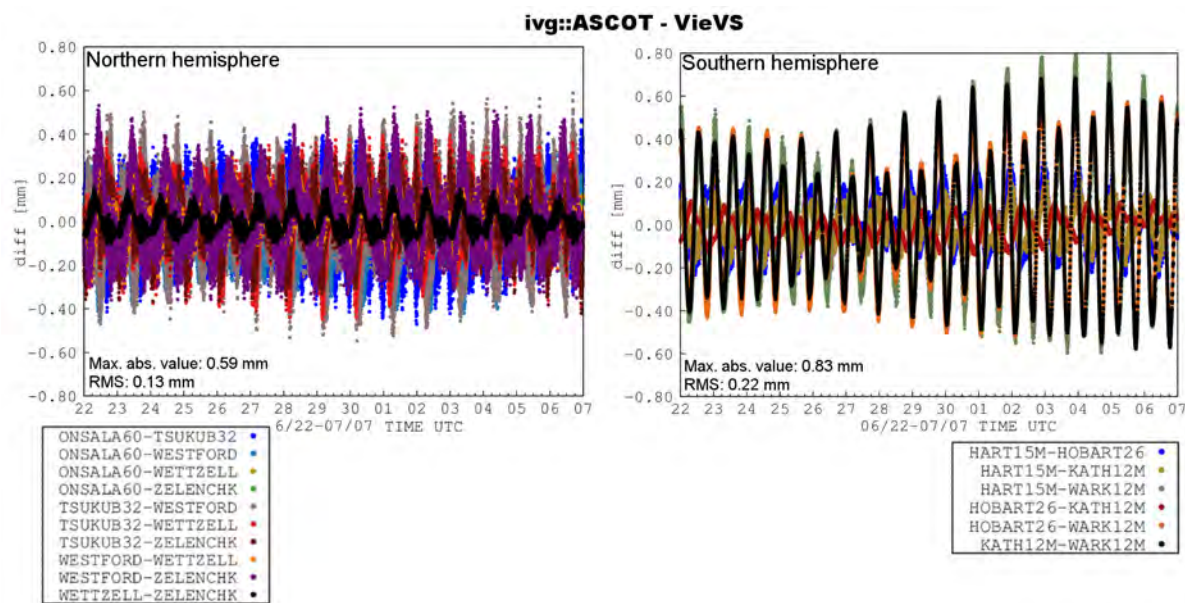


Fig. 2 Agreement between computed theoretical delays (full delay model) from ivg::ASCOT and VieVS over a period of 15 days. The results refer to baselines located in the northern (left) and southern hemisphere (right).

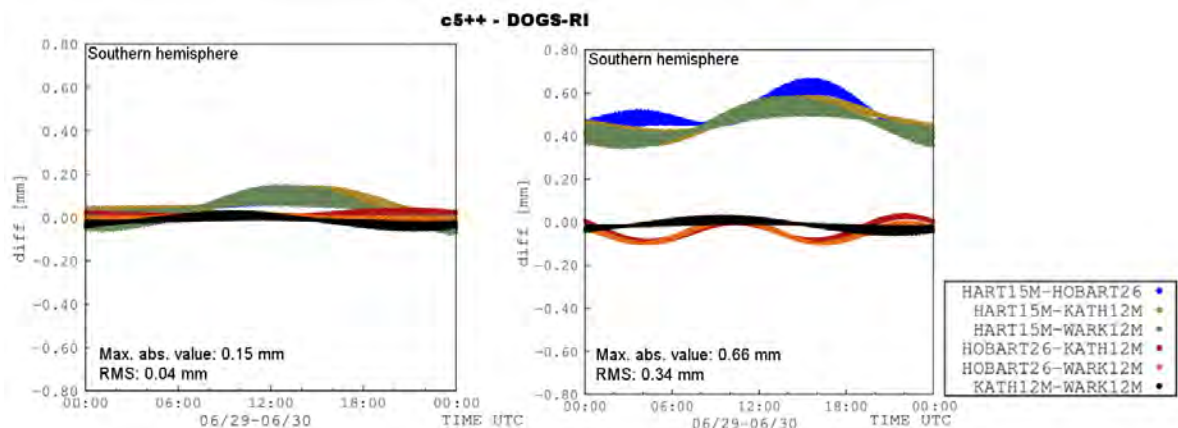


Fig. 3 Effect of tropospheric bending on source elevation angles as shown with the c5++ — DOGS-RI pair over a period of 24 hours. Both plots depict residuals between theoretical delays for the network located in the southern hemisphere. For this particular example, only geometric, gravitational and axis offset delays are considered. The left plot depicts differences when bending delay corrections are applied in both software packages. If such corrections are neglected in c5++, one can notice a significant change of the differences w.r.t. DOGS-RI as depicted in the right plot. These discrepancies can be assigned to the alt-azimuth type antennas having axis offsets of at least 1 m (fictitious $AO_{\text{HART15M}} = 1.4950$ m). Smaller differences occur for antennas with X/Y mount type (e.g., HOBART26).

state-of-the-art VLBI analysis software packages, can be achieved. Nonetheless, this project needs to be continued in order to study remaining discrepancies and to minimize theoretical delay differences. A modification of the network geometry and the use of simulated observations (modeling of stochastic processes) are con-

sidered as further steps in order to enhance the agreement between software packages.

We expect that by continuing this comparison campaign it will be possible to get a better picture of the consistency of delay modeling within the IVS. It is assumed that our results and conclusions are helpful

for VLBI software developers to maintain, update, and improve their analysis software packages. Thus, this project is expected to have an impact on the reliability and consistency of IVS products and subsequent scientific research.

Acknowledgements

G. Klotek would like to thank all participants for their cooperation and commitment to this project. John Gipson and Sergei Bolotin are acknowledged for their feedback concerning the VGOSDB format.

References

1. Artz T., Halsig S., Iddink A., Nothnagel A., ivg::ASCOT: The Development of a new VLBI Software Package. Poster presented at the IVS 2016 General Meeting, Johannesburg, South Africa, 13–19 March, 2016.
2. Bourda G., Charlot P., Biancale R., VLBI analyses with the GINS software for multi-technique combination at the observation level. *Proc. SF2A 2007*, Bouvier J., Chalabaev A., Charbonnel C. (Eds.), Grenoble, France, 2–6 July, 2007.
3. Böhm J., Böhm S., Nilsson T., Pany A., Plank L., Spicakova H., Teke K., Schuh H., The new Vienna VLBI Software VieVS. Kenyon S., Pacino M. C., Marti U. (Eds.), *Geodesy for Planet Earth*, International Association of Geodesy Symposia 136, 1007–1011, 2012, doi: 10.1007/978-3-642-20338-1_126.
4. Böhm J., Niell A. E., Tregoning P., Schuh H., Global Mapping Function (GMF): A new empirical mapping function based on numerical weather model data. *Geophys. Res. Lett.*, 33(7), L07304, 2006, doi: 10.1029/2005GL025546.
5. Fey A. L., Gordon D., Jacobs C. S. (Eds.), The second realization of the International Celestial Reference Frame by Very Long Baseline Interferometry, IERS Technical Note 35, Frankfurt am Main: Verlag des Bundesamts für Kartographie und Geodäsie, 204 pp., 2009.
6. Hobiger T., Otsubo T., Sekido M., Gotoh T., Kubooka T., Takiguchi H., Fully automated VLBI analysis with c5++ for ultra-rapid determination of UT1. *Earth Planets Space*, 62, pp. 933–937, 2010, doi: 10.5047/eps.2010.11.008.
7. Kierulf H. P., Andersen P. H., Böckmann S., Kristiansen O., VLBI analysis with the multi-technique software GEOSAT. *IVS 2010 General Meeting Proceedings*, NASA/CP-2010-215864, pp. 207–211, 2010.
8. Lambert S. B., Status of the GLORIA geodetic VLBI analysis software package. *Proceedings of the Journées 2011 “Systèmes de référence spatio-temporels” (JSR2011): Earth rotation, reference systems and celestial mechanics: Synergies of geodesy and astronomy*, Schuh H., Böhm S., Nilsson T. and Capitaine N. (Eds.), Vienna, Austria, 19–21 September, pp. 47–48, 2010.
9. Niell A., Whitney A., Petrachenko B., Schlüter W., Vandenberg N., Hase H., Koyama Y., Ma C., Schuh H., Tuccari G., VLBI2010: Current and future requirements for geodetic VLBI systems. In: Behrend D., Baver K. (Eds.), *International VLBI Service for Geodesy and Astrometry 2005 Annual Report*, NASA/TP-2006-214136, pp. 13–40, 2006.
10. Nothnagel A., Conventions on thermal expansion modelling of radio telescopes for geodetic and astrometric VLBI. *J. Geod.*, 83(8), pp. 787–792, 2009, doi: 10.1007/s00190-008-0284-z.
11. Petit G., Luzum B. (Eds.), IERS Conventions (2010), IERS Technical Note 36, Frankfurt am Main: Verlag des Bundesamts für Kartographie und Geodäsie, 179 pp., 2010.
12. Schmid R., Zur Kombination von VLBI und GNSS, DGK, C636, Verlag der Bayerischen Akademie der Wissenschaften, 2009.
<http://www.dgk.badw.de/fileadmin/docs/c-636.pdf>
13. Schmid R., Gerstl M., Seitz M., Angermann D., DGF1 Analysis Center Annual Report 2013. In: Baver K.D., Behrend D., Armstrong K.L. (Eds.), *International VLBI Service for Geodesy and Astrometry 2013 Annual Report*, NASA/TP-2014-217522, pp. 263–264, 2014.
14. Shu F., Zheng W., Jiang W., Chen Z., Zhu R., Shanghai VLBI Correlator 2013 Annual Report. In: Baver K. D., Behrend D., Armstrong K. L. (Eds.), *International VLBI Service for Geodesy and Astrometry 2013 Annual Report*, NASA/TP-2014-217522, pp. 224–226, 2014.
15. Skurikhina E., On computation of antenna thermal deformation in VLBI data processing. *Proceedings of 15th Working Meeting on European VLBI for Geodesy and Astrometry*, Barcelona, pp. 124–130, 2001.
16. Sovers O. J., Fanselow J. L., Jacobs C. S., Astrometry and geodesy with radio interferometry: experiments, models, results. *Reviews of Modern Physics*, Vol. 70, No. 4, pp. 1393–1454, 1998, 10.1103/RevModPhys.70.1393.
17. Titov O., Tesmer V., Böhm J., OCCAM v.6.0 software for VLBI data analysis, *IVS 2004 General Meeting Proceedings*, NASA/CP-2004-212255, pp.267–271, 2004.

Simulations of Near Real-time EOP Estimation from a Future VGOS Network

Tobias Nilsson¹, Maria Karbon¹, Benedikt Soja¹, Susanne Glaser², Robert Heinkelmann¹, Harald Schuh^{1,2}

Abstract We describe the Kalman filter implemented in the VieVS@GFZ software which is able to analyze VLBI data in real-time. The filter is tested through simulations of a real-time estimation scenario from a 30 station VGOS network. We obtain a precision of 20–30 μs for polar motion and celestial pole offsets and 1.3 μs for UT1–UTC. The Kalman filter is able to work fully automated and can detect and correct problems like clock breaks automatically.

Keywords VLBI, VGOS, real-time, Kalman filter

1 Introduction

One of the goals of the upcoming VLBI Geodetic Observing System (VGOS) is to reduce the latency between the observations and the availability of the results, e.g., Earth Orientation Parameters (EOP). For the current VLBI system this latency is about two weeks, and the goal of VGOS is to reduce it to less than 24 hours [7]. Ideally, the results should be available in real-time [1]. Achieving this is challenging for all parts of the VLBI processing chain. First of all, the data needs to be sent with e-transfer in real-time from the stations to the correlator. For this it is required that all the stations, and in particular the correlator, are connected to high-speed electronic networks. Then, as

soon as all the data from a scan have arrived at the correlator, the data are correlated in order to produce the VLBI observables, e.g., the group delays. These are then used as input to a VLBI analysis software, where the interesting parameters, like the EOP, are estimated. The possibility of VLBI in near real-time has been demonstrated for one-hour single-baseline sessions, so-called Intensive sessions [2]. However, for VGOS, real-time operation will be more challenging, especially since the data recording rate for VGOS will be 8–16 Gbps. Although the data do not necessarily need to be sent with this speed, since it is planned to also use the time in which the telescopes slew to the next source for the transfer, still a stable connection to the correlator of several Gbps is needed.

In this work we focus on the challenges for the last part of the VLBI processing chain: the VLBI data analysis. This part, just as the other parts, must run completely autonomous and needs to be able to deal with any problem that may occur, e.g., clock breaks. As soon as the observables from a new scan are available from the correlator, a new solution should be calculated in order to get updated estimates for the EOP and other parameters [1]. Thus it seems appropriate to apply a Kalman filter for the parameter estimation. In this work we apply a modified version of the Kalman filter implemented in the VieVS@GFZ software [5, 8]. The implementation is briefly described in Section 2. The software is tested through simulation of a real-time estimation scenario from a 30-station VGOS network. The setup of the simulations is presented in Section 3 and the results in Section 4. Finally, the conclusions are given in Section 5.

1. GFZ German Research Centre for Geosciences, Section 1.1 Space Geodetic Techniques, Telegrafenberg A17, 14473 Potsdam, Germany

2. Technische Universität Berlin, Institute of Geodesy and Geoinformation Science, Straße des 17. Juni 135, 10623 Berlin, Germany

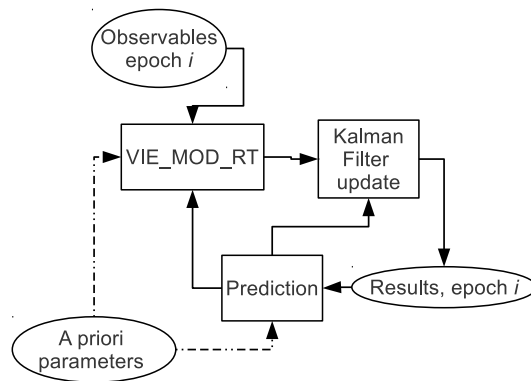


Fig. 1 Flowchart of the real-time VLBI data analysis with VieVS@GFZ.

2 Kalman Filter Implementation

The basic structure of the Kalman filter is shown in Figure 1. Whenever observables from a new scan become available, the theoretical delays and the partial derivatives are calculated using the module VIE_MOD_RT. The a priori parameters needed for these calculations, e.g., the EOP, the station coordinates, and the radio source coordinates, are predicted from the results of the previous epoch, except for the very first epoch where initial guesses of these parameters are used. Then the estimates are updated by the Kalman filter by making an optimal combination of the values predicted from the previous epoch and the observables of the current epoch. For more details, see [5]. For the real-time analysis, the Kalman filter loop only runs forward in time. However, the option also exists to run the filter backwards in time, followed by smoothing where the optimal combination of the forward and backward results is calculated. This will only improve the results at the earlier epochs, not the last one. Hence, this option is only applicable for post-processing.

In the Kalman filter the following parameters are estimated: all five EOP (modeled as integrated random walk processes), station coordinates (highly constrained random walk processes), radio source coordinates (constant offsets), zenith wet delays (random walk), tropospheric gradients (random walk), and clock errors (random walk plus integrated random walk). The datum for the station coordinates is realized by adding No-Net-Rotation (NNR) and No-Net-Translation (NNT) constraints as additional

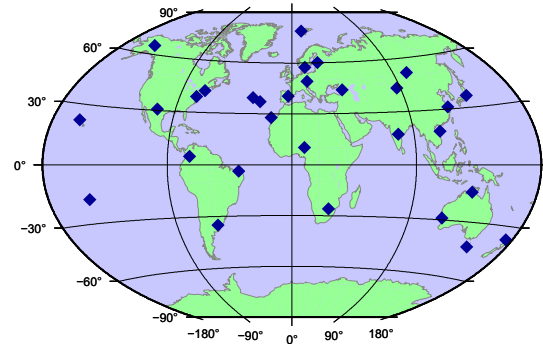


Fig. 2 The 30-station VGOS network used for the simulations.

pseudo-observations. Similarly, the datum for the radio sources is realized by NNR constraints.

3 Simulations

To test the real-time Kalman filter we made simulations. Here we assumed a future observing scenario with a 30-station VGOS network (see Figure 2). For most antennas we assumed a slew rate of $12^\circ/\text{s}$ in azimuth and $6^\circ/\text{s}$ in elevation. The exceptions were existing antennas with different slew rates, i.e., the antennas in Australia, New Zealand, and at the Goddard Geophysical and Astronomical Observatory (GGAO), USA, all of which have slew rates of about $5^\circ/\text{s}$ in azimuth and $1.2^\circ/\text{s}$ in elevation. In these simulations we only considered single telescopes at each site, although at several stations twin telescopes are planned or already exist. We generated an observing schedule with the VIE_SCHED software [9], applying the source-based scheduling strategy with four sources observed simultaneously. With this schedule, the very fast antennas made about 2000 scans/day, the others about 1600 scans/day. The schedule was repeated every sidereal day over the whole 25-day simulation period.

Simulated delays were generated with the VIE_SIM software [6]. First the theoretical delays were calculated, then we simulated random errors due to the clocks, the troposphere, and observation noise, and added these to the theoretical delays. For calculating the theoretical delay we used the observed EOP from a 25 days long period (4–29 September 2015). The clocks were simulated as random walk plus integrated random walk processes with an Allan standard devia-

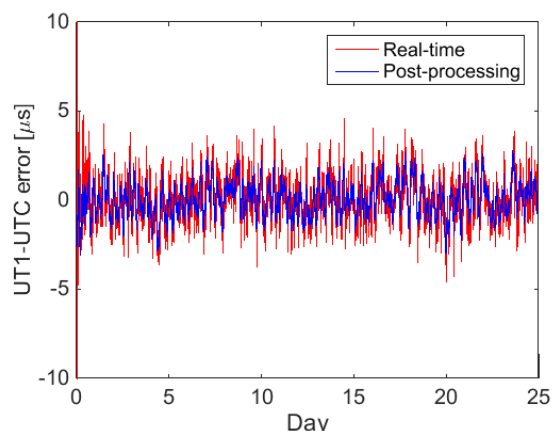


Fig. 3 The differences between the estimated UT1–UTC time series and the time series used as input to the simulations. Shown are both the results for real-time estimation and post-processing.

tion of $1 \cdot 10^{-14}$ @ 50 min, the tropospheric delay according to the algorithms presented in [3] with station specific C_n^2 values obtained from GPS data, and the observation noise was simulated as white noise with a standard deviation of 10 ps. The simulated delays were then used as input to the Kalman filter. As a priori EOP for the first epoch we used the actual EOP of this epoch plus random errors with standard deviations of 100 mas (polar motion), 2 ms (UT1–UTC), and 1 mas (celestial pole offsets). This represents very bad a priori EOP and was used in order to investigate how well the Kalman filter can deal with really poor a priori values.

4 Results

In Figure 3, the UT1–UTC values estimated from the Kalman filter are compared to the values used for creating the simulated delays. Two Kalman filter solutions were investigated: one real-time solution (only forward running Kalman filter) and one post-processed solution (forward and backward Kalman filter + smoothing). For the first epochs, there are large differences between the real-time estimates and the simulated values. The reason is that the a priori values used for the initial epoch contained large errors, thus the Kalman filter needs time in order to converge to the correct value. After a few hours, when the filter has converged, the precision of the estimates is more or less stable. Furthermore, we can see in Figure 3 that the scatter of the

Table 1 WRMS error in the EOP estimated in the real-time analysis and in post-processing.

	x-pole μas	y-pole μas	UT1–UTC μs	dX μas	dY μas
Real-time	27.7	24.6	1.29	20.6	21.3
Post-proc.	18.4	16.7	0.92	14.3	14.8

Table 2 WRMS error in the EOP estimated in the real-time analysis from the reduced data sets.

	x-pole μas	y-pole μas	UT1–UTC μs	dX μas	dY μas
10 stations	52.9	45.1	3.60	40.5	38.4
Every 5th scan	48.1	41.3	2.86	34.4	40.1
Every 10th scan	66.6	56.5	3.76	52.5	48.5

post-processed solution is lower than that of the real-time solution, as expected.

In Table 1 the Weighted Root-Mean-Square (WRMS) differences between the estimated and simulated EOP values are shown. We can see that the WRMS for the real-time estimates are about 40–50% larger than for the ones from the post-processing. A real-time estimate is only determined from the observations at the current and past epochs, while the post-processed estimate is determined also using future observations. Thus, we can say that the post-processed estimates are in principle determined from twice as many observations as the real-time ones. Based on this assumption, we would expect that the precision of the real-time estimates is about a factor of $\sqrt{2}$ worse than the post-processed ones, if we neglect correlations between the observables.

4.1 Reduced Data Set

In reality, it may be difficult to achieve real-time data transfer and correlation for a 30-station VGOS network. For example, some remote stations may not be connected to high-speed networks, or the correlator may not be able to receive all the data from all stations. One solution would be to only e-transfer part of the data, correlate this in real-time and use it to produce an ultra-rapid solution. The rest of the data is then sent later, e.g., by shipping disk modules, correlated, and then used to calculate the more accurate final solution. For example, the real-time e-transfer may be limited to only a few stations and/or selected scans.

We made tests where the real-time solution was calculated using only the observables from ten stations, every fifth scan, or every tenth scan. The WRMS differences between the estimated and simulated values are shown in Table 2. We can see that the WRMS values are much higher than those given in Table 1, as was to be expected due to the lower amount of data. It should be noted that no optimization was applied w.r.t. exactly which scans to include in the real-time solution. Thus, the results can be further improved by an optimal selection of the scans to e-transfer, e.g., instead of simply using scans number 1, 6, 11, and so on, one of the first five scans is chosen, then one of the next five scans, et cetera. Furthermore, it might be possible to make optimizations already in the scheduling w.r.t. the scans used in the real-time solution, although this might slightly degrade the final solution at the same time.

4.2 Clock Breaks and Other Problems

Occasionally, there are problems with the VLBI data, e.g., due to clock breaks. In the real-time analysis, these problems need to be automatically detected and corrected, otherwise the estimates would be affected. We have implemented automated clock break and outlier detection in the VieVS@GFZ real-time software. We make use of the fact that the Kalman filter makes predictions of the observed delays based on the estimates of the previous epoch. When the Kalman filter has converged, the difference between the observed and predicted delays can be expected to be small. Thus if there are large differences it may indicate a problem. It may, however, be difficult to directly determine the type of problem from the observations of just one scan. Thus, whenever large differences occur, we let the Kalman filter run without assimilating any data, i.e., only using predictions, for the next couple of epochs (the following 5 minutes) and compare the predictions at these epochs to the observed delays. If there is a clock break at one station, the difference between the predicted and observed delays will be large and of about the same size for all observations of this station. Hence, it is possible to detect the clock break and at which station it occurred. The clock break is then corrected by increasing the uncertainty of this clock's offset and rate in the Kalman filter; thus, more or less com-

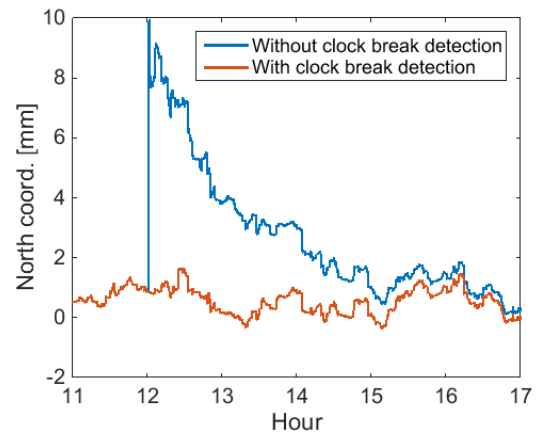


Fig. 4 The north coordinate estimates of the station with a clock break at 12:00. Shown are the results with and without using the automated clock break detection.

pletely new values will be estimated from the observations after the break. If large differences are present at one epoch but not at later epochs, it is an indication of an outlier; thus these observations are removed.

We tested the clock break detection by simulating a clock break of 0.66 ns (20 cm) at 12:00 UTC at one station. The software was able to detect and correct the clock break correctly. In Figure 4 we show the effect of this clock break on the north coordinate of this station. If the clock break detection and correction is not used, there is a jump in the coordinate of the station of almost 1 cm at the epoch of the clock break, and it takes several hours until the solution has converged back to the original level. On the other hand, if the automated clock break detection and correction is used, we see no effect on the north coordinate or any other estimated parameter.

5 Conclusions

Based on the real-time simulation results, the Kalman filter is able to estimate the polar motion and celestial pole offsets with a precision of 20–30 μas and UT1–UTC with a precision of 1.3 μs from a 30 station VGOS network. This is significantly better than what is obtained by the current VLBI system (about 100 μas for standard R1/R4 sessions, 30 μas for the CONT sessions [4]). However, the results are 40–50% worse compared to the results obtained in post-processing.

Thus it will still be beneficial to calculate a final solution with a delay of one or several days, in addition to the ultra-rapid real-time solution.

Acknowledgements

This work was supported by the Austrian Science Fund (FWF), project number P24187-N21 (VLBI-ART).

References

1. H. Hase, D. Behrend, A. Nothnagel, and H. Schuh. A vision for VGOS observations and analysis in 2020. In *Proceedings of the 22nd European VLBI Group for Geodesy and Astronomy Working Meeting*, pages 93–96, 2015. Available from: http://www.oan.es/raege/evga2015/EVGA2015_proceedings.pdf.
2. S. Matsuzaka, H. Shigematsu, S. Kurihara, M. Machida, K. Kokado, and D. Tanimoto. Ultra rapid UT1 experiment with e-VLBI. In A. Finkelstein and D. Behrend, editors, *Proceedings of the Fifth IVS General Meeting: Measuring the Future*, pages 68–71, 2008. Available from: <http://ivscc.gsfc.nasa.gov/publications/gm2008/>.
3. T. Nilsson and R. Haas. Impact of atmospheric turbulence on geodetic very long baseline interferometry. *J. Geophys. Res.*, 115:B03407, 2010. doi:10.1029/2009JB006579.
4. T. Nilsson, R. Heinkelmann, M. Karbon, V. Raposo-Pulido, B. Soja, and H. Schuh. Earth orientation parameters estimated from VLBI during the CONT11 campaign. *J. Geodesy*, 88(5):491–502, 2014. doi:10.1007/s00190-014-0700-5.
5. T. Nilsson, B. Soja, M. Karbon, R. Heinkelmann, and H. Schuh. Application of Kalman filtering in VLBI data analysis. *Earth Planets Space*, 67(136):1–9, 2015. doi:10.1186/s40623-015-0307-y.
6. A. Pany, J. Böhm, D. MacMillan, H. Schuh, T. Nilsson, and J. Wresnik. Monte Carlo simulations of the impact of troposphere, clock and measurement errors on the repeatability of VLBI positions. *J. Geodesy*, 85:39–50, 2011. doi:10.1007/s00190-010-0415-1.
7. B. Petrachenko, A. Niell, D. Behrend, B. Corey, J. Böhm, P. Charlot, A. Collioud, J. Gipson, R. Haas, T. Hobiger, Y. Koyama, D. MacMillan, Z. Malkin, T. Nilsson, A. Pany, G. Tuccari, A. Whitney, and J. Wresnik. Design aspects of the VLBI2010 system. In D. Behrend and K. Baver, editors, *International VLBI Service for Geodesy and Astrometry 2008 Annual Report*, NASA/TP-2009-214183. NASA Technical Publications, 2009.
8. B. Soja, T. Nilsson, M. Karbon, F. Zus, G. Dick, Z. Deng, J. Wickert, R. Heinkelmann, and H. Schuh. Tropospheric delay determination by Kalman filtering VLBI data. *Earth Planets Space*, 67(144):1–16, 2015. doi:10.1186/s40623-015-0293-0.
9. J. Sun, J. Böhm, T. Nilsson, H. Krásná, S. Böhm, and H. Schuh. New VLBI2010 scheduling strategies and implications on the terrestrial reference frames. *J. Geodesy*, 88(5):449–461, 2014. doi:10.1007/s00190-014-0697-9.

Options and Functions of the Revised IVS Combination Web Site

Linda Messerschmitt, Sabine Bachmann, Daniela Thaller

Abstract The World Wide Web is one of the most important communication and information exchange platforms today. Because of the high amount of users and the global accessibility, every business is interested in the Internet. It opens up new possibilities of international cooperation. In geodesy, this aspect of international cooperation is of prime importance.

Keywords International Terrestrial Reference Frame 2014, IVS Combination Center, VLBI, Earth Orientation Parameter, Web site

1 Introduction

The International VLBI Service for Geodesy and Astrometry (IVS, <http://ivscc.gsfc.nasa.gov/>) is a global association of institutions for the VLBI space technique. The IVS is responsible for the determination of the Earth Orientation Parameters (EOP), as well as the contribution to the International Terrestrial Reference-frame (ITRF) based on VLBI observations. A part of the IVS, the Combination Center (CCIVS) based at the Federal Agency for Cartography and Geodesy (BKG, Germany), is the central location for consolidating analyzed VLBI data. Two combined products are generated in an operational mode: a rapid and a quarterly solution.

For the publication of these official IVS products, the CCIVS maintains a Web site, which was recently revised. The new Web site was announced via the IVS mail list in December 2015. Details of the

Bundesamt für Kartographie und Geodäsie (BKG)

combination were offered graphically and numerically at this Web presence. Due to these changes, more options and functions were added to the already available content, which will be presented in Section 3.

The Web site is available on the following link:

<http://ccivs.bkg.bund.de>

2 The Content Management System

The revision of the Web site was realized on the basis of the Content Management System (CMS) ‘GovernmentSiteBuilder’, which was developed by Materna especially for standardizations for Web sites of government departments, public authorities, and other national institutions in Germany. For this purpose, the system offers a large extent of predefined options for language settings, usability, and web accessibility. A login function, a registration mode, service functions, or graphical styles are available and can be integrated or modified for each purpose. The system bundles the information and links it together, so it simplifies the administration effort and the updates of the content. Every step of the process is recorded in layers, so that changes can be monitored individually. The content will only be published after all integrated data and links are available in the system. These security requirements will reduce potential errors.

3 New Functions

The existing content was expanded by more information and functions. Therefore the greatest importance was retaining the structure and the navigation of the initial Web site. Additional contents were added to the menu, e.g., quick links or separate menus.

graphic representation	information
+ Scale of Helmert Transformation	+ combination report
+ ITRF2014 results	+ archive
+ station coordinates	+ news and activities
+ EOP	+ calender
+ baseline	+ publication and poster
	+ observatory map
	+ service functions
	+ sitemap
	+ glossary
	+ contact form
	+ print function
	+ search function

Table 1 Added information and functions in the Web content.

3.1 ITRF2014 Results

The International Terrestrial Reference Frame (ITRF) is being processed in regular time intervals, and VLBI sessions since 1979 are taken into account. The latest version, the ITRF2014, was generated from the results of nine Analysis Centers with a total session count of 5,796 (Bachmann et al. 2016). The results of the VLBI contribution to the ITRF are presented under the menu point 'ITRF2014': station coordinates in X, Y, Z, and North, East, Up; EOP; scale of the Helmert Transformation, and baseline lengths. The data is being extracted from a database and prepared for the graphical plot tool, where each user can choose various settings. The results of the settings can be downloaded as a numerical file.

Figures 1–3 show examples from the IVS combination results for ITRF2014.

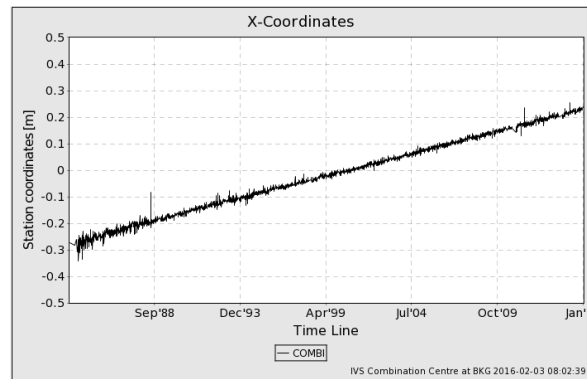


Fig. 1 X-coordinate residuals of station Wettzell from the IVS combination for ITRF2014.

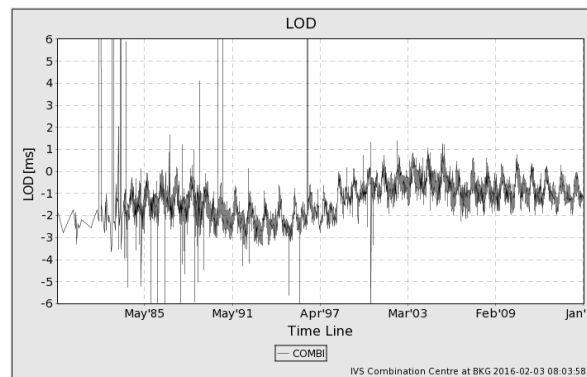


Fig. 2 Session-wise LOD estimates from the IVS combination for ITRF2014.

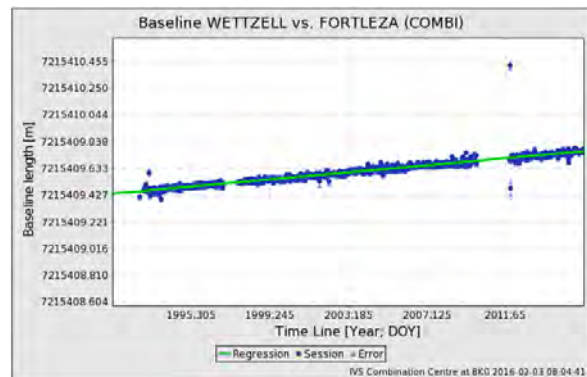


Fig. 3 Baseline length for Wettzell–Fortaleza from the IVS combination for ITRF2014.

3.2 Combination Report

The combination report for the session-wise IVS combination was established to inform all contributing ACs and all interested parties. All required information and

important details of every combination are individually assembled into a report (see Figure 4 for an example). The weight of each AC is given, and a combination statistic for each AC is calculated. The combination report contains offset, rate, and standard deviation parameters for the EOPs of each AC solution w.r.t. the combination. The estimated station coordinates and EOPs of the combination are also listed in the report. Further information can be added at any time. The SINEX file and the report can be found in the archive¹.

The reports are going to be sent out via mail as feedback to every contributing AC.

```

Combination report
SOLUTION
Link to sinexfile
AC contribution
-----
AC      Session details      passed/no contribution/rejected
-----
final weighting factors in COMBI
final weighting factor for AC = 1.57433639536895

COMBI ESTIMATE
-----
NUT_X ---- 13:331:23481 mas -1.48500938695768E-02  3.25226E-02
NUT_Y ---- 13:331:23481 mas  4.40258163545538E-01  3.53980E-02
UT ---- 13:331:23481 ms  -5.67378509982609E+01  1.57231E-03
XPO ---- 13:331:23481 mas  5.82449514956613E+01  2.86124E-02
YPO ---- 13:331:23481 mas  2.9207025520331E+02  3.14850E-02
LOD ---- 13:331:23481 masD  1.58185802098157E+00  5.97890E-03
XPOR ---- 13:331:23481 masD -7.77877100174048E-01  1.11514E-01
YPOR ---- 13:331:23481 masD  7.68777061461013E-01  1.30853E-01
STAX 7531 13:331:25920 m  1.20246251378082E+06  3.83632E-11
STAY 7531 13:331:25920 m  2.52734526780822E+05  3.83632E-11
STAZ 7531 13:331:25920 m  6.23776622316438E+06  3.83632E-11
-----
AC
-----
+SOLUTION/STATISTICS
NUMBER OF OBSERVATIONS      1419
NUMBER OF UNKNOWN          508
WEIGHTED SQUARE SUM OF O-C  2.47538392489028D+15
SQUARE SUM OF RESIDUALS (VTPV) 9.70558975743183D+02
VARIANCE FACTOR             9.4375242222299D-01
WRMS OF POSTFIT RESIDUALS   2.27445074014065D-11
-SOLUTION/STATISTICS
-----
Parameter |value
-----|-----
sc_off_xpol | 0.001572406668811724 |
sc_s_off_xpol | 0.003209469431714736 |
sc_rat_xpol | -0.007049568244237248 |
sc_s_rat_xpol | 0.005493173993903027 |
wrms_xpol | 0.04002459446517018 |
rms_xpol | 0.06189932655994299 |
sc_off_ypol | 0.002850322490411202 |
sc_s_off_ypol | 0.004111618342854179 |
sc_rat_ypol | 0.0032113587817661 |
sc_s_rat_ypol | 0.006987686226265066 |
wrms_ypol | 0.05211058623263043 |
rms_ypol | 0.07856987726178714 |
sc_off_dut1 | 0.0001179112867964599 |
sc_s_off_dut1 | 0.0002171412514138504 |
sc_rat_dut1 | 0.0002985106989019518 |
sc_s_rat_dut1 | 0.000368560883497504 |
wrms_dut1 | 0.002895801239094685 |
rms_dut1 | 0.003169096372250698 |
    
```

Fig. 4 Structure of the combination reports.

¹ http://www.ccivs.bkg.bund.de/EN/FAQs/Archiv/archiv_node.html

3.3 Additional Functions

The new generated calendar shows the important VLBI meetings of the present year. Every month is shown separately, and the event days are affirmed clearly. Additionally, the meetings of each month are sorted alphabetically, and if a meeting is missing, it can be announced by using the contact form.

Publications of the IVS Combination Center—e.g., presentations, posters, abstracts, and proceedings—can be found under the menu ‘Publications & Poster’. Furthermore, a news page introduces and informs all users about the activities of the IVS Combination Center, and details of the latest combination are listed at this page, as well.

3.4 Service Functions

3.4.1 Contact Form

The CMS offers already a wide scope of predefined functions including the contact form. Prescribed input fields make it possible to get in contact with the IVS Combination Center easily. In this case the IVS Combination Center will receive the message with all indicated sender information. Wrong entries or incorrect information will be detected by the system automatically. For contact, please use the main e-mail address (ccivs@bkg.bund.de) of the IVS Combination Center preferably.

Fig. 5 Contact form of the ccivs Web site.

3.4.2 Sitemap, Glossary, and Search Function

The sitemap, the glossary, and the search function are also included in the system and expand the functionality of the Web site.

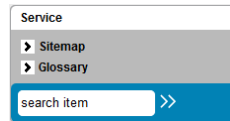


Fig. 6 Separated service menu of the ccivs Web site.

These three functions are introduced to simplify the navigation between all pages. The sitemap is similar to a table of content and describes the structure of the Web site. Every page can be reached by selecting the menu posts. The glossary is like a digital dictionary, which can be extended by the IVS Combination Center. It serves to describe all used abbreviations or technical terms in the page content. Colored letters symbolize valid glossary entries. Missing entries can be pointed out to the IVS Combination Center by using the contact form.

The search function is provided for browsing or searching for special words in the page content. For the search criterion, individual search terms and logical interconnections can be used. To give one example of the search criterion, you can specify the word OR between two search terms. Wildcards (*) stand for any letter and (?) for only one letter. The symbol (~) at the end of a search term provides a less precise search result.

3.4.3 Print Function

The print function can be found at each page in the footer. With this, the information of the current page (full page) can be printed out externally. The function helps to save data or the user specific settings and the results of the plot tool.

3.5 Observatory Map

The observatory map is an embedded Google Earth map for providing data of the VLBI stations. To use this map, a valid Google Earth version must be installed on

your system. Information such as station coordinates, the responsible organization, the location, and if available, a link to the observatory Web site are displayed by choosing a station symbol. The map was realized to show the VLBI network graphically (see Figure 7 for an example).



Fig. 7 VLBI network observatory map from using a Google Earth Plugin.

4 Conclusions

The reconstruction of the IVS Combination Center Web site was realized to standardize the Web presence and to make the handling more convenient. The chosen system provides these necessary conditions and serves methods and functions to implement these features additionally. By this, the content and possible settings are increased.

References

1. S. Bachmann, D. Thaller, O. Roggenbuck, M. Lösler, and L. Messerschmitt (2016) IVS contribution to ITRF2014. J Geod, doi 10.1007/s00190-016-0899-4.

ivg::ASCOT: Development of a New VLBI Software Package

Thomas Artz, Sebastian Halsig, Andreas Iddink, Axel Nothnagel

Abstract The VLBI group of the Institute of Geodesy and Geoinformation of the University of Bonn (IGG) has started implementing a new analysis toolbox for VLBI observations. The main reason is the need for a flexible environment which allows for straightforward implementations of new scientific and software-related ideas for VLBI data analysis. Furthermore, we want to accumulate the developments, which have been performed in Bonn in recent years, under a unified software package. The software is implemented in C++ and should finally be able to perform scheduling of VLBI sessions and simulation of VLBI observations, as well as geodetic data analysis and intra-technique combination. Thus, it is named: IGG VLBI Group–Analysis, Scheduling and Combination Toolbox (ivg::ASCOT). Currently, we are able to perform single-session data analysis, at the stage when the ambiguities have been resolved. Furthermore, global solutions to derive celestial and terrestrial reference frames can be performed on the normal equation level. Intra-technique combinations of several solutions complete the initial functionality of the software package.

Keywords VLBI, C++, software package, scheduling, geodetic VLBI data analysis, intra-technique combination

Institute of Geodesy and Geoinformation, University of Bonn

1 Introduction

There are several VLBI analysis packages that are used in the VLBI community. However, there are quite good reasons to start developing your own software. At the Institute of Geodesy and Geoinformation (IGG) of the University of Bonn, the main goal is to have a flexible and expandable environment at hand to easily develop new scientific projects. This is hardly the case for contemporary packages due to internal structures or the dependence on proprietary libraries or programs. Thus, the IGG VLBI Group (ivg) started the development of the Analysis, Scheduling and Combination Toolbox (ivg::ASCOT) in December 2014. The programming language is C++, and for the graphical user interface Qt¹ is used. The major goal is to merge the code from the PhD theses prepared at our institute in recent years into one consistent environment.

Currently, a basic VLBI least-squares adjustment in a session-by-session mode is possible. Furthermore, a global solution of pre-processed and pre-reduced datum-free normal equations in Solution INdependent EXchange (SINEX) format² can be performed. With very similar functionality, combinations on the normal equation level can be carried out.

The theoretical modeling of the VLBI delay is currently being validated in the VLBI Analysis Software Comparison Campaign 2015 (VASCC2015, [11]). In this way, we can directly ensure the correctness of our implementation w.r.t. other widely-spread VLBI data analysis software packages.

¹ <http://www.qt.io/>

² <http://www.iers.org/ IERS/EN/Organization/ AnalysisCoordinator/SinexFormat/sinex.html>

2 Structure of the Toolkit

The implementation relies on a variety of external code written in different languages. The basis of the theoretical modeling is the Conventions of the International Earth Rotation and Reference Systems Service (IERS Conventions, [14]). The IERS FORTRAN routines³ are compiled into a library and directly linked within `ivg::ASCOT`. This allows convention updates to be easily and directly adopted as the code on the IERS Web site is updated as well.

Furthermore, the SOFA library⁴ is used for the Earth orientation modeling. The JPL ephemeris is accessed via the CSPICE toolkit⁵ or code from Project-Pluto⁶. For the numerical calculations, we make use of ATLAS⁷/LAPACK⁸ or openBLAS⁹.

The basic internal library incorporating most of the functionality is `libivg`. Here, several classes are compiled which represent, e.g., the sessions with scans and observations, as well as the parameters. Furthermore, classes for the Earth Orientation Parameter (EOP) series as well as the terrestrial and celestial reference frames exist, which are made of stations and sources. Finally, the fundamental classes for the parameter adjustment are included in `libivg`.

In addition, there are different libraries for post-analysis tools (`libAnalysisTools` and `libqtplot`). The library `libAnalysisTools` contains classes to analyze station and source position variations; e.g., baseline length repeatabilities can be calculated. Furthermore, transformations between different reference frame realizations can be performed or estimated. In addition, the library `libqtplot` provides an easily accessible plotting environment as well as a graphical user interface (GUI) for various purposes. Thus, the functionality and the presentation of the results are strictly separated.

³ <http://62.161.69.131/iers/convupdt/convupdt.html>

⁴ <http://www.iausofa.org/>

⁵ <http://naif.jpl.nasa.gov/naif/>

⁶ http://www.projectpluto.com/jpl_eph.htm

⁷ <http://math-atlas.sourceforge.net/>

⁸ <http://www.netlib.org/lapack/>

⁹ <http://www.openblas.net/>

3 Single Session Analysis

The single session data analysis is based on VLBI observations given in the `vgosDB` data format [5] or in NGS card files¹⁰. Currently, an analysis can only be performed if the group delay ambiguities are resolved, the ionospheric corrections are calculated, and clock breaks are earmarked.

In an independent solution, a priori station motions are calculated based on the recommendations of the IERS Conventions, and further variations; e.g., non-tidal atmospheric pressure loading [15] or hydrological loading¹¹ could be applied. The theoretical delay including the relativistic corrections are implemented according to the IERS Conventions 2010 [14]. The EOPs can be used in a format according to the IERS C04 series¹² or USNO finals¹³. For the EOP modeling, additionally subdaily variations are taken into account according to the IERS Conventions 2010.

The parameter adjustment is currently solely based on the classical weighted least-squares adjustment. For the parameterization, a polynomial representation of arbitrary degree and/or continuous piece-wise linear functions with arbitrary interval length can be used. The continuous piece-wise linear functions are always referenced to the epoch of the first observation. The following parameters are currently supported:

- clocks,
- zenith wet delays,
- tropospheric gradients,
- station positions,
- source positions, and
- EOPs.

The weights of the observations are based on the standard deviations which result from the fringe fitting process. However, a stochastic refinement can be performed by applying constant and elevation weights [6] or an additional covariance matrix based on turbulence theory [7]. Finally, a simple data snooping procedure based on a Baarda test [3] can be applied to eliminate outliers.

¹⁰ http://lacerta.gsfc.nasa.gov/mk5/help/dbngs_format.txt

¹¹ <http://lacerta.gsfc.nasa.gov/hydro/>

¹² <http://www.iers.org/IERS/EN/DataProducts/EarthOrientationData/eop.html>

¹³ <http://maia.usno.navy.mil/ser7/finals.daily>

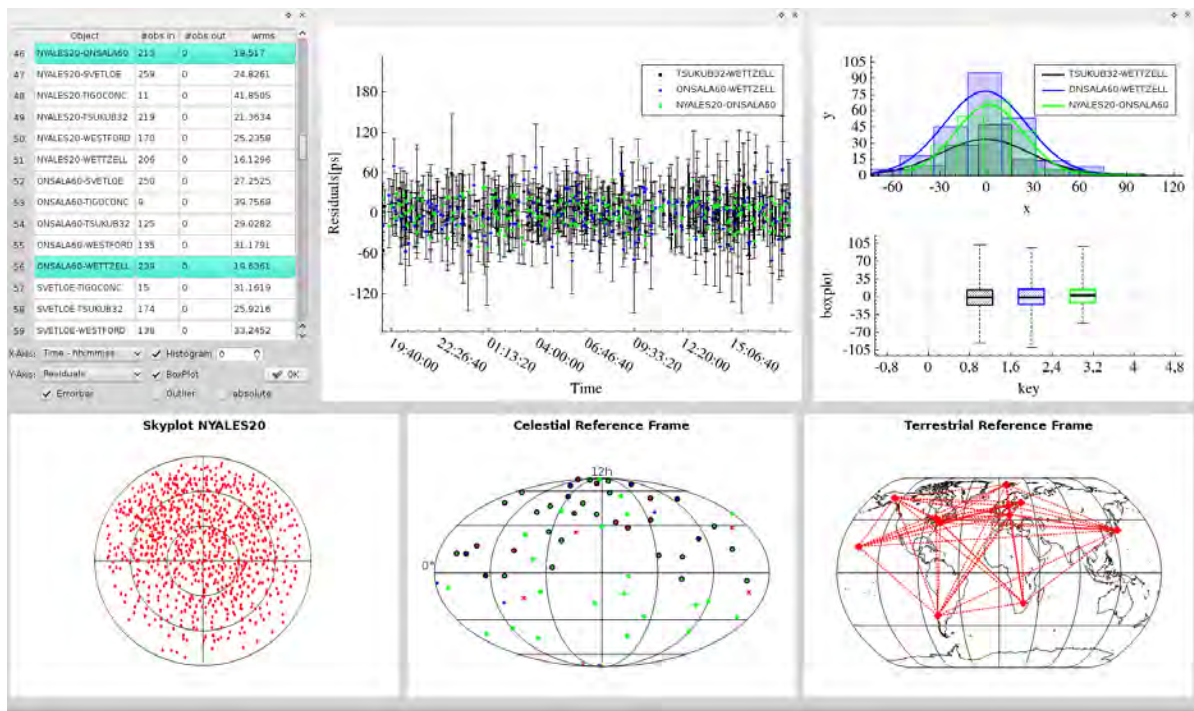


Fig. 1 Window of the residuals plot from a single session analysis including list of stations, baselines, and sources with WRMS of residuals, residual plot, statistical analysis, skyplot, observed sources, and network geometry.

The output of a single session analysis is either datum free normal equations or solutions with covariance matrices in SINEX format. Furthermore, a GUI exists where the residuals can be plotted (see Figure 1) depending on sites, baselines, or sources, and a statistical analysis of the residuals can be performed, e.g., by creating histograms and box plots.

4 Global Solution and Combination

Global solutions are based on pre-processed datum-free normal equations in SINEX format from single-session analysis. Through this functionality, it is also possible to use solutions from other software packages such as regular contributions to the official combined product of the International VLBI Service for Geodesy and Astrometry (IVS, [16]).

It is possible to reduce nuisance parameters and to perform transformations of a priori values. Furthermore, the global solution allows for various manipulations of normal equations such as transformations and

stacking [1]. This would make it possible to easily set up new parameters which are based on original ones such as, e.g., station velocities based on station positions. However, this feature is not implemented at this stage of the development.

Furthermore, session-by-session combination on the normal equation [4] or on the solution level [8] is possible. The major shortcoming at this point of the development is the absence of a reliable weighting procedure for different contributions.

The output of a global solution is again a SINEX file containing the estimates and the corresponding covariance matrix. But, it is also possible to export the stacked datum free normal equations prior to the solution.

5 Analysis Tools

A major feature of ivg::ASCOT is the post-analysis tools, which are based on solutions in SINEX files (see Figure 2). In a GUI, one can select the solutions

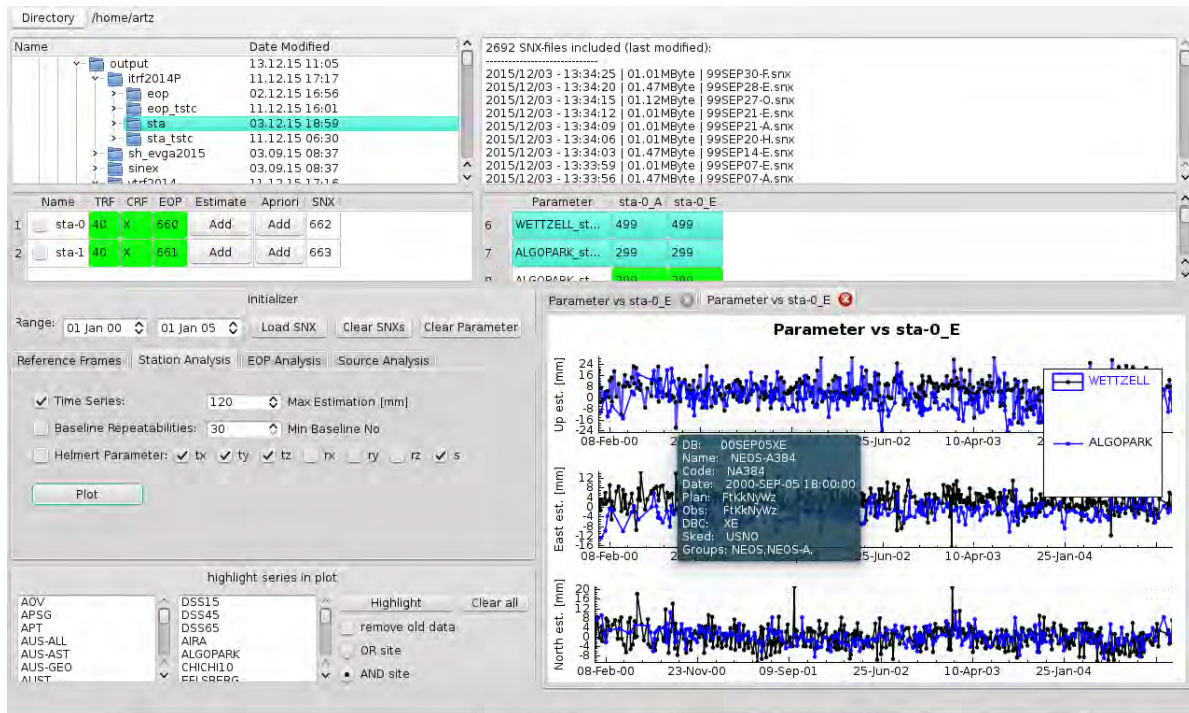


Fig. 2 Post data analysis GUI.

and perform a visualization of time series (stations, sources, and EOPs). Furthermore, a filtering of these time series can be performed based on various criteria, e.g. the session type or individual observing stations. In addition, it is possible to plot terrestrial and celestial reference frames, estimate Helmert parameters between different realizations, and visualize residuals after applying transformations.

6 Scheduling Module

The scheduling is currently not included in ivg::ASCOT. However, the implementation is basically based on the fundamental libraries of ivg::ASCOT.

The philosophy of the scheduling approach is the analysis of impact factors [12] to realize a geometrical optimization based on the parameters to be estimated. For Intensive sessions, the procedure is already used on a routine basis [13].

The input for the scheduling module is SKED catalogs¹⁴. The output is saved in skd-file format.

Porting the scheduling module into the toolbox is planned for the future.

7 Simulation Module

The simulation part is currently based on the vgosDB data format. The simulated delays consist of a deterministic part, according to the theoretical modeling of a single session analysis, and three stochastic components. These are simulated as baseline dependent noise, clock variations by power-law processes [9], and troposphere noise based on turbulence theory [10]. The variances for these processes can be chosen individually. The simulation was described in [2].

¹⁴ <ftp://gemini.gsfc.nasa.gov/pub/sked/catalogs/>

8 Conclusion and Future Work

The implementation of ivg::ASCOT is done in C++ and is thus highly flexible and expandable. Furthermore, using the Qt-library allows for a very intuitive and easy way to create graphical user interfaces. At the present stage of the development, typical VLBI parameters can be estimated in an independent solution, and basic time series analysis can be performed on residuals and estimates. Furthermore, global solutions can be used to estimate celestial and terrestrial reference frames, and even a combination of various analysis centers' input is possible.

Although not yet integrated, the scheduling part is based on the ivg::ASCOT libraries. This standalone scheduling program is currently used to schedule the INT2 sessions. However, porting the scheduling module into the toolbox is planned for the future.

Further developments will be primarily based on themes of PhD theses. Besides these scientific goals, it is planned to start the single session analysis at an earlier stage as is the case now. Thus, we will start with resolving ambiguities and calculating ionospheric corrections. Furthermore, the post-analysis tools will be enhanced, e.g., by implementing more thorough time series analysis.

References

1. T. Artz, S. Tesmer, and A. Nothnagel. Assessment of Periodic Sub-diurnal Earth Orientation Parameter Variations at Tidal Frequencies via Transformation of VLBI Normal Equation Systems. *J GEODESY*, 85(9):565–585, 2011.
2. T. Artz, A. Nothnagel and L. La Porta. VLBI observations of geostationary satellites. In: *Proceedings of the 21st European VLBI Group for Geodesy and Astrometry Working Meeting*, Helsinki, Finland, Reports of the Finnish Geodetic Institute, ISBN: 978-951-711-206-3, 217–221, 2013.
3. W. Baader. *A testing procedure for use in geodetic networks*. Publications on geodesy, Neth. Geod. Comm. Vol. 2, Issue 5, 1968.
4. S. Böckmann. *Robust determination of station positions and Earth orientation parameters by VLBI intra-technique combination*. phd-thesis, Universität Bonn, 6. Sep 2010.
5. S. Bolotin, K. Baver, J. Gipson, D. Gordon, and D. MacMillan. Implementation of the vgosDb format, In: *Proceedings of the 22nd European VLBI Group for Geodesy and Astrometry Working Meeting*, 18-21 May 2015 Ponta Delgada, Azores, Eds: R. Haas and F. Colomer, ISBN 978-989-20-6191-7, 150–152, 2015.
6. J. Gipson, D. MacMillan, and L. Petrov, Improved Estimation in VLBI through Better Modeling and Analysis, In: *IVS 2008 General Meeting Proceedings, "Measuring the Future"*, St. Petersburg, Russia, March 03-06 2008, Eds: A. Finkelstein and D. Behrend, 157–162, 2008.
7. S. Halsig, T. Artz, A. Iddink, and A. Nothnagel. Augmenting the stochastic model in VLBI data analysis by correlations from atmospheric turbulence models. In R. Haas and F. Colomer, editors, *Proceedings of the 22th EVGA working meeting*, 18–21 May 2015, Ponta Delgada, pages 201–204, 2015.
8. A. Iddink, A. Nothnagel, and T. Artz. Rigorous VLBI intra-technique combination strategy for upcoming CRF realizations. In N. Capitaine, editor, *Proceedings of the Journées 2013 Systèmes de Référence Spatio-Temporels* pp 81–83. Observatoire de Paris, 2014. ISBN: 978-2-901057-69-7.
9. N. J. Kasdin. Discrete Simulation of Colored Noise and Stochastic Processes and $1/f^\alpha$ Power Law Noise Generation. In *Proceedings of the IEEE*, volume 83, pages 802–826, May 1995.
10. G. Kerमारrec and S. Schön. On the Matérn covariance family: a proposal for modeling temporal correlations based on turbulence theory. *J GEODESY*, 88(11):1061–1079, 2014.
11. G. Klopotek et al. Results from the VLBI Software Comparison Campaign 2015, In: *IVS 2016 General Meeting Proceedings, "New Horizons with VGOS"*, Johannesburg, South Africa, March 13–19 2016, Eds: D. Behrend, K.D. Baver and K. Armstrong, this volume.
12. J. Leek, T. Artz, and A. Nothnagel. Optimized scheduling of VLBI UT1 Intensive sessions for twin telescopes employing impact factor analysis. *J GEODESY*, 89(9):911–924, 2015.
13. A. Nothnagel, J. Leek, M. Beier, T. Artz, and D. Ullrich. Sophistication in UT1-Intensive Scheduling by Using Impact Factors - First Results of Field Tests, In: *Proceedings of the 22nd European VLBI Group for Geodesy and Astrometry Working Meeting*, 18–21 May 2015 Ponta Delgada, Azores, Eds: R. Haas and F. Colomer, ISBN 978-989-20-6191-7, 185–188, 2015.
14. G. Petit and B. Luzum. IERS Conventions 2010. IERS Technical Note 35, Verlag des Bundesamtes für Kartographie und Geodäsie, Frankfurt am Main, Jul 2010. ISSN: 1019-4568.
15. L. Petrov and J.-P. Boy. Study of the atmospheric pressure loading signal in very long baseline interferometry observations. *J GEOPHYS RES*, 109(B18):B03405, Mar 2004.
16. H. Schuh and D. Behrend. VLBI: A fascinating technique for geodesy and astrometry. *Journal of Geodynamics*, 61, doi: 10.1016/j.jog.2012.07.007, pp. 68–80, 2012.

Transition to the vgosDb Format

Sergei Bolotin, Karen Bayer, John Gipson, David Gordon, Daniel MacMillan

Abstract The IVS Working Group 4 developed a new format to store and exchange data obtained from geodetic VLBI observations. The new data format, vgosDb, will replace existing Mark III databases this year. At GSFC we developed utilities that implement the vgosDb format and will be used routinely to convert correlator output to the new data storage format.

Keywords VLBI data analysis software, vgosDb

1 Introduction

Data produced at a correlator are subject to various changes before they become available to an end user. Historically, the results of correlation and fringe fitting of VLBI observations are stored in a binary self-descriptive file called a *database*. The format of the database file and implementation of input/output operations were developed in the early 1970s. Since then, the databases have been used as a standard for data exchange in the geodetic VLBI community.

The database format has disadvantages, mostly caused by hardware and software limitations that existed in the period when the format was developed. In addition, the format was not well documented. Several attempts to replace the database format with an alternative were made in the last few decades, but none of these were successful. The anticipated vast increase in the number of VLBI observations and the emergence of VLBI Global Observing System

NVI, Inc.

(VGOS) technology prompted the IVS Directing Board to establish the IVS Working Group on Data Structures. Efforts undertaken by the group were eventually realized in the creation of the new VLBI data format, *vgosDb* (see [4]).

In accordance with the vgosDb format, the VLBI data of one session are stored in various files in the form of $\{key \Rightarrow value\}$. Each file represents an atomic piece of data, e.g., observed values with their standard deviations, or station coordinates. An additional feature is that it is possible to keep alternative models or approaches to the editing of observations in the same session data tree. A set of data files that is available to the user is specified in a special file called a *wrapper file*. It is possible to have more than one wrapper file for one VLBI session.

2 vgosDb-compatible VLBI Data Analysis Software

First results of the implementation of the vgosDb format by the GSFC VLBI group were shown in 2013. The legacy VLBI data analysis software, *global solve*, is ready to use data in the vgosDb format [5]. A part of the *solve* distribution package is the utility *db2vgosDB*, which converts data of a VLBI session from the database format into the vgosDb format. The next generation VLBI data analysis software, *vSolve*, is capable of working with the new format [2].

In addition, vgosDb-compatible utilities were developed to support the transition to the vgosDb format. These utilities replace the legacy utilities *dbedit* and *pxxcb/dbcal*. The first utility, *dbedit*, creates database files from correlator output and fringe files. Routinely,

it is executed at a correlator, and the database file for each band is then sent to one of the VLBI data centers. The purpose of the second pair of utilities, `pwxcb` and `dbcal`, is to extract, validate, edit (if necessary), and put into a database the information that is contained in the Field System log files produced by each station that participated in a VLBI session. Usually, two types of data are extracted: cable calibration measurements and meteorological parameters.

The new vgosDb-compatible utilities, `vgosDbMake` (which replaces `dbedit`) and `vgosDbProcLog` (which replaces `pwxcb/dbcal`), are part of the new VLBI data analysis software developed at NASA GSFC [1] and currently distributed in one package under the common name “nusolve”. It is available on the FTP site:

```
ftp://gemini.gsfc.nasa.gov/pub/misc/
  slb/nusolve-latest.tar.gz
```

These utilities have the same design as other `vSolve` software as well as the same software development environment.

The utilities are designed to operate on any POSIX compatible operating system. We use C++ as the programming language due to its power, flexibility, and portability. The GNU Build System is used to make the software distribution portable. The software consists of two parts:

- Space geodesy library: a library where data structures and algorithms are implemented (about 90% of the total source code).
- Executables `vgosDbMake` and `vgosDbProcLog`: drivers that call library functions and organize work with an end user (about 10% of the total source code).

Such organization of the software allows us to share the source code between applications and reuse it in other projects.

The software has a modular structure that makes it flexible and scalable. A module is a logical block of code that is loosely tied with other parts of the software.

Obviously, not all the modules will be used by `vgosDbMake` and `vgosDbProcLog`. On the other hand, the modular design of the software allows us to easily add the functionality of the utilities to the interactive VLBI data editor, `vSolve`.

Modification of the program `calc` to be compatible with vgosDb is done in a different way. A library that mimics the Mark III database handler programming interface has been created. The library replaces database functions with vgosDb input/output operations. In this case we do not need to modify the `calc` source code at all, but just need to link the software with the new library. This approach was realized by Julia Ringsby, an NVI intern in 2013 [6], in the program `vgosDbCalc`. It was written in the C++ programming language, but its design is different from the design of the `vSolve` software. We use `vgosDbCalc` as a prototype for demonstration of the vgosDb format usage, but it will be replaced with a utility based on our common design for the new VLBI data analysis software.

The software `vgosDbCalc` is distributed in a separate package and can be downloaded from the FTP site

```
ftp://gemini.gsfc.nasa.gov/pub/misc/
  slb/vgosDbCalc.tar.gz
```

The distribution contains instructions on how to compile the source code and to run the utility. A collection of necessary files with *a priori* data is also in the distribution. It should be noted that one of these files, the table of the Earth rotation parameters, needs to be updated on a regular basis.

3 Use of the VLBI Data in the vgosDb Format

The vgosDb format is used in routine data analysis utilizing the set of the three vgosDb compatible software packages: `solve`, `vgosDbCalc`, and `vSolve`.

Before switching to the new vgosDb format we made the VLBI observations in this format available for public access in two groups of files. The first is the data that are distributed by the official IVS ftp sites. The vgosDb files for this set can be downloaded from

```
ftp://gemini.gsfc.nasa.gov/pub/
  vgosDB_IVS/
```

The second collection of the vgosDb files corresponds to the GSFC-analyzed VLBI observations. It can be obtained from

```
ftp://gemini.gsfc.nasa.gov/pub/
  vgosDB_GSFC/
```

The main difference between the two data sets is in the data editing options. These publicly accessible data will help users to transition to the new format.

The first practical use of the VLBI observations in the vgosDb format was reported by MIT Haystack Observatory [7]. All VGOS-related observations since January 2016 were analyzed with vgosDb data flow. These observations include broadband VGOS sessions with up to three stations and S/X sessions using mixed Mark IV and broadband stations.

4 Conclusions

Our group will switch to the new VLBI data format in mid-2016. At the time of writing this paper we are performing extensive testing of the software, the legacy solve package, and new utilities from the nusolve distribution. In July 2016, we will perform tests of the entire VLBI data flow using the vgosDb format and then start to release VLBI sessions in the new format routinely. We strongly encourage all Analysis Centers to switch to the new VLBI data format.

Acknowledgements

We are grateful to Tim Morin, Mike Titus, and Arthur Niell of the MIT Haystack Observatory for installing, testing, and helping debug the vgosDb format.

References

1. S. Bolotin, J.M. Gipson and D. MacMillan. *Development of a New VLBI Data Analysis Software*. In D. Behrend, and K.D. Baver, editors, *IVS 2010 General Meeting Proceedings*, NASA/CP-2010-215864, NASA GSFC, Maryland, pages 197–201, 2010.
2. S. Bolotin, K. Baver, J.M. Gipson, D. Gordon and D. MacMillan. *The VLBI data analysis software vSolve: development progress and plans for the future*. In D. Behrend, K.D. Baver, and K. Armstrong, editors, *IVS 2014 General Meeting Proceedings*, ISBN 978-7-03-042974-2, Science Press, Beijing, China, pages 253–257, 2014.
3. J.M. Gipson. *IVS Working Group 4: VLBI Data Structures*. In D. Behrend, and K.D. Baver, editors, *IVS 2012 General Meeting Proceedings*, NASA/CP-2012-217504, NASA GSFC, Maryland, pages 212–221, 2012.
4. J. Gipson, J. Böhm, S. Bolotin, D. Gordon, T. Hobiger, C. Jacobs, S. Kurdubov, A. Nothnagel, O. Sovers, O. Titov, H. Takiguchi. *Final Report of IVS Working Group 4 (WG4) on Data Structures*. In K.D. Baver, D. Behrend, and K. Armstrong, editors, *International VLBI Service for Geodesy and Astrometry 2013 Annual Report*, NASA/TP-2014-217522, NASA GSFC, Maryland, pages 11–25, 2014.
5. J. Gipson. *Practical Uses of VGOSDB Format*. In R. Haas and F. Colomer, editors, *Proceedings of the 22nd European VLBI Group for Geodesy and Astrometry Working Meeting*. ISBN 978-989-20-6191-7, pages 97–101.
6. D. Gordon, C. Ma, D. MacMillan, J. Gipson, S. Bolotin, K. Le Bail, K. Baver. *GSFC VLBI Analysis Center Report*. In K.D. Baver, D. Behrend, and K. Armstrong, editors, *International VLBI Service for Geodesy and Astrometry 2013 Annual Report*, NASA/TP-2014-217522, NASA GSFC, Maryland, pages 272–275, 2014.
7. A. Niell, R. Cappallo, B. Corey, C. Eckert, P. Elosegui, R. McWhirter, G. Rajagopalan, C. Ruzsczyk, M. Titus. *VGOS Observations with Westford, GGAO, and the new station at Kokee, Hawaii*. This volume.

Refinement of the Rapid UT1 Estimation Derived from Tsukuba VLBI Measurements after the 2011 Earthquake

Gerald Engelhardt, Volkmar Thorandt, Dieter Ullrich

Abstract The Tsukuba station in Japan is an essential station in the International VLBI Service for Geodesy and Astrometry (IVS) Intensive series for rapid Universal time (UT1) estimation. The use of this station in rapid UT1 estimation requires a set of best-predetermined station coordinates, but the consequences of the earthquake in Japan in March 2011 were such that the previously known velocity rates of the station Tsukuba were unusable. Since 2012, the VLBI group at BKG has used a method which solves this problem. This procedure was refined with respect to a newly developed extrapolation to get the most probable station positions of Tsukuba for the epochs of the Intensive sessions. The procedure is explained and could be successfully integrated into the technological process of operational analysis of post-quake Intensive sessions with station Tsukuba.

Keywords Rapid UT1 estimation, coordinate series, extrapolation

1 Situation Before and After the 2011 Earthquake

The first successful UT1 Intensive session with the VLBI station Tsukuba in Japan (IVS name Tsukub32) was measured on May 5, 1999. Since then, approximately 823 sessions could be measured until early March 2011. After a big earthquake in the region of the station Tsukuba on March 11, 2011, station displacements up to 67 centimeters occurred. The time series

Bundesamt für Kartographie und Geodäsie (BKG)

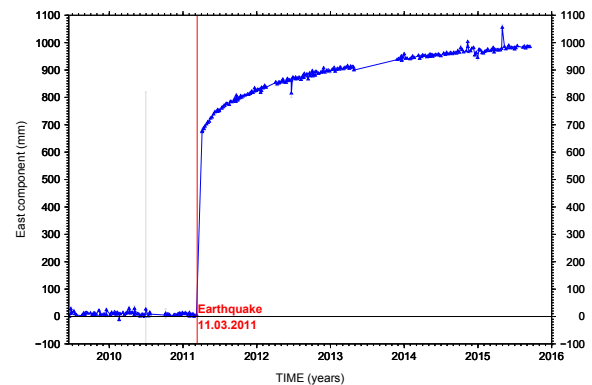


Fig. 1 Station position time series of Tsukub32 (Japan) in east component of VLBI solution bkg00014 in the form of differences to the reference session named R1383 (09JUN15XA).

of the station coordinates about 1.5 years before and 4.5 years after the earthquake can be seen in Figures 1, 2, and 3. You can see a big offset in the east compo-

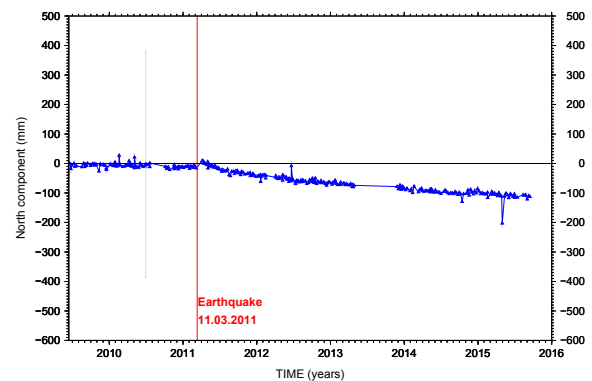


Fig. 2 Station position time series of Tsukub32 (Japan) in north component of VLBI solution bkg00014 in the form of differences to the reference session named R1383 (09JUN15XA).

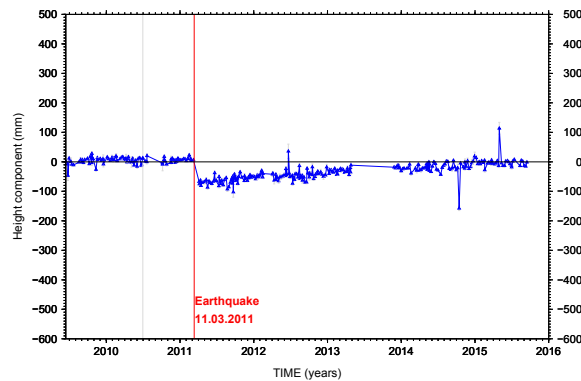


Fig. 3 Station position time series of Tsukub32 (Japan) in the height component of VLBI solution bkg00014 in the form of differences to the reference session named R1383 (09JUN15XA).

ment but also different rates in all components after the earthquake. Therefore, the old velocity rates before the earthquake can no longer be used. A new procedure for getting the best possible coordinates as a prerequisite for a reliable unbiased UT1 estimation is thus necessary.

2 Procedure of Intensive Session Processing (Int2/3)

2.1 Tsukub32 Coordinate Series from BKG Global Solution bkg00014

The BKG global solution bkg00014 [4] for generating terrestrial reference frame (TRF) and celestial reference frame (CRF) realizations, tropospheric parameters, and earth orientation parameter (EOP) series is based on a solution mode with common estimation of all parameter types from 24-hour sessions since 1984. The station coordinates of Tsukub32 are one part of the arc-parameters in sessions with station Tsukub32. The station position time series of Tsukub32 in X , Y , Z coordinate components and their standard deviations are extracted in a first step.

2.2 Tsukub32 Smoothed Pseudo-coordinate Series

The locally determined station coordinates of Tsukub32 and their standard deviations are used

for the estimation of a weighted mean between two sequent station positions at the mid-epoch of both single solutions. Thus, a smoothed pseudo-coordinate series of station Tsukub32 can be generated for all coordinate components (X , Y , Z).

2.3 Linear Interpolation

The smoothed pseudo-coordinate series of Tsukub32 is used for linear interpolation between the epochs of two sequent data points to get the most probable station positions for the epochs of Int2/3 sessions. If epochs of Int2/3 sessions exist after the last estimated Tsukub32 position, coordinates of the last 24-hour session of it were used in the old procedure [2].

2.4 Extrapolation

If you need the most probable station positions for the epochs of Int2/3 sessions after the epoch of the last estimated Tsukub32 position from the global solution, then a rate in each coordinate component is used now for the extrapolation. The starting point for this is the estimates of the last seven Tsukub32 positions from the global solution. The process is illustrated by the example of the X coordinate, see Figure 4, but it is also valid for the coordinate components Y and Z .

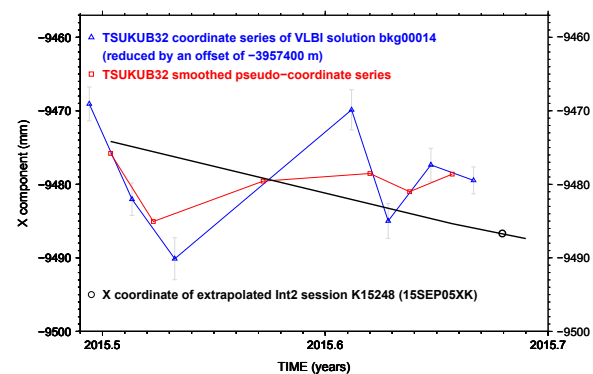


Fig. 4 Example for the extrapolation in coordinate component X for the Int2 session K15248 (15SEP05XK) with actually determined coordinate series and a smoothed pseudo-coordinate series of station Tsukub32 after the March 2011 earthquake.

So:

$$X_{g1}, \dots, X_{g7} \quad sX_{g1}, \dots, sX_{g7}$$

are given, with

X_g : X coordinate of global solution

and

sX_g : standard deviation of X_g .

The process can be divided into four steps:

Step 1: Calculation of smoothed pseudo-coordinates X_{m1}, \dots, X_{m6} by weighted mean between two given sequent coordinate values to the respective mean epochs Em_1, \dots, Em_6

Step 2: Calculation of piecewise rates between two sequent smoothed pseudo-coordinate values to their epochs, so

$$\frac{X_{m2} - X_{m1}}{Em_2 - Em_1}, \dots, \frac{X_{m6} - X_{m5}}{Em_6 - Em_5}$$

Step 3: Conversion to piecewise rates per year and estimation of the average rate $vX(\text{mean})$

Step 4: Based on $vX(\text{mean})$ it is possible to compute the station coordinate for the epoch of the respective Int2/3 session starting from the middle of the period $Em(\text{mean})$ derived from Em_1, \dots, Em_6 and the average coordinate $Xm(\text{mean})$ derived from X_{m1}, \dots, X_{m6} .

An example of the extrapolation of the X coordinate for the Int2 session K15248 (15SEP05XK) is shown in Figure 4.

2.5 UT1 Estimation

After determination of the most probable station positions of Tsukub32 for the epochs of Int2/3 sessions, regular analysis can be executed. The estimated parameter types are the difference between UT1 and international atomic time (TAI), station clock, and zenith

troposphere together with fixed station coordinates in VLBI TRF, realization 2008a [1] and radio source positions from *International Celestial Reference Frame, second realization (ICRF2)* [3]. The reliability of the determination of UT1-TAI depends significantly on the accuracy of the fixed station coordinates. Thus, a coordinate change of one centimeter in the eastern component of Tsukub32 causes a UT1-TAI change of about 15.5 microseconds in the example session K15248.

3 Integration in Technological Process

The above described single steps for handling the Int2/3 sessions with station Tsukub32 were combined into a semi-automatic process. The newly determined a priori station coordinates for each Tsukub32 Intensive session are used as input for the session by session Tsukub32 Intensive cycle run. Finally, an IVS formatted EOP list is created and mixed with the non-Tsukub32 IVS EOP list. These algorithms were included in the BKG post-interactive part of establishing the IVS EOP solutions.

4 Conclusions

On the basis of an interpolation and extrapolation procedure of the station position time series of Tsukub32 derived from a global solution with all 24-hour sessions, the most probable station positions of Tsukub32 for the epochs of the Intensive sessions can be estimated.

A great advantage of this method is that the same VLBI antenna at the station Tsukub32 is used for the 24-hour sessions and Int2/3 sessions. The new extrapolation method prevents the sole use of a specific weak Tsukub32 position from the global solution, resulting in a higher reliability of Tsukub32 coordinate determination at the epochs of Int2/3 sessions.

References

1. Boeckmann S, Artz T, Nothnagel A (2010). VLBI terrestrial reference frame contributions to ITRF2008. *J Geod*, DOI10.1007/s00190-009-0357-7.

2. Engelhardt G, Thorandt V, Ullrich D (2013). Rapid UT1 Estimation Derived from Tsukuba VLBI Measurements after 2011 Earthquake. *In: Proceedings of the 21st Meeting of the European VLBI Group for Geodesy and Astronomy*, Kirkkonummi, Finland; N. Zubko, M. Poutanen (eds.); 85–87.
3. Fey A, Gordon D, Jacobs CS (2009). The Second Realization of the International Celestial Reference Frame by Very Long Baseline Interferometry. *IERS Technical Note No 35*. Verlag des Bundesamtes für Kartographie und Geodäsie, Frankfurt am Main.
4. Thorandt V, Engelhardt G, Ullrich D (2015). VLBI Analysis at BKG. *In: Proceedings of the 22nd European VLBI Group for Geodesy and Astrometry Working Meeting*, Ponta Delgada, Azores; R. Haas, F. Colomer (eds.); 256–258.

Improvement of the IVS-INT01 Sessions through Bayesian Estimation

John Gipson, Karen Baver

Abstract We report on the use of Bayesian estimation in the analysis of IVS INT01 sessions. We demonstrate that the use of a priori knowledge improves the accuracy of the UT1 estimates. We look at two cases—the incorporation of gradients estimated from independent R1 and R4 sessions and the use of an external model of Free Core nutation. In each case we find the magnitude of the change in the UT1 estimates induced by using the a priori information. We also calculate the improvement in the accuracy of the Intensives as measured by the agreement between the Intensive estimate of UT1 and that of a concurrently run R1/R4 session. In both cases, the accuracy is improved, and the amount of improvement is consistent with expectations based on the size of the effect.

Keywords Intensive, UT1, Bayesian estimation

1 Introduction

VLBI makes important contributions to the estimation of Earth Orientation Parameters and is unique in its ability to measure UT1 [1]. Because of this, the IVS schedules bi-weekly 24-hour R1 (Monday) and R4 (Thursday) sessions to measure all components of EOP. The IVS also schedules special one-hour sessions designed specifically to measure UT1. These Intensive sessions have a small number of stations (typically two to four) involving long East-West baselines and run for about one hour, resulting in 15–40 observations. Normally data from these sessions is transmitted electroni-

NVI, Inc.

cally to the correlator, and the final UT1 estimate is often available within < 24 hours after the session ends. But the very characteristics of short duration and small network size that makes rapid transmission, correlation, and analysis possible also means that the precision of the Intensives is much less than that of 24-hour VLBI sessions. Anything that can improve the accuracy and/or the precision of the Intensives is important.

In this paper our data set is the INT01 series which are scheduled by USNO, run Monday–Friday, and use the Kokee–Wettzell baseline. These sessions are scheduled using two alternating strategies. The STN uses a small set of strong sources with uneven sky coverage. The MSS uses a large set of sources that are on average weaker but have good sky coverage. Sessions can behave differently depending on the strategy used to schedule them, so we typically divide the INT01 sessions into STN and MSS subsets for analysis [2]. Ultimately we are interested in the accuracy of the UT1 estimates. Because of this we further restrict our attention to only those Intensives that occur on the same day as an independent R1/R4 session. Our proxy for the accuracy is the difference between the Intensive UT1 estimate and that of the concurrent R1/R4 session interpolated to the same epoch. Figure 1 plots this difference for 2011–2012. The STN estimates differ from the 24-hour estimates by up to $\sim 100 \mu\text{s}$, and the MSS estimates differ by up to $\sim 70 \mu\text{s}$. The standard deviations of the differences are also high— $30.68 \mu\text{s}$ for the STN and $21.04 \mu\text{s}$ for the MSS.

Our primary goal is to improve the a priori models used in the Intensives, and to verify that this results in more accurate UT1 estimates. As a side-effect, we determine the change in the UT1 estimates caused by changing the a priori. This is similar to work done previously by Nothnagel and Schnell [5] who looked at

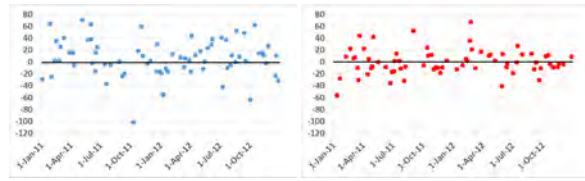


Fig. 1 Differences between UT1 estimates from IVS 24-hour and operational INT01 STN (left) and MSS (right) sessions.

the effect of errors in Polar Motion (PM) and Nutation (FCN) and found they were significant. Gipson et al. [3] redid this work and extended it to include the effect of errors in station position, mapping functions, and atmosphere gradients. They determined which modeling errors have potentially the largest impact on UT1 (East, PM, FCN, gradients) and hence should have a priority on improved modeling, and which error sources had a small effect (e.g., Up and North) and could be ignored.

Gipson et al. [3] also demonstrated that using PM and nutation estimates derived from concurrent 24-hour R1/R4 sessions in Intensive analysis improved the agreement between the Intensive and R1/R4 estimates of UT1. We extend this work by demonstrating that using atmospheric gradients from 24-hour sessions also improves the agreement. Such an approach is not possible operationally, because the results from the R1/R4 sessions are not available until several weeks later. We also looked at improving the a priori modeling by using data which *is* available at the time of the Intensive processing, namely using FCN values from Sébastien Lambert’s FCN series [4]. We find that use of this data improves the agreement between the Intensive and 24-hour session estimates.

In Sections 2 and 3 we discuss our general approach. In Section 4 we look at using gradient estimates from R1/R4 sessions. In Section 5 we look at applying external FCN. Section 6 has some concluding remarks. We find that the use of better a priori information improves the accuracy of Intensive UT1 estimates and that the magnitude is in line with what you would expect based on the effect of the error. But the resulting change in the accuracy is small, 1–2 μ s or less.

2 Augmented Normal Equations

Least squares estimation involves solving the matrix equation $A = N^{-1}B$, where A is the parameter esti-

mate vector, N is the normal matrix of weighted partial derivatives, and B is the ‘ $O-C$ ’ (=“Observed minus Calculated”) vector. INT01 sessions have a small (~ 16 to 25) number of observations and only allow estimation of a few (typically five) parameters which are: atmosphere offsets at Kokee and Wettzell; clock and clock rate at Wettzell; and UT1 offset. Sometimes a quadratic clock term is estimated as well.

An important and often unstated implicit assumption is that the a priori models are correct. We know that this assumption is incorrect, because, for example, when we estimate PM in a 24-hour session we get non-zero values. An error in an underlying model will change the ‘ $O-C$ ’ vector, which in turn will change the estimates.

To address this issue, we construct the normal equations for the Intensives with additional parameters corresponding to possible errors in the a priori. We call these ‘augmented’ normal equations. These may be singular because we may not have enough data to estimate the parameters. To fix this we apply additional information in the form of constraints. We call this approach ‘Bayesian’. Explicitly, let a be the index of an extra parameter A_a , and assume that we know that A_a has the value V_a with an uncertainty of σ_a . We modify the normal equations thus: $N_{aa} \rightarrow N_{aa} + 1/\sigma_a^2$, $B_a \rightarrow B_a + V_a/\sigma_a^2$ with all other components staying the same. Effectively we are introducing extra “observations” corresponding to the constraint. If $V_a = 0$, in the limit $\sigma_a \rightarrow 0$ we recover the usual UT1 estimate. Non-zero values of V_a and σ_a change the UT1 estimate.

3 Effect of Changing a Priori

In this section we establish some notation and derive some results. Let j label an Intensive, and let $UT1_{Def,j}$ (respectively, $UT1_{Mod,j}$) be the UT1 estimate from the default (respectively, modified) processing. Also let $UT1_{24,j}$ be the UT1 estimate from a corresponding 24-hour session, interpolated to the epoch of the Intensive. We are interested in the following quantities:

$$\Delta UT1_{Def,j} = UT1_{Def,j} - UT1_{24,j} \quad (1)$$

$$\Delta UT1_{Mod,j} = UT1_{Mod,j} - UT1_{24,j} \quad (2)$$

$$\delta UT1_{Mod,j} = UT1_{Def,j} - UT1_{Mod,j} \quad (3)$$

The first two are the differences between the Intensive and the 24-hour estimate of UT1, and will be useful in

determining the accuracy of Intensive UT1 estimates. The third defines the effect of modifying the analysis of the Intensive. For any series f, g , define:

$$\langle f \cdot g \rangle = \sum_j^N f_j g_j / N \quad (4)$$

As N goes to infinity this is just the expectation value.

Let $\epsilon_{A,j}$ denote the error in UT1 (here A is one of Def, Mod , or 24). Then we find, for example,

$$\Delta UT1_{Def,j} = \epsilon_{Def,j} - \epsilon_{24,j} \quad (5)$$

Consider

$$\begin{aligned} \langle \Delta UT1_{Def}^2 \rangle &= \langle \epsilon_{Def}^2 \rangle + \langle \epsilon_{24}^2 \rangle \\ &\quad - 2 \langle \epsilon_{Def} \cdot \epsilon_{24} \rangle \end{aligned} \quad (6)$$

The errors in the 24-hour and Intensive UT1 estimates should not be correlated. Hence for large N the last term on the Right Hand Side (RHS) should vanish. Further, because the formal errors for the Intensives are a factor of 5–10 larger than for the 24-hour sessions we expect that $\epsilon_{Def}^2 \gg \epsilon_{24}^2$. This means the second term can be ignored. We are left with:

$$\langle \Delta UT1_{Def}^2 \rangle \simeq \langle \epsilon_{Def}^2 \rangle \quad (7)$$

The symbol \simeq means the equality holds for large N . This means that we can calculate the expected error (ϵ_{Def}) by calculating $\langle UT1_{Def}^2 \rangle$.

Suppose that we modify the analysis of the Intensives in some way. What is the expected error in these new estimates? Analogous to Equation 7, we find:

$$\langle \Delta UT1_{Mod}^2 \rangle \simeq \langle \epsilon_{Mod}^2 \rangle \quad (8)$$

Note that by Equations 2 and 3 we have:

$$\begin{aligned} \Delta UT1_{Mod} &= UT1_{Mod} - UT1_{24} \\ &= UT1_{Def} - \delta UT1_{Mod} - UT1_{24} \\ &= \Delta UT1_{Def} - \delta UT1_{Mod} \end{aligned} \quad (9)$$

Hence

$$\begin{aligned} \langle \Delta UT1_{Mod}^2 \rangle &= \langle (\Delta UT1_{Def} - \delta UT1_{Mod})^2 \rangle \quad (10) \\ &= \langle \Delta UT1_{Def}^2 \rangle + \langle \delta UT1_{Mod}^2 \rangle \\ &\quad - 2 \langle \delta UT1_{Mod} \cdot \Delta UT1_{Def} \rangle \end{aligned}$$

We consider two alternatives. First, suppose that $\delta UT1_{Mod}$ is noise-like. In this case it will be uncorrelated with both $UT1_{Def}$ and $UT1_{24}$:

$$\begin{aligned} \langle \delta UT1_{Mod} \cdot UT1_{24} \rangle &\simeq 0 \\ \langle \delta UT1_{Mod} \cdot UT1_{Def} \rangle &\simeq 0 \end{aligned} \quad (11)$$

Using Equation 1 $\langle \delta UT1_{Mod} \cdot \Delta UT1_{Def} \rangle \simeq 0$. Hence for a noise-like signal we have:

$$\langle \epsilon_{Mod}^2 \rangle \simeq \langle \epsilon_{Def}^2 \rangle + \langle \delta UT1_{Mod}^2 \rangle \quad (12)$$

As expected, adding noise increases the error. At the other extreme, suppose that ϵ_{Mod} removes noise from $UT1_{Def}$. In this case we still expect it to be uncorrelated with $UT1_{24}$, but it should be correlated with $UT1_{Def}$:

$$\begin{aligned} \langle \delta UT1_{Mod} \cdot UT1_{24} \rangle &\simeq 0 \\ \langle \delta UT1_{Mod} \cdot UT1_{Def} \rangle &\simeq \langle \delta UT1_{Mod}^2 \rangle \\ &\quad + 2 \langle \delta UT1_{Mod} \cdot \Delta UT1_{Mod} \rangle \end{aligned} \quad (13)$$

where the last term is effectively zero. Going through the same analysis of Equation 10 as previously:

$$\langle \epsilon_{Mod}^2 \rangle \simeq \langle \epsilon_{Def}^2 \rangle - \langle \delta UT1_{Mod}^2 \rangle \quad (14)$$

hence adding the signal $\delta UT1_{Mod}$ reduces the error.

4 Use of R1/R4 Gradients

In the analysis of the 24-hour and Intensive sessions the *a priori* gradient is the average gradient at a site computed from a numerical weather model. In the 24-hour sessions we estimate residual East-West and North-South gradients as a Piece-Wise-Linear function with rate breaks every six hours. In the Intensives we do not.

To incorporate additional information about gradients into the Intensives we augment the Intensive normal equations to include residual gradients. We restrict attention to only those Intensives that occur on the same day as R1/R4 sessions that include both Kokee and Wettzell. Out of the original 74 STN and 70 MSS sessions we were left with 54 and 53 sessions, respectively. The R1/R4 residual gradient estimates are interpolated to the epoch of the Intensives. The Intensive gradient estimates are constrained to these values with small sigmas.

In analogy with Equation 1, define the following:

$$\begin{aligned}\delta UT1_{Grad,j} &= UT1_{Def,j} - UT1_{Grad,j} \\ \Delta UT1_{Def,j} &= UT1_{Def,j} - UT1_{24,j} \\ \Delta UT1_{Grad,j} &= UT1_{Grad,j} - UT1_{24,j}\end{aligned}\quad (15)$$

The first of these is just the change in UT1 estimates caused by including gradients and is plotted in Figure 2. The second+third items are the distance between the Intensive and 24-hour estimates. Because the errors in the 24-hour sessions are much smaller, these are a measure of the error in the Intensive estimates. Figure 3 plots $|\Delta UT1_{Def,j}| - |\Delta UT1_{Grad,j}|$ which we call the reduction in absolute error. The first term is the distance between the default Intensive and 24-hour estimate of UT1, while the second is the distance when we use gradients. If this is positive, using gradients helped.

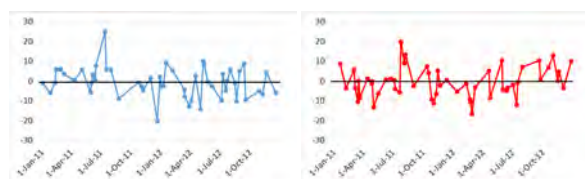


Fig. 2 Effect of using gradient estimates on STN (left) and MSS (right) INT01 UT1 estimates (μs).

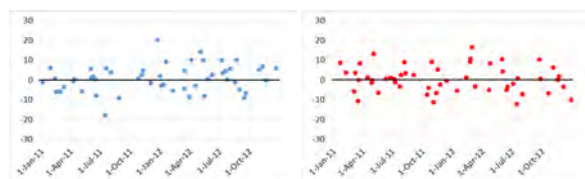


Fig. 3 Reduction in absolute error for STN (left) and MSS (right) INT01 sessions (μs) from using gradients.

As demonstrated in the previous section, the RMS of $\Delta UT1_{Def}$ ($\Delta UT1_{Grad}$) is a measure of the error in the default (gradient) estimate of UT1 from the Intensives. Table 1 lists these values. Using gradients improves the accuracy, although the amount is small. This table also lists the RMS of $\delta UT1_{Grad}$ which is a measure of the size of the ‘gradient signal’ in the UT1 estimate. Gradients change the UT1 estimate by $\sim 7.5 \mu\text{s}$, which is a large effect. This may seem in contradiction to the small change in error. But as shown in the previous section,

$$RMS \delta UT1_{Grad} \simeq \sqrt{\langle \Delta UT1_{Def}^2 \rangle - \langle \Delta UT1_{Grad}^2 \rangle}$$

which relates the size of the gradient signal to a reduction in the variance. Table 1 displays the RHS of this equation. Note that these values are within 20% of $\delta UT1_{Grad}$ which is a reasonable agreement.

Table 1 Effect of atmospheric gradients in μs .

	STN	MSS
RMS $\Delta UT1_{Def}$	29.30	21.73
RMS $\Delta UT1_{Grad}$	28.42	19.84
Improvement in RMS	0.88	1.89
RMS $\delta UT1_{Grad}$	7.46	7.62
$\sqrt{\langle \Delta UT1_{Def}^2 \rangle - \langle \Delta UT1_{Grad}^2 \rangle}$	6.55	8.98
Average reduction in absolute error	0.77	0.58

5 Use of Empirical Free Core Nutation

Sébastien Lambert (SYRTE, Observatoire de Paris) developed and maintains a model of the FCN derived from the IERS EOP 08 C04 series. The nutation values in the IERS C04 come from VLBI estimates of the FCN, and hence Lambert’s model should be consistent with our estimates from the R1s and R4s. The major obstacle to using Lambert’s FCN series directly is that it is given in terms of nutation X and Y, whereas our software used ψ and ε . We wrote software to convert between these two, and Figure 4 shows good agreement between the transformed FCN values from Lambert and our FCN estimates from the R1/R4 series.

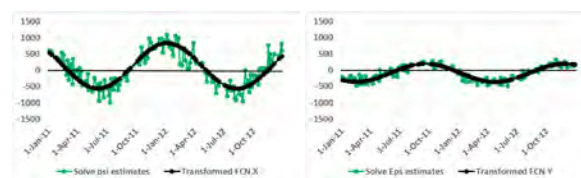


Fig. 4 Left: agreement between transformed FCN X values and Solve ψ estimates (μs). Right: agreement between transformed FCN Y values and Solve ε estimates (μs).

To use this FCN data in analyzing the Intensives we used exactly the same technique as for the gradients. We augmented the Intensive normal equations to include estimates of nutation. We interpolated the ex-

ternal FCN model values to the epoch of the Intensives and then applied these a priori values with tight constraints. In contrast to the previous case where we used gradient values from R1/R4 sessions, in principle we can do this for all sessions. To evaluate the effect of this, however, we limit our attention here to only those sessions which occur on the same day as an R1/R4 session.

Figure 5 plots $\delta UT1_{FCN}$, the change in UT1 estimates caused by incorporating FCN. Figure 6 plots the reduction in absolute error from using external FCN data.

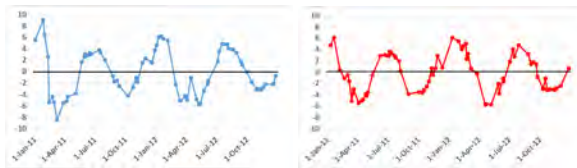


Fig. 5 Effect of using free core nutation on STN (left) and MSS (right) INT01 UT1 estimates (μs).

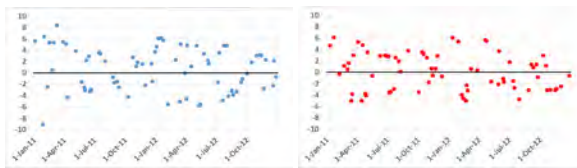


Fig. 6 Reduction in absolute error for STN (left) and MSS (right) INT01 sessions (μs) from using FCN.

Table 2 summarizes the effect of using external FCN in the estimate of UT1 from the Intensives. The use of FCN helps, but the reduction is small, only a fraction of μs . On the other hand this reduction is in line with what you would expect based on the size of δFCN .

Table 2 Effect of Free Core Nutation in μs .

	STN	MSS
RMS $\Delta UT1_{Def}$	31.15	20.89
RMS $\Delta UT1_{FCN}$	30.97	20.60
Improvement in RMS	0.18	0.29
RMS $\delta UT1_{FCN}$	3.80	3.32
$\sqrt{\langle \Delta UT1_{Def}^2 \rangle - \langle \Delta UT1_{FCN}^2 \rangle}$	3.30	3.49
Average reduction in absolute error	0.66	0.12

6 Conclusions

In this note we demonstrated that you can improve the accuracy of UT1 estimates from Intensive sessions by the use of a priori information. We looked at two cases—the use of gradient information from R1/R4 sessions and the use of an external FCN model. The reduction was largest when we used gradient information. But this information is not available for the operational analysis of Intensives because the R1/R4 sessions are not processed until several weeks after the Intensives are. On the other hand, there may be other sources of gradient information which are available during processing, such as from the IGS.

The use of external FCN information improved the accuracy of the UT1 estimates, but the impact was very small. This information is available at the time the Intensives are processed, and we will modify our software to use it.

We also note that in both cases, the reduction in error was larger for the MSS sessions. We believe that this is due to the fact that the error in the MSS sessions is smaller to begin with, and hence they are more sensitive to small changes in the modeling.

Acknowledgement. We thank Daniel MacMillan (NVI, Inc.) for useful comments about Section 3.

References

- Behrend D., “Data Handling within the International VLBI Service”, Data Science Journal, Vol. 12, pp. WDS81–WDS84, ISSN 1683-1470, 17 February 2013. DOI 10.2481/dsj.WDS-011.
- Gipson, John, and Bayer, Karen, “Improvement of the IVS-INT01 Sessions by Source Selection: Development and Evaluation of the Maximal Source Strategy”, J Geod (2016) 90:287-303, DOI 10.1007/s00190-015-0873-6.
- Gipson, John, Strandberg, Ingrid, and Azhirmian, Armin, “A priori Modeling Errors and UT1 Estimates from Intensives”, Fall 2015 AGU Meeting.
- Lambert, Sébastien, “Empirical Modeling of the Earth’s Free Core Nutation”, http://synte.obspm.fr/~lambert/fcn/notice_fcn.pdf.
- Nothnagel, Axel and Dorothee Schnell. “The impact of errors in polar motion and nutation on UT1 determinations from VLBI Intensive observations”, J Geod (2008) 82:863–869, DOI 10.1007/s00190-008-0212-2.

Hard- and Software Tools for the Education of Geodetic VLBI

Thomas Hobiger, Rüdiger Haas, Eskil Varenius

Abstract The Onsala Space Observatory hosts two 2.3-m radio telescopes called SALSA (“Such a lovely small antenna”) which are utilized to bring front-line interactive astronomy to the classroom. Until now SALSA was used for astronomical educational purposes solely, in particular demonstrating the concept of single dish measurements. However, it is possible to combine both SALSAs to form an interferometer by making use of hardware which has been developed for software-defined radio. In doing so, one can utilize the SALSA antenna pair as a student demonstrator for geodetic Very Long Baseline Interferometry. Here is discussed which COTS hardware components are necessary to turn the SALSA installation into an interferometer. A simple Octave-based correlator has been written in order to process SALSA data. Results from a test run during which the Sun was tracked are presented and discussed here.

Keywords Software-defined radio, SALSA, education

1 SALSA

Two small 2.3-m radio telescopes named SALSA (cf. Figure 1) are hosted at the Onsala Space Observatory in Sweden. SALSA is the short form of “Such a lovely small antenna” or, in Swedish, “Sicken Attans Liten Söt Antenn”. After free online registration, anyone may control one or both of these telescopes via the In-

1. Department of Earth and Space Sciences, Onsala Space Observatory, Chalmers University of Technology

ternet and carry out his/her own experiments. SALSA is a part of the European Hands-On Universe project, EU-HOU, to bring front-line interactive astronomy to the classroom. Most SALSA users observe emissions from hydrogen in the spiral arms of the Milky Way, and all observations can be done via a Web browser. Considering the great success concerning education



Fig. 1 Webcam image of the two SALSA antennas at the Onsala Space Observatory, taken on February 22, 2016 at 11:00 UT (<http://vale.oso.chalmers.se/salsa/webcam>).

and outreach with the SALSA telescopes, it was studied whether it would be technically feasible to use the two antennas in interferometric mode in order to mimic a simplified VLBI setup.

2 Turning SALSA into an Interferometer

In order to realize a simple and easy to handle VLBI demonstrator, it was decided to record RF signals with a single hardware tool. In doing so, one can combine both SALSA antennas to form a local interferometer which removes the need to deal with clock differences

or drifts in post-processing. The USRP E310 stand-alone software defined radio (cf. Figure 2) was found to be a suitable solution for realizing such a concept. This small device has two independent RF front-ends



Fig. 2 Photo of the URSP E310 together with a pen for better illustration of the dimensions of the device.

with flexible mixed-signal baseband sections and integrated frequency synthesizers. Overall RF frequencies between 70 MHz and 6 GHz can be translated to complex baseband and sampled with up to 56 MHz of instantaneous bandwidth. Thus, the interferometer can be realized as depicted in Figure 3.

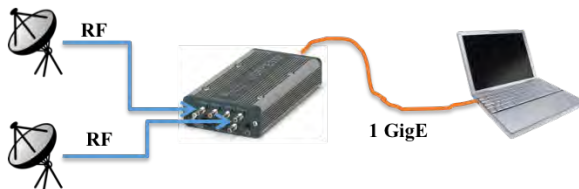


Fig. 3 Signal chain of the SALSA interferometer.

Digitized signals are sent over 1 GbE to an off-the-shelf PC where they are recorded on hard disk. Real-time signal processing is not implemented at the moment but can be realized with minimum efforts. Moreover, one can make use of the FPGA resources and move some of the signal processing stages to the USRP and only deal with light-weight signal processing on the PC.

3 First Light

In order to test the interferometric capability, the two SALSA antennas were pointed towards the Sun on February 10, 2016. Figure 4 depicts the delay resolution function of a 20 millisecond scan observing the Sun at 1410 MHz with 1 Msps/channel around 14:00 UTC. A clear peak in the fringe plot indicates successful correlation. All data were processed with an Octave based correlator which uses a simplified delay and delay-rate model for quick fringe detection on this short baseline.

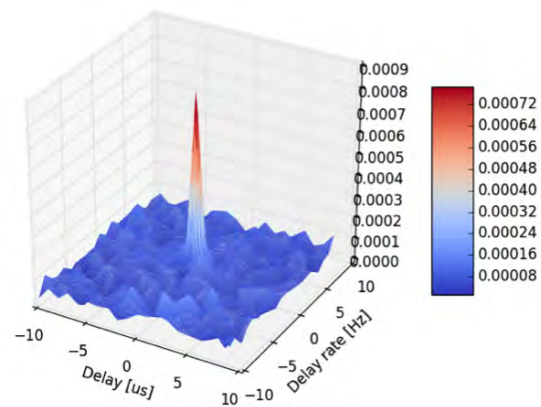


Fig. 4 Delay resolution function of a 20 ms scan of the Sun at 1,410 MHz.

4 Post-processing

A longer (i.e., 300-second) scan of the Sun was recorded a few minutes after the first fringe test. Data were post-processed with another Octave script, and phases, delays, and amplitudes were successfully obtained for accumulation periods of one second. Results are shown in Figure 5 and confirm the expected performance of the narrow-band interferometer setup. Except for an expected drift, interferometer phases appear to be very stable over time, while interferometer delays reveal a scatter of about 6 ns, which agrees well with the anticipated uncertainty corresponding to the 1 MHz bandwidth.

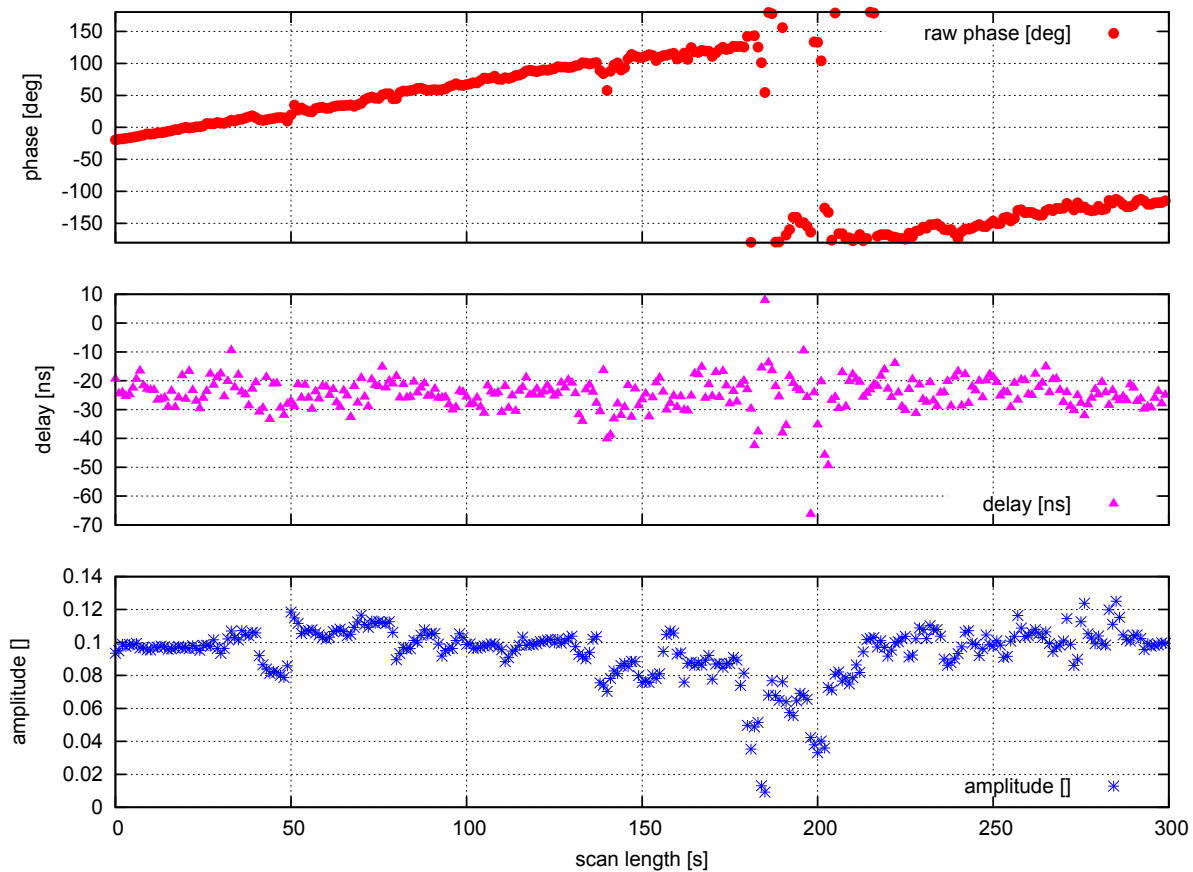


Fig. 5 Phases (upper plot), delays (middle plot), and amplitudes (lower plot) as obtained from a scan of the Sun on February 10, 2016 at 14:03 UT.

5 Next Steps

In order to use the SALSA installation more efficiently for demonstrating the basic concepts of interferometry, a few hard- and software changes are necessary. First, one needs to upgrade the front-ends in order to be able to receive other frequency ranges as well. This goes along with a firmware upgrade of the USRP E310 which enables receiving and processing of a much wider bandwidth. Limitations here are caused by the CPU which runs the embedded system rather than the FPGA processing capabilities. Thus, moving signal processing stages from the USRP to the PC will enable the handling of a wider RF bandwidth. However, one can also think about moving dedicated signal processing steps on the FPGA when dealing with narrow-band signals and thus supporting real-time operations. The USRP E310 supports this by means of RF Network on Chip (RFNoC) which can be developed, implemented,

and tested in the form of undergraduate projects or theses. In general, such a feature can be of special interest for satellite observations, for example GNSS and other communication satellites transmitting in S-band. However, for such applications, one needs to implement also a satellite tracking module in the SALSA control system and make use of two-line element orbit information in order to steer the antennas towards the object of interest.

The post-processing software discussed in the previous section relies on Octave and can also run on Matlab. However, it is necessary to improve the existing software in order to obtain more precise observables. Delay tracking, fringe rotation, and other features have to be considered thoroughly even though the baseline is very short. Thus, longer integration times and correspondingly longer scans can be processed homogeneously while maintaining a high coherence over time. In addition, an interface to standard geodetic observa-

tion formats (VGOSDB, NGS) needs to be created so that data can be handled easily with geodetic analysis software packages.

Considering that all these implementations and developments will be available in the near future, it is anticipated that the SALSA installation can be used as an educational environment that mimics all stages of

VLBI, including antenna control, RF processing, sampling, correlation, and analysis. Moreover, undergraduate and graduate thesis projects are expected to complement and extend the possibilities of the SALSA configuration and pave the way towards prototyping and testing of new observational concepts.

Session 5: Geodetic and Astrometric VLBI Results



March 2016 · Johannesburg · South Africa

IVS Contribution to ITRF2014

Sabine Bachmann¹, Daniela Thaller¹, Ole Roggenbuck², Michael Lösler³, Linda Messerschmitt¹

Abstract Starting with the ITRF2005, the IVS contribution to the ITRF has been an intra-technique combined solution using multiple individual contributions from different institutions. For the IVS contribution to the ITRF2014 nine international institutions were used for a combined solution. The data files contain 24-hour VLBI sessions from the late 1970s until the end of 2014. 5,796 combined sessions in SINEX file format containing datum free normal equations with station coordinates and Earth Orientation Parameters (EOP) have been contributed to the ITRF2014. The overall repeatability for station coordinate time series of the combined solution are 3.3 mm for the north, 4.3 mm for the east, and 7.5 mm for the height component over all stations. The minimum repeatabilities are 1.5 mm for north, 2.1 mm for east, and 2.9 mm for height. A scale difference of 0.11 ppb (i.e., 0.7 mm on the Earth's surface) has been detected between the VTRF2014 and the DTRF2008 (DGFI-TUM realization of ITRS), and a scale difference of 0.44 ppb (i.e., 2.8 mm on the Earth's surface) between the VTRF2014 and ITRF2008. Internal comparisons between the EOP of the combined solution and the individual solutions from the Analysis Center contributions show a WRMS in X- and Y-Pole between 40 and 100 μ s and for dUT1 between 5 and 15 μ s. External comparisons with respect to the IERS-08-C04 series show a WRMS of 132 and 143 μ s for X- and Y-Pole, respectively, and 13 μ s for dUT.

1. Federal Agency for Cartography and Geodesy, Germany

2. Jade Hochschule Wilhelmshaven/Oldenburg/Elsfleth, Germany

3. Frankfurt University of Applied Sciences Faculty of Architecture, Civil Engineering and Geomatics, Germany

Keywords ITRF2014, VLBI, intra-technique combination, station coordinates, terrestrial reference frame, Earth orientation parameters

1 Introduction

The International Terrestrial Reference Frame (ITRF) is the result of an inter-technique combination of all four space geodetic techniques: Doppler Orbitography and Radiopositioning Integrated by Satellite (DORIS), Global Navigation Satellite Systems (GNSS), Satellite Laser Ranging (SLR), and Very Long Baseline Interferometry (VLBI). The International Terrestrial Reference System (ITRS) Center of the International Earth Rotation and Reference Systems Service (IERS) sent out a Call for Participation for the next ITRF containing data until the end of 2013¹. The time span for data was later extended for one additional year until the end of 2014. The ITRF2014 is the latest realization of continuous realizations of the ITRS including all four space geodetic techniques as described in [1] and [9]. All services were requested to submit contributions for the generation of the ITRF2014. Starting with the ITRF2005, the VLBI contribution has consisted of normal equations (NEQs) derived from a combination of different individual contributions from the IVS Analysis Centers [10]. The same strategy was utilized for ITRF2008 [5] and ITRF2014. Since the IVS contribution to the ITRF2008, the VLBI combination procedure has been continuously refined with an increasing number of individual contributions. Figure 1 in [9] shows the schematic representation of the inter-technique combination process for the DTRF-

¹ IERS Message No. 225 in <http://www.iers.org/Messages>

2008 using all space geodetic contributions including the IVS contribution. All contributions are analyzed separately, and the daily/weekly NEQs are accumulated into one NEQ per technique. In a common process, the technique-wise NEQs are then combined into a global TRF (here the DTRF) and EOP.

The VLBI data for the inter-technique combination is provided by the International VLBI Service for Geodesy and Astrometry (IVS) [8]. The IVS is organized under the umbrella of the International Association of Geodesy (IAG) and the International Astronomical Union (IAU) and contributes to the IERS. Since ITRF2008, six years of additional observations have become available, including new sites in the continuously developing network [3].

The combination process of the VLBI contribution to ITRF2014 is described here, focusing on station positions and Earth Orientation Parameters (EOP). Overall 5,796 combined sessions were submitted to the IERS ITRS Center as the IVS contribution to the ITRF-2014. Comparisons of the scale parameter complete the work, because VLBI and SLR are presently the only two space geodetic techniques that are contributing to the scale of the ITRF.

2 Input to the IVS Combination

The IVS contribution to the ITRF2014 contains 24-hour sessions starting in 1979, but in contrast to the regular rapid solution, where only R1 and R4 sessions are used, the IVS contribution to ITRF2014 contains all 24-hour sessions (see the IVS Master Schedule² for more information). The IVS Analysis Centers (ACs) are advised to make use of (at least) all R1 and R4 sessions through December 31, 2014, with contributing ACs responsible for the delivery of the sessions. ACs that are contributing to operational combination EOP products do not always submit a contribution to the IVS combination for the ITRF2014, as well. Table 1 shows the ACs that are contributing to the IVS. It indicates the products to which they are contributing and which software is used to analyze the sessions. It can be seen that five ACs contributed a solution for the ITRF2014 although they do not contribute to the operational combined product. The contribution to the

IVS is open to every interested institute, providing their contribution is in the correct format and meets the pre-defined requirements concerning the analysis method (cf. Section 3).

The input contributions are normal equations stored in the SINEX³ file format, containing station coordinates and EOP, i.e., pole coordinates (including rates), universal time, LOD, and nutation. Several new and independent software packages have also been used, which are currently under review for the operational combined products. For ITRF2008 seven ACs using four different software packages contributed to the combined solution; ten ACs using five different software packages contributed to the combined solution for ITRF2014. The analysis standards, as well as the session characteristics used as input for the combination, are described in this section. The combination process for station coordinates, EOPs and global TRF solutions are then described in the following section.

Figure 2 shows the SINEX file availability for each contributing AC as well as the combined solution. It can be seen that part of the ACs submitted data starting in 1979 and some in 1984, leaving out the very early years of VLBI observations. The number of submitted SINEX files varies between 4,545 and 6,003 sessions, resulting in 5,796 combined sessions containing 158 stations and covering a time span of almost 36 years between 1979.6 and 2015.0.

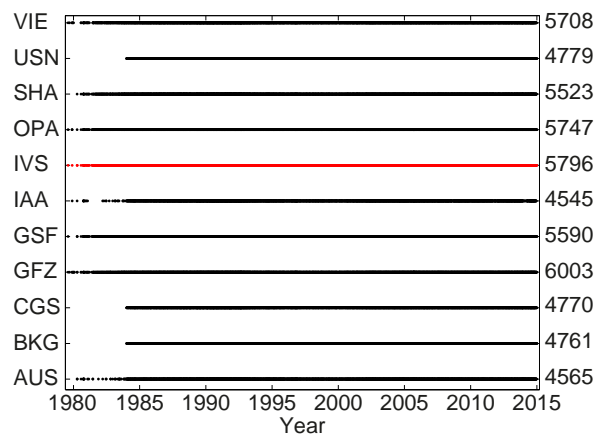


Fig. 2 SINEX file availability for different ACs and the combined contribution (in red/labeled IVS). The total number of sessions delivered are given on the right side.

² <ftp://ivs.bkg.bund.de/pub/vlbi/ivscontrol/>

³ <http://www.iers.org/sinex>

Table 1 IVS Analysis Centers and their contribution to operational IVS products and to the ITRF2014.

AC	Name	Software	Operational AC	ITRF2014	
				submitted	included
AUS	Geoscience Australia, Australia	OCCAM(LSC)	no	yes	no
BKG	Federal Agency for Cartography and Geodesy, Germany	Calc/(nu)Solve	yes	yes	yes
CGS	Centro di Geodesia Spaziale, Italy	Calc/(nu)Solve	under review	yes	yes
DGFI-TUM	German Geodetic Research Institute/TU Munich	OCCAM(LSM)	yes	no	no
GFZ	German Research Center for Geosciences	VieVS@GFZ	under review	yes	yes
GSFC	Goddard Space Flight Center, USA	Calc/(nu)Solve	yes	yes	yes
IAA	Institute of Applied Astrometry, Russia	Quasar	yes	yes	yes
NMA	Norwegian Mapping Authority, Norway	GEOSAT	no	yes	no
OPAR	Observatory of Paris, France	Calc/(nu)Solve	yes	yes	yes
SHAO	Shanghai Observatory, China	Calc/(nu)Solve	no	yes	yes
USNO	U. S. Naval Observatory, USA	Calc/(nu)Solve	yes	yes	yes
VIE	Vienna University of Technology, Austria	VieVS	under review	yes	yes

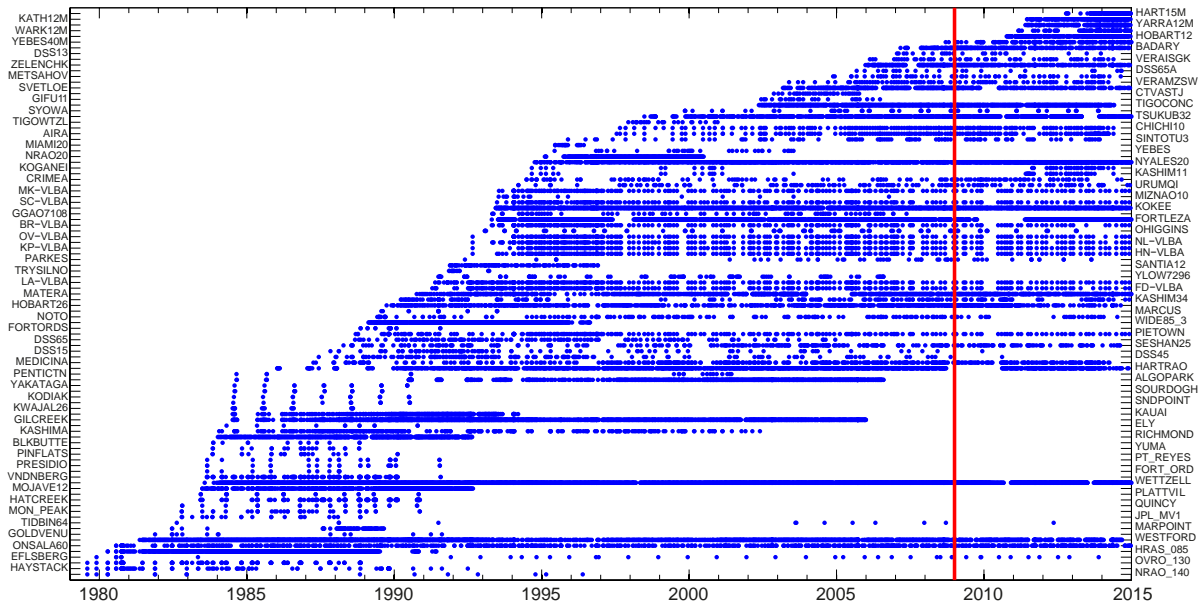


Fig. 1 Station participation. The data on the right hand side of the vertical red line are additional data to the ITRF2014. Only stations with more than ten observed sessions are shown.

Figure 1 shows the station participation stored in the SINEX files. Only stations with more than ten observed sessions are shown. The left hand side of the vertical red line marks the time span of the data included in the preceding ITRF2008. Data on the right hand side are additional data included in the ITRF-2014; thus six years of additional data are included in the latest ITRS realization, coming along with several new stations. Furthermore, stations which started observing a short time before the vertical line and are, thus, not included in the preceding ITRF now have sufficient observations to be included in the ITRF2014.

3 Analysis

The combination process itself has been described in several publications, e.g., [5] and [2]. The underlying hypotheses of the combination approach is that improved statistics for a combined solution compared to the individual solutions are expected. The combination is done on the level of normal equations with predefined analysis conventions (e.g., models, absolute terms, etc.). The major differences between the IVS contribution to the ITRF2008 and ITRF2014 are as follows:

- Transformation on 12h UT for all parameters (ITRF2008: mid-session).
- Improved dynamic outlier test (ITRF2008: static / fixed threshold).
- Solid Earth Tide, Pole Tides: IERS Conventions 2010 (ITRF2008: IERS Conventions 2003).
- Nutation: IAU2006 (ITRF2008: IAU2000A).
- Gradients: Chen-Herring Gradients (ITRF2008: MacMillan (1995) with wet VMF1).
- Source positions: constrained on ICRF2 *a priori* position for defining sources (ITRF2008: Constrained on ICRF1+Ext.1 or individual CRF).

Major differences to IVS routine (rapid / quarterly) combinations are:

- Common epoch 12h UT instead of mid-session as for the routine combination.
- Non-tidal atmospheric loading not applied (annual / semi-annual model applied *a posteriori*).
- Dedicated IVS ITRF2014 axis offset information file.

Figure 3 shows the combination process applied for the IVS contribution to the ITRF2014. The combination is based upon session-wise SINEX files containing datum-free normal equations for station coordinates and EOP.

The first step is an epoch transformation on the same epoch for every contribution. For the ITRF2014 contribution, the IVS decided — for the first time — to transform each session to 12h UT, instead of to mid-session as in operational IVS combinations, in order to conform with the other space geodetic techniques. The second step of the combination processing strategy is a transformation to equal *a priori* station coordinates. Precise *a priori* values are important for the quality and reliability of the combination result. The *a priori* values for station coordinates are taken from the latest combined long-term (quarterly) IVS solution, which is the one with the most up-to-date global VLBI solutions available⁴. Different incidents such as earthquakes or station repairs lead to non-linear antenna displacements, so the determination of accurate station positions can be needed on short notice. This is also the case for newly built telescopes.

The next step of the session-wise combination includes an outlier test for station coordinates. In this

⁴ http://www.ccivs.bkg.bund.de/EN/Quarterly/VTRF-Results/VTRF-Stations/vtrf-stations_node.html

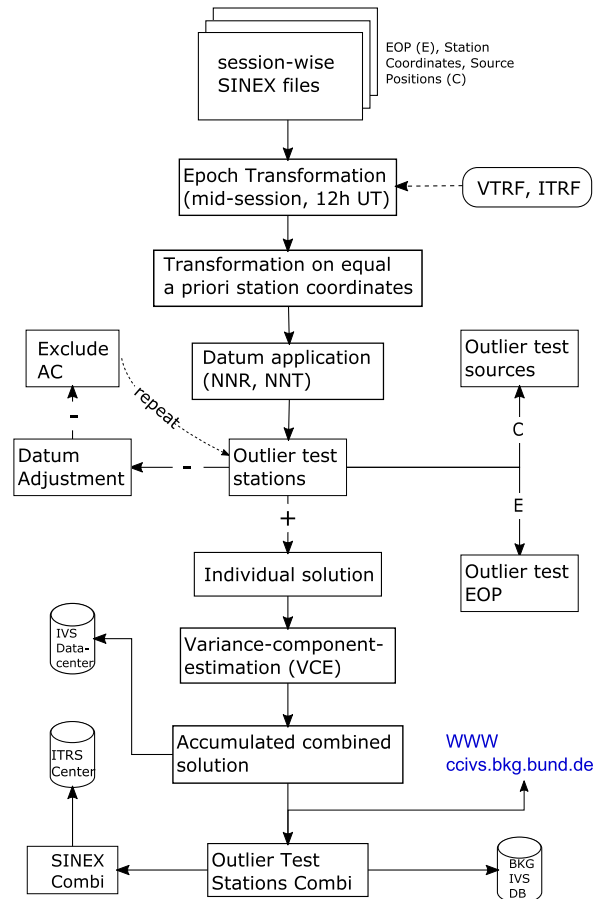


Fig. 3 Schema of the combination procedure.

step, major changes have been applied compared to the precedent procedure for ITRF2008. For ITRF2008, contributions were rejected as outliers in station position if the following two criteria were met [5]:

1. the correction to the *a priori* position was larger than 5 cm in the horizontal and 7.5 cm in the vertical component, and
2. the parameter correction was larger than three times its formal solution error.

This static approach has been replaced by a dynamic approach using the Least Median of Square method (LMS) described in detail in [2]. Based on normal equations with identical epochs and identical *a priori* values, the individual solution for each AC is generated. Comparing these individual solutions, a weighting factor is determined using a variance component estimation (VCE). The median of the weighting factors for each AC vary between 1 and 1.2.

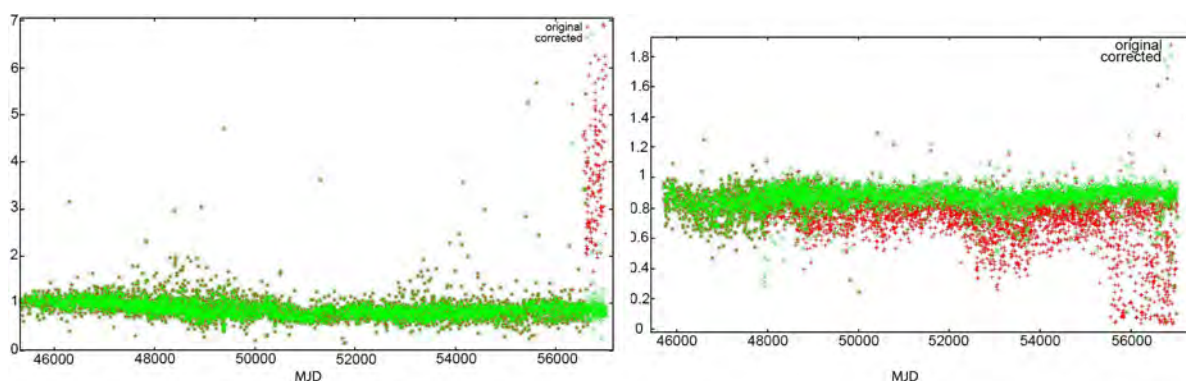


Fig. 4 Variance factor of AC SHAO (left side) and AC USNO (right side) before (red/dark crosses) and after correction (green/light crosses).

The combined normal equation is generated by accumulating the weighted contributions of the ACs. Applying no-net rotation (NNR) and no-net translation (NNT) conditions for station coordinates removes the datum defect of the normal equation and allows its inversion. Stations for which no reliable coordinates can be determined for specific sessions falling in a particular time span (e.g., by reason of station displacements due to earthquakes, maintenance work at the antenna, or too few observations) are excluded from the datum definition and treated as free parameters. As soon as these stations are again stable enough to determine a reliable station coordinate, they are used as datum stations. A SINEX file containing the datum-free normal equations of the combined solution is then submitted to the IERS ITRS Center and the IVS Data Center⁵.

In the beginning of the data collection phase, different problems had to be corrected, e.g., different axis offsets or eccentricity files, problems with writing routines, or inconsistencies in parameter naming. Furthermore, inconsistencies in the variance factors had been found in the pre-analysis of the contributions. Examples are shown in Figure 4. The red/dark crosses show the variance factor as reported in the SINEX files before the corrected analysis and the green/light crosses after the correction was done. The reason for the discrepancies was found in *a priori* station positions for new stations or inconsistent re-analysis of the additional year 2014.

⁵ ftp://ivs.bkg.bund.de/pub/vlbi/ITRF2014/daily_sinex/ivs2014a/

4 Results

4.1 Station Coordinates

Figure 5 shows time series of station coordinates as differences between the combined solution and the individual AC solutions for the east component of station Wettzell, Germany. Figure 6 shows the height component. The station serves as an example for common VLBI station time series. In the early 1990s, station position accuracy became better due to a larger network size, a better global distribution of the stations, and an elevated number of observed sources. While the differences of the east component are in a range of about ± 2 mm, the scatter of the height component is technique-dependent and larger — about ± 3 -4 mm.

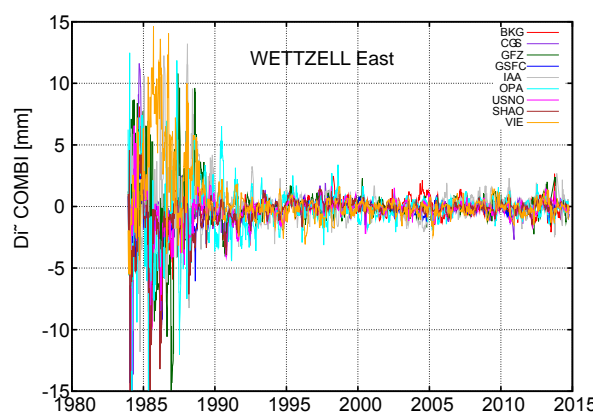


Fig. 5 Time series of the east component differences between the combined solution and the individual solutions for station Wettzell, Germany.

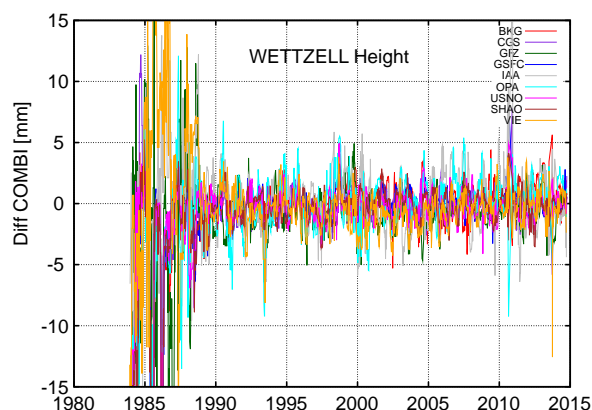


Fig. 6 Time series of the height component differences between the combined solution and the individual solutions for station Wetzell, Germany.

Station precision and repeatability is determined by calculating the WRMS of the session-wise time series of each station, as well as the overall WRMS for all stations. These statistical values give information about the quality of the contributions for every station. The median of station repeatability is better than 4.4 mm in north, 5.8 mm in east, and 9.3 mm in the height component. The minimum repeatability is 1.5 mm in the north component for stations BR-VLBA (Brewster, USA) and NL-VLBA (North Liberty, USA) (using 211 observed sessions each), 2.1 mm in the east component for station ONSALA60 (Onsala, Sweden) (using 839 observed sessions), and 2.9 mm in the height component for station HAYSTACK (Haystack, USA) (using 88 observed sessions). The maximum is 21.2 mm in the north component for station MARPOINT (Maryland Point, USA) (using 76 observed sessions), 28.9 mm in the east component for station SINTOTU3 (Kabato, Japan) (using 88 observed sessions), and 49.9 mm in the height component for station OHIGGINS (O'Higgins, Antarctica) (using 127 observed sessions). These numbers have to be handled with care, because of the station's situation; it is isolated in Antarctica.

The overall WRMS from the session-wise analysis over all stations and for all ACs as well as the combined solution is shown in Figure 7 for the north (violet / left bar), east (green / middle bar), and height (black / right bar) components. The WRMS values are between 3-4 mm for the north component and between 4-6 mm for the east component, while the height component value is about 7-9 mm; this is technique-limited,

due to imperfect observing networks and tropospheric mismodeling.

Comparing the values of the combined solution with the values for the ACs, visualizes the underlying hypothesis of the combination: the combined solution is more accurate than the individual ACs (cf. [5]), although the improvement is hardly visible. The WRMS for the combined solution is 3.3, 4.3, and 7.5 mm for north, east and height, while for the individual solutions the WRMS is between 3.4 and 4.5 mm (with a median of 3.6 mm) for north, between 4.4 and 5.7 mm (with a median of 4.7 mm) for east, and between 7.7 and 9.2 mm (with a median of 8.3 mm) for the height component.

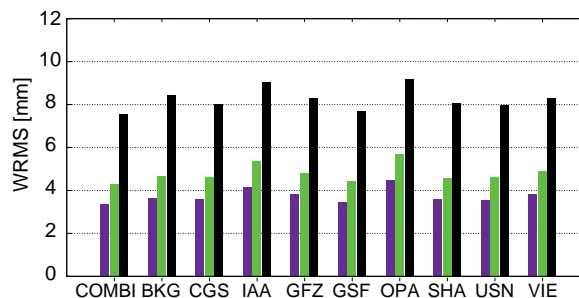


Fig. 7 WRMS over all station for north (violet / left bar), east (green / middle bar), and height (black / right bar) component.

4.2 Scale

Figure 8 shows the smoothed session-wise scale parameter of the combined solution with respect to DTRF2008, ITRF2008, and VTRF2014. In the first years of VLBI data acquisition (before 1994), the scale shows a more scattered behavior with an amplitude between -1 and +1 ppb for all comparisons (cf. red/medium, green/light, and black/dark curves in Figure 8). The scatter of the scale flattens out in the following years, when the VLBI network contains more antennas and more sources are observed within one session. A mean offset of 0.3 ppb can be seen between the DTRF2008 and ITRF2008 starting around 1995. The scale calculated with a Helmert transformation is 0.11 ppb between the VTRF2014 and the DTRF2008 and 0.44 ppb between the VTRF2014 and the ITRF2008.

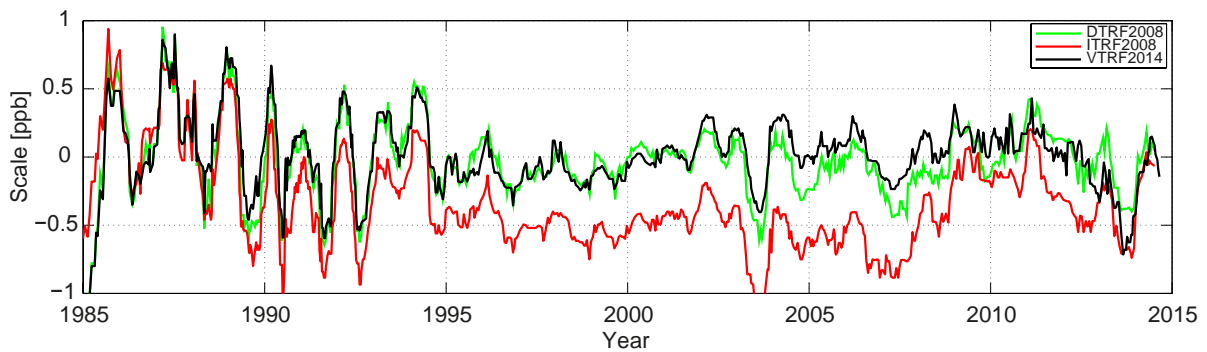


Fig. 8 Smoothed scale parameters between session-wise combined solution and DTRF2008 (green/light), with respect to ITRF2008 (red/medium), and with respect to VTRF2014 (black/dark).

Starting in 2010, the VLBI network experienced significant antenna displacements due to several severe earthquakes in the Chilean and Japanese regions. These changes in the network and the corresponding choice of datum stations for determining Helmert transformation parameters are also visible in the evolution of the scale in Figure 8. The plot shows the same two peculiarities around 2004 and towards the end of the observations in 2014. In the years around 2003/2004, the scale parameter suddenly seems to decrease to -0.6 ppb. Inspecting the sessions included in these two striking years, no particular antenna can be identified to introduce this effect (e.g. with a displacement or a replacement). The corresponding period contains many regional sessions with an unfavorable global station distribution for scale determination. A closer look at the scale parameters for this time period using only R1 or R4 sessions is provided in Figure 9. The dashed line shows the scale containing only R1 sessions and the circled line the scale containing only R4 sessions while the solid line contains all sessions that correspond to the scale shown in Figure 9. The regularly observed (i.e., each once per week) IVS R1 and R4 sessions contain a minimum number of well-distributed participating stations. A reduction of the peculiarities around 2003/2004 are observed for both R1 and R4 sessions. Additionally, investigations have been done on the scale parameter development and dependency on the number of stations within the respective sessions in 2004. It can be observed that for a network with at least seven stations, the irregularity around 2004 disappears. But because sessions with more than seven stations are observed neither frequently nor regularly, the observed scale smoothing

effect should be handled with care. This study corresponds to the assumption made before: the sessions around 2004 seem to be dominated by regional and small networks. Impacts on the regional level are natural effects such as flood or drought, which have to be considered as possible explanations for the visible scale irregularities. Especially, 2003 was a year of exceptional drought in the Northern hemisphere. Investigations to quantify these impacts on the scale parameter have to be done in the future in order to consider them for the weighting model.

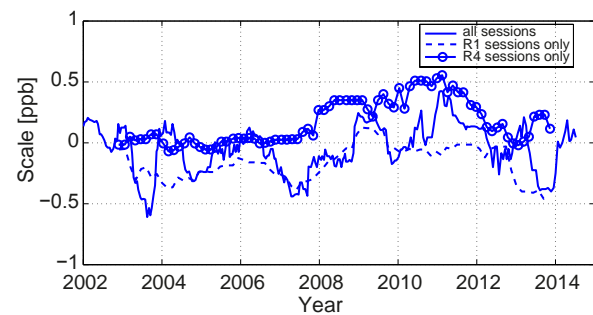


Fig. 9 Detailed view of the smoothed scale parameter between session-wise combined solution and DTRF2008 (solid line, agreeing with Figure 8), when only R1 (dashed line), and when only R4 (circled line) sessions are used.

It could be assumed that the second irregularity around 2014 is influenced by the fact that both reference frames (DTRF2008 and ITRF2008) contain data only until the end of 2008. For sessions observed beyond this period, station coordinates must be extrapolated for several years. Furthermore, the VLBI network contains more new VLBI telescopes (cf. Fig-

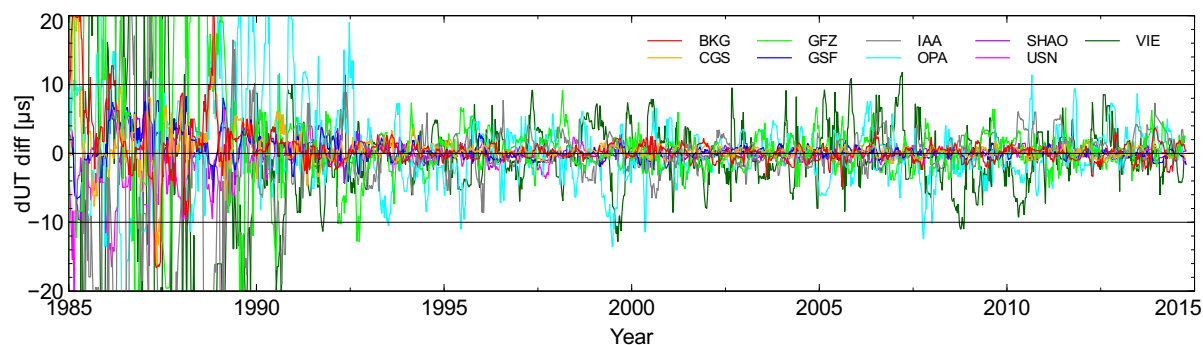


Fig. 10 dUT1 differences between individual and combined solutions smoothed with a 70-day moving median filter.

ure 1) which are not part of DTRF2008 and ITRF2008. This decreases the selection of datum stations for the Helmert transformation. However, the same irregularities can be observed for the scale with respect to the VTRF, where these characteristics do not apply.

4.3 EOP

EOPs are the second parameter type besides station coordinates resulting directly from the combination. The EOPs contain pole coordinates (X- and Y-Pole) and rates, UT1-UTC (dUT1) and the rate LOD (Length of Day), and nutation parameters dX and dY. VLBI is the only geodetic space technique that provides a full set of EOPs, including a link to the celestial reference frame. EOPs are estimated by fixing datum station coordinates to their a priori values within 0.001 mm, which makes it critical to carefully select station a priori values and datum stations. For the first time, all parameters of the combined normal equations are transformed to 12h UT in order to be consistent with the other geodetic space techniques. IVS 24-hour sessions are usually scheduled between 17:00 UT and 17:00 UT of the following day. EOP and station positions determined at 12h UT are shifted by about seven hours compared to the routine IVS combination where all parameters are estimated at mid-session. Therefore, the EOPs estimated at 12h are expected to be degraded compared to what VLBI would be able to deliver in an optimal way.

Figure 10 shows the smoothed time series of the differences between the individual AC solutions and the combined solution for dUT1, which is shown as an example for all EOPs. Similar to the station coordinates, the first years of VLBI data collection were still

very scattered until the VLBI observations' accuracy increased in the early 1990s. The median differences between the individual AC solutions and the combined solution vary between -10 and $10 \mu\text{s}$ for dUT1 and between -50 and $50 \mu\text{s}$ for X-Pole (leaving out the years before 1994) including some peaks.

Figure 11 shows the WRMS of the differences between the individual solutions and the combined solution for X-, Y-Pole (red / left and green / middle bar, respectively) and dUT (blue / right bar). The respective rates (X- and Y-Pole rates and LOD) are shown in Figure 12. Only sessions which were analyzed successfully by all ACs were used for the comparisons.

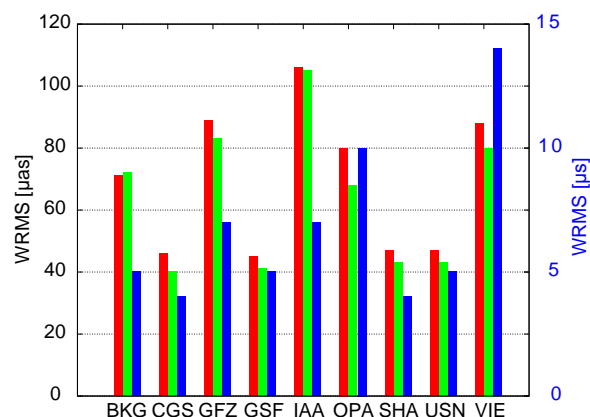


Fig. 11 WRMS of the differences between the individual and combined solutions for X- (red / left bar), Y-Pole (green / middle bar), and dUT (blue / right bar).

The WRMS is between 40 and $100 \mu\text{as}$ for X-Pole, and Y-Pole and between 5 and $15 \mu\text{s}$ for dUT1. Because the VIE AC provided piecewise linear offsets for all EOPs instead of an offset and a rate, a transformation

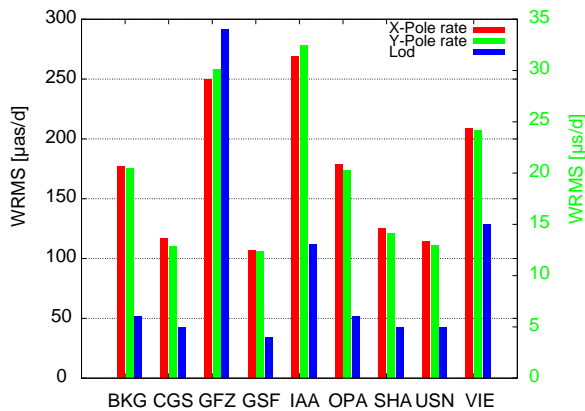


Fig. 12 WRMS of the differences between the individual and combined solutions for X- (red / left bar) and Y-Pole (green / middle bar) rates and LOD (blue / right bar).

to the offset and the rate was included *a priori* to the combination process, which seems to be not as accurate as if the parameterization were directly introduced within the analysis process. The WRMS for X- and Y-Pole rates are between 100 and 250 $\mu\text{s}/\text{d}$ and for LOD between 5 and 15 $\mu\text{s}/\text{d}$. Further studies are required in order to find the reason for the increased LOD WRMS found for the GFZ AC. The WRMS for the nutation parameters (not shown) are between 30 and 80 μs for dX and dY . An elevated WRMS of $\sim 140 \mu\text{s}$ can be found for nutation for the OPA AC. The reason for the increased nutation differences for the OPA AC is still open to investigation.

For an external comparison, the combined EOP results are compared to the IERS C04 series (cf. [4]). Here, the WRMS values for the differences are 132 and 143 μs for X- and Y-Pole, respectively, and 482 and 454 $\mu\text{s}/\text{d}$ for their rates. The WRMS is 13 μs for $dUT1$ and 39 $\mu\text{s}/\text{d}$ for LOD. The WRMS for the nutation parameters are 63 and 67 μs for dX and dY , respectively.

4.4 Presentation of Results

The original IVS contribution to the ITRF2014, including the individual contributions of the ACs as well as the combined solution in SINEX format, are freely available at the three IVS Data Centers at BKG,

CDDIS, and OPAR^{6,7,8}. Results are presented on the newly designed IVS Combination Center's website (<http://ccivs.bkg.bund.de>, see also [6]), comprising time series of station coordinates, baselines, EOP, and time series of the scale parameter of the individual solution as well as of the combined results. Furthermore, a data DOI (10.5880/GFZ.1.1.2015.002, to be cited as [7]), has been established in order to provide the ability to reference the data set and thereby to pay tribute to the contributors, including the complete VLBI data acquisition chain (stations, correlator, analysis, and combination), see Figure 13. The data DOI was established at GFZ, Germany. It contains links to the SINEX files, as well as meta data in the form of an abstract, keywords, contact information, and data description.

Fig. 13 Landing page of DOI.

⁶ ftp://ivs.bkg.bund.de/pub/vlbi/ITRF2014/daily_sinex/ivs2014a/

⁷ ftp://ivsopar.obspm.fr/vlbi/ITRF2014/daily_sinex/ivs2014a/

⁸ ftp://cddis.gsfc.nasa.gov/pub/vlbi/ITRF2014/daily_sinex/ivs2014a/

5 Conclusions

In total 5,796 combined 24-hour sessions for the ITRF-2014 contribution, covering a time span from 1979 to the end of 2014, have been submitted containing 158 stations overall. Eleven IVS Analysis Centers using five different software packages submitted contributions to the combined solution, from which nine contributions using three different software packages were included in the combined solution.

Compared to the IVS contribution to the ITRF-2008, an improved outlier test and weighting strategy was implemented. The station repeatability over all stations (WRMS) is 3-4 mm for the horizontal components (north and east) and 8-9 mm for the height component for all included Analysis Centers. 75 % of the stations have a repeatability of better than 6.9 mm for north, 9.3 mm for east, and 12.7 mm for the height component. Within recent years the VLBI network expanded in size and in quality, so that it can be expected that this will also have a positive impact on the station coordinate quality within the upcoming years. Improving the session weighting by considering the geometric network characteristics for global VTRF solutions is one of the next steps.

Comparisons to the ITRF2008 show a scale offset of 0.44 ppb, while comparisons to the DTRF2008 show a scale offset of only 0.11 ppb. Upcoming developments in the frame of VGOS will provide the opportunity to make further investigations into the VLBI scale parameter.

EOP comparisons show generally a good agreement between the individual contributions and the combined solution. The WRMS of the differences are between 40 and 100 μ as for X- and Y-Pole, between 5 and 15 μ s for dUT1, and between 5 and 35 μ s/d for LOD.

Acknowledgements

We want to thank everyone who contributed within the process of generating the IVS combined contribution to ITRF2014, especially the IVS Analysis Centers that provided the input for the combination process. Furthermore, we want to thank the responsible persons at the IERS ITRS Combination Centers at DGFI-TUM, IGN, and JPL who provided valuable feedback on the

combined sessions. The support by the DFG research unit FOR 1503 for the studies on atmospheric loading is acknowledged, too. We also want to thank R. Bertelmann, R. Heinkelmann, and A. Nothnagel for the work on introducing the data DOI for the VLBI input to the ITRF2014.

References

1. Z. Altamimi, X. Collilieux, and L. Métivier. ITRF2008: an improved solution of the international terrestrial reference frame. *Journal of Geodesy*, Springer Berlin / Heidelberg, doi:10.1007/s00190-011-0444-4, 85, 457-473, 2011.
2. S. Bachmann, D. Thaller, O. Roggenbuck, M. Lösler, and L. Messerschmitt. IVS contribution to ITRF2014. *Journal of Geodesy*, Springer Berlin / Heidelberg, doi:10.1007/s00190-016-0899-4, 2016.
3. D. Behrend, J. Böhm, P. Charlot, T. Clark, B. Corey, J. Gipson, R. Haas, Y. Koyama, D. MacMillan, Z. Malkin, A. Niell, T. Nilsson, B. Petrachenko, A. Rogers, G. Tuccari, and J. Wresnik. M. G. Sideris (Ed.). Recent Progress in the VLBI2010 Development Observing our Changing Earth. Springer Berlin / Heidelberg, 133, doi:10.1007/978-3-540-85426-5_96, 833-840, 2008.
4. C. Bizouard and D. Gambis. The combined solution C04 for Earth Orientation Parameters consistent with International Terrestrial Reference Frame 2008. IERS Earth Orientation Product Centre, 2010.
5. S. Böckmann, T. Artz, and A. Nothnagel. VLBI terrestrial reference frame contributions to ITRF2008. *Journal of Geodesy*, 84, doi: 10.1007/s00190-009-0357-7, 201-219, 2010.
6. L. Messerschmitt, S. Bachmann, and D. Thaller. Options and functions of the revised IVS combination website. To appear in: D. Behrend, K.D. Baver, and K. Armstrong (Eds.), *IVS 2016 General Meeting Proceedings*, 2016, this volume.
7. A. Nothnagel et al. International VLBI Service for Geodesy and Astrometry (IVS). The IVS data input to ITRF2014. International VLBI Service for Geodesy and Astrometry, GFZ Data Services, 2015.
8. W. Schlüter and D. Behrend. The International VLBI Service for Geodesy and Astrometry (IVS): current capabilities and future prospects. *Journal of Geodesy*, Springer Berlin / Heidelberg, 81, doi: 10.1007/s00190-006-0131-z, 379-387, 2007.
9. M. Seitz, D. Angermann, M. Bloßfeld, H. Drewes, and M. Gerstl. The 2008 DGFI realization of the ITRS: DTRF2008. *Journal of Geodesy*, Springer Berlin / Heidelberg, 86, doi:10.1007/s00190-012-0567-2, 1097-1123, 2012.
10. M. Vennebusch, S. Böckmann, and A. Nothnagel. The contribution of Very Long Baseline Interferometry to ITRF2005. *Journal of Geodesy*, Springer Berlin / Heidelberg, doi:10.1007/s00190-006-0117-x, 81, 553-564, 2007.

Vienna Contribution to ITRF2014

Sigrid Böhm¹, Hana Krásná¹, Sabine Bachmann²

Abstract The next realization of the International Terrestrial Reference System, the ITRF2014, was released in the beginning of 2016. The VLBI input to ITRF2014 was provided by the International VLBI Service for Geodesy and Astrometry (IVS) and consists of a combination of all Analysis Center contributions. One of these single solutions was contributed by the Vienna Special Analysis Center of the Department of Geodesy and Geoinformation at TU Wien. In this paper we describe the characteristics of the Vienna contribution (calculated using the Vienna VLBI Software VieVS) to ITRF2014 and VTRF2014, respectively. We give a documentation of the included sessions and stations as well as some statistical information which shows the performance of the Vienna contribution compared to the other contributions in the IVS combination. In addition to that, a single TRF solution, VieTRF2014a, which is based on the Vienna input to ITRF2014, is presented and compared to previous TRF solutions. By and large the Vienna contribution does not exhibit any outstanding features when compared to the other submissions, except for the Earth rotation component dUT1, which shows large residuals with respect to the combined solution. The reason for this discrepancy is probably the different parameterization of EOP in VieVS as piecewise linear offsets, necessitating a transformation prior to the combination.

Keywords ITRF2014, VieVS, data analysis, global solution

-
1. TU Wien, Austria
 2. BKG, Germany

1 Introduction

The International Terrestrial Reference Frame (ITRF) is re-calculated every few years as a combination of solutions from different space-geodetic techniques. The Very Long Baseline Interferometry (VLBI) solution is provided by the IVS and itself is constituted as a combination of normal equations from a number of analysis centers (ACs). The special AC at TU Wien (VIE) contributed to the IVS combination for the first time with single session normal equations in SINEX format computed using VieVS (Böhm et al., 2009, [1]). In the first part of this paper we give a brief overview of the Vienna contribution and comparative plots focusing on the performance of the VIE solution only. For further information on the combination process, details about other ACs, and a more accurate interpretation of results, we refer to Bachmann et al. (2016) [2]. In the second part we introduce the single TRF solution, VieTRF2014a, calculated using the global solution of VieVS.

2 Vienna Contribution to IVS Combination

A total of 5,708 sessions in SINEX format were submitted to the IVS Combination Center, 4,659 of which were successfully used in the combination process. The submission comprises data from 1979.7–2015.0 and includes 145 VLBI stations.

In contrast to common practice, the EOP (Earth orientation parameters) of AC VIE are parametrized as offsets instead of as an offset and a rate. The SINEX files contain EOP as so-called piecewise linear offsets

in 48-hour intervals, which are transformed to an offset and a rate for the combination.

Figure 1 shows the weighted root mean squares (WRMS) of the station position residuals of all ACs with respect to the combined solution. The WRMS of the EOP residuals w.r.t. the combined solution are presented in Figures 2–6. Striking residuals are seen in the VIE dUT1 solution only. This fact can be attributed to the necessary transformation process which needs further investigation.

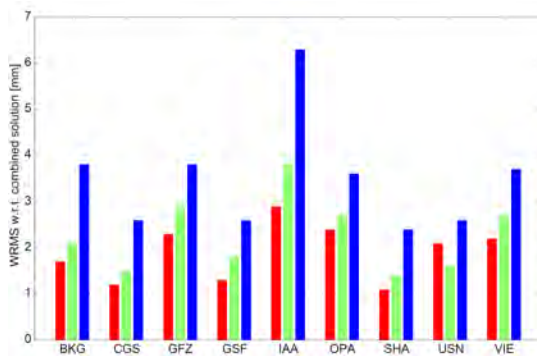


Fig. 1 WRMS of station residuals w.r.t. the combined solution.

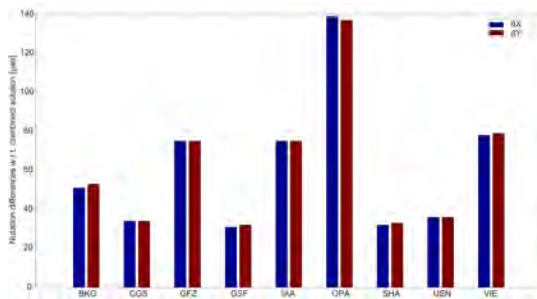


Fig. 2 WRMS of nutation (celestial pole offsets) residuals w.r.t. the combined solution.

For the combination, all individual normal equations are rescaled by a variance factor. These weighting factors for the ACs are estimated by means of variance component estimation. As it is illustrated in Figure 7, the factor for VIE AC is closely aligned to the factor for GFZ AC, due to the fact that both use VieVS for data analysis. Both weighting factors feature a clear annual signal, which could be explained by the use of NGS cards as input for VieVS. For more information about

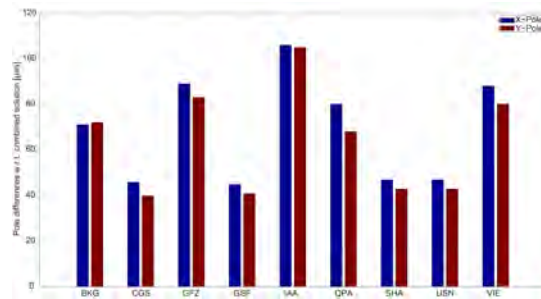


Fig. 3 WRMS of pole residuals w.r.t. the combined solution.

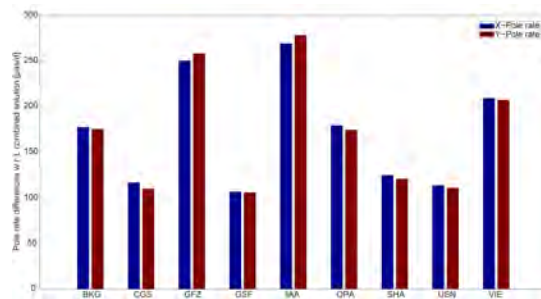


Fig. 4 WRMS of pole rate residuals w.r.t. the combined solution.

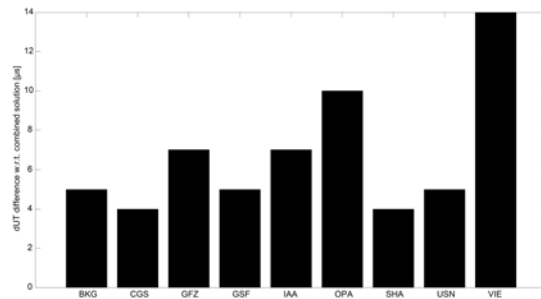


Fig. 5 WRMS of dUT1 residuals w.r.t. the combined solution.

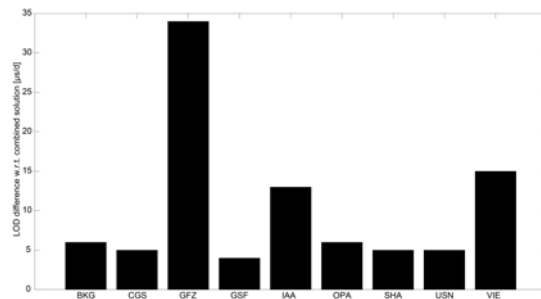


Fig. 6 WRMS of LOD residuals w.r.t. the combined solution.

this phenomenon and the weighting strategy in general we refer to Bachmann et al. (2016) [2].

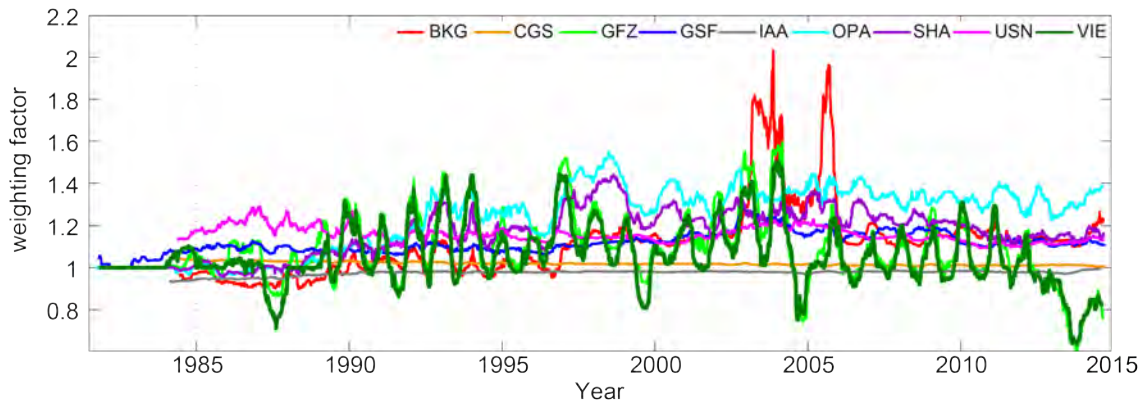


Fig. 7 Session-wise weighting factors for the individual Analysis Centers (ACs).

3 Vienna TRF Solution VieTRF2014a

For the Vienna TRF solution we selected 4,834 sessions spanning the years 1979.7–2015. The solution contains only sessions with more than two stations and more than 200 observations. Sessions for which the single session processing revealed a standard deviation of the unit weight a posteriori of more than 3 or a badly conditioned normal equation matrix were excluded from the global solution. The single sessions were processed using the standard processing settings of VieVS, which are summarized in Table 1.

Table 1 Standard single session processing settings of VieVS.

	Interval (min)	Relative constraints
Clock	60	1.3 cm after 60 min
Zenith wet delay	60	1.5 cm after 60 min
Trop. gradients	360	0.05 cm after 360 min
x-pole, y-pole	1440	0.1 μ as after 1 day
dUT1	1440	0.1 μ as after 1 day
Cel. pole offsets	1440	0.1 μ as after 1 day
Station models	according to IERS Conventions 2010 [3] + non-tidal atmospheric loading (VIENNA)	

The TRF solution called VieTRF2014a contains site positions and velocities of the stations displayed in the global map (Figure 9). Source coordinates were fixed to their ICRF2 positions. Clocks, zenith wet delays, troposphere gradients, and EOP were reduced session-wise. The datum was defined imposing no-net-rotation and no-net-translation conditions on the VTRF2008 (Böckmann et al., 2010, [4]) coordinates of 23 stable long-term observing stations. Antennas which have been observing in fewer than 20 sessions

and for less than two years were reduced and their coordinates estimated session-wise. The activity of the antennas included in the TRF is plotted in Figure 10.

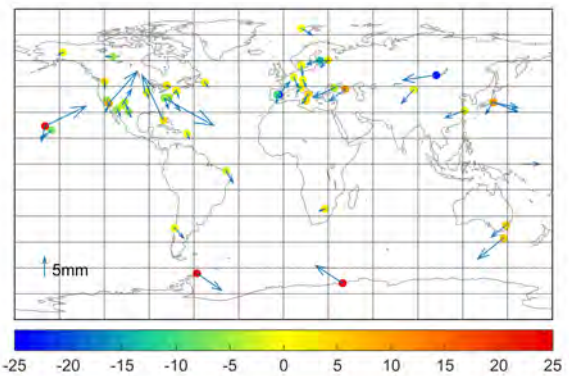


Fig. 8 Position differences between VieTRF2014a and VTRF2008 at epoch 2000.0. Only stations with an RMS of less than 5 mm are shown. The color bar represents the height difference in mm

Table 2 gives the weighted Helmert parameters including formal errors from VieTRF2014a to VTRF2008 at epoch 2000.0 for stations with a position RMS of less than 5 mm and for all stations, respectively. The position differences between VieTRF2014a and VTRF2008 at epoch 2000.0 are shown in Figure 8.

4 Summary and Conclusions

The present paper provides basic information about the contribution of the special AC VIE to the IVS combina-

Table 2 Weighted Helmert parameters from VieTRF2014a to VTRF2008 (epoch 2000.0).

T_x [mm]	T_y [mm]	T_z [mm]	R_x [mas]	R_y [mas]	R_z [mas]	Scale [ppb]
dT_x [mm/yr]	dT_y [mm/yr]	dT_z [mm/yr]	dR_x [μ as/yr]	dR_y [μ as/yr]	dR_z [μ as/yr]	Scale rate [ppb/yr]
Stations with position RMS < 5 mm						
2.28 \pm 0.72	1.60 \pm 0.70	-2.72 \pm 0.67	-0.03 \pm 0.03	0.04 \pm 0.03	0.02 \pm 0.02	0.26 \pm 0.10
-0.18 \pm 0.24	0.01 \pm 0.24	-0.26 \pm 0.23	0.49 \pm 9.35	-2.73 \pm 9.52	-5.66 \pm 7.28	0.01 \pm 0.03
All stations						
2.16 \pm 2.91	1.06 \pm 2.83	-3.17 \pm 2.70	-0.01 \pm 0.11	0.04 \pm 0.11	0.01 \pm 0.09	0.29 \pm 0.40
-0.13 \pm 0.99	-0.09 \pm 0.96	-0.31 \pm 0.94	3.96 \pm 37.87	-1.57 \pm 38.59	-5.02 \pm 29.54	0.01 \pm 0.14

tion solution for ITRF2014. In general, the VIE input does not show any distinctive features w.r.t. the other ACs or the combined solution, except for large WRMS of the dUT1 residuals. The EOP submitted by VIE are represented as piecewise linear offsets and have to be transformed to offset and rate to be consistent with the parametrization of the other ACs. The transformation prior to the combination is presumably responsible for this deviation (see also Bachmann et al. (2016), [2]).

A Vienna TRF solution, VieTRF2014a, was presented in the second part of the paper. This TRF is a preliminary solution and will be refined in terms of datum definition and handling of stations where earthquakes occurred. At present the software is not able to reduce a station only for a certain period of time (for example after a break due to an earthquake). It is also planned to estimate future TRF solutions consistently and therefore simultaneously to the Vienna celestial reference frame solution (refer to the paper, “Vienna Contribution to the ICRF3” by Mayer et al. in this volume).

References

1. J. Böhm, S. Böhm, T. Nilsson, A. Pany, L. Plank, H. Spcakova, K. Teke, and H. Schuh. The new Vienna VLBI Software VieVS. In S. Kenyon, M. C. Pacino, and U. Marti, editors, *International Association of Geodesy Symposia Series*, 136, pages 1007–1011, 2012.
2. S. Bachmann, D. Thaller, O. Roggenbruck, M. Lösler, and L. Messerschmitt. IVS contribution to ITRF2014. *Journal of Geodesy*, doi: 10.1007/s00190-016-0899-4, 2016.
3. IERS Conventions (2010). G. Petit and B. Luzum, editors, *IERS Technical Notes*, 36, Frankfurt am Main: Verlag des Bundesamts für Kartographie und Geodäsie, 2010.
4. S. Böckmann, T. Artz, and A. Nothnagel. VLBI terrestrial reference frame contributions to ITRF2008. *Journal of Geodesy*, 84, pages 201–219, doi: 10.1007/s00190-009-0357-7, 2010.

Comparison of a VLBI TRF Solution Based on Kalman Filtering and Recent ITRS Realizations

Benedikt Soja¹, Tobias Nilsson¹, Susanne Glaser², Kyriakos Balidakis², Maria Karbon¹, Robert Heinkelmann¹, Richard Gross³, Harald Schuh^{1,2}

Abstract Terrestrial reference frames (TRFs) of high quality are indispensable for many geoscientific and geodetic applications including very long baseline interferometry (VLBI) data analysis. While secular station coordinate changes, for instance due to tectonic plate motion, are well represented by a linear model, current accuracy requirements demand modeling of non-linear signals such as surface deformations due to mass loading or post-seismic deformations. In this paper, we portray a TRF solution solely based on VLBI data, employing Kalman filtering and smoothing for the computation of session-wise coordinates of 104 VLBI radio telescopes over more than 30 years. We compare our VLBI TRF to the multi-technique ITRF solutions ITRF2014 and JTRF2014, focusing on the different approaches of modeling non-linear signals. Overall, a good agreement is found for strong post-seismic deformations, but the three solutions diverge in terms of seasonal signals.

Keywords VLBI, Kalman filter, terrestrial reference frames, post-seismic deformations

1 Introduction

Terrestrial reference frames (TRFs) are important for several applications, for example in the fields of navigation, geophysics, and climate investigations. There-

fore, determining TRFs with utmost accuracy and stability is one of the primary tasks of geodesy. In previous generations of International Terrestrial Reference Frame (ITRF) solutions, such as the ITRF2008 [1], the station coordinate model for every segment consisted of an offset and a velocity. In order to take into account non-linear effects and thus satisfy growing accuracy demands, the ITRS (International Terrestrial Reference System) combination centers of the IERS (International Earth Rotation and Reference Systems Service) followed different strategies to extend the coordinate model for the most recent ITRF solutions, comprising data until the end of 2014. For example, all Combination Centers decided to estimate seasonal signals. The two ITRF solutions considered in this study, the ITRF2014¹ by IGN and the JTRF2014 by JPL are discussed in greater detail in Section 3.

At GFZ Potsdam, we have calculated TRF solutions solely based on the data from very long baseline interferometry (VLBI, [2, 3]). VLBI is very important for the determination of TRFs since it is very sensitive to the network scale. Similar to the ITRF solution by JPL, our approach is based on Kalman filtering. More details are provided in Section 2 as well as in Soja et al. (2016) [4].

The aim of this study is to compare these three TRF solutions. In particular, it is of interest how strong non-linear effects, such as post-seismic deformations and seasonal signals, are handled. Therefore, the comparisons of this preliminary study are restricted to stations that are strongly affected by these phenomena.

1. GFZ German Research Centre for Geosciences, Potsdam, Germany

2. Technische Universität Berlin, Berlin, Germany

3. Jet Propulsion Laboratory, California Institute of Technology, Pasadena, United States of America

¹ http://itrf.ign.fr/ITRF_solutions/2014/

2 Kalman Filter VLBI TRF Solution

The Kalman filter VLBI TRF solution (from here on KF VTRF) produced at GFZ is based on 4,239 VLBI sessions between 1980 and the end of 2013. Only sessions with four or more radio telescopes participating and with the volume of the polyhedron defined by the network exceeding more than 10^{15} m^3 were considered to ensure that the network geometry is suitable for TRF determination. In the future, it would be worthwhile to consider the inclusion of regional sessions in order to increase the temporal resolution. As input data the session-wise coordinates computed with the VieVS@GFZ software [5, 6], a fork from the Vienna VLBI Software [7], were used. In total, the coordinates of 104 radio telescopes were processed.

For this study, the standard solution portrayed in [4] was used. The state vector of the Kalman filter comprised offsets and velocities of all considered stations. The coordinate offsets were modeled as random walk processes, with the station-specific process noise derived from time series of the geophysical loading effects that were not corrected for in the VLBI analysis, namely non-tidal atmosphere, non-tidal ocean, and continental water storage loading displacements [8]. In order to increase the short-term stability of the frame, the coordinate noise model was scaled by a factor of 0.1. No seasonal signals were estimated, since it was shown [4] that in the presence of process noise, the resulting time series are identical. In order to take into account the non-linear deformations after strong earthquakes, the noise directly after such an event was increased by a factor of 10 for coordinate jumps of 3 m (and scaled linearly for different sizes of jumps). This scaling factor was steadily reduced to the original noise level over a time span of one year.

3 ITRF2014 and JTRF2014

Both ITRF2014 and JTRF2014 are based on the combined SINEX files submitted by the combination centers of the International Association of Geodesy services of the four primary space-geodetic techniques. For both TRFs, the combination was performed on the parameter level, which means that the datum-free normal equations of the VLBI contribution had to be inverted beforehand. Both solutions include annual and

semi-annual signals and inferred the scale information from the average of the VLBI and satellite laser ranging scales (weighted in the case of JTRF2014).

The selection of data was significantly different between these two solutions. While for ITRF2014 an extensive set of stations was used, a large portion was eliminated for JTRF2014. For example, in the case of VLBI only 71 stations were used (ITRF2014: 140). Regional sessions were excluded for JTRF2014, similar to the KF VTRF solution. On the other hand, the ITRF2014 creators were selective regarding the local ties, while a comprehensive set of 234 tie vectors, properly weighted by their co-variances, was adopted for JTRF2014.

Still, the main difference lies in the fact that ITRF2014 was computed by least-squares adjusting the parameters of the coordinate model (which also includes exponential and/or logarithmic functions for post-seismic deformations), whereas a Kalman filter and smoother was used for JTRF2014. In the latter, the solution is represented by a time series of weekly station coordinates. Similar to the KF VTRF, the coordinates are modeled as random walk processes with the noise derived from geophysical loading models [9].

4 Comparison of TRF Solutions

As the input data sets are different, even between the two multi-technique solutions due to the heavy data screening and editing, it is difficult to select a reference. Consequently, the comparisons have been kept on a qualitative and visual level. The station coordinates in all graphs are shown in local topocentric coordinate systems, with no trends or other functions subtracted, and thus reflect only the differences between the solutions.

In Figure 1, all three TRF solutions are plotted for station Tsukuba, Japan. Clearly visible is the large displacement and strong post-seismic deformation due to the 2011 Tōhoku earthquake, which all solutions are able to account for. Figure 2 portrays the temporal changes in the east coordinate component after the earthquake in greater detail. It becomes evident that the agreement of these current solutions with the observations is much better than what would be possible with the classical linear model. Nevertheless, small dis-

crepancies between the solutions are visible, in particular during the first months of the post-seismic period, where the ITRF2014 disagrees with the two Kalman filter solutions by up to 1.5 cm.

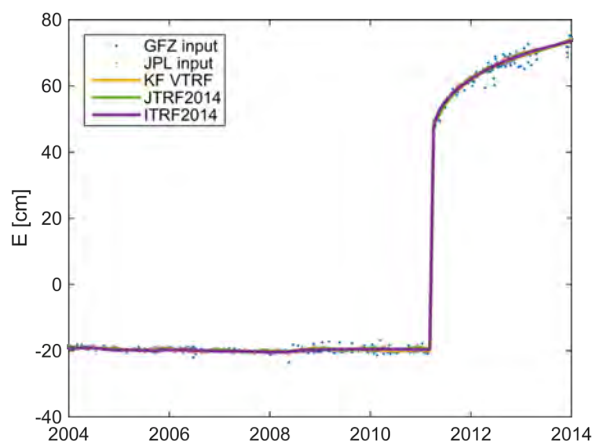


Fig. 1 East coordinates of station Tsukuba from 2004 until 2014 for the KF VTRF solution (yellow), ITRF2014 (green), and ITRF2014 (purple). Additionally, the input coordinates for the VTRF (blue dots) and JTRF2014 (light red dots) are provided.

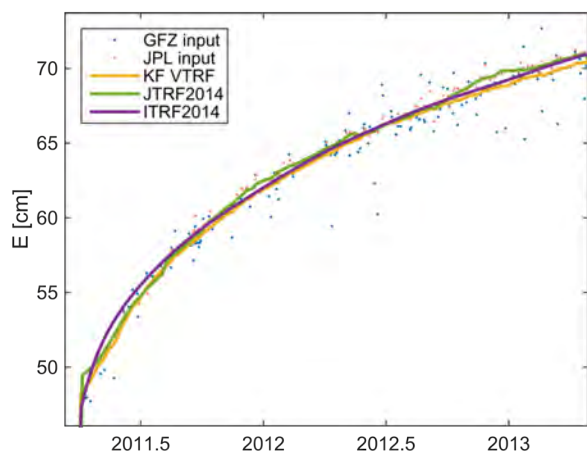


Fig. 2 For the east coordinate of Tsukuba the same data and solutions as in Figure 1 are depicted with a focus on the period after the earthquake.

Figure 3 exhibits the situation of station Tsukuba before the earthquake. Starting from the first half of 2008, a weak seismic signal is visible in all solutions, with coordinates slightly diverging from the long-time trend. The seasonal signals are, however, very different between the three solutions. The annual oscillation

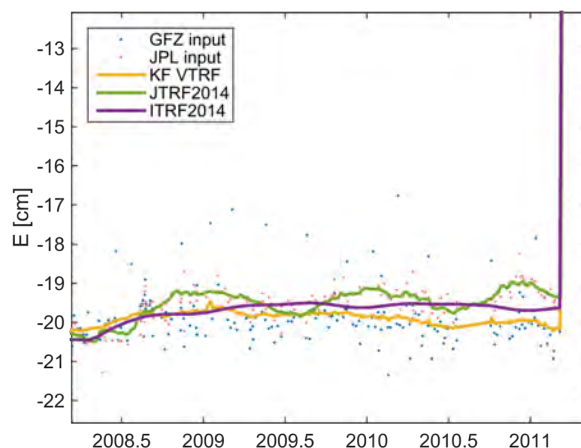


Fig. 3 East coordinates of Tsukuba in the period before the earthquake, otherwise similar to Figure 2.

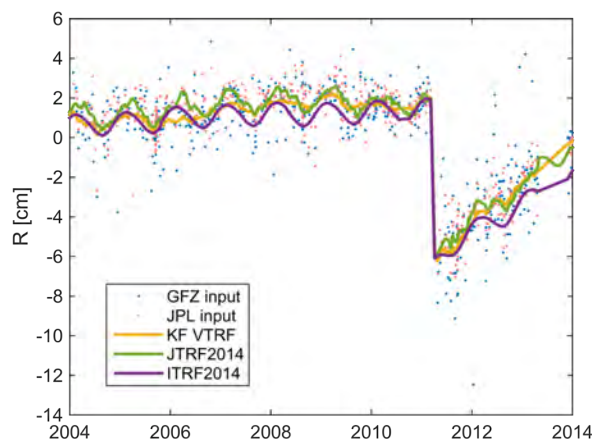


Fig. 4 Height component of Tsukuba between 2004 and 2014 (for details see Figure 1).

in JTRF2014 is significantly larger than in ITRF2014 and seems to be out of phase by about 180° . The phase of the VTRF signals is similar to JTRF2014, but the amplitude fits the one of ITRF2014. A better agreement in terms of seasonal signals is found in the radial component (Figure 4). Here, only the KF VTRF shows smaller amplitudes, however, supported by the input data. In the two multi-technique solutions, a reason for the larger seasonal signals could be co-motion constraints imposed on the co-located GNSS station TSKB, the input data of which shows a distinct annual signal. The trend after the earthquake is different between the Kalman filter solutions and ITRF2014, what is surprising since the agreement is much better in the east component.

In Figure 5, the coordinates of station Gilmore Creek, Alaska, are examined. Similar to the east coordinates of Tsukuba, the three solutions diverge in terms of seasonal signals. Here, the annual signals of irregular amplitudes seen in the two Kalman filter solutions are out of phase. ITRF2014 shows distinct semi-annual signals that are not found in the other solutions. Nevertheless, the seismic effects are well represented in all solutions. A positive effect of the extended coordinate models is that fewer breaks need to be introduced. For example, ITRF2008 introduced six breaks to capture the complex seismic displacements, whereas for the current solutions, it is sufficient to apply just a single break at the epoch of the earthquake.

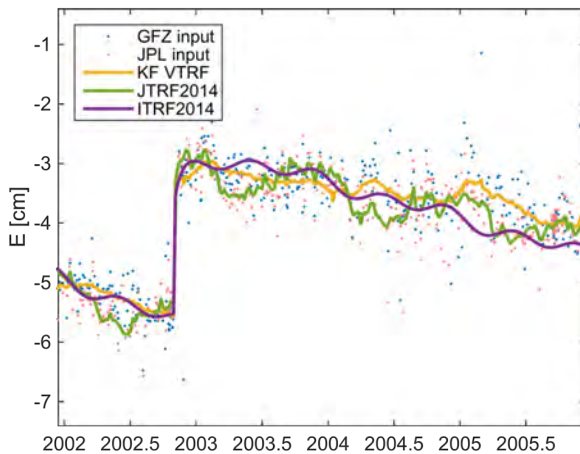


Fig. 5 East coordinates of station Gilmore Creek are shown for the time period 2002–2006. The same TRF solutions as in Figure 1 are included.

Finally, Figure 6 depicts the complex post-seismic behavior of the coordinates of the station in Concepción, Chile, due to the 8.8 M_w earthquake in 2010 and an aftershock in 2011. The JTRF2014 coordinates directly after the earthquake are only based on observations during very few weeks and are therefore mostly predictions, which obviously cannot account for the post-seismic deformations. Once observations are integrated again in mid-2011, JTRF2014 agrees with the other solutions very well. The temporal changes in the coordinates of the KF VTRF and ITRF2014 fit very well over the whole period, although a bias is present.

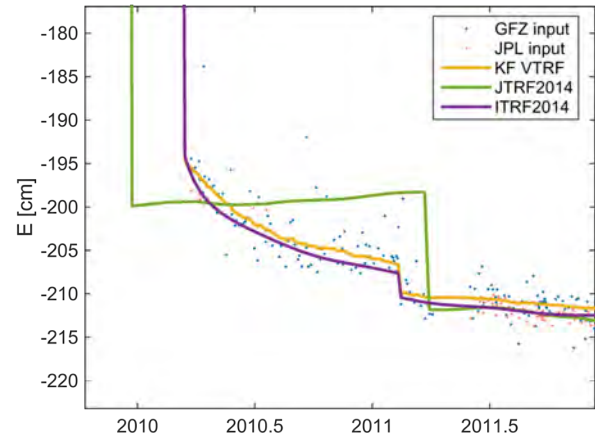


Fig. 6 For station TIGO Concepción, east coordinates during the first years after the 2010 Chile earthquake are given. The same graphical elements as in Figure 1 are shown.

5 Conclusions

In this paper, a VLBI TRF solution based on Kalman filtering and the two International Terrestrial Reference System realizations ITRF2014 and JTRF2014 were compared focusing on non-linear signals. Overall, a good agreement was found during periods of post-seismic deformations. Here, the extension of the coordinate model (in a functional or stochastic sense) allows to closely follow the observed variations, what would not be the case for the classical linear approach. While the seasonal signals from the different solutions are mostly consistent with each other for the height component, striking differences are found in the horizontal components for the considered stations. Considering the different approaches and data sets, the performance of our KF VTRF solution is promising. In the future, the comparisons should be extended to include additional stations as well as the DTRF2014, the ITRF solution by DGFI, Munich.

Acknowledgements

The authors thank the IVS for observing, correlating, and providing the VLBI data used in this work and the ITRS Combination Centers of the IERS at IGN and JPL for providing ITRF solutions. Benedikt Soja works under FWF project P 24187-N21. The work of RG described in this paper was carried out at the Jet Propul-

sion Laboratory, California Institute of Technology, under a contract with the National Aeronautics and Space Administration.

References

1. Z. Altamimi, X. Collilieux, and L. Métivier. ITRF2008: an improved solution of the international terrestrial reference frame. *Journal of Geodesy*, 85(8):457–473, 2011.
2. H. Schuh and D. Behrend. VLBI: A fascinating technique for geodesy and astrometry. *J. Geodyn.*, 61:68–80, 2012.
3. A. Nothnagel, International VLBI Service for Geodesy and Astrometry (IVS), et al. The IVS data input to ITRF2014. International VLBI Service for Geodesy and Astrometry, GFZ Data Services, DOI 10.5880/GFZ.1.1.2015.002, 2015.
4. B. Soja, T. Nilsson, K. Balidakis, S. Glaser, R. Heinkelmann, and H. Schuh. Determination of a Terrestrial Reference Frame via Kalman Filtering of Very Long Baseline Interferometry Data. *Journal of Geodesy*, submitted.
5. T. Nilsson, B. Soja, M. Karbon, R. Heinkelmann, and H. Schuh. Application of Kalman filtering in VLBI data analysis. *Earth, Planets and Space*, 67(1):136, 2015.
6. B. Soja, T. Nilsson, M. Karbon, F. Zus, G. Dick, Z. Deng, J. Wickert, R. Heinkelmann, and H. Schuh. Tropospheric delay determination by Kalman filtering VLBI data. *Earth, Planets and Space*, 67(1):144, 2015.
7. J. Böhm, S. Böhm, T. Nilsson, A. Pany, L. Plank, H. Spicakova, K. Teke, and H. Schuh. The new Vienna VLBI Software VieVS. In S. Kenyon, M. C. Pacino, and U. Marti, editors, *Proceedings of IAG Scientific Assembly 2009*, volume 136 of *International Association of Geodesy Symposia*, pages 1007–1011. Springer-Verlag, Berlin Heidelberg, 2012.
8. IERS Conventions. G. Petit and B. Luzum (eds.). IERS Technical Note 36, Frankfurt am Main: Verlag des Bundesamtes für Kartographie und Geodäsie, 2010.
9. X. Wu, C. Abbondanza, Z. Altamimi, T. M. Chin, X. Collilieux, R. S. Gross, M. B. Heflin, Y. Jiang, and J. W. Parker. KALREF – A Kalman filter and time series approach to the International Terrestrial Reference Frame realization. *Journal of Geophysical Research: Solid Earth*, pages 3775–3802, 2015.

VLBI Processing at ESOC

Claudia Flohrer, Erik Schönemann, Tim Springer, René Zandbergen, Werner Enderle

Abstract ESOC's Navigation Support Office (NavSO) is currently extending its expertise to VLBI processing and analysis by enhancing the processing capabilities of its software package NAPEOS, used for all activities requiring the highest accuracy. The processing of VLBI data will extend ESOC's capabilities of determining the absolute orientation of the Earth and thereby enables NavSO to provide a fully independent set of Earth orientation parameters for ESA missions. Hence, it will allow enhancement of the contribution to the IERS (International Earth Rotation and Reference Systems Service) whilst at the same time reducing the dependency on this service. In addition, NAPEOS is capable of combining all four space-geodetic techniques at the observation level and thus supporting GGOS, the Global Geodetic Observing System, to get a better understanding of our living planet. This paper gives an overview of the current status of the VLBI processing capability at ESOC and provides an outlook on future plans.

Keywords ESOC, NAPEOS, UT1–UTC, VLBI analysis, combination at observation level

1 Introduction

ESOC's Navigation Support Office (NavSO) is providing the geodetic reference for ESA missions and is the coordinator of a European Consortium that provides the Galileo Geodetic Reference Frame. NavSO has demonstrated its expertise in the processing of var-

ious space-geodetic techniques, such as GNSS, SLR, and DORIS, and their combination on the observation level. Nevertheless, the last piece missing for the generation of independent Earth Orientation Parameters (EOPs), required for the definition of the Earth's orientation, is VLBI.

In the following, NavSO is introduced, and its interest in VLBI data analysis is explained. An overview is provided of the current status of the VLBI implementation done so far in NAPEOS and of the next intended steps.

2 ESOC's Navigation Support Office - NavSO

ESA's European Space Operations Centre ESOC, located in Darmstadt, Germany, tracks and controls European spacecraft, and develops and manages ground systems. NavSO is an integral part of the Ground Systems Engineering Department of ESOC, under the directorate of operations.

The main objectives of NavSO are the provision of expertise for high-accuracy navigation, satellite geodesy, and the generation of related products and services for all ESA missions and for third-party customers, as well as supporting the European GNSS programs: Galileo and EGNOS. NavSO's main areas of expertise are:

- NavSO is providing the geodetic reference for ESA missions.
- NavSO is the coordinator of the Galileo Geodetic Service Provider (GGSP) consortium.
- NavSO is operating ESA's global GNSS sensor station network, currently consisting of 16 sites as



Fig. 1 ESA's GNSS Sensor Station Network operated by the Navigation Support Office.

shown in Figure 1. Several new sites are currently under implementation.

- NavSO is an IGS, ILRS, and IDS Analysis Center and thus contributes to the geodetic reference frame realization ITRF.
- NavSO does precise orbit and clock determination for GNSS and LEO satellites using its own software package NAPEOS (NAavigation Package for Earth Orbiting Satellites) [1]. It is capable of processing data from the various satellite-geodetic techniques, such as GNSS, SLR, DORIS, and altimetry, individually but also combined at the observation level. State-of-the-art models and algorithms are used and developed further to ensure high-precision products.
- NavSO has developed and is operating a UTC realization at ESOC, which can be used as time reference for ESA missions. The start of the official contribution to UTC is foreseen within 2016.

Currently NavSO is extending its expertise to be able to process and analyze VLBI observations. The processing of VLBI tracking data will complete ESOC's capabilities in generating EOPs to ensure the operational capability of ESOC. It will enable NavSO to enhance its contribution to the IERS service and to contribute to the IVS service as an analysis center. Finally, it will enable NAPEOS to combine all space-geodetic tech-

niques at the observation level, bringing together the strengths of the individual techniques.

Table 1 shows the contribution of the individual techniques to the celestial and terrestrial reference frame (CRF and TRF) parameters and the EOPs, allowing conversion between the CRF and the TRF. While GNSS, SLR, and DORIS are contributing to polar motion and length-of-day (LOD), VLBI is the only technique able to determine the celestial pole offsets w.r.t. the IAU precession and nutation model (labeled as nutation parameter) and UT1-UTC.

Table 1 Contribution of the individual space-geodetic techniques to reference frames and EOPs.

	Parameter	GNSS	SLR	DORIS	VLBI
CRF	Quasar positions				x
	Satellite orbits	x	x	x	
EOP	Nutation				x
	UT1-UTC				x
	LOD	x	x	x	x
	Polar motion	x	x	x	x
TRF	Station positions	x	x	x	x
	Geocenter	x	x	x	

3 VLBI Implementation in NAPEOS

This section presents the implementation steps to enable the VLBI data processing in NAPEOS. The following list summarizes the different steps. The current status of each implementation step is given in brackets.

- Read observations (**implemented**)
 - Observations are read from the NGS card format. In the future the format can be replaced by vgosDB format based on netCDF files.
- Set up database (**partially implemented**)
 - Station and source coordinates are converted to the NAPEOS database format.
 - Site eccentricities, axis offsets, and mounting types have still to be incorporated.
- Set up new observation type (**implemented**)
 - A new observation type “VLBI group delay” is introduced.
- Set up observation equation (**implemented**)
 - The observation equation for the VLBI group delay is set up. The formulation from Schuh [2], which is consistent with the *Consensus model* of the IERS conventions [3], is used.
- Apply observation corrections (**partially implemented**)
 - Relativistic corrections: So far only terms larger than a maximum order of magnitude of $2 \cdot 10^{-10}$ s are considered; smaller terms still have to be added.
 - Clock synchronization: Clock offsets w.r.t. a reference clock are estimated, but clock breaks are not yet handled.
 - Tropospheric delay: Is taken into account using the meteorological data of each station.
 - Ionospheric delay: Is taken into account using the value provided in the NGS data files.
 - Instrumental delays: Axis offsets and cable delays still have to be implemented.
- Compute partial derivatives to enable parameter estimation (**partially implemented**)
 - The partial derivatives of the parameters to be estimated (e.g., tropospheric wet delay and gradients, station coordinates and clocks, EOPs)

have to be set up w.r.t. the VLBI observation equation. This implementation step is still ongoing. The estimation of source coordinates will not be part of the current implementation but will still be possible at a later stage.

- Enable combination at observation level (**partially implemented**)
 - The combination of EOPs from different observation types is already possible with NAPEOS. Some implementation effort is still needed to combine troposphere parameters, station coordinates, and clocks, as local ties and biases have to be taken into account between VLBI and the other geodetic techniques.
- Apply observation weighting (**implemented**)
 - An elevation-dependent observation weighting can already be applied in NAPEOS.
 - When combining different observation types proper technique-specific weighting factors reflecting the different observation accuracies of each technique have to be applied.

4 Initial Results and Next Steps

The implementation of the presented steps into NAPEOS started in the end of 2015. The VieVS software [4] was used to validate the observation model and to compare the results. The current state of implementation allows the generation of O–C residuals at the 0.5 m level. An example is given in Figure 2, showing a screenshot of the NAPEOS graphical user interface with O–C residuals of one VLBI session with three baselines. The current order of magnitude is fully in line with the expectations, as antenna axis offsets are not yet taken into account and troposphere parameters are not yet estimated.

It is planned to finalize the parameter estimation part for VLBI observations within 2016, which will allow a proper VLBI data analysis and the comparison of results with other VLBI analysis groups. NavSO will take part in the *VLBI Analysis Software Comparison Campaign 2015* (VASCC 2015) performed by the Chalmers University of Technology, in order to validate the implementation of the observation model.



Fig. 2 Screenshot of the NAPEOS graphical user interface showing O–C residuals in meters for one session with three baselines.

In the long term NavSO plans to combine VLBI data with GNSS, SLR, and DORIS data on the observation level and to actively participate in the IVS.

References

1. ESA/ESOC, DOPS-SYS-TN-0100-OPS-GN, NAPEOS Mathematical Models and Algorithms, 2009.
2. Harald Schuh, Die Radiointerferometrie auf langen Basen zur Bestimmung von Punktverschiebungen und Erdrotationsparametern, C: Dt. Geodät. Komm. bei d. Bayer. Akad. d. Wiss., 1987.
3. Gérard Petit and Brian Luzum (eds.), IERS Conventions (2010), IERS Technical Note 36, Frankfurt am Main: Verlag des Bundesamts für Kartographie und Geodäsie, 2010.
4. Johannes Böhm, Sigrid Böhm, Tobias Nilsson, Andrea Pany, Lucia Plank, Hana Spicakova, Kamil Teke, Harald Schuh, The New Vienna VLBI Software VieVS, in Proceedings of IAG Scientific Assembly 2009, International Association of Geodesy Symposia Series Vol. 136, edited by S. Kenyon, M. C. Pacino, and U. Marti, pp. 1007–1011, 2012.

Combination of Two Radio Space-Geodetic Techniques with VieVS during CONT14

Younghee Kwak¹, Johannes Böhm¹, Thomas Hobiger², Lucia Plank³, Kamil Teke⁴

Abstract Unlike CONT11, CONT14 does not have official information on common frequency standards for co-located sites. Nevertheless, according to Kwak et al. (2015) [1], we have the possibility to find the co-located sites that used the same clocks through comparing clock rates from single technique solutions. Moreover, CONT14 includes co-located VLBI radio telescopes, i.e., HOBART26 and HOBART12. Therefore, it is also a good test bed to develop the analysis strategy for future twin/sibling telescopes. In this study, we compute VLBI-like GNSS delays (GNSS single differences) between the ranges from two stations to a satellite, using phase measurements with most of the errors corrected by the c5++ software. We estimate station coordinates and site common parameters (i.e., zenith wet delays, troposphere gradients, and clock parameters) with the Vienna VLBI Software. Common clock parameters are limited to the sites sharing the same frequency standard and having good performance of it during CONT14. Local tie vectors are introduced as fictitious observations for co-located instruments: GNSS–VLBI and at Hobart even VLBI–VLBI. In this paper, we show the comparison results between the combination solutions and the single technique solutions in terms of station position repeatability during 15 days.

Keywords VLBI, GNSS, combination at the observation level, CONT14

1. Technische Universität Wien
2. Chalmers University of Technology
3. University of Tasmania
4. Hacettepe University

1 Introduction

The local tie vectors of co-located sites with several space-geodetic techniques play a key role to tie different terrestrial reference frames. However, the local tie vectors at many sites show doubtful quality and, furthermore, there is no independent method to validate them. In order to address this vulnerability, the International VLBI Service for Geodesy and Astrometry (IVS) has organized a working group on Satellite Observations with VLBI which studies possibilities to observe Earth satellites with the VLBI ground network affiliated with the IVS (<http://ivsvcc.gsfc.nasa.gov/about/wg/wg7>). Other than technical issues, it also puts a premium on developing the geometric model of satellites for analysis. The geometric model for GNSS satellites has been implemented in the Vienna VLBI Software (VieVS [2]) according to Klioner (1991) [3] and Plank et al. (2014) [4], and it was tested by Kwak et al. (2015) [5] using real GNSS data. The current accuracy of the model involved for GNSS data in VieVS is at the cm-level [5].

IVS schedules CONT campaigns, which are sets of continuous VLBI sessions during 15 days having well balanced the geographical distribution of the observation sites. Most of the CONT sites have co-located International GNSS Service (IGS) stations and simultaneously receive GNSS data. Therefore, the CONT campaign is a proper test bed for handling both VLBI and GNSS data in a common analysis software, e.g., VieVS in this study. Of course, GNSS data, usually GNSS phase measurements, need to be distilled for processing with VieVS. For more details, see Kwak et al. (2015) [5].

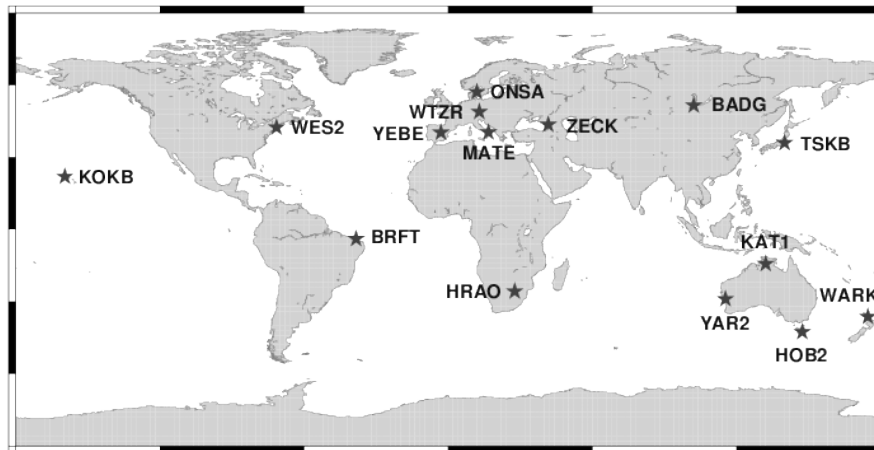


Fig. 1 A global network of co-located sites of IVS and IGS during CONT14. The station codes are written following IGS station code names.

2 Data

CONT14 was observed between May 6 and May 20, 2014. For the 15-day period of CONT14, there were 15 sites co-located with IGS stations (Figure 1). Especially Hobart (HOB2) had two IVS stations and one IGS station co-located.

We process group delays from CONT14 sessions for VLBI data as usual. In order to process and combine GNSS data together with VLBI data in VieVS, we generate VLBI-like GNSS delays (GNSS single differences) based on real GNSS phase measurements. For more details on production of GNSS delays, see Kwak et al. (2015) [5]. Two kinds of data (group delays for quasars and VLBI-like GNSS delays for GNSS satellites) are merged into single files per 24-hour session.

3 Common Clock Check

Unlike CONT11, CONT14 has no information about common frequency standards for co-located sites. However, according to Kwak et al. (2015) [1], it is possible to gauge which co-located sites shared the common clocks by way of comparing clock rates from single technique solutions. Figure 2 shows the comparison of clock rates. Here, the clock rates are relative rates with respect to the reference clock of Wettzell (WTZR). During 15 days, the clock rates of each site except HRAO look comparable between

the two techniques and are mostly in the range of ± 20 cm/day, which corresponds to around 0.008 ps/s. Some instant peaks of HOB2, KAT1, MATE, and ZECK signify clock breaks which are revealed through simple least-squares estimation (clock offsets and a ZWD). We exclude these sites and HRAO, which did not share the clock, for clock rate combination. The sites, which do not appear in Figure 2, are initially excluded from the clock rate combination. Meanwhile, clock offsets cannot be used for comparison, because the cable delay variations and other instrumental delays are also absorbed into the clock parameters. We also do not consider quadratic terms in this study.

4 Combination and Results

In the combination, we do not deal with products (estimated parameters) or normal equations but construct a combined design matrix which contains the partial derivatives of VLBI and GNSS with common geophysical models (Figure 3).

All the parameters are estimated separately and the constraints for common parameters (i.e., ZWD, troposphere gradients, and clock rates) are additionally given. ZWDs greatly depend on the height, because they signify the vertical delay values while the radio signals go through the wet troposphere. Hence, ZWD corrections have to be introduced to account for the height differences between the co-located techniques.

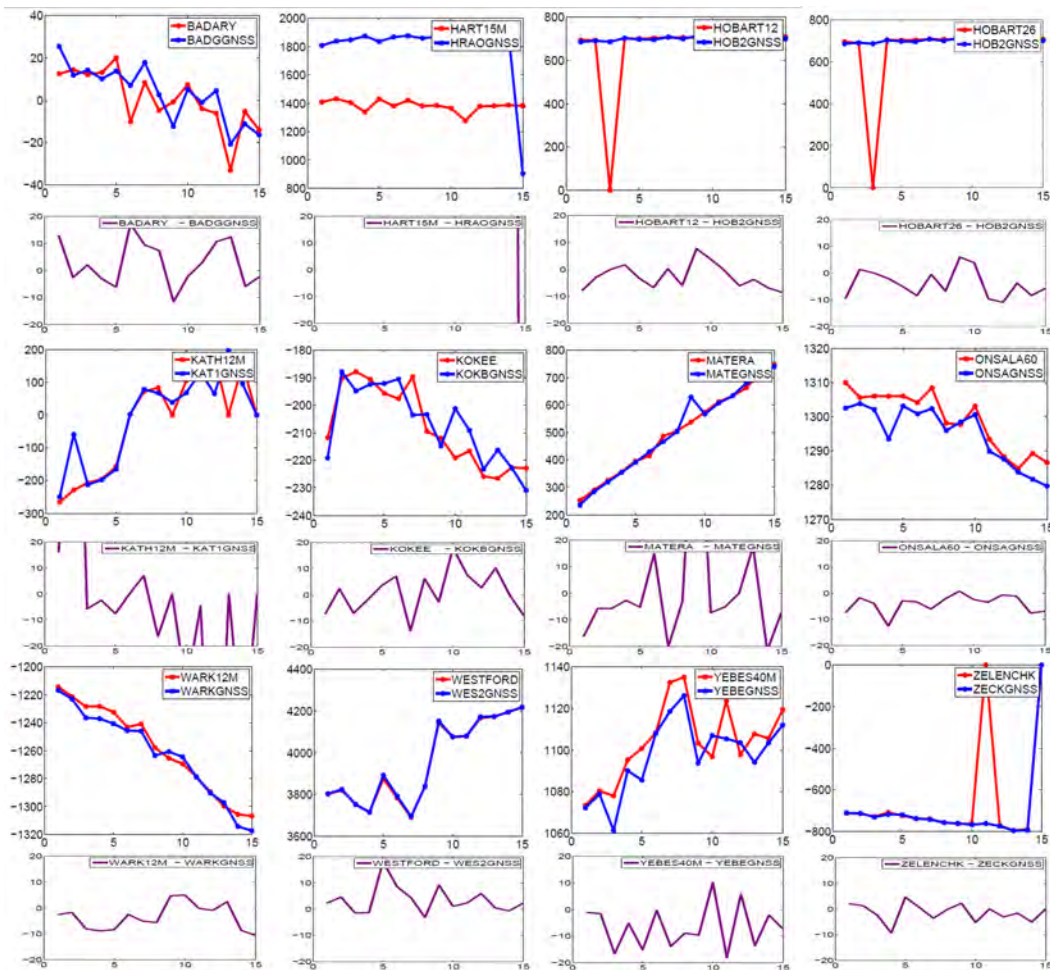


Fig. 2 Clock rates of each site which are derived from single technique solutions (red: VLBI, blue: GNSS, purple: difference) during the 15 days of the CONT14 campaign. The units of the horizontal and vertical axes are days and cm/day, respectively. The clock of WTZZ is set as reference clock. Except for HRAO, the clock rate differences are in the range of ± 20 cm/day corresponding to ± 0.008 ps/s. The instant peaks indicate clock breaks at HOB2, KAT1, MATE, and ZECK. The sites that have been excluded in the analysis at least once because of their data quality do not appear in this figure.

We apply mean ZWD correction values in accordance with Teke et al. (2011) [7] and use 1-cm constraints. When the horizontal distances between the co-located techniques are close enough, troposphere gradients are supposed to be the same [6]. For troposphere gradients, we apply loose constraints (2 cm). For all the sites, common parameter constraints of ZWDs and troposphere gradients are applied while common clock rates are constrained (10 cm/day) only for chosen sites due to sharing and/or performance of the common clock (Section 3 and Figure 2) during CONT14.

Besides, we add extra fictitious observations with known local tie vectors (survey measurements) only for

several stations: HRAO, KOKB, ONSA, WES2, and HOB2 (only for VLBI–VLBI). We apply 3 cm for the constraints, since the formal errors of the local tie measurements are usually too optimistic.

We have implemented the above combination features in VieVS also for general purposes, e.g., co-located twin/sibling telescopes.

An overview of the general analysis strategies is shown in Table 1. The EOP values are fixed to IERS 08 C04, since the partial derivatives of the EOP have not been introduced in the GNSS part.

In order to evaluate the combination performance, we compare the mean station position repeatabilities

Table 1 Models and a prioris used in this work.

Geometric models	VLBI: Consensus model GNSS: Klioner (1991) [3]
Satellite position	IGS final orbit (http://www.igs.org)
Station position	ITRF2014 [8]
Solid Earth tide	IERS 2010 Conventions [9]
Ocean loading	FES2004 [10]
Earth orientation parameters	IERS 08 C04 (http://hpiers.obspm.fr)
Troposphere delay	Zenith hydrostatic delays from GPT [11] VMF [12]
	No a priori for troposphere gradient
Ionosphere	Corrected by using ionospheric linear combination in the PPP processing

of the single solutions and the combinations. As mentioned in Section 1, the current accuracy of the model involved for GNSS data in VieVS is at the cm-level [5] and thus the station position repeatability of GNSS stations is worse than the repeatability of standard GNSS solutions. Therefore, in this paper, we focus on the comparison between single and combination solutions of each technique and the impact of common parameter constraints on combination solutions.

As a result of the combination, the mean station position repeatabilities of the GNSS solutions are improved by 5, 9, and 13% for the north, east, and up components, while the VLBI solutions are improved by 4, 6, and 16% for each component (Figure 4). The results indicate that both techniques benefit equally from the combination.

5 Conclusions

In this paper, we combined VLBI data and VLBI-like GNSS delays for 15 co-located sites during CONT14. Both data types were analyzed with the VLBI software VieVS individually and combined. Comparing clock rates, we could assess if co-located instruments shared the clock at the CONT14 sites. For the combination, the common site parameters (ZWD, troposphere gradients, and clock rates) were constrained between the two techniques. Furthermore, the local ties of the reference points at the co-located site were selectively introduced. The combination solutions improve the mean station position repeatability in comparison with the single technique solutions. The analysis strategy of common parameter constraints and local ties can also be applied to co-located VLBI observations with

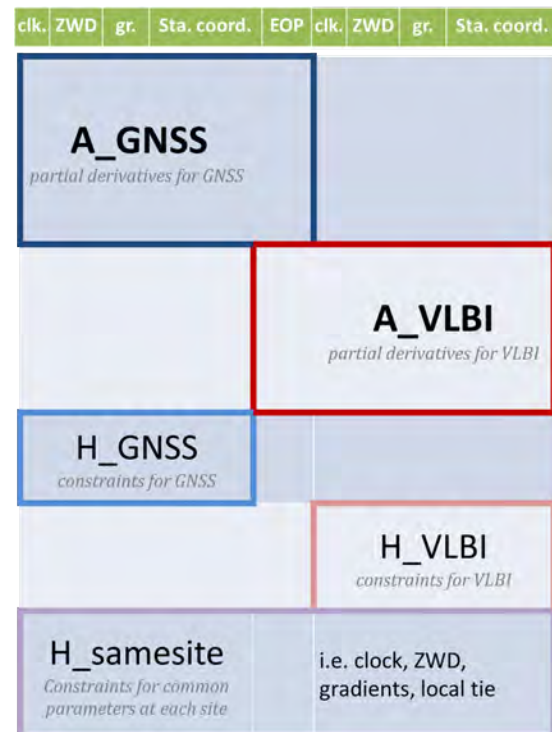


Fig. 3 Construction of the design matrix which consists of partial derivatives (**A_GNSS** and **A_VLBI**) of GNSS and VLBI with respect to clock (column clk.), zenith wet delays (column ZWD), troposphere gradients (column gr.), station coordinates (column Sta. coord.), and Earth orientation parameters (column EOP) and constraints (**H_GNSS** and **H_VLBI**) for them. The partial derivatives with respect to EOP for GNSS have not been implemented yet. The constraints (**H_samesite**) for common parameters and fictitious observations for local ties can be additionally attached for co-located sites.

twin/sibling telescopes in the future. As we see from the GNSS results, the GNSS geometric model (near-field model) in VieVS still needs to be improved. Furthermore, the partial derivatives with respect to EOP

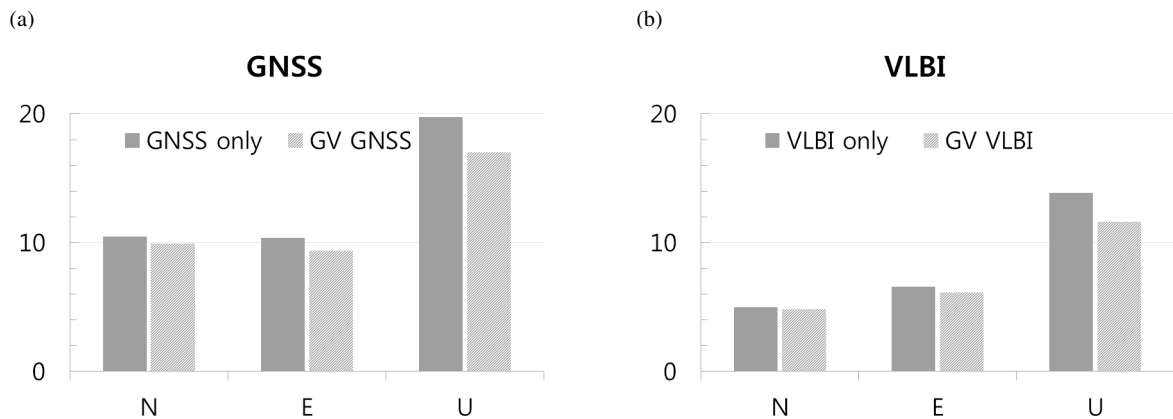


Fig. 4 Mean station position repeatabilities of single solutions (solid box) and combination solutions (box with a pattern of diagonal lines) for north, east, and up components. Plot (a) shows the results of GNSS stations and plot (b) the results of VLBI stations. The unit is mm.

for GNSS need to be implemented in VieVS and then one can estimate EOPs and expect better GNSS single solutions and combination results.

Acknowledgements

This work has been supported by the Austrian Science Fund (FWF, project No.: M1592-N29 and J3699-N29).

References

1. Y. Kwak, J. Böhm, T. Hobiger, L. Plank and K. Teke, "Observation Level Combination of GNSS and VLBI with VieVS: a Simulation Based on CONT11", AGU Fall Meeting 2015, San Francisco, USA; 2015-12-14 – 2015-12-18, 2015.
2. J. Böhm, S. Böhm, T. Nilsson, A. Pany, L. Plank, H. Spicakova, K. Teke, H. Schuh, "The New Vienna VLBI Software VieVS", In S. Kenyon, M. C. Pacino, U. Marti, editors, Geodesy for Planet Earth, International Association of Geodesy Symposia, vol 136, Springer Berlin Heidelberg, doi:10.1007/978-3-642-20338-1-126, pages 1007–1011, 2012.
3. S. Klioner, "General relativistic model of VLBI observables", In W. E. Carter, editors, Proceedings of the AGU Chapman Conference on Geodetic VLBI: Monitoring Global Change, NOAA Technical Report NOS 137 NGS 49, pages 188–202, 1991.
4. L. Plank, J. Böhm, H. Schuh, "Precise station positions from VLBI observations to satellites: a simulation study", *Journal of Geodesy*, 88, doi:10.1007/s00190-014-0712-1, pages 659–673, 2014.
5. Y. Kwak, J. Böhm, T. Hobiger and L. Plank, "The Processing of Single Differenced GNSS Data with VLBI Software", In Proceedings of IAG Commission 1 Symposium 2014, Springer Berlin Heidelberg, Berlin, Heidelberg, pages 1–8, 2015.
6. T. Hobiger and T. Otsubo, "Combination of GPS and VLBI on the observation level during CONT11 - common parameters, ties and inter-technique biases", *Journal of Geodesy*, 88(11), doi:10.1007/s00190-014-0740-x, pages 1017–1028, 2014.
7. K. Teke, J. Böhm, T. Nilsson, H. Schuh, P. Steigenberger, R. Dach, R. Heinkelmann, P. Willis, R. Haas, S. Garcia Espada, T. Hobiger, R. Ichikawa, and S. Shimizu, "Multi-technique comparison of troposphere zenith delays and gradients during CONT08", *Journal of Geodesy*, 85(7), doi:10.1007/s00190-010-0434-y, pages 395–413, 2011.
8. Z. Altamimi, P. Rebischung, L. Metivier and X. Collilieux, "ITRF2014: Main Results", AGU Fall Meeting 2015, San Francisco, USA; 2015-12-14 – 2015-12-18, 2015.
9. G. Petit and B. Luzum, "IERS Conventions (2010)", IERS Technical Note 36, Verlag des Bundesamtes für Kartographie und Geodäsie, 2010.
10. F. Lyard, F. Lefevre, T. Letellier, and O. Francis, "Modelling the global ocean tides: modern insights from FES2004" *Ocean Dynamics*, 56(5-6), doi:10.1007/s10236-006-0086-x, pages 394–415, 2006.
11. J. Böhm, R. Heinkelmann, and H. Schuh, "Short Note: A global model of pressure and temperature for geodetic applications", *Journal of Geodesy*, 81(10), doi:10.1007/s00190-007-0135-3, 679–683, 2007.
12. J. Böhm, B. Werl, and H. Schuh, "Troposphere mapping functions for GPS and very long baseline interferometry from European Centre for Medium-Range Weather Forecasts operational analysis data", *Journal of Geophysical Research*, 111(B2), doi:10.1029/2005JB003629, 2006.

Aspects of ICRF-3

Chopo Ma¹, Daniel MacMillan², Karine Le Bail², David Gordon²

Abstract The Second Realization of the International Celestial Reference Frame (ICRF2) used dual-frequency VLBI data acquired for geodetic and astrometric purposes from 1979–2009 by organizations coordinated by the IVS and various precursor networks. Since 2009 the data set has been significantly broadened, especially by observations in the southern hemisphere. While the new southern data have ameliorated the north/south imbalance of observations, they appear to produce a systematic zonal declination change in the catalog positions. Over the 35 years of the ICRF data set the effect of galactic aberration may be significant. Geophysical and tropospheric models also may affect the source positions. All these effects need to be addressed in preparation for ICRF-3.

Keywords ICRF, observing program, declination, troposphere, galactic aberration

1 Data Distribution

ICRF2 was dominated by data from northern hemisphere stations. Figure 1 shows the evolution of the distribution of observations between northern and southern hemisphere stations from 1980 to 2015. As more southern hemisphere stations were added, the distribution has evolved from mainly northern to ~35% southern. Figure 2 shows the evolution of the observation distribution between northern hemisphere, south-

ern hemisphere, and mixed baselines. The distribution has evolved from mainly northern to ~20% mixed and ~20% southern.

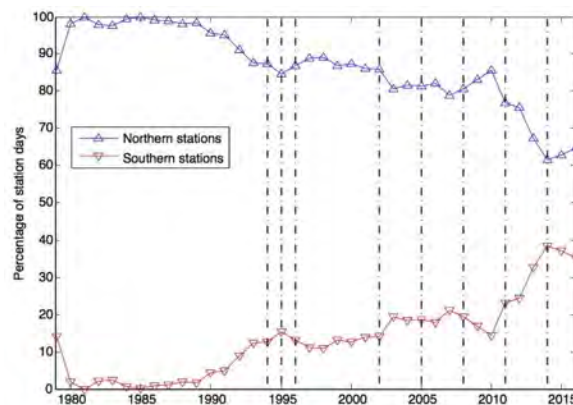


Fig. 1 Site observation distribution from 1980 to 2015 between northern sites (blue triangles) and southern hemisphere sites (red inverted triangles) as percentage of station days.

Figure 3 shows the growth of observations from 1980 to 2015. When ICRF2 was implemented in 2009, there were ~6.7 million observations from 4,726 sessions. Currently (as of 2016), there are ~10.7 million observations from 5,889 sessions. Southern hemisphere only and N-S baselines have increased noticeably in recent years but still represent only ~15% of the total.

Figure 4 shows the distribution of sources by number of sessions in the current (February 2016) solution. The largest group of sources (mostly VCS) has been observed in only two sessions. This however is a significant improvement over ICRF2, where ~2/3 of the sources (also mostly VCS) were observed only once.

1. NASA GSFC
2. NVI Inc./NASA GSFC

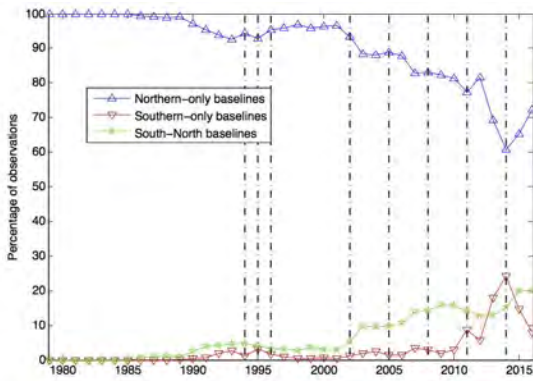


Fig. 2 Baseline observation distribution from 1980 to 2015 between baselines with only northern hemisphere stations (blue triangles), only southern hemisphere stations (red inverted triangles), and both northern and southern stations (green stars).

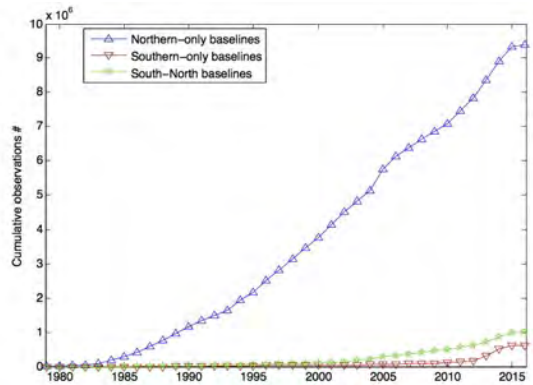


Fig. 3 Cumulative observations from 1980 to 2015. Currently there are ~ 9.16 million observations from purely northern hemisphere baselines (blue triangles), ~ 0.61 million from purely southern hemisphere baselines (red inverted triangles), and ~ 0.98 million from mixed baselines (green stars).

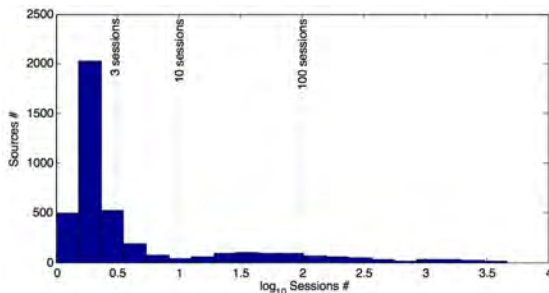


Fig. 4 Number of sources observed by session count in the current solution. Each histogram category shows the number of sources that were observed in a given number of sessions.

Recently it was found that 500 ICRF2 sources had not been reobserved since ICRF2. These sources are

predominantly weaker non-VCS sources, with 310 in the north and 190 in the south. An effort is underway to reobserve them; 65 have now been reobserved from a set of 100 sources added to the source monitoring program in October 2015. More of these sources will soon be added to the monitoring list.

2 Precision Improvement Since ICRF2

Figures 5a and b show the precision of the current (February 2016) solution, in μs . The distribution is much narrower than in ICRF2, with most sources better than $150 \mu\text{s}$ in right ascension (RA) and $250 \mu\text{s}$ in declination (DEC).

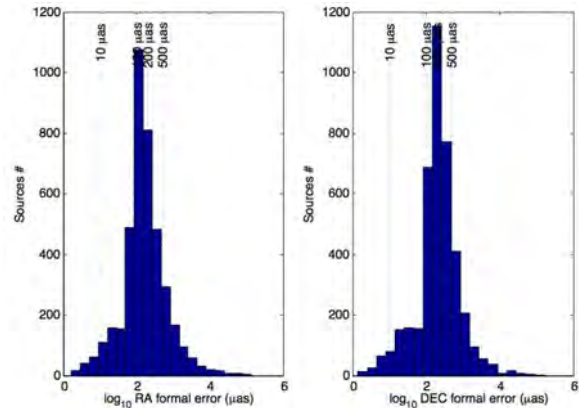


Fig. 5 Precision of sources in the current (February 2016) solution, in μs . Histograms show how many sources were observed at a given precision in right ascension (a) and declination (b).

Efforts have been made to improve the observations of the defining sources since ICRF2. Figures 6a and b compare the precision of the ICRF2 defining sources from the ICRF2 solution with the current solution. In ICRF2, 53 defining sources were observed in 18 or fewer sessions. By the end of 2015, all have been observed in at least 19 sessions due to the IVS VLBI source monitoring program.

Decimation tests were made to estimate the improvement of position uncertainties for non-VCS sources since ICRF2. Sessions were divided chronologically into two groups (even and odd sessions) and solutions were performed for each group for the ICRF2 data set and the current data set. The variance of the differences in source position estimates from the

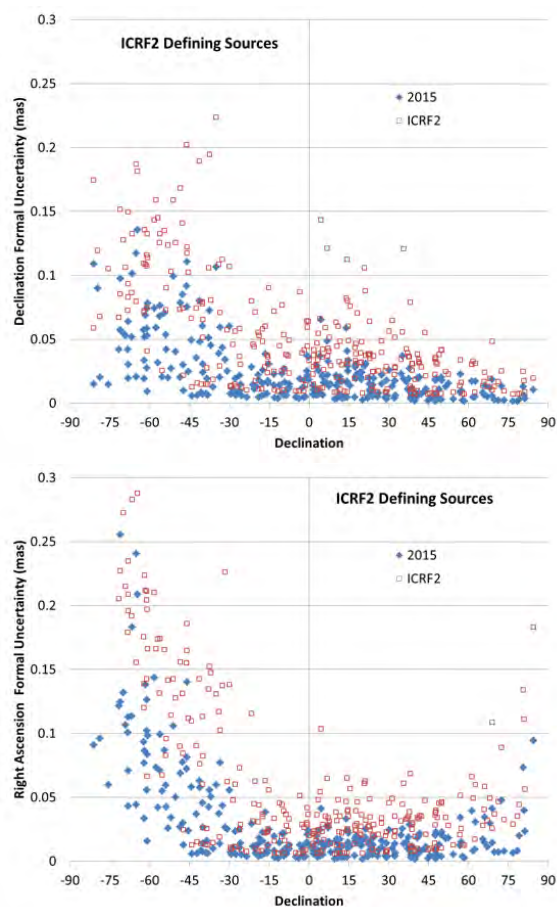


Fig. 6 Observations of ICRF2 defining sources in ICRF2 (open red squares) and after 2015 (filled blue diamonds). a) Declination formal uncertainty (mas) vs. declination. b) Right ascension formal uncertainty (mas) vs. declination.

two solutions gives an estimate of the average source position noise (uncertainty). For the ICRF2 data set we get RA and DEC. WRMS's of 52 and 62 μas for 794 sources. For the current dataset, it decreases to 32 and 43 μas for 883 sources.

Table 1 Average and median improvement in the precision of ICRF2–*Gaia* transfer sources. From Le Bail et al., 2016 [1].

Group	#	RA (mas)		DEC (mas)	
		2011b	2015a	2011b	2015a
1	89	0.017/0.011	0.011/0.007	0.017/0.013	0.011/0.008
2	66	0.032/0.020	0.022/0.015	0.032/0.027	0.021/0.018
3	16	0.052/0.053	0.033/0.033	0.080/0.064	0.037/0.033
4	24	0.869/0.251	0.128/0.066	1.903/0.345	0.163/0.092

Efforts have been made to improve the uncertainties of a set of 195 optically bright sources for use in aligning *Gaia* with ICRF-3. Table 1 shows the average and median precision improvement of these ICRF2–*Gaia* transfer sources since the start of this effort (RA uncertainties are not corrected for cosine DEC).

3 Systematic Effects

3.1 Zonal Declination

Figure 7 compares the positions of the defining sources from a recent solution with their ICRF2 positions. Each plot subtracts the ICRF2 positions from the current solution values for declination (a) and right ascension (b). The comparison reveals a zonal systematic in declination estimates with a peak of ~ 0.1 mas at $20\text{--}30^\circ\text{S}$. This systematic is apparently caused by data from the four AUST stations that started observing in 2010. Figure 8 shows the resulting differences after excluding all data from the AUST network sessions as well as all AUST observations in other networks. The systematic is removed. Additional solutions have shown that removing either KATH12M or HOBART12 removes a significant part, but not all, of the zonal systematic. It is not clear from these tests whether there is a systematic error in ICRF2, a systematic instrumental effect from the AUST antennas, or a systematic effect due to the geometry of the AUST observing network.

3.2 Troposphere Delay Modeling

Figures 9a and b show the results of changing the elevation cutoff in (a) a 1980–2014 solution, and (b) the ICRF2 solution. Each solution was run with both a 15° cutoff and a 5° cutoff. The differences between the resulting declination estimates are plotted. The difference between the estimated parameters from the solutions is a measure of the troposphere model error, since the troposphere error at 15° is very small and it increases strongly as elevation decreases to 5° . The test shows that there is no clear systematic difference between the two cutoffs.

Three other tests were run. First, gradient constraints were weakened by a factor of 100. Next

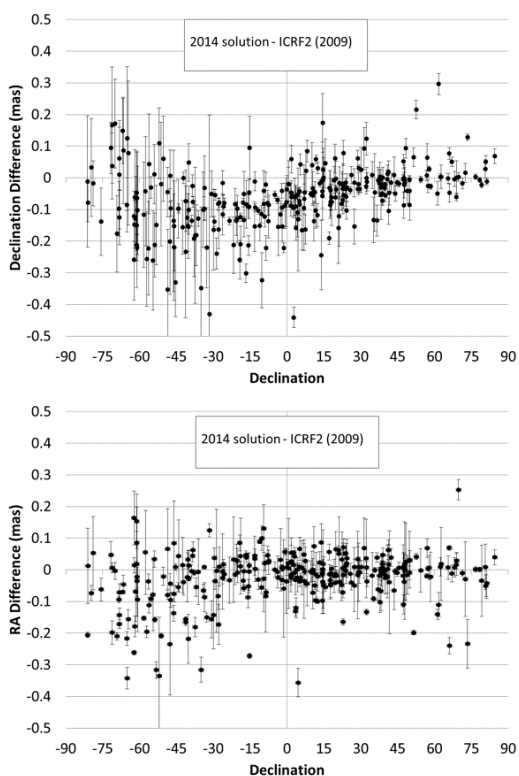


Fig. 7 Current CRF solution vs. ICRF2 solution: current values minus ICRF2 values. a) Declination differences and b) right ascension differences.

the results of elevation-dependent weighting were compared to results from using an elevation cutoff. Finally, a solution was run with ITRF2014 modeling of earthquakes instead of session-by-session estimation of post-seismic displacements. None of these tests produced a significant change in the systematic zonal declination effect.

3.3 Aberration

Figure 10a plots the proper motion due to the component of the galactic acceleration vector towards the Galactic center. MacMillan [2] estimated this component in a VLBI solution to be $5.3 \pm 0.3 \mu\text{as}/\text{year}$. For comparison, one can compute this acceleration from the radial distance to the Galactic center and the circular rotation speed of the solar system around the Galactic center, which can be determined from parallax mea-

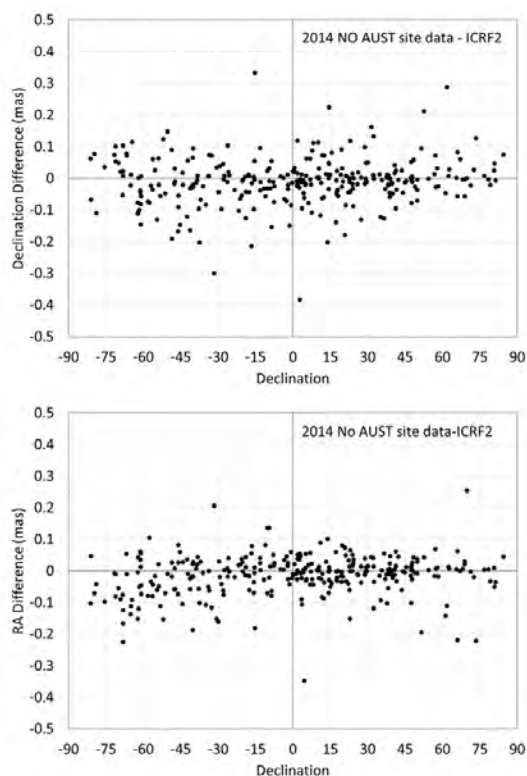


Fig. 8 Effect of removing the AUST stations from the current solution: current values (without AUST) minus ICRF2 values. a) Declination differences and b) right ascension differences.

surements. Using the values from Reid et al. [3] leads to an aberration vector magnitude of $4.9 \pm 0.4 \mu\text{as}/\text{year}$.

For contrast, Figure 10b plots the raw proper motion field computed from a source position time series for sources with right ascension and declination proper motion uncertainties less than $50 \mu\text{as}$ per year. The plot shows that the aberration effect is much smaller than the random apparent motions, which are likely due to source structure.

4 Conclusions

The cumulative number of observations when ICRF2 was generated in 2009 was 6.7 million. This number has increased to 10.7 million observations in the present solution. The strongest 100 sources from the 500 sources not reobserved since ICRF2 are now being reobserved. At least 65 have been observed since Oc-

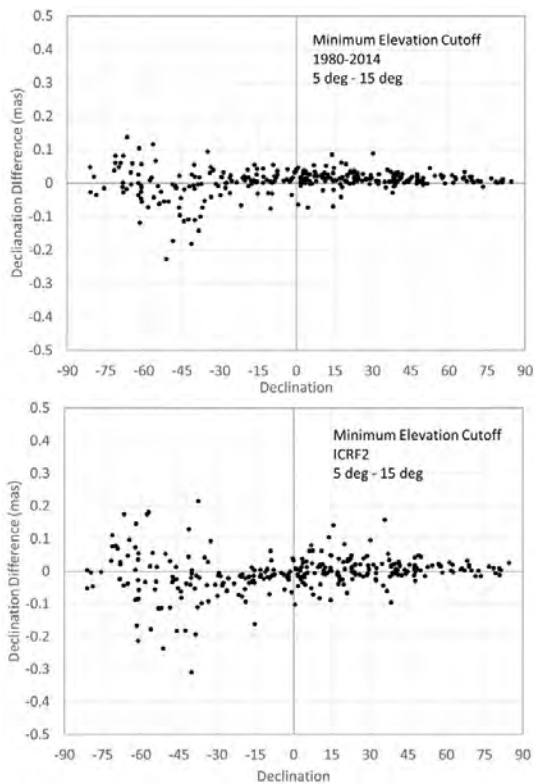


Fig. 9 Declination estimates from a solution with a 5° minimum elevation cutoff minus declination estimates from a solution with a 15° cutoff. a) 2014 solution and b) the ICRF2 solution.

tober 2015. The average source position uncertainty of the non-VCS sources has improved since ICRF2. The most recent solution has decreased the average right ascension uncertainty from $52 \mu\text{s}$ to $32 \mu\text{s}$ and the average declination uncertainty from $62 \mu\text{s}$ to $43 \mu\text{s}$. The ICRF2–*Gaia* transfer source precision has also improved significantly since 2011. The precision for 295 ICRF2 defining sources has improved for all declinations. Comparing declinations from a current CRF solution to declinations from the ICRF2 solution reveals a systematic zonal dependence, with a maximum of ~ 0.1 mas at $20\text{--}30^\circ\text{S}$. Tests of troposphere modeling do not appear to explain this. But removing data from four AUST stations removes the systematic. It is unclear whether there is a systematic error in ICRF2 or a systematic instrumental effect due to the AUST antennas or a systematic effect due to the geometry of AUST observing.

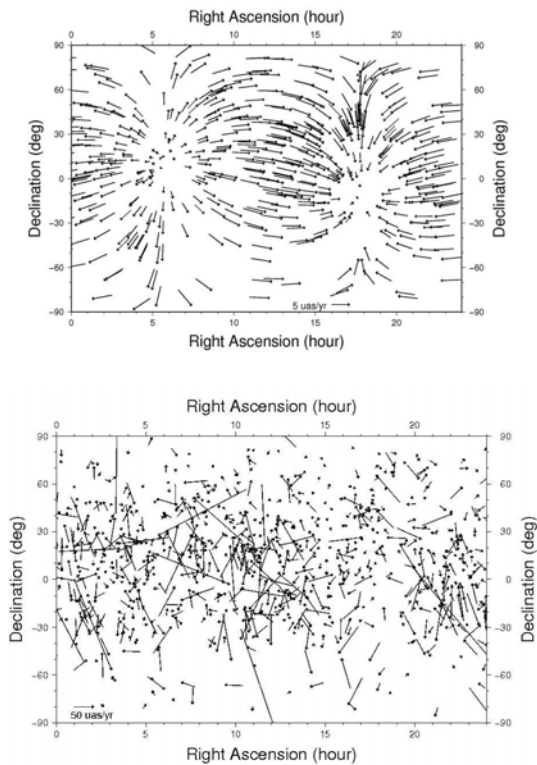


Fig. 10 a) Proper motion due to the component of acceleration vector towards the Galactic center. b) Raw proper motion field for sources with uncertainties better than $50 \mu\text{m}/\text{year}$.

References

1. K. Le Bail, J. M. Gipson, D. Gordon, D. S. MacMillan, D. Behrend, C. C. Thomas, S. Bolotin, W. E. Himwich, K. D. Baver, B. E. Corey, M. Titus, G. Bourda, P. Charlot, and A. Collioud, “IVS Observation of ICRF2–*Gaia* Transfer Sources”, In *The Astronomical Journal*, 151:79, 2016, doi:10.3847/004-6256/151/3/79.
2. D. S. MacMillan, “Determination of Galactic Aberration from VLBI Measurements and Its Effect on VLBI Reference Frames and Earth Orientation Parameters”, American Geophysical Union Meeting, Fall 2014.
3. M. J. Reid, K. M. Menten, A. Brunthaler, X. W. Zheng, T. M. Dame, Y. Xu, Y. Wu, B. Zhang, A. Sanna, M. Sato, K. Hachisuka, Y. K. Choi, K. Immer, L. Moscadelli, K. L. J. Rygl, and A. Bartkiewicz, “Trigonometric Parallaxes of High Mass Star Forming Regions: The Structure and Kinematics of the Milky Way”, *Astrophysical Journal*, vol. 783, Num. 2, p. 130, 2014.

Vienna Contribution to the ICRF3

First results

David Mayer, Hana Krásná, Johannes Böhm

Abstract The current realization of the ICRS, the ICRF2, was published in 2009. New stations were implemented, and the amount of data from the southern hemisphere increased dramatically. The demands on the accuracy of the celestial reference frame are higher than ever, with the GAIA mission providing a catalog in the visible spectrum with comparable accuracy. These advances in VLBI and new demands on accuracy entail the necessity of a new version of the celestial reference frame which will be called ICRF3. We will report on the progress and plans of the Vienna group to estimate such a reference frame. Differences in our solution (especially in declination) compared to other groups are discussed. Furthermore, we examine issues which arise during the estimation process such as a declination bias (a maximal offset of about 150 μ as in declination).

Keywords ICRF, VLBI

1 Introduction

The latest release, the International Celestial Reference Frame 2 (ICRF2) (Fey *et al.*, 2015), is the official realization of the International Celestial Reference System (ICRS). It was created in 2009 and utilizes Very Long Baseline Interferometry (VLBI) data from 1979 to 2009. Since the creation of the ICRF2, the number of S/X-band group delays almost doubled from about 6.5 million to about 10 million. This massive increase

Technische Universität Wien, Austria

in data points is due to advances in the VLBI technique and an ever growing network of participating stations.

In the near future the recently launched Global Astrometric Interferometer for Astrophysics (GAIA) satellite will provide first results. GAIA will map objects in the sky in the visible part of the electromagnetic spectrum and will do that with an accuracy comparable to VLBI, see Bourda *et al.* (2012) for more information. Hence, the reference frame provided by VLBI can be compared with the frame provided by GAIA. This comparison will shed light on the inherent systematic effects of the techniques and will provide insight into astrophysical phenomena such as the core shift. Consequently, the need for a reference frame in the radio domain with the best possible accuracy is high.

Because the demands on the reference frame provided by VLBI and the large amount of new data are steadily increasing, the community decided to work on a new release which will incorporate the new data and state-of-the-art analysis techniques.

1.1 Motivation

The motivation of this work is to create a comparable Celestial Reference Frame (CRF) with data analyzed by the Vienna group using the software Vienna VLBI Software (VieVS) (Böhm *et al.*, 2012). On the one hand, it is important to compare independent (in terms of analysis strategy and software) solutions in order to find bugs in the individual solutions and, on the other hand, having more people analyze the same data leaves less room for error and should yield better results. Furthermore, it is good to have as many different solutions as possible, if the ICRF3 working group

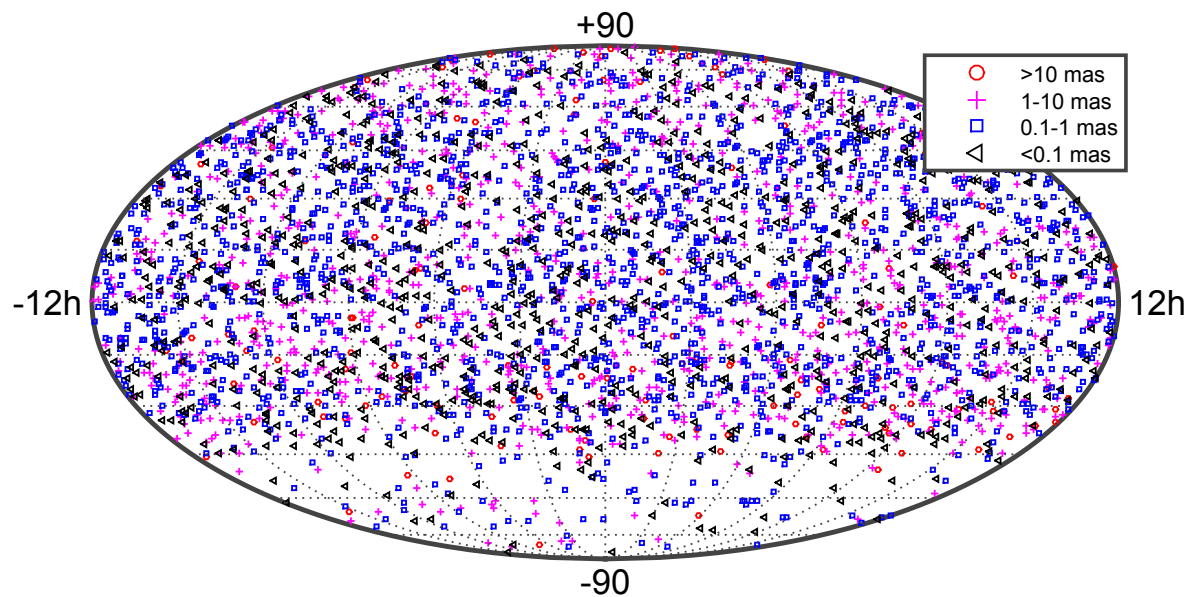


Fig. 1 Map of all source estimates of the Vienna CRF solution w. r. t. the ICRF2. The individual estimates are grouped according to their size and depicted with different markers.

of the International Astronomical Union (IAU) decides to stack more than one solution in a similar approach to the terrestrial reference frame estimation (different Analysis Centers submitting normal equation systems which are then stacked), see Bachmann *et al.* (2016) for more details.

2 Methodology

In order to estimate a CRF from VLBI data a couple of process steps have to be applied.

First, the data have to be selected. In this solution, we used data which were corrected for the ionospheric delay and for which the ambiguities were resolved. The data are provided by the International VLBI Service (IVS) in the form of NGS cards. Not all sessions are suitable for CRF estimation. Therefore, a selection of adequate sessions has to be carried out (see Section 2.2 for details on the selection of sessions). In a second step the whole history of VLBI data has to be analyzed session-wise (see Section 2.1 for details on the selected parameters). From this analysis, normal equation matrices are saved for each session. The final step is to stack all the normal equation systems into one global

system and estimate a global CRF (see Section 2.1 for details on the selection of global parameters).

In order to validate the resulting CRF it has to be compared to solutions from other groups. A well-tested way to realize that is by estimating transformation parameters between different CRFs. Such a comparison can be found in Section 4.1.

2.1 Parameter Selection

A standard single session analysis with state-of-the-art geodetic parameterization incorporating the IERS 2010 conventions (Petit & Luzum, 2010) was conducted. Additionally, atmospheric loading was applied. Parameters, such as zenith wet delays (piecewise linear offsets every 20 minutes with a relative constraint of 1 cm), gradients (piecewise linear offsets every six hours with a relative constraint of 0.05 cm), clock parameters (piecewise linear offsets every one hour with a relative constraint of 1.3 cm, one rate, and one quadratic term), Earth Orientation Parameters (one offset per session) and station and source coordinates (one offset per session) were estimated, and normal equation matrices were created.

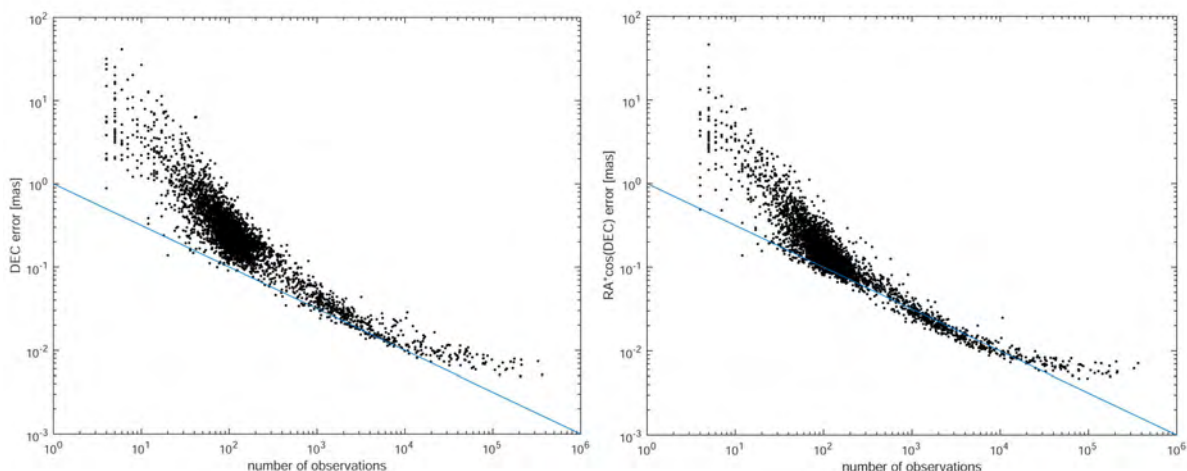


Fig. 2 Formal errors (DEC on the left and RA on the right) of the sources from the Vienna CRF solution plotted over their number of observations.

Following the single session analysis the normal equation matrices must be rearranged and stacked. Certain parameters must be reduced, which means that they are estimated session wise. In our solution those parameters are EOP, special handling sources (unstable sources), stations which only observe in a few sessions, and auxiliary parameters (clock and troposphere). In order to get an invertible equation system sources with fewer than three observations have to be fixed to their a priori values. Global parameters, such as station positions, velocities, and source positions are then estimated with a No-Net-Rotation (NNR)/No-Net-Translation (NNT) (on datum stations) and NNR (on defining sources) approach, respectively.

2.2 Session Selection

Not all VLBI sessions are created equal. Therefore, it makes sense to only select sessions which are suitable for the task. We decided to base our session selection on a few criteria. First, we only wanted sessions where the chi-square is above 3 (no reweighting was applied), which means that the measurements fit well to our models and a priori values. Secondly, we discarded sessions which have a low (in our case 200) number of observations. Lastly, we removed some sessions by hand. After this process we ended up with 4,776 VLBI sessions. Additionally, the 24 VCS-I and the eight VCS-II sessions were added.

3 Results

In this section we will present the results of our current Vienna solution.

Figure 1 depicts the estimates of the Vienna solution w.r.t. the ICRF2. Most (46.2%) of the estimates are between 0.1 and 1 mas, 26.4% are between 1 and 10 mas, 23.5% are smaller than 0.1 mas, and 3.9% are larger than 10 mas.

In Figure 2, the formal errors of RA and DEC over the number of observations are illustrated. One can see that in principle the formal errors get better with a larger number of observations (the ideal case would be the $1/\sqrt{N}$ rule, where N is the number of observations, which is depicted as a line though the plot). The exceptions from the rule are sources which are observed the most. After approximately 10^4 observations, the formal error does not seem to get smaller with more observations.

4 Discussion

4.1 Comparison with Other Catalogs

In order to validate the Vienna solution with other state-of-the-art CRF solutions, a comparison was conducted. The methodology is similar to the catalog comparison found in Lambert, S. (2014). In general the

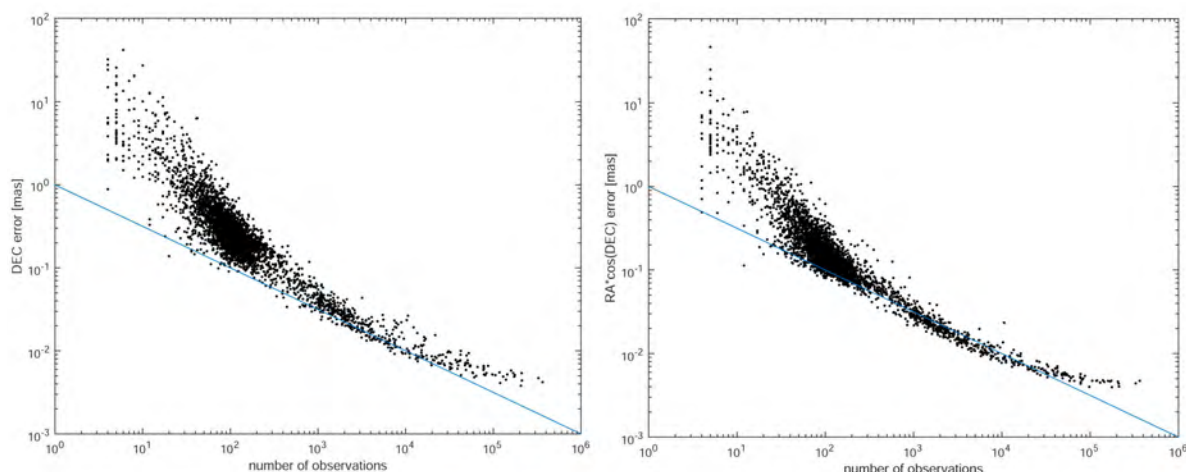


Fig. 3 Formal errors (DEC on the left and RA on the right) of the sources from the Vienna CRF solution with fixed EOP for regional sessions plotted over their number of observations.

295 defining sources were used to calculate rotations in three directions (A_1 , A_2 , and A_3), slopes in right ascension (RA) and declination (DEC) over DEC (D_α and D_δ), and a bias in DEC (B_δ) between the Vienna solution and a recent solution provided by USNO (Fey, personal communication) and GSFC¹. The resulting parameters are listed in Table 1.

Table 1 Catalog comparison between the Vienna solution and recent solutions from GSFC and USNO.

	A_1 [μ as]	A_2 [μ as]	A_3 [μ as]	D_α [μ as/rad]	D_δ [μ as/rad]	B_δ [μ as]
VIE vs GSFC	-4 ± 5	-36 ± 4	21 ± 6	-6 ± 8	-45 ± 8	41 ± 6
VIE vs USNO	-6 ± 5	-10 ± 4	13 ± 6	-18 ± 8	-40 ± 8	46 ± 6

The Vienna CRF does differ from solutions provided by other groups. In particular, the Vienna solution has a rather large slope in DEC over DEC and a large bias in DEC compared with the other solutions (see Table 1 for details). We are still not sure where this difference originates from. One explanation would be the session selection. In our solution a larger number of sessions was excluded which in turn resulted in a significant reduction in observations for some of the rarely observed defining sources. We did not weight the defining sources before doing the comparison, which means

¹ http://gemini.gsfc.nasa.gov/solutions/2015a_astro/2015b_astro.html

that uncertainties in these rarely observed source coordinates propagate directly into the transformation. We will fix this in the near future and do the comparison again.

4.2 Formal Errors of Vienna Solution

Another effect which is present in the Vienna CRF is that our formal errors are too large compared to other solutions. In principle, this deviation could be due to the fact that our individual solutions are not reweighted in the single session analysis, but further investigation is necessary.

Malkin (2009) showed that EOP quality is dependent on the size of the network. We decided to create a solution where we fix the EOP for regional (such as the AUSTRALS) sessions and found that it has a significant impact on the formal errors of sources, see Figure 3. One can see that, compared to Figure 2, the formal errors of frequently observed sources (right side of the plot) are significantly reduced. More investigation concerning this effect will be done in the future.

4.3 Declination Bias

Figure 4 depicts the difference in DEC of the Vienna solution w. r. t. the ICRF2 over DEC. This bias, from

here forth called declination bias, was so far only found to be present in current CRF solutions based on the software Calc/Solve. Because the declination bias can also be seen in the Vienna solution, which uses VieVS, we can conclude that the effect is real and most likely not software dependent. We did several tests in order to find the origin of the declination bias and arrived at very similar conclusions (the bias is due to the new Australian telescopes etc.) to what was presented (Ma, personal communication) by the GSFC group.

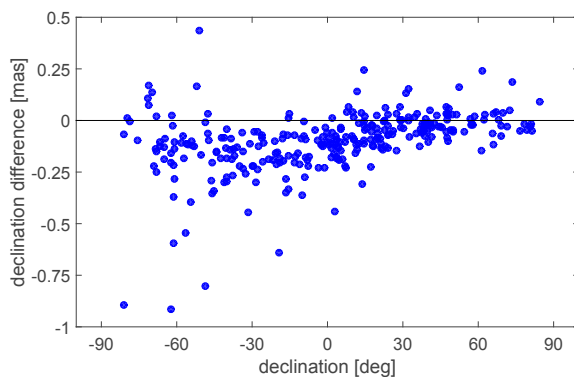


Fig. 4 Declination bias as seen between the Vienna solution and ICRF2.

4.4 Outlook

In the future we will focus our research on the declination bias. Furthermore, we will test the influence of new troposphere analysis strategies, such as a more refined gradient model and ray-traced delays, on the CRF.

Acknowledgements

This work was supported by the Austrian Science Fund (FWF, project I2204).

References

- BACHMANN, S., THALLER, D., ROGGENBUCK, O., LÖSLER, M. AND MESSERSCHMITT, L. (2016). Ivs contribution to itr2014. *Journal of Geodesy*, 1–24.
- BÖHM, J., BÖHM, S., NILSSON, T., PANY, A., PLANK, L., SPICAKOVA, H., TEKE, K. AND SCHUH, H. (2012). The new Vienna VLBI Software VieVS. In *Proceedings of the 2009 IAG Symposium, Buenos Aires, Argentina*, Vol. 136, 1007–1011, International Association of Geodesy Symposia, 31 August – 4 September 2009.
- BOURDA, G., COLLIOD, A., CHARLOT, P., PORCAS, R. AND GARRINGTON, S. (2012). Towards an accurate alignment of the vlbi frame and the future gaia optical frame: Global vlbi imaging observations of a sample of candidate sources for this alignment. In D. Behrend and K. Baver, eds., *IVS 2012 General Meeting Proceedings*, 334–338, NASA/CP-2012-217504.
- FEY, A.L., GORDON, D., JACOBS, C.S., MA, C., GAUME, R.A., ARIAS, E.F., BIANCO, G., BOBOLTZ, D.A., BÖCKMANN, S., BOLOTIN, S., CHARLOT, P., COLLIOD, A., ENGELHARDT, G., GIPSON, J., GONTIER, A.M., HEINKELMANN, R., KURDUBOV, S., LAMBERT, S., LYTVYN, S., MACMILLAN, D.S., MALKIN, Z., NOTHNAGEL, A., OJHA, R., SKURIKHINA, E., SOKOLOVA, J., SOUCHAY, J., SOVERS, O.J., TESMER, V., TITOV, O., WANG, G. AND ZHAROV, V. (2015). The second realization of the international celestial reference frame by very long baseline interferometry. *The Astronomical Journal*, 150, 58.
- LAMBERT, S. (2014). Comparison of vlbi radio source catalogs. *Astronomy & Astrophysics*, 570, A108.
- MALKIN, Z. (2009). On comparison of the Earth orientation parameters obtained from different VLBI networks and observing programs. *Journal of Geodesy*, 83, 547–556.
- PETIT, G. AND LUZUM, B., eds. (2010). IERS Conventions 2010. Frankfurt am Main: Verlag des Bundesamts für Kartographie und Geodäsie, IERS Technical Note No. 36.

Status of the X/S Source Catalog

David Gordon, Karine Le Bail

Abstract We summarize the current status of the X/S source catalog as preparations are being made for ICRF3 in 2018. The current X/S catalog has $\sim 20\%$ more sources than ICRF2 and has considerably better and more homogeneous precision. Additional observations since 2009, including a second epoch VCS campaign, have resulted in precision improvements of ~ 1.7 times for the ICRF2 non-VCS sources and ~ 7 times for the ICRF2 VCS-only sources. But similar to ICRF2, the X/S catalog today is still relatively sparse and noisy in the south. Efforts are underway to provide a set of high precision, optically bright sources for alignment of the *Gaia* optical frame with ICRF3 in the coming years.

Keywords X/S catalog, ICRF2, ICRF3

1 Introduction

The second realization of the International Celestial Reference Frame (ICRF2) [1, 2] contained positions for 3,414 sources, obtained from X and S band dual-frequency geodetic and astrometric VLBI sessions. The sources in ICRF2 were divided into two groups because approximately $2/3$ of them came exclusively from the six Very Long Baseline Array (VLBA) Calibrator Survey (VCS) campaigns [3, 4, 5, 6, 7, 8], had mostly been observed in only one VLBI session, and had average formal errors approximately five times larger than the other one-third. Of the 3,414 sources,

NVI, Inc.

1,217 were classified as regular or ‘non-VCS’ sources, and 2,197 were classified as ‘VCS-only’ sources.

ICRF2 was a tremendous improvement over ICRF1. It used four times as much data (1.6 million vs. 6.5 million observations), contained 5.6 times as many sources (608 vs. 3,414), had a sixfold improvement in the noise floor (250 vs. 40 μ arc-sec), and had twice better axis stability (20 vs. 10 μ arc-sec). As we approach ICRF3 in 2018, we must realize that such huge gains are no longer possible. But ICRF3 will be significantly better in other ways.

2 X/S Progress Since ICRF2

Since mid-2009, RDV VLBA sessions have been used to reduce the position uncertainties of ~ 400 of the noisiest ICRF2 sources and to detect many new sources. Additional new sources have also been added in other IVS sessions, mostly in the southern hemisphere. Overall, as of March 2016, some 384 new sources have been added through the regular RDV and other IVS sessions since ICRF2.

In 2012, an IAU working group was formed to generate a third realization of the International Celestial Reference Frame by 2018. One of the goals for ICRF3 is to provide the highest accuracy reference frame possible for alignment of the *Gaia* optical reference frame with the radio reference frame. But in 2012, about two-thirds of the X/S sources were still single-epoch sources with much larger average position errors than the other $1/3$. For the future alignment between the radio reference frame (ICRF3) and the optical (*Gaia*) reference frame, a more uniform precision in ICRF3 would be needed. Therefore, re-observing the single-

epoch sources to improve their position errors became a high priority for ICRF3. In response, a small group was formed to request VLBA observing time to re-observe these sources in a second epoch VLBA Calibrator Survey Campaign (VCS-II).

The VCS-II campaign consisted of eight 24-hour VLBA sessions, run between January 2014 and March 2015. The recording rate was 2 Gbit/s, with 1.5 Gbit/s at X-band and 0.5 Gbit/s at S-band. By contrast, the original VCS1-6 sessions used only 128 Mbit/s for most of the sessions. Thus the VCS-II sessions were some 3–5 times more sensitive than the original VCS1-6 sessions. The VCS-II sessions observed 2,400 target sources, plus 182 ICRF2 defining sources for atmosphere calibration and alignment with ICRF2. Of these, 2,062 single-epoch sources were successfully re-observed, and their average inflated errors were reduced by a factor of 4.8. Also, 324 new sources were detected, all being sources that had been observed but not detected in the original VCS1-6 sessions. Only 14 sources were not detected. Results are reported in [9].

At the time of ICRF2, the two classes of sources had average inflated errors of .55/.81 milli-arc-second (mas) (non-VCS) and 2.11/3.56 mas (VCS-only) in RA/Dec. With all the new observations since ICRF2, the average inflated errors for the two groups are now .33/.45 mas (non-VCS) and .29/.50 mas (VCS-only). Being nearly the same, there is no longer any need for a two-class distinction between them. However, the new sources added since ICRF2 do have considerably larger average inflated errors, and so some distinction may still be necessary. There are currently 515 single-epoch sources in the X/S catalog, so a second class of sources would be a much smaller fraction in ICRF3 (less than 15%), compared to the large fraction ($\sim 2/3$) in ICRF2. These new sources are generally very weak but there is hope of re-observing many of them before ICRF3.

3 The Current X/S Catalog

As of March 2016, there are 4,121 sources in the X/S catalog at GSFC, or $\sim 20\%$ more than in ICRF2. Of these, 1,991 (48%) are the ‘regular’ or ‘non-VCS’ sources, i.e., sources that were **not** observed **only** in the VCS1-6 and/or VCS-II campaigns. The rest, 2,130 (52%), are ‘VCS-only’ sources, i.e., they were observed **only** in the VCS1-6 and/or VCS-II cam-

paigns. Average inflated errors are actually smaller for the current VCS-only group compared to the current non-VCS group: 0.44/0.76 mas vs. 1.23/1.67 mas. However, the non-VCS group has a few single epoch sources that are very noisy and which skew the averages. Median inflated errors are similar for the two groups: 0.20/0.34 mas (current VCS-only) vs. 0.16/0.26 mas (current non-VCS).

Also, of the current ‘non-VCS’ sources, 784 were actually observed **only** in other VLBA sessions, mostly the RDVs. So in fact, 2,915 sources come exclusively from VLBA sessions, and only 1,207 were observed in non-VLBA sessions. This means that the VLBA has had a huge impact on the X/S catalog, accounting for 71% of the total number of sources.

4 Distribution of the X/S Sources

A deficiency in both ICRF1 and ICRF2 is that most of the sources were north of $\sim -30^\circ$ declination. Unfortunately this situation has not changed, and will not change, in ICRF3. The VLBI networks available in the southern hemisphere cannot approach the sensitivities of the VCS and VCS-II campaigns. There is some hope that an African network of large antennas will become available in a few years, but this would not be in time for ICRF3. Figure 1 shows the relative density of X/S sources in two degree declination strips. One can see that the density is fairly even in the $+90^\circ$ to -30° range, then drops to $\sim 1/3$ as much in the -50° to -90° range. Source uncertainties are also very unevenly distributed between the north and the south. Figure 2 shows the distribution of inflated formal errors averaged in two degree declination strips. South of $\sim -30^\circ$, the inflated errors increase dramatically and show much greater scatter.

5 Ongoing Work

Several efforts are currently underway to improve the upcoming ICRF3 and its usefulness to the scientific community. A group of 195 ICRF3–*Gaia* optically bright intercomparison sources are being observed regularly [10] to improve their positions and thus improve the alignment between ICRF3 and the *Gaia* optical

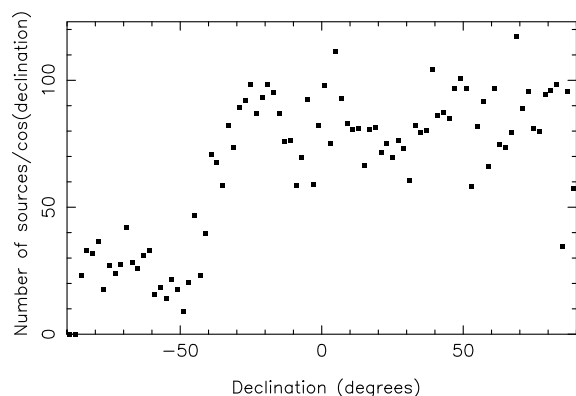


Fig. 1 Relative source density in 2° declination bins.

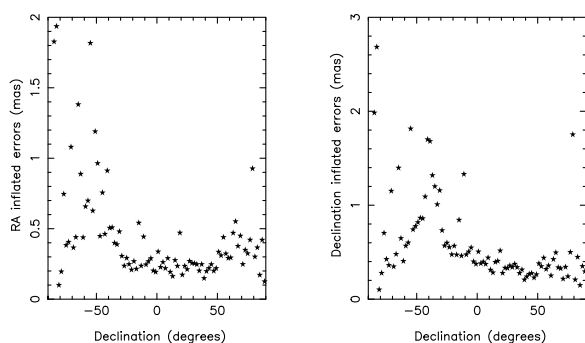


Fig. 2 Average inflated errors in 2° declination bins.

reference frame. Precision goals of 0.1 mas or better have already been obtained for most of them and will be obtained for all of them before ICRF3. Also, as of mid-2015, some 500 ICRF2 sources had not been re-observed since 2009 or earlier. These sources are now being added to the source monitoring program, and as of May 2016, 74 of them have already been re-observed.

6 Summary

ICRF3 will contain a large X/S catalog and maybe smaller catalogs at other radio frequencies (Ka/X and K bands). The X/S catalog will be at least 20% larger than in ICRF2, and the positions will be more precise and more homogeneous. There will also be no large second class of sources, as in ICRF2. Because of the increased precision, ICRF3 will also likely have a smaller noise floor than ICRF2. The current X/S catalog has

more southern sources than ICRF2, but unfortunately the southern one-third of the sky will still be sparsely represented in ICRF3.

Acknowledgements

The VLBA is operated by the National Radio Astronomy Observatory, which is a facility of the National Science Foundation, and operated under cooperative agreement by Associated Universities, Inc.

References

1. Fey, A.L., Gordon, D. & Jacobs, C.S. (editors), 2009, 'The Second Realization of the International Celestial Reference Frame by Very Long Baseline Interferometry', IERS Technical Note No. 35. (<http://www.iers.org/TN35>).
2. Fey, A.L., Gordon, D., Jacobs, C.S., Ma, C., Gaume, R.A., et al., 'The Second Realization of the International Celestial Reference Frame by Very Long Baseline Interferometry', *Astronomical Journal*, 150, 58, 2015. doi:10.1088/0004-6256/150/58.
3. Beasley, A.J., Gordon, D., Peck, A.B., Petrov, L., McMillan, D.S., Fomalont, E.B. & Ma, C., 'The VLBA Calibrator Survey—VCS1', *Astrophysical Journal Supplement*, 141, 13, 2002. doi:10.1086/339806.
4. Fomalont, E.B., Petrov, L., McMillan, D.S., Gordon, D. & Ma, C., 'The Second VLBA Calibrator Survey: VCS2', *Astronomical Journal*, 126, 2562, 2003. doi:10.1086/378712.
5. Petrov, L., Kovalev, Y.Y., Fomalont, E.B. & Gordon, D., 'The Third VLBA Calibrator Survey: VCS3', *Astronomical Journal*, 129, 1163, 2005. doi:10.1086/426920.
6. Petrov, L., Kovalev, Y.Y., Fomalont, E.B. & Gordon, D., 'The Fourth VLBA Calibrator Survey', *Astronomical Journal*, 131, 1872, 2006. doi:10.1086/499947.
7. Kovalev, Y.Y., Petrov, L., Fomalont, E.B. & Gordon, D., 'The Fifth VLBA Calibrator Survey: VCS5', *Astronomical Journal*, 133, 1236, 2007. doi:10.1086/511157.
8. Petrov, L., Kovalev, Y.Y., Fomalont, E.B. & Gordon, D., 'The Sixth VLBA Calibrator Survey: VCS6', *Astronomical Journal*, 136, 58, 2008. doi:10.1088/0004-6256/136/2/580.
9. Gordon, D., Jacobs, C., Beasley, A., Peck, A., Gaume, R., Charlot, P., Fey, A., Ma, C., Titov, O. & Boboltz, D., 'Second Epoch VLBA Calibrator Survey Observations: VCS-II', *Astronomical Journal*, in press, 2016.
10. Le Bail, K., Gipson, J.M., Gordon, D., MacMillan, D.S., Behrend, D., Thomas, C.C., Bolotin, S., Himwich, W.E., Bayer, K.D., Corey, B.E., Titus, M., Bourda, M., Charlot, P. & Collioud, A., 'IVS Observation of ICRF2—*Gaia* Transfer Sources', *Astronomical Journal*, 151, 79, 2016. doi:10.3847/0004-6256/151/3/79.

Estimating the Celestial Reference Frame via Intra-Technique Combination

Andreas Iddink, Thomas Artz, Sebastian Halsig, Axel Nothnagel

Abstract One of the primary goals of Very Long Baseline Interferometry (VLBI) is the determination of the International Celestial Reference Frame (ICRF). Currently the third realization of the internationally adopted CRF, the ICRF3, is under preparation. In this process, various optimizations are planned to realize a CRF that does not benefit only from the increased number of observations since the ICRF2 was published. The new ICRF can also benefit from an intra-technique combination as is done for the Terrestrial Reference Frame (TRF).

Here, we aim at estimating an optimized CRF by means of an intra-technique combination. The solutions are based on the input to the official combined product of the International VLBI Service for Geodesy and Astrometry (IVS), also providing the radio source parameters. We discuss the differences in the setup using a different number of contributions and investigate the impact on TRF and CRF as well as on the Earth Orientation Parameters (EOPs). Here, we investigate the differences between the combined CRF and the individual CRFs from the different analysis centers.

Keywords VLBI, ICRF, intra-technique combination, datum-free normal equations, full variance-covariance information

Institute of Geodesy and Geoinformation, University of Bonn

1 Introduction

Very Long Baseline Interferometry (VLBI) is the unique space-geodetic technique for the generation of the International Celestial Reference Frame (ICRF), one of the fundamental products of the International VLBI Service for Geodesy and Astrometry [8]. To date, two realizations of the International Celestial Reference System (ICRS) have been computed, and the third one [7] is under construction. The latest realization, the ICRF2 [4], consists of precise positions of 3,414 sources, including 295 defining sources. Furthermore, 2,197 out of the 3,414 sources were observed only in VLBA Calibrator Survey (VCS, e.g., [2]) sessions, which are special astrometric survey sessions, optimized to observe a huge number of new radio sources. Both previous realizations were computed by a single analysis center, the VLBI group at the NASA Goddard Space Flight Center (GSFC), using a single software package, Calc/Solve.

While the benefit of the intra-technique combination of various analysis centers for the Terrestrial Reference Frame (TRF) and Earth Orientation Parameters (EOPs) is well known [3] and has been utilized for the official IVS products for many years, only comparisons between source catalogs of different analysis centers were made for the computation of the ICRF2. Due to the fact that today most of the IVS analysis centers routinely produce contributions containing radio source positions, an intra-technique combination is equally feasible for the generation of a CRF. For this reason, a rigorous combination procedure for CRF determinations has been proposed in Iddink et al. [5, 6].

The developed approach is based on the combination at the level of datum-free normal equation systems (NEQs), which enables the rigorous transfer of the full

variance-covariance information of all individual input contributions and all related parameters. Furthermore, it is guaranteed that the contributions are not distorted by any constraints before combining them. Thus, the same a priori frames and an identical datum can be applied to all contributions within the combination process. Since high precision geodetic VLBI started operating in 1979, over 5,500 sessions have been observed and analyzed by several analysis centers. These sessions are freely available on the server of the IVS and can be used for the combination on a session-by-session level.

Additionally, various campaigns have been performed to sample the southern hemisphere with a better density, and the VCS has been redone. Further optimizations of the ICRF3 [7] with respect to the previous versions will be obtained on the analysis side. Following IUGG Resolution No. 3 (2011) this approach can then easily be extended to a consistent estimation of CRF, TRF, and the EOPs, based on the observations of different space-geodetic techniques. Based on all these NEQs generated by different analysis centers, individual CRFs can be computed and assessed.

In this paper we focus on the usability of the different contributions in terms of generating a reliable combined CRF. This includes the investigation of the differences between the combined CRF and the individual CRFs from the different analysis centers. The whole combination process as well as the illustration and assessment is done with our new VLBI software package `ivg::ASCOT` [1]. Here we also give an insight into the main capabilities of our SINEX analyzer toolbox.

2 Combination Setup

At the beginning it is sensible to use a set of sessions that is small and only comes from a few different analysis centers. This gives us the opportunity to detect blunders within the combination process and the individual contributions.

The rough combination procedure can be summarized as follows:

- selection of sessions,
- selection of analysis centers,
- stacking of related NEQs,

- defining the datum and solving the system,
- illustration and interpretation of the results.

In order to assess the general functionality of the combination procedure implemented in `ivg::ASCOT`, we started using the contributions of two well-known and established analysis centers: the United States Naval Observatory (USNO) and the Goddard Space Flight Center (GSFC). Both analysis centers are using the software package `Calc/Solve`. For further simplification only 15 sessions from CONT14 were used to generate a short-term CRF, TRF, and corresponding EOPs. Hence, in our initial combination only 30 NEQs were stacked using the freely available SINEX files containing the pre-reduced datum-free NEQs. The station coordinates were set up as global parameters in order to obtain a single station position over the whole period of CONT14. All EOPs as well as all special handling sources were set up on a daily basis. The remaining sources were stacked and set up as global parameters. In order to be able to solve the stacked monolithic system, an NNR/NT datum was applied to the stations and an NNR datum to the sources.

Finally, we obtained a combined CRF, TRF, and corresponding EOPs. Additionally, we performed the same procedure twice only using the sessions of each Analysis Center individually. Thus, we were able to compare the individual CRFs and TRFs to the combined one by means of a Helmert transformation. With respect to the CRF, the transformation was based on the ICRF2 defining sources and w.r.t. the TRF on a set of well-established stations. After transforming the catalogs onto each other, the residuals between corresponding sources/stations can be computed and illustrated. In the following we focus on the CRF.

3 Initial Results

The solution residuals of GSFC are illustrated in blue (dark), and the residuals of USNO are shown in green (light) (see Figure 1). As one would expect, the residuals are perfectly symmetrical and always point into the opposite direction. This is because only two contributions were used, and both contributions were weighted equally. Furthermore, due to the fact that both analysis centers used the same software package and only a short time period was selected, it is reasonable that

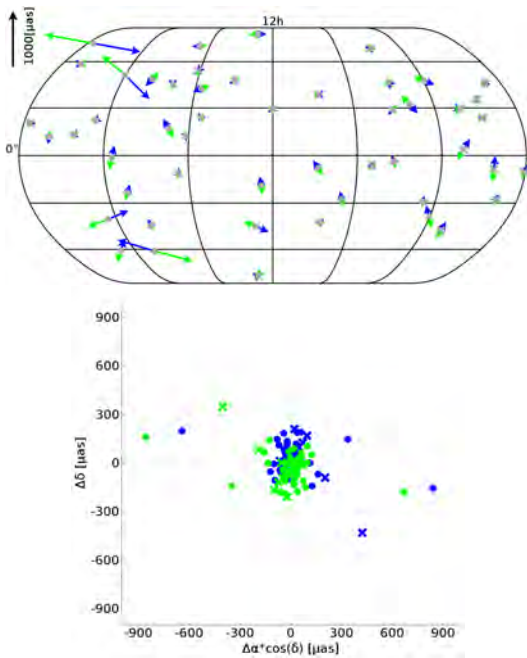


Fig. 1 Residuals between the combined and individual solutions using CONT14: GSFC (blue/dark), USNO (green/light).

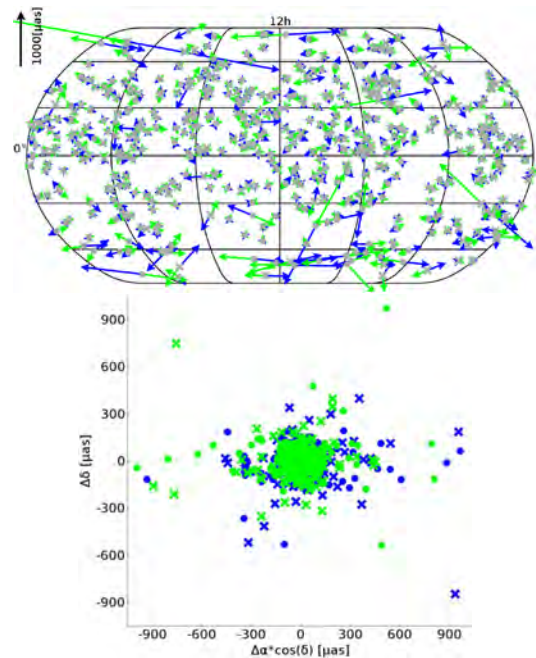


Fig. 2 Residuals between the combined and individual solutions using R1/R4 between 2010 and 2014: GSFC (blue/dark), USNO (green/light).

all residuals are quite small and even not visible at this scale.

In the next step the whole solution setup was retained, but the time period was expanded. In the next solution setup (see Figure 2), we used all official R1 and R4 sessions between 2010 and 2014 analyzed at GSFC and USNO, and we performed the same combination procedure as already explained. Additionally to the CRF plot using arrows for illustrating the differences, the lower plots in Figure 1 and Figure 2 show the same residuals in a more vivid way. Here we also see the same expectable symmetric behavior of the differences between the individual solutions and the combined one after the transformation onto each other. The defining sources are represented by a disc while all other types of sources are illustrated by a cross.

In general, the estimated rotation angles (see Table 1) and their standard deviations as well as the big residuals of some weak sources in the far southern and northern hemispheres match the expectations. In summary, the results in Figure 1 and Figure 2 should demonstrate the successful performance of the general combination procedure and the subsequent analysis and plotting toolbox of `ivg::ASCOT`.

After the step of expanding the time period for two analysis centers, more analysis centers needed to

Table 1 Rotation angles and their standard deviations between combined catalog and individual catalogs related to Figure 2 and Figure 4.

Anal. Center	x [mas]	y [mas]	z [mas]
GSFC	-0.002 ± 0.003	0.001 ± 0.003	-0.002 ± 0.003
USNO	0.001 ± 0.003	0.000 ± 0.003	0.002 ± 0.003

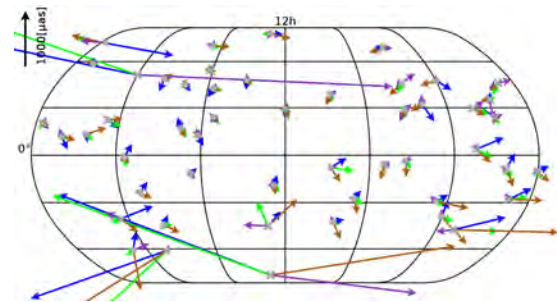


Fig. 3 Residuals between the combined and individual solutions using CONT14: GSFC (blue), USNO (green), DGFI (brown), CGS (purple).

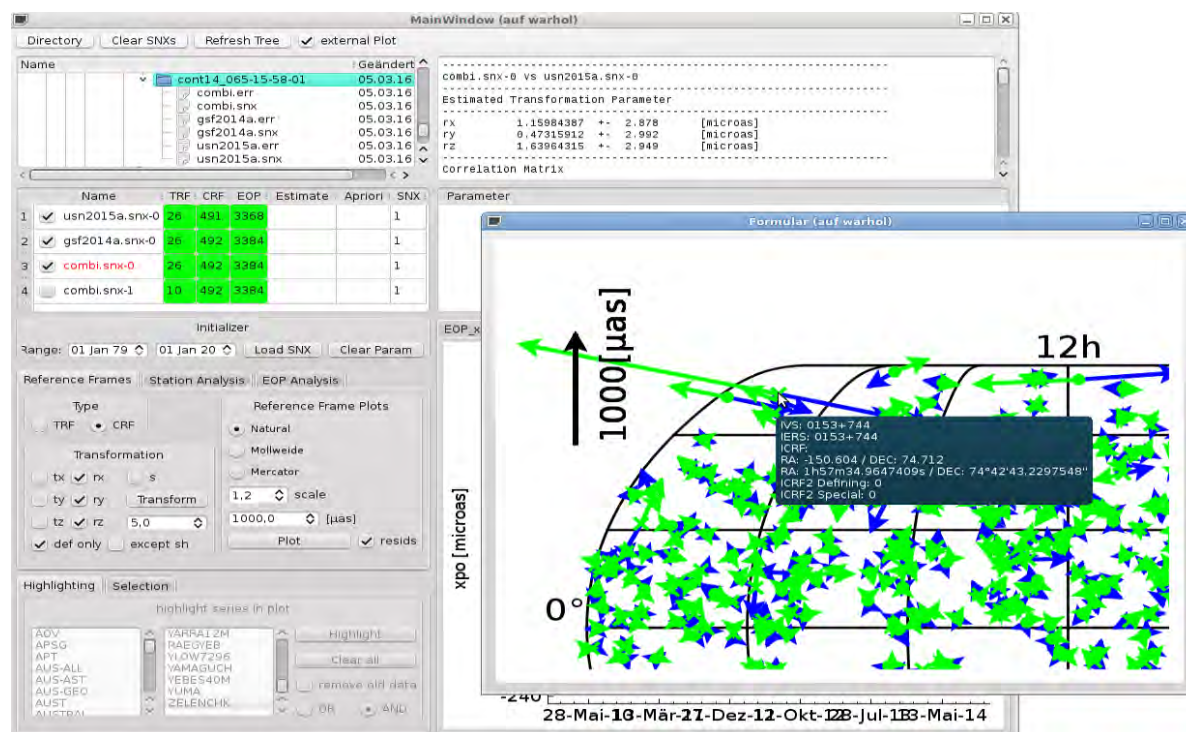


Fig. 4 Example of using the ivg::ASCOT SINEX analyzer. Individual (USNO, GSFC) and combined results are loaded and transformed on each other by means of a Helmert transformation. The residuals are illustrated in an external plot. The zoom functionality and the tooltips enable the analysis of source specific information (e.g., position, different names, defining or special handling).

be included in the combination. For this purpose the time range was again limited to only 15 sessions of CONT14, but now two additional analysis centers were used: the German Geodetic Research Institute (DGFI) and the Centro di Geodesia Spaziale (CGS). Hence, four analysis centers contributed to the combined CRF solution illustrated in Figure 3, using the same combination setup as in the previous cases.

When comparing the residuals of Figure 1 and Figure 3, it becomes obvious that most of the residuals are comparable in terms of their magnitude. Nevertheless there are about five sources with big striking residuals pointing in different directions. After some deeper investigations into this issue using the ivg::ASCOT SINEX analyzer toolbox (see Figure 4) it has become clear that all of these sources have only a few observations within CONT14.

The resulting problem is that the use of Calc/Solve combined with an unsuitable configuration setup leads to the issue that these specific sources are not stored in the NEQs and therefore not saved in the SINEX files. Because of this, these weak sources with only a

few observations lead to hidden constraints within the affected NEQs. Hence, the in-the-proper-sense datum-free NEQs are not datum-free anymore and cannot be rigorously combined with other contributions.

In the case of the combined results illustrated in Figure 3, the exclusion of the CGS contribution from the combination prevents the occurrence of the huge residuals because of this issue.

4 Conclusion and Future Work

We have shown that we are able to generate a combined CRF based on different contributions using our newly developed VLBI software package ivg::ASCOT. Between two and four analysis centers were used, and between 15 and 400 sessions were stacked. In order to generate a reliable combined CRF, investigations concerning the features and properties of a combined CRF based on more sessions and more analysis centers have to be made. Furthermore we found out that

it is absolutely mandatory to store all observed sources within the NEQs and the SINEX files, independent of the number of observations.

References

1. T. Artz, S. Halsig, A. Iddink, and A. Nothnagel. ivg::ASCOT: The Development of a new VLBI Software Package. In *IVS 2016 General Meeting Proceedings, "New Horizons with VGOS"*, Johannesburg, South Africa, March 13-19 2016, Eds: D. Behrend, K. D. Baver, and K. L. Armstrong, this volume.
2. A.J. Beasley et al. The VLBA Calibrator Survey-VCS1 (2002). In *The Astrophysical Journal Supplement Series*, Volume 141, Issue 1, pp. 13–21. doi: 10.1086/339806.
3. S. Böckmann, T. Artz, A. Nothnagel, and V. Tesmer (2010). International VLBI Service for Geodesy and Astrometry: Earth orientation parameter combination methodology and quality of the combined products. In *Journal of Geophysical Research*, 115, B04404 doi: 10.1029/2009JB006465.
4. IERS (2009). The second realization of the international celestial reference frame by very long baseline interferometry. In A.L. Fey, D. Gordon, and C.S. Jacobs (Eds.): *IERS Technical Note 35*, presented on behalf of the IERS/IVS Working Group, Verlag des Bundesamtes für Geodäsie und Kartographie, Frankfurt am Main.
5. A. Iddink, A. Nothnagel, and T. Artz. Rigorous VLBI intra-technique combination strategy for upcoming CRF realizations. In N. Capitaine, editor, *Proceedings of the Journées 2013 Systèmes de Référence Spatio-Temporels*, pp. 81–83. Observatoire de Paris, 2014. ISBN: 978-2-901057-69-7.
6. A. Iddink, T. Artz, and A. Nothnagel (2015). Development of a Combination Procedure for Celestial Reference Frame Determination. *IAG Scientific Assembly, Potsdam*, 2015. doi: 10.1007/1345-2015-22.
7. Z. Malkin et al (2014). The ICRF-3: Status, Plans, and Progress on the next generation international celestial reference frame. In *Proceedings of the Journées 2014 "Systèmes de référence spatio-temporels"*, St. Petersburg, Russia.
8. H. Schuh and D. Behrend. VLBI: A fascinating technique for geodesy and astrometry. *Journal of Geodynamics*, 61, doi: 10.1016/j.jog.2012.07.007, pp. 68–80, 2012.

Selecting Sources that Define a Stable Celestial Reference Frame with the Allan Variance

Karine Le Bail¹, David Gordon¹, Chopo Ma²

Abstract The ICRF2 was adopted by the IAU in 2009 and was based on the positions of 3,414 radio sources determined by VLBI. Discussions on the next realization of the ICRF (ICRF3) have been underway within the IAU and IVS since 2012. VLBI has made significant advances since ICRF2. From the latest GSFC solution, we extract a set of sources that defines a stable celestial reference frame, as shown by Feissel-Vernier 2003 [1] using tools such as the Allan variance and the drift of the position time series. This method also allows us to highlight a set of the least stable sources that may need special handling.

Keywords ICRF, radio sources, source selection, Allan variance, defining sources, special handling sources

1 Introduction

In this paper, we investigate two questions of interest for the realization of the ICRF3. The first objective is to select a set of sources that define a stable celestial reference frame. The method used is inspired by the study of Feissel-Vernier 2003 [1] using the Allan variance and the drift of the position time series. The second objective is to identify sources that degrade the stability of the celestial reference frame to be able to handle them in the same way as the set of sources that were called the ‘special handling’ sources in ICRF2. The method proposed here uses the results of the previous method,

1. NVI, Inc., NASA GSFC, Greenbelt Rd, Greenbelt, MD 20701
2. NASA Goddard Space Flight Center

but also takes into account the type of noise determined by the Allan variance.

In the second section of this paper, we discuss the solution of source position time series we studied. In the third section, we detail our analysis as well as the tools used. The fourth section shows the results obtained and proposes tools and criteria organized in a detailed method to determine different sets of sources: “stable” sources and sources that would need to be handled differently in the analysis because they degrade the celestial reference frame (called special handling sources in ICRF2).

2 Data

The set of VLBI position time series we analyzed in this paper was produced with the Calc/Solve software by D. Gordon at GSFC. It used VLBI sessions from August 1979 through October 2015. It contains 4,081 sources, including the VCS sources.

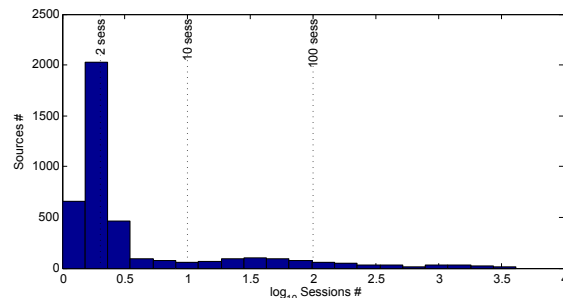


Fig. 1 Distribution of the number of sessions each source was observed in for the 4,081 sources studied in this paper.

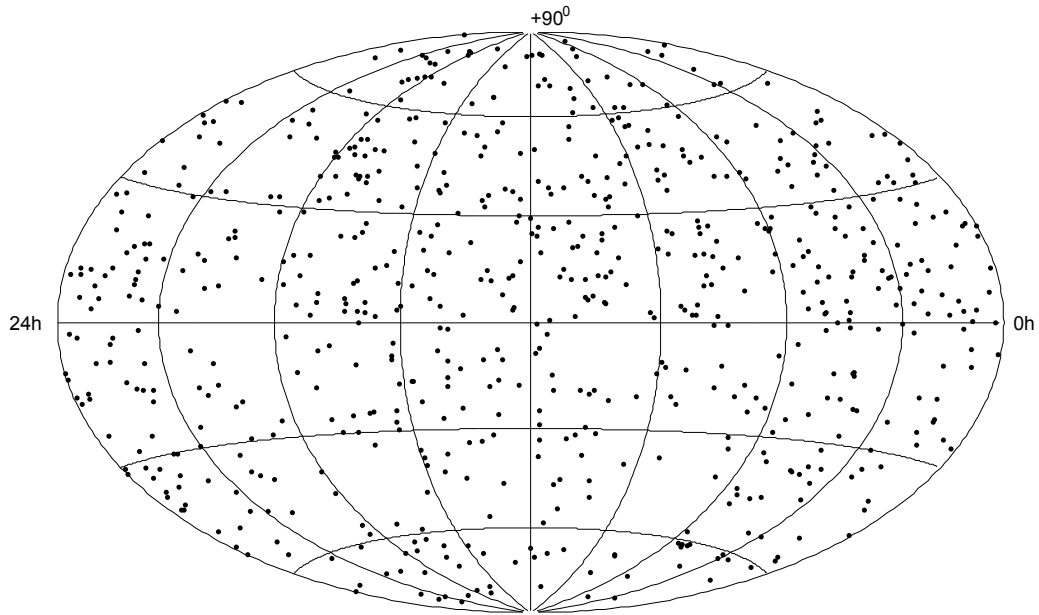


Fig. 2 Map of the 724 sources studied in this paper.

To be significant, the Allan variance analysis needs to be done on a reasonable number of points. For this reason, we used only 724 sources that were observed in more than ten sessions, shown in Figure 1. These sources are still reasonably distributed as seen in Figure 2.

In previous studies (Feissel-Vernier 2003 [1], Le Bail and Gordon 2010 [2], Le Bail et al. 2014 [3]), the analysis was done independently on Right Ascension and Declination, and then a stability index was built by combining the values obtained on each coordinate.

To take into account both coordinates at the same time, we decided to convert the series (Right Ascension, Declination) into Arc Lengths (see Bolotin and Lytvyn 2009 [4]). We compute the Arc Length as the angular distance between the position $P_i(\alpha_i, \delta_i)$ of a given source at time t_i and its average position over time $P_m(\alpha_m, \delta_m)$. As this distance is rather small, we use the haversine formula which is better conditioned:

$$l_{im} = 2 \arcsin \left\{ \sin^2 \left(\frac{\delta_m - \delta_i}{2} \right) + \cos(\delta_i) \cos(\delta_m) \sin^2 \left(\frac{\alpha_m - \alpha_i}{2} \right) \right\}^{0.5}$$

Figure 3 illustrates an example for the source 0642+449.

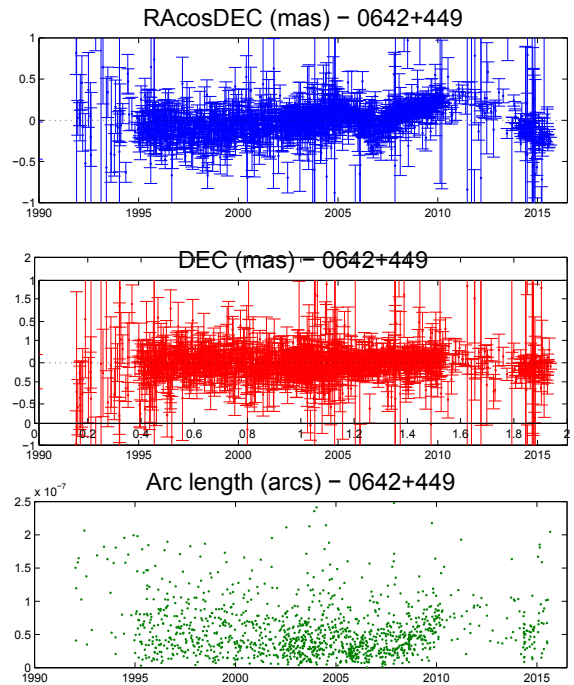


Fig. 3 Right Ascension, Declination and Arc Length of the source 0642+449.

Stability test

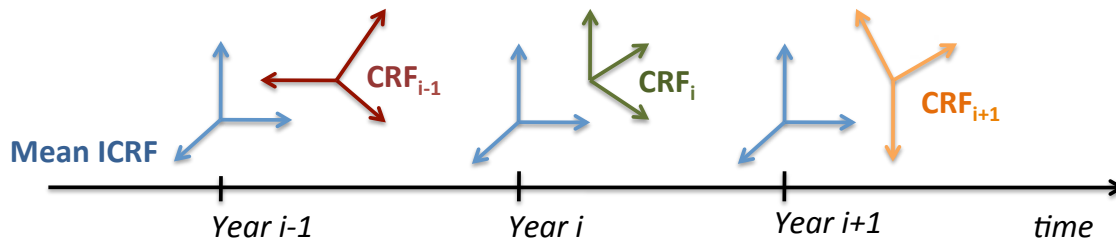


Fig. 4 Stability test scheme (see [2]).

$$\left\{ \begin{aligned} (\alpha_m - \alpha_i) \cos \delta_m &= A_1(i) \tan \delta_i \cos \alpha_i + A_2(i) \tan \delta_i \sin \alpha_i - A_3(i) \\ \delta_m - \delta_i &= -A_1(i) \sin \alpha_i + A_2(i) \cos \alpha_i + dz(i) \end{aligned} \right.$$

To obtain the type and the level of noise, we use the Allan variance. If $(x_i)_i$ are the measurements and τ the sampling time, the Allan variance at τ is defined by: $\sigma^2(\tau) = \frac{1}{2} \langle (\widehat{x}_{i+1} - \widehat{x}_i)^2 \rangle$. The type of noise is obtained by computing the slope of the Allan variance curve in a plot $(\log_{10}(\sigma^2(\tau)), \log_{10}(\tau))$. A slope of -1 indicates white noise, 0 indicates flicker noise, and $+1$ indicates random walk.

where α_i and α_m are the Right Ascension of the source at year i and mean, respectively; δ_i and δ_m are the Declination of the source at year i and mean, respectively.

This scheme is applied to (Right Ascension, Declination) and then to the series (Arc Length).

The time series are analyzed over the period January 1990 to October 2015. The 724 remaining sets of time series are not all suitable for our analysis with the Allan variance (e.g., data span not long enough, large gaps in between consecutive data, poor number of points in a year). So we eliminated the time series of 207 sources. Our method is applied on a reduced set of 517 sources.

We construct a source stability index *SIndex* inspired by Feissel-Vernier 2003 [1] as the combination of the normalized value of the drift and the Allan standard deviation at one-year sampling time ($\sigma^2(\tau = 1 \text{ year})$). We derived two *SIndex* per source: one studying the series (Right Ascension, Declination) and a second one obtained from the Arc Length time series.

The sources are then sorted depending on the *SIndex* from the less stable to the most stable. To test the stability of a given subset of sources, we calculate the rotation parameters between two celestial reference frames realized by this subset: one is the yearly mean realization and the other one is the mean computed over the entire period (see Equation below and Figure 4). We obtain $(A_1(i), A_2(i), A_3(i), dz(i))_i$ for each year i and we look at the standard deviation and the mean of the quantity $(A_1(i), A_2(i), A_3(i), dz(i))_i$ for each subset.

4 Results

The standard deviations and means for each subset are presented in Figure 5. The study made when analyzing Right Ascension and Declination independently is shown in blue circles, and when analyzing Arc Length in red diamonds.

The two approaches give similar results, especially for the smallest subsets of sources (right side of the plots).

If we choose the 270 most stable sources, 201 sources are common for both selection methods.

The less stable sources seem to impact significantly the frame. As the source stability indices are computed as a combination of the drift and the level of noise (Allan variance for a sampling time of one year), this may be due to the instability of the source (e.g., structure) and/or poor accuracy due to the small number of points in the time series. It tends to show that this stability index may not be sufficient to detect sources that need special handling. However, we said previously that the Allan variance gives also an indication on the type of noise: sources exhibiting flicker noise or random walk can be considered as unstable and should be studied in more details.

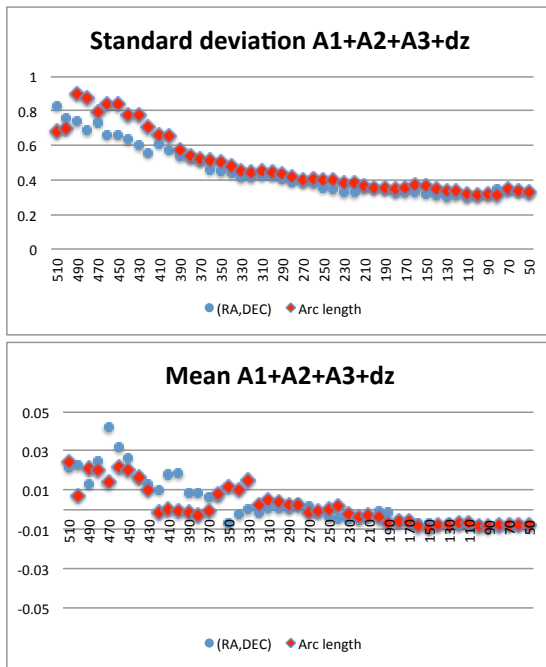


Fig. 5 Standard deviation and mean of the quantity $A1+A2+A3+dz$.

We have then two criteria on which to judge the stability of a source: the stability index and the type of noise.

Let's take the set of 39 special handling sources that were listed in ICRF2. Thirty of them are studied in this paper. All 30 sources are considered unstable: eight are considered unstable by the stability index $SIndex$, fifteen by the type of noise, and seven by both criteria.

But this study permitted the detection of other non-special handling sources in ICRF2, that are unstable. An example is the source 0642+449 which coordinates are represented in Figure 3. When computing the Allan variance on each coordinate (Right Ascension, Declination, and Arc Length), the corresponding slopes are respectively 0.23 ± 0.24 , 0.08 ± 0.35 , and 0.41 ± 0.03 , which points on flicker noise in the time series. This is a very important conclusion, especially because 0642+449 is an ICRF2 defining source.

5 Conclusions

The methods used in this study allows us to select sources that would define a stable celestial reference

frame. When combining the source stability index and the study of the type of noise with the Allan variance, the selection can be also extended to sources that need special handling.

The limitation of this method is that it depends greatly on the Allan variance which is statistically significant when the sources are regularly observed. When averaging yearly, 336 of the 724 sources had less than ten points per year each year.

To remedy the problem and to be able to investigate all sources of a set, more criteria should be considered:

1. criteria that could be computed even with a low number of observations: level of noise using the regular standard deviation, drift of the time series;
2. criteria that are significant when the source is sufficiently observed: level of noise using the Allan variance at different sampling time, type of noise using the Allan variance on regularized series averaged in different periods from 7 days to 1 year;
3. criteria that indicate the physical nature of structure: Structure Index SI from Fey & Charlot 1997 [5], time series of flux values.

References

1. M. Feissel-Vernier, "Selecting stable extragalactic compact radio sources from the permanent astrometric VLBI program", In *A&A*, 403, doi:10.1051/0004-6361:20030348, pages 105–110, 2003.
2. K. Le Bail, and D. Gordon, "Time-dependent Selection of an Optimal Set of Sources to Define a Stable Celestial Reference", In D. Behrend and K. D. Baver, editors, *International VLBI Service for Geodesy and Astrometry 2010 General Meeting Proceedings*, NASA/CP-2010-215864, pages 280–284, 2010.
3. K. Le Bail, D. Gordon, and J. M. Gipson. Evaluation of the Stability of ICRF2 in the Past Five Years Using the Allan Variance. In D. Behrend, K. Baver, and Kyla Armstrong editors, *IVS 2014 General Meeting Proceedings*, "VGOS: The New VLBI Network", Science Press (Beijing), ISBN 978-7-03-042974-2, pages 395–398, 2014.
4. S. Bolotin, and S. Lytvyn, "Investigation of stability of radio sources from arc-length method", In *Proc. Journées 2008*, Dresden, Germany, 22-24 Sep 2008, Ed. M. Soffel, N. Capitaine, 207–210, 2009.
5. A. L. Fey, and P. Charlot, "VLBA Observations of Radio Reference Frame Sources. II. Astrometric Suitability Based on Observed Structure", In *The Astrophysical Journal Supplement Series*, 111:1, doi:10.1086/313017, pages 95–142, 1997.

Defining Source Selection and Celestial Reference Frame Stability

C. Gattano, S. Lambert

Abstract The celestial reference frames are conceptually materialized by point-like sources with no motion on the sky. But with the accuracy of our observations increasing, to fulfill those conditions becomes more and more difficult. In this study, we first present the danger of taking into account unstable sources in the set of defining sources of a celestial reference frame. Then, based on a previous study where we classified radio sources observed by Very Long Baseline Interferometry with respect to their position stability using a statistical tool called Allan Variance (see “Source Characterization by the Allan Variance”, this volume), we constructed several celestial reference frames by choosing sets of defining sources using the new classification. We studied the stability of the frames in three ways: (1) statistically and temporally, (2) inspired by Lambert [6], and (3) using Earth precession-nutation as a stability indicator, as it was not done before.

Keywords Defining sources, celestial reference frame stability, precession-nutation

1 Introduction

The purpose of the celestial reference system (CRS) is to represent the Universe that is hypothetically non-rotating. Such a system is necessary in order to apply the physical laws of the nature and study motions, e.g., variations of the Earth orientation. Since 1991, it is defined by a structure carried by the directions of extra-

SYRTE, Observatoire de Paris, PSL Research University, CNRS, Sorbonne Universités, UPMC Univ

galactic radio sources. Without other information, this principle stays theoretical, and the only way to use it is to materialize it, i.e., to use observations to create the structure. By doing so, we realize a celestial reference frame (CRF), as was done in 1998 with the release of the ICRF1 [7].

Given this idea, other studies have been done since then to refine the structure by selecting more and more stable directions, and therefore stabilizing the celestial reference frame with always a greater accuracy of its stability [3, 5, 1, 2]. Currently, the most stable realization is the ICRF2 [4]. I invite you to read the introductory section of “Source Characterization by the Allan Variance” in these proceedings to get some details about the methodologies used in those studies.

ICRF2 was produced in 2009, and since then no real improvements have been done to refine the structure. We worked on this and got a classification with respect to position stability of sources observed using Very Long Baseline Interferometry (VLBI). The details are explained in “Source Characterization by the Allan Variance” in these proceedings. In summary, the classification divides the VLBI sources into three groups based on the behavior of their Allan Variance (AV). Inside each group, the sources are sorted by a score computed from minima of the Allan Variance in both $d\alpha \cos \delta$ and $d\delta$ with respect to the mean position.

This refinement is needed, because one of the main goals of the CRF is to study the orientation of the Earth and particularly the precession-nutation, i.e., displacements of the instantaneous Earth rotation axis’ direction on the celestial sphere. To illustrate this link between CRF and precession-nutation, we first present in Section 2 consequences of a non-linear source¹ (NL)

¹ A non-linear source has a radio center showing motion under the view of VLBI that cannot be modeled by a linear function.

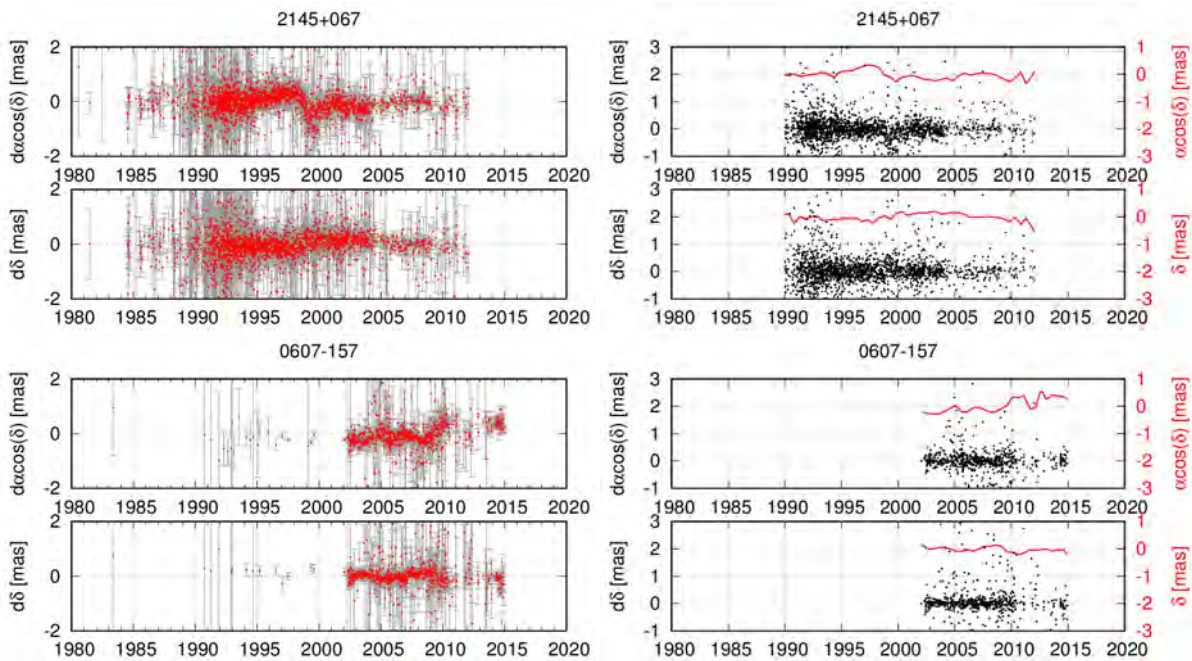


Fig. 1 Examples of two coordinate time series of non-linear sources obtained in a VLBI analysis (left) and the decomposition low/high frequency (right).

mistakenly selected as a defining source² (DS) for CRF and for precession-nutation.

Then, using our source classification, we select several subsets of defining sources and estimate the stability of CRFs derived from the subsets' structure. The method is inspired by Lambert (2013) [6] and explained in Section 3. The goal is to determine which criteria are predominant in the definition of a stable CRF between the behavior of the Allan Variance and the threshold value of the computed score related to the Allan Variance minima. To compare, we also add the adjustment of precession-nutation based on each CRF and study the residuals to use them as another criterion of stability. Finally, in Section 4, we draw some conclusions.

2 Contamination by Non-linear Sources

From the coordinate time series from VLBI analysis, we selected some non-linear sources (NL) whose time series present variations that cannot be modeled by a

² A defining source is how we called a source whose line-of-sight direction defines an axis of the frame.

linear function. In general, every coordinate time series can be characterized in two ways. On the one hand, we can study the high frequency components of their series composed of a thermal noise which is instrumental, of the badly modeled atmospheric component, and of the non-modeled source structure signal. On the other hand, the low frequency components gather intrinsic information about the radio center motion (e.g., periodic variations, jumps, or linear drift).

So, we selected several sources that present non-linear patterns on the low frequency part of their time series in order to study their contributions to the CRF instability and to variations in the precession-nutation time series. The sources selected are 0014+813, 0528+134, 1044+719, 2145+067 (see Figure 1), 4C39.25, 0607-157 (see Figure 1), 0642+449, 0955+476, and 1739+522.

In this study, all solutions produced from the adjustment of VLBI observations are based on the analysis strategy applied at Paris Observatory that produces the OPA solution³. We only played with the subset for the no-net-rotation constraint (NNR) applied during the weighted least-squares adjustment of source coordinates. Because we compared the solutions among

³ <ftp://ivsopar.obspm.fr/vlbi/ivsproducts/eops/opa2015a.eops.txt>

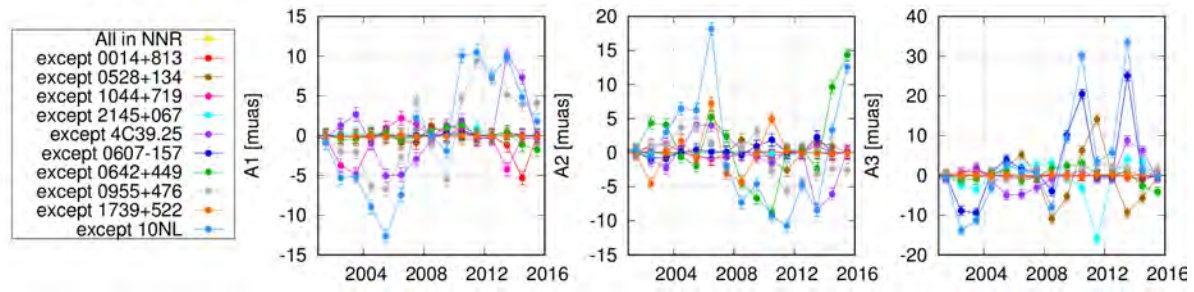


Fig. 2 Annual rotations between the CRF of the reference solution (202 sources as defining sources) and annual CRFs constructed from the CRFs of test solutions ($202 - N_{rejected}$ sources as defining sources) plus the coordinate time series of the removed sources.

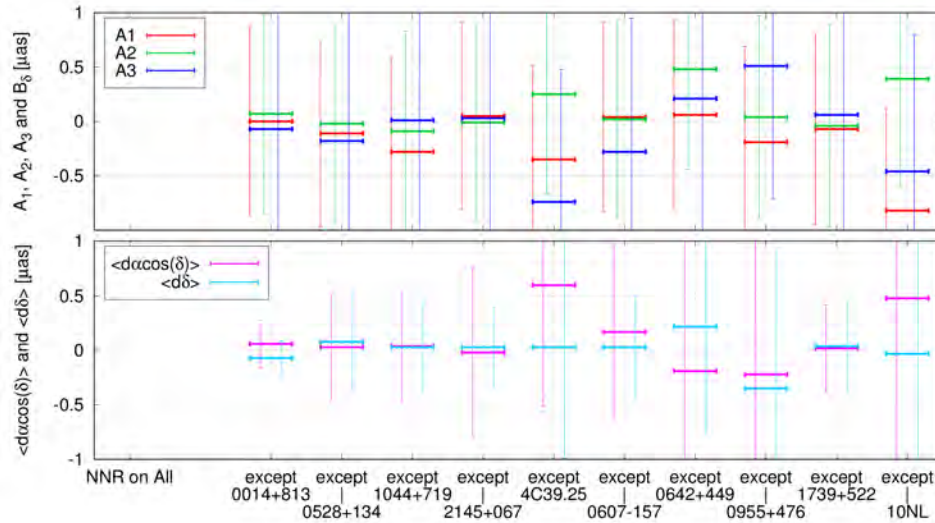


Fig. 3 Rotations and average coordinate differences between common sources of the CRFs from the reference solution (202 sources as defining sources) and test solutions ($202 - N_{rejected}$ sources as defining sources).

each other, the rest of the strategies are irrelevant as they are common for every solution and will thus not be detailed. We used the R1 and R4 sessions as the set of delays in our adjustments.

As the reference solution, we used a solution based on a subset of the defining sources; i.e., we applied the NNR to a set of 202 VLBI sources that were observed in more than 100 sessions in the VLBI history. Then all other solutions, called test solutions, were produced by removing one of the NL listed above. A final test solution was produced by removing all NL sources plus an additional source, i.e., ten in total. When a source is rejected from the DS subset, it is adjusted locally during the analysis, i.e., with one set of coordinates for each session in which it is observed.

To get an idea of the potential mistakes that an NL can bring if it is incorrectly chosen as a DS, we

computed annual coordinates of the rejected sources in each test solution. Then we computed an annual CRF for each test solution from the fixed coordinates of the DS sources to which we added the annual positions of the corresponding rejected source(s). Therefore, we got an annual CRF composed of 202 sources that we can compare to the CRF of the reference solution and get annual rotations $A_1(t)$, $A_2(t)$, $A_3(t)$ for each test solution as follows:

$$\begin{aligned} A_1 \tan \delta_1 \cos \alpha_1 + A_2 \tan \delta_1 \sin \alpha_1 - A_3 &= \alpha_1 - \alpha_2 \\ -A_1 \sin \alpha_1 + A_2 \cos \alpha_1 &= \delta_1 - \delta_2 \end{aligned} \quad (1)$$

Figure 2 shows the results, and we can see that most sources have an impact of a few microseconds of arc (μas) on the CRF rotations (tens of μas for the most agitated). If you look carefully at the light blue curve

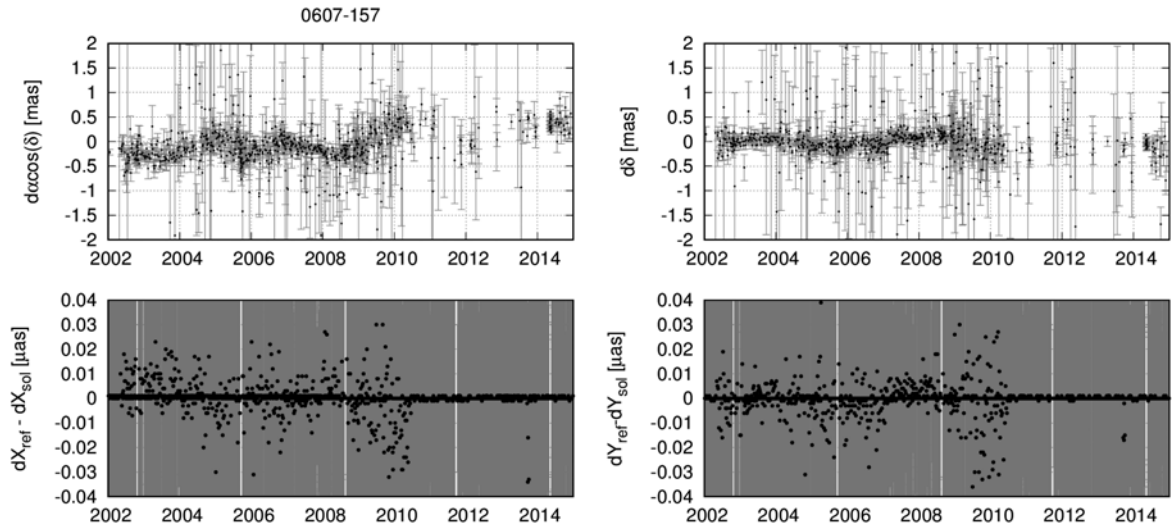


Fig. 4 Differences between the precession-nutation time series obtained from the reference solution and the test solution where 0607–157 was removed from the DS subset.

corresponding to the test solution with ten sources removed from the DS subset, it appears that the value of rotations $A_1^{10NL}(t)$, $A_2^{10NL}(t)$, $A_3^{10NL}(t)$ may be the sum of the individual rotations $A_1^{NLi}(t)$, $A_2^{NLi}(t)$, $A_3^{NLi}(t)$ for all other test solutions i , with only one rejected source. That means that the effect of NL on annual CRF is additive.

One can also ask if mistakenly taking out an NL source from the DS subset of the VLBI solution can affect the position of all the other sources of the DS subset. To answer this question, we took the CRFs from the test solutions, composed of 201 sources for the first nine solutions and 192 for the last, and we compared them with the reference CRF, composed of 202 sources, using Equation (1) as before but applying it to the common sources between the CRFs—that is, 201 sources (192 for the last).

Figure 3 shows the results, and the effect seems negligible, less than the μas level. But, again, although small, the effect seems additive. If we took out a significant number of animated sources (e.g., one hundred) in our DS subset, the degradation in the position of the stable sources could rise to the μas level, maybe even tens of μas .

Finally, what can be the effect on the precession-nutation? In our solution, we adjusted Earth Orientation Parameters (EOP) so we could compute dif-

ferences between precession-nutation from our reference solution and from the test solutions. In Figure 4, we present the example of 0607–157. The effect, at the level of hundredths of μas , is lower than the one on CRF. Therefore, to affect significantly precession-nutation by erroneously including NL in the DS subset, the amount of such mistakes should be large, even larger than the typical size of a DS subset (200~300). But it is to be noted that the effect we see is due to the motion of the NL, because the shape of the coordinate time series is clearly recognizable in the precession-nutation difference time series.

3 Testing Allan Variance by Precession-Nutation Residuals

Knowing that, with respect to Allan variance behavior, there are only 40 good sources among the 202 sources observed more than 100 times (see “Source Characterization by the Allan Variance” in these proceedings), we would like to test this classification in order to get confidence in its utilization.

For this purpose we composed several DS subsets for the VLBI analysis adjustment (Table 1). The different types in the Allan Variance

Table 1 Summary of the various compositions of subsets for defining sources (DS), standard sources (Std), and non-linear sources (NL) in several VLBI solutions. Glo=Global means the position of the source is estimated once for all sessions. Loc=Local means the position of the source is estimated for each session. NNR means we applied the no-net-rotation constraint on the corresponding source subset.

	DS (Glo+NNR)	Std (Glo)	NL (Loc)
Ref.	ICRF2 DS	ICRF2 Std	ICRF2 NL
Tnt1	AV_0	AV_1	AV_2
Tnt2	$AV_0 + AV_1$	-	AV_2
Tnt3	AV_0	-	$AV_1 + AV_2$
Twt1	$AV_0^- + AV_1^- + AV_2^-$	-	$AV_0^+ + AV_1^+ + AV_2^+$
Twt2	$AV_0^- + AV_1^- + AV_2^-$	AV_0^+	$AV_1^+ + AV_2^+$
Twt3	$AV_0^- + AV_1^- + AV_2^-$	$AV_0^+ + AV_1^+$	AV_2^+
Twt4	$AV_0^- + AV_1^-$	AV_2^+	$AV_0^+ + AV_1^+ + AV_2^+$

classification refer to different behaviors of the Allan Variance coordinates time series as follows:



and attributes $^+$ and $^-$ refer to:

$$AV^+ \Rightarrow \sqrt{\min(AV_{\alpha \cos \delta}(t)) + \min(AV_{\delta}(t))} > 0.05 \text{mas}$$

$$AV^- \Rightarrow \sqrt{\min(AV_{\alpha \cos \delta}(t)) + \min(AV_{\delta}(t))} < 0.05 \text{mas}$$

Then, we got from these adjustments precession-nutation time series on which we adjusted a nutation signal from a MHB2000-based model [8] composed of 42 luni-solar principal components with corrected amplitudes to fit the adjustments plus a Free Core Nutation (FCN) signal at 430.21 days. The details of such an adjustment can be found in “The Annual Retrograde Nutation Variability” in these proceedings. Finally, we analyzed the root mean square of the residuals for both $\alpha \cos \delta$ and δ and compared their values for the different solutions. The values are displayed in Table 2.

Table 2 Root mean square of the nutation residuals after adjustment of an MHB2000-base model corrected to fit the results of the solution adjustment.

ID Sol.	$\sigma^{(res.dX)}$	$\sigma^{(res.dY)}$	ID Sol.	$\sigma^{(res.dX)}$	$\sigma^{(res.dY)}$
Ref.	0.390	0.787	Twt1	0.428	0.799
Tnt1	0.299	0.839	Twt2	0.412	0.804
Tnt2	0.297	0.840	Twt3	0.405	0.809
Tnt3	0.254	0.753	Twt4	0.429	0.800

We can see that the best residuals we got are from the solution Tnt3 where the 40 best sources with respect to Allan Variance are taken to define the axes of the CRF, and all the other sources are estimated locally. Such a result goes for a selection of stable sources from an Allan Variance point-of-view.

4 Conclusions

This study is at its beginning and should be pursued to get more results and gain more confidence in what we do. At this time, we can only say that the worst non-linear sources can have an effect on the order of tens of μas if they are used by mistake in the defining sources of a VLBI solution. The consequences for the estimation of other sources are on the level of tenths of μas and at the level of hundredths of μas for the precession-nutation. But effects are additive. It means that the more mistakes we make in selecting our defining sources, the higher is the impact on astrometry and geodesy. Finally, we briefly tested our Allan Variance classification. The first results are in favor of its goodness, and we get a little more confidence in the fact that only 40 well-observed sources are currently stable.

References

1. M. Feissel-Vernier, Selecting stable extragalactic compact radio sources from the permanent astrogeodetic VLBI program, In Astronomy and Astrophysics, 2003, 403, 105–110.
2. M. Feissel-Vernier et al., Analysis strategy issues for the maintenance of the ICRF axes, In Astronomy and Astrophysics, 2006, 452, 1107–1112.
3. A.L. Fey et al., The Second Extension of the International Celestial Reference Frame: ICRF-EXT.1, In Astronomical Journal, 2004, 127, 3587-3608.
4. A.L. Fey et al., The Second Realization of the International Celestial Reference Frame by Very Long Baseline Interferometry, In Astronomical Journal, 2015, 150, 58.
5. A.M. Gontier et al., Stability of the extragalactic VLBI reference frame, In Astronomy and Astrophysics, 2001, 375, 661–669.
6. S. Lambert, Time stability of the ICRF2 axes, In Astronomy and Astrophysics, 2013, 553, A122.
7. C. Ma et al., The International Celestial Reference Frame as Realized by Very Long Baseline Interferometry, In Astronomical Journal, 1998, 116, 516–546.
8. P. M. Mathews et al., In Journal of Geophysical Research (Solid Earth), 107, 2068, 2002.

About the Modeling of Radio Source Time Series as Linear Splines

Maria Karbon¹, Robert Heinkelmann¹, Julian Mora-Diaz¹, Minghui Xu², Tobias Nilsson¹, Harald Schuh¹

Abstract Many of the time series of radio sources observed in geodetic VLBI show variations, caused mainly by changes in source structure. However, until now it has been common practice to consider source positions as invariant, or to exclude known misbehaving sources from the datum conditions. This may lead to a degradation of the estimated parameters, as unmodeled apparent source position variations can propagate to the other parameters through the least squares adjustment. In this paper we will introduce an automated algorithm capable of parameterizing the radio source coordinates as linear splines.

Keywords VLBI, radio sources, linear splines, MARS

1 Introduction

Within geodetic VLBI only one global source position for a source's whole VLBI history is estimated. However, many of the observed sources show systematic linear or non-linear behavior and thus influence the stability of the Celestial Reference Frame (CRF), e.g., [1]. Such instabilities, if left unmodeled, will distort the estimated values of the other parameters [2, 3]. To minimize these effects, only sources considered to be stable are entered into the celestial datum definition, the so called ICRF2 (second realization of the International Celestial Reference Frame: [4]) defining sources. Their selection was based on statistical properties of the time series, the observational history, and their position in

the sky to guarantee an optimal geometric distribution. However, not all defining sources remain stable over longer time spans, and statistics can be misleading [5, 6]. Thus, we decided to parameterize the source coordinates with linear splines to allow variations, which additionally will allow us to include the so called special handling sources in the datum, making use of the long observational history of these sources.

2 Data and Data Analysis

For our study we used 4,170 VLBI sessions observed within the years 1980 and 2013. We restricted the sessions to those which have a globally distributed station network that includes more than 10^{15} m³. For each session we estimated the positions of all sources which had more than three observations; otherwise they were constrained to their a priori positions. In the first step the NNR condition for the celestial datum definition was applied to the ICRF2 defining sources. The parameterization for the other parameters was similar to what is described in [7]. From this we were able to get time series of 38 special handling sources and 3,048 sources which are neither defining nor special handling sources, the so called 'other' group. To get the positions of the 265 defining sources within our solution free of datum constraints, we divided the datum sources into two groups (Figure 1). To estimate the positions of one group, the other was included into the NNR condition, and vice versa.

1. GFZ German Research Centre for Geosciences

2. Shanghai Astronomical Observatory

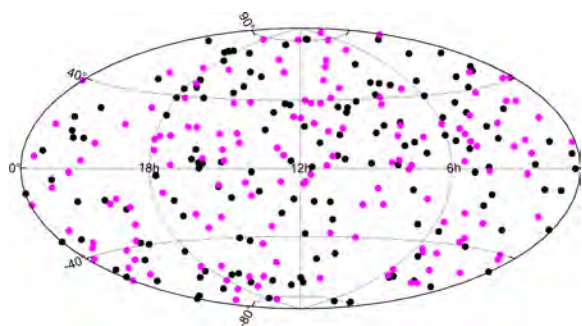


Fig. 1 ICRF2 defining sources, in magenta (light gray) and black, the two groups used for the datum definition to estimate the respective other group.

3 Time Series of the Sources

80% of the sources contained in our data set are observed in fewer than five sessions, with 2,660 sources falling in the ‘other’ group but also two defining sources being that poorly observed. Figure 2 shows a pie chart of the relative and absolute numbers of sources observed in more than five but less than 100 sessions (15% of the total number of sources), and sources observed in more than 100 sessions (less than 7% out of the total). As one can see, the biggest group (47%) is formed again by sources from the ‘other’ category observed in five to 100 sessions. However, the 131 defining sources which are well-observed (in more than 100 sessions), only amount to 19%, and almost exactly the same number is observed in fewer than 100 sessions. Further, most of the special handling sources are very well-observed, but due to the fact that source position variations are not modeled, they cannot be introduced as datum sources.

Within ICRF2 the assessment of the stability of the source positions was done through statistics, e.g. weighted root mean square, standard deviation, and χ^2 per degree of freedom, while other authors, e.g. [5], use the Allan deviation [8]. That is problematic as these measures depend on the size of the sample, and further, especially in the case of the Allan variance, on the sampling length. The number of sessions per source, or the observation period of a source in years (criteria used for ICRF2), alone do not guarantee that either necessity is fulfilled.

To illustrate that issue, we plotted in Figure 3 three sources which are well-observed; in red (left plots) are $d\alpha$ and $d\delta$ for the special handling source 4C39.25

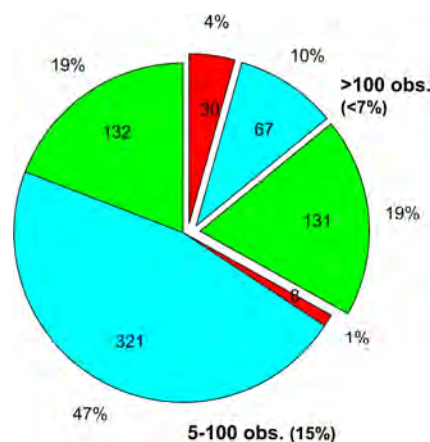


Fig. 2 Number of sources which are observed in 5—100 sessions and more than 100, color coded regarding their class; green (intermediate shading): defining, red (darkest shading): special handling, cyan (lightest shading): other.

observed in 3,098 sessions, in green (middle plots) are plots for the defining source 0420-014 observed in 1,032 sessions, and in cyan (right plots) are plots of 0602+673 of the ‘other’ group observed in 759 sessions. In black the semi-annual mean values are plotted. The special handling source is very well-sampled within the whole time span, although more sparsely within the first and last years. Nevertheless, the evolution of the source position variation is well resolved. The defining source for which we have position estimates for the same time span, however, shows huge gaps in the time series. For such a time series the mean values might still give reasonable results as the sample size is big enough. Still, the investigation of spectral characteristics using the whole time span is destined to fail due to the large gaps. This source further shows from the mid ‘80s until the mid ‘90s clear systematics in the $d\alpha$ coordinate, comparable in magnitude and time span to the special handling source 4C39.25 — a characteristic we do not want for defining sources. The ‘other’ source 0602+673 on the right, however, shows a very stable behavior for both components from 2002 until 2008; then systematics in $d\delta$ emerge.

Considering all of this, we suggest to abandon the classification of sources into special handling and defining sources. Not only is the determination of the stability of the source position highly dependent on the properties of the time series and the statistics applied, but also a source which shows no systematics during one time period can exhibit variations at other

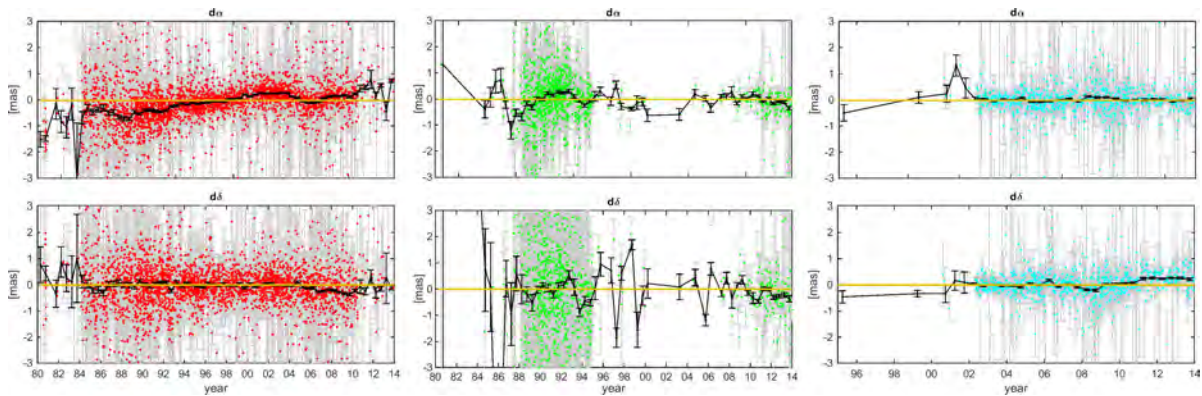


Fig. 3 In red (left plots) are the coordinates of special handling source 4C39.25, in green (middle) are defining source 0420-014's plots, and in cyan (right) are 'other' source 0602+673's plots. All have their error bars in gray. The semi-annual mean values are in black, with corresponding error bars.

times, and vice versa. Also, with increasing precision of the VLBI technique, the demands on the accuracy of the sources are increasing. Thus, holding onto such stability criteria will inevitably lead to a shrinking number of sources suitable for the datum definition. Instead we propose to parameterize the source position variations with linear splines, allowing them the freedom to change — an approach similar to what has been successfully used for years for the station positions.

4 Parameterization of Source Positions with Linear Splines

When parameterizing the source positions with linear splines, one faces the practical problem of the large number of sources. As any manual approach is out of the question when confronted with more than 6,600 time series, we looked for an adequate automated tool. We found what we needed in the MARS algorithm [9], which is a method for flexible regression modeling delivering continuous linear splines. The model consists of a weighted sum of basis functions $B_i(x)$, where each c_i is a constant coefficient.

$$\hat{f}(x) = \sum_{i=1}^n c_i B_i(x), \quad (1)$$

Each basis function $B_i(x)$ is a constant, a hinge function, or a product of two or more hinge functions. Hinge functions take the form of

$$\max(0, x - \text{const}) \quad \text{or} \quad \max(0, \text{const} - x). \quad (2)$$

To find the ideal set of basis functions, it relies on a fast least squares update technique, trying to minimize the sum-of-squares residual error. The only input data the algorithm needs is the time series and its error information, in our case the single estimates for each source coordinate for each session with its standard deviation.

5 The Linear Splines Determined by MARS

Figure 4 shows the estimates of the source positions of the special handling source 4C39.25 in red (left plots) and estimates of the 'other' source 0602+673 in cyan (right), overlaid with the spline determined by MARS in blue. Both are determined by entering all ICRF2 defining sources into the NNR condition, which is the most robust procedure. As one can see, the MARS spline follows to great extent the semi-annual mean values (plotted in gray). Only where the estimates show larger uncertainties does the algorithm downweight the positions considerably; thus the segmentation of the spline remains unaffected. This can be seen at the beginning of the time series of 4C39.25, where the data is not only more sparse, but also less reliable.

In magenta (lightest thick horizontal line) and black (darkest line) the splines determined through the time series produced by the two different groups of defining sources are plotted. The overall agreement for both sources is good, as expected, although in the first years of 4C39.25 larger differences appear. This is linked to

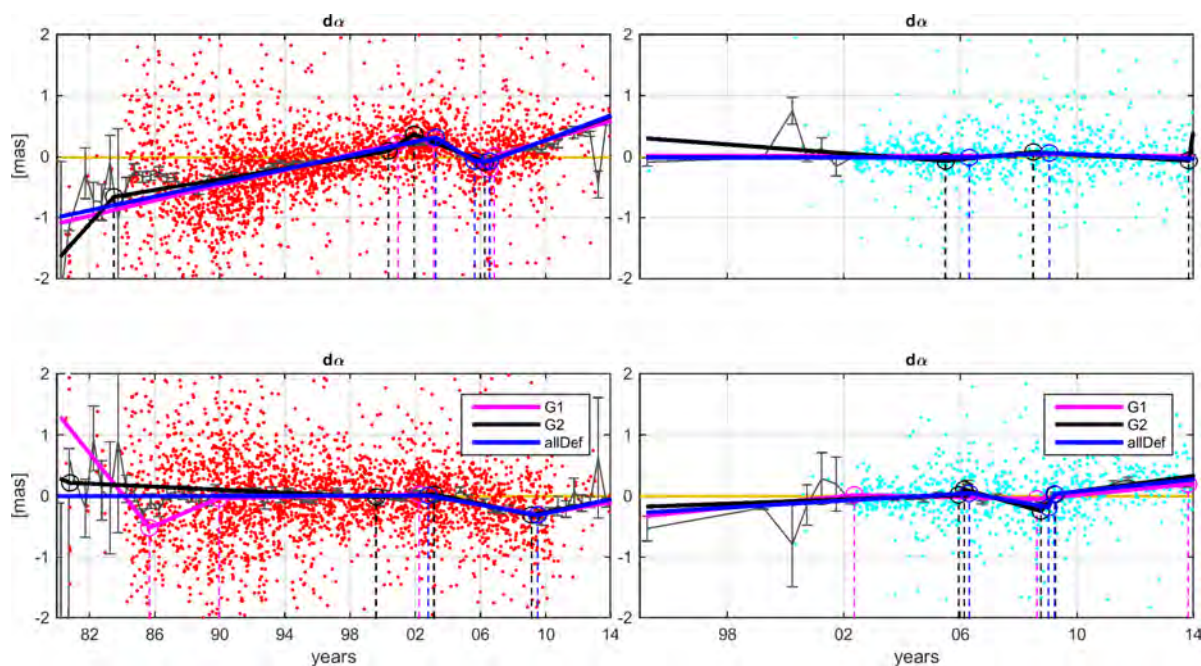


Fig. 4 In red (left) are the coordinates of special handling source 4C39.25, in cyan (right) are the ‘other’ source 0602+673’s coordinates, and in gray are the semi-annual mean values. The time series is determined with all ICRF2 defining sources in the datum, overlaid with the corresponding MARS spline in blue (horizontal line with intermediate shading). The MARS spline when using Group 1 as datum is in magenta (lightest horizontal line) and when using Group 2 is in black (darkest horizontal line).

the generally worse geometry due to the little number of sources observed in the early years of VLBI. Hence, the geometry suffers when halving the datum sources, as it is done within the grouping. A similar effect cannot be seen in the splines determined for source 0602+673, where the splines agree also well when the data is sparse. Here, we look at a source which was introduced to the VLBI observing schedule much later, where the accuracy of the VLBI system was much higher and the geometry, both in the celestial and terrestrial networks, more stable. Anyway, for sources which are not defining, such problems do not appear, as the best datum definition, i.e., all ICRF2 defining sources, is chosen. However, it comes into play when determining the splines for said defining sources.

To assess this effect, we calculated for the defining source 0420-014 an additional solution, where all ICRF2 defining sources are in the NNR condition, except this one. This additional spline is plotted in Figure 5 in cyan (dashed line). The spline which shows the least movement is the one in magenta (lightest horizontal line). This one is produced with the time series determined when Group 1 defines the datum; source 0420-014 is part of this group. This seems to be the net-

work configuration which allows this source the least movement. However, Group 2 (black) and the solution where only this source was excluded from the ICRF2 defining sources (cyan) deliver the exact same spline (alternating, dashed line). This proves that our grouping of the defining sources does not deteriorate the spline determination. The solution where all ICRF2 defining sources are entered into the NNR condition (blue, darker solid line), including 0420-014, meanders between the others, but shows similar features as the black and cyan spline.

6 Conclusions

VLBI analysis can acknowledge the fact that sources have structure that changes over time. Instead of excluding such sources from the datum, which would inevitably lead to a declining number of defining sources as the capabilities of the VLBI system increase, we could model these variations. In this work we present one possible approach to how to parameterize source positions with linear splines. In conclusion, it can be

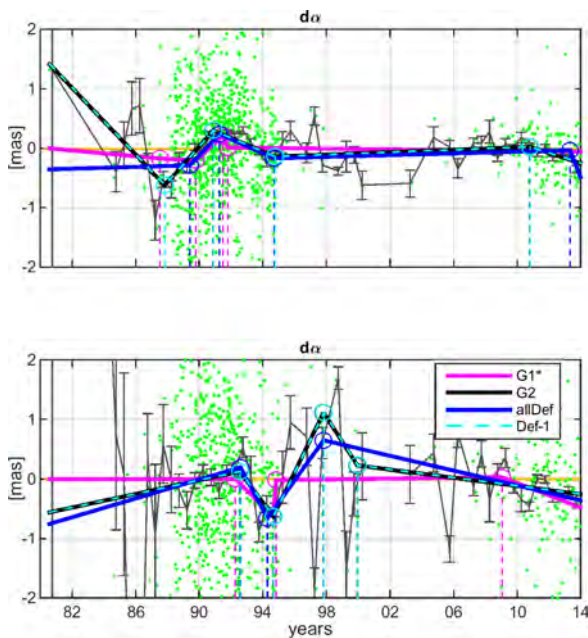


Fig. 5 In green the coordinates of the defining source 0420-014, in gray the semi-annual mean values. Time series determined with Group 2 in the datum (0420-014 is in Group 1); overlaid with the corresponding MARS spline in black (dark part of dashed line). The MARS spline when using Group 1 as datum is in magenta (lighter solid line), when using ICRF2 defining is in blue (darker solid line), and when only excluding this source from the ICRF2 defining is in cyan (light part of dashed line).

said that the crucial aspect of the definition of such splines is the sampling of the data. Whenever the time resolution is good, all the splines, independent of the datum definition and the type of source, agree at a reasonable level. However, whenever the observations get sparse and the reliability of the estimated positions low, the spline depends more on the definition of the datum. Thus, if we want to model the time evolution of the sources the continuous monitoring of VLBI radio sources is indispensable. Results of the application of such splines in the VLBI data analysis are planned to be presented in a paper in the Special Issue of the Journal of Geodesy: VLBI contribution to reference frames and Earth's rotation studies.

Acknowledgements

This work was supported by the Deutsche Forschungsgemeinschaft, DFG. Project number: HE 5937/2-1

References

- [1] P. Charlot, D. A. Boboltz, A. L. Fey, E. B. Fomalont, B. J. Geldzahler, D. Gordon, C. S. Jacobs, G. E. Lanyi, C. Ma, C. J. Naudet, J. D. Romney, O. J. Sovers, and L. D. Zhang. THE CELESTIAL REFERENCE FRAME AT 24 AND 43 GHz. *Astronomical Journal*, 139(5), 2010.
- [2] M. Feissel-Vernier, C. Ma, A. M. Gontier, and C. Barache. Sidereal orientation of the Earth and stability of the VLBI celestial reference frame. *Astron Astrophys*, 438:1141–1148, 2005.
- [3] D. S. MacMillan and C. Ma. Radio source instability in VLBI analysis. *J Geod*, 81:443–453, 2007.
- [4] A. L. Fey, D. Gordon, C. S. Jacobs, C. Ma, R. A. Gaume, E. F. Arias, G. Bianco, D. A. Boboltz, S. Boeckmann, S. Bolotin, P. Charlot, A. Collioud, G. Engelhardt, J. Gipson, A. M. Gontier, R. Heinkelmann, S. Kurdubov, S. Lambert, S. Lytvyn, D. S. MacMillan, Z. Malkin, A. Nothnagel, R. Ojha, E. Skurikhina, J. Sokolova, J. Souchay, O. J. Sovers, V. Tesmer, O. Titov, G. Wang, and V. Zharov. The Second Realization of the International Celestial Reference Frame by Very Long Baseline Interferometry. *The Astronomical Journal*, 150(2), 2015.
- [5] A. M. Gontier, K. Le Bail, M. Feissel, and T. M. Eubanks. Stability of the extragalactic VLBI reference frame. *A&A*, 375:661–669, 2001.
- [6] M. Karbon, R. Heinkelmann, Julian Mora-Diaz, Minghui Xu, Tobias Nilsson, and Harald Schuh. About the extension of the parametrization of the radio source coordinates in geodetic VLBI and its impact on the time series analysis. *J Geod*, 2016. submitted.
- [7] R. Heinkelmann, T. Nilsson, M. Karbon, L. Liu, C. Lu, J. A. Mora-Diaz, E. Parselia, V. Raposo-Pulido, B. Soja, M. Xu, and H. Schuh. *IVS 2014 General Meeting Proceedings* chapter The GFZ VLBI solution—characteristics and first results. Science Press, Shanghai, China, ISBN 978-7-03-042974-2, 2014.
- [8] D. W. Allan. Statistics of atomic frequency standards. *Proc IEEE*, 54, 1966.
- [9] J. H. Friedman. Multivariate Adaptive Regression Splines. *The Annals of Statistics*, 19(1):1–141, 1991.

Completing the K-band Celestial Reference Frame in the North

A. de Witt¹, A. Bertarini², C.S. Jacobs³, J. Quick¹, S. Horiuchi⁴, T. Jung⁵, J. Lovell⁶, J. McCallum⁶, G. Bourda⁷, P. Charlot⁷

Abstract 22 GHz (K-band) radio observations have the potential to form the basis for the most accurate celestial reference frame ever constructed. Relative to the standard 2.3/8.4 GHz (S/X) observing bands, K-band is expected to exhibit a reduction in extended source morphology and core-shift. This reduction in astrophysical systematics should allow for a more stable celestial reference frame at K-band and should also be advantageous in tying the VLBI radio frame to the Gaia optical frame. The current K-band catalog consists of only 279 sources from ten Very Long Baseline Array (VLBA) sessions producing uncertainties in source positions at the $\sim 100 \mu\text{s}$ level. Given that southern K-band observations in the mid-south and over the south polar cap are under way, this paper returns attention back to the north. Further, given that the VLBA's 2 Gbps data rate is now 16 times better than that used in the original northern K-band observations, the resulting four-fold increase in sensitivity makes now an opportune time to re-visit K-band celestial frame work in the north. Therefore, we have initiated a new program of astrometric and imaging observations in the north using the VLBA to improve K-band astrometric precision and spatial coverage as well as to map the intrinsic source structure so that their astrometric quality can be evaluated. Our goal is to have at least 500 sources in the final K-band reference frame. This paper discusses the ini-

tial results from the first two of four approved K-band VLBA sessions.

Keywords Celestial frame, K-band, VLBA, source structure, ICRF-3.

1 Background

At the standard S/X frequencies, many ICRF radio sources exhibit spatially extended structure that may vary in both time and frequency, degrading the accuracy of estimated source positions.

On VLBI scales sources tend to become more compact and show reduced core-shift at shorter wavelengths (higher frequencies). Both of these improvements allow for a more well-defined and stable reference frame at higher frequencies, such as K-band. This will be particularly advantageous in tying the VLBI reference frame to future optical reference frames such as Gaia. Astrometric and imaging observations by Lanyi et al. (2010) and Charlot et al. (2010) provide a foundation for the development of a reference frame at K-band.

The current K-band catalog (see Figure 1) consists of only 279 sources with weak coverage in the southern hemisphere, several localized regions with no sources, and median uncertainties in source positions at the $\sim 100 \mu\text{s}$ level. Dedicated observations to improve the precision and spatial coverage of the K-band CRF are currently underway.

1. Hartebeesthoek Radio Astronomy Observatory, Krugersdorp, South Africa

2. IGG & MPIfR, Bonn, Germany

3. JPL, California Institute of Technology/NASA, Pasadena, CA

4. CSIRO/NASA, Tidbinbilla, Australia

5. Korea Astronomy and Space Science Institute, Daejeon, Korea

6. University of Tasmania, Hobart, Tasmania, Australia

7. Laboratoire d'Astrophysique de Bordeaux, Floirac, France

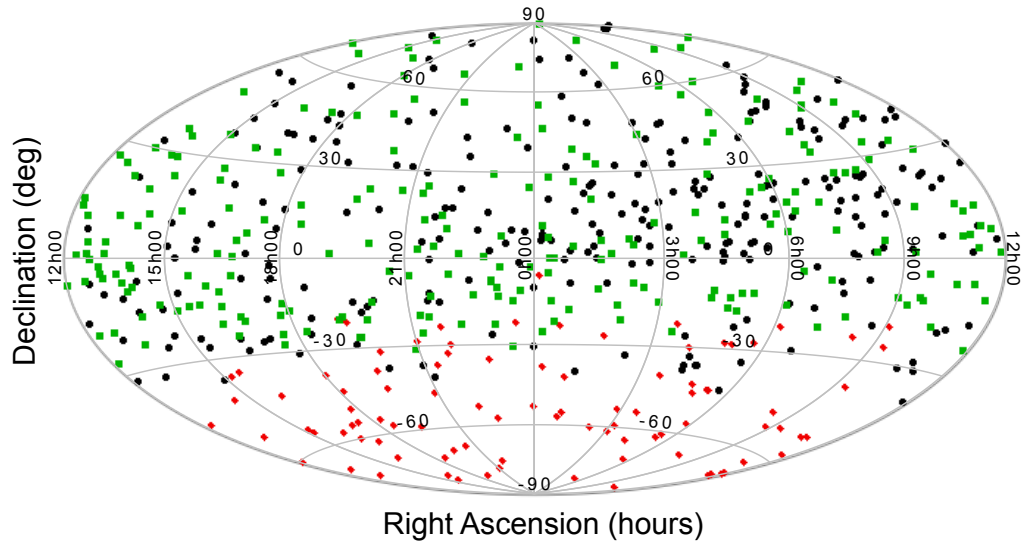


Fig. 1 The 279 sources from Lanyi et al. (2010) and Charlot et al. (2010) are shown in black. The 246 sources being observed using the VLBA are shown in green. The 106 sources from the southern astrometric observations are shown in red (de Witt et al. 2015).

2 Goals

Our goal is to realize by 2018 a full-sky, K-band celestial frame with accuracy better than $70 \mu\text{s}$ to match the Gaia predicted accuracy for visual magnitudes at $V \approx 18$. We are also aiming to densify the K-band frame in the north using the Very Long Baseline Array (VLBA) and to produce a sky coverage in the southern hemisphere comparable in density and accuracy to that obtained from the astrometry done with the VLBA in the northern hemisphere. Figure 1 shows the sky coverage at K-band of previously observed sources plus the additional sources that we are in the process of observing. In black are the 279 sources previously observed by Lanyi et al. (2010) and Charlot et al. (2010); in green are the 246 sources currently under observation using the VLBA; in red the 106 sources coming from the southern hemisphere observation program using South Africa to Australia baselines (de Witt et al. 2015). Thus Figure 1 shows the need for improving the sky coverage both in the south (red sources) and the north (green sources).

3 K-band CRF in the North

We have partially completed a project, BJ083, with the VLBA to observe 264 sources. The source list is based

upon the 8.4/32 GHz (X/Ka) catalog (Jacobs, 2014). The selection criteria were set to have sources above about -30° declination and flux cut-off of $\sim 100 \text{ mJy}$. Two of the four 24-hour sessions scheduled were already observed. There are two additional VLBA observing sessions already approved which will be used to observe the rest of the sources from our list of 264 total candidates.

4 Preliminary Imaging Results from the VLBA

Our imaging pipeline started with correlation using DiFX (Deller et al, 2007), fringe fitting with PIMA (Petrov, 2011), and finally the imaging itself used DIFMAP (Shepherd, 1997). For the astrometric observable extraction, the data were fringe fitted using the Haystack Observatory Postprocessing System (HOPS). Physical modeling and parameter estimation will use JPL's MODEST software (Sovers, Fanelow, Jacobs, 1998).

We now have initial results for 108 sources from our first VLBA session (BJ083a: 2015 Jul 21). Figure 2 shows images and visibility plots (north is up and east is to the left) for a representative sample of six out of the total of 108 sources analyzed so far.

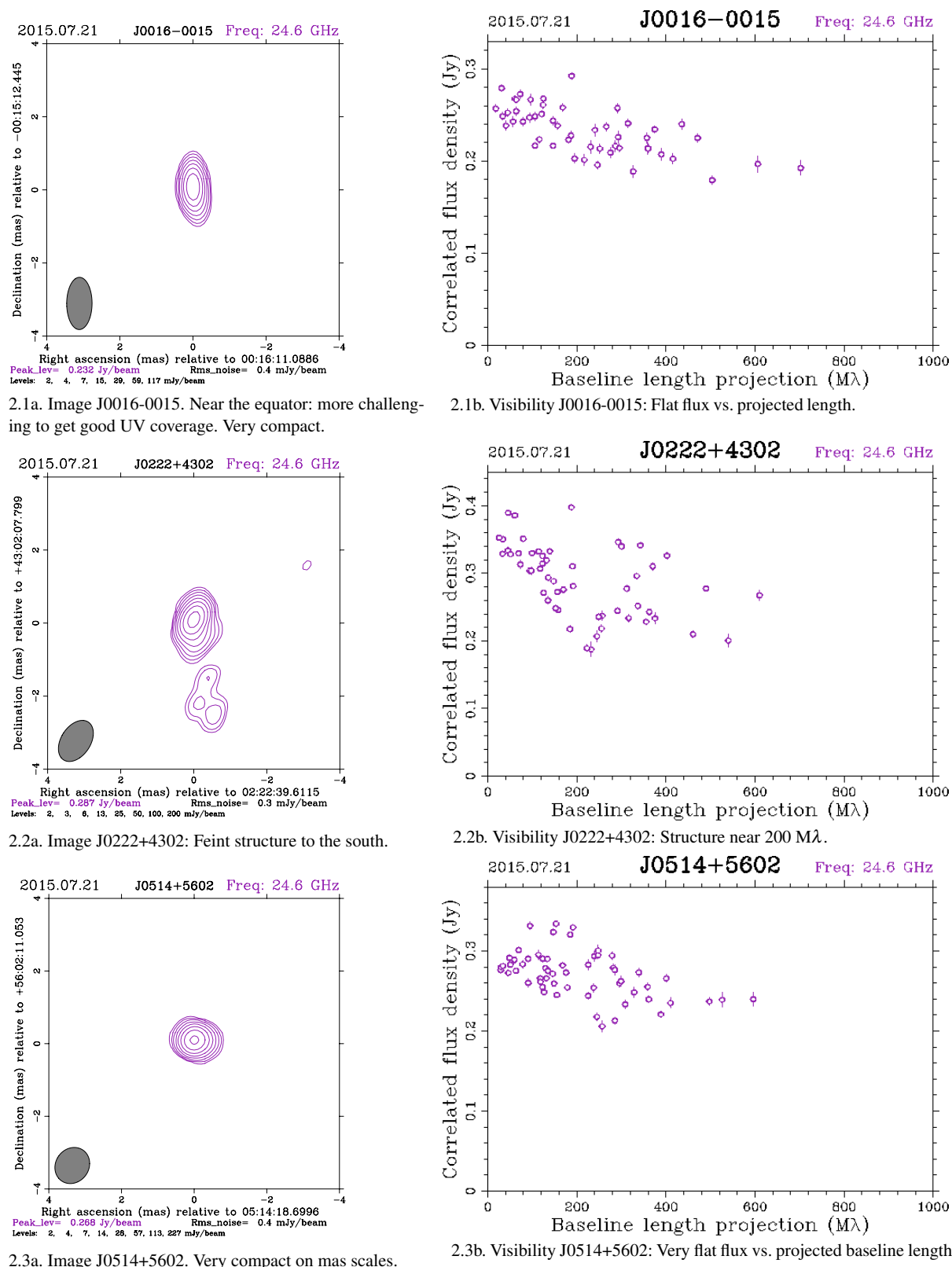
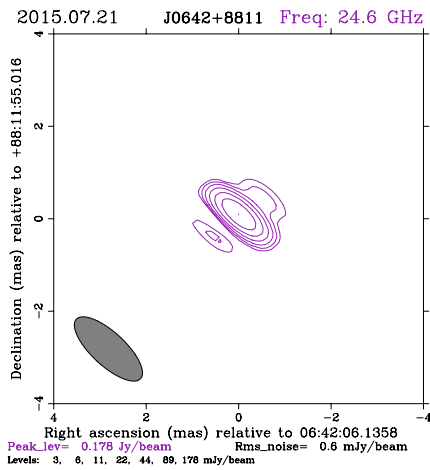
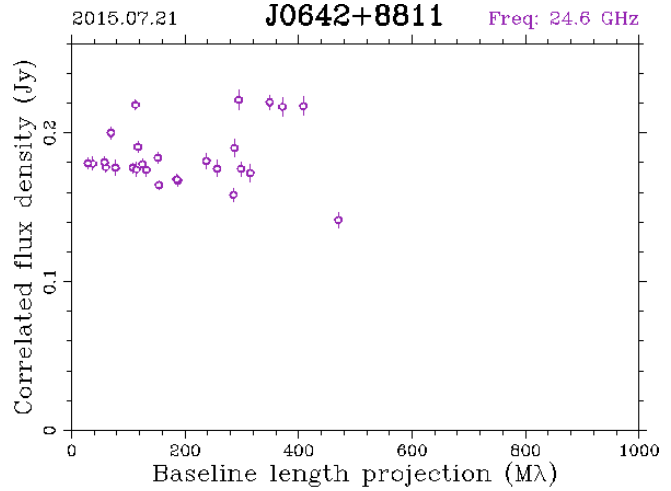


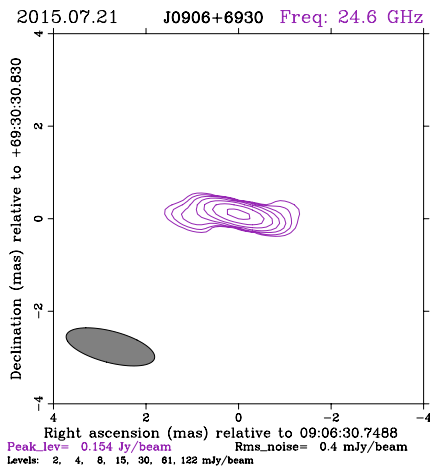
Fig. 2 Images and visibility plots from VLBA K-band CRF data.



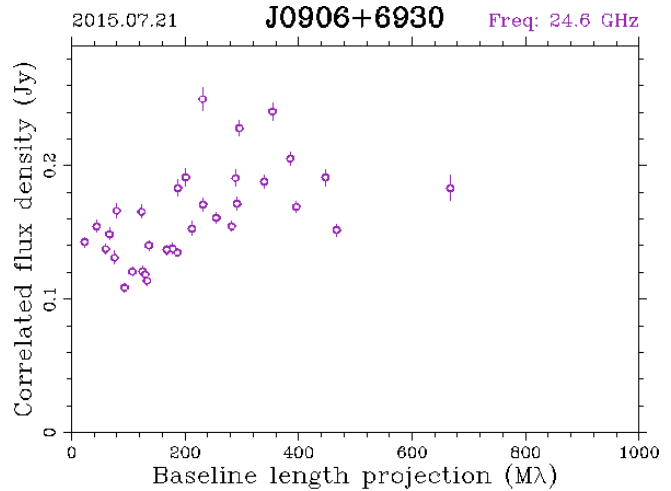
2.4a. Image J0642+8811. Extended to NE. Source is within 2° of North pole: potential for excellent UV coverage.



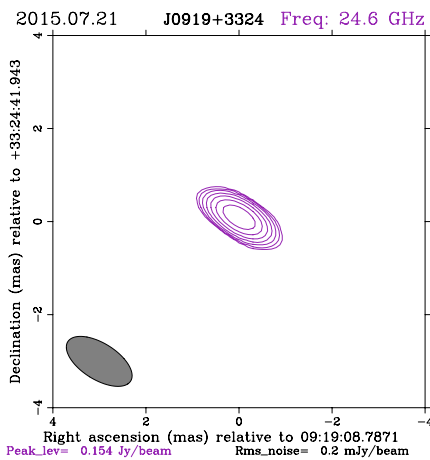
2.4b. Visibility J0642+8811.



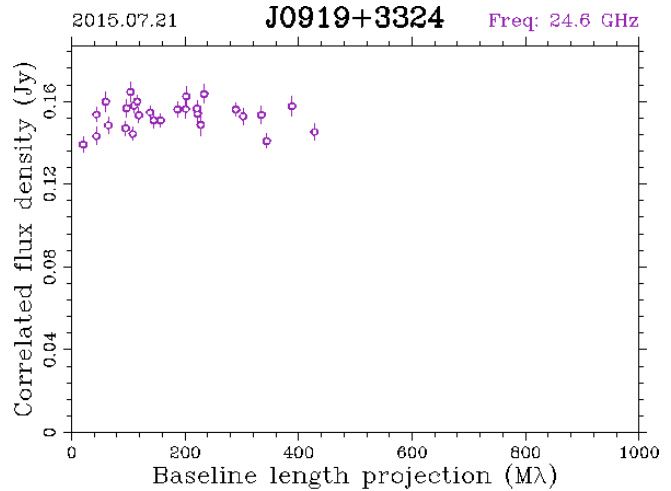
2.5a. Image J0906+6930. At redshift 5.5 this is the most distant quasar in our celestial frame. Circumpolar sources allow good UV coverage. Note anti-symmetric extension.



2.5b. Visibility J0906+6930. Redshift 5.5. Note the increasing flux vs. projected baseline length.



2.6a. Image J0919+3324. Very compact on mas scales.



2.6b. Visibility J0919+3324. Very flat flux vs. projected length.

Fig. 2 Images and visibility plots from VLBA K-band CRF data (cont'd).

These six sources were chosen to represent a wide range of declinations ($\delta = 0^\circ$ to $\delta = 88^\circ$) which leads to wide range of potential UV coverages. In particular, sources north of $\delta \approx 60^\circ$ will be above the horizon at all times and thus have potential for excellent UV coverage from the rotation of the baselines through the 24-hour session. On the other hand, given that the VLBA is an all northern array, sources near the equator such as J0016–0015 will be visible for a rather limited range of hour angles and thus the UV coverage in general will be at a disadvantage compared to circumpolar sources. We have also included some sources at mid-northern declinations (J0919+3324, J0222+4302) and a near circumpolar source (J0514+5602) to give a wide sampling of the expected quality of UV coverages.

5 Conclusions

In an effort to realize a more accurate celestial reference frame by leveraging more compact source structures and smaller core shifts, we have begun a program of observations at K-band.

We report here on our northern K-band VLBA program from which 108 of 264 planned sources have now been mapped. Work to complete images of all 264 sources and to estimate astrometric positions is underway. This northern data, when combined with our complementary southern program using HartRAO, AuScope, and Tidbinbilla, is expected to produce a full-sky K-band reference frame with a median precision of $\approx 70 \mu\text{as}$ by 2018 in order to be considered the ICRF-3 (radio) and to be ready for comparison with the Gaia (optical) frame.

Acknowledgements

HartRAO is a facility of the National Research Foundation, South Africa. U.S. government sponsorship is acknowledged for NASA portions of this work. The Na-

tional Radio Astronomy Observatory's VLBA is a facility of the National Science Foundation operated under cooperative agreement by Associated Universities, Inc. This work made use of the Swinburne University of Technology software correlator, developed as part of the Australian Major National Research Facilities Programme and operated under license. ©2016: All rights reserved.

References

1. P. Charlot, et al., The Celestial Reference Frame at 24 and 43 GHz. II. Imaging, *AJ*, 139, 1713, 2010.
2. A. T. Deller, S. J. Tingay, M. Bailes and C. West, DiFX: A Software Correlator for Very Long Baseline Interferometry Using Multiprocessor Computing Environments *PASP*, 119, 318, 2007.
3. A. de Witt et al., A Celestial Reference Frame at 22 GHz (K-band), in *Proceedings of the 22nd European VLBI Group for Geodesy and Astrometry Working Meeting*, 18–21 May 2015, Ponta Delgada, Azores, 2015.
4. C. S. Jacobs et al., The X/Ka Celestial Reference Frame: Results from combined NASA-ESA baselines including Malargüe, Argentina, in *Proceedings of the 8th IVS General Meeting*, Shanghai, China, 2014.
5. G. E. Lanyi et al., The Celestial Reference Frame at 24 and 43 GHz. I. Astrometry, *AJ*, 139, 1695, 2010.
6. Y. Petrov, Y. Y. Kovalev, E. B. Fomalont and D. Gordon, The Very Long Baseline Array Galactic Plane Survey–VGaPS, *AJ*, 142, 35, 2011.
7. M. C. Shepherd, Difmap: an Interactive Program for Synthesis Imaging, *ASP Conf. Series*, 125, 77, 1997.
8. O. J. Sovers, J. L. Fanselow and C. S. Jacobs, Astrometry and geodesy with radio interferometry: experiments, models, results, *Reviews of Modern Physics*, 70, 1393, 1998.

Source Characterization by the Allan Variance

C. Gattano, S. Lambert

Abstract Until now, the main criteria for selecting geodetic sources were based on astrometric stability and structure at 8 GHz [6]. But with more observations and the increase of accuracy, the statistical tools used to determine this stability become inappropriate with regards to sudden motions of the radiocenter. In this work, we propose to replace these tools by the Allan Variance [1], first used on VLBI sources by M. Feissel-Vernier [3], leading to a new classification of sources into three groups according to the shape of the Allan Variance. In parallel, we combine two catalogs, the Large Quasar Astrometric Catalogue [13] and the Optical Characteristics of Astrometric Radio Sources [10], in order to gather most physical characteristics known about these VLBI targets. By doing so, we may reveal physical criteria that may be useful in the selection of new targets for future VLBI observations.

Keywords VLBI, Allan Variance, source stability, source classification

1 Introduction

The need for stable sources on the celestial sphere has existed for a long time, because they are used to materialize a non-rotating universe around the Earth and realize a so-called quasi-inertial reference frame. Such a frame is fundamental, because the physical laws are expressed only through it—otherwise inertial forces have to be applied to explain observed motions. One princi-

pal application of the celestial reference frames is the study of the Earth orientation parameters (EOP), five in total, which characterize the change of Earth orientation with respect to the non-rotating universe due to solar system objects' attraction and to geophysical response.

In 1999, the commonly approved celestial reference frame (CRF) changed from a catalog of stars to a catalog of extragalactic objects seen through Very Long Baseline Interferometry (VLBI), the ICRF1 [9]. During its construction, a particular interest was put on the selection of the defining sources (DS), which are the most stable sources that carry the axes of the frame. The method used was based on arbitrary thresholds of observation time history and uncertainties of position adjustments through VLBI analysis. Then, a source was rejected if it showed significant position differences when two random subsets were statistically oriented in the same directions. Sources presenting a non-linear motion or a large source structure were also rejected. By doing so, 212 DS were selected out of 608 sources. A first extension added 59 sources to the catalog. A second extension added 109, and the DS subset was reconsidered to 207 [5].

In 2001, Gontier et al. [7] investigated the stability of the CRF and produced an automatic algorithm to iteratively deselect sources from the DS subset based on the time behavior and statistical approach. They got 242 DS for their most stable frame. In 2003, Feissel-Vernier [3] introduced the use of the Allan Variance in conjunction with the observation history and linear drift. She obtained 199 DS, and in 2006 an extension was released based on this method, in order to increase the number of DS [4]. This extension competed with ICRF work.

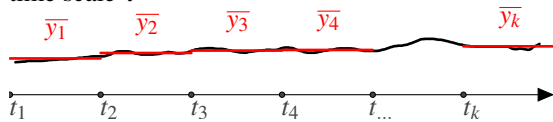
SYRTE, Observatoire de Paris, PSL Research University, CNRS, Sorbonne Universités, UPMC Univ.

In 2009, the second realization of the ICRF [6] was released based on a method close to the ICRF1 approach but taking the time behavior into account. However, in the process the Allan Variance was replaced by the classical variance of the position time series. In this context, it can also be noted that one improvement of the ICRF2 was to take into account the declination coverage in the DS subset.

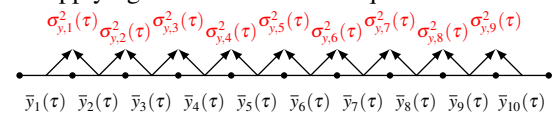
Since then, the ICRF2 has been used as reference frame. But seven years have passed, new source observations have been added to the observational history, and no study has been presented to refine the DS subset with respect to stability. It is obvious that things must have changed, and we propose here to again use the Allan Variance to determine the stability of the VLBI sources with more than 100 observing sessions, i.e., 202 sources, and select the stable ones. In Section 2, we explain the principle of the Allan Variance and its modified form. In Section 3, we present its application to the 202 most observed VLBI sources and detail the three subsets based on Allan Variance tendencies. In Section 4, we analyze our results together with the physical characteristics from the Large Quasar Astrometric Catalogue (LQAC [13]) and the Optical Characteristics of Astrometric Radio Sources (OCARS [10]), and finally we draw some conclusions.

2 The Tool: Allan Variance

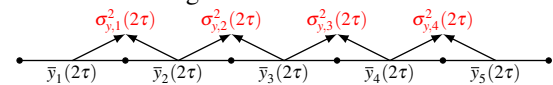
A. Regular sampling of the function with a minimal time scale τ



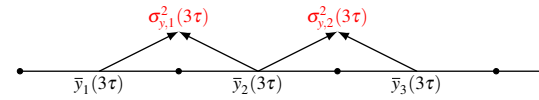
B. Applying the Allan Variance equation



C. Increasing the time scale $\tau \rightarrow 2\tau$ and applying the Allan Variance again



D. Further increasing the time scale



E. Average all $\sigma_{y,i}^2(k\tau)$ for each time scale $k\tau$

Let $y(t)$ be a continuous time function. Given a time scale τ , samples can be computed using

$$\bar{y}_k = \overline{y(t_k)} = \frac{1}{\tau} \int_{t_k}^{t_k+\tau} y(u) du$$

In the case of VLBI data \bar{y}_k is obtained by averaging the observations inside a sliding window of width τ , using as weights the squares of the formal uncertainties.

The Allan Variance [1] is a statistical tool that can study the dispersion of a signal between peers:

$$\sigma_y^2(\tau) = \frac{1}{2} \langle (\bar{y}_{k+1} - \bar{y}_k)^2 \rangle \quad (1)$$

Rather than study the dispersion around the mean, as with the true variance, we study the variation between two successive samples given a time sampling $k\tau$.

Table 1 Connection between the type of noise, its spectral density behavior, and the Allan Variance tendency.

White noise	$\Rightarrow S_y(f) \propto f^0 \Rightarrow \sigma_y^2(\tau) \propto \tau^{-1}$
Flicker noise	$\Rightarrow S_y(f) \propto f^{-1} \Rightarrow \sigma_y^2(\tau) \propto \tau^0$
Random Walk noise	$\Rightarrow S_y(f) \propto f^{-2} \Rightarrow \sigma_y^2(\tau) \propto \tau^{+1}$

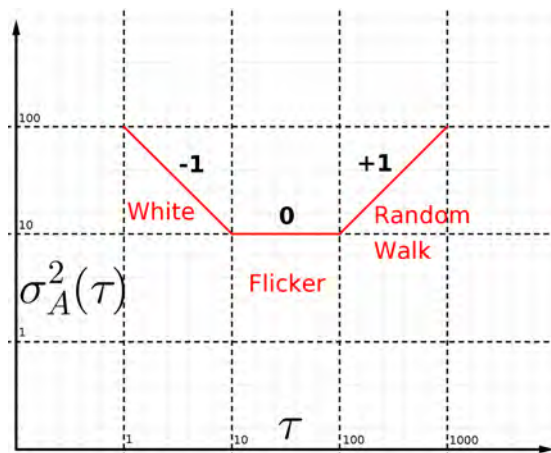


Fig. 1 Allan Variance tendencies with respect to the type of noise.

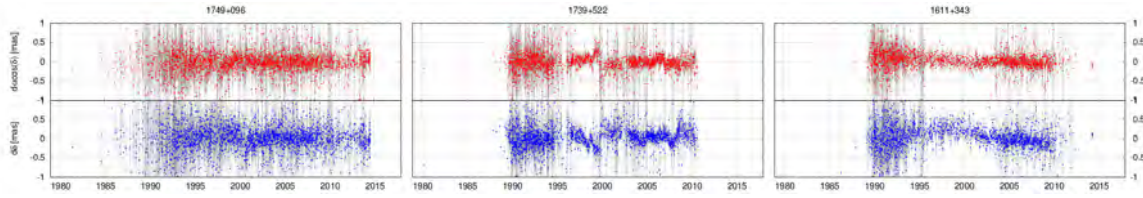


Fig. 2 Examples of radio source coordinate time series from CALC/SOLVE VLBI data analysis. The upper graph shows $d\alpha \cos(\delta)$ with respect to the temporal mean position, while the lower graph shows $d\delta$ with respect to the mean position.

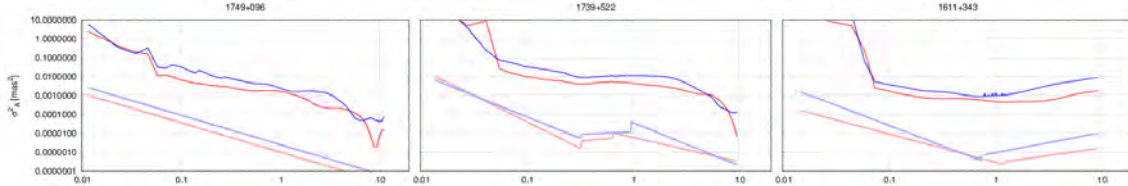


Fig. 3 Allan Variance in $d\alpha \cos(\delta)$ in red (lighter lines) and $d\delta$ in blue (darker lines) of the previous sources and their linear piece-wise adjustment (from left to right): Allan 0 example, Allan 1 example, and Allan 2 example.

VLBI time series can show several types of noise from white noise (or thermal noise) to colored noise such as flicker noise (random jump at random time) and random walk noise. These noise types differ in their spectral density $S_y(f)$ by a different exponent in the power law that leads to different behavior of the Allan Variance.

It is to be noted that in this work we used the modified Allan Variance with the particularity that we do not fill the observation gaps present in most of the time series.

$$\begin{aligned} \text{mod } \sigma_y^2(n\tau) &= \frac{1}{2n^4(M-3n+2)} \times \\ &\sum_{j=1}^{M-3n+2} \left\{ \sum_{i=j}^{j+n-1} \left(\sum_{k=i}^{i+n-1} \bar{y}_{k+n} - \bar{y}_k \right) \right\}^2 \end{aligned} \quad (2)$$

3 The Coordinates Time Series

In order to study the stability of the VLBI radio sources, we worked on the coordinate time series of those targets. We used CALC/SOLVE to analyze all the VLBI non-Intensive sessions available from the IVS Data Centers, and we applied a special treatment to get the time series rather than obtaining them from the independent solution mode.

We obtained time series from ten different solutions where 9/10 of the sources are estimated globally (i.e., one position for all sessions) and 1/10 locally (i.e., one

position per session). These ratios were applied separately to defining sources and standard sources (others except the non-linear ones) in order to keep the no-net-rotation constraint (NNR) on 9/10 of the ICRF2 defining sources for a solution with a common subset of at least 8/10 DS when we compare two solutions. A supplementary solution, similar to a typical CRF solution from IVS analysis, enables us to get time series for 39 non-linear sources (NL).

In Figure 2, we show examples of three most observed VLBI sources: 1749+096, 1739+522, and 1611+343. The red (lighter) points are offset in $\alpha \cos \delta$ from the mean position, and the blue (darker) points are offset in δ .

4 Results

We applied the Allan Variance (AV) to VLBI sources present in more than 100 sessions after removing outliers. Then, we modeled AV tendencies by linear piece-wise functions between local minima and maxima. In Figure 3, we show the results for our three examples. AV tendencies are down-shifted, represented by straight red (lighter) lines for $\alpha \cos \delta$ and by blue (darker) lines for δ .

We defined three subsets characterized by the shape of the AV tendencies. The first case, called Allan 0 (e.g., Figure 3 left), gathers sources with a decreasing behavior with respect to an increasing time scale on both $\alpha \cos \delta$ and δ data. It means that we increase the

accuracy of position adjustment if we take into account more and more observations. Such sources are the most suited to define axes of a CRF.

The second case, Allan 1 (e.g., Figure 3 middle), gathers sources that keep a decreasing behavior for a large time scale but at lower ones show a reverse tendency and therefore a degradation of the dispersion on position. It means that the sources have presented some sort of motion, but if we take a sufficiently large observation time range, the phenomenon is averaged, and we get improvements back on position adjustment accuracy. Because of the motion, their usefulness for defining the frame axes is questionable.

The last case and the worst one, called Allan 2 (e.g., Figure 3 right), gathers sources that present an increasing tendency over large time scales. For those sources, adding observations foretell a degradation of the accuracy of its adjustment, and such sources seem not suited for defining the axes of a frame.

In the case of getting different statuses from $\alpha \cos \delta$ and δ , the worst one is selected and associated with the source. In Figure 4, we resume the classification of our sample. A score is also determined by the quadratic sum of the global minima of the Allan Variance in both coordinates, in order to sort them inside each group.

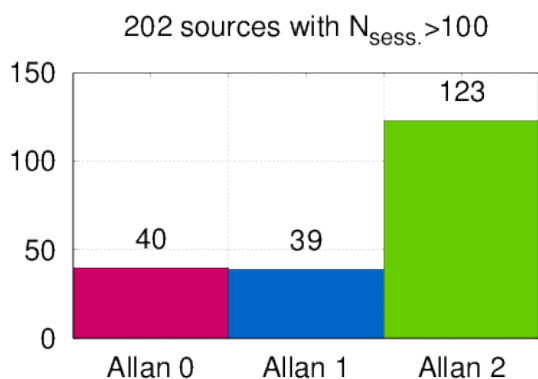


Fig. 4 Number of sources with more than 100 observing sessions in each category in our new classification w.r.t. stability.

5 Analysis and Discussion

In Figure 5, we present the comparison of our classification with respect to the ICRF2 repartition: defining sources (DS), non-linear sources (NL), other sources

(Std). In Figure 6, the comparison is made with respect to the redshift taken from the third version of the LQAC [13], which is a compilation of large quasar surveys for several parts of the sky. Note that not all VLBI source redshifts are known. And then, Figure 7 shows the result of the comparison with respect to the type of the object taken from OCARS [10].

The first thing to notice is that this new classification seems not to be in agreement with the repartition of the ICRF2. This can be an effect of the new sessions observed between 2010 and 2016, or it can show that one or the other method is not relevant to determine the stability of a radio source. We plan to apply our methodology to the ICRF2 data, i.e., stop the observation in 2009 in order to conclude if the two methodologies are truly different.

On the other hand, we see that stability with respect to the Allan Variance does not show a dependence on the type of the AGN, i.e., on different orientations of the sources with respect to the line of sight [2, 14]. There may be a dependence on redshift with an optimum between 1 and 2, but it is difficult to conclude because of the low number of sources with redshift greater than 2. Nevertheless, this is not a surprise because cosmology theory tells us that at some redshift, the angular diameter distance of an object increases instead of decreases [8]. For an Einstein-de-Sitter model, the value is between 1 and 1.5.

The stability of the sources may be strongly linked to what happens around the black hole(s), resulting in (multiple-)core emission or (multiple-)beam emission as it is, for instance, shown by the numerical model of Roland et al. [11]. An instability may be seen directly in the observations by the luminous variability of the radio-center, explained in detail by Shabala et al. [12].

6 Conclusions

This work introduces a method to classify VLBI sources by means of the Allan Variance. The result is in disagreement with the ICRF2 classification with regard to stability, and we have to understand why. It could be a divergence between methodologies, or it could be a consequence of the new observations from 2010 to 2016 not available at the time of the ICRF2. We do not succeed in finding a common physical characteristic, especially on the type of the source,

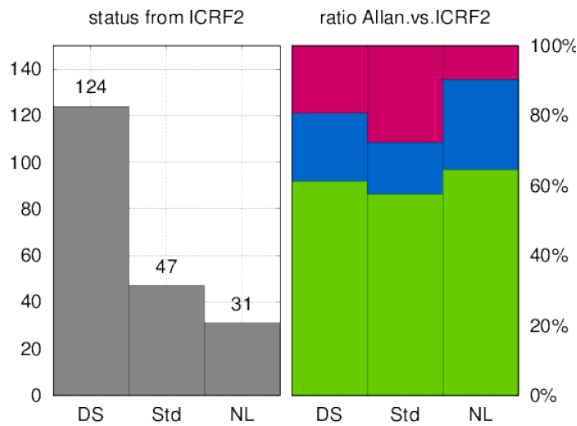


Fig. 5 Repartition of our new classification with respect to the ICRF2 classification: histogram (left); ratio (right). DS = defining sources, Std = standard sources, NL = non-linear sources.

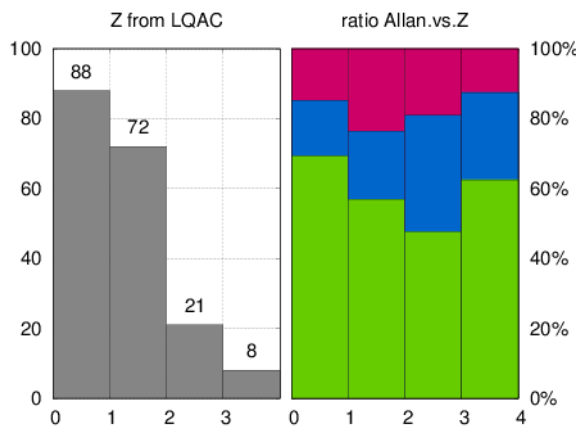


Fig. 6 Repartition of our new classification with respect to the redshift: histogram (left); ratio (right).

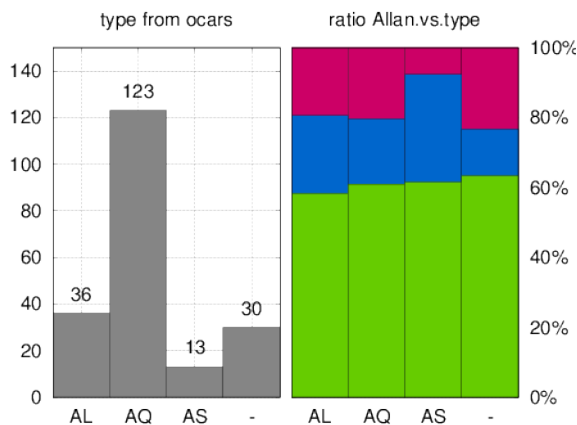


Fig. 7 Repartition of our new classification w.r.t. the type of Active Galactic Nuclei: histogram (left); ratio (right). AL = Blazar, AQ = quasar, AS = Seyfert.

whereas it is advised to select BL-Lacs and Blazars as geodetic VLBI targets to get stable sources because of a collimated beam in the line of sight. The study reveals a preferred redshift value of $1 \sim 1.5$ as good targets as the cosmology theory tells us.

In another work presented in these proceedings, we study the effect of using this classification in the selection of defining sources for the celestial reference frame construction.

References

1. D.W. Allan, Statistics of atomic frequency standards, In IEEE Proceedings, 1966, 54, 221–230.
2. R. Antonucci, Unified models for active galactic nuclei and quasars, In Annual Review of Astron and Astrophys, 1993, 31, 473–521.
3. M. Feissel-Vernier, Selecting stable extragalactic compact radio sources from the permanent astrometric VLBI program, In Astronomy and Astrophysics, 2003, 403, 105–110.
4. M. Feissel-Vernier et al., Analysis strategy issues for the maintenance of the ICRF axes, In Astronomy and Astrophysics, 2006, 452, 1107–1112.
5. A.L. Fey et al., The Second Extension of the International Celestial Reference Frame: ICRF-EXT.1, In Astronomical Journal, 2004, 127, 3587–3608.
6. A.L. Fey et al., The Second Realization of the International Celestial Reference Frame by Very Long Baseline Interferometry, In Astronomical Journal, 2015, 150, 58.
7. A.M. Gontier et al., Stability of the extragalactic VLBI reference frame, In Astronomy and Astrophysics, 2001, 375, 661–669.
8. D.W. Hogg, Distance measures in cosmology, In ArXiv Astrophysics e-prints, 1999.
9. C. Ma et al., The International Celestial Reference Frame as Realized by Very Long Baseline Interferometry, In Astronomical Journal, 1998, 116, 516–546.
10. Z. Malkin, Optical Characteristics of Astrometric Radio Sources OCARS, In Izvestiia Glavnoi rossiiskoi astronomicheskoi observatorii, 2013, 220, 507–510.
11. J. Roland et al., Structure of the nucleus of 1928+738, In Astronomy and Astrophysics, 2015, 578, A86.
12. S.S. Shabala et al., The effects of frequency-dependent quasar variability on the celestial reference frame, In Journal of Geodesy, 2014, 88, 575–586.
13. J. Souchay et al., The third release of the Large Quasar Astrometric Catalog (LQAC-3): a compilation of 321 957 objects, In Astronomy and Astrophysics, 2015, 583, A75.
14. C.M. Urry, P. Padovani, Unified Schemes for Radio-Loud Active Galactic Nuclei, In Publications of the ASP, 1995, 107, 803.

How Good is the Deep Southern Sky

S. Basu^{1,2,3}, A. de Witt², S. Shabala³, J. McCallum³, J. Quick², A. Bertarini^{4,5}

Abstract The Celestial Reference Frame Deep South (CRDS) observing sessions are part of a program to strengthen the International Celestial Reference Frame (ICRF) in the South and are coordinated by the International VLBI Service for Geodesy and Astrometry (IVS). The aim of the CRDS sessions is to provide astrometric results from Very Long Baseline Interferometric (VLBI) observations for improving the current ICRF, but also to extend and densify the ICRF by observing new sources. The effect of source structure variability on VLBI astrometric positions can be significant, and it is important to map these sources on a regular basis. In this paper we present our most recent results from our efforts to provide VLBI maps from the CRDS astrometric observations. In the future, continual analysis of CRDS observations will allow us to monitor the sources for structural changes so that their astrometric quality can be evaluated regularly.

Keywords VLBI, IVS, ICRF: quasars, CRDS, imaging

1 Introduction

High-precision Very Long Baseline Interferometry (VLBI) measurements of positions of extra-galactic radio sources are used to define and maintain celestial reference frames (CRF) with sub-milliarcsecond (sub-mas) precision. Early efforts at defining a celestial reference frame using VLBI observations of extra-galactic radio sources led to the realization of the International Celestial Reference Frame (ICRF) [10]. The second extension of the ICRF (ICRF-Ext.2) [4] contained 212 ‘defining’ sources (sources of high astrometric quality) along with 294 ‘candidate’ sources (sources with insufficient observations) and 102 ‘other’ sources (sources with excessive position variations).

The current realization of the celestial reference frame (ICRF-2) [6] is based on dual frequency 2.3-GHz (S-band) and 8.4-GHz (X-band) VLBI observations of 3,414 extra-galactic radio reference sources, including 295 ‘defining’ sources which determine the orientation of the frame axes. In 2012, the need for a more uniform spatial coverage of sources and uniform accuracy in source coordinates led to the formation of an International Astronomical Union (IAU) working group, with the goal of the realization of the next generation celestial reference frame (ICRF-3) [9], to be completed by 2018.

The primary sources used to define and maintain the ICRF are radio-loud quasars. To maintain the highest accuracy in astrometry and geodesy, it is desired to use sources where the radio emission is compact or core-dominated with a point-like structure. However, many of the extra-galactic sources that make up the ICRF exhibit spatially extended intrinsic structures on mas scales. The extended emission structures in these

1. University of South Africa, Pretoria, South Africa
2. Hartebeesthoek Radio Astronomy Observatory, Krugersdorp, South Africa
3. School of Physical Sciences, University of Tasmania, Australia
4. Institute for Geodesy and Geoinformatics, University of Bonn, Germany
5. Max Planck Institute for Radioastronomie, Germany

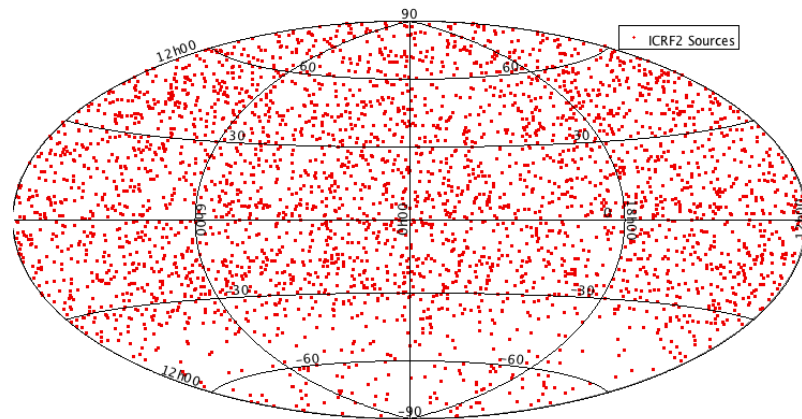


Fig. 1: Distribution of sources in the ICRF-2 catalog on an Aitoff equal plane projection of the celestial sphere. The deficit of sources south of -30° can clearly be seen.

sources may also change with observing frequency and can evolve significantly over timescales of months to years. It is well-known that the effect of source structure on astrometric VLBI positions can be significant and that structure and flux density variability are directly related to the precision of geodetic solutions [14]. It is therefore important to map the structures of these sources on a regular basis.

Another method to assess astrometric source quality for application to the ICRF is the source structure index (SI), which is the median value of the structure delay corrections computed from VLBI source maps [3]. The ICRF sources are categorized according to their SI value, where the best astrometric sources receive a structure index of 1 and sources with an SI of 3 and 4 are considered not suitable for geodetic or high-precision astrometric VLBI observations. A list of SI values for all ICRF-2 sources can be found in Fey et al. [5]. Flux density information can also be used as an estimate of the compactness of a source, e.g. [11], where source compactness (SC) is defined as the ratio of core flux density to total flux density.

Catalogs of compact radio sources, including the ICRF-2, are weak in the south (see Figure 1), especially at declinations south of -45° , the limit of the reach of northern baselines. There have been many efforts in recent years to increase the number of known reference sources and to densify the ICRF in the south e.g. [13, 8]. There have, however, only been a few imaging observations of reference sources in the south, e.g.

[7, 11, 12], and dedicated campaigns to map and monitor source structure prove to be difficult, with the availability of antennas being one of the most limiting factors in the south. As a result, we investigated the possibility of imaging source structure from existing astrometric and geodetic observations in the south. We identified the Celestial Reference Frame Deep South (CRDS¹) astrometric VLBI observations to be suitable for mapping purposes, and first imaging results were obtained in 2014 [1].

In this paper we present multi-epoch imaging results as well as the calculated structure indices and source compactness values for two of the sources in our sample. Results were obtained from CRDS astrometric observations at both 2.3 and 8.4 GHz.

2 Session Selection

We selected the CRDS astrometric sessions for imaging purposes based on the following criteria:

- The majority of sources observed are south of -40° declination.
- Sessions from 2013 onwards have at least four stations per scan, as opposed to more typical astrometric sessions where only two-station scans are required.

¹ Information about the CRDS is available on the Web at <http://ivscc.gsfc.nasa.gov/program/master>



Fig. 2: Map of station positions from the CRDS experiments.

- All sessions have at least two scans per source, with a maximum of seven scans per source.
- The scan duration is not based on minimum SNR per baseline, but set at a minimum of five minutes per scan.
- On average, most sources are observed in at least two to three sessions per year.

The CRDS observing program started in 2011 with six sessions scheduled per year. Since 2013, from CRDS63 onwards, observations have been scheduled using a regular network of six southern stations. In June 2013 the bandwidth was also increased from 4 to 8 MHz (CRDS66 onwards). The telescopes that

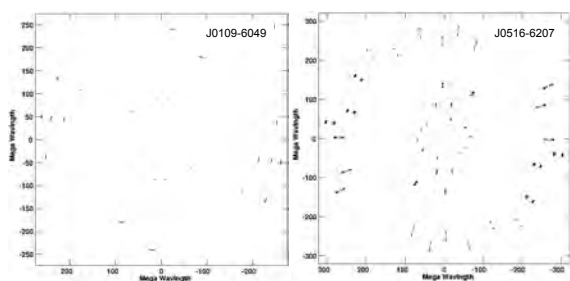


Fig. 3: The u - v plane coverage for two sources at similar declinations but from different CRDS sessions. The u - v coverage plot on the left is from the CRDS63 session in which only four antennas participated, resulting in very poor sampling in the u - v plane. The u - v coverage plot on the right is from the CRDS68 session in which all six antennas participated. The gap in the u - v coverage clearly shows the missing intermediate baseline lengths that results from the absence of telescopes between Australia and South Africa.

telescope in South Africa, the Hobart 12- and 26-m and the Katherine and Yarragadee 12-m telescopes in Australia, and the Warkworth 12-m telescope in New Zealand. A map of CRDS station positions is shown in Figure 2. Representative plots of the u - v coverage for two sources at similar declinations but from different CRDS sessions are shown in Figure 3.

For the purpose of this study we reduced and analyzed data from the CRDS66 session as well as the CRDS68 session for both 2.3 and 8.4 GHz. Observations for CRDS66 were made on 30–31 July 2013, and observations for CRDS68 were made on 27–28 November 2013. Data was recorded at right circular polarization (RCP) with six IFs at S-band and ten IFs at X-band with a bandwidth of 8 MHz per IF. Data was correlated at the Washington Correlator (WACO) in Washington, DC.

3 Data Reduction and Results

The data reduction was done using the NRAO’s Astronomical Image Processing System (AIPS) [2] and included data inspection, editing, and fringe-fitting. Our earlier work on VLBI imaging of CRDS63 proved to be successful, and hence we followed a similar approach in reducing the data for CRDS66 and CRDS68 [1].

In Figure 4 we show representative contour plots at both 2.3 and 8.4 GHz for two of our sources, J0450-8101 and J0538-4405. Plots from two epochs, July 2013 (CRDS66) and November 2013 (CRDS68) are shown. The contour plots for both sources, at both frequencies and epochs, show a compact central object with no extended structure or additional components. Both of these sources are among the ICRF-2 defining sources.

Observations from the LCS experiments at 8.4 GHz also show J0450-8101 to be a very compact source with no extended structures. For J0538-4405, imaging results from the Bordeaux VLBI Image Database (BVID)² using the Very Long Baseline Array (VLBA) show a central compact object with no extended structure at both frequencies.

In Table 1 we also list the SI and SC values for each of the sources, at both frequencies and epochs.

² The Bordeaux VLBI Image Database (BVID) is available from <http://www.obs.u-bordeaux1.fr/BVID/>

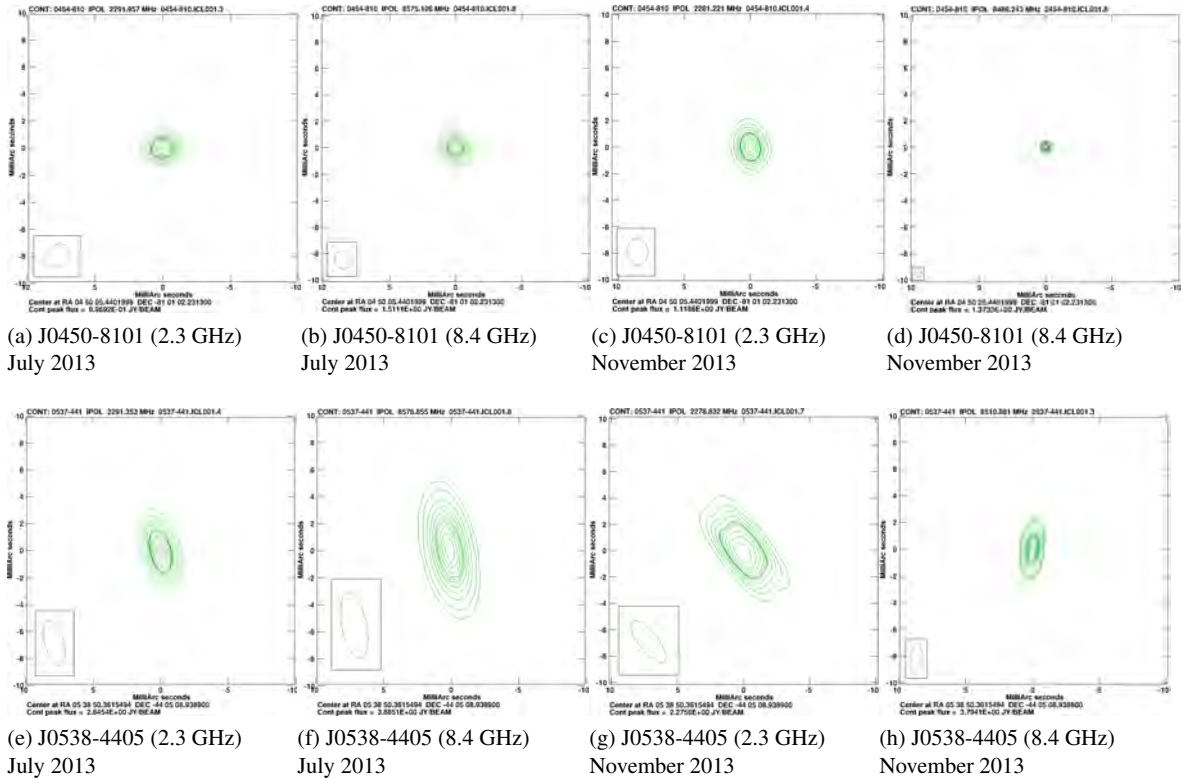


Fig. 4: Contour plots for J0450-8101 (top) and J0538-4405 (bottom) at 2.3 and 8.4 GHz, both for two epochs, July 2013 (CRDS66) and November 2013 (CRDS68). North is up, and East is to the left. The FWHM beamsize is graphically indicated in the bottom left corner. The contour levels are a percentage of the peak brightness and are at 5, 10, 20, 30, 40, 50, 60, 70, 80, and 90%, with the 50% level represented by a thick contour.

For the SC we have taken the core flux density as the CLEANed flux density within one synthesized beam (labelled as Jy/beam for each source in Figure 4) and the total flux density as the sum of all CLEANed components. It should be noted that the source compactness can be greater than 1 for inclusion of negative CLEAN components.

Table 1: SC and SI values for J0450-8101 and J0538-4405 at 2.3 and 8.5 GHz for both epochs, July and November 2013.

Source Name	2.3 GHz (July)	2.3 GHz (Nov.)
J0450-8101	SI=1.48, SC=0.95	SI=1.68, SC=0.85
J0538-4405	SI=1.78, SC=0.85	SI=1.90, SC=0.48
Source Name	8.5 GHz (July)	8.5 GHz (Nov.)
J0450-8101	SI=1.42, SC=1.04	SI=1.07, SC=1.07
J0538-4405	SI=2.03, SC=0.91	SI=1.96, SC=0.90

4 Conclusions

In this paper we provided an overview of the CRDS astrometric observing sessions and we presented some results from our efforts to image sources structure. In order to verify the reliability of our results it is important that we continue to compare the images of those sources also observed in other VLBI programs. In order to further verify the astrometric quality of these sources we will also take into consideration the visibility plots as well as the size of the source. A reasonable estimate of the source size can be obtained by fitting a Gaussian model to the visibility data. Considering all aspects of the CRDS experiment, we believe this project will contribute significantly to future work regarding ICRF source densification in the Southern Hemisphere.

Acknowledgements

We thank Alan Fey, Maria Davis, and David Hall from the United States Naval Observatory (USNO) for use of the data from the CRDS observing sessions. The first author wishes to thank HartRAO, NRF-DST, and University of South Africa for financial support. The research has made use of the IVS database.

References

1. S. Basu, A. de Witt, J. F. H. Quick, A. Bertarini, and L. Leeuw, Multi-epoch Study of Source Morphology in the Southern Hemisphere, In D. Behrend, K. D. Baver, and K. L. Armstrong (eds.), *IVS 2014 General Meeting Proceedings*, Science Press (Beijing), ISBN 978-7-03-042974-2, 426—430, 2014.
2. A. H. Bridle and E. W. Greisen, The NRAO AIPS Project - a Summary, NRAO, Charlottesville, aips memo 87 edn, 1994.
3. P. Charlot. Radio-source structure in astrometric and geodetic very long baseline interferometry, *AJ*, 99, 1309, 1990.
4. A. L. Fey et al. The Second Extension of the International Celestial Reference Frame: ICRF-Ext.1, *AJ*, 127, 3587, 2004.
5. A. Fey, D. Gordon, and C. Jacobs (eds.), The Second Realization of the International Celestial Reference Frame by Very Long Baseline Interferometry, Presented on behalf of the IERS/IVS Working Group, *IERS Technical Note 35*, 29, 2009.
6. A. L. Fey et al. The Second Realization of the International Celestial Reference Frame by Very Long Baseline Interferometry, *AJ*, 150, 58, 2015.
7. F. Hungwe et al. Characterization of long baseline calibrators at 2.3 GHz., *MNRAS*, 418, 2113, 2011.
8. J. Lovell, J. McCallum, S. Shabala, J. Dickey, C. Watson, O. Titov, S. Tingay, C. Reynolds, and J. Morgan, The AuScope VLBI Array, In D. Behrend and K. D. Baver (eds.), *IVS 2012 General Meeting Proceedings*, NASA/CP-2012-217504, 176—180, 2012.
9. Z. Malkin et al. The ICRF-3: Status, plans, and progress on the next generation International Celestial Reference Frame, In Z. Malkin and N. Capitaine (eds.), *Journées 2014 “Systèmes de référence spatio-temporels”*, 3, 2015.
10. C. Ma et al. The International Celestial Reference Frame Realized by VLBI, *IERS Technical Note*, 23, 1997.
11. R. Ojha et al. VLBI Observations of Southern Hemisphere ICRF Sources. I., *AJ*, 127, 3609, 2004.
12. R. Ojha et al. VLBI Observations of Southern Hemisphere ICRF Sources. II. Astrometric Suitability Based on Intrinsic Structure., *AJ*, 130, 2529, 2005.
13. L. Petrov et al. The LBA Calibrator Survey of southern compact extragalactic radio sources - LCS1, *MNRAS*, 414, 2528, 2011.
14. S. Shabala, O. Titov, J. Lovell, J. McCallum, J. Blanchard, C. Watson, and J. Dickey, Quasar Structure Effects on the VLBI Reference Frame: The Case of 1144-379, In D. Behrend and K.D. Baver (eds.), *IVS 2012 General Meeting Proceedings*, NASA/CP-2012-217504, 329—333, 2012.

Source Structure of 0642+449 Derived from CONT14 Observations

M. H. Xu^{1,2}, R. Heinkelmann¹, J. M. Anderson¹, J. Mora-Diaz¹, H. Schuh¹, Guangli Wang²

Abstract The CONT14 campaign features state-of-the-art VLBI data. Therein, the radio source 0642+449 was observed with about one thousand observables each day during the continuous observing period of fifteen days, providing tens of thousands of closure delays, the sum of the delays around a closed loop of baselines. The closure delay is independent of the instrumental and propagation delays and provides valuable additional information about the source structure. An example of the use of this new “observable” for the determination of source structure is given for the radio source 0642+449. This source, as one of the defining sources in the second realization of the International Celestial Reference Frame (ICRF2), is found to have two point-like components with a separation of 425 microarcseconds in right ascension and 47 microarcseconds in declination. The two components are almost equally bright with the flux-density ratio up to 0.92. With the help of recent space VLBI observations at 1.6 GHz, the morphology of 0642+449 could be identified to some extent. The closure delays larger than 1 ns are found to be caused by source structure as well, demonstrating that the structure effect of a source with this simple structure could reach up to tens of nanoseconds, which is at least one magnitude larger than expected. We anticipate our study to be a starting point for more effective determination of the structure effect in VLBI observations without the involvement of radio source images.

Keywords Astrometry, VLBI, galactic nuclei, individual quasar 0642+449

1 Introduction

It is well known that radio source structures are generally asymmetric, time dependent, and frequency dependent. The effect of source structure, however, has been ignored as noise in routine geodetic VLBI data analysis so far. The source structure effect is still very important and challenging for astrometric VLBI, as shown in simulation studies [4, 5]. If VLBI is to achieve its full potential of the realization of the extragalactic Celestial Reference Frame with accuracy at the microarcsecond level and that of the Terrestrial Reference Frame with accuracy of the millimeter level, it is necessary to study and handle the source structure effect more effectively based on the astrometric observations themselves. This is the purpose of this research.

We make use of the closure delay, the sum of the delays around a closed loop of baselines, as a new observable and propose a method to use this new observable for the determination of the source structure effect on the astrometric VLBI observable. We calculate the closure delays, investigate the characteristics of the source structure, and then solve for the source structure effect on each observable. The source 0642+449, one of the ICRF2 defining sources, is selected as a demonstration case for this method. This work has been presented in our journal paper [7].

1. Deutsches GeoForschungsZentrum (GFZ)

2. Shanghai Astronomical Observatory, Chinese Academy of Sciences

2 Data

The data from CONT14¹ observations [3] at X band were used. CONT14, as a campaign of continuous VLBI observations over 15 days with 17 globally distributed stations, was intended to acquire state-of-the-art VLBI data with the highest accuracy of which the then existing VLBI system was capable. Because only 71 radio sources were observed in this campaign, one could expect that most of these radio sources would have enough observations with good uv coverage to get meaningful statistical information from closure delays.

Closure delay is the sum of the delays around a closed loop of baselines. To the accuracy of the second order in delay, the closure delay $\tau_{abc}(t)$ at reference epoch t for three stations a , b , and c , is calculated from geodetic VLBI observations² by using

$$\tau_{abc}(t) = \tau_{ab}(t) + \tau_{bc}(t) - \tau_{ac}(t) + [\dot{\tau}_{bc}(t) \cdot \tau'_{ab}(t) + \frac{1}{2} \ddot{\tau}_{bc}(t) \cdot \tau''_{ab}(t)^2], \quad (1)$$

where, for instance, τ_{ab} is the group delay observable from station a to station b , and τ_{bc} is the group delay observable from station b to station c , for the same wavefront received by three stations. A prime on a delay symbol indicates an absence of dependence on station clock offset, that is, referring to the geometric delay, and a superposed dot and double superposed dots denote differentiation with respect to time once and twice, respectively. The definition and model of closure delay was discussed in detail in our original paper [7]. In geodetic VLBI measurements, by convention, the time tag of VLBI observables is referred to the epoch when the wavefront passes the first station in the baseline. In order to have the three delay observables in the closure refer to the same wavefront, Equation 1 includes the corrections in brackets for the delay for the second baseline in the triangle.

¹ <http://ivscc.gsfc.nasa.gov/program/cont14/>

² For astronomical observations that reference all observables in one scan to the same wavefront, the model of closure delay is quite simple: $\tau_{abc}(t) = \tau_{ab}(t) + \tau_{bc}(t) - \tau_{ac}(t)$.

3 Measurement Noise in VLBI Group Delays

Closure delay is a direct and important criterion of how much the source structure affects delay observables. It also demonstrates the measurement noise in geodetic VLBI observables and thus indicates the accuracy level of delay observables. For a comparison to demonstrate the measurement noise in VLBI observables, the standard deviations of closure delays for unresolved sources, such as 0016+731 and 0727-115, were calculated as well. Source 0016+731 has about 23~300 closure delays and 0727-115 has about 11~200 closure delays. The standard deviation for source 0016+731, which showed a little resolved structure, is about 11 ps, and that for source 0727-115 is about 8 ps. The closure delays for source 0727-115 over 15 days are shown in Figure 1. This figure demonstrates that the closure delays for this source are exclusively smaller than 30 ps.

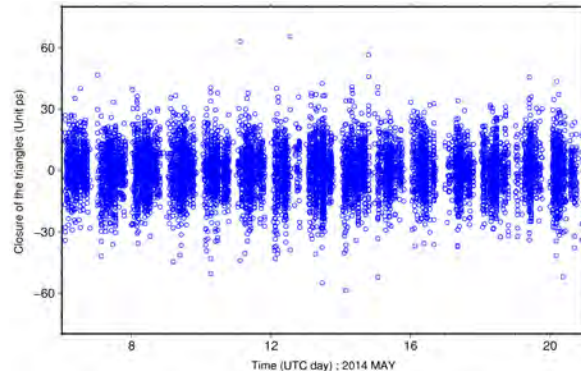


Fig. 1 The closure delays for source 0727-115.

4 Structure of Source 0642+449

The closure delays for source 0642+449 are shown in Figure 2. There are 21~400 closure delays. The mean value and the standard deviation of closure delays is 0.3 ps and 139 ps, respectively, for the closure delays in the range 0 to 1.0 ns. Variations in the closure delays for source 0642+449 sufficiently far away from zero, so that they are unlikely to be caused by random mea-

surement noise, should, in principle, only be observed for sources with significant structure.

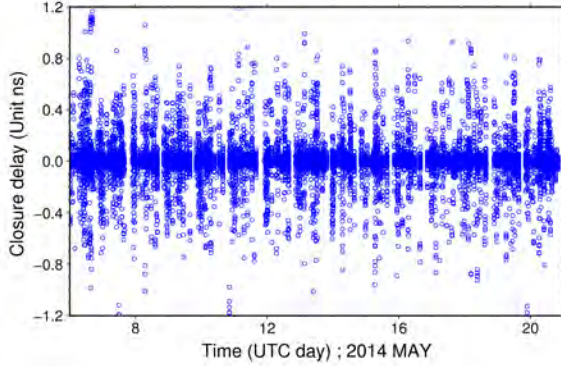


Fig. 2 The closure delays for source 0642+449.

A method was developed to determine the structure delay for each observable based on the closure delays. In an array of N stations, there are at most $N(N-1)/2$ baselines and $N(N-1)(N-2)/6$ closure delay relations. But only $(N-1)(N-2)/2$ of these relations are independent. There are therefore $(N-1)$ too few closure delays to determine the source structure effect for each standard baseline-delay observable, and an independent estimate of the structure delay on $(N-1)$ baselines has to be derived. The investigations in Section 3 give some insight into this; the proposed method uses the assumption that source 0642+449 is a point-like source with respect to the baselines shorter than a certain value. We then choose 7,100 km as the threshold and select a necessary and minimum number of $< 7,100$ km baselines to connect as many stations as possible in each scan. The structure effects on these selected baselines are assumed to be zero. Taking a fifteen-station array as an example, ideally there are fourteen baselines shorter than 7,100 km connecting fifteen stations as a complete connection. Setting the source structure effect on these selected baselines to be zero allows us to solve for the structure effects on other baselines utilizing the closure delays. The next step is to solve as many triangles as possible based on the connection with the threshold of 7,100 km, scan by scan.

Finally, 16~941 triangles were solved, and the source structure effects on 8,492 baseline delays were determined. In this solution, 2,179 observables of short ($< 7,100$ km long) baselines were assumed to have no source structure effect to build up the connection.

Figure 3 shows the uv coverage with color marking the magnitude of the derived source structure effect on each point. In general, the source structure has a strong effect on long baselines along two opposite directions of, approximately, the u axis. The results are divided into two groups for the detailed study of learning the source structure effect.

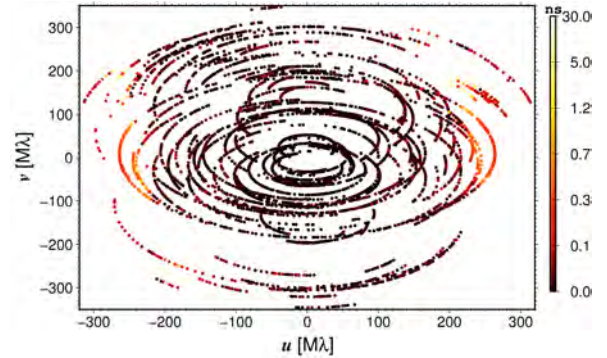


Fig. 3 Coverage of the Fourier domain (uv coverage) of the CONT14 observations of 0642+449 at 8.4 GHz ($\lambda = 3.6$ cm), plotted in units of Mega lambda. Color marks the absolute magnitude of the source structure effect on each of 8,492 observables derived from closure delays [7].

We can determine that the source exhibits a structure with two compact components on baselines with lengths of around 9,000 km. The ratio of the flux densities of the weaker component to the stronger one, K , is about 0.92, because the peak structure effect for these baselines is approximately 0.7 ns.

Thomas (1980) referred the source position in his model to the middle point of the separation between the two components [6], while Charlot (1990) took the centroid point of brightness as the reference point [1]. The reference point does not matter for the closure delay, but we apply the centroid model here, because we assume that observables of short baselines have zero source structure effect, and in practice they are referred very closely to the center of brightness. According to this model, the structure delay τ_s on baseline \mathbf{B} is given as

$$\tau_s = \frac{K(1-K)[1 - \cos(2\pi R)]R}{f(1+K)[K^2 + 2K\cos(2\pi R) + 1]}, \quad (2)$$

where f is the observing frequency, $R = \mathbf{B} \cdot \mathbf{S}_{12}/\lambda$, λ is the wavelength, and \mathbf{S}_{12} is the relative position vector in the uv plane of the weaker component P_2 with respect to the stronger one P_1 .

Because the closure delay is not sensitive to the reference point in the source structure at all, this study lets all observables refer to an unknown point, in this case to the centroid of brightness by the choice of the model, per scan. This reference point will finally be determined through VLBI data analysis. We further assume that the source structure does not change within the fifteen days of observations. A “guess” estimation for the unknown parameters in Equation 2 was made from the results of baselines with lengths from 8,400 km to 9,600 km derived in Section 5. The final estimation was done by model-fitting the closure delays based on the a priori values from the guess estimation. The flux-density ratio is then estimated to be 0.916 ± 0.012 and the relative position vector to be $-426 \pm 12 \mu\text{as}$ in right ascension and $-66 \pm 19 \mu\text{as}$ in declination. According to the detected morphology, a baseline with a length of 7,100 km has $R = 0.41$, and the peak structure effect is only 13 ps, which explains the foundation of the assumption that short baselines have no structure effect, which is used for the connection.

One can easily compute the source structure effect for each observable based on Equation 2 and the two-component model. After using the model to correct the structure effect, the standard deviation of the closure delay was decreased from 139 ps to 90 ps for all triangles, with a closure delay less than 1 ns, which is a significant improvement.

5 Discussion and Conclusions

Using CONT14 observations, the source structure effect is demonstrated at the level of each individual VLBI group delay for the first time. The study reveals that at X band (8.4 GHz) during the CONT14 sessions, the source had two point-like components. The standard deviation of the corrected closure delay was reduced by 36%. Recently, space-VLBI (RadioAstron) observations of this source at 1.6 GHz in 2013 with a resolution of 0.8 mas, \sim four times better than that of ground VLBI images at this wavelength, found that this source has two compact cores separated by 0.76 mas [2] with a position angle of 81° in the sky plane. Because the space VLBI observations were made fourteen months earlier than the CONT14 observations, one may not expect that they were necessarily observing the same blob, but the position angle of the two com-

ponents should be approximately in the same direction. Our result demonstrates that the two components are in the direction of position angle about 261.2° , which is the same direction detected by space VLBI.

It is still challenging to implement the identified source structure to correct the effect in VLBI data analysis. First, an accurate model for the BWS group delay to the level of at least 10 ps needs to be derived. This model should be able to reduce the magnitudes of the closure delays of triangles with the longest baselines to the level of that of small triangles, a few tens of ps. Second, a careful re-study of the linear combination of S and X band data with the presence of source structure would be essential to have an accurate correction for the source structure effect on the combined S/X observable. The attempt to correct structure effect in VLBI data analysis recently has been made by Xu et al. (2016b) [8]. This significant effect should and will be handled in geodetic VLBI.

Acknowledgements

Ming Hui would like to thank the IAG for supporting his travel to South Africa to attend the IVS General Meeting.

References

1. Charlot, P., 1990b, *AJ*, 99, 1309
2. Lobanov, A. P., Gómez, J. L., Bruni, G., et al., 2015, *A&A*, 583, A100
3. Nothnagel, A., 2015, The IVS data input to ITRF2014, International VLBI Service for Geodesy and Astrometry, DOI: <http://doi.org/10.5880/GFZ.1.1.2015.002>
4. Plank, L., Shabala, S. S., McCallum, J. N., et al., 2016, *MNRAS*, 455, 343
5. Shabala, S. S., McCallum, J. N., Plank, L., et al., 2015, *J. Geod.*, 89, 873
6. Thomas, J. B., 1980, “An analysis of source structure effects in radio interferometry measurements”, JPL publication 80-84, JPL, Pasadena, California Dec 15
7. Xu, M. H., Heinkelmann, R., Anderson, J. M., et al., The source structure of 0642+449 detected from the CONT14 observations, 2016, submitted to *AJ*
8. Xu, M. H., Heinkelmann, R., Anderson, J. M., et al., The impacts of source structure on geodetic parameters demonstrated by the radio source 3C371, 2016, submitted to *JoG*

Images of VLBI Calibrators from the BeSSeL Survey

Bo Zhang

Abstract The BeSSeL Survey is a VLBA Key Science project. The primary goal of the survey is to study the spiral structure and kinematics of the Milky Way, by measuring distances and proper motions to masers in regions of massive star formation across large portions of the Milky Way. To measure the distances of Masers via trigonometric parallaxes, the relative positions between the masers and extragalactic VLBI calibrators are determined with phase-referencing at different epochs spanning at least one year. The Masers usually serve as phase reference since they are much stronger than the calibrators, allowing integration times about one hour for the weak calibrators. In addition, the calibrators are often observed through the whole observing program, providing excellent uv-coverage for imaging. From the BeSSeL survey, there will be about 4,000 high-quality images of about 200 VLBI calibrators distributed near the Galactic plane. In this report, we present basic information of the VLBI calibrator images from the BeSSeL survey.

Keywords VLBI, calibrators, astrometry, phase referencing

1 Introduction

Calibrators are important for both absolute and relative VLBI astrometry. For absolute astrometry, VLBI calibrator surveys will help to improve the International Celestial Reference Frame (ICRF), by adding new sources (i.e., QSOs) to densify the grid of the

frame and monitoring the mass structures of the current sources. The space astrometry satellite Gaia has an ambitious aim to construct a dense optical celestial reference frame based on QSOs with unprecedented position accuracy. Aligning the Gaia frame to the ICRF with the highest accuracy will be crucial for ensuring consistency between the measured radio and optical positions. However, only a small number of the current ICRF sources are suitable for this alignment, more common sources from a calibrator survey are important for the optical and radio frame link [2].

For relative astrometry, the achievable accuracy of a differential VLBI measurement is approximately proportional to the angular separation between the calibrator and the target [5]. In other words, the relative astrometry accuracy and image quality of the weak radio source using phase-referencing relies on a dense and accurate grid of bright radio sources [4].

2 VLBI Calibrators

2.1 VLBI Calibrators from Absolute Astrometry

Currently there are about 10,000 calibrators and 45,000 images of 8,000 calibrators (<http://astrogeo.org>). However, most of the calibrators are from absolute astrometry and geodesy programs in snapshot observing mode, which observe the calibrators for a few scans with minutes of integration time. The primary Web sites of image database VLBI calibrators are listed below,

- Radio Reference Frame Image Database (RRFID)
URL: <http://rorf.usno.navy.mil/rrfid.shtml>

The RRFID contains snap-shot VLBA S/X band and K/Q band images and some LBA X band images.

- Bordeaux VLBI Image Database (BVID)
URL: <http://www.obs.u-bordeaux1.fr/m2a/BVID>
The BVID contains a total of 4,499 VLBI images of 1,212 extragalactic radio sources, including VLBI images at S/X and K/Q band.
- Astrogeo VLBI Image Database
URL: <http://astrogeo.org>
On this Web site, the VLBI image database of compact radio sources provides 45,000 images of active galactic nuclei in radio waves, including images from many calibrator surveys using the VLBA, EVN, KVN, KaVA, and LBA.

2.2 VLBI Calibrators from Relative Astrometry

For relative astrometry, phase referencing is one of the most important observing modes which observe a weak target and one or more nearby calibrators alternately or simultaneously, using the derived delay, delay rate, and phase corrections from the calibrators to remove their effects from the target source visibility, increasing the integration time to hours for weak target sources. This technique allows relative position measurements of target-calibrator source pairs, and imaging weaker objects [1]. VLBI phase-referencing is widely applied in a wide range of astrophysics studies and space navigation. However, currently there are no image databases for calibrators from VLBI relative astrometry, i.e., phase-referencing.

3 Calibrators from the BeSSeL Survey

3.1 BeSSeL Survey

The BeSSeL Survey (Bar and Spiral Structure Legacy Survey) is a VLBA Key Science project. Detailed information about BeSSeL can be found on its Web site (<http://bessel.vlbi-astrometry.org>). The primary goal of the survey is to study the spiral structure and kinematics of the Milky Way, by measuring distances

and proper motions to masers (6.7 and 12 GHz CH₃OH and 22 GHz H₂O masers) in regions of massive star formation across large portions of the Milky Way. To measure the distances of masers via trigonometric parallaxes, the relative positions between the masers and extragalactic VLBI calibrators are determined with phase-referencing at different epochs spanning at least one year. As shown in Figure 1, over 100 distances to high-mass star-forming regions have been measured with trigonometric parallaxes by the VLBA, VERA, and EVN [6]; the shapes and widths of the spiral arms of the Milky Way were determined by these measurements.

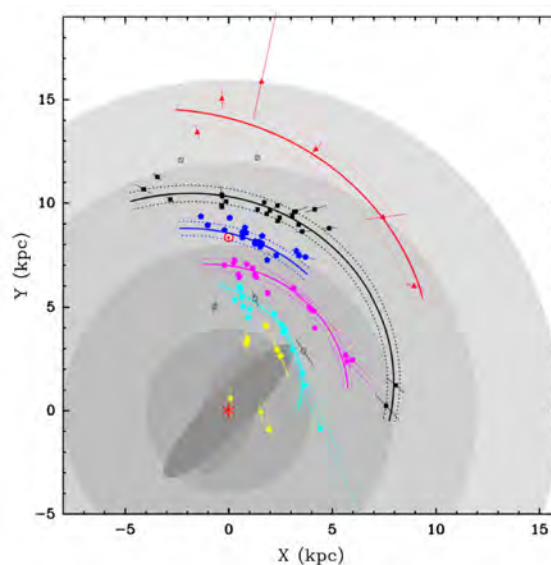


Fig. 1 Plane view of the Milky Way showing the locations of high-mass star forming regions with trigonometric parallaxes measured by the VLBA, VERA, and the EVN [6].

An important byproduct of the BeSSeL survey would be the images of VLBI calibrators. Except for searching new calibrators in snapshot mode [3], BeSSeL also monitors many VLBI calibrators at different frequencies and different epochs. The masers usually serve as phase reference since they are much stronger than the calibrators, allowing several hours' integration times for the weak calibrators. In addition, the calibrators are often observed throughout the whole observing program, providing excellent uv-coverage for imaging. Therefore, BeSSeL will provide a high

quality VLBI calibrator image database, which is very important for astrometric and astrophysical studies.

3.2 BeSSeL Calibrators

There are about 200 VLBI calibrators observed in BeSSeL, and about 40% of them have no VLBI images. For each calibrator at different frequencies, there are at least four images obtained at different epochs spanning at least one year. There are about 130 and 110 calibrators to be observed at K- and C-band, respectively. Whereas for Ku band, there are about 15 calibrators. For some calibrators, the numbers of observing epochs are larger than 60. In total, BeSSeL has about 500 VLBA programs at different epochs as shown in Table 1. For each epoch, there are about eight calibrators. Thus, there are about 4,000 images for all calibrators.

Table 1 BeSSeL VLBA programs.

Program code	Sub-code	Epochs	Freq. Band	Time range
BR145	B-Y	189	K/Ku	2010.4–2013.12
BR149	B-U	83	K	2012.9–2014.4
BR198	A-V	131	C/K	2013.9–2015.4
BR210	A-F	96	C/K	2015.2–2016.10

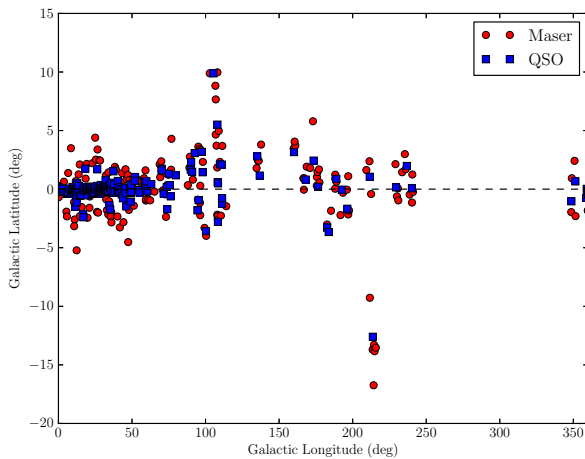


Fig. 2 Sky distribution of Maser sources and calibrators from the BeSSeL survey in Galactic coordinates.

3.2.1 An Example of VLBI Calibrator Images

Here, we show an example of the calibrator images from VLBI phase-referencing observations under the VLBA program BR198C4 at C-band (6.7 GHz). In this program, we observed three group of target and calibrators. Figure 3 shows the sky distribution of one target and three calibrators in the first group.

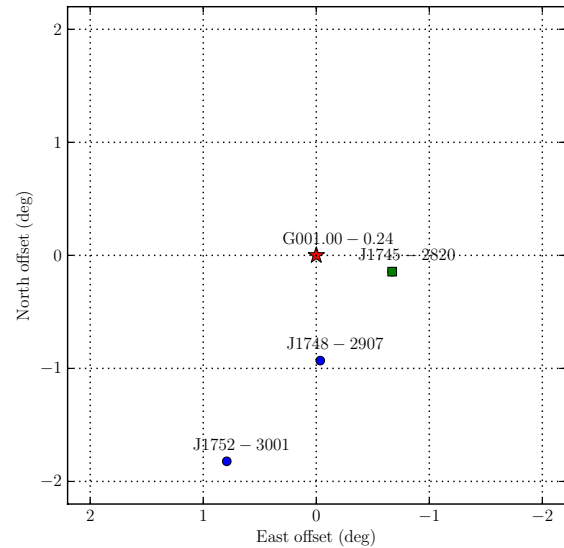


Fig. 3 Relative position of target and calibrators in an example of VLBI relative astrometry under the VLBA program BR198C4.

In this program, we obtained the first VLBI image of J1752-3001, and the first images of J1745-2820 and J1748-2907 at C-band (6.7 GHz). The image qualities of the latter two are much better than their previous images, mainly due to the better uv-coverage and longer integration time of about one hour. The RMS noise in the images, as shown in Figure 4, is close to the theoretical thermal noise. Figure 5 shows the correlated flux densities of the calibrators versus the uv-distance, which indicates the compactness of the radio sources.

4 Future Work

We started to create images of the VLBI calibrators in early 2016. We plan to finish the imaging of all BeSSeL VLBI calibrators close to the galactic plane by the end of 2016, and then the remainder by July 2017. There

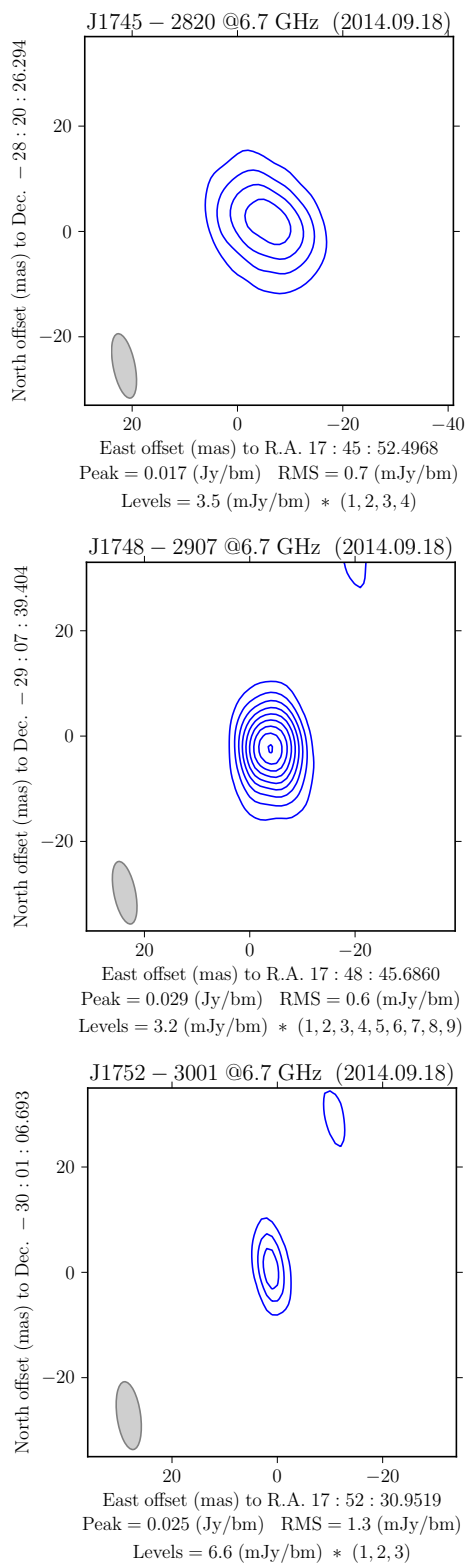


Fig. 4 VLBI images of three calibrators at C-band on 18 September 2014 under the VLBA program BR198C4.

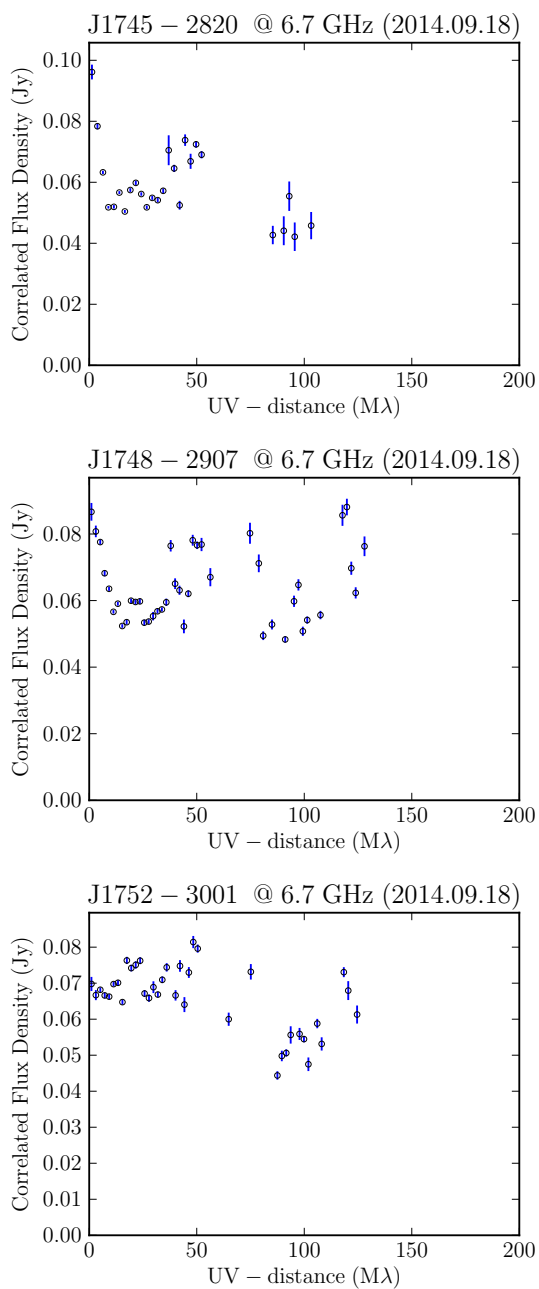


Fig. 5 Correlated flux versus uv-distance of three calibrators at C-band on 18 September 2014 under the VLBA program BR198C4.

are also some BeSSeL-like phase-reference VLBI program archived data from the VLBA, VERA, and the EVN. The images from these archived data are also very important for monitoring the source structures. We will make images for these calibrators in the future.

Acknowledgements

This work was sponsored by the 100 Talents Project of the Chinese Academy of Sciences and the Natural Science Foundation of Shanghai.

References

1. Beasley, A. J. & Conway, J. E. 1995, in *Astronomical Society of the Pacific Conference Series*, Vol. 82, *Very Long Baseline Interferometry and the VLBA*, ed. J. A. Zensus, P. J. Diamond, & P. J. Napier, 327.
2. Bourda, G., Charlot, P., & Le Campion, J.-F. 2008, *A&A*, 490, 403.
3. Immer, K., Brunthaler, A., Reid, M. J., et al. 2011, *ApJS*, 194, 25.
4. Petrov, L., Kovalev, Y. Y., Fomalont, E. B., & Gordon, D. 2008, *AJ*, 136, 580.
5. Reid, M. J. & Honma, M. 2014, *ARA&A*, 52, 339.
6. Reid, M. J., Menten, K. M., Brunthaler, A., et al. 2014, *ApJ*, 783, 130.

An Inequality Constrained Least-Squares Approach as an Alternative Estimation Procedure for Atmospheric Parameters from VLBI Observations

Sebastian Halsig, Thomas Artz, Andreas Iddink, Axel Nothnagel

Abstract On its way through the atmosphere, radio signals are delayed and affected by bending and attenuation effects relative to a theoretical path in vacuum. In particular, the neutral part of the atmosphere contributes considerably to the error budget of space-geodetic observations. At the same time, space-geodetic techniques become more and more important in the understanding of the Earth's atmosphere, because atmospheric parameters can be linked to the water vapor content in the atmosphere. The tropospheric delay is usually taken into account by applying an adequate model for the hydrostatic component and by additionally estimating zenith wet delays for the highly variable wet component. Sometimes, the Ordinary Least Squares (OLS) approach leads to negative estimates, which would be equivalent to negative water vapor in the atmosphere and does, of course, not reflect meteorological and physical conditions in a plausible way. To cope with this phenomenon, we introduce an Inequality Constrained Least Squares (ICLS) method from the field of convex optimization and use inequality constraints to force the tropospheric parameters to be non-negative allowing for a more realistic tropospheric parameter estimation in a meteorological sense. Because deficiencies in the a priori hydrostatic modeling are almost fully compensated by the tropospheric estimates, the ICLS approach urgently requires suitable a priori hydrostatic delays. In this paper, we briefly describe the ICLS method and validate its impact with regard to station positions.

Institute of Geodesy and Geoinformation, University of Bonn

Keywords VLBI, inequality constraints, ICLS, zenith wet delay, atmospheric parameters

1 Introduction

Variable conditions in the neutral atmosphere contribute considerably to the error budget of space-geodetic techniques, such as Global Navigation Satellite Systems (GNSS) or Very Long Baseline Interferometry (VLBI). At the same time, space-geodetic observations play a steadily increasing role in the understanding of the Earth's atmosphere and become more and more important in interdisciplinary studies of climatology or meteorology. For instance, atmospheric parameters from Global Positioning System (GPS) observations are used for data assimilation procedures in global numerical weather models. VLBI observations are not used for these purposes, because the observations are not continuous and the global distribution and spatial coverage lags behind GPS observations. However, with regard to the VLBI Global Observing System (VGOS, [7]), the next generation VLBI system, which leads to an increasing number of observations as well as a better sky coverage and, therefore, a better sampling of the atmosphere, a more valuable contribution to atmospheric sciences could be possible, at least for calibration purposes.

On its way through the atmosphere, the signals of space-geodetic techniques are delayed and affected by bending and attenuation effects relative to a theoretical path in vacuum. The tropospheric delay is usually taken into account by applying an adequate model (e.g., the modified Saastamoinen formula [3]) for the hydrostatic component (index h) and by additionally

estimating a correction parameter for the highly variable wet component (index w) within the VLBI parameter estimation process. Both components are modeled by a zenith delay (ΔL_h^z and ΔL_w^z) and a corresponding mapping function ($m_{f_h}(\varepsilon)$ and $m_{f_w}(\varepsilon)$) for the transformation from zenith to an arbitrary elevation angle ε . In addition, troposphere gradients in the North-South and East-West directions (G_{ns} and G_{ew}) can be estimated to overcome azimuthal asymmetries in the refractive index (second line of Equation 1, where α denotes the azimuth) [6],

$$\Delta L_t(\alpha, \varepsilon) = m_{f_h}(\varepsilon)\Delta L_h^z + m_{f_w}(\varepsilon)\Delta L_w^z + m_{f_g}(\varepsilon)[G_{ns}\cos(\alpha) + G_{ew}\sin(\alpha)]. \quad (1)$$

Unfortunately, the Ordinary Least Squares (OLS) approach sometimes leads to negative zenith wet delay (ZWD) estimates. Because ZWD parameters can be directly linked to the integrated water vapor content in the atmosphere, and there is of course nothing like negative water vapor, these atmospheric parameters obviously do not reflect meteorological and physical conditions in a plausible way. To overcome this issue, an Inequality Constrained Least Squares (ICLS) approach from the field of convex optimization [2] is introduced as an alternative estimation procedure for the determination of atmospheric parameters. Thus, the tropospheric parameters are constrained to non-negative values allowing for more realistic zenith wet delay estimates.

Special consideration should be given to the a priori hydrostatic delay, because mis-modeling a priori tropospheric data is compensated by the zenith wet delay estimates by almost 100%. If prohibited by inequality constraints, the erroneous hydrostatic delays can not be compensated by the ZWDs anymore, which then directly affects other correlated parameter groups such as the vertical component of the station positions. The influence of different inequality constraints for certain ZWD parameters and VLBI stations on the zenith wet delay estimates of the same station as well as on other parameter types is investigated in this study.

2 The Inequality Constrained Least Squares Method

The OLS model can be written as

$$\mathbf{l} = \mathbf{A}\mathbf{x} + \mathbf{v}, \quad (2)$$

$$\boldsymbol{\Sigma}_{ll} = \sigma_0 \mathbf{Q}_{ll}, \quad (3)$$

where \mathbf{l} denotes the vector of observations with corresponding variance-covariance matrix $\boldsymbol{\Sigma}_{ll}$ as the product of the a priori variance factor σ_0 and the cofactor matrix \mathbf{Q}_{ll} . The matrix \mathbf{A} is the Jacobian matrix which contains the partial derivatives of the observation equations with respect to the parameters and \mathbf{x} is the vector of unknown parameters to be estimated ($\tilde{\mathbf{x}}$ denotes the adjusted parameters). The vector

$$\mathbf{v} = \mathbf{A}\tilde{\mathbf{x}} - \mathbf{l} \quad (4)$$

contains the residuals. The optimal solution is obtained by minimizing the objective function, the (possibly weighted) square sum of residuals

$$\mathbf{v}^T \boldsymbol{\Sigma}_{ll}^{-1} \mathbf{v} \dots \min. \quad (5)$$

In case of the ICLS method, the concept is extended by linear inequality constraints of the form

$$\mathbf{B}^T \mathbf{x} \leq \mathbf{b}, \quad (6)$$

which have to be fulfilled strictly. Because it is not known in the beginning, which inequality constraints will become active and will influence the result, the ICLS problem can only be solved iteratively. In each iteration, the corresponding sets of active and inactive constraints change. In general, there are several iterative methods to solve such an ICLS problem. In this study, we made use of the so-called Active Set method [4], a simplex algorithm, which follows the boundary of the feasible set, i.e., the region where all inequality constraints are fulfilled, until the optimal solution is reached. For more details, see [5] or [10].

Due to the missing analytic relationship between observations and parameters, the calculation of standard deviations in the Least Squares sense is not possible anymore. Thus, to allow for a suitable quality description of the derived parameters, we make use of Monte Carlo simulations to obtain a discrete approximation of the probability density function. Instead of standard deviations, so-called highest probability density intervals are calculated to overcome asymmetric probability density functions caused by inequality constraints [9].

3 Results

In order to validate the ICLS method, we make use of about 125 VLBI sessions provided by the International VLBI Service for Geodesy and Astrometry (IVS, [11], [8]). The databases are processed using the VLBI data analysis software `ivg::ASCOT` [1], which is being developed by the VLBI group of the Institute of Geodesy and Geoinformation of the University of Bonn. The modeling and analysis setup described in [5] is used for all solutions.

In Figure 1, the zenith wet delay estimates are exemplarily illustrated for the VLBI station GILCREEK (Gilmore Creek, Alaska) and a VLBI session on November 28, 2001. The ZWD parameters derived from the Least Squares solution are represented as black triangles while the ICLS estimates are depicted as gray circles. The second OLS parameter, for instance, is negative by about 3 mm and is shifted to a non-negative value in the ICLS approach. Because continuous piece-wise linear functions are used for the parametrization of the atmospheric parameters, all zenith wet delay estimates of the same VLBI station are correlated and, as a consequence, many of the ZWDs shown in Figure 1 are also shifted. However, the ZWD differences between the OLS and ICLS solution are not significant, except for the parameter where the inequality constraint is active. This holds for the general case as well.

Even more interesting is the influence of this single inequality constraint (applied for one atmospheric

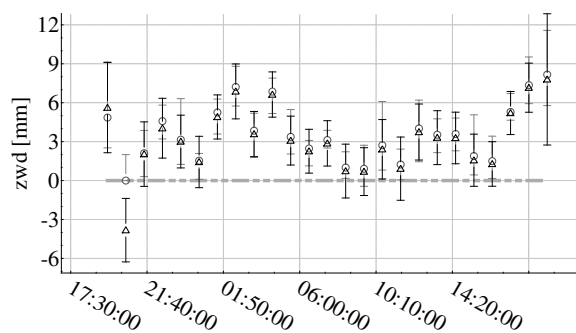


Fig. 1 Zenith wet delay parameters for the VLBI station GILCREEK (Gilmore Creek, Alaska) on November 28, 2001. The Least Squares estimates are represented as black triangles and the Inequality Constrained Least Squares solution is depicted as gray circles.

parameter) on other parameter groups, especially because different parameter types, such as clock parameters, zenith wet delays, and the vertical component of the stations positions, are correlated within the VLBI parameter estimation procedure. This effect is shown in Figure 2.

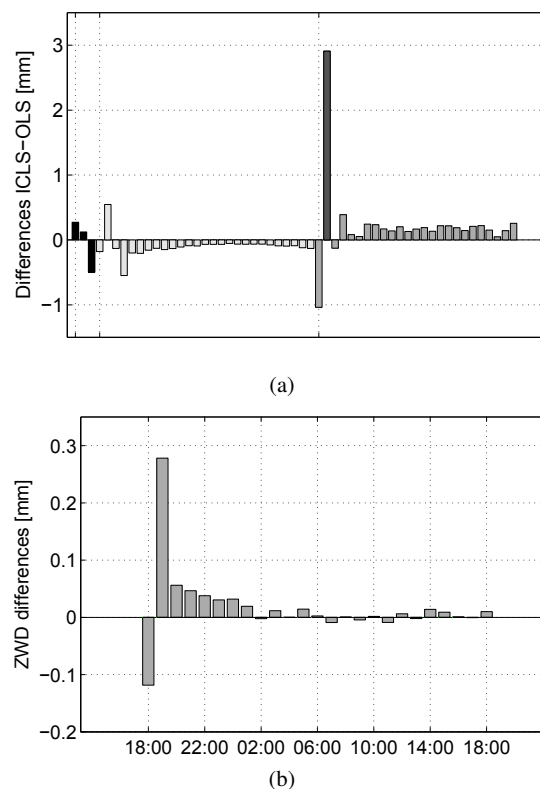


Fig. 2 (a) The influence of a single ZWD inequality constraint (dimmed gray) on station coordinates (black), clocks (light gray), and zenith wet delays (dark gray) of the same station (Gilmore Creek, Alaska). (b) The influence of the same inequality constraint on zenith wet delay parameters (dark gray) of another station (Matera, Italy).

The influence of a single inequality constraint applied to only one zenith wet delay of the station GILCREEK (dimmed gray) on the station coordinates (black), the clock model correction parameters (light gray), and the zenith wet delays (dark gray) of the same station is depicted in Figure 2(a). Here, it becomes obvious that less than one millimeter of the difference between the ICLS and OLS solution of approximately 3 mm is compensated by the vertical component of the telescope coordinates. The maximum difference can be

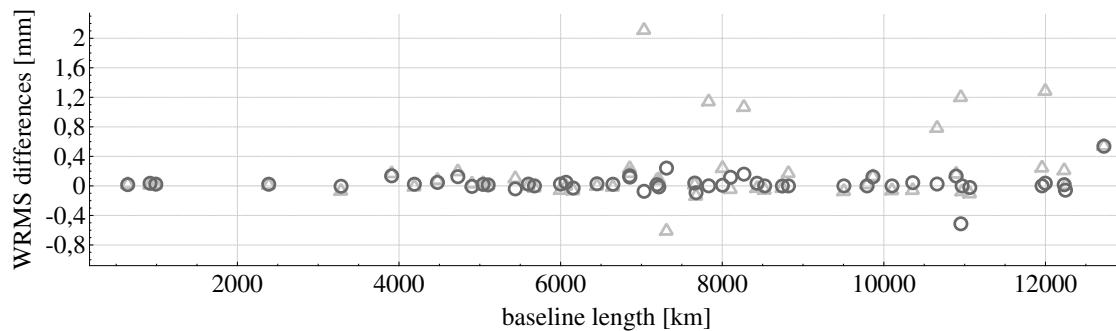


Fig. 3 Baseline length repeatability differences with respect to the OLS solution. The light gray triangles represent an ICLS solution, where the meteorological data used for the calculation of the hydrostatic delay only results from in-situ measurements, while dark gray circles depict an ICLS solution using atmospheric a priori data derived from a combination of in-situ observations and a numerical weather model of the ECMWF.

found in one of the ZWD estimates (about 1 mm). The remaining part is evenly distributed between the other parameters, although the differences are on the order of tenths of a millimeter and of course not significant. Figure 2(b) shows the influence of the same inequality constraint on the zenith wet delay estimates of another station, here exemplarily for MATERA (Matera, Italy). The differences between both solutions are again on the order of tenths of a millimeter, which indicates that the use of the ICLS method only leads to an effect on estimates of the same station for which inequality constraints are applied.

In the following, particularly the effect of inequality constraints on station coordinates will be investigated in more detail. Thus, the differences in baseline length repeatabilities between the Least Squares and the ICLS method are calculated for 125 VLBI sessions in 2002. For about 20% of these sessions automatically inequality constraints are applied for at least one station and one zenith wet delay parameter. The results are depicted in Figure 3, where the baseline length repeatability differences of two ICLS realizations with respect to the Least Squares solution are represented by light gray triangles and dark gray circles, respectively. Both ICLS solutions only differ in the meteorological data (i.e., temperature and pressure) used for the modified Saastamoinen formula [3]. In the first solution, meteorological data from in-situ measurements as observed at the VLBI sites are applied (light gray triangles). However, these data may contain data gaps and outliers. As a consequence, mis-modeling in the a priori data occurs, which is compensated by the zenith wet delay estimates by almost 100%. When introducing in-

equality constraints, this compensation effect is suppressed and affects other correlated parameter groups like the vertical component of the telescope positions. This then leads to a degradation of the baseline length repeatabilities (light gray triangles). Thus, special attention has to be paid to the a priori modeling of the zenith hydrostatic delays.

In the second solution (dark gray circles) a numerical weather model of the European Center for Medium Weather Forecast (ECMWF) is used to define the level of the meteorological data, while their variability is taken from the in-situ observations after removing outliers and filling data gaps. As a consequence, the differences between this realization and the OLS solution are not significant anymore, although inequality constraints are introduced to allow for a more reliable estimation of tropospheric parameters.

Please note that approximately the same number of inequality constraints is needed for both ICLS realizations, although the constrained parameters can be different and the order of magnitude in the differences between the ICLS and OLS can vary. Thus, it has to be concluded that the negative zenith wet delay estimates result not only from a priori mis-modeling. In fact, there are several other “dirt” effects on the ZWD parameters, such as mis-modeling of geophysical effects as well as certain impact due to instrumental delays or the clock parametrization. This has to be investigated in more detail in the future. In addition, the tropospheric parameters in cold regions derived alternatively have to be validated with regard to numerical weather models or other space-geodetic techniques like GPS or GNSS in general.

4 Conclusion and Future Work

Sometimes, the OLS method leads to negative zenith wet delay parameters. In a meteorological sense, that would be equivalent to negative water vapor in the atmosphere. In order to constrain these parameters to non-negative estimates and, therefore, to allow for more realistic tropospheric parameters, an ICLS approach is introduced. The influence of inequality constraints on zenith wet delay parameters as well as on other parameter groups has been investigated leading to the following results. The use of the ICLS method solely affects parameters of the same station, where inequality constraints are active. The differences between the ICLS and OLS solutions due to the inequality constraints are partly compensated by the vertical component of the station coordinates. However, the differences in baseline length repeatabilities between both solutions are not significant if the a priori hydrostatic model is not affected by outliers, data gaps, or mis-modeling issues. Thus, the use of inequality constraints is, in principle, possible without disturbing the VLBI target parameters. However, further investigations need to be carried out concerning other “dirt” effects compensated by the ZWD parameters. Additionally, an external validation for the newly derived tropospheric parameters is necessary, which can be achieved using either numerical weather models or ZWD time series from GPS observations.

Due to the discontinuous nature of VLBI observations, the tropospheric parameters can, of course, not yet be used for atmospheric purposes in terms of a data assimilation process. However, zenith wet delay estimates could, in fact, act as calibration parameters for numerical models or other space-geodetic techniques, at least as soon as a better coverage of the atmosphere becomes reality within the scope of VGOS networks.

Acknowledgements

S. Halsig thanks the German Research Foundation (Deutsche Forschungsgemeinschaft, DFG) for its financial support (contract NO 318/10-1).

References

1. T. Artz, S. Halsig, A. Iddink, A. Nothnagel. ivg::ASCOT: The Development of a new VLBI Software Package., In: *IVS 2016 General Meeting Proceedings, “New Horizons with VGOS”*, Johannesburg, South Africa, March 13-19 2016, Eds: D. Behrend, K. D. Baver and K. Armstrong, this volume.
2. S. Boyd, L. Vandenberghe. *Convex Optimization.*, Cambridge University Press, 2004.
3. J. L. Davis, T. A. Herring, I. I. Shapiro, A. E. E. Rogers, G. Elgered. Geodesy by radio interferometry: Effects of atmospheric modeling errors on estimates of baseline length. *Radio Sci*, 20(6), pp. 1593 - 1607, 1985.
4. P. E. Gill, W. Murray, M. H. Wright MH. *Practical Optimization*, Academic Press, London, 1981.
5. S. Halsig, L. Roese-Koerner, T. Artz, A. Nothnagel, and W.-D. Schuh. Improved Parameter Estimation of Zenith Wet Delays Using an Inequality Constrained Least Squares Method. *International Association of Geodesy Symposia*, Springer Berlin Heidelberg, doi: 10.1007/1345_2015_171, 2015.
6. D. S. MacMillan, C. Ma. Atmospheric gradients and the VLBI terrestrial and celestial reference frames. *GEOPHYS RES LETT*, 24(4):453 - 456, doi: 10.1029/97GL00143, 1997.
7. A. Niell, C. Beaudoin, R. Cappallo, B. Corey, M. Titus. First results with the GGAO12m VGOS system. In: *Proceedings of the 21th EVGA Working Meeting*, Espoo, Finland, March 5-8 2013, Eds: N. Zubko and M. Poutanen, Reports of the Finnish Geodetic Institute, pp. 29 - 32, 2013.
8. A. Nothnagel, International VLBI Service for Geodesy and Astrometry (IVS). The IVS data input to ITRF2014. International VLBI Service for Geodesy and Astrometry. *GFZ Data Services*. doi: 10.5880/GFZ.1.1.2015.002, 2015.
9. L. Roese-Koerner, B. Devaraju, N. Sneeuw, W. D. Schuh. A stochastic framework for inequality constrained estimation. *J Geodesy* 86(11):1005–1018, doi: 10.1007/s00190-012-0560-9, 2012.
10. L. Roese-Koerner, I. Krasbutter, W. D. Schuh. A Constrained Quadratic Programming Technique for Data-Adaptive Design of Decorrelation Filters. In: VII Hotine-Marussi Symposium on Mathematical Geodesy, Springer Berlin Heidelberg, pp. 165 - 170, 2012.
11. H. Schuh and D. Behrend. VLBI: A fascinating technique for geodesy and astrometry. *Journal of Geodynamics*, 61, doi: 10.1016/j.jog.2012.07.007, pp. 68 - 80, 2012.

On the Impact of Different Mapping Functions on Geodetic and Tropospheric Products from VLBI Data Analysis

Kyriakos Balidakis¹, Florian Zus², Jan Douša³, Tobias Nilsson², Susanne Glaser¹, Benedikt Soja², Maria Karbon², Robert Heinkelmann², Harald Schuh^{1,2}

Abstract We assess the impact of mapping functions on geodetic very long baseline interferometry (VLBI). The results from the analysis of 13 years of VLBI data processed by employing different mapping functions are intercompared. One of these is the newly developed Potsdam mapping function (PMF). The PMF performs slightly better than the VMF1 in terms of baseline length repeatability and Earth orientation parameters. Additionally, we investigated the impact of the underlying spatial resolution of the numerical weather model employed for the ray-tracing on the geodetic estimates, and we found millimeter level differences in the height estimates during severe weather events.

Keywords VLBI, troposphere, mapping functions, ray-tracing, Earth orientation parameters

1 Introduction

In data analysis of space geodetic techniques, such as Very Long Baseline Interferometry (VLBI) and Global Navigation Satellite Systems (GNSS), including observations spanning a wide range of elevations improves the de-correlation of the estimated position height from the estimates of the residual zenith delay and the clock parameters, hence enhancing the precision of these parameters. Unlike low elevation GNSS observations, the

VLBI observations are unaffected by the effects of multi-path scattering and phase center variations. Thus the adoption of an elevation dependent weighting strategy as well as an elevation mask angle ($\approx 7^\circ$) is inessential. This allows VLBI analysis to benefit from fully utilizing low elevation observations. Nevertheless, as the elevation angle decreases, the mapping function (MF) uncertainties rapidly increase, degrading the positioning precision. Therefore, it is imperative that accurate mapping functions be applied and that their uncertainties be described stochastically in the adjustment.

Throughout the years, several tropospheric MF have been developed --- the interested reader is referred to Nilsson et al. (2013) for a review. To date, the most accurate and widely globally applied MF are the Vienna Mapping Functions 1 (VMF1) (Böhm et al., 2006), because the functional formulation and the underlying data set (ECMWF operational analysis) are very accurate. Therefore, they are recommended by the latest IERS Conventions (Petit and Luzum, 2010). However, the climatological approach adopted for the description of coefficients b and c prevents parametrized mapping from representing short-term and anomalous atmospheric behavior (cf. Section 2). In addition to this, as the underlying numerical weather model (NWM) is intended to produce the best state estimate, it is subject to system changes (e. g., February 2006, January 2010, and March 2016) which consequently lead to inhomogeneities in the time series of the products. In an effort to address these issues, we used our in-house ray-trace software package (Zus et al., 2012) to determine the a , b , and c coefficients utilizing the ERA-Interim reanalysis (Dee et al., 2011). Hereinafter, this rigorous MF will be referred to as the PMF.

In this paper, we study the benefit of applying the PMF in VLBI analysis. Section 2 outlines the develop-

1. Technische Universität Berlin, Institute of Geodesy and Geoinformation Science, Berlin, Germany

2. Helmholtz Centre Potsdam, GFZ German Research Centre for Geosciences, Space Geodetic Techniques, Potsdam, Germany

3. Geodetic Observatory Pečný of the Research Institute of Geodesy, Topography and Cartography, Czech Republic

ment of the PMF. In Section 3, we perform a series of VLBI solutions and elaborate on the geodetic results. Section 4 recapitulates the results and provides an outlook.

2 The Potsdam Mapping Functions (PMF)

In essence, the total delay that radio signals experience when traversing the neutral atmosphere is approximated as a function of elevation ε and azimuth α :

$$\tau_{trop}(\varepsilon, \alpha) = mf_h d_h^z + mf_w d_w^z + mf_g (G_{NS} \cos(\alpha) + G_{EW} \sin(\alpha)) \quad (1)$$

where the subscript h stands for hydrostatic and w for wet. The zenith delays are denoted by d_i^z , and G_{NS} and G_{EW} are the total linear horizontal delay gradients. The fitting ansatz for both symmetric MF (mf_i) follows the continued fraction form normalized to yield unity at zenith (Herring, 1992). Here, the total gradient MF mf_g follows Chen and Herring (1997).

$$mf_i = \begin{cases} \frac{1 + \frac{a_i}{1 + \frac{b_i}{1 + c_i}}}{\sin(\varepsilon) + \frac{a_i}{\sin(\varepsilon) + \frac{b_i}{\sin(\varepsilon) + c_i}}}, & \text{for } i = h \vee w \\ \frac{1}{\sin(\varepsilon) \tan(\varepsilon) + 0.0032}, & \text{for } i = g \end{cases} \quad (2)$$

For our investigations, we employ ERA-Interim at the original resolution (six-hourly $1^\circ \times 1^\circ$ fields on 60 model levels) and the ray-trace algorithm proposed by Zus et al. (2012). In essence, for the considered VLBI stations we compute tropospheric delays for various elevation and azimuth angles in order to estimate the a , b , and c coefficients of the MF and the total linear horizontal delay gradients by a least-squares fit. A detailed description can be found in Douša et al. (2016).

We compare our product (PMF_1.0 hereafter) with the original VMF1 (VIE-VMF1) and UNB-VMF1¹ (from NCEP reanalysis 1) in terms of slant total delays (STD) for $\varepsilon = 5^\circ$ (cf. Figure 1). Because differences in the MF coefficients are overshadowed by discrepancies

¹ unb-vmf1.gge.unb.ca/About.html

in both hydrostatic and non-hydrostatic zenith delays between different providers, we follow Balidakis et al. (2016) to extract the necessary data for the calculation of the zenith delays. The rule of thumb suggests that the STD difference at the lowest elevation angle a station observed during a session equals approximately five times the expected estimated station height difference (Böhm, 2004). Considering the rather large bias present in the UNB-VMF1 differences, we have opted not to consider it in the subsequent VLBI analysis.

3 VLBI Data Analysis and Results

We perform two series of VLBI solutions. Initially, we utilize the classical Gauß-Markov least-squares adjustment module of the VieVS@GFZ VLBI software (Böhm et al., 2012; Nilsson et al., 2015) to analyze observations from the IVS-R1 and IVS-R4 sessions (1,326 24-hour multi-baseline sessions), spanning the period 2002-2015 and featuring in total a 32-station global network. We produce three solutions, varying only the MF applied: (1) VIE-VMF1, (2) GPT2w (Böhm et al., 2015), and (3) PMF_1.0.

To study sub-daily variations and the impact of the resolution of the underlying NWM on the geodetic results, the Kalman filter module of VieVS@GFZ is better suited (Soja et al., 2015). We analyze the best existing continuous VLBI data set, CONT14². The filter is run forwards and backwards, followed by a smoother. We produce four solutions, with a solution employing PMF from ray-tracing in $0.5^\circ \times 0.5^\circ$ fields (PMF.0.5 hereafter) and another from ray-tracing in CMC-GDPS³ (UNB-VMF1 hereafter), additionally to the above-listed MF, excluding GPT2w.

In all solutions we employ homogenized in situ data (Balidakis et al., 2016). In addition to the conventional displacement models (Petit and Luzum, 2010), we correct for deformations induced by non-tidal atmospheric pressure loading (NTAL⁴) and continental water storage loading (Dill and Dobsław, 2013), to reduce correlations. Station coordinates and Earth orientation parame-

² Fifteen consecutive 24-hour sessions in May 2014, featuring a 17 station global network.

³ dd.weather.gc.ca/model_gem_global/25km

⁴ The NTAL series are calculated employing the operational model of ECMWF, utilizing MOG2D-G to describe the dynamic ocean response to pressure and wind forcing.

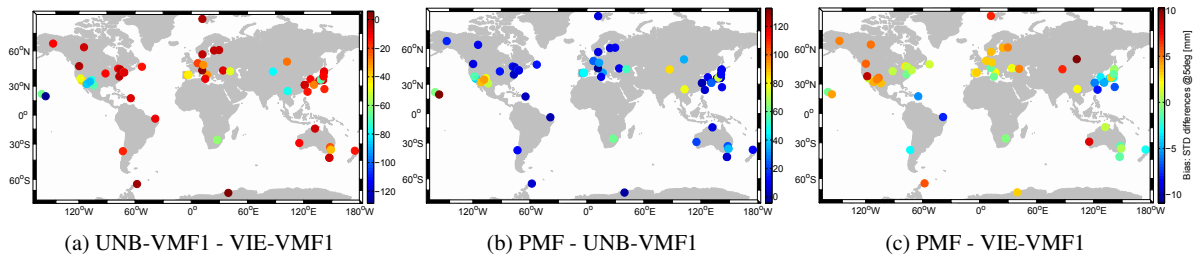


Fig. 1: Shown are the average STD differences in mm at $\epsilon = 5^\circ$ between the VIE-VMF1, UNB-VMF1 and PMF.1.0, calculated from 14 years of data, utilizing the same zenith delays for all three cases.

ters (EOP) are estimated at 24-hourly intervals, whereas ZWD are estimated at hourly and linear horizontal delay gradients at six-hourly intervals.

In VLBI analysis, varying the MF mainly impacts the height coordinate component. We find that when the PMF.1.0 is applied instead of VIE-VMF1, the estimated height changes by more than 1 mm at only two sites, whereas GPT2w biases 35% of the sites considered, w. r. t. VIE-VMF1. The weighted root-mean-square (WRMS) differences between VIE-VMF1 and PMF.1.0 indicate marginal changes. When GPT2w is applied, the WRMS increase can be as large as 16% w. r. t. VIE-VMF1 (cf. Figure 2).

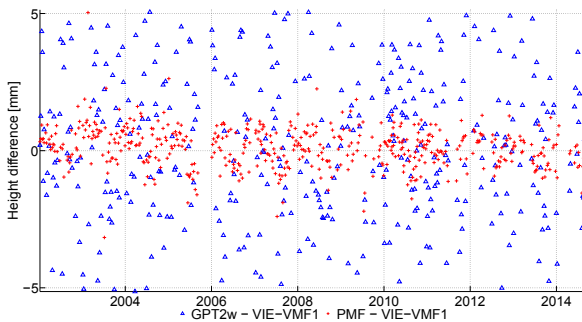


Fig. 2: Differences of the residual height estimates at Westford, USA, between the solutions applying VIE-VMF1, PMF.1.0, and GPT2w.

Figure 3 illustrates that in the presence of severe weather events, solutions obtained using MF that differ only in the resolution of the underlying NWM may diverge significantly. In this example, there was a severe weather event at Tsukuba, Japan, on May 18, corresponding to day of year 138 in 2014.

Another quantitative measure of the impact of employing different MF on the geodetic results is provided

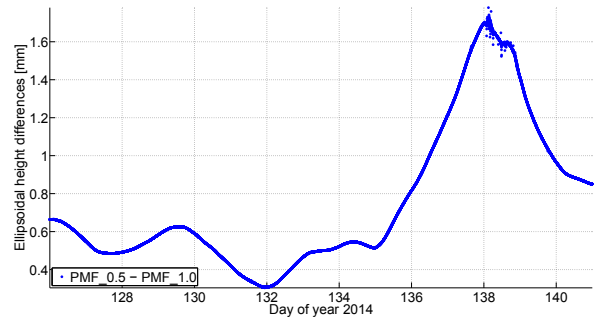


Fig. 3: Differences of the residual height estimates at Tsukuba, during CONT14, between the solutions applying PMF.1.0 and PMF.0.5.

by studying the changes in the baseline length repeatability. Therefore, we calculate the WRMS scatter of baseline length estimates. Given a baseline length time series $\{b\}_{i=1}^N$, the formula we used reads:

$$WRMS = \sqrt{\sum_{i=1}^N \frac{v_{b_i}^2}{\sigma_{v_{b_i}}^2} / \sum_{i=1}^N \frac{1}{\sigma_{v_{b_i}}^2}}, \quad (3)$$

where v_{b_i} are the baseline length residuals from a straight-line fit solved by a rigorous evaluation of the non-linear Gauß-Helmert model and $\sigma_{v_{b_i}}$ are their formal errors. We find that PMF performs slightly better than VIE-VMF1 (for $\approx 60\%$ of baselines longer than 1,000 km), and improves the repeatability for $\approx 65\%$ of the baselines compared to GPT2w.

To assess the impact of varying the MF on the resulting terrestrial reference frame (TRF), the seven-parameter similarity transformation is performed, in a session-wise manner. Figure 4c portrays that the scale factor between the VIE-VMF1 and the PMF.1.0 solutions yields sub-mm changes. The slightly positive bias

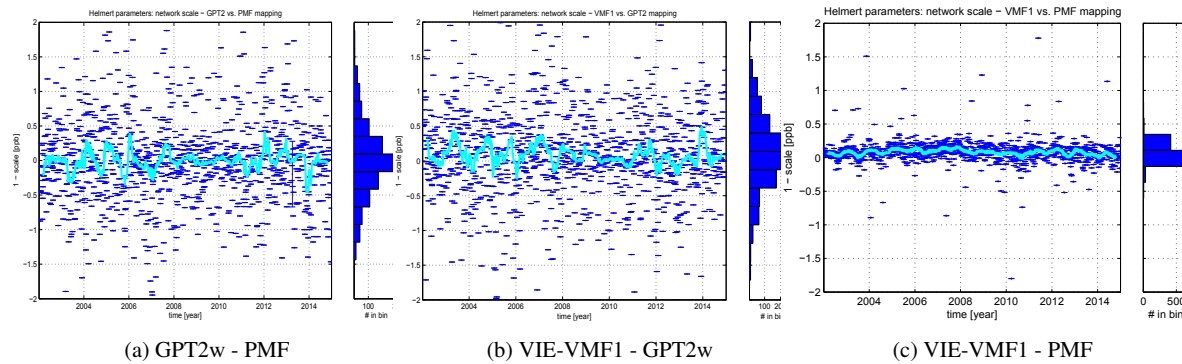


Fig. 4: Time series of scale difference estimates from the epoch-wise Helmert transformation among all solutions are shown in blue (dark) ($1 \text{ ppb} \approx 6.4 \text{ mm}$). The cyan (light) line represents a 90-day moving median.

can be explained by (1) the different underlying NWM data, i. e., the ECMWF ERA-Interim reanalysis versus the ECMWF operational analysis, (2) the difference between a rigorous MF and a MF based on the VMF1 concept, (3) the differences in the underlying ray-trace algorithms, e. g., the PMF utilizes a local (Gaussian) curvature radius of the Earth whereas the VMF1 utilizes a constant curvature radius for the Earth, and finally (4) the different boundary conditions considered. On the contrary, Figures 4a and 4b demonstrate that using an empirical MF considerably distorts the scale at the cm-level, depending on weather conditions.

Differences between the MF tested here propagate rather moderately to the estimated EOP. Nevertheless, it has to be noted that the WRMS of all EOP series marginally increases when GPT2w is applied in lieu of VIE-VMF1. In particular, the WRMS of the polar motion components inflates by $\approx 2\%$, and an offset as large as $3 \mu\text{as}$ and $-20 \mu\text{as}$ ($\approx 1 \text{ mm}$ at a 10,000 km baseline) appears in x_{pole} and y_{pole} , respectively. Applying the PMF reduces the WRMS of the celestial pole offset x_{CIP} by $\approx 3.6\%$ compared to VIE-VMF1. The standard deviation in the time series of the differences of ZWD, NS, and EW gradients between the VIE-VMF1 solution and GPT2w, is 3, 2.8, and 2.7 times larger compared to the differences between PMF and the VIE-VMF1 solution (cf. Figure 5). An annual signal is visible in the differences between PMF and VIE-VMF1.

In Figure 6, the discrepancies in the estimated ZWD at Tsukuba during CONT14 are shown. The best agreement is found between PMF_0.5 and PMF_1.0, whereas the largest discrepancies lie between VIE-VMF1 and PMF_0.5 (e. g., the bias in the ZWD series of Fortaleza, Brazil exceeds 1 mm—not shown here).

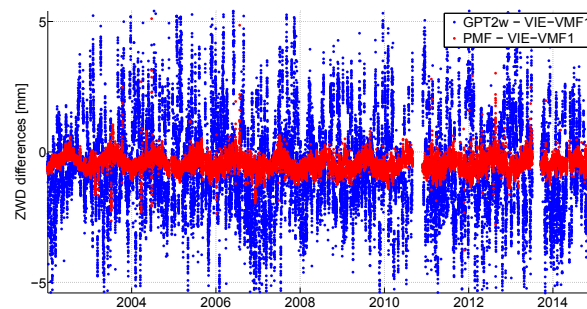


Fig. 5: The differences of the ZWD estimates at Wettzell, Germany, between the solutions applying VIE-VMF1, PMF_1.0, and GPT2w.

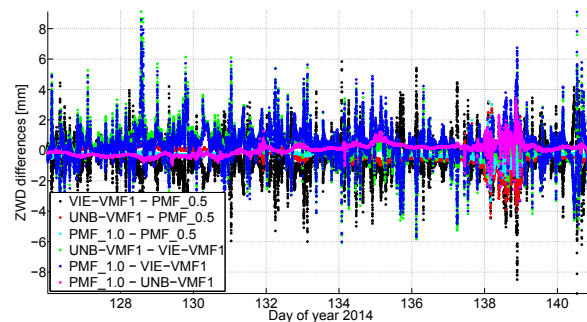


Fig. 6: The differences of the ZWD estimates at Tsukuba during CONT14 between VIE-VMF1, UNB-VMF1, PMF_1.0, and PMF_0.5.

4 Conclusions and Outlook

In this study, we address the MF that are employed for VLBI data analysis. The PMF was developed from rigorous ray-tracing in ERA-Interim, based on the ad-

vanced mapping concept. Two series of VLBI solutions were generated employing the least-squares method and a Kalman filter, to study long and short term effects, respectively. Intercomparing the estimates, we find that the scale is distorted (up to the cm-level) when employing the empirical GPT2w model, whereas the differences between VIE-VMF1 and PMF are at the sub-mm level. PMF marginally improves the estimated EOP series and the baseline length repeatability compared to GPT2w and VIE-VMF1. For CONT14, mm-level differences in the height estimates can stem from the resolution of the underlying NWM used for the ray-tracing. A more thorough analysis spanning the entirety of VLBI data is foreseen.

Acknowledgements

We acknowledge the IVS (Schuh and Behrend, 2012) for coordinating the VLBI experiments analyzed in this study. DWD and ECMWF are acknowledged for granting access to the NWM data used in this study. Thalia Nikolaidou is acknowledged for providing data from ray-tracing in NCEP reanalysis 1 and CMC-GDPS. KB works under DFG project HE 5937/2-1.

References

- Balidakis K, with seven co-authors (2016) On the impact of inhomogeneities in meteorological data on VLBI data analysis. In: Behrend D, Baver K, Armstrong K (eds), IVS 2016 General Meeting Proceedings, this volume.
- Böhm J, Werl B, Schuh H (2006) Troposphere mapping functions for GPS and very long baseline interferometry from European Centre for Medium-Range Weather Forecasts operational analysis data. *J Geophys Res Solid Earth* 111(B2).
- Böhm J (2004) Troposphärische Laufzeitverzögerungen in der VLBI. *Geowissenschaftliche Mitteilungen, Geowissenschaftliche Mitteilungen* 68.
- Böhm J, with seven co-authors (2012) The New Vienna VLBI Software VieVS. In: Kenyon S, Pacino MC, Marti U (eds) *Geodesy for Planet Earth, International Association of Geodesy Symposia*, vol 136, Springer Berlin Heidelberg, pp 1007–1011.
- Böhm J, Möller G, Schindelegger M, Pain G, Weber R (2015) Development of an improved empirical model for slant delays in the troposphere (GPT2w). *GPS Solut* 19(3):433–441.
- Chen G, Herring TA (1997) Effects of atmospheric azimuthal asymmetry on the analysis of space geodetic data. *J Geophys Res Solid Earth* 102(B9):20,489–20,502
- Dee DP, with 35 co-authors (2011) The ERA-Interim reanalysis: configuration and performance of the data assimilation system. *Quarterly Journal of the Royal Meteorological Society* 137(656):553–597.
- Dill R, Dobsław H (2013) Numerical simulations of global-scale high-resolution hydrological crustal deformations. *J Geophys Res Solid Earth* 118:5008–5017.
- Douša J, with eight co-authors (2016) Benchmark campaign and case study episode in Central Europe for development and assessment of advanced GNSS tropospheric models and products. *Atmos Meas Tech Discuss* 2016:1–40.
- Herring TA (1992) Modeling atmospheric delays in the analysis of space geodetic data. In: De Munck JC, Spoelstra TAT (eds) *Proceedings of Refraction of Transatmospheric signals in Geodesy*, vol 36, Netherlands Geodetic Commission Publications on Geodesy, p 157–164.
- Nilsson T, Böhm J, Wijaya DD, Tresch A, Nafisi V, Schuh H (2013) *Atmospheric Effects in Space Geodesy*, Springer Berlin Heidelberg, Berlin, Heidelberg, chap Path Delays in the Neutral Atmosphere, pp 73–136.
- Nilsson T, Soja B, Karbon M, Heinkelmann R, Schuh H (2015) Application of Kalman filtering in VLBI data analysis. *Earth, Planets and Space* 67(1):1–9.
- Petit G, Luzum B (eds) (2010) *IERS Conventions (2010)*, IERS Technical Note, vol 36. Verlag des BKG, Frankfurt am Main, Germany.
- Schuh H, Behrend D (2012) VLBI: A fascinating technique for geodesy and astrometry. *J Geodyn* 61:68–80.
- Soja B, with eight co-authors (2015) Tropospheric delay determination by Kalman filtering VLBI data. *Earth, Planets and Space* 67(144):1–16.
- Thayer GD (1974) An improved equation for the radio refractive index of air. *Radio Sci* 9(10):803–807.
- Zus F, with six co-authors (2012) A methodology to compute GPS slant total delays in a numerical weather model. *Radio Sci* 47(2).

El Niño and VLBI Measured Length of Day

John Gipson

Abstract VLBI is unique in its ability to measure UT1 and is an important contributor to measuring the Length of Day (*LOD*). In this paper I study *LOD* and demonstrate that it has structure at all time scales, and decompose it into Tidal, Seasonal, and Long Period and Residual terms. I show that the Multivariate Enso Index is strongly correlated with the Residual *LOD*. I compare the impact of the current El Niño with that of the 1997–98 El Niño. Both events result in an increase in *LOD* of 750 μ s and a cumulative impact on UT1 of 0.1 seconds.

Keywords El Niño, *LOD*, AAM

1 Introduction

“Never underestimate the joy people derive from hearing something they already know.” —Enrico Fermi

This paper reviews some of the properties of Length of Day (*LOD*). There is no new science here—the key results have been known since the 1980s and 1990s. The motivation for this paper is the current El Niño, which is the strongest one since the 1997–98 El Niño. In 1998, Gipson and Ma [1] wrote a paper on the impact of the 1997–98 El Niño on *LOD*. It caused an increase in *LOD* of 750 μ s. As the El Niño dissipated, so did the change in *LOD*. I was interested in the impact of the current El Niño on *LOD*. The two events are very similar, and the current El Niño is on track to have a similar or larger impact. To demonstrate this we

NVI Inc.

need to decompose *LOD* into various pieces to isolate the impact of the El Niño.

2 Angular Momentum and *LOD*

It is useful to decompose the angular momentum of the Earth system as follows:

$$J_{Earth} + J_{Ocean} + J_{Atmosphere} + J_{Core} = J_{Total}. \quad (1)$$

Here J_{Earth} is the Earth’s Angular Momentum (*EAM*), J_{Ocean} is the Oceanic Angular Momentum (*OAM*), $J_{Atmosphere}$ is the Atmospheric Angular Momentum (*AAM*), and J_{Core} is the Earth’s Core’s Angular Momentum (*CAM*). In the absence of external torques, the total angular momentum is conserved:

$$\frac{dJ_{Total}}{dt} = 0 \quad (2)$$

which leads to

$$\Delta J_{Earth} + \Delta J_{Ocean} + \Delta J_{Atmosphere} + \Delta J_{Core} = 0. \quad (3)$$

If the angular momentum of one component changes, the others must compensate. The Sun and Moon (and to a lesser extent the planets) do exert torques on the Earth which lead to nutation and precession of the Earth spin axis. But over short time scales these effects can be ignored, and the above equation is a reasonable approximation.

VLBI does not directly measure the angular momentum of the Earth. Instead it measures the *LOD* which is related to J_{Earth} and the Earth’s moment of inertia I_{Earth} by:

$$J_{Earth} = \omega I_{Earth} = \frac{2\pi}{LOD} I_{Earth}. \quad (4)$$

Small changes in *LOD* cause changes in J_{Earth} :

$$\Delta J_{Earth} = -\Delta LOD \left(\frac{2\pi}{LOD^2} I_{Earth} \right). \quad (5)$$

3 VLBI Measured *LOD*

Figure 1 shows VLBI measured *LOD* since early 1980. The curve appears smoother at the start because the data was sparse. The *LOD* appears to be a quasi-periodic signal superimposed over long term variation. Figure 2 is a close-up of the data since 2010. Two striking features of both figures are the seasonal signals and the regular ‘spikes’. Both of these are evident when we Fourier transform the data to the time domain as shown in Figure 3. The ‘spikes’ show up as sharply defined peaks in the spectrum, whereas the seasonal signal shows up as broad peaks centered around the annual and semi-annual periods.

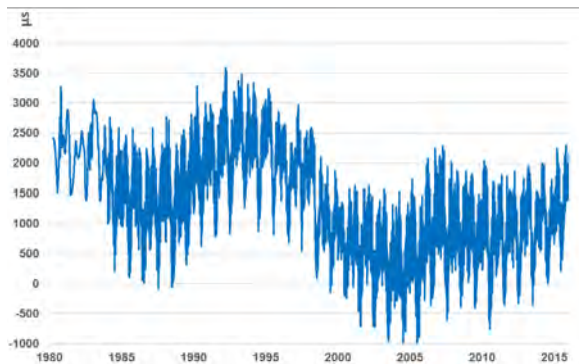


Fig. 1 VLBI measured *LOD* (with tidal terms).

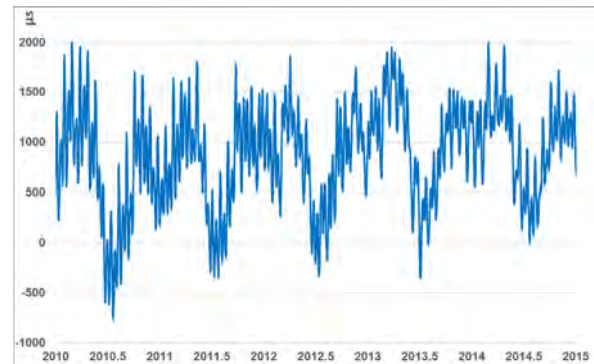


Fig. 2 Close-up of *LOD* with tidal terms.

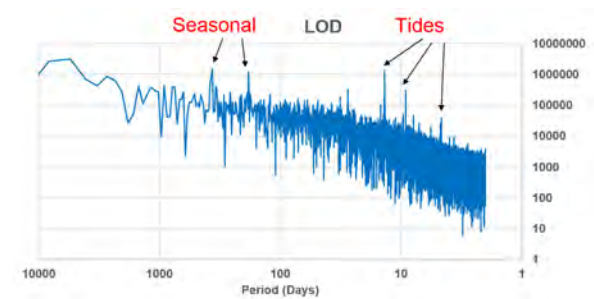


Fig. 3 *LOD* spectrum.

4 Decomposition of *LOD*

One of our goals in this note is to decompose *LOD* into terms which are separated by cause and/or period.

$$LOD = \text{Tidal Terms} + \text{Seasonal Terms} + \text{Long Period} + \text{Residual}$$

In the remainder of this section we do this separation.

4.1 Tidal Terms

The sharp peaks in the spectrum of *LOD* occur at tidal frequencies. The gravitational force of the Sun and the Moon changes the ocean heights and currents. This results in a change in the *OAM*, and the *EAM* changes to compensate for this so that the total Angular Momentum is conserved. The tidal behavior of *LOD* is well understood, and the IERS provides a good model for it [2]. If we subtract the IERS model from the VLBI measured data we obtain the series shown in Figure 4 and the corresponding spectrum shown in Figure 5. In the remainder of this note *LOD* will mean *LOD* with the tidal terms removed.

4.2 Seasonal Terms

Figure 4 exhibits strong seasonal behavior superimposed on a slowly varying signal. To extract the seasonal component we calculate the average *LOD* as a function of the Day of the Year (*DOY*). For leap years

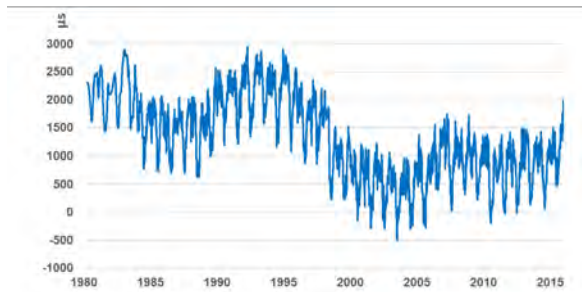


Fig. 4 VLBI measured LOD with tidal terms removed.

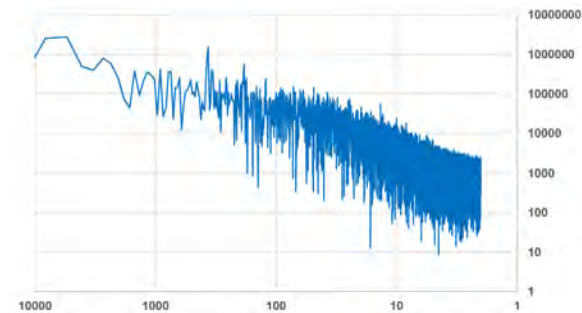


Fig. 5 Spectrum of LOD with tidal terms removed.

we assume that $LOD(366) = LOD(365)$. This seasonal behavior is plotted in Figure 6.

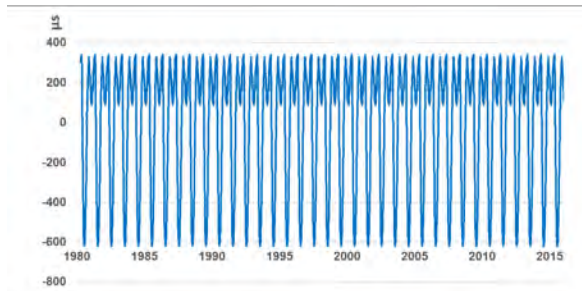


Fig. 6 LOD 's seasonal dependence in microseconds.

4.3 Atmospheric Angular Momentum

The atmosphere plays a vital role in exciting small but measurable changes in the rotation of our planet. Recognizing this, the International Earth Rotation and Reference Systems Service invited the U.S. National Meteorological Center to organize a Sub-bureau for

Atmospheric Angular Momentum for the purpose of collecting, distributing, archiving, and analyzing atmospheric parameters relevant to Earth rotation/polar motion. These parameters are calculated from the output of numerical weather models, and have been publicly available since 1989 [3]. Figure 7 plots the AAM calculated using as input the NCEP re-analysis model and is scaled so that it can be interpreted in terms of LOD . On time scales of one to two years, this looks very similar to Figure 4.

Figure 8 plots the VLBI measured LOD together with AAM since 2014. I removed a constant offset from LOD . The correlation between the two series over this period is 0.96. The striking level of agreement is testimony to the accuracy of the numerical weather models on which the calculation of AAM is based and to the accuracy of measurements of LOD .

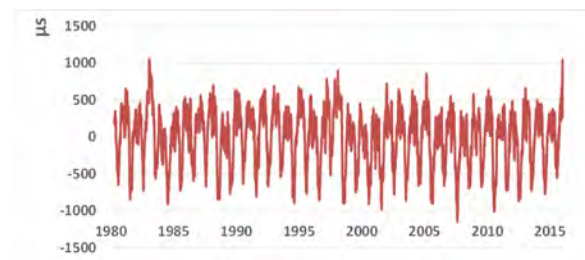


Fig. 7 AAM calculated from the NCEP re-analysis model.

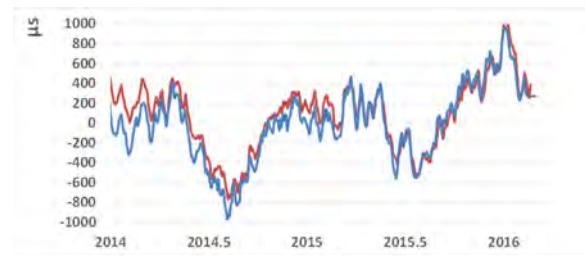


Fig. 8 LOD (bottom line) and AAM (top line).

4.4 Long Period and Residual LOD

Figure 9 plots the difference between the VLBI measured LOD and the rescaled AAM values. Apart from the noise in the signal, the dominant structure is a long-

period variation of the *LOD*. This is thought to be due predominantly to changes in the interior angular momentum of the earth, that is, changes in J_{Core} .

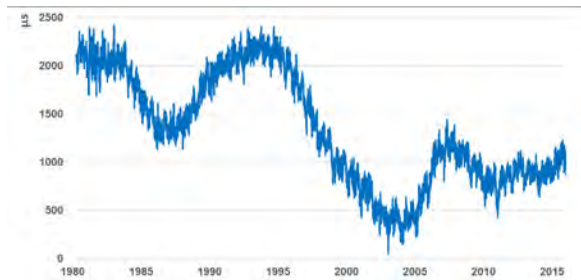


Fig. 9 “Long period” *LOD* obtained by subtracting AAM from *LOD*.

Figure 10 plots the Residual *LOD* obtained from the measured *LOD* by removing: 1.) Tidal Terms; 2.) Seasonal Terms; 3.) Long Period Terms.

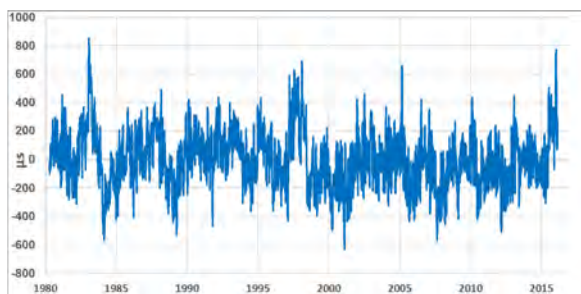


Fig. 10 Residual *LOD*.

5 EL Niño and *LOD*

El Niño is a global phenomenon affecting the weather all over the world. One measure of the strength of El Niño is the Multivariate Enso Index (MEI) which depends on six weather related variables observed over the Pacific. These variables are: sea level pressure, zonal and meridional components of the surface wind, sea surface temperature, surface air temperature, and cloudiness [4]. The values for the MEI are available from 1950 through the current time at <http://www.esrl.noaa.gov/psd/enso/mei/table.html>. Figure 11 plots the MEI between 1980 and 2015.

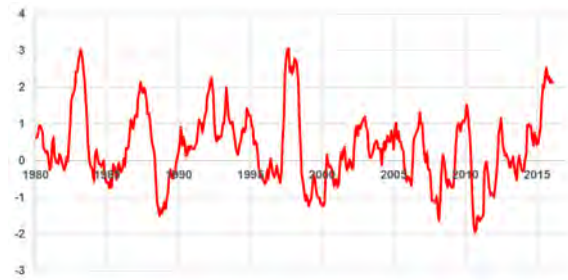


Fig. 11 The Multivariate ENSO Index.

Figure 12 combines Figures 10 and 11 to show the similarity between MEI and residual *LOD*. Three El Niño events and two La Niña events are circled. The 1996–97 El Niño caused an increase in *LOD* of about 750 μ s, and the affect of the current one is similar.

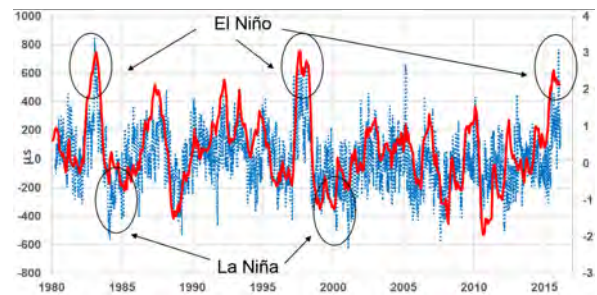


Fig. 12 MEI (solid line) and residual *LOD* (dotted line).

6 Earth as a Clock and the Relationship Between *LOD* and *UT1*

One can view the Earth as a clock. *LOD* is related to the rate of the clock by $LOD=1/Rate$. If the $LOD > 86400s$, then the clock is running slow, whereas if $LOD < 86400s$ the clock is running fast. In this analogy *UT1* is the accumulated error in time and is given by:

$$UT1 = \int (86400s - LOD)dt \quad (6)$$

To illustrate these concepts, consider Figure 13 which shows *LOD*'s seasonal behavior over a two-year period. This has peaks in Northern Hemisphere (NH) Winter and troughs in NH Summer. The difference

between Winter and Summer is due to the North-South asymmetry of the continents, which leads to more storms in NH Winter. These storms increase the *AAM*, which results in a slowing down of the Earth. The NH Winter days are about 1 ms longer than Summer days.

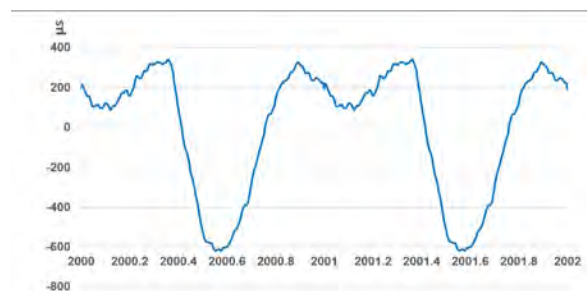


Fig. 13 *LOD*'s seasonal behavior in μs .

Figure 14 shows the seasonal effect on *UT1* over two years. This is obtained by integrating the seasonal *LOD* starting on January 1. *UT1* has a maximum of +30 ms around June 1, and a minimum of -18 ms around October 1.

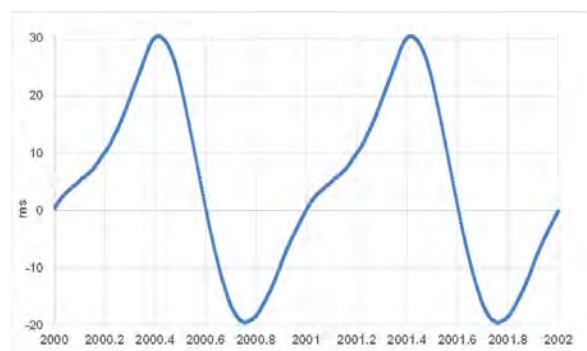


Fig. 14 Seasonal *UT1* in milliseconds.

In the previous section we saw that the 1997–98 and the current El Niño events caused an increase in *LOD* of about 750 μs in the residual *LOD*. If we integrate this we can find the impact on *UT1*. Figure 15 shows the change in *UT1* for the two El Niños. The 1997–98 El Niño had a cumulative effect of 0.1 seconds, and the current event is on track to repeat this. This is three times larger than the normal seasonal changes in *UT1*.

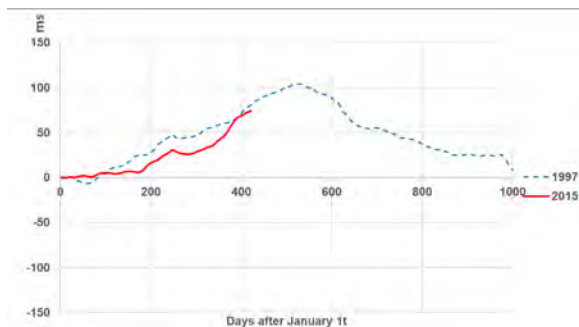


Fig. 15 Change in *UT1* in milliseconds from the 1997 El Niño (dashed line) and the 2015 El Niño (solid line). The X-axis shows days after January 1.

7 Conclusions

In this note we looked at VLBI measured *LOD*. The spectrum of *LOD* demonstrates that there is structure at all time scales. We decomposed *LOD* into several components based on their period and the origin of the effect. We also showed that there is clear correlation between *MEI* and the residual *LOD*. Lastly we looked at the impact of the El Niño on *LOD*. The current El Niño results in a significant increase in *LOD* (the day gets longer). As the 1997–98 El Niño dissipated, *LOD* returned to its baseline value, and we expect the same to happen with the current event.

References

1. Gipson, J. and C. Ma, "Signature of El Niño in Length of Day as Measured by VLBI", IERS Technical Note 26, 1999, pp. 17–29.
2. Petit, G. and B. Luzum, editors, "IERS Conventions 2010", IERS Technical Note No. 36, "Tidal variations in the Earth's rotation".
3. Salstein, D.A., D.M. Kann, A.J. Miller, and R.D. Rosen, (1993). The sub-bureau for atmospheric angular momentum of the International Earth Rotation Service (IERS); a meteorological data center with geodetic applications. Bull. Am. Meteorol. Soc., 74, 67–80.
4. Wolter, K., and M. S. Timlin, 2011: El Niño/Southern Oscillation behaviour since 1871 as diagnosed in an extended multivariate ENSO index (MEI.ext). Intl. J. Climatology, 31, 14pp., 1074–1087.

The Annual Retrograde Nutation Variability

C. Gattano, S. Lambert, C. Bizouard

Abstract Very Long Baseline Interferometry is the only technique that can estimate Earth nutations with an accuracy under the milliarcsecond level. With 35 years of geodetic VLBI observations, the principal nutation terms caused by luni-solar tides and geophysical response have been estimated. We focus on the variability. Two of them present very significant amplitude and phase variations: the retrograde Free Core Nutation (FCN) with a period of around 430 days and the Annual Retrograde Nutation (ARN). Despite progress made in global circulation models, the atmospheric and ocean excitation cannot account for that. In particular the ARN shows an amplitude modulation of approximately six years, reminiscent of the six-year geomagnetic oscillation in the Length-of-Day (LOD). As to the latter, we suggest that the nutation term variability may have deep Earth causes, and we estimate an order of magnitude of Earth internal structure parameters to explain this variability.

Keywords Nutation, least-squares adjustment, ARN

1 Introduction

The last approved nutation model, MHB2000 [14], was derived from VLBI data. They have adjusted 1365 luni-solar and planetary terms, associating constant amplitudes and phases with each of them. But this model was unsuccessful in explaining the free core nutation (FCN) that increases by more than 100 μas at some

times. This nutation arises from a geophysical response to luni-solar attraction, and it finds its source in the coupling between the fluid outer core and the mantle. This coupling can be of viscous nature, of electromagnetic nature, or due to the topography of the boundary.

Therefore, to estimate correctly the variation of the FCN is important for the understanding of the inner structure of the Earth. Many studies have been published on its estimation, and several models exist: Malkin (2013) [12], Krásná et al. (2013) [10], Belda et al. (2016) [1]. One of them has been selected as reference by the IERS: the Lambert model¹ [16]). These works have in common that they estimate the variability using a window with a width on the order of the FCN period. The proximity of the annual retrograde nutation (ARN) with the FCN can be dangerous because of the beat phenomenon. Given the variability of the FCN and possibly of the ARN, a least-squares adjustment approach may not succeed.

2 Data

We carried out a comparison of several nutation time series provided by different Analysis Centers of the IVS (see Table 1). The nutation time series used in this study are offsets according to the IAU2000A/2006 precession-nutation model [14, 5] in dX, dY parametrization. Despite the divergence between the nutation time series that may be associated with differences in analysis strategies², the Analysis Center products are in agreement on the Free Core

SYRTE, Observatoire de Paris, PSL Research University, CNRS, Sorbonne Universités, UPMC Univ.

¹ http://syrtte.obspm.fr/~lambert/fcn/notice_fcn.pdf

² We do not present an analysis comparison in this study. But if you are interested, you can find all technical files for each IVS so-

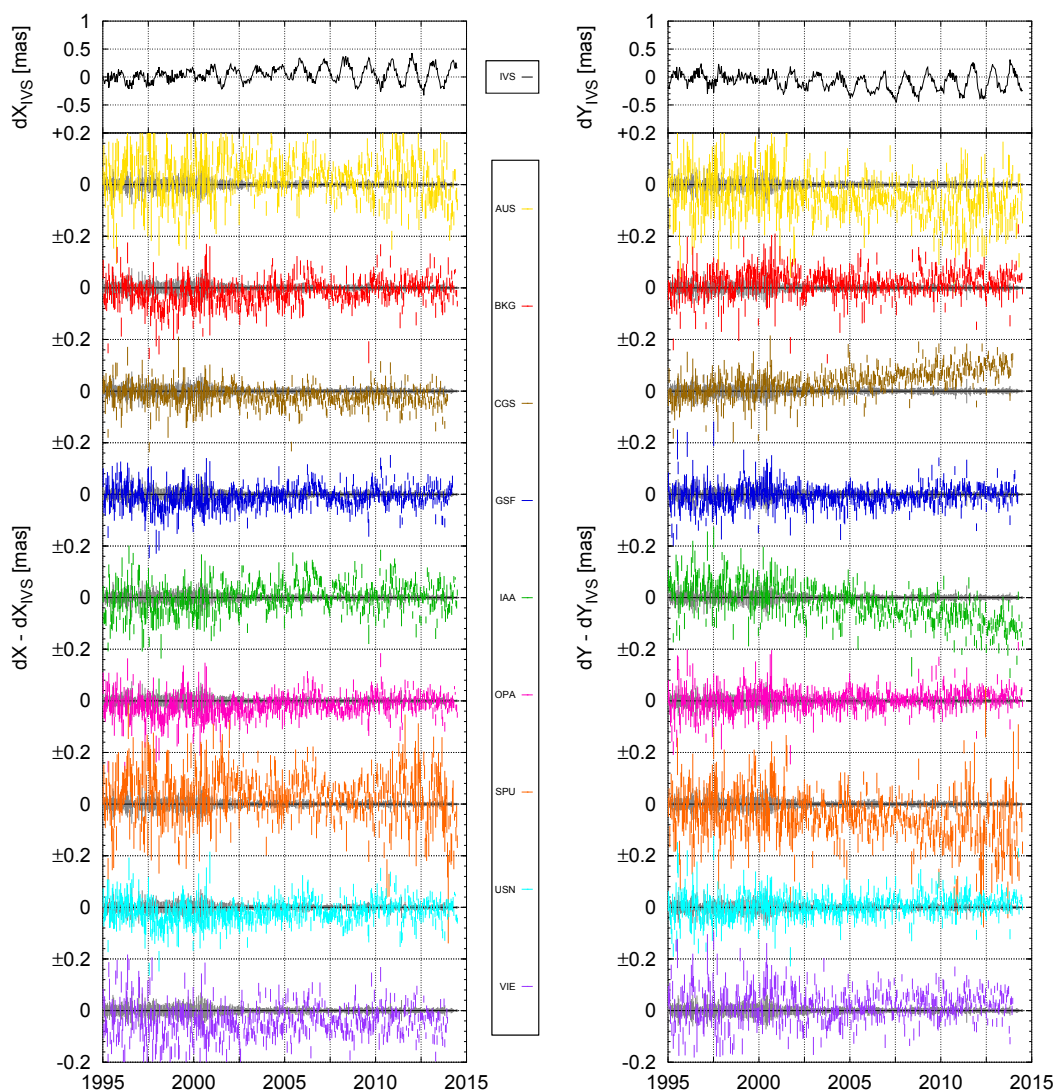


Fig. 1 Comparison of dX, dY from several IVS Analysis Centers with respect to the IVS combination solution.

Nutation (FCN) and the Annual Retrograde Nutation (ARN) products and their variability at the level of about $30 \mu\text{as}$.

3 Analysis

Earth nutations can be of luni-solar(-planetary) origin, e.g., the Annual Retrograde Nutation (ARN), or can

be a response of the Earth structure, from inner core to superficial fluid layers, to external gravitational perturbation and show up at different frequencies that the latter one, as is the case for FCN. It is common to state that the luni-solar nutations are constant in amplitude, phase, and frequency, whereas those produced by geophysical response are known to be variable in amplitude and phase (e.g., Lambert model [16]) and in frequency (e.g., Gubanov 2010 [8]).

lution in one of three primary IVS Data Centers (CDDIS, BKG, OPA) or see Gattano et al. [7].

In this study, we suppressed the hypothesis of constance for the luni-solar nutation, especially for the ARN, and we adjusted it simultaneously with the FCN

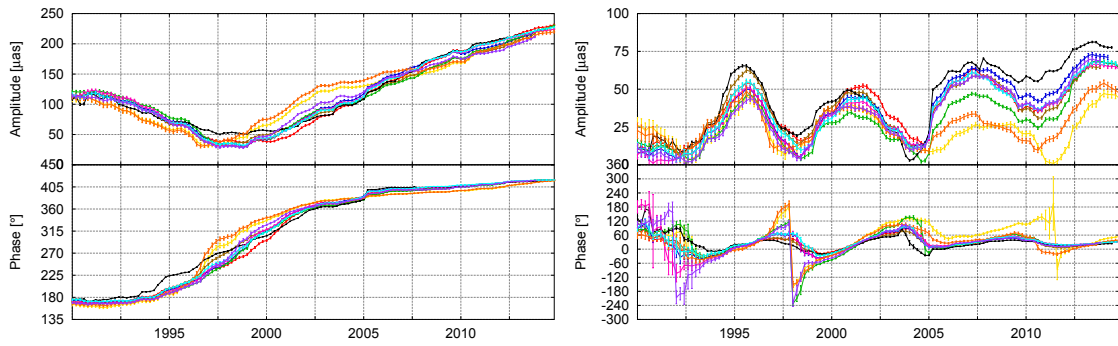


Fig. 2 Free Core Nutation and Annual Retrograde Nutation simultaneous adjustments using a seven-year sliding window least-squares approach.

Table 1 Nutation time series of several IVS Analysis Centers.

Solution	Analysis Center
aus00007	Geoscience Australia, Canberra
bkg00014	Bundesamt für Kartographie und Geodäsie, Leipzig, Germany
cgs2014a	Centro di Geodesia Spaziale, Matera, Italy
gsf2014a	NASA Goddard Space Flight Center (GSFC), Greenbelt, MD, USA
iaa2007a	Institute of Applied Astronomy, Saint Petersburg, Russia
opa2015a	Paris Observatory, France
spu00004	Saint-Petersburg University, Russia
usn2015a	United States Naval Observatory (USNO), Washington, DC
vieeop13	Vienna University of Technology, Austria
ivs14q2X	IVS Combination Center, Germany

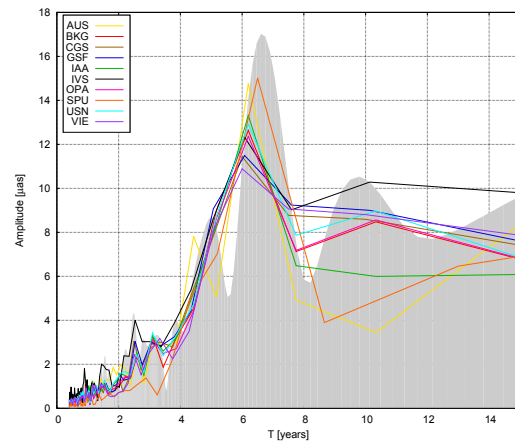


Fig. 4 Spectrum comparison of the ARN least-squares adjustment of the IVS nutation time series. The gray area shows the oversampled spectrum of the IVS, to investigate the details of the spectrum.

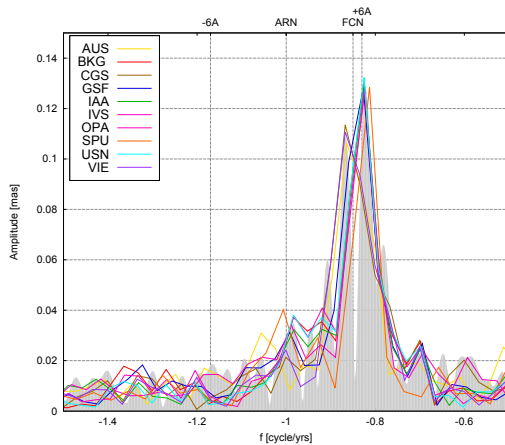


Fig. 3 Spectrum comparison of the IVS nutation time series around the annual retrograde range. The gray area shows the oversampled spectrum of the IVS, to investigate the details of the spectrum.

by means of a seven-year sliding window in a least-squares approach, to ensure the demodulation due to the beat, and decayed every 0.2 year. The rigid Earth model [18] predicts an amplitude of 24 mas, amplified by a factor ≈ 1.3 in the non-rigid Earth model [14]. Our analysis of the ARN products of the IVS Analysis Centers clearly shows a periodical modulation with a period of about six years and an intensity of about 20 μas , confirmed when we look at the spectrum (Figure 4).

Can this variability be an artefact from our analysis? Indeed, the sum of two periodic signals, one at the ARN period and the other at the FCN period, leads to a single modulated signal with a modulation period of 6.62 years, suspiciously close to the period of the

peak in Figure 4. In the spectral domain, if the ARN is truly modulated in amplitude with a six-year period, the spectrum should present two symmetric peaks around the ARN frequency: one at the right place of the FCN and thus invisible because of the dominance of the latter, one on the other side. By studying the spectrum of several IVS solutions (Figure 3), we see no evidence of such a second peak around -313 days (-1.17 cycle/year in frequency), even if we see a dissymmetry of the FCN pattern, amplified by about $20 \mu\text{as}$ at the right place where the ARN modulation peak should be. But the surroundings also show that fluctuations are also at the level of $20 \mu\text{as}$, and the amplitude modulation we see in the least-squares adjustment would be hidden in those fluctuations. So it is difficult to conclude anything from the spectral domain.

Following the IVS General Meeting we tested our least-squares adjustment approach on artificial data and tried to recover the FCN and ARN amplitude variations from the constructed dX, dY series. We cannot show the results in this paper, but we can give the preliminary conclusions. The least-squares adjustment is perfect in the case of constant nutation. But when we make the ARN and/or the FCN vary, things are more complicated. When the FCN varies, which is a known fact nowadays, some pseudo-oscillations of about five to six years appear, even if the ARN is constant. Furthermore, if the ARN truly varies at these periods, it creates a false signal of about three years in the FCN, when adjusting it using a smaller width window. For example, in a recent study [1], a comparison of various FCN models adjusted with a window size in the range of the FCN period is presented. In their amplitude series, we see some bumps of several years width that can be an effect of an ARN variation. Another work [13] uses a similar algorithm associating these features to geomagnetic jerks whereas it can just be an effect of an ARN variation that has been missed.

Currently, it is still unclear to us what happened between the FCN and the ARN, but it seems that the least-squares adjustment is not suitable for a correct estimation of both of them.

4 Geophysical Interpretation

Whether the retrograde annual nutation is variable in amplitude may have consequences for our understand-

ing of the Earth's deep interior. Mechanisms driving such a variability would be searched at the surface of the Earth or inside the Earth. Surface fluids, especially the atmosphere which dominates at the diurnal frequencies, exert a variable torque on the Earth. Nevertheless, in absence of reliable or consistent data sets, it is today difficult to make conclusions about their contribution (see, e.g., [6, 11]). Inside the Earth, the main source of excitation is the tidally (or electromagnetically) driven core flow interacting at the core-mantle boundary (CMB) and the inner core boundary (ICB). The core flow is tied to the walls of the cavity by viscous, topographic, or electromagnetic couplings. The former occur when, e.g., the fluid is trapped in incursions of the CMB in the mantle. The latter comes up if there is a thin metallic layer at the base of the mantle that can be permeated by the toroidal magnetic field [17, 2, 3]. Another source of excitation is the gravitational coupling between the inner-core and the mantle (e.g., [4, 3, 15]). Recently, a six-year oscillation detected in the length-of-day (LOD) was possibly accounted for by a combination of the above mechanisms [15], while Holme & de Viron [9] suggested that observed jumps in the LOD were direct signatures of geomagnetic jerks.

In the diurnal band, the amplitude of the nutation is mainly governed by the FCN resonance occurring near -430 days. The resonant frequency is

$$\sigma_{\text{FCN}} = -\Omega - \Omega \frac{A}{A_m} \left(e_f - \beta + K_{\text{CMB}} + \frac{A_s}{A_f} K_{\text{ICB}} \right),$$

where $A, A_{m,f,s}$ are the mean moment of inertia of the whole Earth, the mantle, the fluid outer core, and the solid inner core, respectively; e_f is the core flattening; β is a compliance expressing the deformation at the surface when a pressure is applied to the CMB; and $K_{\text{CMB,ICB}}$ are coupling constants at the CMB and the ICB (see Mathews et al. 2002). Note that K_{CMB} is directly proportional to the radial component of the magnetic field at the CMB.

We used the transfer function of Mathews et al. (2002) to constrain a possible departure of the global constant $K_{\text{CMB}} + A_s/A_f K_{\text{ICB}}$ with respect to the model and allowing the observed variability of the annual retrograde nutation. Results are reported in Figure 5. The coupling constant remains within $\sim 10^{-6}$ which is actually the order of magnitude of the uncertainty given by Mathews et al. (2002) for

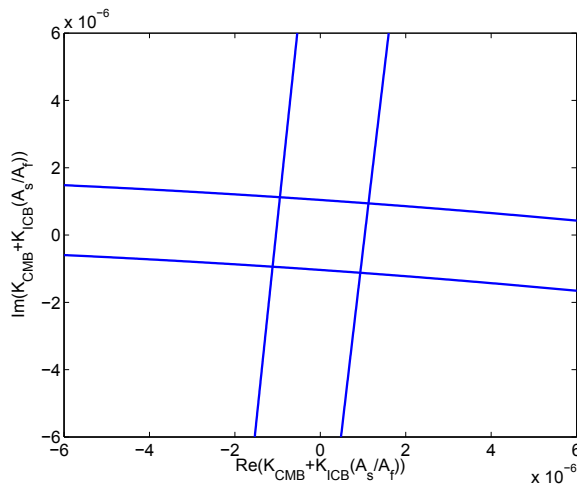


Fig. 5 The region where the global coupling constant $K_{\text{CMB}} + A_s/A_T K_{\text{ICB}}$ can vary to account for the observed variability of the retrograde annual nutation.

$\text{Im}K_{\text{CMB}}$ but smaller than the uncertainty for K_{ICB} . Such a change would push the FCN period by a few hours only, which is hardly detectable by direct observation of the free motion or indirect determination of the resonance through VLBI or superconducting gravimeter data (e.g., Rosat & Lambert 2009).

5 Conclusions

We decided to suppress the hypothesis of the constance of the luni-solar nutation, especially for the Annual Retrograde Nutation (ARN). We used dX, dY data from several IVS Analysis Centers and adjusted for FCN and ARN simultaneously using a seven-year sliding window least-squares adjustment approach. The result for the ARN was to find a variation of a six-year period in the amplitude and phase time series.

But the configuration is complicated here because of the proximity of the frequencies between ARN and FCN. A modulation phenomenon arises from this closeness and impacts the least-squares algorithm. Testing this algorithm on artificial data reveals that the periodic signal we see in ARN, but also some periodic features we can see in FCN in the literature (e.g.,

[1, 13]), could be a contamination of the variability of one or the other. Spectral analysis is also not conclusive about the trueness of the ARN variability.

Furthermore, the study of the geophysical consequence of such a variability, in the inner structure of the Earth, reveals changes in parameters that are actually on the order of magnitude of the error bars given by the current reference model of Mathews et al. [14]. This means that we have to clarify the situation between FCN and ARN from the data, and the least-squares adjustment may become useless and should be replaced by a more refined technique.

References

1. S. Belda et al., In *Journal of Geodynamics*, 94, 59–67, 2016.
2. B. A. Buffett, In *Journal of Geophysics Research*, 97, 19, 1992.
3. B. A. Buffett et al., In *Journal of Geophysical Research (Solid Earth)*, 107, 2070, 2002.
4. B. A. Buffett, In *Geophysics Research Letters*, 23, 2279–2282, 1996.
5. N. Capitaine et al., In *Astronomy & Astrophysics*, 432, 355–367, 2005.
6. O. de Viron et al., In *Journal of Geophysical Research (Solid Earth)*, 110, 11404, 2005.
7. C. Gattano et al., In *SF2A-2015: Proceedings of the Annual meeting of the French Society of Astronomy and Astrophysics*, pages 115–119, 2015.
8. V. S. Gubanov, In *Astronomy Letters*, 36, 444–451, 2010.
9. R. Holme, O. de Viron, In *Nature Letter*, 499, 202–204, 2013.
10. H. Krásná et al., In *Astronomy and Astrophysics*, 555, A29, 2013.
11. S. B. Lambert, In *Astronomy and Astrophysics*, 457, 717–720, 2006.
12. Z. Malkin, In *Journal of Geodynamics*, 72, 53–58, 2013.
13. Z. Malkin, In *ArXiv e-prints*, 2016.
14. P. M. Mathews et al., In *Journal of Geophysical Research (Solid Earth)*, 107, 2068, 2002.
15. J. E. Mound, B. A. Buffett, In *Journal of Geophysical Research (Solid Earth)*, 108, 2334, 2003.
16. G. Petit et al., In *IERS Conventions (2010)*, IERS Technical Note 36, 2010.
17. M. G. Rochester, In *Journal of Geophysics Research*, 67, 4833–4836, 1962.
18. J. Souchay et al., In *Astronomy and Astrophysics, Supplement*, 135, 111–131, 1999.

Tidal Atmospheric Loading and VLBI

Anastasiia Girdiuk, Michael Schindelegger, Johannes Böhm

Abstract This study is dedicated to the influence of diurnal atmosphere-ocean dynamics on Earth rotation and loading effects as observed by Very Long Baseline Interferometry (VLBI). In the first part, we investigate loading signals caused by atmospheric tides and the associated mass variations in the ocean. Different models are compared by means of baseline length repeatability; furthermore, consistent corrections for the atmosphere and the ocean are discussed. We also show VLBI results for two gravitational ocean tide models (FES2004 and FES2012), where the latter benefits from a much finer horizontal resolution and an improved description of hydrodynamic processes. As a result of the comparisons, the effect of changing loading is insignificant with respect to baseline length repeatability. The second part focuses on the Earth rotation variations associated with atmospheric tides, comprising small but non-negligible oscillations on the order of $10 \mu\text{s}$. Here, we compare tidally analyzed VLBI observations against estimates from different providers of numerical weather models. In summary, changing atmospheric and ocean models in VLBI analysis does not affect the tidal terms analysis. For example, the principal atmospheric diurnal radiational S_1 tide shows a small variability for applied loads.

Keywords Geodetic VLBI analysis, tidal terms analysis, VLBI reduction, atmospheric loading, ocean loading

TU Wien, Geodesy and Geoinformation, Research Group of Advanced Geodesy

1 Introduction

Tidal atmospheric loading provides a small contribution to station coordinate changes, but it should not be neglected due to its periodic behavior. Diurnal S_1 and semi-diurnal S_2 present periodic signals of the tidal atmospheric loading in the routine VLBI analysis as recommended by the IERS Conventions [8]. At the same time, the Earth's crust is affected by the irregular atmospheric non-tidal loading which is calculated based on atmospheric pressure fields as provided by meteorological models. Although this contribution to station coordinate changes is not recommended by the IERS Conventions, it causes large ground surface deviations and is thus usually corrected for in VLBI solutions. In the following we assess the impact of atmospheric tidal and non-tidal loadings as well as ocean tidal loading on baseline length repeatability (Section 3) and on tidal terms in Earth rotation parameters (Section 3.1).

2 Data

Geodetic 24-hour VLBI sessions with at least five antennas in the time span from May 1995 to May 2015 are processed by using the Vienna VLBI Software (VieVS) [7] as follows:

1. Outlier detection of observed residuals;
2. Celestial pole offset estimation to get *a priori* daily Earth Orientation Parameter (EOP) values based on the daily final EOP time series [8];
3. Generation of long hourly Earth Rotation Parameters (ERP) time series making use of the *a priori* EOP model as described above;

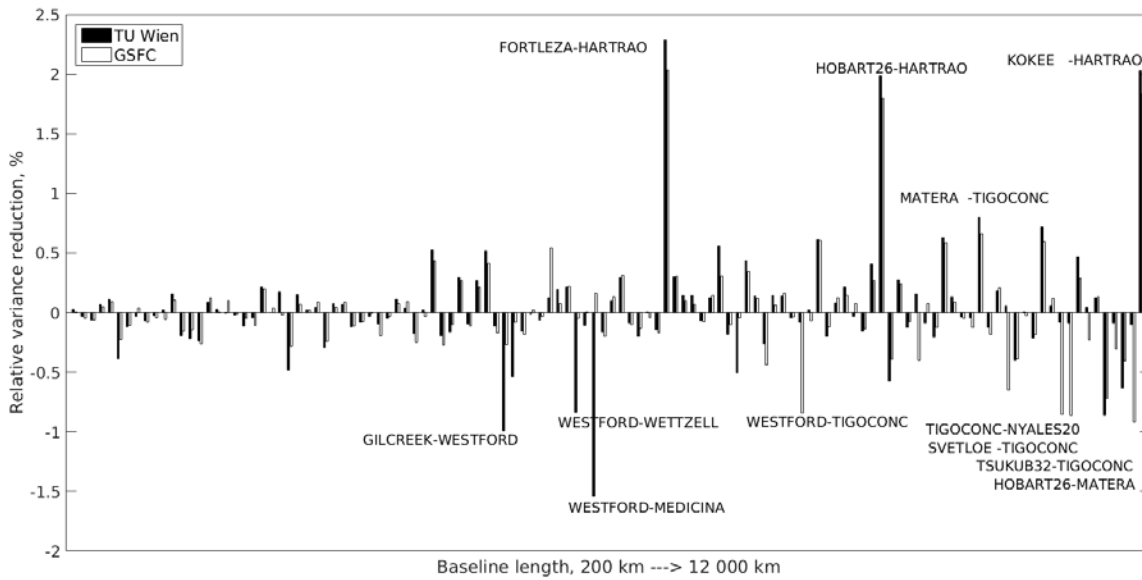


Fig. 1 Relative variance reduction for VLBI baseline length repeatabilities when using the models by TU Wien and GSFC w.r.t. not correcting for atmospheric tidal loading.

4. Estimation of baseline length repeatability in a separate run. The station coordinates are fixed to the realization by [3] in the other solutions.

A priori models, methods, and constraints are widely used and are described in detail in [3] and [13]. Usually, a global solution, which accumulates normal equations of all sessions available, is carried out for the determination of tidal terms in Earth rotation parameters. In spite of the extensive application of the global solution the single session time series approach is employed in this study and provides the hourly ERP values (max. 25 points per session) derived by inverting each VLBI session separately in VieVS.

3 Analysis

Tidal atmospheric loading as provided by TU Wien (Vienna University of Technology) [15] and Goddard Space Flight Center (GSFC) models [10] are compared in this study. A description of these models is presented in Table 1. The main differences are in the calculation methods, the weather models, and the land-sea masks. The calculation of atmospheric pressure fields is divided into two parts [11] for both models: the tidal part as recommended by the IERS Conventions

Table 1 Description of the atmospheric and ocean models.

Model	Weather Model	Land-sea Mask
TU Wien	Tidal: European Centre for Medium-Range Weather Forecasts (ECMWF) delayed cut-off stream (DCDA) every 3 h Non-tidal: ECMWF 6h with 1° resolution	determined from Earth TOPOgraphic terrain model ETOPO5 1° resolution
GSFC	National Center for Environmental Prediction (NCEP) Reanalysis 6 h with 2.5° resolution	from Finite Element Solution FES99 0.25° resolution
Model	Weather Model	Uniform Grid
FES2004	S ₁ : from R. Ray, operational (op.) ECMWF 6 h	1/8°
FES2012	S ₁ : op. ECMWF DCDA 3 h anal.	1/16°

and the non-tidal part, which is not accounted for in the IERS Conventions. The underlying weather models have different providers and grid resolutions: the TU Wien model uses a finer resolution. The implemented land-sea mask has a better resolution in the case of the GSFC model. However, both are not consistent with the uniform grid of the two ocean models.

Changes in loads are analyzed by means of relative variance reduction expressed as percentage. The variance reduction is calculated for the baseline length repeatability, and, thus, the relative variance is the differ-

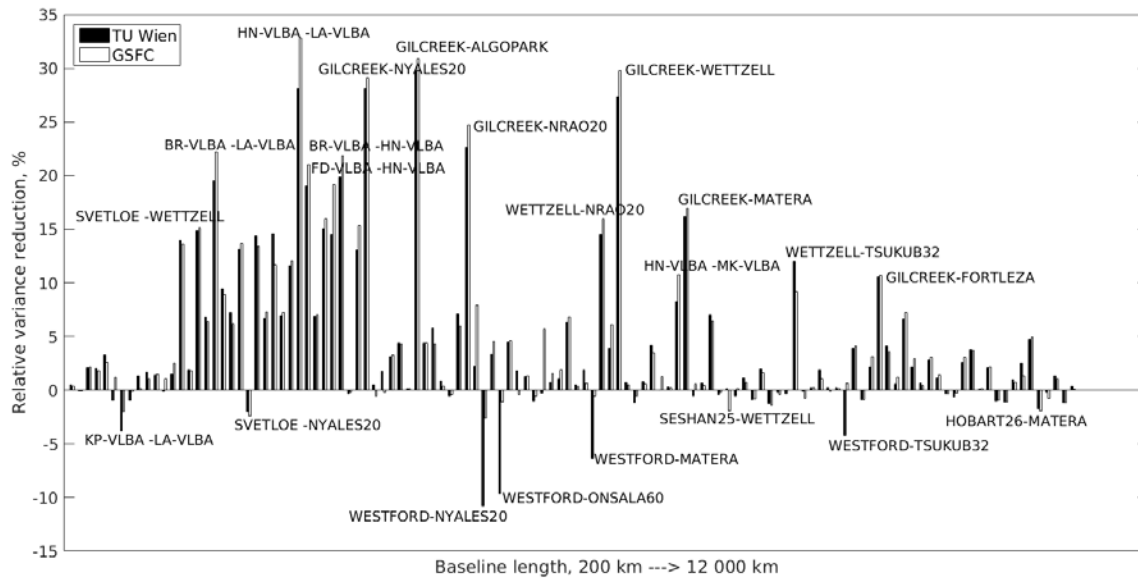


Fig. 2 Relative variance reduction for VLBI baseline length repeatabilities when using the models by TU Wien and GSFC w.r.t. not correcting for atmospheric non-tidal loading.

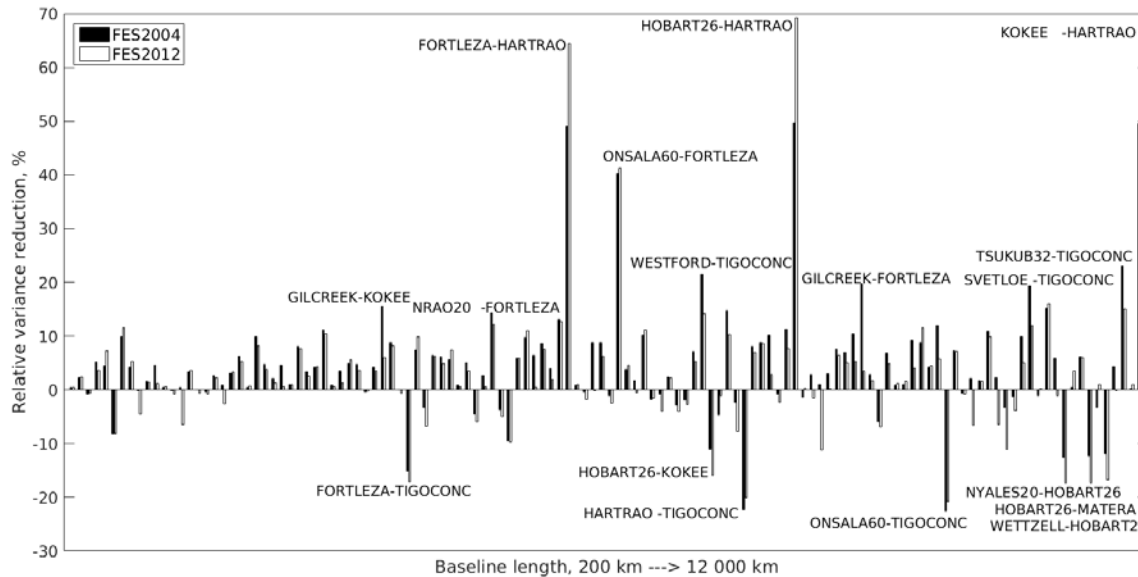


Fig. 3 Relative variance reduction for VLBI baseline length repeatabilities when using the models FES2004 and FES2012 w.r.t. not correcting for tidal ocean loading.

ence between the squared repeatabilities of the same baseline normalized by a reference one. For this reason the station coordinates are calculated in a separate run, and several solutions are obtained: two solutions with respect to both TU Wien and GSFC (tidal and non-tidal loadings included) and two solutions (for each provider) disregarding tidal and (two solutions as well)

non-tidal loading. As the major condition, the baselines observed in at least 100 sessions are assembled, and, also, the tidal and non-tidal loadings are available from both models during these sessions. In this setup some baselines had to be excluded in the comparison because of missing loading data.

Figure 1 shows a comparison of the atmospheric tidal loading and Figure 2 of the atmospheric non-tidal loading, where positive values represent improvements in baseline length repeatability with the corrections applied. The scattering of the relative variance reduction is smaller in the case of atmospheric tidal loading (Figure 1) than for atmospheric non-tidal loading (Figure 2). Therefore, the non-tidal part of atmospheric loading should not be neglected but taken into account as well. This is still not recommended by the IERS Conventions due to having no agreement on adopted models of non-tidal displacement. However, the statistical tests performed in this study prove that the models by TU Wien and GSFC do not have statistically significant discrepancies.

Additionally, the large ocean tidal loading influence comparably to atmosphere in station coordinate changes is tested between two models listed in Table 1: FES2004 and FES2012. In the case of ocean loading calculation the underlying weather model has a better agreement with the weather model used to calculate atmospheric corrections as provided by TU Wien; nevertheless, the uniform grid is improved for FES2012 and disagrees with both atmospheric models. The station displacements were calculated by M. S. Bos and H.-G. Scherneck (Ocean tide loading provider [1]) for FES2004 and by Leonid Petrov (International Mass Loading Service [9]) for FES2012. The relative variance reduction is used similar to the comparison of atmospheric loadings. The reference solution does not account for ocean loading at all and is compared with solutions in Figure 3 where FES2004 or FES2012 are applied. In the same way, the positive numbers depict baseline repeatability improvement when introducing the FES2004 or FES2012 models. Also, several baselines show degradation of the model performance and demand further investigation as well as identical behavior of atmospheric models. Again, there is no evidence that one ocean model has a statistically better value.

3.1 Tidal Terms Analysis

Hourly original ERP time series of polar motion and length-of-day (converted from Universal Time difference (dUT1)) are processed by means of a single session time series approach. Least-squares adjustment is

employed for processing of the ERP time series with standard deviations as provided by VieVS introducing a stochastic model as well.

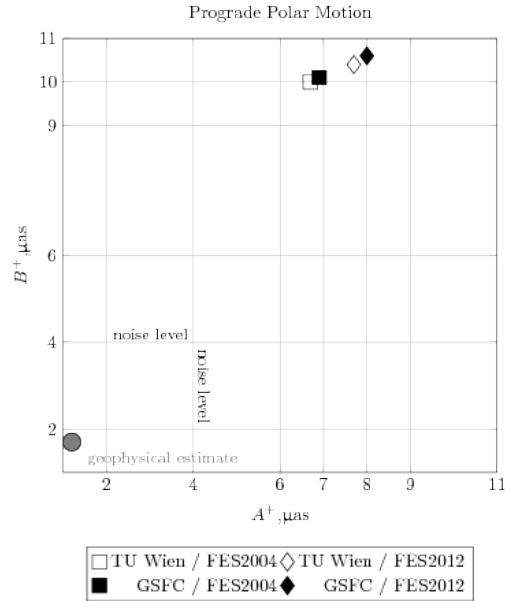


Fig. 4 Tidal terms analysis for prograde polar motion at S1.

Diurnal and semi-diurnal prograde A_j^+ , B_j^+ and retrograde A_j^- , B_j^- coefficients are estimated in a standard harmonic model, e.g., for pole coordinates at epochs t_i :

$$\begin{aligned} x_p &= \sum_{j=1}^n (-A_j^+ - A_j^-) \cos \alpha_j + (B_j^+ - B_j^-) \sin \alpha_j, \\ y_p &= \sum_{j=1}^n (B_j^+ + B_j^-) \cos \alpha_j + (A_j^+ - A_j^-) \sin \alpha_j, \end{aligned} \quad (1)$$

where $\alpha_j = \alpha_j(t_i)$ are the angular (fundamental) arguments [14]. All in all 70 tides (neglecting gravitational S_1 , i.e., only radiational S_1 are estimated) as published in the IERS Conventions plus six zero tides, where no excitation signals are expected, are estimated based on a high-frequency (HF) ocean model. The HF ocean model from the IERS Conventions is applied as a priori in the single session VieVS processing and consistent with the FES2004 ocean model. In case of FES2012 the a priori HF ocean model (26 tides) has been calculated by Matthias Madzak (PhD thesis [6]) and applied consistently with FES2012 ocean tidal loading.

Tidal terms analyses were performed for every solution differing in atmospheric and ocean loading corrections to investigate inconsistencies (about 10 μas)

with geophysical estimates (about 2 μs) obtained by M. Schindelegger et al. [12]. For this reason we focus on the principal diurnal atmospheric tide S_1 shown in Figure 4. Zero tides are introduced in the model additionally and used to mark noise levels in the obtained time series. The differences between the S_1 estimates in Figure 4 with respect to the underlying atmospheric and ocean models for station corrections are on the noise level of the obtained time series and seem to be insignificant, similar to the comparison of these models by means of baseline repeatability. Unfortunately, the efforts undertaken in this study focusing on the changes in different loads do not solve the problem of an approximately 10 μs discrepancy between the geophysical estimate and the VLBI derived estimates as obtained in this work (see Figure 4).

4 Conclusions

The tidal atmospheric loading is applied in VLBI reductions as a small correction for station coordinates; however, the atmospheric non-tidal loading is still not accounted for in the IERS Conventions and improves baseline length repeatability significantly (3% for tidal loading vs. up to 35% for non-tidal loading). Atmospheric corrections for station positions were varied between two models as provided by TU Wien and GSFC, with the two models having a very good agreement. Additionally, ocean tidal loading was tested between the models FES2004 and FES2012 because of its large contribution to station coordinate changes (improving the baseline length repeatability by up to 70%). The discrepancies when using these models are not significant, similar to the atmospheric models. In the same way, tidal terms analysis does not reveal any differences between solutions obtained in this study, where the loads are replaced by different providers. Thus, this topic requires further investigation because of the big discrepancy with geophysical estimates.

Acknowledgements

Financial support for this study was made available by the IAG travel grant and the Austrian Science Fund under project ASPIRE (I1479).

References

1. M. S. Bos, H. G. Scherneck, "Free ocean tide loading provider", <http://www.oso.chalmers.se/loading>, 2007.
2. L. Carrère, F. Lyard, M. Cancet, A. Guillot, L. Roblou, "FES2012: A new global tidal model taking advantage of nearly 20 years of altimetry", Proceedings of meeting "20 Years of Altimetry", Venice, 2012.
3. H. Krásná, J. Böhm, L. Plank, T. Nilsson, H. Schuh, "Atmospheric Effects on VLBI-derived Terrestrial and Celestial Reference Frames", In C. Rizos and P. Willis, editors, *Earth on the edge: science for a sustainable planet*, International Association of Geodesy Symposia, Springer, Melbourne, Australia, pages 203–208, 2014.
4. F. Lyard, F. Lefevre, T. Letellier, O. Francis, "Modelling the global ocean tides: modern insights from FES2004", *J Ocean Dyn* 56:394–415, 2006.
5. P. Mathews, T. Herring, B. Buffett, "Modeling of nutation and precession: New nutation series for nonrigid Earth and insights into the Earth's interior", *J Geophys Res* 107:B42068, 2002.
6. M. Madzak, "Short period ocean tidal variations in Earth rotation", PhD thesis, Vienna University of Technology, 2015.
7. M. Madzak, S. Böhm, H. Krásná, L. Plank, "Vienna VLBI Software Version 2.1 User Manual", <http://vies.geo.tuwien.ac.at/fileadmin/editors/VieVS/documents/viesDoc.pdf>
8. G. Petit, B. Luzum, "IERS Conventions (2010)", Frankfurt am Main: Verlag des Bundesamts für Kartographie und Geodäsie, 2010.
9. L. Petrov, "The International Mass Loading Service", <http://arxiv.org/abs/1503.00191>, 2015.
10. L. Petrov, J. P. Boy, "Study of the atmospheric pressure loading signal in very long baseline interferometry observations", *J Geophys Res* 109:B03405, 2004.
11. R. M. Ponte, R. D. Ray, "Atmospheric pressure corrections in geodesy and oceanography: A strategy for handling air tides", *Geophys Res Lett* 29:2153, 2002.
12. M. Schindelegger, D. Einšpigel, D. Salstein, J. Böhm, "The global S_1 tide in Earth's nutation", *Surv Geophys*, pages 1–38, 2016.
13. H. Schuh, J. Böhm, "Very long baseline interferometry for geodesy and astronomy", In G. Xu, editors, *Sciences of geodesy—II: innovations and future developments*, Springer, New York, pages 339–376, 2013.
14. J. Simon, P. Bretagnon, J. Chapront, M. Chapront-Touze, G. Francou, J. Laskar, "Numerical expressions for precession formulae and mean elements for the Moon and the planets", *Astron Astrophys* 282:663–683, 1994.
15. D. Wijaya, J. Böhm, M. Karbon, H. Krásná, H. Schuh, "Atmospheric pressure loading", In J. Böhm and H. Schuh, editors, *Atmospheric effects in space geodesy*, Springer-Verlag Berlin Heidelberg, pages 137–158, 2013.

Progress on the VLBI Ecliptic Plane Survey

Fengchun Shu¹, Leonid Petrov², Wu Jiang¹, Jamie McCallum³, Sang-oh Yi⁴, Kazuhiro Takefuji⁵, Jinling Li¹, Jim Lovell³

Abstract We launched the VLBI Ecliptic Plane Survey program in 2015. The goal of this program is to find all compact sources within 7.5° of the ecliptic plane which are suitable as phase calibrators for anticipated phase referencing observations of spacecrafts. We planned to observe a complete sample of the sources brighter than 50 mJy at 5 GHz listed in the PMN and GB6 catalogs that have not yet been observed with VLBI. By April 2016, eight 24-hour sessions had been performed and processed. Among 2,227 observed sources, 435 sources were detected in three or more observations. We also ran three eight-hour segments with the VLBA for improving the positions of 71 ecliptic sources.

Keywords Radio astrometry, catalogs, ecliptic plane, high sensitivity observations

1 Introduction

This paper presents the status report of the ongoing VLBI Ecliptic Plane Survey (VEPS) program. The first goal of the program is to search for more ecliptic calibrators using a minimum network of three stations. We consider a source that is brighter than 30 mJy at a baseline projection length of 5,000 km as a calibrator. We have selected all objects within 7.5° of the eclip-

tic plane, with single dish flux densities brighter than 50 mJy at 5 GHz from the PMN (Parkes-MIT-NRAO) and GB6 (Green Bank 6 cm) catalogs except for those:

- that have been detected with VLBI before or
- that were observed with VLBI in a high sensitivity mode (detection limit better than 20mJy), but have not been detected.

As the number of target sources is more than 7,000, we planned to observe in two phases:

- Phase-A — Observations of 2,216 sources that have total flux densities at 5 GHz > 100 mJy
- Phase-B — Observations of 4,802 sources that have total flux densities at 5 GHz in the range [50, 100] mJy

More details about the observations of this large sample of target sources are given in Sections 2–4.

The second goal of the VEPS program is to improve the position accuracy to better than 1.5 nrad for those ecliptic calibrators detected in various VLBI experiments, but with large position uncertainties. This type of observation should be performed at S/X dual band and use a large network such as the VLBA, EVN, or IVS in a high-sensitivity mode. We will address this issue in Section 5.

2 Observations

The Phase-A observations began in February 2015. The participating stations include the three core Chinese VLBI stations: Seshan25, Kunming, and Urumqi. However, sometimes they are not available at the same time, or occasionally one or two of them have a risk of

1. Shanghai Astronomical Observatory, Chinese Academy of Sciences

2. Astrogeo Center

3. University of Tasmania

4. National Geographic Information Institute

5. National Institute of Information and Communication Technology

failure. In that case, one or two international stations are required.

Figure 1 shows the geographical distribution of all participating stations. Kashima34, Sejong, and Hobart26 have contributed to the past VEPS observations. They have middle-sized antennas and good common visibility for the ecliptic zone. Before joining in the VEPS survey, we made fringe tests to Sejong, Hobart26, and Kashima34 in December 2014, July 2015, and January 2016 respectively.

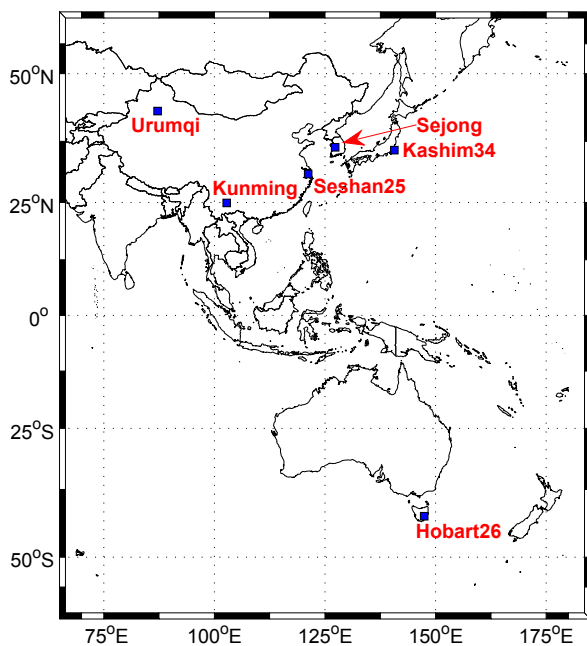


Fig. 1 Distribution of participating stations.

So far eight sessions have been observed, as summarized in Table 1. Each target source was observed in two scans of 90 seconds. Four calibrators were observed every hour for the reduction of atmospheric effects and amplitude calibration.

Figure 2 shows the frequency sequence used in the Phase-A observations. Eight USB channels and eight LSB channels spread over about an 800-MHz frequency range at X-band result in 16 IF channels, and the bandwidth for each IF channel is 32 MHz, so the total data rate is 2048 Mbps with two-bit sampling. The data volume is close to 16 TB for each station in one 24-hour session.

For the Sejong station, the maximum rate is 1024 Mbps, so the data sampling was changed to one bit. For

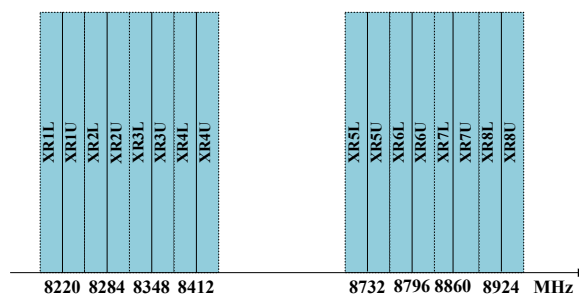


Fig. 2 Frequency sequence used in the VEPS observations.

Hobart26, its 32 MHz bandwidth had not been tested at that time, so we observed the first 16-MHz bandwidth for each IF channel instead. In the case of a 1024-Mbps data rate, the data volume is close to 8 TB for each station in one session.

3 Data Processing

The data from the Chinese domestic stations were recorded on 16-TB diskpucks and then shipped to Shanghai, while the data from international stations were transferred to Shanghai via high-speed network. The data volume for each session is much bigger than that of regular geodetic sessions, so the data processing is very time-consuming. Another technical issue is the correlation of mixed observing modes with different bandwidths or sampling bits. This could be supported by the DiFX correlator installed at Shanghai, which also serves as one of the IVS correlators.

For the correlation of one-bit sampled data from Sejong against two-bit sampled data from the other stations, a different treatment was implemented in the station-based processing module, and it turned out to have the same results after the data were transformed to the frequency domain.

For the correlation of 16-MHz bandwidth data from Hobart26 against 32-MHz bandwidth from the other stations, the zoom mode was selected to pick up the overlapped frequency band. Moreover, it was optional to correlate only on the 16-MHz bandwidth on the baselines to Hobart26, while the other stations with 32-MHz bandwidth went through an independent correlation pass, the same as the usual correlation procedures.

Table 1 Summary of the VEPS observations.

Date (yyyy-mm-dd)	Time UT	Dur hrs	Code	Stations	Frequency	Data rate (Mbps)	Channels	Sampling (bits)	Data volume (TB)	# Targets
2015-02-13	05h00m	24	VEPS01	ShKmUr	X	2048	16	2	48	293
2015-02-14	06h00m	24	VEPS02	ShKmUr	X	2048	16	2	48	338
2015-04-23	05h00m	24	VEPS03	ShKmUrKv	X	2048	16	2	56	300
2015-04-24	06h00m	24	VEPS04	ShKmUrKv	X	2048	16	2	56	400
2015-08-10	05h00m	25	VEPS05	ShKmKvHo	X	2048	16	2	42	252
2015-08-19	05h00m	25	VEPS06	ShKmKvHo	X	2048	16	2	42	277
2016-03-02	08h30m	24	VEPS07	ShKmUrKb	X	2048	16	2	52	333
2016-03-11	05h00m	24	VEPS08	ShKmUrKb	X	2048	16	2	60	477

Note 1. — Sh: Seshan25; Km: Kunming; Ur: Urumqi; Kv: Sejong; Kb: Kashim34; Ho: Hobart26.

Note 2. — The mode 1024 (data rate) — 16 (channels) — 1 (bit) was used at Sejong.

Note 3. — The mode 1024 (data rate) — 16 (channels) — 2 (bit) was used at Hobart26.

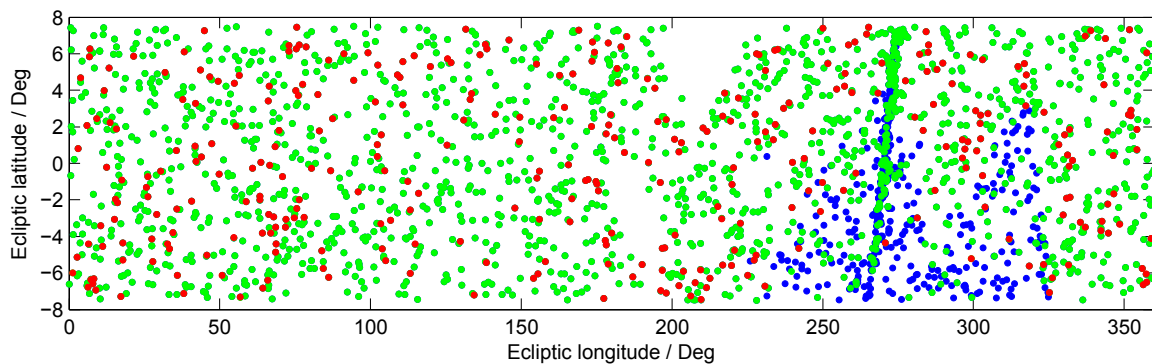


Fig. 3 Distribution of Phase-A sources. Among 2,216 target sources (blue, darkest), 1,903 sources (green, lightest) have been observed, and 363 sources (red, intermediate) were detected in three or more observations.

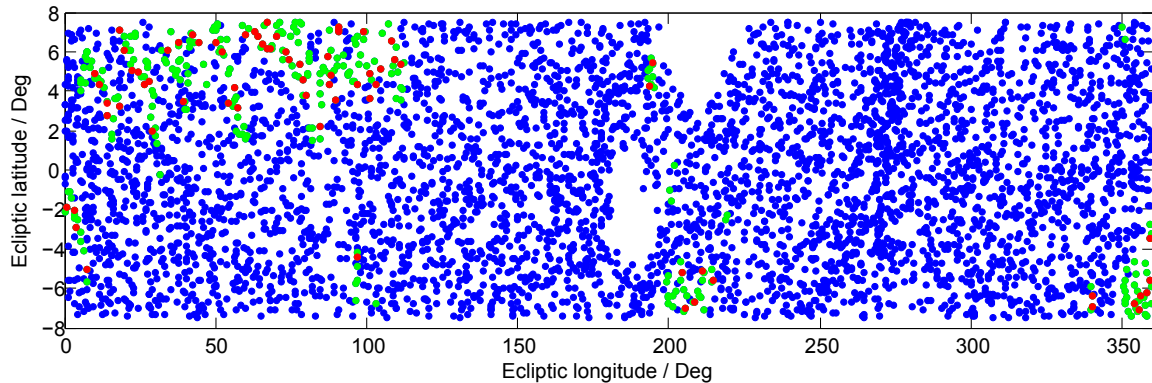


Fig. 4 Distribution of Phase-B sources. Among 4,802 target sources (blue, darkest), 324 sources (green, lightest) have been observed, and 72 sources (red, intermediate) were detected in three or more observations.

4 Preliminary Results

In general, the VEPS observing sessions were successful, although Urumqi had no fringes in the first half of the VEPS01 session due to a receiver problem, and Se-

shan25 and Kunming had no fringes in VEPS03 due to an incorrect use of B1950 source positions.

We have processed all of the observed sessions. Based on the data analysis, there are 435 target sources that were detected in three or more observations among 2,227 observed. The detection rate is about 20%. Their

median position precision is about 18 nrad. The estimation of the correlated flux densities is better than 15%.

Except for the baselines to Sejong, the other baselines have detection limits better than 30 mJy. Deduced from the four VEPS sessions, the SEFD of Sejong varied from 3000 to 5000, which can also be confirmed by the IVS sessions in which it participated. The causes are under investigation and may be related to the antenna pointing model, aperture efficiency as a function of frequency, or the receiver system.

Figure 3 and Figure 4 show the distribution of Phase-A sources and Phase-B sources, respectively. Most Phase-A sources have now been observed. We can see there are two holes in the plots beside 200 degrees of ecliptic longitude. In the PMN surveys, these small regions were severely affected by solar contamination when the sidelobes of the antenna were encountering the Sun, so those data have been expunged from the survey [1]. In the next VEPS sessions, we will try to fill the two holes with sources from other radio catalogs.

In order to finish the survey of the remaining sources, an additional 400 hours of observing time will be required. We expect that Sejong will have a better performance with improved SEFDs and that Hobart26 will use the DBBC2 2-Gbps mode.

5 High-Sensitivity Astrometry

As of April 2016, we have observed 73 ecliptic sources with the VLBA in three eight-hour segments at 2.3 and 8.6 GHz at 2 Gbps (project code: BS250). The targets are the weakest calibrators with a correlated flux density at baseline project lengths of 5,000 km in the range [30, 50] mJy. A priori positions of one half the targets were derived from single-band VLBI observations at 4 or 8 GHz. We scheduled each target in three scans that were 180 seconds long. Two targets have not been detected at S-band. Position uncertainties of 71 remaining targets before our VLBA observations were in the range of [0.8, 294] nrad with a median of 6.2 nrad. After our VLBA observations, the position uncertainties dropped to [0.7, 5.6] nrad, with a median of 1.8 nrad (see Figure 5).

Statistics of VLBI-detected sources within $\pm 7.5^\circ$ of the ecliptic plane are shown in Table 2. The number of known calibrators in the ecliptic plane is grow-

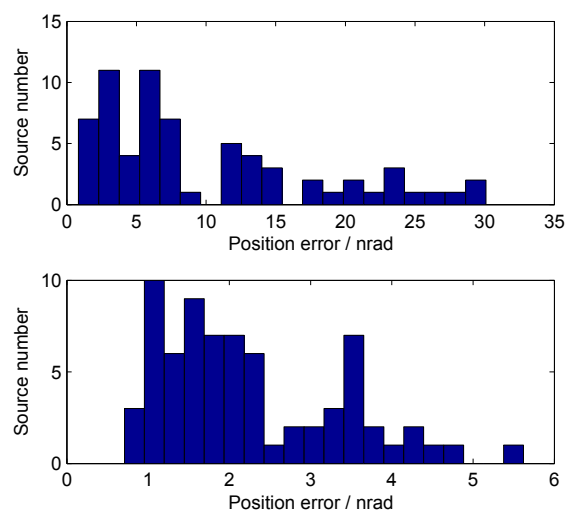


Fig. 5 Top: histogram of position errors of 71 sources before the VLBA observations. Please note that four sources with position errors larger than 35 nrad are not included in the statistics. Bottom: histogram of position errors of 71 sources after the VLBA observations.

ing rapidly and reached 1,167 recently. Positions of only 23% have been determined with accuracy better than 1.5 nrad using S/X dual-band VLBI. Changes on 2016-04-01 with respect to 2016-02-01 are contributed by some VEPS, VCS9, and VCS-II experiments [2]. Changes on 2016-05-01 with respect to 2016-04-01 are contributed by the project BS250.

In order to improve the positions of known calibrators, we plan to observe them with the VLBA, EVN, or IVS. In a more practical sense, it might be a good idea to form a high-sensitivity network with Asian and Oceanian antennas. In such a network, a compatible observing mode using S/X band at 2 Gbps needs to be defined and tested. With the inclusion of Tianma or Parkes, even the baselines to the small antennas of AuScope will have a sensitivity comparable to the VLBA.

6 Conclusions

The VEPS observations for detecting more ecliptic calibrators are running smoothly and have become routine work now. More than 400 sources have been detected on VLBI baselines for the first time.

Table 2 Statistics of sources detected with VLBI within $\pm 7.5^\circ$ of the ecliptic plane.

	2015-01-01	2016-02-01	2016-04-01	2016-05-01
# Calibrators with errors < 1.0 nrad	130	133	143	155
# Calibrators with errors < 1.5 nrad	187	191	261	293
# Calibrators with errors < 2.0 nrad	279	283	405	449
# Calibrators with errors < 2.5 nrad	336	349	479	533
# Calibrators with errors < 3.0 nrad	402	423	518	574
# Calibrators with errors < 5.0 nrad	521	549	625	681
Total # calibrators	772	969	1167	1167
Total # sources including non-calibrators	1154	1450	1710	1732

The VEPS observations for improving positions of known calibrators will benefit from a proposed high sensitive network with Asian and Oceanian antennas.

Acknowledgements

The work is carried out with the support of the National Natural Science Foundation of China (U1331205).

References

1. Griffith, Mark R., Wright, Alan E., Burke, B. F., Ekers, R. D., The Parkes-MIT-NRAO (PMN) surveys. 6: Source catalog for the equatorial survey, *Astrophysical Journal Supplement Series* (ISSN 0067-0049), vol. 97, no. 2, pp. 347–453, 1995.
2. David Gordon, Revisiting the VLBA Calibrator Surveys: VCS-II, *Proceedings of the 22nd European VLBI Group for Geodesy and Astronomy Working Meeting*, edited by R. Haas and F. Colomer, pp. 198–200, 2015.

On the Impact of Inhomogeneities in Meteorological Data on VLBI Data Analysis

Kyriakos Balidakis¹, Robert Heinkelmann², Apurva Phogat¹, Benedikt Soja², Susanne Glaser¹, Tobias Nilsson², Maria Karbon², Harald Schuh^{1,2}

Abstract In this study, we address the issue of the quality of meteorological data employed for VLBI data analysis. We use data from six numerical weather models (NWMs) to form references on which the homogenization process is based. We explore the impact of the choice of NWM as well as the way to extract data from it. Among our findings is that data from the surface fields of NWMs are not suitable for either geodetic analysis or homogenization efforts, whether they are in their original form or after they have been compensated for the height difference between the orography of the NWM and the actual elevation. The reason lies in the fact that for 77% of the VLBI stations a height bias larger than 2.5 mm appears, as well as an average bias in the zenith wet delay estimates of 12.2 mm. Should the proposed extraction approach be followed, the difference between operational and reanalysis NWMs is not significant for such an application. Our conclusions are based on the analysis of VLBI data over 13 years.

Keywords VLBI, numerical weather models, homogenization, Earth orientation parameters, reference frames

1 Introduction

Due to the highly volatile character of the neutral atmosphere, the modeling of the related propagation delay is challenging. This poses the most prominent limitation in

the precision and accuracy of the parameters estimated by microwave-based space geodetic techniques.

The work presented in this paper is restricted to the potential accuracy limitation that the mismodeling of the nuisance effects of *neutral atmospheric propagation delay* and the *thermal deformation of antennas* poses to the Very Long Baseline Interferometry (VLBI) technique due to erroneous meteorological records employed to mitigate them. As both effects are considered at the observation level, any errors not described in the observation covariance matrix will propagate in the estimated parameters and their accuracies. Being a function of surface pressure, the zenith hydrostatic delay (ZHD) is subject to inhomogeneities in the related observations, which could result in spurious trends in the zenith wet delays (ZWDs) and consequently render the physical interpretation of trends in integrated water vapor (IWV) uncertain. Moreover, they can bias the height time series and thus finally distort the scale of the estimated terrestrial reference frame (TRF) (Heinkelmann et al., 2009). As far as the thermal deformation is concerned, inaccurate temperature values allow site motions closely following the temperature anomalies, whereas an artificial offset in the temperature induces a virtual height displacement (Nothnagel, 2008).

The other microwave-based space geodetic techniques currently contributing to the ITRF customarily acquire the necessary meteorological data by either empirical or numerical weather models (NWMs). Conversely, VLBI analysis enjoys the advantage that the aforementioned nuisance effects can be potentially eliminated more effectively by employing in situ observations, because in principle all VLBI stations are equipped with meteorological sensors. Nevertheless, there are cases where erroneous meteorological records

1. Technische Universität Berlin, Institute of Geodesy and Geoinformation Science

2. Helmholtz-Zentrum Potsdam, Deutsches GeoForschungsZentrum GFZ, Space Geodetic Techniques

yield unacceptable results which have a dubious traceability at the parameter level.

In this work, we homogenize the meteorological observations recorded in the vicinity of VLBI stations. In order to meet this objective, reference series which experience all broad climatic influences of the candidate sites but none of their artificial biases, trends, or drifts are required. We resort to NWMs to obtain such series, following the procedure outlined in Section 2. For our investigations we test the following NWMs:

1. ECMWF's atmospheric operational analyses,
2. ECMWF's ERA-Interim (Dee et al., 2011),
3. NOAA/OAR/ESRL PSD's NCEP-DOE AMIP-II reanalysis (Kanamitsu et al., 2002),
4. NASA's MERRA-1 (Rienecker et al., 2011),
5. NASA's MERRA-2, and
6. JMA's JRA-55 reanalysis¹.

We performed a *penalized maximal t test* (e.g. Wang et al., 2007) on the formed pressure and temperature difference time series to detect abrupt shifts in the recursive average. Afterwards, we investigated the effect on time series of the station positions, Earth orientation parameters (EOP), and ZWDs from a reprocessing of 13 years of VLBI data while applying the different meteorological data sets.

2 Extracting Data from Numerical Weather Models

As proven in Heinkelmann et al. (2016), performing the hypsometric adjustment on values extracted from surface fields yields unacceptable results, specifically in regions with steep topographic gradients.

Therefore, we choose to work with model level (σ -pressure coordinate system) data. An alternative would be to employ pressure level data. The reason for choosing the model level lies mainly in the fact that most NWMs (e.g., ECMWF's products) are generated on model levels and at the surface; the transformation to pressure levels introduces a deterioration in the vertical resolution.

A potential source of bias in the pressure time series is that in the transformation from ellipsoidal heights to dynamic heights, the geoid undulation N , is currently

not considered. This results inescapably in a logarithmic bias proportional to N as large as 5 hPa w.r.t. reliable in situ pressure records. For our investigations, we extract N from EIGEN---6C4 (Förste et al., 2014) using full-degree spherical harmonic synthesis.

Utilizing the 3D temperature and specific humidity fields as well as the pressure and geopotential number surface fields, we calculate the pressure and temperature at the points of interest following the procedure outlined here, which largely follows ECMWF (2015). Initially, the 3D pressure field is calculated:

$$p_k = \frac{1}{2} \left(p_{k-\frac{1}{2}} + p_{k+\frac{1}{2}} \right), \quad \text{for } 1 \leq k \leq k_{max} \quad (1)$$

$$p_{k+\frac{1}{2}} = A_{k+\frac{1}{2}} + B_{k+\frac{1}{2}} p_s, \quad \text{for } 0 \leq k \leq k_{max}$$

where k is the generalized vertical index, k_{max} is the number of vertical levels, p_s is the surface pressure, p_k is the full-level pressure, $p_{k\pm\frac{1}{2}}$ is the pressure at the interfaces, and $A_{k+\frac{1}{2}}$ and $B_{k+\frac{1}{2}}$ are constants. The next step includes the calculation of full-level values of the geopotential in a finite difference form:

$$\phi_k = \phi_s + \sum_{j=k+1}^{k_{max}} R_{dry}(T_v)_j \ln \left(\frac{p_{j+\frac{1}{2}}}{p_{j-\frac{1}{2}}} \right) + \alpha_k R_{dry}(T_v)_k$$

$$\alpha_k = \begin{cases} \ln 2, & \text{for } k = 1 \\ 1 - \frac{p_{k-\frac{1}{2}}}{p_{k-\frac{1}{2}} + p_{k+\frac{1}{2}}} \ln \left(\frac{p_{k+\frac{1}{2}}}{p_{k-\frac{1}{2}}} \right), & \text{for } k > 1 \end{cases} \quad (2)$$

where ϕ_s denotes the geopotential at the orography and $(T_v)_k$ stands for the virtual temperature on level k (to account for moisture fluctuations):

$$T_v = T \left(1 + \left(\frac{R_{vap}}{R_{dry}} - 1 \right) q \right), \quad (3)$$

q is the specific humidity, T is the temperature, and R_{vap} and R_{dry} denote the gas constant for water vapor and dry air, respectively. Following this robust extraction approach the bias between different models almost vanishes (Figure 1 and Figure 2).

As far as the temperature is concerned, the reference temperature of each VLBI site is of crucial importance for the thermal deformation correction. Currently these values are extracted from GPT (Boehm et al., 2007), the finite resolution of which introduces a bias in some cases (Figure 3).

¹ jra.kishou.go.jp/JRA-55/index_en.html

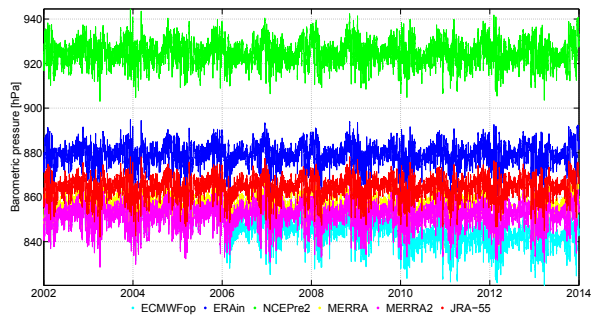


Fig. 1: Surface pressure time series at Zelenchukskaya, Russia, from ECMWF’s operational model, ERA-Interim, NCEP-DOE_AMIP-re2, MERRA, MERRA2, and JRA-55.

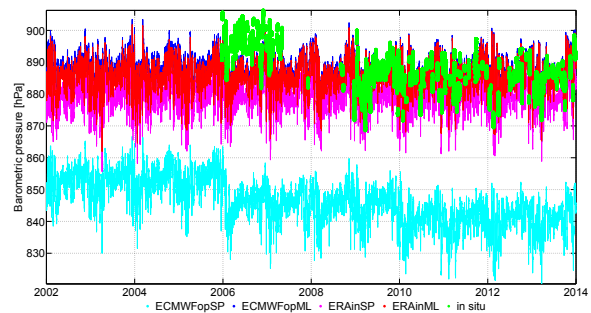


Fig. 2: Pressure time series at Zelenchukskaya, Russia. The suffix “SP” describes data extracted from the surface pressure fields and the suffix “ML” describes data from model levels. Data labeled “in situ” were retrieved from the pressure sensor mounted in the vicinity of the VLBI station.

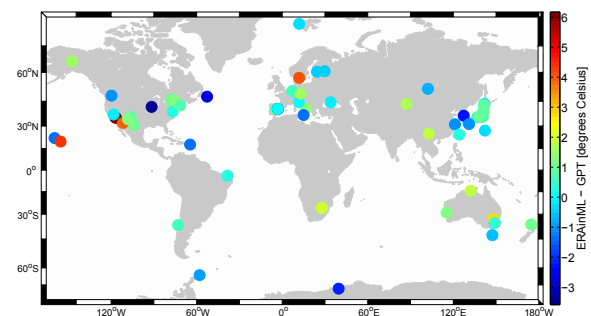


Fig. 3: The bias between the reference temperature currently in use for the thermal deformation calculation (GPT) and our estimation from ERAinML data.

3 VLBI Data Analysis and Results

We utilize the Least Squares Adjustment module of the VieVS@GFZ VLBI software (Nilsson et al., 2015) to analyze interferometric group delay data (Nothnagel et al., 2015) from the IVS-R1 and IVS-R4 rapid turnaround VLBI experiments (1,326 24-hour multi-baseline sessions), spanning the period from 2002 until 2015 and featuring in total a global 32 station network. We indicatively produce five solutions, with the meteorological parameters (pressure and temperature) being the only point of difference. These use meteorological data from:

1. in situ, as recorded at the VLBI sites (when unavailable, GPT2 (Lagler et al., 2013) is used),
2. GPT2,
3. hourly MERRA2 surface fields (MERRA2sfc),
4. six-hourly ECMWF’s ERA-Interim reanalysis model level data (ERAinML), and
5. homogenized in situ data adjusted for the height difference between the meteorological sensor and the VLBI reference point, with ERAinML serving as a reference.

For the sites where information is available, we compensate for the height difference between the VLBI reference point and the level each meteorological data set refers to. In all solutions, we compensate for deformations induced by non-tidal atmospheric pressure loading (NTAL) and continental water storage loading² (CWSL), in addition to the conventional displacement models (Petit and Luzum, 2010), to reduce correlations. Furthermore, we employ the Potsdam mapping functions which utilize the advanced mapping concept and a rigorous ray-tracing approach using ERA-Interim (Balidakis et al., 2016). Station coordinates and EOPs are estimated at daily intervals, whereas ZWDs are estimated at hourly and linear horizontal delay gradients at six-hourly time intervals.

The largest effect of alternating meteorological data sets in VLBI data analysis is expected in the height coordinate component. For solutions 2, 4, and 5, the station heights change by more than 2.5 mm in 22% of the VLBI stations, whereas 77% of the VLBI stations

² CWSL series were calculated from the LSDM, forced by the ECMWF operational model (Dill and Dobsław, 2013). We calculate the NTAL series consistently, utilizing the ECMWF’s operational model, assuming a dynamic ocean response to pressure and wind forcing from the barotropic model MOG2D-G.

are biased for the third solution (Figure 4). We find that employing meteorological data homogenized with ERAInML reduces the weighted root mean square of the height time series by 6.2% on average.

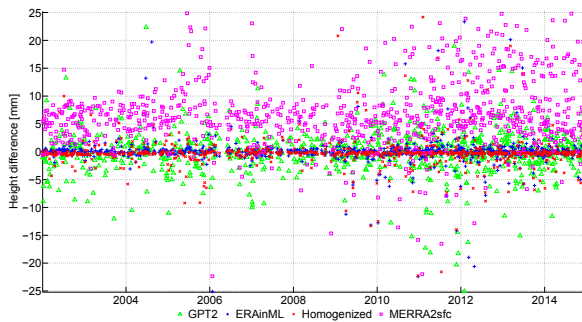


Fig. 4: Differences between the residual height estimates at Ny-Ålesund, Svalbard w. r. t. the first solution.

Mismodeling the ZHD is partly compensated by the ZWD estimates. For instance, if the recorded pressure series at a certain site has a significant³ positive bias w. r. t. the actual one, the sign of the estimated ZWDs could be negative, indicating the modeling error. In such a case (e.g., Sejong, South Korea), the impact of the blunder is partly mitigated in all other parameters, but the inference of long term trends of IWV is not reliable. Here, a bias is found in the ZWD series of 5.4 mm, 12.2 mm, and 4.0 mm for solutions 2, 3, and 4 (over all stations) w. r. t. the first. When we employ the homogenized data set, the average bias is only 1.7 mm (Figure 5).

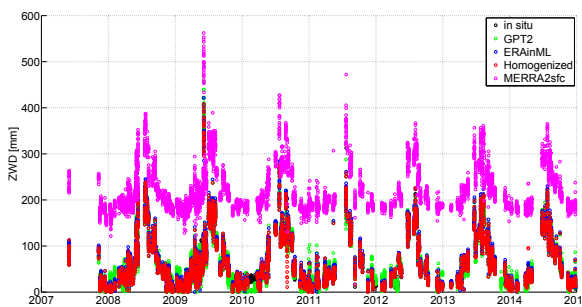


Fig. 5: Zenith wet delays at Badary, Russia.

³ This is not a constant either over the VLBI sites or over time; e.g., for Wettzell, an artefact pressure increment larger than 30 hPa during summer will result in negative ZWDs.

We perform the seven-parameter Helmert transformation between the first solution and all others, in a session-wise manner. As illustrated in Figure 6, the scale factor is considerably distorted, when either GPT2 or MERRA2sfc are employed, as in addition to the scatter increase (2.5 mm, 7 mm) a bias is introduced (1 mm, 4 mm). On the contrary, respectively the impact of ERAInML is at the sub-millimeter level. The EOPs are not largely affected except for the MERRA2sfc solution where an increase in the WRMS of all series is observed, as well as a bias of 0.2 mas and -0.1 mas in the x and y terrestrial pole coordinates.

4 Conclusions

In this study, we address the inhomogeneities in the raw meteorological data available in the VLBI archive that are employed for VLBI data analysis, i.e. pressure and temperature. Five VLBI solutions were generated and the estimates intercompared. Data either from empirical models or the surface fields of NWMs bias the heights and consequently distort the scale of the resulting TRF. We recommend the use of a data set homogenized in a manner similar to the one presented here (ideally) or data extracted from the model levels of spatio-temporally dense (meso-beta scale) NWMs.

Acknowledgements

We acknowledge the IVS (Schuh and Behrend, 2012) for coordinating the VLBI experiments analyzed in this study. DWD, ECMWF, JMA, NASA-GES, and NOAA/OAR/ESRL PSD are acknowledged for granting access to the NWM data used in this study. KB thankfully acknowledges the financial support of the DFG under grant HE 5937/2-1.

References

Balidakis K, Zus F, Douša J, Nilsson T, Glaser S, Soja B, Karbon M, Heinkelmann R, and Schuh H (2016) On the impact of different mapping functions on geodetic and tropospheric products from VLBI data analysis.

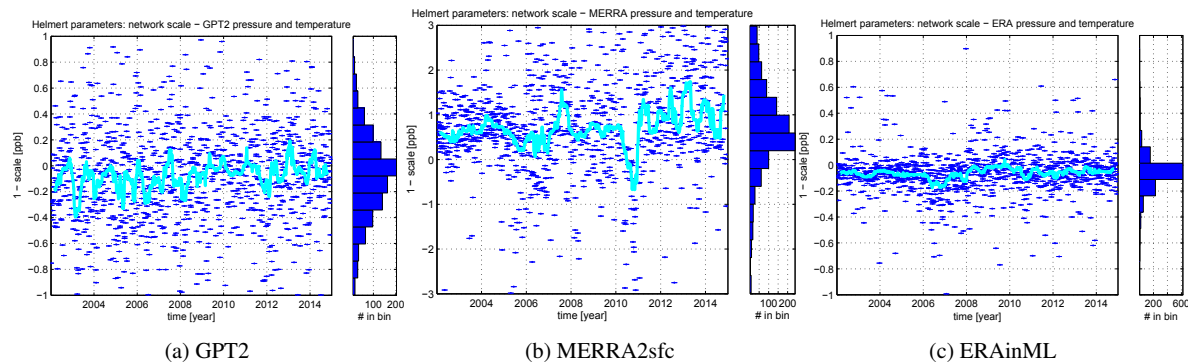


Fig. 6: The scale difference from the epoch-wise Helmert transformation between solutions w. r. t. the 1st.

- In: Behrend D, Baver K, Armstrong K (eds), IVS 2016 General Meeting Proceedings, this volume.
- Boehm J, Heinkelmann R, Schuh H (2007) Short note: A global model of pressure and temperature for geodetic applications. *Journal of Geodesy* 81(10):679–683.
- Dee DP, with 35 co-authors (2011) The ERA-Interim reanalysis: configuration and performance of the data assimilation system. *Quarterly Journal of the Royal Meteorological Society* 137(656):553–597.
- Dill R, Dobsław H (2013) Numerical simulations of global-scale high-resolution hydrological crustal deformations. *Journal of Geophysical Research: Solid Earth* 118:5008–5017.
- ECMWF (2015) Part III: Dynamics and Numerical Procedures, ECMWF. IFS Documentation, operational implementation 12 May 2015.
- Förste C, with eight co-authors (2014) EIGEN-6C4 the latest combined global gravity field model including GOCE data up to degree and order 2190 of GFZ Potsdam and GRGS Toulouse.
- Heinkelmann R, Boehm J, Schuh H, Tesmer V (2009) The effect of meteorological input data on the VLBI reference frames. In: Drewes H (ed) *Geodetic Reference Frames: IAG Symposium Munich, Germany, 9–14 October 2006*, Springer Berlin Heidelberg, Berlin, Heidelberg, p 245–251.
- Heinkelmann R, Balidakis K, Phogat A, Lu C, Moradiaz J, Nilsson T, Schuh H (2016) Effects of meteorological input data on the VLBI station coordinates, TRF and EOP. In: Freymueller J (ed) *International Association of Geodesy Symposia, Prague 2015, submitted*.
- Kanamitsu M, Ebisuzaki W, Woollen J, Yang SK, JHJ, Fiorino M, L PG (2002) NCEP–DOE AMIP-II Reanalysis (R-2). *Bulletin of the American Meteorological Society* 83:1631–1643.
- Lagler K, Schindelegger M, Böhm J, Krásná H, Nilsson T (2013) GPT2: Empirical slant delay model for radio space geodetic techniques. *Geophysical Research Letters* 40(6):1069–1073.
- Nilsson T, Soja B, Karbon M, Heinkelmann R, Schuh H (2015) Application of Kalman filtering in VLBI data analysis. *Earth, Planets and Space* 67(1):1–9.
- Nothnagel A (2008) Conventions on thermal expansion modelling of radio telescopes for geodetic and astrometric VLBI. *Journal of Geodesy* 83(8):787–792.
- Nothnagel A, International VLBI Service for Geodesy and Astrometry (IVS) et al (2015) The IVS data input to ITRF2014. International VLBI Service for Geodesy and Astrometry, GFZ Data Services.
- Petit G, Luzum B (eds) (2010) IERS Conventions (2010), IERS Technical Note, vol 36. Verlag des Bundesamts für Kartographie und Geodäsie, Frankfurt am Main, Germany.
- Rienecker MM, with 28 co-authors (2011) MERRA: NASA’s Modern-Era Retrospective Analysis for Research and Applications. *Journal of Climate* 24:3624–3648.
- Schuh H, Behrend D (2012) VLBI: A fascinating technique for geodesy and astrometry. *Journal of Geodynamics* 61:68–80.
- Wang XL, Wen QH, Wu Y (2007) Penalized maximal t test for detecting undocumented mean change in climate data series. *Journal of Applied Meteorology and Climatology* 46(6):916–931.

Session 6: VLBI Observations of Space Vehicles



March 2016 · Johannesburg · South Africa

APOD Mission Status and Observations by VLBI

Geshi Tang¹, Jing Sun¹, Xie Li¹, Shushi Liu¹, Guangming Chen¹, Tianpeng Ren¹, Guangli Wang²

Abstract On September 20, 2015, 20 satellites were successfully launched from the TaiYuan Satellite Launch Center by a Chinese CZ-6 test rocket and are, since then, operated in a circular, near-polar orbit at an altitude of 520 km. Among these satellites, a set of four CubSats, named APOD (Atmospheric density detection and Precise Orbit Determination), are intended for atmospheric density in-situ detection and derivation via precise orbit. The APOD satellites, manufactured by DFH Co., carry a number of instruments including a density detector, a dual-frequency GNSS (GPS/BD) receiver, an SLR reflector, and a VLBI S/X beacon. The APOD mission aims at detecting the atmospheric density below 520 km. The ground segment is controlled by BACC (Beijing Aerospace Control Center) including payload operation as well as science data receiving, processing, archiving, and distribution. Currently, the in-orbit test of the nano-satellites and their payloads are completed, and preliminary results show that the precision of the orbit determination is about 10 cm derived from both an overlap comparison and an SLR observation validation. The in-situ detected density calibrated by orbit-derived density demonstrates that the accuracy of atmospheric mass density is approximately $4.191 \times 10^{-14} \text{ kgm}^{-3}$, about 5.5% of the measurement value. Since three space-geodetic techniques (i.e., GNSS, SLR, and VLBI) are co-located on the APOD nano-satellites, the observations can be used for combination and validation in order to detect systematic differences. Furthermore, the observations of the APOD satellites by VLBI radio telescopes can be used in an ideal fashion to link the dynamical reference frames of the

satellite with the terrestrial and, most importantly, with the celestial reference frame as defined by the positions of quasars. The possibility of observing the APOD satellites by IVS VLBI radio telescopes will be analyzed, considering continental-size VLBI observing networks and the small telescopes with sufficient speed.

Keywords APOD, atmospheric density, VLBI

1 Introduction

The precise orbit prediction of LEO spacecraft is very important for space debris collision avoidance, orbit maneuvers of LEO spacecraft, and rendezvous and docking of the space station. But it is still a huge challenge for the spacecraft operators. One of the main reasons is that the atmospheric density is known not accurately enough. At the altitude of LEO spacecraft, atmospheric density variations are driven by variations in the solar ultraviolet irradiance, electrical energetic particles from the magnetosphere, and solar wind and waves originating in the lower atmosphere that propagate upward. There are many atmosphere models describing the variations of the density, including empirical and physical models. Improving the accuracy of these models is a very challenging task and needs high-quality observations of mass density (direct or indirect) with sufficient spatial and temporal resolutions and coverage. Since the 1960's, many techniques have been developed to measure the atmospheric mass density and composition, including drag-derived means by orbit of spacecraft, in-situ measurements

1. Aerospace Flight Dynamic Laboratory

2. Shanghai Astronomical Observatory

Table 1 APOD payload system.

		nano-sat
Atmosphere density detector	Detection range [km]	120 ~ 550
	Pressure measure range [Pa]	$1.0^{-6} \sim 1.0^{-2}$
	Temperature range [$^{\circ}\text{C}$]	-20 ~ 60
	Sampling rate [s]	1
GNSS receiver	Mode	GPS/BDS
	GPS frequency [MHz]	L1: 1575.42, L2: 1227.60
	BDS frequency [MHz]	B1: 1561.098, B3: 1250.618
	Sampling rate [s]	8
Laser retro reflector	Type	Pyramid
	Number of cube corner prisms	9
VLBI beacon	S-Band frequency [MHz]	$f_{carrier}=2262.01, f_{S_{dor1}}=2256.87, f_{S_{dor2}}=2260.98,$ $f_{S_{dor3}}=2263.04, f_{S_{dor4}}=2267.15$
	X-Band frequency [MHz]	$f_{carrier}=8424.02, f_{X_{dor1}}=8404.87, f_{X_{dor2}}=8420.19,$ $f_{X_{dor3}}=8427.85, f_{X_{dor4}}=8431.66$

by neutral mass spectrometers, ultraviolet remote sensing and other techniques as rocket payload or ground based [1]. Especially, both CHAMP and GRACE have generated an unprecedented volume of high-quality measurements of the mass density and contributed to great achievements in atmospheric density research and modeling. Still, more extensive spatial and temporal coverage is needed to improve the accuracy of the models because of the complexity of the variations of atmosphere. The cost to meet this requirement is huge. But the development of low-cost CubSat provides a very good opportunity to detect atmospheric density with a more extensive spatial coverage. Thus BACC/AFDL (Beijing Aerospace Control Center/Aerospace Flight Dynamic Laboratory) proposed the APOD project to test the technology of in-situ detection by a payload instrument and to derive precise orbits on CubSats.

2 Satellites and Payload Overview

Inside the APOD family, there are one nano-satellite called APOD-A and three pico-satellites called APOD-B/C/D. The four satellites are flying in a circular, near-polar orbit with an inclination of about 97° . All four satellites were orbiting at an altitude of 520 km directly after launch. Then APOD-A descended to 470 km altitude two weeks later. The designed lifetime is twelve months. In order to obtain atmospheric density by the in-situ detector and from the precise orbits, the instruments used for the precise orbit determination and

density detection are mounted on the APOD satellites (Figure 1). The instrumentation includes a the dual-frequency GNSS receiver, an atmospheric density detector, an SLR Reflector, and a VLBI beacon. The APOD payload is listed in Table 1; it was a great challenge to integrate these instruments in such a miniature satellite.

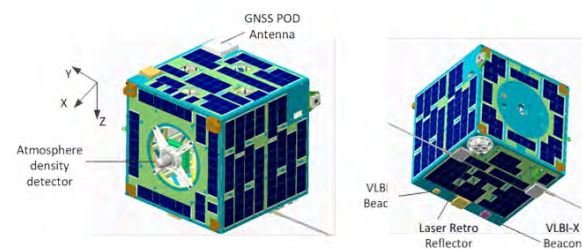


Fig. 1 Physical layout of the APOD nano-sat with the location of the scientific instruments: front side view (left) and bottom side view (right).

3 Preliminary Results

3.1 Precise Orbit Determination (POD)

Since the launch of APOD, the in-orbit commissioning of the platform and payload have been finished, and now APOD is in ordinary operation. The POD is performed by GPS L1/L2 double differences carrier phase data. The data rate is about 1/8 Hz or lower because of lost lock of carrier phase. BACC produces precise

orbit products by a POD software with independent intellectual property rights. The orbit precision is verified by the XiAn Satellite Control Center (XSCC) using the Bernese software. For POD based on GNSS L1/L2, a batch processing using 30 hours with a 12-hour overlap is employed. To avoid boundary effects, we only consider ten hours of these overlaps. Figure 2 shows the standard deviation of the GNSS L1/L2 POD solution of APOD-A. Losing lock of the signal in L2 is serious, leading to negative influences on the orbit precision.

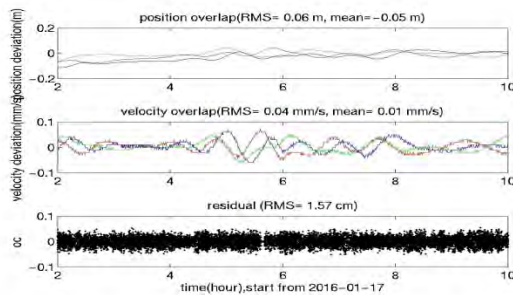


Fig. 2 Overlap comparisons of nano-sat: position (top), velocity (middle), and O-C in POD of GPS L1/L2 carrier phase (bottom).

The orbit precision has been validated independently by Satellite Laser Ranging (SLR). The International Laser Ranging Service (ILRS) provides SLR measurements to the APOD satellites. BACC is responsible for guiding the SLR stations by uploading satellite prediction files to the ILRS Web site in Consolidated Prediction Format (CPF). At the time of writing, APOD nano-sat had been tracked by 13 SLR stations all over the world. More than 4000 normal point data have been accessed since the first normal point data was obtained on 2 October 2015 by CHAL and SHA2 SLR stations. The SLR measurements are used for an independent validation of the GNSS-derived orbits. The names of the APOD satellites in the ILRS are PN-1A, PN-1B, PN-1C, and PN-1D, respectively. A detailed description of the LRR and the measurement conditions of the APOD satellites are described on ILRS Web site at (http://ilrs.gsfc.nasa.gov/missions/satellite_missions/future_missions/pn1a_general.html). ITRF2008 coordinates are used for the SLR stations, the CoM offset of the LRR array is corrected according to the parameters described on the ILRS Web site. The normal point

data, whose residuals are larger than 30 cm and whose elevation angles are less than 15° , are removed. Figure 3 shows the differences between the SLR measured ranges and the ranges derived from the GPS L1/L2 carrier phase POD.

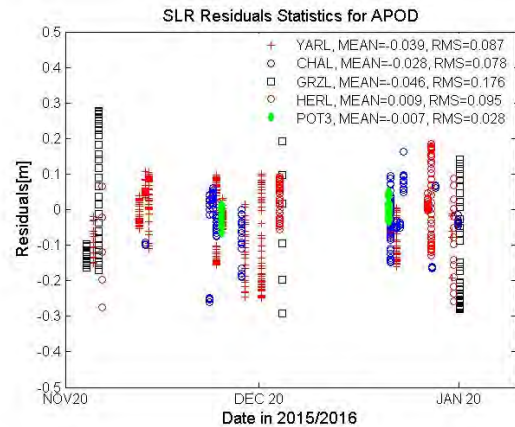


Fig. 3 SLR residuals for POD. The mean residual and standard deviation of every station are marked in the figure. Their values for all stations are -2.93 cm and 9.85 cm, respectively.

From the overlap comparison of the GNSS derived orbit and the independent validation by SLR measurement, the POD accuracy of the APOD-A satellite is at the 10-cm level, which can meet the requirement of the mission.

APOD is the first LEO satellite with a VLBI S/X beacon. The APOD orbit was also validated independently by the Chinese CEI (Connected-Element Interferometry). On March 10, 2016, a CEI constituted by a three-meter antenna and a 12-meter antenna observed the APOD satellites, where the S-band radio signals including the main-carrier, DOR beacons are tracked and recorded. The local oscillators of the recording channels are 2262 MHz, 2267.15 MHz, and 2256.85 MHz, respectively. The bandwidth is 1 MHz and the quantization digit is 8 bits, being the same for all recording channels. According to the traditional signal processing algorithm, the interferometric delay (DOR, Differential One-way Range) is completed. Following the DOR processing algorithm, the interferometric delay of the APOD satellite is obtained. Figure 4 shows the VLBI observations of the APOD nano-sat with respect to the APOD orbit.

From a VLBI observational point-of-view, the APOD satellite constitutes a challenge since the

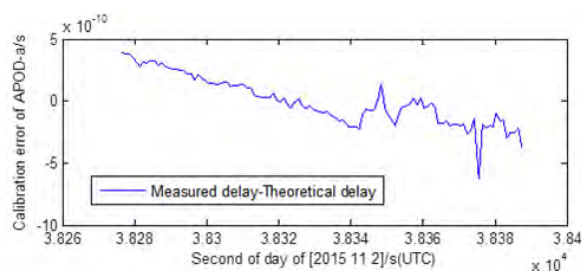


Fig. 4 O-C of VLBI observations for the APOD nano-sat.

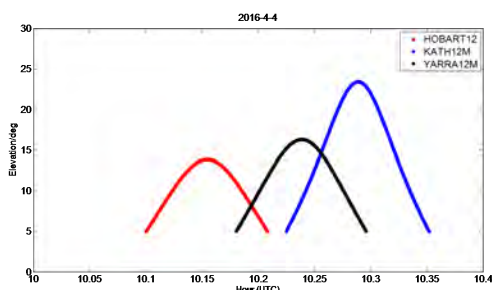


Fig. 5 Elevation plot of APOD as seen from AuScope.

mutual visibility depends on the altitude of the APOD satellite and the separation of the radio telescopes [2]. Further, the APOD satellite travels very fast through the field of view. The first VLBI observations to APOD were carried out successfully with the three AuScope VLBI observatories on April 4, 2016. The good condition to co-view APOD with AuScope can be found in Figure 5. BACC generated the schedule in VEX format using VieVS [3] in the stepwise tracking mode, i.e., each satellite observation was given as a source in (RA, Dec) coordinates with an update every 12 seconds. The maximum az/el velocity was $30^\circ/\text{min}$ and $6^\circ/\text{min}$ for the APOD observation, respectively. Observations to quasars were scheduled before and after the observations to the APOD satellites [4]. The VLBI data was transferred to BACC, where the correlation and processing of the APOD data was started by the VLBI team of BACC.

4 Atmospheric Density

In the APOD mission, two independent methods are designed to obtain the atmospheric mass density. One method is the drag-derived mass density and

the other is in-situ Atmospheric Density Detector (hereafter ADD). Drag-derived densities from LEO satellite orbits are the most common and direct method to determine atmospheric mass density. The basic principle of this method is that the primary effect of the atmospheric drag acceleration reduces the semi-major axis of the LEO satellite monotonically. ADD, manufactured by National Space Science Center (NSSC), is a space-borne device which consists of a spherical gold-plated stainless steel antechamber with a knife-edged orifice inlet, an electron impact ion source, and electronics. Figure 6 gives a comparison between the verified in-situ atmospheric density and the drag-derived atmospheric density with respect to the NRLMSISE-00 model.

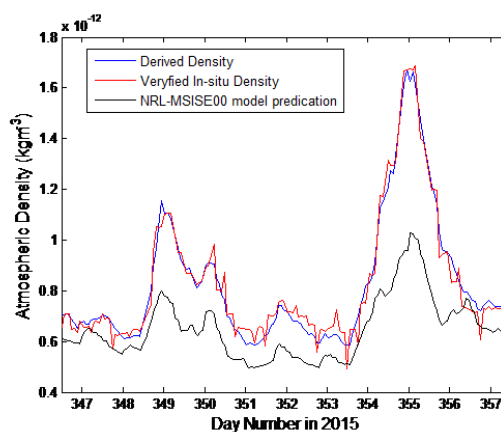


Fig. 6 Comparison between the verified in-situ atmospheric density and the orbit-derived atmospheric density.

5 Summary

The APOD project demonstrated excellent prospects for low-cost CubeSat in detecting atmospheric density in a much more extensive spatial coverage and much higher temporal resolution. The preliminary result about the orbit precision was validated independently by different methods. It shows that the three-dimensional position precision of the APOD satellite is about 10 cm. With the precise orbit, the in-situ Atmospheric Density Detector data was calibrated by orbit-derived density and the fitting precision of the detected density is approximately $4.191 \times 10^{-14} \text{ kgm}^{-3}$, which is about 5.5% of the orbit-derived value. Further VLBI

observations with IVS antennas would provide more possibilities to study systematic differences and to link the reference frames.

Acknowledgements

The authors would like to thank our colleagues from AuScope for the observations to APOD.

References

1. J.T. Emmert, “Thermospheric mass density: A review”, *Advances in Space Research*, doi:<http://dx.doi.org/10.1016/j.asr.2015.05.038>, 2015.
2. TORNATORE, V., HAAS, R., DUEV, D., POGREBENKO, S., CASEY, S., MOLERA CALVÉS, G. AND KEIMPEMA, A.. Single baseline GLONASS observations with VLBI: data processing and first results. In W. Alef, S. Bernhart and A. Nothnagel, eds., *Proceedings of the 20th Meeting of the European VLBI Group for Geodesy and Astrometry*, Vol. 22, 162–165, Institut für Geodäsie und Geoinformation der Universität Bonn, 2011.
3. Matthias Madzak, Sigrid Böhm, Hana Krásná, and Lucia Plank. Vienna VLBI Software Version 2.1 User Manual. Web document <http://vievs.geo.tuwien.ac.at/fileadmin/editors/VieVS/documents/vievsDoc.pdf>
4. Sun J, Böhm J, Nilsson T, Krásná H, Böhm S, Schuh H. New VLBI2010 scheduling strategies and implications on the terrestrial reference frames. *J Geod*, 88:449–461, 2014.

E-GRIP: A Highly Elliptical Orbit Satellite Mission for Co-location in Space

Benjamin Männel¹, Markus Rothacher¹, Philippe Jetzer², Steve Lecomte³, Pascal Rochat⁴

Abstract The Einstein Gravitational Red-shift Probe (E-GRIP) will be a new satellite mission allowing detailed studies for relativistic and geodetic purposes. The scientific objectives of E-GRIP are the measurement of the space-time curvature around the Earth, multiple tests of general relativity, and special geodetic applications. E-GRIP will fly in a highly eccentric orbit ($e > 0.6$, apogee > 35000 km) and will carry a narrow- and a wide-angle microwave link (at both X- and K-band), two GNSS antennas, SLR retro-reflectors, a photon counter unit, and a space hydrogen maser. Consequently, E-GRIP could act as a co-location satellite with suitable observation conditions for VLBI. Beyond a mission overview, we provide results from extended VLBI simulations concerning link budget, visibilities, and achievable station coordinate results. In addition, we present also some basic considerations concerning the feasibility of co-located GNSS and SLR observations for E-GRIP's highly elliptical orbit.

Keywords VLBI, E-GRIP, co-location, satellite-tracking

1 Introduction

In recent years much effort has been undertaken to combine space geodetic observations on-board

satellites, known as co-location in space. Whereas co-locations on-board Low Earth Orbiters (LEO) and on-board GNSS satellites already exist for SLR and GNSS, no such satellites are allowing at present for VLBI observations. In order to cure this situation new satellite missions such as JPL/CNES's Geodetic Reference Antenna in Space (GRASP, Bar-Sever et al., 2009) are considered, new observation concepts such as tracking of GNSS L-band signals were implemented (e.g. Tornatore et al., 2014; Haas et al., 2014), and at some telescopes, receiver chains were modified (Kodet et al., 2014). Evaluating today's situation, three possibilities for a near-future co-location satellite are feasible: a dedicated LEO mission, GNSS satellites, and a dedicated satellite in a highly elliptical orbit. Table 1 lists the main advantages/disadvantages concerning the VLBI tracking for each of these possibilities. According to Table 1, a LEO is an easy way to implement a dedicated co-location satellite due to the low costs regarding launch and spacecraft bus. However, as the low altitude limits the VLBI observability, elliptical orbits become interesting. When speaking of highly elliptical orbits within this paper, an eccentricity $e > 0.3$ is assumed. The advantage of such an orbit is obvious: due to the high altitude close to the apogee, VLBI tracking with long baselines becomes possible, and, as the apparent satellite speed is slow, no requirements on the slew rates have to be fulfilled. However, three major concerns have to be addressed (1) VLBI tracking close to the perigee might be as challenging as it is for LEOs, (2) GNSS and SLR observations are challenging during apogee crossings, and (3) the tracking statistics will be inhomogeneous due to the orbit geometry. Within this paper we introduce E-GRIP as a highly elliptical orbit mission including a description of the planned microwave link

1. ETH Zürich, Switzerland

2. University of Zürich, Switzerland

3. Centre Suisse d'Electronique et de Microtechnique, Neuchâtel, Switzerland

4. Spectratime, Neuchâtel, Switzerland

Table 1 Comparison of different satellite/orbit types for co-location in space concerning VLBI satellite tracking.

	(near-circular) LEO	GNSS satellite	satellite in a highly elliptical orbit
space segment	low costs	already existing	costs are higher than for LEO
scheduling aspects	short baselines, short and fast passes require high slew rates	long passes, switching between spacecraft for better sky coverage	up to max. baseline length, very long and slow passes exist
observed signals	mission-dep. (S-,X-,K-Band)	L-Band	mission-dep. (S-,X-,K-Band)
coordinate results	≈ 1 cm (Plank et al., 2014) for single-satellite tracking	2-10 cm for single-satellite tracking, <1 cm for constellation tracking	1-2 cm single-satellite tracking (dur- ing apogee)
conclusion	challenging due to short baselines and short passes	limitation due to L-Band signals	challenging for stations observing the perigee region

(Section 2). In Section 3 we present results of our VLBI satellite tracking simulation studies for E-GRIP.

2 E-GRIP: Mission and Status

E-GRIP is a joint mission study of ETH Zürich, University of Zürich, Centre Suisse d'Electronique et de Microtechnique, and Spectratime. Currently E-GRIP is within an extended Phase 0/A, which will be finished in June 2016. E-GRIP has three major scientific objectives:

- testing of the local position invariance (i.e. testing Earth, Sun, and Lunar gravitational red-shift),
- tests of higher-order effects such as the Schwarzschild space curvature, the Shapiro time delay, and frame dragging, and
- tests of special geodetic applications:
 - inter/continental time comparison,
 - relativistic geodesy, and
 - co-location in space.

In order to perform these tasks E-GRIP will fly in a highly elliptical orbit. For our initial studies we selected two orbits:

- **EGRIP-A:** $a = 24450$ km, $e = 0.636$, $d_p = 2540$ km
- **EGRIP-B:** $a = 35000$ km, $e = 0.800$, $d_p = 700$ km.

The core of E-GRIP's scientific payload is an active space hydrogen maser stable to $1 \cdot 10^{-15}$ @ 10000 s. This on-board time and frequency standard is connected to two microwave communication antennas which will be described later. Also one high-quality space-proofed GNSS receiver will be part of the payload. This receiver will be connected to a nadir-

and a zenith-facing antenna allowing GNSS observations during apogee and perigee crossings. For SLR a retro-reflector array and a photon counting unit will be part of the payload.

The microwave link required for the ground-to-space clock comparison will allow the VLBI tracking of E-GRIP. In order to have a stable link during the entire revolution two antennas—one narrow-beam high-gain antenna (antenna 1) and one wide-beam low-gain antenna (antenna 2)—have been selected. Table 2 provides the characteristics of both antennas. Figure 1 shows an estimation of the received power for the microwave links listed in Table 2 depending on the orbit altitude. The minimal received power is -125 dBW and -136 dBW for an altitude of 20000 km and 50000 km, respectively. For comparison, -114 dBW can be received, when observing GNSS L_1 signals (Tornatore and Haas, 2009). Two conclusions can be drawn from Figure 1: (1) the signal loss due to

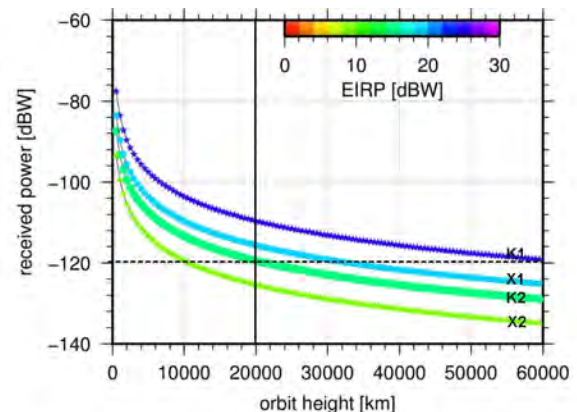


Fig. 1 Link budget for the two microwave links (K1, X1 = antenna 1; K2, X2 = antenna 2).

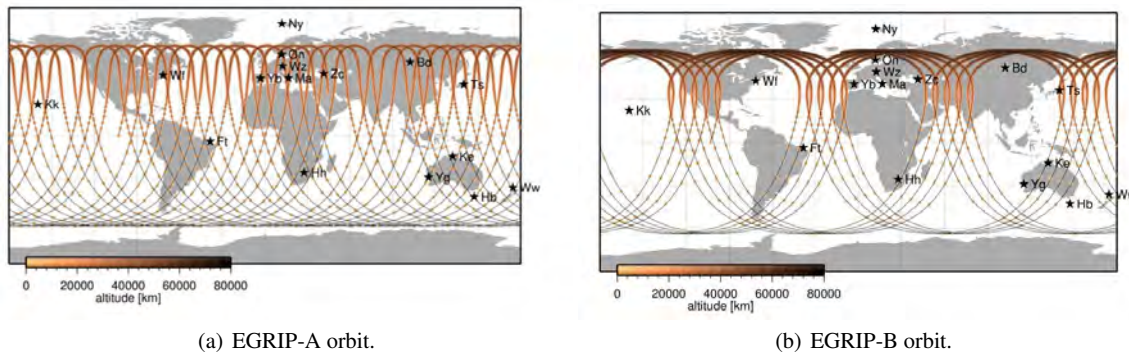


Fig. 2 E-GRIP ground tracks; GLOBAL station network; time period January 4 – January 18, 2015.

Table 2 E-GRIPs antenna and microwave link characteristics.

Ant.	working area	beam-width	frequency [GHz]	gain [dBi]
1	>20000 km	$\pm 13.6^\circ$	K0: 22.96 ± 0.25	>15.9
			K1: 25.69 ± 0.25	>15.9
2	<20000 km	$\pm 42^\circ$	X2: 8.458 ± 0.10	>15.9
			K0: 22.96 ± 0.25	>6.1
			K2: 25.69 ± 0.25	>6.1
			X2: 8.458 ± 0.10	>6.1

the larger distance is not critical and (2) the received signals are still strong compared to quasar signals.

Looking at the considered apogee heights, it is obvious that GNSS and SLR observations are challenging for E-GRIP. Within two studies we addressed this topic and found that (1) by carrying a zenith- and a nadir-facing GNSS antenna, a minimum number of four GPS and GLONASS satellites is observable for nearly each epoch (max. nadir angle 23°) and (2) by carrying a retro-reflector array, SLR observations are challenging but possible over the entire arc.

3 Satellite Tracking Simulation

The simulations presented here were performed using a modified version of the Bernese GNSS Software (5.2) able to simulate and process VLBI satellite tracking data (Männel et al., 2014). For the simulation procedure we followed the IVS guidelines (Böhm et al., 2006), i.e., tropospheric wet zenith delays were generated using a turbulence model, and receiver clock errors were produced with a random walk and an integrated random walk process. Additionally, a white

noise of 42 ps (≈ 1.4 cm) was applied to each observation (one observation per minute). We selected two station networks, one regional (EUROPE, 1) and one global (GLOBAL, 2):

- **EUROPE:** Matera, Metsähovi, Ny-Ålesund, Onsala, Svetloe, Wettzell, Yebes, and Zelenchukskaya
- **GLOBAL:** Badary, Fortleza, Hartebeesthoek, Hobart (both telescopes), Katherine, Matera, Ny-Ålesund, Onsala, Tsukuba, Warkworth, Westford, Wettzell, Yarragadee, Yebes, and Zelenchukskaya.

Figure 2 shows the ground tracks of the E-GRIP orbits including the GLOBAL station network.

In the first step we considered the visibility conditions for the individual satellite orbits. Figure 3 shows the number of epochs per week for which different satellites (LEO, GPS, EGRIP-A, EGRIP-B) are above the horizon for the individual stations. Additionally, also elevation cutoffs at 10° and 20° were considered. Obviously, for circular orbits the number of epochs will nearly be equal for all stations. Consequently, about the same number of epochs can be found for LEO and GPS satellite tracking. In the case of E-GRIP, the northern stations have significantly more observations than those in southern regions. This is explained by the orbit geometry, especially by the location of the apogee which is above the northern hemisphere (see Figure 2). To quantify the results shown in Figure 3, one can say that LEO is observable in 10% of all epochs and a GPS satellite in 40% of all epochs (cutoff = 0°). For the highly elliptical orbits these numbers range from 80 to 10% and from 90 to 2.5% for EGRIP-A and EGRIP-B, respectively. However, we did not consider satellite-specific effects such as the beam-width and station-

specific limitations such as slew rates at this point. It has to be mentioned that this type of study has been done for individual stations and not for baselines, i.e., station-dependent visibilities and not visibilities in the VLBI sense were analyzed.

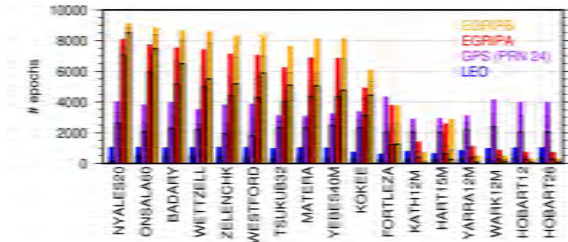


Fig. 3 Number of epochs per week (January 4 – January 10, 2015) with spacecraft above horizon (cutoff elevation resp.); the column order is LEO ($a=2000$ km), GPS, E-GRIP-A, EGRIP-B; border line represents cutoff elevation: no border = 0° , normal border = 10° , and thick border = 20° ; the stations are sorted in accordance to their latitude.

From the simulated observations we generated weekly solutions while estimating station coordinates, receiver clocks, and tropospheric zenith delays. The datum was defined by an NNT and NNR condition. The individual coordinate solutions x_i were then compared by computing their repeatability, i.e., comparing the weekly solution against a combined long-term solution x_m . The repeatabilities are obtained for the north (n), east (e), and height (h) component by using the formula

$$\sigma_x = \sqrt{\frac{1}{n-1} \sum_{i=1}^n (x_i - x_m)^2} \text{ with } x \in \{n, e, h\}. \quad (1)$$

Figure 4 shows the derived station coordinate repeatabilities for the network EUROPE including the number of simulated observations per station. We use the term observation in this context as one satellite observation; thus the number of baseline observations is much higher. Obviously, the number of observations depends on the station latitude. In accordance with Figure 3, a difference of about 300 observations per day (corresponding to 30% of the total amount) can be found for the European network. The derived repeatabilities are in the range of 10 mm for all EUROPE stations. There is no latitudinal dependence of the repeatabilities visible in the EGRIP-A case. For EGRIP-B increased repeatabilities were found for stations situated in the South. In that case the 3D-repeatabilities

reach 20 mm. The results are much more inhomogeneous for the GLOBAL network. As shown in Figure 4, comparable results can be derived in the EGRIP-A case for stations in the northern hemisphere (10 to 20 mm). However, due to the much lower number of observations in the southern hemisphere, the derived repeatabilities for such stations are incredibly large. In the case of EGRIP-B, similar results were found with slightly larger 3D-repeatabilities in the northern hemisphere (up to 30 mm); for some stations in the southern hemisphere, station coordinates could not be obtained due to missing observations.

Comparing the derived repeatabilities against related simulation studies for LEO and GNSS satellites, values similar to the achieved results can be found for the EUROPE and northern GLOBAL stations (e.g., Plank et al., 2014).

4 Conclusions

We presented the new satellite mission E-GRIP aiming for tests of general relativity and co-location in space. Based on visibility simulation studies we showed the good observation conditions for VLBI satellite tracking, especially in the apogee region. Based on weekly solutions, we discussed the potential advantages for the obtained station coordinates when observing E-GRIP or other highly elliptical satellite orbits. Reaching repeatabilities comparable to LEO or GNSS orbits (i.e., 1–2 cm), also very long VLBI baselines are observable in a single-satellite tracking mode. However, the considered extreme eccentricities ($e > 0.6$) might be ideal for relativity tests but too large for a pure co-location mission as we could not derive coordinates for several stations in southern regions due to the very low number of observations associated with the perigee region.

References

- Bar-Sever, Y. E., Haines, B., Wu, S., Lemoine, F., and Willis, P. (2009). Geodetic Reference Antenna in Space (GRASP): A Mission to Enhance the Terrestrial Reference Frame. In *COSPAR colloquium: scientific and fundamental aspects of the Galileo program*. Padua, 2009.

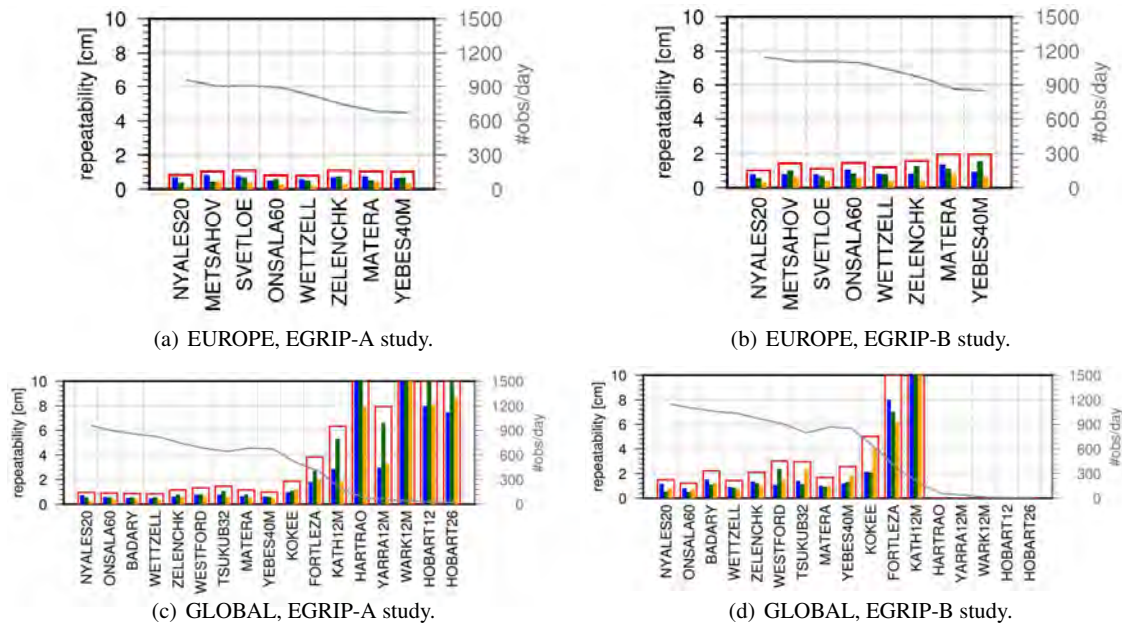


Fig. 4 Station coordinate repeatabilities; the column order is north, east, up with 3D encasing bar. The stations are sorted in accordance to their latitude; average number of daily observations.

Böhm, J., Wresnik, J., and Pany, A. (2006). Simulation of wet zenith delays and clocks. IVS Memorandum 2006-013v03.

Haas, R., Neidhardt, A., Kodet, J., Plötz, C., Schreiber, U., Kronschnabl, G., Pogrebenko, S., Duev, D., Casey, S., Marti-Vidal, I., Yang, J., and Plank, L. (2014). The Wettzell-Onsala G130128 Experiment - VLBI observations of a GLONASS satellite. In Behrend, D., Baver, K., and Armstrong, K., editors, *IVS 2014 General Meeting Proceedings*, pages 451–455. Science Press (Beijing), ISBN 978-7-03-042974-2.

Kodet, J., Schreiber, U., Plötz, C., Neidhardt, A., Kronschnabl, G., Haas, R., Calvés, G. M., Pogrebenko, S., Rothacher, M., Männel, B., Plank, L., and Hellschmied, A. (2014). Co-locations of Space Geodetic Techniques on Ground and in Space. In Behrend, D., Baver, K., and Armstrong, K., editors, *IVS 2014 General Meeting Proceedings*, pages 446–450. Science Press (Beijing), ISBN 978-7-03-042974-2.

Männel, B., Rothacher, M., Kodet, J., Schreiber, U., and Schmid, R. (2014). GLONASS Satellites Simultaneously Observed by VLBI, GNSS and SLR. In Behrend, D., Baver, K., and Armstrong, K., editors, *IVS 2014 General Meeting Proceedings*, pages 461–465. Science Press (Beijing), ISBN 978-7-03-

042974-2.

Plank, L., Böhm, J., and Schuh, H. (2014). Precise station positions from VLBI observations to satellites: a simulation study. *J Geod.* 88:1–15.

Tornatore, V. and Haas, R. (2009). Considerations on the observation of GNSS-signals with the VLBI2010 system. In *Proceedings of the 19th European VLBI for Geodesy and Astrometry Working Meeting*.

Tornatore, V., Haas, R., Duev, D., Pogrebenko, S., Casey, S., and Calvés, G. M. (2014). Direct VLBI Observations of Global Navigation Satellite System Signals. In Rizos, C. and Willis, P., editors, *Earth on the Edge: Science of a Sustainable Planet*. doi:10.1007/978-3-642-37222-3_32.

VLBI Observations of GNSS Signals on the Baseline Hobart–Ceduna

First Results

Andreas Hellerschmied¹, Johannes Böhm¹, Younghee Kwak¹, Jamie McCallum², Lucia Plank²

Abstract Observing GNSS satellites with geodetic VLBI opens a variety of new possibilities, which include promising applications in the field of inter-technique frame ties. Considering GNSS satellites as co-location platforms in space, such observations provide possibilities to directly connect the dynamic GNSS and the kinematic VLBI reference frames, which may result in improved future ITRF realizations. In our research we are trying to apply observation strategies that are commonly used in geodetic VLBI, i.e., the main observables are group delays derived from direct observations of GNSS satellite signals. However, clear strategies for the data acquisition and the geodetic analysis are still missing. To pave the way towards an operational application we established a workflow to plan, correlate, observe, and analyze VLBI observations to GNSS satellites. Based on these processes we carried out several successful experiments on the Australian baseline Hobart–Ceduna in 2015 in which we observed GLONASS and GPS satellites in the L1 and L2 bands. For the first time a connected processing chain from scheduling, to correlation, to data analysis has been realized. In this contribution we introduce our workflow and present first results.

Keywords VLBI satellite observations, GNSS, VieVS

1. Technische Universität Wien, Austria

2. University of Tasmania, Australia

1 Introduction

The use of co-location platforms in space for the realization of frame ties between the key space-geodetic techniques, as a supplement to the earthbound localities, is a hot topic in the geodetic community. As dedicated satellite missions, such as the GRASP mission proposed in 2011 (Nerem & Draper, 2011), are rare and not suitable for extensive testing, VLBI observations to GNSS satellites provide a promising alternative to connect the dynamic GNSS and the kinematic VLBI reference frames. In a broader context, observations of GNSS satellites can also be considered as a preparation for observations to future dedicated co-location satellites, such as E-GRASP or E-GRIP (Männel *et al.*, 2016).

In our research we focus on direct observations of GNSS satellite signals with the geodetic VLBI system, trying to apply observation schemes which are commonly used in geodetic VLBI. Hence, our main observables are group delays derived from direct observation and subsequent correlation of GNSS satellite signals, which are treated in the geodetic analysis similarly to delays derived from standard observations of quasars.

Compared to previous experiments carried out within recent years (e.g., Tornatore *et al.*, 2014; Hellerschmied *et al.*, 2014) we also incorporated the correlation, fringe fitting, and analysis in one seamless processing chain. In this paper we first introduce the established workflow and then show initial results for actual GNSS observations on the baseline Hobart–Ceduna (Australia) carried out in 2015.

2 Observations

2.1 Scheduling

The starting point of each VLBI session is a precise observation schedule, defining which sources are observed by which antennas at a given time. The scheduling of satellite observations is a complex task, taking into account numerous observation restrictions caused by the observation geometry, satellite orbit characteristics (e.g., low orbit altitude restricts the common visibility from widely separated stations) and antenna capabilities (e.g., tracking features, slew rate limits, observable frequency range).

For the scheduling of the GNSS observations the VieVS satellite scheduling program (Hellerschmied *et al.*, 2015) was used, which is included as a module in the Vienna VLBI Software (VieVS; Böhm *et al.*, 2012). Basically, it is a convenient tool for the scheduling of real VLBI satellite observations and the creation of the required VEX-formatted schedule files. The orbit determination is based on Two-Line Element (TLE) data sets, which are widely available online. The program also allows generation of combined schedules with observations of satellites and natural sources within one session. The station-specific VEX files can then be used to control GNSS VLBI sessions in an automated manner.

This tool was used to schedule the experiments listed in Table 1 for the baseline Hobart–Ceduna (see Section 2.2) in 2015. During all sessions GLONASS and GPS satellites were observed in the L1 and L2 bands, along with some quasars for calibrations.

2.2 Observation Network

All discussed observations were carried out by the 26-m antenna at Hobart (Ho), Tasmania, and the 30-m antenna at Ceduna (Cd), South Australia, realizing a single baseline of $\sim 1,700$ km length. Both antennas were equipped with linearly polarized (X and Y) L-band receivers with a nominal operating range from 1.35 to 1.65 GHz. Although the GNSS L2 signals (GPS: 1227.6 MHz; GLONASS: 1246.0 MHz) were out of the nominal receiver range and therefore

Table 1 GNSS VLBI experiments on the baseline Ho–Cd in 2015.

Exp. name	Date	Dur.	Obs. GNSS	Sat. scans
g179a	2015-06-28	2h	GPS, GLONASS	13@5min
g236a	2015-08-24	4h	GPS	23@5min
g238a	2015-08-26	4h	GPS, GLONASS	23@5min

attenuated, a signal reception was still possible due to the high power level of the observed signals.

To keep track of the moving satellites during data acquisition, a so-called stepwise satellite tracking approach (described in detail by e.g. Hellerschmied *et al.*, 2015) was implemented in the observation schedules. Basically, satellite orbits are converted to sequences of discrete positions defined by topocentric right ascension and declination. These station dependent tracking points are then used to track the satellites by repositioning the antennas—virtually stepwise—in a time interval of 10 seconds. The recording of data is practically continuous.

2.3 The ‘g236a’ Experiment

As a representative example we describe one of the sessions observed in 2015, the ‘g236a’ session, in detail. First results are presented in the following sections. The g236a experiment was carried out on August 24 from 12:00 to 16:00 UTC. Four GPS satellites (PRN: 02, 12, 24, 24) were observed along with two natural sources (1921–293 and 0208–512). Data was recorded in four 16-MHz channels, centered at the L1 and L2 GPS carrier frequencies, respectively, X- and Y-polarized in each case ($L1_x$, $L1_y$, $L2_x$, $L2_y$).

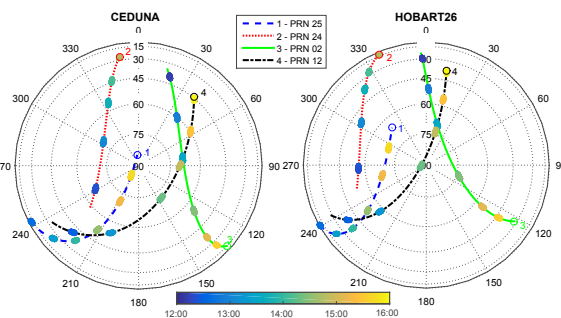


Fig. 1 Skyplots for the participating stations of the ‘g236a’ experiment (August 24, 2015; 12:00–16:00 UTC).

The scan sequence is illustrated in the skyplots for Ho and Cd in Figure 1. Satellites were observed in scans of five minute duration each, switching the observation target after each scan. With this configuration each satellite was observed in several scans well-distributed over the visible arcs. In Figure 1 the observation time is color-coded. Single quasar scans were scheduled roughly every hour between the satellite scans and at the start and end of the session.

3 Correlation and Fringe Fitting

For the correlation (input model) and the data analysis we needed the ability to calculate near field a priori delays for the VLBI observations of GNSS satellites. Therefore, VieVS was upgraded with a near field delay model (Plank *et al.*, 2014), which implements an iterative solution of the light time equation applying relativistic corrections according to Klioner (1991). Satellite positions used for the delay modeling were interpolated from IGS final orbits¹.

The data was correlated with the DiFX software (Deller *et al.*, 2007). As the standard correlator input model generated by the supplied Calc-Server was designed for sources at a virtually infinite distance (e.g. quasars), we calculated dedicated near field delay models for the observed satellites in VieVS and enter them into the control files.

For fringe fitting the FRING task in AIPS and al Fourfit, which is the standard tool in geodesy, were applied successfully. The drawback of using FRING AIPS for geodetic purposes is that the delay epochs are referred to the geocenter, rather than the signal reception at the first network station, which is the common practice in geodesy. On the other hand, AIPS provides more possibilities for manipulating and investigating the data than Fourfit.

The ‘g236a’ data presented in this paper was correlated with a 10 second integration time in DiFX. Therefore we derived one delay solution every 10 seconds within each satellite scan of five minute duration in total. The SNR values after fringe fitting in Fourfit were very high, with values larger than 7000 for the L1 data and between 500 and 700 for the L2 data. The SNR for

¹ <https://igscb.jpl.nasa.gov/components/prods.html>

the L2 data is lower, because these signals were out of the receiver range and therefore attenuated.

Figure 2 depicts fringe delays of the ‘g236a’ experiment calculated in AIPS. Fringe delays basically represent the deviation between actual observations and the a priori delays derived from the correlator input model. We calculated single band delays of the in-phase correlation products (XX and YY) of the recorded L1 and L2 channels. This results in four delay solutions ($L1_{XX}$, $L1_{YY}$, $L2_{XX}$, $L2_{YY}$) per solution epoch (10 second interval)—one per recorded channel (color-coded in Figure 2). As the delays are plotted versus observation time individual five minute scans can clearly be discerned. The RMS scatter within these five minute scans is in the range of several tens of ps. We find large systematic offsets between the recorded channels with up to 40 ns (e.g., in scan 20). Due to this issue a combination of the two recorded orthogonal polarizations (X, Y) was not successful so far. Hence, we only use the $L1_{XX}$ delays for our further discussions.

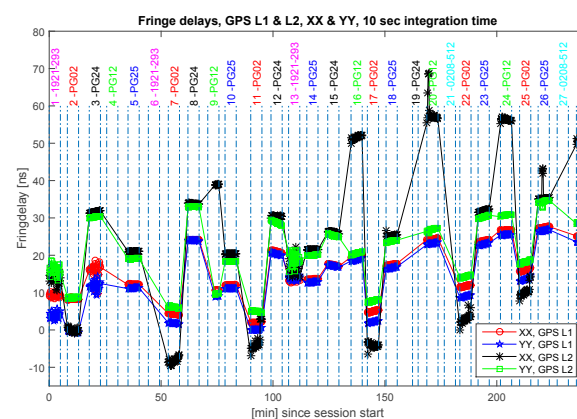


Fig. 2 Fringe delays of experiment ‘g236a’ calculated in AIPS. The names of the observed sources are shown in the top line. Delays for the natural sources (1921–293, 0208–512) are missing or noisy, because the applied 10 second integration time was too short for good results from these comparably weak sources.

4 Data Analysis

A preliminary data analysis was carried out in VieVS, based on single band group delays of the observed GNSS satellites calculated in Fourfit.

Due to the systematic channel offsets ionospheric delay corrections could not be determined directly from the satellite observations in two bands (L1+L2) so far. Alternatively, ionospheric corrections for all observations were calculated from Global Ionospheric Maps (GIM, e.g., IGS TEC maps²) using dedicated functions in VieVS (Tierno Ros *et al.*, 2011). For the ‘g236a’ experiment these corrections were in a range between 1 and 5 ns.

Figure 3 depicts observed minus computed (O–C) values calculated for satellite observations in the ‘g236a’ experiment. O–C values are used as input for a subsequent least-squares adjustment. The observed values (O) are calculated as fringe delays from the $L1_{XX}$ correlation products plus a priori delays from the correlator input model (= total delays). Computed values (C) were calculated with near field delay modeling in VieVS (see Section 3). All O–C values range from -1 to $+4$ ns. In the O–C plot the tracks of the four observed satellites show characteristic signature with variations between 1 and 4 ns per track. Underlying reasons for these satellite track signals and the O–offsets in general (e.g., model inaccuracies, clocks, troposphere) are still the subject of investigations. With individual five minute scans the accuracy is quite good at this point with an RMS scatter between ~ 10 and 100 ps. Figure 4 depicts two scans (8 and 23) in detail.

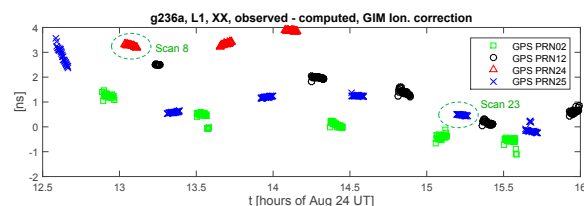


Fig. 3 Observed-minus-computed values for satellite observations of the ‘g236a’ experiment. Scans 8 and 23 are shown in detail in Figure 4.

Based on the O–C values described above we estimated clock parameters for Ho using least-squares adjustment in VieVS. Estimated parameters were hourly piece-wise linear offsets, one rate, and one quadratic term. The resulting post-fit residuals are shown in Figure 5. They are in a range of ± 50 cm, and the post-fit weighted RMS is 29.6 cm. In principle VieVS is able to estimate further geodetic parameters based on VLBI

² <https://igsceb.jpl.nasa.gov/components/prods.html>

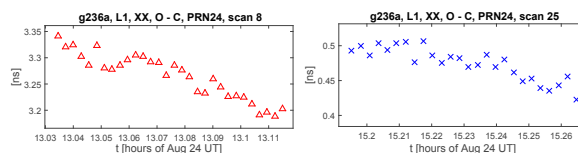


Fig. 4 Observed-minus-computed values of scans 8 and 23 of the ‘g236a’ experiment.

satellite observations analogous to the analysis of standard geodetic VLBI sessions with observations of natural sources. However, at this point the residuals between observations and theoretical delays are still quite large as shown above. Therefore, our preliminary conclusion is that observations and models have to be improved to be able to estimate further parameters (e.g., tropospheric zenith wet delays) meaningfully.

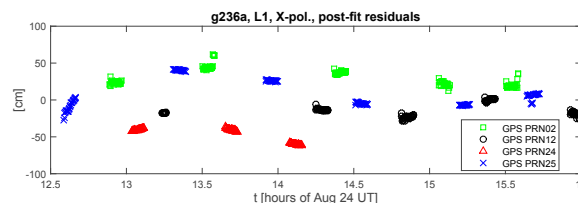


Fig. 5 Post-fit residuals of satellite observations during the ‘g236a’ experiment (WRMS = 29.6 cm).

5 Summary and Outlook

We established a processing chain to plan, observe, correlate, and analyze VLBI near field observations to (GNSS) satellites. For the scheduling the VieVS satellite scheduling module was used, providing convenient features for creating VEX files for satellite observations. Furthermore, VieVS was upgraded with a near field delay model to calculate a priori delays for GNSS satellite observations. Additional modifications allow VieVS to input delay observables from satellite observations and to use them as the basis for geodetic analysis and parameter estimation. DiFX was used for correlations, applying dedicated correlator input models for near field observations calculated directly in VieVS. For the fringe fitting we successfully applied both AIPS and Fourfit, the latter being the standard tool in geodesy.

The VLBI antennas at Ceduna and Hobart, which are directly operated by the University of Tasmania (UTAS), are a great test bed for VLBI satellite observations, because they are equipped with L-band receivers, capable of recording GNSS L1 and L2 signals.

Based on the introduced workflow we carried out several successful GNSS VLBI experiments in June and August 2015 on the baseline Ho–Cd. For the ‘g236a’ experiment, which was discussed as a representative example, the resulting post-fit WRMS was 29.6 cm after estimating clock parameters in VieVS. Although the residuals are still quite large, it shows that our observation and analysis schemes in principle work. Currently, the main issues are the elimination of systematic offsets between the recorded channels and the rigorous combination of the recorded X- and Y-polarized signals to get one single and unambiguous delay for the L1 and L2 band per solution epoch.

Nevertheless, these observations for the first time combined all steps in a connected processing chain: scheduling (including the provision of VEX files for the observation and correlation), the creation of correlator input models, the derivation of total delays, and finally the actual data analysis. This workflow tremendously eases the implementation of such VLBI observations of GNSS satellites, opening up the field for further investigations and improvements.

Acknowledgements

This work was supported by the Austrian Science Fund (FWF, projects I2204 and J3699-N29).

References

- BÖHM, J., BÖHM, S., NILSSON, T., PANY, A., PLANK, L., SPICAKOVA, H., TEKE, K., AND SCHUH, H. (2012). The New Vienna VLBI Software VieVS. In S. Kenyon, M. C. Pacino, and U. Marti, eds., *Geodesy for Planet Earth*, Vol. 136 of *International Association of Geodesy Symposia*, 1007–1011, Springer Berlin Heidelberg.
- DELLER, A., TINGAY, S., BAILES, M., AND WEST, C. (2007). DiFX: A Software Correlator for Very Long Baseline Interferometry Using Multiprocessor Computing Environments. *The Publications of the Astronomical Society of the Pacific*, 119, 318–336.
- HELLERSCHMIED, A., PLANK, L., NEIDHARDT, A., HAAS, R., BÖHM, J., PLÖTZ, C., AND KODET, J. (2014). Observing satellites with VLBI radio telescopes - practical realization at Wettzell. In D. Behrend, K. Baver and K. Armstrong, eds., *IVS 2014 General Meeting Proceedings*, 441–445, Science Press (Beijing). ISBN 978-7-03-042974-2.
- HELLERSCHMIED, A., BÖHM, J., NEIDHARDT, A., KODET, J., HAAS, R., AND PLANK, L. (2015). Scheduling VLBI Observations to Satellites with VieVS. In C. Rizos and P. Willis, eds., *Proc. IAG Commission 1 Symposium 2014: Reference Frames for Applications in Geosciences (REFAG2014)*, International Association of Geodesy Symposia, Springer Berlin Heidelberg, available online.
- KLIONER, S. (1991). General Relativistic Model of VLBI Observables. In W. Carter, ed., *Proc. of AGU Chapman Conference on Geodetic VLBI: Monitoring Global Change*, NOAA Technical Report NOS 137 NGS 49, 188–202, American Geophysical Union, Washington D.C.
- MÄNNEL, B., ROTHACHER, M., JETZER, P., LECOMTE, S., AND ROCHAT, P. (2016). E-GRIP: A Highly Elliptical Orbit Satellite Mission for Co-location in Space. In *Proceedings of the 9th IVS General Meeting, Johannesburg*, this volume.
- NEREM, R.S. AND DRAPER, R.W. (2011). Geodetic Reference Antenna in Space. *GRASP proposal submitted in response to NNH11ZDA0120*, prepared for National Aeronautics and Space Administration Science Mission Directorate September 29, 2011.
- PLANK, L., BÖHM, J., AND SCHUH, H. (2014). Precise station positions from VLBI observations to satellites: a simulation study. *J Geod.*, 88, 659–673.
- TIERNO ROS, C., BÖHM, J., AND SCHUH, H. (2011). Use of gnss-derived tec maps for vlbi observations. In *Proceedings of the 20th Meeting of the European VLBI Group for Geodesy and Astrometry, Bonn*, 114–117.
- TORNATORE, V., HAAS, R., CASEY, S., POGREBENKO, S., AND MOLERA CALVÉS, G. (2014). Direct VLBI Observations of Global Navigation Satellite System Signals. In C. Rizos and P. Willis, eds., *Earth on the Edge: Science for a Sustainable Planet, Proc. IAG General Assembly, 2011*, Vol. 6 of *International Association of Geodesy Symposia*, 247–252, Springer Berlin Heidelberg.

Accurate Spacecraft Positioning by VLBI Imaging

Weimin Zheng^{1,2}, Fengxian Tong¹, Fengchun Shu^{1,2}

Abstract VLBI is a radio astronomy technique with very high space angle resolution, and the Chinese VLBI Network has played an important role in the Chang'E series lunar mission. In the upcoming Chinese lunar and deep space missions, the ability to achieve higher resolution angular positions will be necessary. For these reasons, we have carried out research into accurate spacecraft positioning and have conducted several space vehicle phase-referencing positioning experiments using the Chinese VLBI Network and other VLBI antennas. This paper shows the VLBI spacecraft imaging position experiment results for the Chang'E lunar probes, the Mars Express probe, and the Rosetta probe. The results have validated phase reference VLBI with the milli-arcsecond level position resolution for deep space probes.

Keywords Phase reference VLBI, Chang'E lunar probes, MEX, Rosetta

1 Introduction

Very Long Baseline Interferometry (VLBI) has played an important role in spacecraft positioning during the past decades. Higher accuracy VLBI measurements will be necessary for the future of deep space explorers. Phase reference VLBI is a technique whose accuracy can reach the milli-arcsecond (mas) level or even higher. For this reason, it has been used in high accuracy spacecraft positioning [1]~[10].

1. Shanghai Astronomical Observatory, CAS

2. Key Laboratory of Radio Astronomy, CAS

China has launched probes for lunar exploration, and the positioning accuracy of the lunar spacecraft is on the order of 100 m (~50 mas) [11]. Future Chinese deep space exploration will require more accurate positioning results. For the research into high accuracy phase reference VLBI positioning, some experiments using lunar probes (CE-2, CE-3, and CE-5T1), the Mars Express (MEX), and the comet 69P probe (Rosetta) have been carried out.

In this paper, we give some VLBI phase reference experimental results for the deep space probes mentioned above.

2 VLBI Imaging Theory

According to the VLBI imaging theory (Figure 1), the brightness distribution of the observed target can be restored from observed visibilities sampled on the UV plane by the inverse Fourier transform [12]~[14]:

$$I(l, m) = \iint V(u, v) e^{j2\pi(ul+vm)} du dv \quad (1)$$

where the UV plane is a plane that is perpendicular to the line of sight, and l and m are the cosines of the target unit vector along the U-axis and the V-axis, respectively.

When doing phase reference VLBI, the observed target phase is calibrated using a nearby calibrator. Because the most common system errors will be removed, the accurate target position with respect to the calibrator will be obtained.

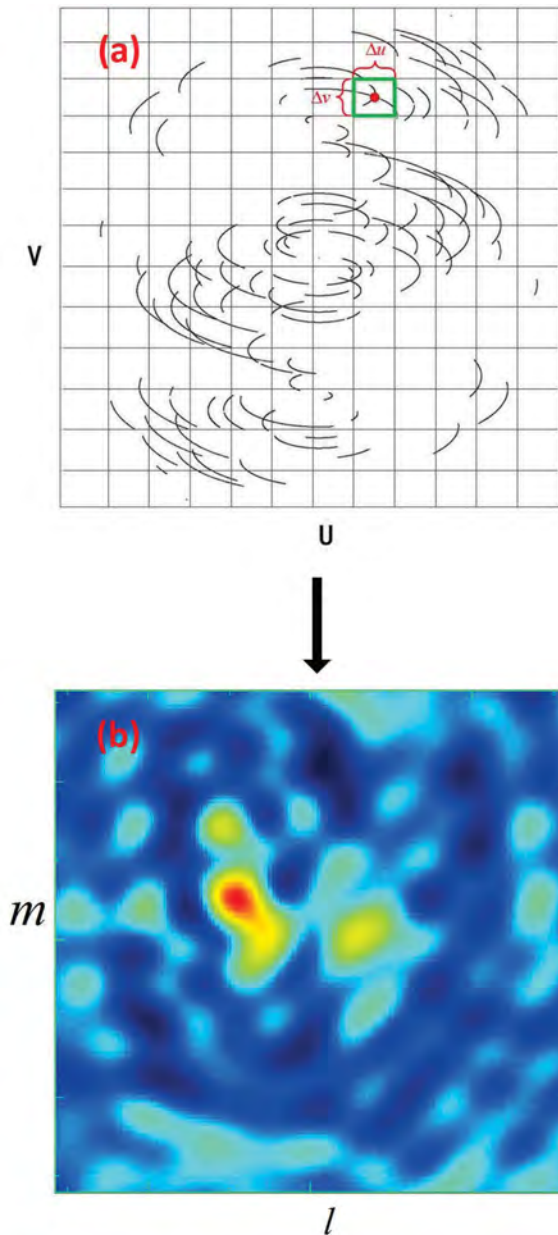


Fig. 1 UV sampling and raw image. (a) UV coverage; (b) raw image.

3 Data and Analysis

To study the spacecraft phase reference VLBI, several experiments (Table 1) have been carried out using the Chinese VLBI Network (CVN).

In these experiments, three CVN antennas joined the CE-2 observing; four CVN antennas joined the

Table 1 Information of spacecraft phase reference VLBI experiments.

Spacecraft	Date (UTC)	Duration	Distance	Frequency
CE-2	2013-05	~6h	$\sim 5 \times 10^7$ km	S band
CE-3	2013-12	~30h	$\sim 4 \times 10^5$ km	X band
CE-5T1	2014-12	~6h	$\sim 4 \times 10^5$ km	X band
MEX	2015-01	~2h	~ 1.9895 AU	X band
Rosetta	2015-09	~10h	~ 1.7889 AU	X band

CE-3 and CE-5T1 observing; four CVN antennas and one Russian antenna (BADARY) joined the MEX observing; and three CVN antennas, three Russian antennas (SVETLOE, ZELENCHK, and BADARY), two New Zealand antennas (WARK12M and WARK30M), two South African antennas (HART15M and HARTRAO), three Australian antennas (KATH12M, YARRA12M, and HOBART26), and two German antennas (WETTZELL and WETTZ13N) joined the Rosetta observing. The imaging results are shown in Figure 2 through Figure 4. The brightest peak position of each image is the angular offset that is related to the target a priori position.

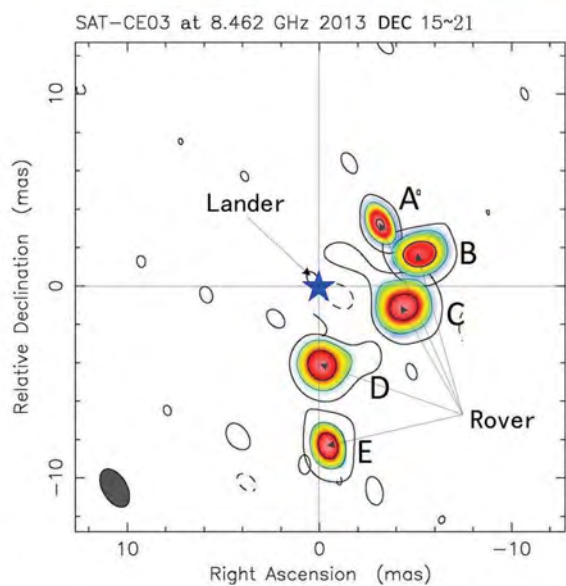
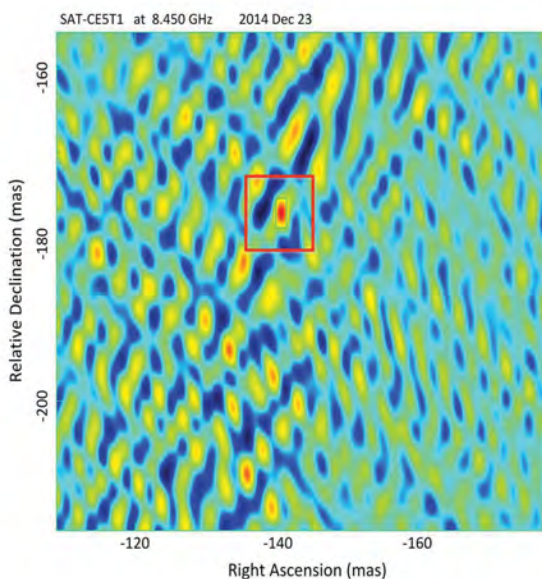
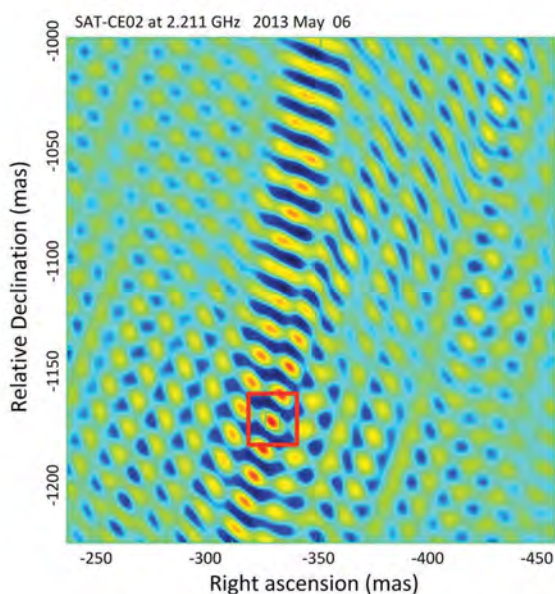
Figure 2 shows the imaging results of CE-2 and CE-3. Five CE-3 Rover relative positions were measured at the lunar surface sites A~E. The CE-2 angular position accuracy is within the CE-2 orbital accuracy. The angular accuracy of the CE-3 Rover relative to the Lander is ~ 0.5 mas, which is consistent with the position results measured with the onboard camera and the Inertial Measurement Unit (IMU).

Figure 3 shows the imaging results of CE-5T1 and Rosetta. The CE-5T1 and Rosetta position accuracies are within their respective orbital accuracies.

Figure 4 shows the imaging results of MEX. The top figure is the CVN result, and the bottom figure is the JIVE (Joint Institute for VLBI in Europe) result. The discrepancy between the CVN and the JIVE imaging positioning results is less than 2 mas. Both results are consistent with the MEX micro-arcsecond (μ as) orbital accuracy.

4 Conclusions

In this paper, we showed the successful spacecraft phase reference VLBI experiments. Spacecraft phase reference VLBI can obtain mas-level positioning results. Phase reference VLBI does not need a specially



Dirty RR Map. Array: CVN
ROSETTA at 8.422 GHz 2015 Sep 20

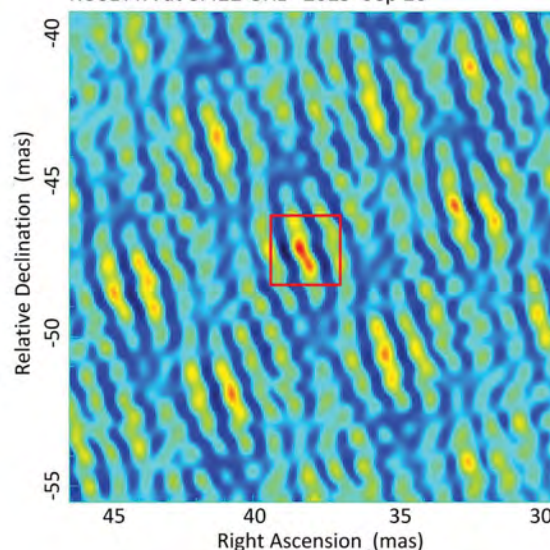


Fig. 2 Phase reference VLBI imaging results of CE-2 (top) and CE-3 (bottom).

Fig. 3 Phase reference VLBI imaging results of CE-5T1 (top) and Rosetta (bottom).

designed radio beacon, and the observation sessions are short compared with the normal VLBI sessions. These are the merits of phase reference VLBI. The experimental results indicate that the VLBI phase reference can be used for spacecraft positioning of higher accuracy in the upcoming lunar and martian missions.

Acknowledgements

This work is sponsored by the Natural Science Foundation of China General Program (11173052, 11373061, 11573057, and 11403082), the Key Laboratory of Radio Astronomy of Chinese Academy of Sciences, the Science & Technology Commission project of Shang-

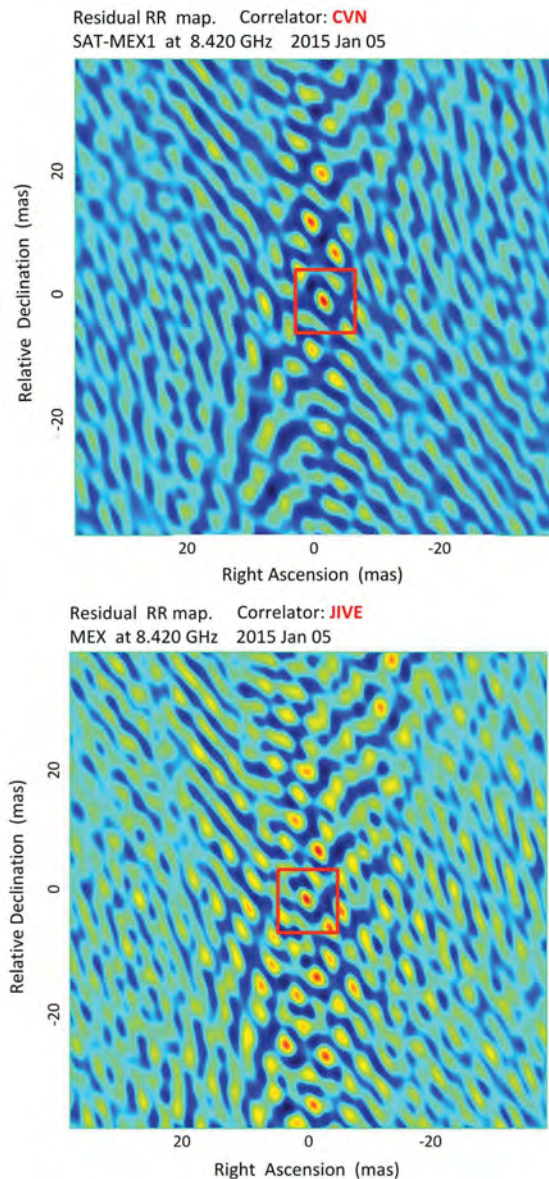


Fig. 4 CVN (top) and JIVE (bottom) phase reference VLBI imaging results of MEX.

hai Municipality (06DZ22101), the Program of Shanghai Subject Chief Scientist (14XD1404300), and the Chinese lunar exploration project. We would like to thank Dr. Sergei Pogrebenko for the MEX result comparisons, Alexander Neidhardt and Christian Plötz for the Rosetta observations, and the observations of Russian antennas, New Zealand antennas, South African antennas, Australian antennas, and the CVN.

References

1. Jones D L, Fomalont E, Dhawan V, et al. VLBA Astrometric Observations of the Cassini Spacecraft at Saturn. *The Astronomical Journal*, pages 29–38, 2011.
2. G. Lanyi, J. Border, J. Benson, et al. Determination of Angular Separation Between Spacecraft and Quasars with the Very Long Baseline Array. JPL IPN Progress Report 42-162, 2005.
3. D. S. Bagri. A Proposed Frequency Synthesis Approach to Accurately Measure the Angular Position of a Spacecraft. JPL IPN Progress Report 42-163, 2005.
4. W. Majid, D. Bagri. Availability of Calibration Sources for Measuring Spacecraft Angular Position with Sub-Nanoradian Accuracy. JPL IPN Progress Report 42-165, 2006.
5. Gabor Lanyi, Durgadas S. Bagri, James S. Border. Angular Position Determination of Spacecraft by Radio Interferometry. *Proceedings of IEEE*, pages 2193–2201, 2007.
6. D. S. Bagri, W. A. Majid. Estimating Accurate Relative Spacecraft Angular Position from Deep Space Network Very Long Baseline Interferometry Phases Using X-Band Telemetry or Differential One-Way Ranging Tones. JPL IPN Progress Report 42-172, 2008.
7. Ed Fomalont, Tomas Martin-Mur, James Border, et al. Spacecraft Navigation Using the VLBA. 10th European VLBI Network Symposium and EVN Users Meeting: VLBI and the new generation of radio arrays, 2010.
8. T. J. Martin-Mur, G. L. Kruizinga, P. D. Burkhart, et al. Mars Science Laboratory Interplanetary Navigation. *Journal of Spacecraft and Rockets*, pages 1014–1028, 2014.
9. Jones D L, Fomalont E, Dhawan V, et al. VLBA Astrometric Observations of the Cassini Spacecraft at Saturn. *The Astronomical Journal*, pages 29–38, 2011.
10. Duev D A, Calves G M, Pogrebenko S V, et al. Spacecraft VLBI and Doppler Tracking: Algorithms and Implementation. *Astronomy and Astrophysics*, pages 849–858, 2012.
11. Huang Yong, Chang Sheng Qi, Li Pei Jia, et al. Orbit determination of Chang'E-3 and positioning of the lander and the rover. *Chin Sci Bull*, pages 3858–3867, 2014.
12. Thompson A. Richard, James M. Moran, George W. Swenson. *Interferometry and synthesis radio in astronomy*, Second Edition. John Wiley and Sons, pages 86–90, 2008.
13. B. G. Clark. *Interferometers and Coherence Theory*. ASP Conference Series, pages 3–16, 1995.
14. A. Richard Thompson, James M. Moran, George W. Swenson Jr. *Interferometry and Synthesis in Radio Astronomy* (Second Edition). Wiley-VCH: 2004.

Venus and Mars Express Spacecraft Observations with Wettzell Radio Telescopes

Guifré Molera Calvés^{1,2}, Alexander Neidhardt³, Christian Plötz⁴, Gerhard Kronschnabl⁴, Giuseppe Cimó^{2,5}, Sergei Pogrebenko²

Abstract The ESA Venus, Mars Express, and Rosetta spacecraft were observed at X-band with the Wettzell radio telescopes Wn and Wz in the framework of an assessment study of the possible contribution of the European VLBI network to the upcoming ESA deep space missions and further projects. These observations were extended to regular weekly sessions to routinely run the processing and analysis pipeline. Recorded data were transferred from Wettzell to the JIVE cooperation partners for correlation and analysis. A high dynamic range of the detections allowed us to achieve a mHz level of the spectral resolution accuracy and extract the phase of the spacecraft signal carrier line. Several physical parameters can be determined from these observational results with more observational data collected. Apart from other results, the measured phase fluctuations of the carrier line at different time scales can be assessed to determine the influence of the Solar wind plasma density fluctuations on the accuracy of the astrometric VLBI observations.

Keywords VLBI, radio telescope, spacecraft signal, solar wind

1 Introduction

The combination of Very Long Baseline Interferometry (VLBI) and Doppler spacecraft tracking has been successfully exploited in a number of space science missions, including VLBI tracking of the descent and landing of the Huygens Probe in the atmosphere of Titan [2] and VLBI observations of ESA's Venus Express and of the Mars Express Phobos flyby [7].

Based on the experience acquired in these projects, the Planetary Radio Interferometry and Doppler Experiment (PRIDE) concept has been developed. PRIDE is an international enterprise led by the Joint Institute for VLBI in Europe (JIVE). It focuses primarily on tracking planetary and space science missions through radio interferometric and Doppler measurements [3]. PRIDE provides precise estimations of the spacecraft state vectors based on Doppler and VLBI phase-referencing techniques [1]. These can be applied to a wide range of research fields.

Figure 1 shows the basic configuration for the PRIDE observations, where the observations of planetary spacecraft are combined with observations of natural radio sources.

Table 1 shows the main characteristics of the radio telescopes at the Wettzell observatory used for spacecraft observations. The 20-m Radio Telescope Wettzell (RTW) with station code Wz was finished in 1983 and is one of the main systems of the International VLBI Service for Geodesy and Astrometry (IVS). It is equipped with an S/X-receiving system. The antenna Wn with a 13.2-m dish is the northern telescope of the newly built TWIN Radio Telescope Wettzell (TTW), which was finished and inaugurated in 2013. TTW is a fast-slewing broadband telescope following the specifications of the VLBI Global Observing System

1. Aalto University, School of Electrical Engineering, Department of Radio Science and Engineering

2. Joint Institute for VLBI ERIC

3. Technische Universität München, Geodätisches Observatorium Wettzell

4. Bundesamt für Kartographie und Geodäsie

5. ASTRON, the Netherlands Institute for Radio Astronomy

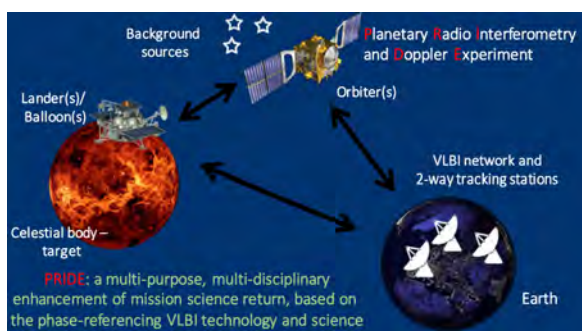


Fig. 1 Scheme of the Planetary Radio Interferometry and Doppler Experiments (PRIDE) observations.

(VGOS). The antenna Wn is currently equipped with a standard S/X-receiving system, which is extended with a Ka-band receiver.

Table 1 The radio telescopes at Wettzell used for the spacecraft observations.

Station code	latitude	longitude	altitude (m)	dish (m)	SEFD-X (Jy)
Wettzell Wz	49°08'42.0"	12°52'37.9"	661.20	20.0	700
Wettzell Wn	49°08'38.1"	12°52'39.7"	672.57	13.2	840

2 Observations

The PRIDE team initiated systematic observations of planetary spacecraft in 2009. ESA’s VEX spacecraft was selected due to its high-quality signal, suitable transmission frequency, and possibility of being observed by European VLBI radio telescopes. The 20-m RTW (Wz) has participated since 2010 in 57 sessions involving VEX until the mission ended in 2014 and in 23 sessions involving MEX between 2014 and 2016. In 2015, the Wn was additionally included into the network of planetary spacecraft observations. A total number of 17 sessions were arranged since then with Wn. In our observations, the spacecraft signals are observed in X-band ($\lambda = 3.6$ cm, $f_0 = 8.4$ GHz).

On 20 May 2015, we operated the first simultaneous observation of spacecraft using both Wn and Wz. After that, eight similar experiments were arranged. Figure 3 shows the relative power to noise ratio, the Doppler frequency residuals, and the difference between the telescopes’ residuals detected on 26 October 2015.

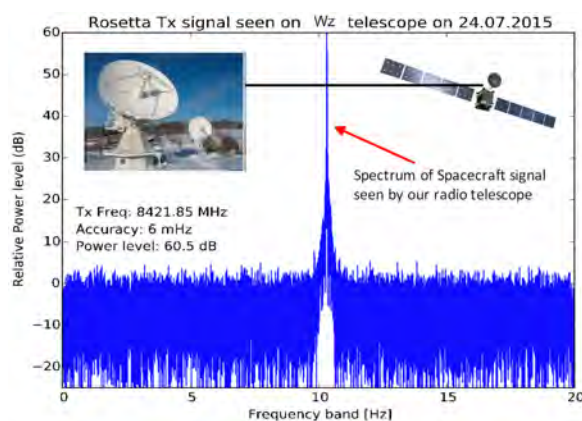


Fig. 2 Detection of the spacecraft signal transmitted by Rosetta by the Wettzell radio telescopes on 24 July 2015.

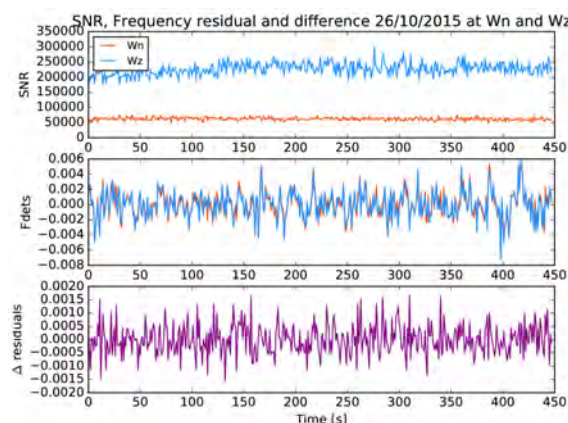


Fig. 3 Upper panel: relative power Wz (blue/upper line) and Wn (red/lower line). Middle panel: residual frequencies for same data. Lower panel: difference between both telescopes’ residuals. The MEX data were observed at Wz and Wn on 26 October 2015. The standard deviations of the frequency detections are 1.78 mHz for Wn, 1.76 for Wz, and 0.5 mHz for the difference.

Spacecraft observations are research and development approaches to open new domains for geodetic VLBI. The geodetic benefit is the interrelation to other techniques to tie the different reference frames. VGOS supports spacecraft tracking, while mostly Earth orbiting satellites in the near field are in the focus [6]. But the IVS encourages developments which use VLBI on sources besides quasars (see different volumes of the past IVS General Meetings Proceedings). It opens doors to spacecraft navigation which is strongly related to the application of reference frames. Besides this, the observations of spacecraft are checks of the accuracy

of the techniques at the location of the antennas and throughout the whole processing chain. Additionally, they are technical tests for possible future domains of VLBI, which are currently already possible. Another aspect is that one of the pillars of geodesy is gravity and the gravitational field [10]. In a wider sense, spacecraft observations with VLBI enable the determination of gravitational fields of planetary objects. From the point of view of a geodetic observatory the observations are quite valuable. Using two telescopes provides the possibility of more observations, because one telescope might be able to observe while the other is occupied by another session. It would also offer possibilities of new observation modes for differential VLBI, so that one telescope observes quasars close to the spacecraft while the other tracks the spacecraft itself. Current implementations do not take enough account of these possibilities.

3 Analysis

The data processing is conducted using the on-purpose software developed for multi-tone tracking of planetary spacecraft signals. The software is divided into three parts: the SWspec, the SCtracker, and the digital Phase-Locked-Loop. All three software packages were described in [7]. Figure 4 shows a block diagram of the spacecraft tracking software.

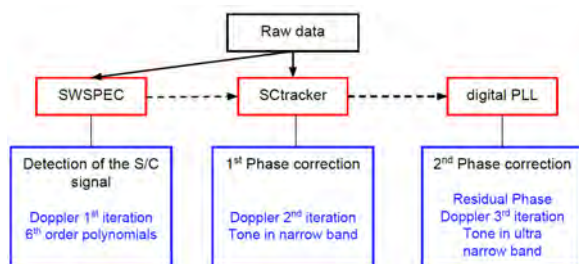


Fig. 4 Illustration of the data analysis steps and software modules used for spacecraft tracking purposes: SWspec, SCtracker, and digital PLL. The complete software is developed and maintained jointly by JIVE and Aalto University.

The three most important parameters out of our detections are Doppler noise, the Signal-to-Noise Ratio (SNR) of the carrier, and the phase scintillation indices.

The output results for the first two parameters from a regular observation are shown in Figure 3. The results are utilized for a wide field of research:

- studies of the interplanetary scintillation caused by the solar wind at different solar elongations and positions with respect to the Sun [7].
- characterization of the properties of Coronal Mass Ejections (CME) and monitoring of similar events in almost real-time [8].
- determination of the speed of the solar wind using VLBI techniques.
- studies of the planetary atmosphere on Venus, using radio signal and aerobreaking techniques [9].
- determination of gravitational fields of planetary objects (moons, comets) by using fly-by techniques [5].
- radio occultation experiments to evaluate ingress and egress phenomena.
- orbit determination of the space missions, such as Radio Astron [3].
- enhancement and support of future planetary space missions: JUICE, ExoMars, Bepi-Colombo, etc.

4 Conclusions

Planetary spacecraft as targets for radio observations by ground-based radio telescopes provide a unique opportunity to investigate a wide range of scientific fields.

Tracking observations of spacecraft, ESA's MEX and Rosetta, will continue in order to improve detection measurements and the processing pipeline. Future space missions, such as ESA's Jupiter Icy Moon Explorer (JUICE), will benefit from such precise knowledge.

Radio science studies such as this one allow us to disentangle the contributions from the interplanetary plasma and the Earth's ionosphere. The research will continue with the goals of characterizing the atmospheric and ionospheric structure of planets and media, small body fly-by missions, atmospheric drag campaigns, radio occultations, detection of coronal mass ejections, or precise orbit determination of satellites. Besides the scientific output, the tests provide a technical feasibility study of the technical workflow from scheduling to analysis.

Acknowledgements

We would like to thank the operators at each of the supporting stations for making the observations possible. We are also thankful to the project team of the ESA VEX and MEX missions for their support and assistance of our research.

References

1. BEASLEY, A.J., & CONWAY, J.E. (1995). VLBI Phase-Referencing, eds. ASP, 82, 327.
2. BIRD, M. K., ALLISON, M., ASMAR, S. W. ET AL. (2005). *Nature*, 438, 8.
3. DUEV, D.A., MOLERA CALVÉS, G., POGREBENKO, S.V. ET AL. (2012). Spacecraft VLBI and Doppler tracking: algorithms and implementation, *A&A*, 541, A43.
4. DUEV, D.A., ZAKHVATKIN, M.V., STEPANYANTS, S.V. ET AL. (2015). Radio Astron as a target and as an instrument: Enhancing the Space VLBI mission's scientific output, *A&A* 573, A99.
5. DUEV, D.A., S.V. POGREBENKO, G. CIMÓ, ET AL. (2016). Planetary Radio Interferometry and Doppler Experiment (PRIDE), submitted to *A&A*. technique: a test case of the Mars Express Phobos fly-by.
6. PLANCK, L. (2013). VLBI satellite tracking for the realization of frame ties, Dissertation, Technische Universität Wien, http://ww2.erdrotation.de/SharedDocs/Downloads/EN/Publications/Dissertations/Plank_Dissertation.pdf?__blob=publicationFile, Download 2016-05-15.
7. MOLERA CALVÉS, G., CIMÓ, G., POGREBENKO, S.V. ET AL. (2014). Observations and analysis of phase scintillation of spacecraft signal on the interplanetary plasma, *A&A*, Vol. 564, id.A4, 7.
8. MOLERA CALVÉS, G., KALLIO, E., CIMÓ, G. ET AL. (2016). Exploring Interplanetary Coronal Mass Ejections with spacecraft radio signals, submitted to *A&A*.
9. ROSENBLATT, P., BRUINSMA, S.L., MÜLLER-WODARG, I.C.F. ET AL. (2012). First ever in situ observations of Venus' polar upper atmosphere density using the tracking data of the Venus Express Atmospheric Drag Experiment (VExADE), vol. 217, 831-838.
10. ROTHACHER, MARKUS, PLAG, HANS-PETER, NEILAN, RUTH (2015). The Global Geodetic Observing System. Geodesy's contribution to Earth Observation. GGOS. International Association of Geodesy. http://www.ggosportal.org/lang_en/nn_261454/SharedDocs/Publikationen/EN/GGOS/Introduction...to...GGOS,templateId=raw,property=publicationFile.pdf/Introduction_to_GGOS.pdf, Download 2015-09-27.

About the Meeting



March 2016 · Johannesburg · South Africa

Registered Participants

Name	Institution	City	Country
Jim Lovell	University of Tasmania	Hobart	Australia
Lucia Plank	University of Tasmania	Hobart	Australia
Stanislav Shabala	University of Tasmania	Hobart	Australia
Johannes Böhm	TU Vienna	Vienna	Austria
Anastasiia Girdiuk	TU Vienna	Vienna	Austria
Andreas Hellerschmied	TU Vienna	Vienna	Austria
Younghee Kwak	TU Vienna	Vienna	Austria
David Mayer	TU Vienna	Vienna	Austria
Bill Petrachenko	DRAO, NRCan Penticton	Penticton	Canada
Guifei Jing	NRSCC	Beijing	China
Zhong Chen	SHAO	Shanghai	China
Jiangying Gan	SHAO	Shanghai	China
Yidan Huang	SHAO	Shanghai	China
Wu Jiang	SHAO	Shanghai	China
Fengchun Shu	SHAO	Shanghai	China
Guangli Wang	SHAO	Shanghai	China
Minghui Xu	SHAO	Shanghai	China
Shuangjing Xu	SHAO	Shanghai	China
Zhijun Xu	SHAO	Shanghai	China
Bo Zhang	SHAO	Shanghai	China
Weimin Zheng	SHAO	Shanghai	China
Renjie Zhu	SHAO	Shanghai	China
Jyri Näränen	Finnish Geospatial Research Institute	Masala	Finland
Nataliya Zubko	Finnish Geospatial Research Institute	Masala	Finland
Richard Biancale	CNES/GRGS	Toulouse	France
Patrick Charlot	LAB Bordeaux	Floirac	France
César Gattano	Observatoire de Paris	Paris	France
Sabine Bachmann	BKG Frankfurt	Frankfurt/Main	Germany
Gerald Engelhardt	BKG Leipzig	Leipzig	Germany
Dieter Ullrich	BKG Leipzig	Leipzig	Germany
Gerhard Kronschnabl	BKG Wettzell	Bad Kötzing	Germany
Christian Plötz	BKG Wettzell	Bad Kötzing	Germany
Torben Schüler	BKG Wettzell	Bad Kötzing	Germany
Claudia Flohrer	ESA/ESOC	Darmstadt	Germany
Alexander Neidhardt	FESG Wettzell	Bad Kötzing	Germany

Name	Institution	City	Country
Robert Heinkelmann	GFZ Potsdam	Potsdam	Germany
Maria Karbon	GFZ Potsdam	Potsdam	Germany
Tobias Nilsson	GFZ Potsdam	Potsdam	Germany
Harald Schuh	GFZ Potsdam	Potsdam	Germany
Benedikt Soja	GFZ Potsdam	Potsdam	Germany
Thomas Artz	IGG Bonn	Bonn	Germany
Sebastian Halsig	IGG Bonn	Bonn	Germany
Andreas Iddink	IGG Bonn	Bonn	Germany
Arno Müskens	IGG Bonn	Bonn	Germany
Axel Nothnagel	IGG Bonn	Bonn	Germany
Richard Porcas	MPIfR Bonn	Bonn	Germany
Eberhard Sust	MT Mechatronics	Mainz	Germany
Hans-Thomas Zimmerer	MT Mechatronics	Mainz	Germany
Kyriakos Balidakis	TU Berlin	Berlin	Germany
Emmanuel Proven-Adzri	Space Science and Technology Institute	Accra	Ghana
Simona di Tomaso	E-Geos	Matera	Italy
Matteo Stagni	IRA - INAF	Bologna	Italy
Gino Tuccari	IRA - INAF	Bologna	Italy
Vincenza Tornatore	Politecnico di Milano	Milano	Italy
Ryoji Kawabata	GSI Tsukuba	Tsukuba	Japan
Takaaki Jike	NAOJ	Oshu	Japan
Tomoaki Oyama	NAOJ	Oshu	Japan
Mamoru Sekido	NICT	Kashima	Japan
Martin Mutie		Nairobi	Kenya
Antone Orege	AVN	Nairobi	Kenya
Felix Omonya	NACOSTI	Nairobi	Kenya
Nancy Omollo	Newton Fund	Nairobi	Kenya
Willice Obonyo	Rongo University College	Sare	Kenya
Calvince Juma	Technical University of Kenya	Nairobi	Kenya
Amos Chepkwony	University of Nairobi	Nairobi	Kenya
Samson Mutunga	University of Nairobi	Nairobi	Kenya
Ann Njeri Ng'Endo	University of Nairobi	Nairobi	Kenya
Jephter Ondieki	University of Nairobi	Nairobi	Kenya
René Vermeulen	ASTRON	Dwingeloo	Netherlands
Bob Campbell	JIVE	Dwingeloo	Netherlands
Harro Verkouter	JIVE	Dwingeloo	Netherlands
Per Erik Opseth	NMA Norway	Hønefoss	Norway
Leif Morten Tangen	NMA Norway	Hønefoss	Norway
Halfdan Pascal Kierulf	NMA Norway	Oslo	Norway

Name	Institution	City	Country
Ann-Silje Kirkvik	NMA Norway	Oslo	Norway
Anne Kristin Frivold	NMA Norway	Røyse	Norway
Jungho Cho	KASI	Daejeon	Rep. Korea
Sang Oh Yi	NGII	Sejong	Rep. Korea
Alexander Ipatov	IAA RAS	St. Petersburg	Russia
Evgeny Nosov	IAA RAS	St. Petersburg	Russia
Gladness Baloyi	HartRAO	Krugersdorp	South Africa
Paul Mmtoni Barasa	HartRAO	Krugersdorp	South Africa
Michael Bietenholz	HartRAO	Krugersdorp	South Africa
Roelf Botha	HartRAO	Krugersdorp	South Africa
Glenda Coetzer	HartRAO	Krugersdorp	South Africa
Ludwig Combrinck	HartRAO	Krugersdorp	South Africa
Aletha de Witt	HartRAO	Krugersdorp	South Africa
Khadija El Bouchefry	HartRAO	Krugersdorp	South Africa
Hubert Mathebula	HartRAO	Krugersdorp	South Africa
Lisa Mbwia	HartRAO	Krugersdorp	South Africa
Webby Miyoba	HartRAO	Krugersdorp	South Africa
Marisa Nickola	HartRAO	Krugersdorp	South Africa
George Nicolson	HartRAO	Krugersdorp	South Africa
Jonathan Quick	HartRAO	Krugersdorp	South Africa
Pfesesani van Zyl	HartRAO	Krugersdorp	South Africa
Marion West	HartRAO	Krugersdorp	South Africa
Sayan Basu	HartRAO	Pretoria	South Africa
Mbali Mlangeni	HartRAO	Pretoria	South Africa
Ivan Farayi Muzondo	HartRAO	Pretoria	South Africa
Sphumelele Ndlovu	HartRAO	Pretoria	South Africa
Nokwazi Purity Nkosi	HartRAO	Pretoria	South Africa
Malebo Sharon Rakgalakane	HartRAO	Pretoria	South Africa
Nkululeko Qwabe	SKA South Africa	Cape Town	South Africa
Lerothodi Leeuw	University of South Africa	Unisa	South Africa
Pablo de Vicente Abad	IGN Spain	Madrid	Spain
Sten Bergstrand	SP Technical Research Institute	Borås	Sweden
Rüdiger Haas	Chalmers University of Technology	Onsala	Sweden
Thomas Hobiger	Chalmers University of Technology	Onsala	Sweden
Niko Kareinen	Chalmers University of Technology	Onsala	Sweden
Grzegorz Kłopotek	Chalmers University of Technology	Onsala	Sweden
Markus Rothacher	ETH Zurich	Zurich	Switzerland
Graham Appleby	NERC Space Geodesy Facility, Herstmonceux	Hailsham	U.K.
Richard Gross	Jet Propulsion Laboratory	Pasadena, CA	U.S.A.

Name	Institution	City	Country
Christopher Jacobs	Jet Propulsion Laboratory	Pasadena, CA	U.S.A.
Brian Corey	MIT Haystack Observatory	St. Petersburg, FL	U.S.A.
Roger Cappallo	MIT Haystack Observatory	Westford, MA	U.S.A.
Arthur Niell	MIT Haystack Observatory	Westford, MA	U.S.A.
Ganesan Rajagopalan	MIT Haystack Observatory	Westford, MA	U.S.A.
Chet Ruszczyk	MIT Haystack Observatory	Westford, MA	U.S.A.
Frank Lemoine	NASA GSFC	Greenbelt, MD	U.S.A.
Chopo Ma	NASA GSFC	Greenbelt, MD	U.S.A.
Dirk Behrend	NVI, Inc./NASA GSFC	Greenbelt, MD	U.S.A.
John Gipson	NVI, Inc./NASA GSFC	Greenbelt, MD	U.S.A.
David Gordon	NVI, Inc./NASA GSFC	Greenbelt, MD	U.S.A.
Ed Himwich	NVI, Inc./NASA GSFC	Greenbelt, MD	U.S.A.
Karine Le Bail	NVI, Inc./NASA GSFC	Greenbelt, MD	U.S.A.
Daniel MacMillan	NVI, Inc./NASA GSFC	Greenbelt, MD	U.S.A.
Cynthia Thomas	NVI, Inc./NASA GSFC	Greenbelt, MD	U.S.A.
Christopher Dieck	U.S. Naval Observatory	Washington, DC	U.S.A.
Nicole Geiger	U.S. Naval Observatory	Washington, DC	U.S.A.
John Spitzak	U.S. Naval Observatory	Washington, DC	U.S.A.
Careen Mutembo	AVN Student, Zambia Bureau of Standards	Lusaka	Zambia
Noah Lumbwe Chanka	AVN Trainee, Newton Fund Zambia	Ndola	Zambia
Esther Musambo Kunaka	Astronomy for Africa-Zambia	Kitwe	Zambia
Kando Hamiyanze Moonga	University of Zambia, SKA	Lusaka	Zambia
Mubela Mutale	University of Zambia	Lusaka	Zambia
Nchimunya Mwiinga	University of Zambia	Lusaka	Zambia
Namakau Mwiya	University of Zambia	Lusaka	Zambia
Naomi Simumba	University of Zambia	Lusaka	Zambia
Misheck Sinyangwe	University of Zambia	Lusaka	Zambia
Peter Banda	University of Zambia	Petauke	Zambia

Author Index

[First author papers printed in **bold face**.]

Ah, Ki-duk: p. 139, Activities at Sejong Station

Alef, Walter: p. 34, BRAND EVN

————— p. 171, New DiFX Software Correlator Cluster at Bonn and Summary of Recent Activities

Ambrosini, Roberto: p. 166, The First Geodetic VLBI Field Test of LIFT: A 550-km-long Optical Fiber Link for Remote Antenna Synchronization

Anderson, J.: p. 149, First Local Ties from Data of the Wettzell Triple Radio Telescope Array

————— p. 317, Source Structure of 0642+449 Derived from CONT14 Observations

Aoki, Tetsuro: p. 25, An Overview of the Japanese GALA-V Wideband VLBI System

Appleby, Graham M.: p. 15, **Current Trends and Challenges in Satellite Laser Ranging**

Artz, Thomas: p. 96, First Results of the FAST-S/X Sessions with New VGOS Antennas

————— p. 166, The First Geodetic VLBI Field Test of LIFT: A 550-km-long Optical Fiber Link for Remote Antenna Synchronization

————— p. 193, **Constraining Least-Squares VLBI Solutions**

————— p. 203, Results from the VLBI Analysis Software Comparison Campaign 2015

————— p. 217, **ivg::ASCOT: Development of a New VLBI Software Package**

————— p. 283, Estimating the Celestial Reference Frame via Intra-Technique Combination

————— p. 326, An Inequality Constrained Least-Squares Approach as an Alternative Estimation Procedure for Atmospheric Parameters from VLBI Observations

Bachmann, Sabine: p. 213, Options and Functions of the Revised IVS Combination Web Site

————— p. 241, **IVS Contribution to ITRF2014**

————— p. 251, Vienna Contribution to ITRF2014

Balidakis, Kyriakos: p. 256, Comparison of a VLBI TRF Solution Based on Kalman Filtering and Recent ITRS Realizations

————— p. 331, **On the Impact of Different Mapping Functions on Geodetic and Tropospheric Products from VLBI Data Analysis**

————— p. 356, **On the Impact of Inhomogeneities in Meteorological Data on VLBI Data Analysis**

Basu, S.: p. 312, **How Good is the Deep Southern Sky**

Baver, Karen: p. 222, Transition to the vgosDb Format

————— p. 229, Improvement of the IVS-INT01 Sessions through Bayesian Estimation

Behrend, Dirk: p. 3, Strategic Plan of the IVS for the Period 2016–2025

————— p. 69, **Implementation of the VGOS Trials**

————— p. 127, From CONT to VGOS: the Evolution of the CONT Campaigns

Bellanger, A.: p. 203, Results from the VLBI Analysis Software Comparison Campaign 2015

Bergstrand, Sten: p. 113, **Activities of the IERS Working Group on Site Survey and Co-location**

————— p. 154, Automated Simultaneous Local Ties with GNSS and Robot Tacheometer

Bernhart, Simone: p. 171, New DiFX Software Correlator Cluster at Bonn and Summary of Recent Activities

Bertarini, Alessandra: p. 3, Strategic Plan of the IVS for the Period 2016–2025

————— p. 96, First Results of the FAST-S/X Sessions with New VGOS Antennas

————— p. 149, First Local Ties from Data of the Wettzell Triple Radio Telescope Array

- p. 166, The First Geodetic VLBI Field Test of LIFT: A 550-km-long Optical Fiber Link for Remote Antenna Synchronization
- p. 171, New DiFX Software Correlator Cluster at Bonn and Summary of Recent Activities
- p. 302, Completing the K-band Celestial Reference Frame in the North
- p. 312, How Good is the Deep Southern Sky
- Bezrukov, Ilya:* p. 96, First Results of the FAST-S/X Sessions with New VGOS Antennas
- p. 106, New Generation VLBI: Intraday UT1 Estimations
- Bianco, Giuseppe:* p. 15, Current Trends and Challenges in Satellite Laser Ranging
- p. 132, The Italian VLBI Network: First Results and Future Perspectives
- Bizouard, C.:* p. 341, The Annual Retrograde Nutation Variability
- Bolotin, Sergei:* p. 222, **Transition to the vgosDb Format**
- Bondarenko, Yu.:* p. 96, First Results of the FAST-S/X Sessions with New VGOS Antennas
- Bortolotti, Claudio:* p. 166, The First Geodetic VLBI Field Test of LIFT: A 550-km-long Optical Fiber Link for Remote Antenna Synchronization
- Bourda, G.:* p. 203, Results from the VLBI Analysis Software Comparison Campaign 2015
- p. 302, Completing the K-band Celestial Reference Frame in the North
- Briskan, Walter:* p. 171, New DiFX Software Correlator Cluster at Bonn and Summary of Recent Activities
- p. 187, Difxcalc – Calc11 for the DiFX Correlator
- Bruni, Gabriele:* p. 171, New DiFX Software Correlator Cluster at Bonn and Summary of Recent Activities
- Byon, Do-young:* p. 139, Activities at Sejong Station
- Böer, Armin:* p. 101, Current Status of an Implementation of a System Monitoring for Seamless Auxiliary Data at the Geodetic Observatory Wettzell
- Böhm, Johannes:* p. 96, First Results of the FAST-S/X Sessions with New VGOS Antennas
- p. 265, Combination of Two Radio Space-Geodetic Techniques with VieVS during CONT14
- p. 275, Vienna Contribution to the ICRF3
- p. 346, Tidal Atmospheric Loading and VLBI
- p. 373, VLBI Observations of GNSS Signals on the Baseline Hobart–Ceduna
- Böhm, Sigrid:* p. 251, **Vienna Contribution to ITRF2014**
- Calonico, Davide:* p. 166, The First Geodetic VLBI Field Test of LIFT: A 550-km-long Optical Fiber Link for Remote Antenna Synchronization
- Cappallo, Roger:* p. 44, VGOS Observations with Westford, GGAO, and the New Station at Kokee, Hawaii
- p. 61, **Delay and Phase Calibration in VGOS Post-Processing**
- Charlot, Patrick:* p. 3, Strategic Plan of the IVS for the Period 2016–2025
- p. 82, VGOS Source Selection Criteria
- p. 302, Completing the K-band Celestial Reference Frame in the North
- Chen, Guangming:* p. 363, APOD Mission Status and Observations by VLBI
- Chen, Zhong:* p. 176, Current Status of the Shanghai VLBI Correlator
- Chung, Moon-hee:* p. 139, Activities at Sejong Station
- Cimó, Giuseppe:* p. 382, Venus and Mars Express Spacecraft Observations with Wettzell Radio Telescopes
- Clivati, Cecilia:* p. 166, The First Geodetic VLBI Field Test of LIFT: A 550-km-long Optical Fiber Link for Remote Antenna Synchronization
- Collioud, Arnaud:* p. 82, VGOS Source Selection Criteria
- Combrinck, Ludwig:* p. 3, Strategic Plan of the IVS for the Period 2016–2025
- p. 118, Optimizing the African VLBI Network for Astronomy and Geodesy
- Corey, Brian:* p. 44, VGOS Observations with Westford, GGAO, and the New Station at Kokee, Hawaii
- p. 65, How to Register a VGOS Radio Telescope at ITU and Why It Is Important
- de Vicente, Pablo:* p. 40, First 2-Gbps Observations between the KVAZAR VGOS Antennas and the YebeS RAEGE Antenna
- p. 96, First Results of the FAST-S/X Sessions with New VGOS Antennas
- p. 123, **A Technical Overview of the EVN**
- de Witt, A.:* p. 118, **Optimizing the African VLBI Network for Astronomy and Geodesy**
- p. 302, **Completing the K-band Celestial Reference Frame in the North**

- p. 312, How Good is the Deep Southern Sky
- DLR DFD Team:* p. 146, The German Antarctic Receiving Station O’Higgins and Its VLBI Capabilities
- Douša, Jan:* p. 331, On the Impact of Different Mapping Functions on Geodetic and Tropospheric Products from VLBI Data Analysis
- Eckert, Chris:* p. 44, VGOS Observations with Westford, GGAO, and the New Station at Kokee, Hawaii
- Elosegui, Pedro:* p. 44, VGOS Observations with Westford, GGAO, and the New Station at Kokee, Hawaii
- Enderle, Werner:* p. 261, VLBI Processing at ESOC
- Engelhardt, Gerald:* p. 225, **Refinement of the Rapid UT1 Estimation Derived from Tsukuba VLBI Measurements after the 2011 Earthquake**
- Eschelbach, Cornelia:* p. 149, First Local Ties from Data of the Wettzell Triple Radio Telescope Array
- p. 154, Automated Simultaneous Local Ties with GNSS and Robot Tacheometer
- Fedotov, Leonid:* p. 106, New Generation VLBI: Intraday UT1 Estimations
- Flohner, Claudia:* p. 261, **VLBI Processing at ESOC**
- Frittelli, Matteo:* p. 166, The First Geodetic VLBI Field Test of LIFT: A 550-km-long Optical Fiber Link for Remote Antenna Synchronization
- Gan, Jiangying:* p. 180, Hardware Correlator Development at SHAO
- p. 183, **High-speed Data Playback of the VLBI Hardware Correlator**
- Gattano, C.:* p. 292, **Defining Source Selection and Celestial Reference Frame Stability**
- p. 307, **Source Characterization by the Allan Variance**
- p. 341, **The Annual Retrograde Nutation Variability**
- Gayazov, Iskander:* p. 106, New Generation VLBI: Intraday UT1 Estimations
- Gerstl, M.:* p. 203, Results from the VLBI Analysis Software Comparison Campaign 2015
- Gipson, John:* p. 3, Strategic Plan of the IVS for the Period 2016–2025
- p. 222, Transition to the vgosDb Format
- p. 229, **Improvement of the IVS-INT01 Sessions through Bayesian Estimation**
- p. 336, **El Niño and VLBI Measured Length of Day**
- Girdiuk, Anastasiia:* p. 346, **Tidal Atmospheric Loading and VLBI**
- Glaser, Susanne:* p. 208, Simulations of Near Real-time EOP Estimation from a Future VGOS Network
- p. 256, Comparison of a VLBI TRF Solution Based on Kalman Filtering and Recent ITRS Realizations
- p. 331, On the Impact of Different Mapping Functions on Geodetic and Tropospheric Products from VLBI Data Analysis
- p. 356, On the Impact of Inhomogeneities in Meteorological Data on VLBI Data Analysis
- Gordon, David:* p. 187, **Difxcalc – Calc11 for the DiFX Correlator**
- p. 203, Results from the VLBI Analysis Software Comparison Campaign 2015
- p. 222, Transition to the vgosDb Format
- p. 270, Aspects of ICRF-3
- p. 280, **Status of the X/S Source Catalog**
- p. 288, Selecting Sources that Define a Stable Celestial Reference Frame with the Allan Variance
- Gross, Richard:* p. 256, Comparison of a VLBI TRF Solution Based on Kalman Filtering and Recent ITRS Realizations
- Guo, Shaoguang:* p. 180, Hardware Correlator Development at SHAO
- p. 183, High-speed Data Playback of the VLBI Hardware Correlator
- Haas, Rüdiger:* p. 3, Strategic Plan of the IVS for the Period 2016–2025
- p. 154, Automated Simultaneous Local Ties with GNSS and Robot Tacheometer
- p. 198, Robust Ambiguity Estimation for an Automated Analysis of the Intensive Sessions
- p. 203, Results from the VLBI Analysis Software Comparison Campaign 2015
- p. 234, Hard- and Software Tools for the Education of Geodetic VLBI
- Halsig, Sebastian:* p. 96, First Results of the FAST-S/X Sessions with New VGOS Antennas
- p. 149, First Local Ties from Data of the Wettzell Triple Radio Telescope Array
- p. 193, Constraining Least-Squares VLBI Solutions
- p. 203, Results from the VLBI Analysis Software Comparison Campaign 2015

- p. 217, *ivg::ASCOT: Development of a New VLBI Software Package*
- p. 283, *Estimating the Celestial Reference Frame via Intra-Technique Combination*
- p. 326, **An Inequality Constrained Least-Squares Approach as an Alternative Estimation Procedure for Atmospheric Parameters from VLBI Observations**
- Hanado, Yuko*: p. 25, *An Overview of the Japanese GALA-V Wideband VLBI System*
- Hase, Hayo*: p. 65, **How to Register a VGOS Radio Telescope at ITU and Why It Is Important**
- Hasegawa, Shingo*: p. 25, *An Overview of the Japanese GALA-V Wideband VLBI System*
- Heinkelmann, Robert*: p. 208, *Simulations of Near Real-time EOP Estimation from a Future VGOS Network*
- p. 256, *Comparison of a VLBI TRF Solution Based on Kalman Filtering and Recent ITRS Realizations*
- p. 297, *About the Modeling of Radio Source Time Series as Linear Splines*
- p. 317, *Source Structure of 0642+449 Derived from CONT14 Observations*
- p. 331, *On the Impact of Different Mapping Functions on Geodetic and Tropospheric Products from VLBI Data Analysis*
- p. 356, *On the Impact of Inhomogeneities in Meteorological Data on VLBI Data Analysis*
- Hellerschmied, Andreas*: p. 96, *First Results of the FAST-S/X Sessions with New VGOS Antennas*
- p. 373, **VLBI Observations of GNSS Signals on the Baseline Hobart–Ceduna**
- Himwich, Ed*: p. 3, *Strategic Plan of the IVS for the Period 2016–2025*
- p. 69, *Implementation of the VGOS Trials*
- Hjelle, G.A.*: p. 203, *Results from the VLBI Analysis Software Comparison Campaign 2015*
- Hobiger, Thomas*: p. 198, *Robust Ambiguity Estimation for an Automated Analysis of the Intensive Sessions*
- p. 203, *Results from the VLBI Analysis Software Comparison Campaign 2015*
- p. 234, **Hard- and Software Tools for the Education of Geodetic VLBI**
- p. 265, *Combination of Two Radio Space-Geodetic Techniques with VieVS during CONT14*
- Horiuchi, S.*: p. 302, *Completing the K-band Celestial Reference Frame in the North*
- Hugentobler, U.*: p. 203, *Results from the VLBI Analysis Software Comparison Campaign 2015*
- Ichikawa, Ryuichi*: p. 25, *An Overview of the Japanese GALA-V Wideband VLBI System*
- Iddink, Andreas*: p. 193, *Constraining Least-Squares VLBI Solutions*
- p. 203, *Results from the VLBI Analysis Software Comparison Campaign 2015*
- p. 217, *ivg::ASCOT: Development of a New VLBI Software Package*
- p. 283, **Estimating the Celestial Reference Frame via Intra-Technique Combination**
- p. 326, **An Inequality Constrained Least-Squares Approach as an Alternative Estimation Procedure for Atmospheric Parameters from VLBI Observations**
- IGN Yebes Observatory Staff*: p. 135, **RAEGE Project Update: Yebes Observatory Broadband Receiver Ready for VGOS**
- Ikeda, Takatoshi*: p. 25, *An Overview of the Japanese GALA-V Wideband VLBI System*
- Ilin, Gennadiy*: p. 106, *New Generation VLBI: Intraday UT1 Estimations*
- Ipatov, Alexander*: p. 3, *Strategic Plan of the IVS for the Period 2016–2025*
- p. 106, **New Generation VLBI: Intraday UT1 Estimations**
- Ivanov, Dmitriy*: p. 96, *First Results of the FAST-S/X Sessions with New VGOS Antennas*
- p. 106, *New Generation VLBI: Intraday UT1 Estimations*
- Jacobs, C.S.*: p. 302, *Completing the K-band Celestial Reference Frame in the North*
- Je, Do-heung*: p. 139, *Activities at Sejong Station*
- Jetzer, Philippe*: p. 368, *E-GRIP: A Highly Elliptical Orbit Satellite Mission for Co-location in Space*
- Jiang, Tianyu*: p. 176, *Current Status of the Shanghai VLBI Correlator*
- Jiang, Wu*: p. 176, **Current Status of the Shanghai VLBI Correlator**
- p. 351, *Progress on the VLBI Ecliptic Plane Survey*
- Jike, Takaaki*: p. 159, **VERA Geodetic VLBI with a Newly Developed High-speed Sampler and Recorder**
- Jung, Tae-hyun*: p. 139, *Activities at Sejong Station*
- p. 302, *Completing the K-band Celestial Reference Frame in the North*

- Kallio, Ulla*: p. 143, Metsähovi Geodetic Fundamental Station in Finland — New VGOS Site, Plans, and Current Status
 ——— p. 154, **Automated Simultaneous Local Ties with GNSS and Robot Tacheometer**
- Karbon, Maria*: p. 208, Simulations of Near Real-time EOP Estimation from a Future VGOS Network
 ——— p. 256, Comparison of a VLBI TRF Solution Based on Kalman Filtering and Recent ITRS Realizations
 ——— p. 297, **About the Modeling of Radio Source Time Series as Linear Splines**
 ——— p. 331, On the Impact of Different Mapping Functions on Geodetic and Tropospheric Products from VLBI Data Analysis
 ——— p. 356, On the Impact of Inhomogeneities in Meteorological Data on VLBI Data Analysis
- Kareinen, Niko*: p. 198, **Robust Ambiguity Estimation for an Automated Analysis of the Intensive Sessions**
- Kawabata, Ryoji*: p. 3, Strategic Plan of the IVS for the Period 2016–2025
- Kawai, Eiji*: p. 25, An Overview of the Japanese GALA-V Wideband VLBI System
- Ken, Voytsekh*: p. 106, New Generation VLBI: Intraday UT1 Estimations
- Kirkvik, A.S.*: p. 203, Results from the VLBI Analysis Software Comparison Campaign 2015
- Kirschbauer, Katharina*: p. 101, Current Status of an Implementation of a System Monitoring for Seamless Auxiliary Data at the Geodetic Observatory Wettzell
- Klopotek, G.*: p. 203, **Results from the VLBI Analysis Software Comparison Campaign 2015**
- Klügel, T.*: p. 146, The German Antarctic Receiving Station O’Higgins and Its VLBI Capabilities
 ——— p. 149, First Local Ties from Data of the Wettzell Triple Radio Telescope Array
- Kodet, Jan*: p. 49, The VGOS TWIN Radio Telescope TTW2 at Wettzell
- Koenig, Daniel*: p. 73, Generation of Global Geodetic Networks for GGOS
- Komuro, Jun-ichi*: p. 25, An Overview of the Japanese GALA-V Wideband VLBI System
- Kondo, Tetsuro*: p. 25, An Overview of the Japanese GALA-V Wideband VLBI System
- Koyama, Yasuhiro*: p. 25, An Overview of the Japanese GALA-V Wideband VLBI System
- Kronshnabl, Gerhard*: p. 49, **The VGOS TWIN Radio Telescope TTW2 at Wettzell**
 ——— p. 96, First Results of the FAST-S/X Sessions with New VGOS Antennas
 ——— p. 382, Venus and Mars Express Spacecraft Observations with Wettzell Radio Telescopes
- Krásná, Hana*: p. 251, Vienna Contribution to ITRF2014
 ——— p. 275, Vienna Contribution to the ICRF3
- Kurdubov, Sergei*: p. 40, First 2-Gbps Observations between the KVAZAR VGOS Antennas and the Yebes RAEGE Antenna
 ——— p. 96, First Results of the FAST-S/X Sessions with New VGOS Antennas
 ——— p. 106, New Generation VLBI: Intraday UT1 Estimations
- Kuzmicz-Cieslak, Magda*: p. 73, Generation of Global Geodetic Networks for GGOS
- Kwak, Younghee*: p. 265, **Combination of Two Radio Space-Geodetic Techniques with VieVS during CONT14**
 ——— p. 373, VLBI Observations of GNSS Signals on the Baseline Hobart–Ceduna
- Lambert, S.*: p. 203, Results from the VLBI Analysis Software Comparison Campaign 2015
 ——— p. 292, Defining Source Selection and Celestial Reference Frame Stability
 ——— p. 307, Source Characterization by the Allan Variance
 ——— p. 341, The Annual Retrograde Nutation Variability
- La Porta, Laura*: p. 171, New DiFX Software Correlator Cluster at Bonn and Summary of Recent Activities
- Le Bail, Karine*: p. 270, Aspects of ICRF-3
 ——— p. 280, Status of the X/S Source Catalog
 ——— p. 288, **Selecting Sources that Define a Stable Celestial Reference Frame with the Allan Variance**
- Lecomte, Steve*: p. 368, E-GRIP: A Highly Elliptical Orbit Satellite Mission for Co-location in Space
- Levi, Filippo*: p. 166, The First Geodetic VLBI Field Test of LIFT: A 550-km-long Optical Fiber Link for Remote Antenna Synchronization
- Li, Jinling*: p. 351, Progress on the VLBI Ecliptic Plane Survey
- Li, Jiyun*: p. 163, Progress on the VLBI Data Acquisition System of SHAO

- Li, Xie:* p. 363, APOD Mission Status and Observations by VLBI
- Lim, Hyung-chul:* p. 139, Activities at Sejong Station
- Liu, Shushi:* p. 363, APOD Mission Status and Observations by VLBI
- Lovell, Jim:* p. 3, Strategic Plan of the IVS for the Period 2016–2025
- p. 87, Observing with Sibling and Twin Telescopes
- p. 92, **Prototyping Automation and Dynamic Observing with the AuScope Array**
- p. 302, Completing the K-band Celestial Reference Frame in the North
- p. 351, Progress on the VLBI Ecliptic Plane Survey
- Lösler, Michael:* p. 149, First Local Ties from Data of the Wettzell Triple Radio Telescope Array
- p. 154, Automated Simultaneous Local Ties with GNSS and Robot Tacheometer
- p. 241, IVS Contribution to ITRF2014
- Ma, Chopo:* p. 3, Strategic Plan of the IVS for the Period 2016–2025
- p. 270, **Aspects of ICRF-3**
- p. 288, Selecting Sources that Define a Stable Celestial Reference Frame with the Allan Variance
- Maccaferri, Giuseppe:* p. 166, The First Geodetic VLBI Field Test of LIFT: A 550-km-long Optical Fiber Link for Remote Antenna Synchronization
- MacLeod, G.:* p. 118, Optimizing the African VLBI Network for Astronomy and Geodesy
- MacMillan, Daniel:* p. 73, **Generation of Global Geodetic Networks for GGOS**
- p. 127, From CONT to VGOS: the Evolution of the CONT Campaigns
- p. 222, Transition to the vgosDb Format
- p. 270, Aspects of ICRF-3
- Mardyshkin, Vyacheslav:* p. 106, New Generation VLBI: Intraday UT1 Estimations
- Marshall, Dmitriy:* p. 53, Operating Experience with the Broadband Acquisition System on the RT-13 Radio Telescopes
- p. 96, First Results of the FAST-S/X Sessions with New VGOS Antennas
- p. 106, New Generation VLBI: Intraday UT1 Estimations
- Max-Moerbeck, Walter:* p. 187, Difxcalc – Calc11 for the DiFX Correlator
- Mayer, David:* p. 87, Observing with Sibling and Twin Telescopes
- p. 92, Prototyping Automation and Dynamic Observing with the AuScope Array
- p. 96, First Results of the FAST-S/X Sessions with New VGOS Antennas
- p. 118, Optimizing the African VLBI Network for Astronomy and Geodesy
- p. 275, **Vienna Contribution to the ICRF3**
- McCallum, Jamie:* p. 87, Observing with Sibling and Twin Telescopes
- p. 92, Prototyping Automation and Dynamic Observing with the AuScope Array
- p. 302, Completing the K-band Celestial Reference Frame in the North
- p. 312, How Good is the Deep Southern Sky
- p. 351, Progress on the VLBI Ecliptic Plane Survey
- p. 373, VLBI Observations of GNSS Signals on the Baseline Hobart–Ceduna
- McWhirter, Russ:* p. 44, VGOS Observations with Westford, GGAO, and the New Station at Kokee, Hawaii
- Melnikov, Alexey:* p. 40, **First 2-Gbps Observations between the KVAZAR VGOS Antennas and the Yeves RAEGE Antenna**
- p. 53, Operating Experience with the Broadband Acquisition System on the RT-13 Radio Telescopes
- p. 96, First Results of the FAST-S/X Sessions with New VGOS Antennas
- p. 106, New Generation VLBI: Intraday UT1 Estimations
- Messerschmitt, Linda:* p. 213, **Options and Functions of the Revised IVS Combination Web Site**
- p. 241, IVS Contribution to ITRF2014
- Mikhailov, Andrey:* p. 40, First 2-Gbps Observations between the KVAZAR VGOS Antennas and the Yeves RAEGE Antenna
- p. 96, First Results of the FAST-S/X Sessions with New VGOS Antennas
- p. 106, New Generation VLBI: Intraday UT1 Estimations
- Miyauchi, Yuka:* p. 25, An Overview of the Japanese GALA-V Wideband VLBI System

- Molera Calvés, Guifré*: p. 382, **Venus and Mars Express Spacecraft Observations with Wettzell Radio Telescopes**
- Mora-Diaz, Julian*: p. 297, About the Modeling of Radio Source Time Series as Linear Splines
 — p. 317, Source Structure of 0642+449 Derived from CONT14 Observations
- Mura, Alberto*: p. 166, The First Geodetic VLBI Field Test of LIFT: A 550-km-long Optical Fiber Link for Remote Antenna Synchronization
- Mähler, S.*: p. 149, First Local Ties from Data of the Wettzell Triple Radio Telescope Array
- Männel, Benjamin*: p. 368, **E-GRIP: A Highly Elliptical Orbit Satellite Mission for Co-location in Space**
- Müskens, Arno*: p. 171, **New DiFX Software Correlator Cluster at Bonn and Summary of Recent Activities**
- Namba, Kunitaka*: p. 25, An Overview of the Japanese GALA-V Wideband VLBI System
- Nanni, Mauro*: p. 166, The First Geodetic VLBI Field Test of LIFT: A 550-km-long Optical Fiber Link for Remote Antenna Synchronization
- Negusini, Monia*: p. 132, The Italian VLBI Network: First Results and Future Perspectives
 — p. 166, The First Geodetic VLBI Field Test of LIFT: A 550-km-long Optical Fiber Link for Remote Antenna Synchronization
- Neidhardt, Alexander*: p. 49, The VGOS TWIN Radio Telescope TTW2 at Wettzell
 — p. 96, **First Results of the FAST-S/X Sessions with New VGOS Antennas**
 — p. 101, **Current Status of an Implementation of a System Monitoring for Seamless Auxiliary Data at the Geodetic Observatory Wettzell**
 — p. 146, The German Antarctic Receiving Station O'Higgins and Its VLBI Capabilities
 — p. 149, First Local Ties from Data of the Wettzell Triple Radio Telescope Array
 — p. 382, Venus and Mars Express Spacecraft Observations with Wettzell Radio Telescopes
- Nickola, M.*: p. 118, Optimizing the African VLBI Network for Astronomy and Geodesy
- Niell, Arthur*: p. 3, **Strategic Plan of the IVS for the Period 2016–2025**
 — p. 44, **VGOS Observations with Westford, GGAO, and the New Station at Kokee, Hawaii**
- Nilsson, Tobias*: p. 208, **Simulations of Near Real-time EOP Estimation from a Future VGOS Network**
 — p. 256, Comparison of a VLBI TRF Solution Based on Kalman Filtering and Recent ITRS Realizations
 — p. 297, About the Modeling of Radio Source Time Series as Linear Splines
 — p. 331, On the Impact of Different Mapping Functions on Geodetic and Tropospheric Products from VLBI Data Analysis
 — p. 356, On the Impact of Inhomogeneities in Meteorological Data on VLBI Data Analysis
- Noll, Carey E.*: p. 15, Current Trends and Challenges in Satellite Laser Ranging
- Nosov, Evgeny*: p. 53, **Operating Experience with the Broadband Acquisition System on the RT-13 Radio Telescopes**
- Nothnagel, Axel*: p. 3, **Strategic Plan of the IVS for the Period 2016–2025**
 — p. 96, First Results of the FAST-S/X Sessions with New VGOS Antennas
 — p. 149, First Local Ties from Data of the Wettzell Triple Radio Telescope Array
 — p. 193, Constraining Least-Squares VLBI Solutions
 — p. 217, ivg::ASCOT: Development of a New VLBI Software Package
 — p. 283, Estimating the Celestial Reference Frame via Intra-Technique Combination
 — p. 326, An Inequality Constrained Least-Squares Approach as an Alternative Estimation Procedure for Atmospheric Parameters from VLBI Observations
- Näränen, Jyri*: p. 143, Metsähovi Geodetic Fundamental Station in Finland — New VGOS Site, Plans, and Current Status
- Oh, Hong-jong*: p. 139, Activities at Sejong Station
- Okamoto, Yoshihiro*: p. 25, An Overview of the Japanese GALA-V Wideband VLBI System
- Pavlis, Erricos C.*: p. 15, Current Trends and Challenges in Satellite Laser Ranging
 — p. 73, Generation of Global Geodetic Networks for GGOS
- Pearlman, Michael R.*: p. 15, Current Trends and Challenges in Satellite Laser Ranging
- Perini, Federico*: p. 166, **The First Geodetic VLBI Field Test of LIFT: A 550-km-long Optical**

- Fiber Link for Remote Antenna Synchronization**
- Petrachenko, Bill*: p. 3, Strategic Plan of the IVS for the Period 2016–2025
- p. 78, Operational VGOS Scheduling
- p. 82, **VGOS Source Selection Criteria**
- Petrov, Leonid*: p. 118, Optimizing the African VLBI Network for Astronomy and Geodesy
- p. 351, Progress on the VLBI Ecliptic Plane Survey
- Phogat, Apurva*: p. 356, On the Impact of Inhomogeneities in Meteorological Data on VLBI Data Analysis
- Plank, Lucia*: p. 87, **Observing with Sibling and Twin Telescopes**
- p. 92, Prototyping Automation and Dynamic Observing with the AuScope Array
- p. 203, Results from the VLBI Analysis Software Comparison Campaign 2015
- p. 265, Combination of Two Radio Space-Geodetic Techniques with VieVS during CONT14
- p. 373, VLBI Observations of GNSS Signals on the Baseline Hobart–Ceduna
- Plötz, Christian*: p. 49, The VGOS TWIN Radio Telescope TTW2 at Wettzell
- p. 96, First Results of the FAST-S/X Sessions with New VGOS Antennas
- p. 101, Current Status of an Implementation of a System Monitoring for Seamless Auxiliary Data at the Geodetic Observatory Wettzell
- p. 146, **The German Antarctic Receiving Station O’Higgins and Its VLBI Capabilities**
- p. 149, First Local Ties from Data of the Wettzell Triple Radio Telescope Array
- p. 382, Venus and Mars Express Spacecraft Observations with Wettzell Radio Telescopes
- Pogrebenko, Sergei*: p. 382, Venus and Mars Express Spacecraft Observations with Wettzell Radio Telescopes
- Poutanen, Markku*: p. 143, Metsähovi Geodetic Fundamental Station in Finland — New VGOS Site, Plans, and Current Status
- Quick, J.*: p. 302, Completing the K-band Celestial Reference Frame in the North
- p. 312, How Good is the Deep Southern Sky
- Rajagopalan, Ganesh*: p. 44, VGOS Observations with Westford, GGAO, and the New Station at Kokee, Hawaii
- Ren, Tianpeng*: p. 363, APOD Mission Status and Observations by VLBI
- Rochat, Pascal*: p. 368, E-GRIP: A Highly Elliptical Orbit Satellite Mission for Co-location in Space
- Roggenbuck, Ole*: p. 241, IVS Contribution to ITRF2014
- Roma, Mauro*: p. 166, The First Geodetic VLBI Field Test of LIFT: A 550-km-long Optical Fiber Link for Remote Antenna Synchronization
- Rothacher, Markus*: p. 368, E-GRIP: A Highly Elliptical Orbit Satellite Mission for Co-location in Space
- Rottmann, Helge*: p. 171, New DiFX Software Correlator Cluster at Bonn and Summary of Recent Activities
- Ruszczuk, Chet*: p. 44, VGOS Observations with Westford, GGAO, and the New Station at Kokee, Hawaii
- Saaranen, Veikko*: p. 143, Metsähovi Geodetic Fundamental Station in Finland — New VGOS Site, Plans, and Current Status
- Salnikov, Alexander*: p. 106, New Generation VLBI: Intraday UT1 Estimations
- Sarti, Pierguido*: p. 132, The Italian VLBI Network: First Results and Future Perspectives
- Schindelegger, Michael*: p. 346, Tidal Atmospheric Loading and VLBI
- Schmid, Ralf*: p. 113, Activities of the IERS Working Group on Site Survey and Co-location
- p. 203, Results from the VLBI Analysis Software Comparison Campaign 2015
- Schuh, Harald*: p. 208, Simulations of Near Real-time EOP Estimation from a Future VGOS Network
- p. 256, Comparison of a VLBI TRF Solution Based on Kalman Filtering and Recent ITRS Realizations
- p. 297, About the Modeling of Radio Source Time Series as Linear Splines
- p. 317, Source Structure of 0642+449 Derived from CONT14 Observations
- p. 331, On the Impact of Different Mapping Functions on Geodetic and Tropospheric Products from VLBI Data Analysis
- p. 356, On the Impact of Inhomogeneities in Meteorological Data on VLBI Data Analysis
- Schönberger, Matthias*: p. 101, Current Status of an Implementation of a System Monitoring for Seamless Auxiliary Data at the Geodetic Observatory Wettzell

- Schönemann, Erik*: p. 261, VLBI Processing at ESOC
- Schüller, Torben*: p. 3, Strategic Plan of the IVS for the Period 2016–2025
- p. 49, The VGOS TWIN Radio Telescope TTW2 at Wettzell
- p. 146, The German Antarctic Receiving Station O’Higgins and Its VLBI Capabilities
- p. 149, **First Local Ties from Data of the Wettzell Triple Radio Telescope Array**
- p. 171, New DiFX Software Correlator Cluster at Bonn and Summary of Recent Activities
- Searle, Anthony*: p. 78, **Operational VGOS Scheduling**
- p. 82, VGOS Source Selection Criteria
- Sekido, Mamoru*: p. 25, **An Overview of the Japanese GALA-V Wideband VLBI System**
- Serna Puente, J.*: p. 146, The German Antarctic Receiving Station O’Higgins and Its VLBI Capabilities
- Shabala, Stas*: p. 92, Prototyping Automation and Dynamic Observing with the AuScope Array
- p. 312, How Good is the Deep Southern Sky
- Shen, Zhiqiang*: p. 176, Current Status of the Shanghai VLBI Correlator
- Shu, Fengchun*: p. 176, Current Status of the Shanghai VLBI Correlator
- p. 203, Results from the VLBI Analysis Software Comparison Campaign 2015
- p. 351, **Progress on the VLBI Ecliptic Plane Survey**
- p. 378, Accurate Spacecraft Positioning by VLBI Imaging
- Smolentsev, Sergei*: p. 106, New Generation VLBI: Intraday UT1 Estimations
- Soja, Benedikt*: p. 208, Simulations of Near Real-time EOP Estimation from a Future VGOS Network
- p. 256, **Comparison of a VLBI TRF Solution Based on Kalman Filtering and Recent ITRS Realizations**
- p. 331, On the Impact of Different Mapping Functions on Geodetic and Tropospheric Products from VLBI Data Analysis
- p. 356, On the Impact of Inhomogeneities in Meteorological Data on VLBI Data Analysis
- Springer, Tim*: p. 261, VLBI Processing at ESOC
- Stagni, Matteo*: p. 132, **The Italian VLBI Network: First Results and Future Perspectives**
- p. 166, The First Geodetic VLBI Field Test of LIFT: A 550-km-long Optical Fiber Link for Remote Antenna Synchronization
- Stempkovski, Victor*: p. 106, New Generation VLBI: Intraday UT1 Estimations
- Sun, Jing*: p. 363, APOD Mission Status and Observations by VLBI
- Sung, Yun-mo*: p. 139, Activities at Sejong Station
- Surkis, Igor*: p. 106, New Generation VLBI: Intraday UT1 Estimations
- Suzuyama, Tomonari*: p. 25, An Overview of the Japanese GALA-V Wideband VLBI System
- Takahashi, Rumi*: p. 25, An Overview of the Japanese GALA-V Wideband VLBI System
- Takefuji, Kazuhiro*: p. 25, An Overview of the Japanese GALA-V Wideband VLBI System
- p. 351, Progress on the VLBI Ecliptic Plane Survey
- Tagiguchi, Hiroshi*: p. 25, An Overview of the Japanese GALA-V Wideband VLBI System
- Tang, Geshi*: p. 363, **APOD Mission Status and Observations by VLBI**
- Tangen, Leif Morten*: p. 37, **Ny-Ålesund Observatory: What Has Been Done?**
- Tegtmeier, Corinna*: p. 193, Constraining Least-Squares VLBI Solutions
- Teke, Kamil*: p. 265, Combination of Two Radio Space-Geodetic Techniques with VieVS during CONT14
- Terada, Kenjiro*: p. 25, An Overview of the Japanese GALA-V Wideband VLBI System
- Thaller, Daniela*: p. 213, Options and Functions of the Revised IVS Combination Web Site
- p. 241, IVS Contribution to ITRF2014
- Thomas, Cynthia*: p. 69, Implementation of the VGOS Trials
- p. 127, **From CONT to VGOS: the Evolution of the CONT Campaigns**
- Thorandt, Volkmar*: p. 225, Refinement of the Rapid UT1 Estimation Derived from Tsukuba VLBI Measurements after the 2011 Earthquake
- Titov, O.*: p. 203, Results from the VLBI Analysis Software Comparison Campaign 2015
- Titus, Mike*: p. 44, VGOS Observations with Westford, GGAO, and the New Station at Kokee, Hawaii
- Tong, Fengxian*: p. 203, Results from the VLBI Analysis Software Comparison Campaign 2015
- p. 378, Accurate Spacecraft Positioning by VLBI Imaging

- Tornatore, Vincenza*: p. 65, How to Register a VGOS Radio Telescope at ITU and Why It Is Important
- Tsutsumi, Masanori*: p. 25, An Overview of the Japanese GALA-V Wideband VLBI System
- Tuccari, Gino*: p. 34, **BRAND EVN**
- Ujihara, Hideki*: p. 25, An Overview of the Japanese GALA-V Wideband VLBI System
- Ullrich, Dieter*: p. 225, Refinement of the Rapid UT1 Estimation Derived from Tsukuba VLBI Measurements after the 2011 Earthquake
- Vaquero Jiménez, B.*: p. 146, The German Antarctic Receiving Station O’Higgins and Its VLBI Capabilities
- Varenius, Eskil*: p. 234, Hard- and Software Tools for the Education of Geodetic VLBI
- Virtanen, Jenni*: p. 143, Metsähovi Geodetic Fundamental Station in Finland — New VGOS Site, Plans, and Current Status
- Vytnov, Alexander*: p. 106, New Generation VLBI: Intraday UT1 Estimations
- Wang, Guangli*: p. 3, Strategic Plan of the IVS for the Period 2016–2025
- p. 203, Results from the VLBI Analysis Software Comparison Campaign 2015
- p. 317, Source Structure of 0642+449 Derived from CONT14 Observations
- p. 363, APOD Mission Status and Observations by VLBI
- Watabe, Ken-ichi*: p. 25, An Overview of the Japanese GALA-V Wideband VLBI System
- Wettzell VLBI Team*: p. 101, Current Status of an Implementation of a System Monitoring for Seamless Auxiliary Data at the Geodetic Observatory Wettzell
- p. 146, The German Antarctic Receiving Station O’Higgins and Its VLBI Capabilities
- Wojdziak, R.*: p. 146, The German Antarctic Receiving Station O’Higgins and Its VLBI Capabilities
- Wu, Yajun*: p. 163, Progress on the VLBI Data Acquisition System of SHAO
- Xu, Minghui*: p. 203, Results from the VLBI Analysis Software Comparison Campaign 2015
- p. 297, About the Modeling of Radio Source Time Series as Linear Splines
- p. 317, **Source Structure of 0642+449 Derived from CONT14 Observations**
- Xu, Zhijun*: p. 180, **Hardware Correlator Development at SHAO**
- p. 183, High-speed Data Playback of the VLBI Hardware Correlator
- Yi, Sang-oh*: p. 139, **Activities at Sejong Station**
- p. 351, Progress on the VLBI Ecliptic Plane Survey
- Zandbergen, René*: p. 261, VLBI Processing at ESOC
- Zhang, Bo*: p. 321, **Images of VLBI Calibrators from the BeSSeL Survey**
- Zheng, Weimin*: p. 203, Results from the VLBI Analysis Software Comparison Campaign 2015
- p. 378, **Accurate Spacecraft Positioning by VLBI Imaging**
- Zhu, Renjie*: p. 163, **Progress on the VLBI Data Acquisition System of SHAO**
- Zubko, Nataliya*: p. 143, **Metsähovi Geodetic Fundamental Station in Finland — New VGOS Site, Plans, and Current Status**
- Zucco, Massimo*: p. 166, The First Geodetic VLBI Field Test of LIFT: A 550-km-long Optical Fiber Link for Remote Antenna Synchronization
- Zus, Florian*: p. 331, On the Impact of Different Mapping Functions on Geodetic and Tropospheric Products from VLBI Data Analysis